

INDENTATION OF BILLETS IN CONTINUOUS EXTRUSION

By

Ali Najafi Sani

April 1980

A thesis submitted for the degree of  
Doctor of Philosophy of the University  
of London and for the Diploma of  
Imperial College.

Mechanical Engineering Department  
Imperial College  
London, S.W.7.

*To Imam Khomeini  
the mighty leader of the  
oppressed people of the entire world.*

*To memory of my father's soul.*

*To my mother, brothers and sisters.*

## SYNOPSIS

A comprehensive survey of the continuous extrusion processes is first given. Amongst the many possibilities, the newly developed method of 'Context' is favoured for its sheer advantage of extruding almost any size and configuration of billet at any conceivable extrusion ratio. The importance is then discussed of the indenting mechanism by which the billet is gripped and dragged forward in a Context type process. The indentation process is put forward as a subject to be investigated in order to explore the real potential of Context, or in principle, any other type of friction-actuated continuous extrusion which uses the same mechanism of indenting the billet.

The finite element technique is the main tool for predicting the deformation during the indentation process under the conditions when plane strain prevails. The usefulness of the finite element technique for detailed studies of deformation-characteristics is demonstrated in a number of suggested problems. The load-displacement curve, geometrical change of the billet, stress and strain distribution are computed and are shown to predict well the actual behaviour of the material. Evidently the finite element method is an extremely powerful tool for analysis.

As a further study, an analytical solution for the process of Context itself is developed. Using a simplified small scale model, the relevant experiments are conducted and the experimental and theoretical findings are presented and compared. The experimental findings reveal the great potential of Context in generating a

considerable amount of drag-force to enable large extrusion ratios to be achieved.

ACKNOWLEDGEMENTS

I sincerely express my deepest gratitude to Dr. B. Lengyel for suggesting the topic and for his guidance and invaluable advice without which this project would have not been completed. I also would like to thank professor J. M. Alexander for his kind permission to use the metal working facilities in the course of experiments.

Thanks are due also to Mr. H. Ramsey for his kind permission to use the work-shop facilities without which the experimental set-ups would have not been possible. Special thanks are also due to Mr. G. Yantian for reading the text and to Miss Amanda Scarrott who patiently typed the manuscript.

The financial support from the Iranian institute of technology of Isfahan is gratefully acknowledged and highly appreciated.

Last but not least the constant encouragement of my late father and also of my mother, and brother Mr. Hussein Najafi Sani, is acknowledged and highly appreciated.

Ali Najafi Sani

April 1980.

Contents

	<u>Page</u>
Synopsis . . . . .	1
Acknowledgements . . . . .	3
Contents . . . . .	4
Notations . . . . .	9
1. <u>Introduction</u> . . . . .	11
1.1 Literature survey . . . . .	11
1.2 Continuous hydrostatic extrusion . . . . .	12
1.2.1 Continuous hydrostatic extrusion with stationary chamber . . . . .	12
1.2.2 Continuous hydrostatic extrusion with moving chamber (Gear Extruder) . . . . .	14
1.3 Continuous conventional extrusion . . . . .	14
1.3.1 Conform . . . . .	15
1.3.2 Extrolling . . . . .	18
1.3.3 Linex . . . . .	20
1.3.4 Context . . . . .	23
1.4 Critical assessment of the indentation process in Context .	29
1.5 Aims of the present work . . . . .	32
2. <u>A finite element formulation for the elastic-plastic analysis of small strains and small displacements</u> . . . . .	34
2.1 Introduction . . . . .	34
2.2 Literature survey . . . . .	35
2.3 Concept of the finite element . . . . .	45
2.4 Basic formulation . . . . .	46

2.4.1	Displacement function	46
2.4.2	Strains	47
2.4.3	Stresses	47
2.4.4	Equivalent nodal forces	48
2.4.5	Equilibrium condition	49
2.5	Non-linear material formulation	51
2.5.1	Derivation of the elastic-plastic stress-strain matrix $[D]^{EP}$	54
2.6	Solution algorithms	60
2.6.1	Tangential stiffness method	61
2.6.1.1	Calculation of the rating factor	68
2.6.2	Initial strain method	69
2.6.3	Initial stress method	71
2.7	Comparison of algorithms	73
2.8	Elements implemented in the computer programs	74
2.8.1	Constant strain triangle elements	74
2.8.2	Quadrilateral elements (consisting of four constant strain triangles)	77
2.8.3	Quadrilateral isoparametric elements	79
2.9	Conclusion	84
3.	<u>The computer programs</u>	86
3.1	Introduction	86
3.2	Computation procedure	86
3.3	Description of the programs	90
3.4	Analysis of the program EPFEAL	90
3.4.1	Subroutine GDATA	90
3.4.2	Subroutine SKFORM	92

3.4.3	Subroutine BOND1	.	.	.	.	.	.	92
3.4.4	Subroutine YIELD1	.	.	.	.	.	.	93
3.4.5	Subroutine CHANGE	.	.	.	.	.	.	94
3.4.6	Subroutine BOND2	.	.	.	.	.	.	94
3.4.7	Subroutine YIELD2	.	.	.	.	.	.	96
3.5	Analysis of the program EPFEA2	.	.	.	.	.	.	97
3.5.1	Subroutine GDATA	.	.	.	.	.	.	98
3.5.2	Subroutine SKFORM	.	.	.	.	.	.	99
3.5.3	Subroutine YIELD1	.	.	.	.	.	.	99
3.5.4	Subroutine YIELD2	.	.	.	.	.	.	99
3.6	Analysis of the program EPFEA3	.	.	.	.	.	.	100
3.6.1	Subroutine GDATA	.	.	.	.	.	.	100
3.6.2	Subroutine YIELD1	.	.	.	.	.	.	101
4.	<u>Experimental work</u>	.	.	.	.	.	.	102
4.1	Introduction	.	.	.	.	.	.	102
	Part 1: <u>Study of the indentation process</u>	.	.	.	.	.	.	103
4.2	Introduction	.	.	.	.	.	.	103
4.3	Design considerations	.	.	.	.	.	.	105
4.4	Experimental set-up	.	.	.	.	.	.	105
4.5	Specimens	.	.	.	.	.	.	107
4.6	Instrumentation	.	.	.	.	.	.	109
4.6.1	Data logger	.	.	.	.	.	.	109
4.6.2	Measurement of dimension and area	.	.	.	.	.	.	109
4.6.3	Surface profile measurements	.	.	.	.	.	.	110
4.7	Parameters defining the state of deformation	.	.	.	.	.	.	110
4.8	Experimental procedure	.	.	.	.	.	.	113
4.9	Experimental results and discussions	.	.	.	.	.	.	114



Part II:	<u>Study of the maximum drag-force induced at the interface of the billet and the chamber in Context continuous extrusion</u>	
		159
4.10	Introduction	159
4.11	Design considerations	160
4.12	Experimental set-up	160
4.13	Specimens	162
4.14	Experimental procedure	163
4.15	Theoretical solution	164
4.16	Experimental and theoretical results and discussions	180
4.17	Conclusions and further work	185
5	<u>Results and discussions</u>	187
5.1	Introduction	187
5.2	A study of case (a)	190
5.2.1	Results obtained by the finite element method	196
5.2.2	Results obtained from volume constancy	208
5.2.3	Results obtained from slip-line theory	216
5.2.4	Comparison of the results	222
5.3	A study of case (b)	225
5.3.1	Results obtained by the finite element method	227
5.3.2	Results obtained from volume constancy	239
5.3.3	Results obtained by the upper-bound theorem	245
5.3.4	Comparison of the results	250
5.3.5	Supplementary computer runs	254
5.3.5.1	Problem I	254
5.3.5.2	Problem II	261
5.4	A study of case (c)	274

5.4.1	Results obtained by the finite element method	. . . . .	276
5.4.2	Results obtained from volume constancy	. . . . .	288
5.5	A study of case (d)	. . . . .	294
5.5.1	Results obtained from the finite element method	. . . . .	297
5.5.2	Upper-bound solution	. . . . .	301
5.6	Conclusions	. . . . .	306
Appendix A	. . . . .	. . . . .	308
Appendix B	. . . . .	. . . . .	325
Appendix C	. . . . .	. . . . .	346
References	. . . . .	. . . . .	362

NOTATIONS

$\{ \}$	column vector
$[ ]$	row vector, or rectangular or square matrix
$[ ]^T, \{ \}^T$	transpose of a matrix or column vector
$[ ]^{-1}$	inverse of a square matrix
$\det [ ]$	determinant of a square matrix
$[B]$	strain-displacement matrix
$[D]^E$	elastic stress-strain matrix
$[D]^P$	plastic stress-strain matrix
$[D]^{EP}$	elastic-plastic stress-strain matrix
$\{f\}_e$	displacement matrix associated with an element
$\{F\}_e$	elemental nodal forces matrix
$\{F\}_{\epsilon 0}$	load matrix due to initial strain $\epsilon_0$
$\{F\}_{\sigma 0}$	load matrix due to initial stress $\sigma_0$
$[I]$	identity matrix
$[J]$	Jacobian matrix
$[K]$	structure stiffness matrix
$[K]_e$	element stiffness matrix
$[N]$	shape function matrix
$\{P\}$	load matrix due to distributed body force
$\{\epsilon\}$	strain matrix
$\{\epsilon\}_0$	initial strain matrix
$\{\sigma\}$	stress matrix
$\{\sigma\}_0$	initial stress matrix
$a$	length
$A$	area
$b$	width

$D$	diameter of billet
$D_0$	initial diameter of billet
$E$	elastic modulus of material
$F$	indenting force applied to billet by the container
$F_d$	axial drag-force applied to billet by the container
$F_e$	axial end-force applied to pressure pad
$H$	height of billet, or slope of stress-strain curve
$H_0$	initial height of billet
$k$	yield shear stress of material
$l$	length
$L$	length of billet
$L_0$	initial length of billet
$P$	mean normal pressure applied to billet by the platens
$\bar{P}$	axial mean pressure
$r$	rating factor, or radius
$T$	interfacial frictional force
$Y$	yield stress of material
$\nu$	Poisson's ratio
$\mu$	coefficient of friction
$\bar{\epsilon}$	equivalent strain
$\epsilon_{ij}$	strain component
$\dot{\epsilon}_{ij}$	strain rate component
$\bar{\sigma}$	equivalent stress
$\sigma_m$	hydrostatic stress
$\sigma_{ij}$	stress component
$\sigma'_{ij}$	deviatoric stress component
$\tau_{xy}$	shear stress component

CHAPTER 1  
INTRODUCTION

1.1 Literature Survey

Present day production processes tend towards automation, requiring little or no skilled labour. This obvious trend is sought especially in the heavy metal forming industry.

Ever since the first continuous extrusion was introduced remarkable attention has been directed towards developing new concepts which can simply and effectively impart a desirable shape to an unlimited length of metal. In view of the fact that supply and cost of material is becoming critical, the expansion of continuous extrusion has been given considerable priority. As to the industrial applications, continuous extrusion is highly recommended for its remarkably low running cost and the continuity of its product which effectively reduce waste.

In the past few years numerous concepts have been presented and their practical feasibility have also been verified. From an economical point of view, however, these concepts have not yet found extensive industrial application owing to such clear disadvantages as: large capital investment, limited extrusion pressure and limited capacity in utilising feedstocks having various shapes and sizes.

Development of the continuous extrusion process falls into two distinct categories, namely:

- (a) Continuous hydrostatic (or viscous drag actuated) extrusion.
- (b) Continuous conventional (or friction actuated) extrusion.

## 1.2 Continuous hydrostatic extrusion

Briefly, in viscous actuated systems, the feedstock is pushed against the die by the motion of a viscous medium which envelopes the feedstock. There are two known versions of such systems, both basically hydrostatic in operation:

- (1) Viscous drag with stationary chamber.
- (2) Viscous drag with moving chamber.

### 1.2.1 Continuous hydrostatic extrusion with stationary chamber

Fuchs (1) of the Western Electric Company developed a new continuous hydrostatic extrusion process which utilized a pressurised flowing fluid (such as beeswax) to move the feedstock into a chamber and through the extrusion die. The basic principle is illustrated in Fig. 1-1. This system consists of an extrusion compartment and several feed compartments. Extrusion pressure  $P_1$  is maintained continuously in the extrusion compartment by two rams, working alternately. Similarly, viscous fluid is pumped into the first feed compartment continuously. As the viscous fluid is forced along axially in the feed compartment, the viscous-drag forces the billet into the extrusion compartment. Clearly the difference between the pressure of the extrusion fluid and that of the viscous fluid must be less than the yield stress of the billet material, in order to prevent plastic flow of the billet at the separating wall between the two compartments. Since the same principle is applicable for the pressure difference at the entry to the first feed compartment, a series of steps is needed until the pressure is reduced to the atmospheric pressure. Heating liners are used in the bore of the feed compartments to reduce the viscous drag along the walls and this

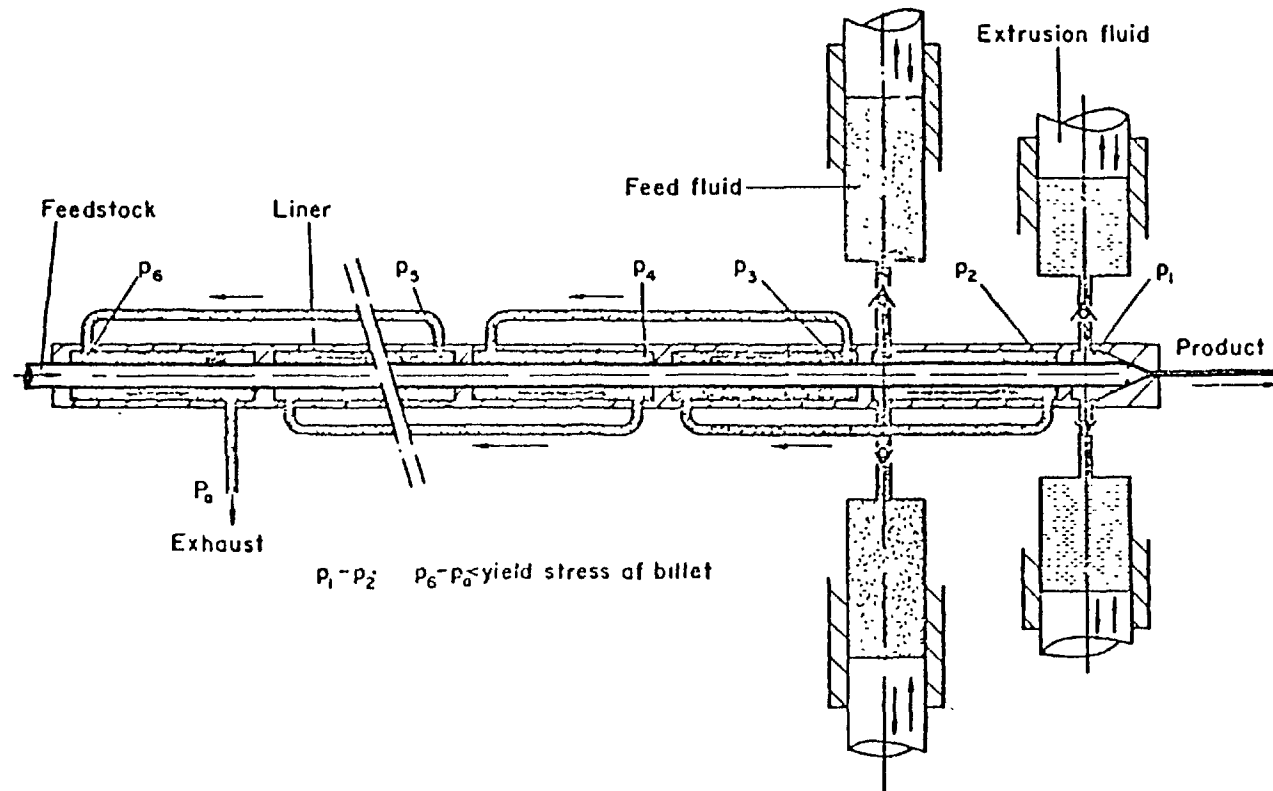


Fig. 1-1. Continuous hydrostatic extrusion.

improves the efficiency of the process.

### 1.2.2 Continuous hydrostatic extrusion with moving chamber (Gear Extruder)

This second process, also developed by Fuchs (2), employs a moving chamber with the viscous fluid dragging the feedstock to the extrusion die.

Essentially, the device has an endless travelling block consisting of circumferentially quartered segments divided into short axial lengths. A rack, machined on each side of the two corners of the segments, provides a means of driving them through the machine. The moving segments are coupled to the wire rod by a viscous medium which moves through the machine towards a fixed die. The viscous medium is a low molecular weight polyethylene which is coated on the billet before it enters the pressure chamber. The basic principle of the process is as follows:

The rod is inserted into the travelling segments through the straightener and coating head. It is then dragged into the pressure chamber at the centre of the continuous extruder. As the members pass over the die, the rod is forced to extrude through the die. The moving container is then split into four segments and transported back to the front-end of the extruder for re-use.

### 1.3 Continuous conventional extrusion

To date three types of friction actuated machines have been developed for commercial use. They are:

- (a) Conform
- (b) Extrolling
- (c) Linex



### 1.3.1 Conform

The concept of Conform can be best explained by referring to the earliest method of conventional extrusion.

In direct conventional extrusion considerable friction exists between the surface of the billet and the bore of its container. The magnitude of the frictional force is greatest at the commencement of the extrusion process, when the billet is of maximum length. Consequently, there is a limit to the length of billet in relation to its diameter. It is of interest to note that this limiting feature, which has motivated the development of hydrostatic extrusion, is now used in the new concept to allow the extrusion of billet of any length.

Fig. 1-2 shows a conventional extrusion system consisting of a punch, container, die and billet. Extrusion can be brought about either by forcing the punch into the container (direct extrusion) or by forcing the die into the container keeping the punch stationary relative to the container (indirect extrusion). In the latter case, the frictional force mentioned does not have to be overcome by the die because the billet does not move relative to the container. If, in fact, the billet was above a certain critical length to diameter ratio the frictional force alone would be sufficient to hold the billet in the container against the force of the die during extrusion. In such circumstances, extrusion would continue only until the billet shortened to a critical length at which point it would then slide away through the container in front of the advancing die (hence one of the reasons for the punch). However, despite this advantage of indirect extrusion the length of billet that may be extruded is still limited.

Green (3) was the first to use this understanding of the

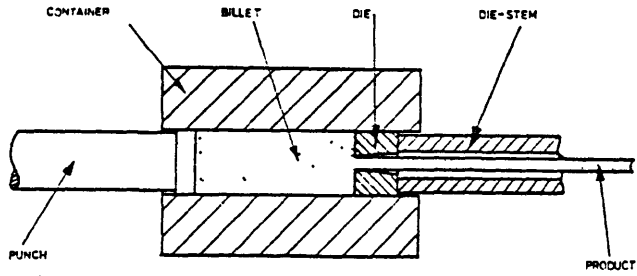


FIG. 1-2. Conventional extrusion system.

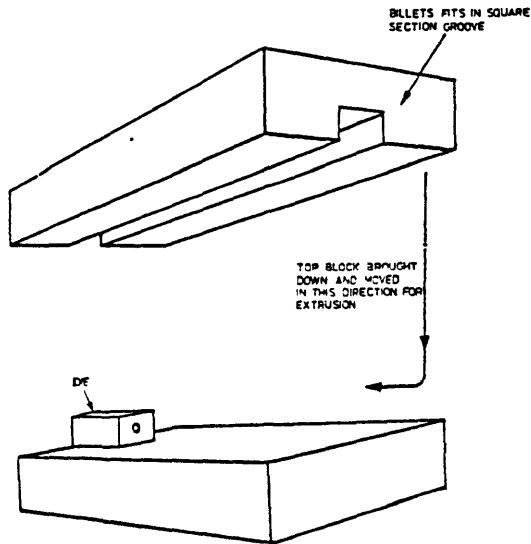


FIG. 1-3. Container concept.

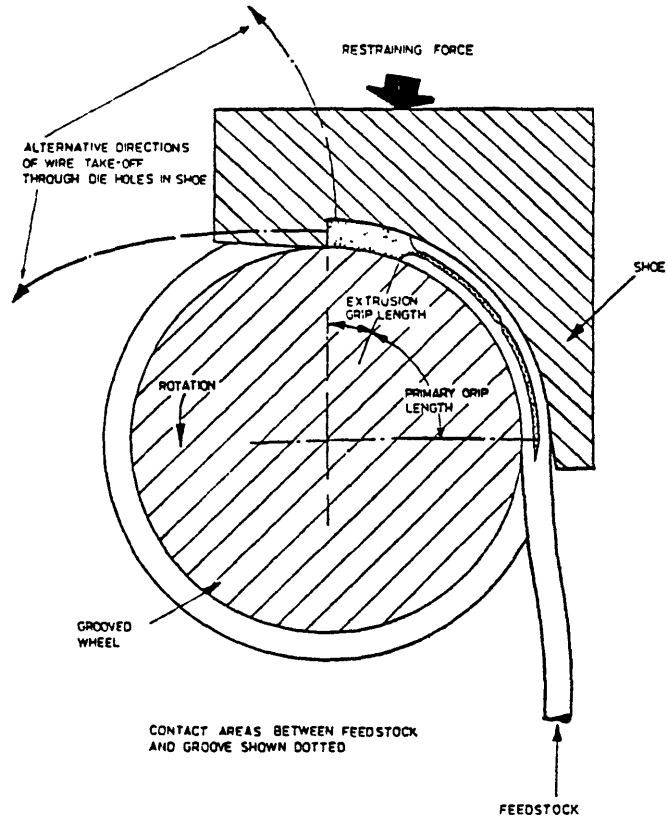


FIG. 1-4. Diagrammatic arrangement of continuous extruder.

indirect extrusion process to develop a continuous extruder, Conform. As shown in Fig. 1-3, the container, having a rectangular-section, is made up of two pieces, one of them incorporating a rectangular groove and the other being just a plain rectangular slab. When put together they form a square-section block with a square-section hole. A square die is fixed into the plain slab in such a way that it protrudes into and effectively blocks off one end of the square hole in the composite container. With this arrangement, the slab portion of the container may be held stationary while the other portion may slide along, and over, the stationary die. Thus three sides of the container may move relative to the remaining fourth side.

In such a model one can consider a billet of round-section, partially contacting all four sides of the container. If the container is now moved as described, the frictional force existing between its three sides and the billet will provide a force tending to move the billet against the die. Clearly the frictional force between the fourth side and the billet will tend to oppose billet movement. Therefore, there will remain a residual force equal to that arising from friction between the billet and two sides. The whole of this residual force is available for use in extruding the billet through the die.

In the die region the compressive stress in the workpiece is likely to be many times greater than the yield stress of the workpiece material. Consequently, the workpiece will flow until it completely fills the rectangular container over a proportion of its length immediately before the die. The length that is filled has similarities with the critical billet length in normal indirect extrusion already referred to. Now, if the contact length is

sufficient and the container is operated as described, extrusion will commence and continue until the length of the contact drops to a critical value. At this point slip will occur. For continuous extrusion, it is therefore necessary to ensure that the length of the contact is by some means constantly maintained greater than a certain critical length. The requirement for truly continuous extrusion is to provide for a continuous length of grooved container and this requirement is most easily and simply met by a disc or wheel having a groove machined around its perimeter. The fourth side of the containment is the inner curved surface of a 'shoe' arranged to fit closely up against the wheel perimeter as shown in Fig. 1-4. In this method the shoe, which resembles an external drum brake, carries the extrusion die. It can be visualized that several separate shoes could be coupled on a rotating disc and also that a number of wheels could be assembled on a single main rotating axle. Either of these techniques could be employed so as to produce multiple products in one machine.

### 1.3.2 Extrolling

Combining extrusion and rolling Avitzur (4) invented a new continuous conventional extrusion called Extrolling. This process combines the continuity of the rolling operation with the high reduction possible in extrusion. The deficiencies of rolling and extrusion, namely, small reduction per pass and finite length are eliminated.

This concept is basically the same as Conform except that the sliding shoe is replaced by a roller. As shown in Fig. 1-5, the rollers provide the forward-moving chamber, as the billet enters the groove,

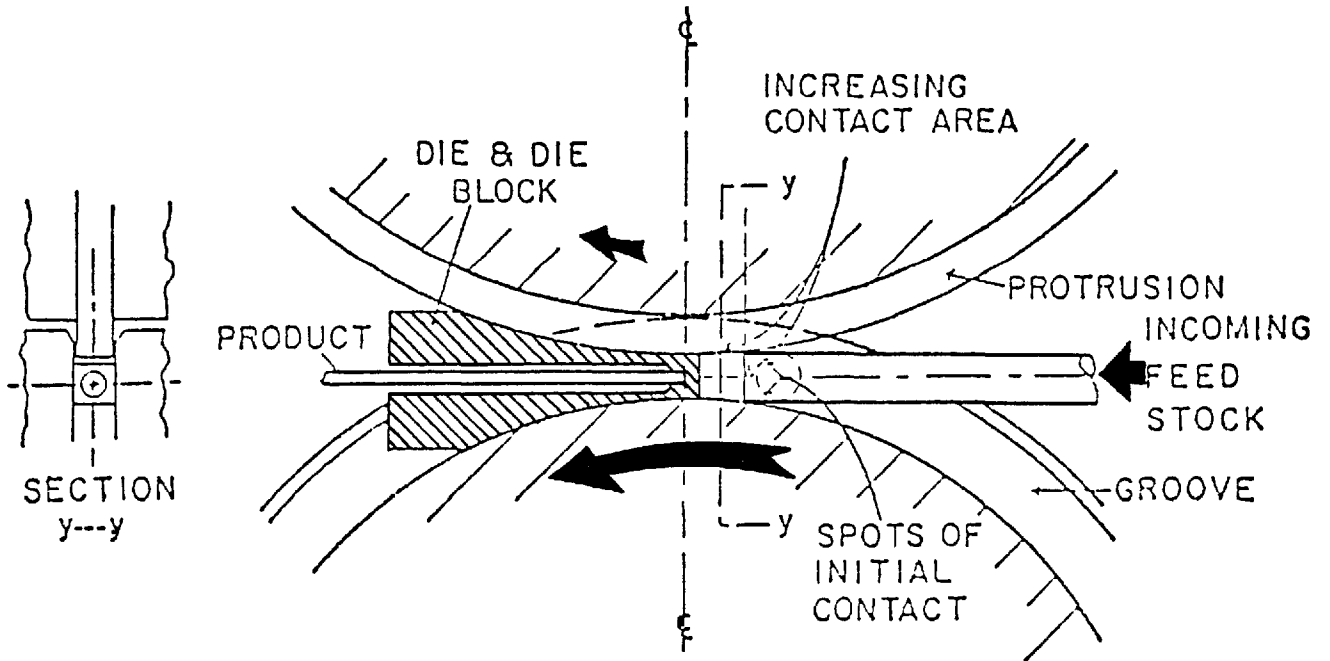
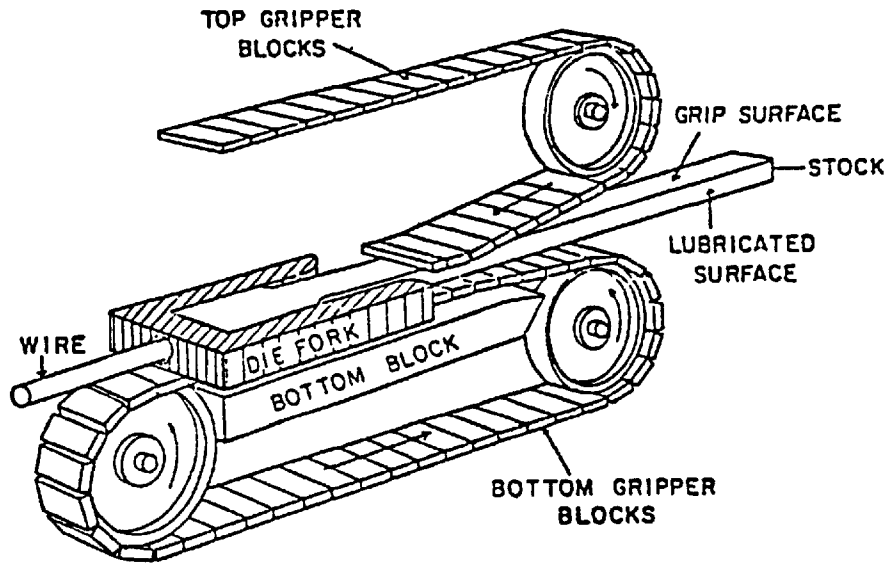


Fig. 1-5. Side view schematic of Extrolling process showing similarity to Conform. Section view y-y of a grooved wheel with protrusion segment.

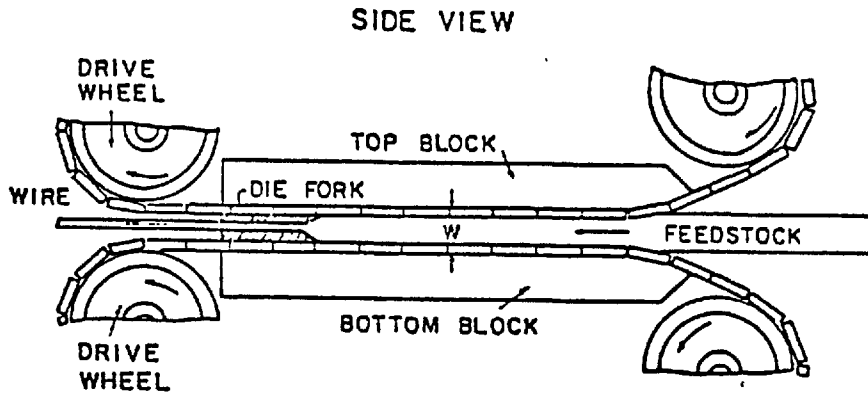
it is dragged forward by friction. As in Conform, for extrusion to occur continuously, a minimum length of contact must be maintained between the workpiece and the chamber. Most materials that can be either rolled or extruded can also be Extrolled. The process can also be adapted at elevated temperatures.

### 1.3.3 Linex

The process of continuous extrusion can be performed in a linear fashion rather than circular as previously described in Conform. Voorhes (5) discovered that two-sided gripping and advancement of the feedstock may be utilized in a continuous extrusion process. The opposing ungripped surfaces of the feedstock are lubricated before the stock upsets against the constraining walls of a chamber. This is shown schematically in Fig. 1-6. Two sides of the chamber are fixed and are composed of the legs of a unique fork-shaped die element. Gripping surfaces make up the other two sides of the chamber, whilst supported by two guiding blocks as shown in Fig. 1-6. Usually, the stock is roughly rectangular in cross section. Round stock is deformed into rectangular feedstock by a preform stage. The objective is to increase the grip area and thus the friction drag. During operation, the stock is carried into the die by two gripping surfaces. The gripping surfaces are hardened steel blocks assembled on two chains which are pulled by drive sprockets past the die. The blocks compress the stock and deform it plastically to a point beyond its yield stress and then carry it into the die fork. The ungripped sides of the feedstock are lubricated to reduce the coefficient of sliding friction between the upset feedstock and the legs of the die fork. As in Conform the upset length stabilizes when sufficient pressure for



Overview of LINEX friction actuated linear continuous extruder.



Side view cross section of linear continuous extruder.

Fig. 1-6. Linex.

extrusion has been developed. When this occurs the process runs in a steady state manner. Comparing Conform and Linex, there are some differences in extrusion characteristics between the two processes. In Linex, the feedstock is lubricated before entering the legs of the die. This cuts down the amount of frictional heat going into the stock prior to extrusion. In Conform there is no lubrication where the feedstock upsets against the shoe. The frictional heat causes the stock temperature to increase significantly as it approaches the die. As a result, Linex operates at some-what lower temperatures. Lower output temperatures mean that the product will not self-anneal, but will exhibit an increase in hardness approximately equivalent to that obtained by wire drawing to the same reduction ratio.

The Linex and Conform processes should have the following economic advantages over wire drawing: 1) Rapid change-over in die and wire sizes; 2) One die versus many dies to achieve the same reduction; 2) Wire breakage less likely; 4) One stage of reduction; 5) Lower initial investment cost for a totally new system; 6) Production of complex sections and tubing in a continuous manner.

The lubricator section of the Linex machine is designed to provide continuous application of lubricant to the two ungripped sides of the feedstock. A variety of lubricants may be used but solid lubricants are preferable since they are easy to handle on a continuous basis and can be applied relatively easily and tend to remain where applied.



#### 1.3.4 Context

The most recent idea for continuous extrusion is that proposed by Lengyel (6). The arrangement shown in Fig. 1-7 shows the basic principle of this concept. When the container walls are moved parallel to the billet axis. In this case only friction drags the stock forward towards the die.

The moving container comprises a number of members. Each member of the container is built up from four parts, but alternative arrangements are feasible (such as those illustrated in Fig. 1-8) to accommodate favourably various shapes of feedstocks. These stock shapes would be useful when extruding products of intricate geometry, for example very wide thin sections which nowadays must be produced from round billets either at very large extrusion ratios or in several steps. It might often be cheaper to cast or roll the billets to a cross-section considered most favourable for a particular product and extrude them from a specially shaped container.

The parts shown in Fig. 1-7 could be moved towards the axis and away from it, always forming a fully enclosed channel between them. A major advantage of this present configuration is its ability to accommodate not only stock of various sections but also many sizes of stock, since each part can slide on both its adjacent parts to create a smaller chamber. With the outer tube empty, a long billet of circular or other cross-section is moved into position coaxially with the outer tube. The four parts of the first member of the container are then placed into position and forced towards the axis, plastically deforming the billet material as shown in section B-B. This member together with the billet is then forced towards the die, then the four parts of the second member are placed into position behind the first

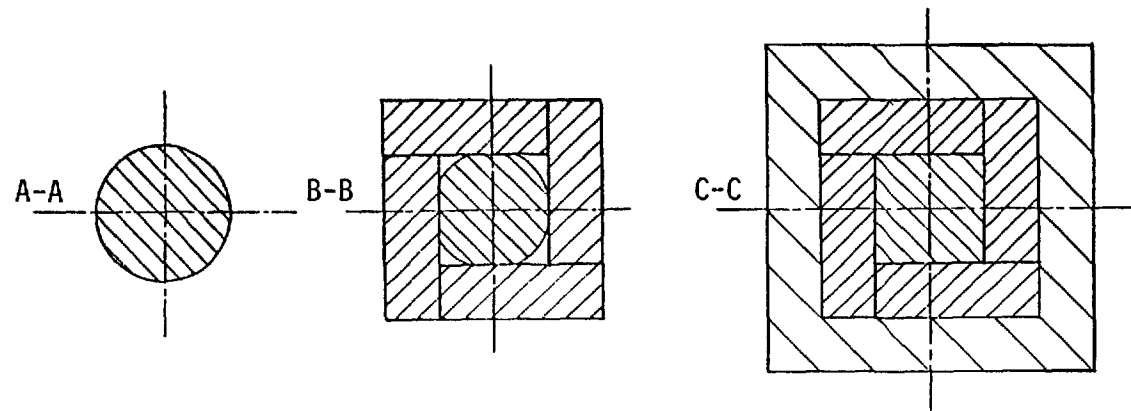
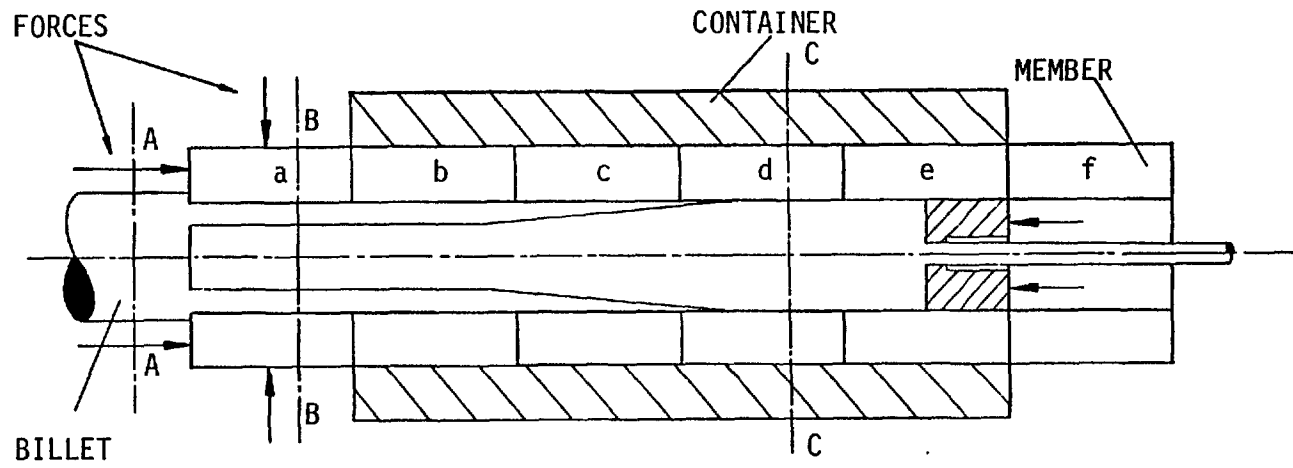


Fig. 1-7. Context.

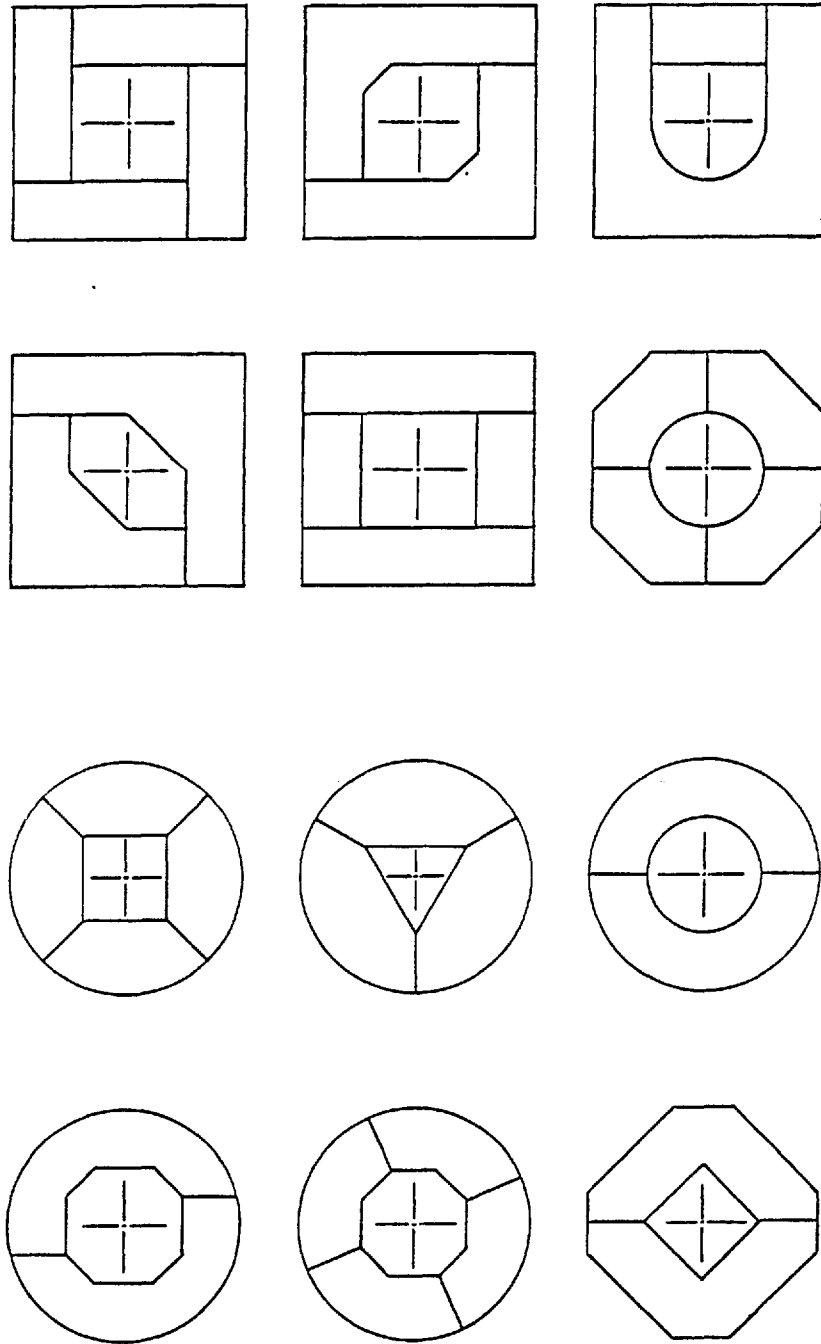


Fig. 1-8. Alternatives in chamber section.

one and forced towards the axis deforming the billet. The process is repeated with the subsequent members until the front-end-face of the billet reaches the die, with one member of the container supporting the die in position 'e'. The container is then forced towards the die with the die exerting pressure on the billet-end. Provided the frictional force between the billet and the container is sufficiently large, the billet material near the die-face suffers further plastic deformation and fills the cross-section of the container completely (section C-C). The area of the interface and the interfacial pressure between billet and container is thus increased. The frictional force dragging the billet forward will also increase until the pressure between the die and the billet material becomes so large as to extrude the latter through the die orifice. As the foremost member clears the outer tube (position 'f') it is returned to continue the process behind the last one (position 'a'). As the back-end of the billet reaches the entry section, a second billet is placed behind the back-end of the first one and the process continues for as long as desired, without interruption or change of speed.

In Fig. 1-9 another possible version of Context continuous extrusion is shown. Here the members are placed in position 'a' at an angle ' $\alpha$ ' to the axis. The billet is indented at this angle and then the members are forced towards the die on a path parallel to the container axis. When the members reach the die in position 'd' they must continue to travel at angle ' $\alpha$ ' to the axis in order to by-pass the die, on a diverging path.

In the diverging version not only friction, but also the indenting forces assist the forward moving of the billet in building up pressure over the die-face. Clearly the members in positions 'b'

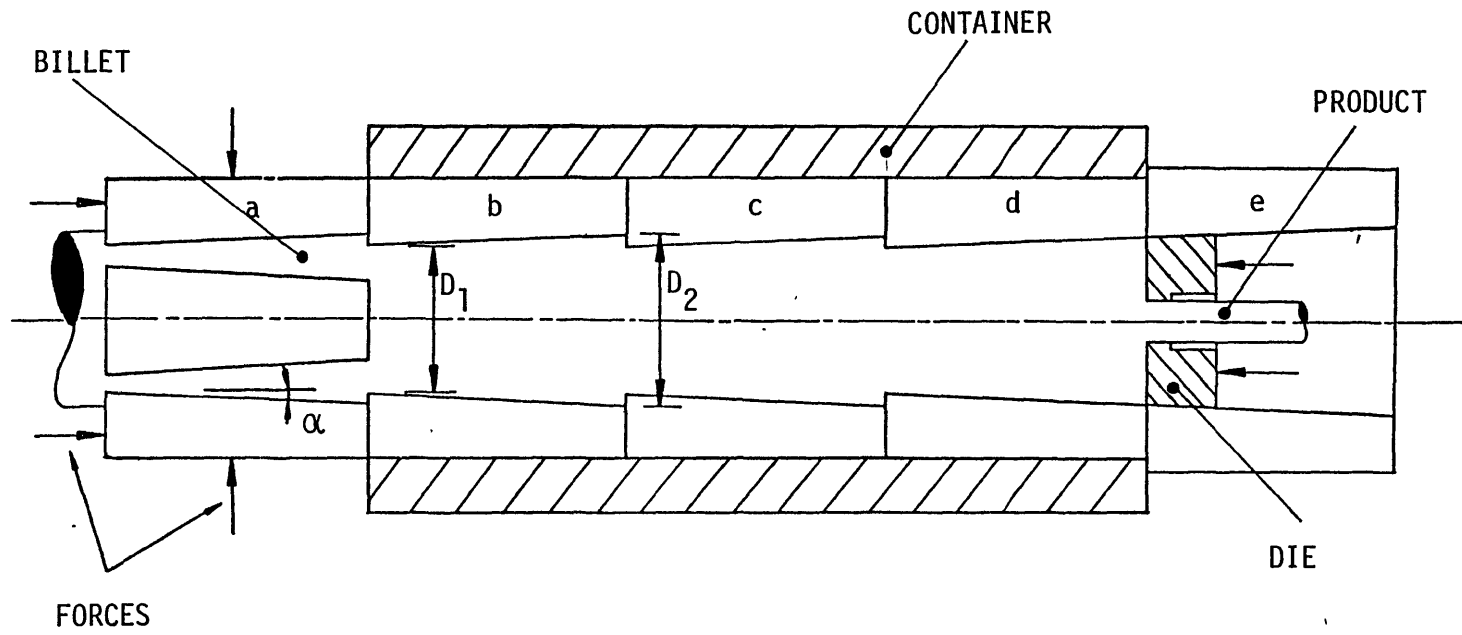


Fig. 1-9. Another version of Context.

and 'c' where they are completely filled with the stock material, could be regarded as dies of square cross sectional area. Before slip could occur between these members and the feedstock not only must the stock/container friction be exceeded but also the stock must be reduced from size  $D_2$  to  $D_1$ . Consequently, a shorter container would be sufficient to build up a particular pressure. Even if the stock/container friction is small, the required pressure could be built up and thus lubricated extrusion would be feasible. From a technical point of view Context offers a wide range of advantages compared with the other methods of conventional continuous extrusion.

Viscous actuated systems are not suitable for hot extrusion. A hot billet reduces the viscous drag in the feed compartment (viscosity is inversely proportional to temperature) where the viscosity is needed most. Energy is also wasted in the transportation of the feed fluid in the bore of the feed compartment where the viscosity must be as low as possible. This means that the process is considerably inefficient. In the Gear Extruder, also a cold process, the problem of sealing between the members is apparent. The extrusion ratio of both these processes is limited.

Conform and Linex were developed mainly for the extrusion of wire, i.e. feedstock of small diameter is reduced in one step into wire of the required dimension.

In Conform, the billet material has to be bent and dragged towards the die. Clearly Conform cannot be modified to use large diameter feedstock as the work done in bending the billet would be significant and wasted. Furthermore, it would be difficult to design a drive to deliver the load needed for extrusion. Additionally there is a

stationary shoe which opposes the forward movement of the feedstock, which further increases the load.

In Linex, a worse situation arises. There are only two gripping faces dragging the billet forward while the arms of the diefork oppose it. Even for wire extrusion, the side faces have to be lubricated to ensure no slippage. In the continuous process, there is no guarantee that the lubricant would not spread to the gripping faces. If this were to occur, the effectiveness of the gripping force would be markedly reduced and so also the extrusion force. Above all, on an industrial scale, continuous lubrication of the feedstock might present an economic problem in view of the cost of lubricant.

The concept of Context is simple and quite effective, if it is proved to be commercially and technically viable. In Context, all faces in contact with the billet are used to drag the billet forward. This automatically means that a much larger extrusion force can be achieved and a larger feedstock can be used.

Comparing viscous actuated continuous extrusion and Context the latter is clearly more efficient due to the direct contact between the container and the feedstock. The problem of sealing the viscous fluid does not exist in a Context type process. It is also clear that this process requires a shorter grip length than the viscous fluid actuated process due to its direct contact with the stock. Its advantage over Linex is apparent as there are not forces between the container walls and the feedstock, to oppose the motion of the feedstock.

#### 1.4 Critical assessment of the indentation process in Context

The possibility of utilising a wide range of billets having various shapes and sizes is one of the most distinguishing features of Context.

In addition, in Context, the arrangement of the segments comprising the chamber can also be altered to accommodate a particular shape of billet in a favourable manner.

For a given chamber length and surface condition, the shape of billet and the arrangement of indenting segments together with the amount of indentation, entirely control the magnitude of the feasible extrusion pressure. In order to calculate the extrusion pressure, therefore, the analysis of the indentation process seems of vital importance. This is appreciated when noting that the friction forces responsible for gripping the billet are related to the indenting forces by some unknown friction coefficient.

By its very nature, the indentation process lacks a well-defined analytical treatment, since the conditions under which the metal flows are unpredictable and may vary enormously. During indentation, configuration of the feedstock and the surface friction may vary considerably. Plastic flow may not only occur in a plane perpendicular to the axis of billet but it may also occur in a direction along the billet. The situation is even more complex when the indenting segments perform their duties at an angle to the axis of the billet.

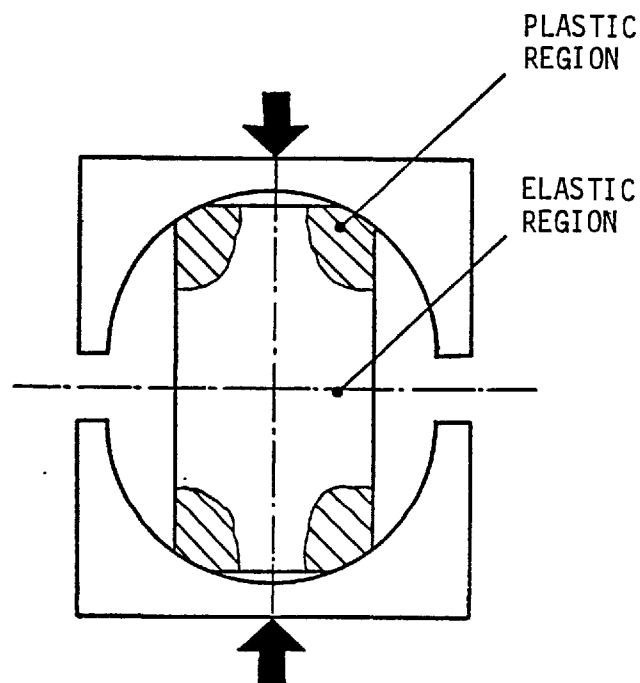
In the indentation process, nevertheless, there are a number of phenomena which tend to retard the axial flow of the material, such as:

(i) Elastic constraint

Usually (but not always) when the amount of indentation is moderate, the plastic flow occurs only in the material adjacent to the indenting segments (such as shown in the illustration). Thus the remaining elastic region extending through the depth of indentation tends to prevent the plastic material from spreading. This kind of constraint is frequently encountered when the billet section is not



uniformly strained, in which case the plastic flow may not spread throughout the section.



(ii) Frictional forces induced at the billet/container interface

An obvious tendency of frictional forces is to prevent the material moving relative to the surface of the indenting segments. When the length of indenting segments in relation to the diameter of billet is sufficiently large it is reasonable to neglect the plastic deformation of the billet in the axial direction relative to that occurring in the cross-sectional area.

(iii) Axial compressive pressure

Due to the mechanism of indentation in Context, which combines both indentation and forward moving of the billet, an axial compressive pressure exists which retards the plastic flow of the billet in the axial direction.

In the indentation process the state of stress and strain is three dimensional. However, when the effects of the foregoing phenomena

combine to eliminate the axial extension of the billet, the deformation can be said to be taking place under plane strain conditions. In such circumstances the study of indentation under conditions of plane strain will result in useful and instructive information on the behaviour of the stock during a three-dimensional indentation process.

#### 1.5 Aims of the present work

So far as the subject of interest is concerned the main two objectives for further investigations should be:

- (i) To study the indentation process
- (ii) To study the maximum frictional force built up at billet/container interface

This present work is an attempt to meet some of these objectives. For the study of the indentation process, the finite element method was selected. This selection was based on the strong capability of the finite element method in the analysis of metal working processes.

A finite element formulation is presented. Based on this formulation, a computer program is developed and its applicability is demonstrated by examining a number of indentation processes. Its extensive validity is also demonstrated by comparing the theoretical results and the corresponding experimental findings.

The finite element program presented is restricted by the following assumptions:

- (a) The magnitude of deformations remain small throughout the indentation process.
- (b) Absence of Bauschinger effect.
- (c) Isotropic material behaviour.

- (d) Plane strain deformation.
- (e) Absence of thermal strains.

To meet the second objective an analytical solution was chosen, to predict simply and effectively the maximum frictional forces built up at billet/container interface, because the finite element approach would have been highly demanding in terms of computing time in view of the immense three dimensional problem involved.

For a particular example, the process is simulated using a simplified model in the laboratory. Experiments are carried out and the effect of the relevant parameters, on the maximum frictional force built up at billet/container interface, are investigated. The process is then analysed theoretically and the theoretical and experimental results are presented and compared.

## CHAPTER 2

### A FINITE ELEMENT FORMULATION FOR THE ELASTIC-PLASTIC ANALYSIS OF SMALL STRAINS AND SMALL DISPLACEMENTS

#### 2.1 Introduction

The finite element method has been applied quite successfully to a wide range of linear structural problems and recently, the method has been extended to include material and geometric non-linearities. While the analysis of linear problems is relatively straightforward, the non-linear problem is considerably more difficult. Although a great number of papers have been published on the analysis of non-linear behaviour, a thorough survey of the available literature indicates that there is considerable uncertainty regarding important questions such as, which solution approach is the best, which flow rule is correct, how should unloading be treated, and so on. Perhaps the most disturbing point has been that most of the computational procedures currently available are very inefficient and require excessive amounts of computer time when applied to practical, large scale problems. The long computer run times (ranging from minutes to several hours) severely limit the use of these non-linear approaches as design tools for the majority of users.

The present study is concerned with presenting the solution techniques for the material non-linear problem with regard to accuracy and computational economy. The equations of equilibrium are first developed. Various solutions, restricted to small strains and displacements, which follow directly from the equilibrium equations are described. Based on the nature of solutions, some general comments and recommendations are made with regard to the accuracy and economy of each

method.

## 2.2 Literature survey

The first applications of finite element method to elastic-plastic problems appeared over a decade ago and were restricted to infinitesimal strains, in general describing only the onset of plastic deformation.

Based on the equilibrium equations, Mendelson and Manson (7) treated the plastic strain increments as thermal strains and developed a method called by them 'the thermal strain approach'. Subsequent papers eventually refer to the initial strain method or, in a modified form, to the initial stress approach. The basic concept of this method is that the equations of equilibrium can be modified to compensate for the fact that the plastic strains do not cause any change in stress. Gallagher (8) used this approach in the stress analysis of heated plates of complex shapes. Argyris (9) also used the method successfully in the analysis of the structural problems encountered.

The tangent modulus approach was first used by Pope (10) and Marcal (11) and extensively used by Marcal and his associates (12-14). Later, Akyuz and Merwin (15) considered contact problems and improved the accuracy of the solutions by using a half-step Runge-Kutta type procedure. Lee and Kobayashi (16) also considered contact problems and compared the experimental and computed results. The same authors, in another work (17), attempted the problem of axisymmetric upsetting and the problem of plane strain side-pressing of solid cylinders (this latter problem will be included amongst many others considered in this present thesis), using the same formulation. In both cases they refer to possibilities of the finite element method for such a class of problems, but remark that there are questions still to be solved, in order to

improve the accuracy of the solutions, especially when large strains are present. Scharpf (18) also uses a finite element formulation for elastic-plastic problems. There, application is made to the spreading of the plastic zone in a plate with a central straight crack. However, as changes in geometry were not considered, the computation had to be interrupted when the deformation became considerable. In (19) the subject is expanded and the tangential stiffness, initial strain and initial stress methods are again compared, by studying the convergence of each of them in one particular application.

Using the tangent modules method, Marcal and King (14) developed a computer program, which they used to investigate a number of problems. Among many problems they attempted were: thick cylinder subjected to internal pressure; flat tension specimen with a central hole; notched tension specimens under conditions of plane strain and plane stress. The computed results were compared with known solutions obtained by other methods. Although in general good agreement was obtained, the analysis of the deformation had to be interrupted at some stage because negative plastic strains were obtained. Later, Yamada and Yoshimura (20) modified their approach and the computer programs presented in this thesis are essentially based on this. In their formulation, for the first time, an explicit expression for the elasto-plastic stress-strain matrix (corresponding to the inverse of the complete stress-strain relations of Prandtl-Reuss) was derived. There, application was made to the analysis of notched tension specimens under conditions of plane stress. In each application they considered various mesh patterns (incorporating only triangular elements) and concluded that the results were highly dependent on the mesh pattern rather than on the mesh size. Again the procedure had limited application for the same reason as mentioned above.

A closer comparison of the algorithms used by Marcal and King (14) and Yamada and Yashimura (20) will be given in the theoretical formulation presented elsewhere.

Blomfield (21) has shown the similarity of the thermal strain and tangent modulus approaches, by deriving them both in terms of rate rather than incremental equations. Results obtained in the elastic-plastic analysis of pipe bends show no significant discrepancies when one or the other approach is used. Marcal (22) compared the two approaches in the case of a flat plate and compared them with existing solutions. He has shown that although the constitutive tensor must be recomputed for every load increment, the tangent modulus approach can be more economical in computation time than the thermal strain approach. In the specific example, in order to obey the prescribed stress-strain curve, only 10 increments in load were required by the tangent modulus against 2300 required by thermal strain approach. Marcal has also shown that, whilst the thermal strain approach is not applicable for perfect plasticity, not even for nearly perfect plasticity, the tangent modulus method does not present such restriction.

Using Yamada's approach several Japanese investigators presented solutions to a number of problems. Iwata (23) applied the same formulation to the analysis of hydrostatic extrusion. The effect of frictional coefficient on the spread of plastic zone, on the pressure-displacement curve, and on the stress distributions were studied in non-steady state plane-strain and axisymmetric extrusions. In the case of the plane-strain extrusion, the computed extrusion pressure and stress states in the plastic zone agreed with the slip-line field solution. The extrusion pressure for the axisymmetric condition was higher than that for plane strain condition, and it was significantly affected by the

coefficient of friction. Although, in general, their results seem to be in good agreement with the slip-line field solution the need for improvements in the method is stressed by the authors.

Nagamatsu (24) studied the compression of a block under conditions of plane-strain. The end-face of the block was supposed to stick to the tool surface (sticking friction). Since the onset of plastic deformation was only considered, the influence of shape changes on the stiffness matrix was neglected. Besides, to shorten the computing time, the changes in the elasto-plastic strain-stress matrix was also neglected. At early stages of deformation the appearance and growth of the plastic region, shape of the bulge, load of compression, distribution of normal pressure and of tangential stress at the interface were calculated. Although the plastic zone propagated over nearly the whole block, the maximum strain achieved was less than 0.13%. In a subsequent work (25) the same authors investigated the axial compression of circular solid and hollow cylinders. The deformation was examined from the elastic through partially plastic to totally plastic stages, considering the geometrical change of the nodal coordinates (such consideration was neglected in the earlier work). Again at various stages of deformation, the shape of the bulge in the inside (for a hollow cylinder) and outside surfaces, load, distribution of pressure and tangential stress on the contact surface between the tool and the cylinder, distribution of strain and stress, and the growth of plastic zone were calculated under various conditions. They were able to analyse the deformation for strains up to the order of 5% for solid, and 4% for hollow cylinders. The authors claim that still large values of strain could be considered at the cost of more computing time. Unusual large values of computed friction coefficients are



contributed to the improper implementation of boundary condition at the cylinder/tool interface.

Geometric non-linearities, as considered by Nagamatsu (25), were also treated by Argyris (9), Mallet and Marcal (26), Felippa (27) and Turner (28), but their solutions were restricted to small strains. Zienkiewicz (29) introduced the initial stress method to overcome the computing difficulties of the tangent modulus approach and the limitations of the thermal strain approach at nearly perfect plasticity. The method was implemented in a computer program and a number of problems such as perforated tension strip with and without strain hardening, cantilever beam subjected to cycling load, plastic yield during metal cutting, and a few others were investigated, showing generally good agreement. A subsequent work by Nayak and Zienkiewicz (30) presents a general formulation which includes: associated and non-associated plasticity; strain hardening and also strain softening behaviour. Advantage of the initial stress method is emphasized for a wide range of problems. Amongst many problems attempted are: cyclic loading of a composite bar, notched tension specimen, thick sphere and cylinder subjected to internal pressure, plane strain extrusion, and plane strain indentation (strain softening and strain hardening behaviour). The authors emphasize the possibility of including in one program a variety of iterative procedure, as they believe the best efficiency lies in a combination of various methods. Finally, they remark on those classes of problems, such as strain softening or collapse where the tangential matrix ceases to be positive definite whilst on the contrary the initial stress method presents no difficulty of that sort. On this same topic, Nayak's work (31) provides an extensive review of literature and covers

applications of the finite element method to a wide variety of fields; elastic-plastic problems, plate theory, complex material behaviour and analysis of large deformation in structural elements.

Most of the literature reviewed so far was concerned with small strain plasticity, therefore predicting the onset of yielding and the early spreading of the plastic zone with satisfactory levels of accuracy. Larger strains can either not be tackled or, as in Nagamatsu's approach (25), incur a heavy penalty in terms of computing time.

In recent years a trend towards the use of non-linear equations of continuum mechanics has been observed in papers on finite element analysis. Pian and Pin Tong (32) have shown that the finite method can be formulated from the variational principles in solid mechanics by relaxing the continuity requirements. The combination of different variational principles and different boundary continuity conditions yield numerous types of approximation methods. In their paper, bending problems are used to compare the relative merits of the various methods. Yaghmai (33) develops a general incremental variational method for the analysis of geometrically and physically non-linear problems in continuum mechanics. His variational method is applicable to any type of material properties, in particular non-linear constitutive laws for elastic and elastic-plastic materials are considered. For the elastic-plastic materials, an incremental constitutive law is considered where deformations are infinitesimal but rotations are finite. There, applications are made to the analysis of elastic-plastic shells of revolution and of circular plate, and the convergence and accuracy of the method is presented. Oden (34) provides a general continuum mechanics theory for the finite element

method, which is then demonstrated with reference to a number of applications. These include the generation of finite element models in the time domain and certain problems in wave propagation, non-linear continuum mechanics, and fluid dynamics. Marcal (35) develops incremental stiffness matrices for the small-strain large displacement analysis of combined non-linear (material and geometry) problems. The theory is demonstrated with reference to a three-dimensional problem of an imperfect hemisphere under external pressure, showing very good agreement with previous known solutions.

Hibbit, Marcal and Rice (36) derive an incremental and piece-wise linear finite element theory for large displacement and large strain problems with particular reference to elastic-plastic behaviour in metals. The resulting equations, though more complex, are in a similar form to those previously developed by Marcal (35) for large displacement and small strain problems, the only additional term being an initial load stiffness matrix which is dependent on current loads. According to the authors, this similarity in form means that existing non-linear general-purpose programs may easily be extended to include finite strains. The general formulation is subsequently reduced to handle those classes of problems with large displacement and small strain. A similar approach is presented by Gordon and Weinstein (37). They examine plane strain sheet drawing, considering smooth and friction boundary conditions, using a Lagrangeon description based on a variational approach presented by Biot (38).

In recent years extensive work in the field of elastic-plastic analysis by the finite element method has been carried out by Japanese investigators. An interesting survey, together with the analysis of the typical difficulties encountered has been presented by Kudo and

Matsubara (39). Special reference must be made to a paper by Kitagawa, Seguchi and Tomita (40), which analyses the problem of a finite element formulation, similar to the one presented by Hibbit (36), but referred to the current configuration of the continuum. They use a convected coordinate system embedded in the body and follow approximately the same path described in (36).

Ostias (41-43) also contributes to the subject and expands previous work for infinitesimal strains by Swedlow (44-45), using an Eulerian approach, assuming isotropic work-hardening material. Flow is analysed as a history dependent process, for which a computer program is developed. Numerical solution is obtained for a number of problems; simple tension, simple torsion and combined tension and torsion in a prismatic element under plane stress and plane strain conditions, and later for the problem of necking in flat tensile bars. Results in the first cases agree closely with known solutions. The necking results agree quantitatively with previous results on the subject, listed by the author.

Swedlow (46) develops an elastic-plastic theory in a fairly general manner so that it may accommodate features such as work-hardening, anisotropy, plastic compressibility, non-continuous loading including local or global unloading, and others. In another paper (47), the formulation is restricted to a Von-Mises work-hardening material and the tension of a prismatic bar is studied. Perfect plasticity and rigid elasticity are not covered. Computer programs based on this formulation are claimed to be economical.

Different approaches have been tried in recent papers by Zienkiewicz and his associates (48-50). Zienkiewicz and Godbole (48) use a stream function formulation to describe large deformation in

plastic and visco-plastic conditions. A finite element solution is found for the non-Newtonian flow problem and application is made to the analysis of steady state extrusion and non-steady state punch indentation. In the extrusion case they improve results obtained by Nayak and Zienkiewicz (30-31), although at cost of using a finer mesh. The extrusion pressure is however still above that given by the slip-line solution. The indenting pressure, in the non-steady state application, is shown to be linearly dependant on the depth of penetration, and above the slip-line solution.

Zienkiewicz and Corneau (49) derive plasticity and creep solutions using a visco-plastic model of the continuum, coupled with the initial strain method. This allows the treatment of non-associated plasticity and strain softening solutions which present difficulties in conventional plasticity approaches. Thus a standard program permits the treatment of a wide range of material non-linear problems. The paper discusses various applications of their general formulation and introduces certain numerical information on solution stability.

Gotch (51) proposes a polynomial shape function of triangular element for finite element analysis of general deformation of sheet metals with or without orthotropic anisotropic. Based on that, a general formulation for large deformation and large strain analysis with non-linearity of material property is derived and some numerical examples are examined with respect to circular sheet metals subjected to hydraulic pressure. Values of strain are not presented, but the whole area of the circular sheet specimens are brought into the plastic range.

Dieterle (52) recently studied the compression of tubular rings

using a finite element formulation as developed by Zienkiewicz (29), but introducing several simplifying features. Although strains are of the order of 0.45 and good agreement with experimental results are claimed to have been achieved, the use of large values of poisson's ratio and the use of unrealistic boundary conditions to improve the results seem to represent too many simplifying assumptions to retain the reliability of the solutions.

Gunasekera and Alexander (53) employ a formulation which highly resembles that of Hibbit (36), being however described in terms of the instantaneous frame of reference, by systematic updating of nodal coordinates and recomputation of the geometrical matrices. The authors claim to be able to obtain a solution for large deformation in the problem of the elastic-plastic expansion of a hole in a plate.

Most recently Blass (54) presented a finite element formulation, considering both material and geometrical non-linearities, for the elastic-plastic analysis of the metal working problems. The restrictions imposed are those of isotropic material behaviour, isothermal deformation, absence of Bauschinger effect and infinitesimal elastic deformation. The analysis is performed in a Lagrangeon frame of reference. There, application is made to the radial upsetting problem. The computed and experimental results and also upper bound solution (due to the author) are presented and compared. The computed results represent a slight improvement over the upper bound solution, but in general they are rather poor in accuracy, despite the generality of his formulation. In his conclusion, he refers to the difficulty in prescribing appropriate boundry conditions to the finite element model. He also refers to his improper model (which gives rise to a complex three-dimensional problem) being highly expensive in view of the

computing time.

### 2.3 Concept of the finite element

In the finite element method a continuous body is considered as a collection of a finite number of elements connected together at various nodal points. A typical element can be isolated from the collection and its behaviour can be studied independently of the behaviour of other elements in the collection. This is similar to ordinary mathematical analysis in which an infinitely small element is isolated to establish a differential or integral equation. In the finite element method a finite element of some standard type is selected according to a particular problem. The choice of element type is very important as clearly there are many families of elements for each type of problem depending upon the interpolation function. For the element selected, variation of the required functions (such as in solid mechanics displacement and stress fields) are approximated uniquely in terms of their values at the element nodal points. The behaviour of the element is then approximated by the use of the principles of mechanics. The process of connecting elements together to form the complete model is purely topological and is independent of the physical nature of the problem at hand or its linearity or non-linearity. The assemblage of elements fitted together at the element nodal points makes a final discrete model of the continuum and its overall behaviour is then described by a system of linear or non-linear algebraic equations depending upon the linear or non-linear continuum behaviour.

## 2.4 Basic formulation

To start, it is advisable to review some of the basic concepts and definitions of finite element method which will be required later. It is also worthwhile to present some considerations regarding the notations to be used.

Rectangular Cartesian coordinates is used throughout. Incremental variables are characterised by the prefix '*d*'. Vectors affected by the super-indices '*E*', '*P*' and '*EP*' are referred to as elastic, plastic or elastic-plastic conditions, respectively. Finally, vectors associated with element nodal points are identified by subscript '*e*'.

### 2.4.1 Displacement function

In the finite element method a displacement assumption is made, expressing displacements of any point within an element as a linear combination of the displacements at a finite number of nodal points in the same element, i.e. in matrix language

$$\{f\} = [N] \{\delta\}_e \quad (2.1)$$

in which matrix  $[N]$  defines the nature of the assumed displacement field and  $\{\delta\}_e$  represents nodal displacements for a particular element. In the case of plane strain or plane stress,  $\{f\}$  represents horizontal and vertical

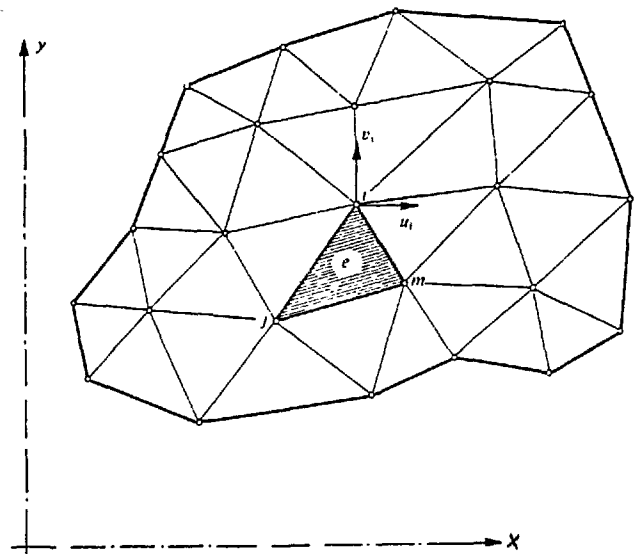


Fig. 2-1.



movements of a typical point within the element and  $\{\delta\}_e$  the corresponding displacements of the element nodal points, Fig. 2-1.

### 2.4.2 Strains

With displacements known at all points within the element, strains at any point can be determined. These always result in a relationship which can be written in matrix form as

$$\{\epsilon\} = [B] \{\delta\}_e \quad (2.2)$$

Strains are, however, defined in terms of displacements and are given by

$$\{\epsilon\} = \begin{Bmatrix} \epsilon_x \\ \epsilon_y \\ \epsilon_z \\ \epsilon_{xy} \\ \epsilon_{xz} \\ \epsilon_{yz} \end{Bmatrix} = \begin{Bmatrix} \frac{\partial u}{\partial x} \\ \frac{\partial v}{\partial y} \\ \frac{\partial w}{\partial z} \\ \frac{\partial u}{\partial y} + \frac{\partial v}{\partial x} \\ \frac{\partial u}{\partial z} + \frac{\partial w}{\partial x} \\ \frac{\partial v}{\partial z} + \frac{\partial w}{\partial y} \end{Bmatrix} \quad (2.3)$$

Thus from Eq. (2.1), with matrix  $[N]$  already determined, the matrix  $[B]$  will be easily obtained. Clearly, if a linear form of matrix  $[N]$  is adopted, the strains will be constant throughout the element.

### 2.4.3 Stresses

In general, the material within the element boundaries may be

subjected to initial strains such as may be due to temperature changes, shrinkage, crystal growth, and so on. If such strains are denoted by  $\{\epsilon\}_0$  then the stresses will be caused by the difference between the actual and initial strains.

In general it is convenient to assume that at the outset of analysis the body is stressed by some unknown system at initial residual stresses  $\{\sigma\}_0$ , which for instance could be measured but cannot be predicted without the full knowledge of the material's history. These stresses can simply be added on to the general definition. Assuming general elastic behaviour, the relationship between stresses and strains will be linear and of the form

$$\{\sigma\} = [D]^E (\{\epsilon\} - \{\epsilon\}_0) + \{\sigma\}_0 \quad (2.4)$$

where  $[D]^E$  is an elasticity matrix containing the appropriate material properties, and is given by

$$[D]^E = \frac{E}{(1+\nu)(1-2\nu)} \begin{bmatrix} 1-\nu & & & & & & \\ \nu & 1-\nu & & & & & \\ \nu & \nu & 1-\nu & & & & \\ 0 & 0 & 0 & (1-2\nu)/2 & & & \\ 0 & 0 & 0 & 0 & (1-2\nu)/2 & & \\ 0 & 0 & 0 & 0 & 0 & (1-2\nu)/2 & \end{bmatrix} \quad (2.5)$$

*Symmetric*

in which  $E$  is the elastic modulus and  $\nu$  is the poisson's ratio.

#### 2.4.4 Equivalent nodal forces

The nodal forces, which are equivalent statically to the boundary

stresses and distributed loads on the element, are expressed by  $\{F\}_e$ . The distributed loads  $\{P\}$  are defined as those acting on unit volume of material.

#### 2.4.5 Equilibrium condition

To make the nodal forces statically equivalent to the actual boundary stresses and distributed loads, the simplest procedure is to impose an arbitrary nodal displacement and to equate the external and internal work done by the various forces and stresses during that displacement.

If such a virtual displacement is defined by  $d\{\delta\}_e$ , Eqs. (2.1) and (2.2) can be expressed as

$$d\{f\} = [N] d\{\delta\}_e \quad \text{and} \quad d\{\epsilon\} = [B] d\{\delta\}_e \quad (2.6)$$

The work done by the nodal forces is equal to the sum of the products of the individual force components and corresponding displacements

$$(d\{\delta\}_e)^T \cdot \{F\}_e$$

Similarly, the internal work per unit volume done by the stresses and distributed forces is

$$d\{\epsilon\}^T \cdot \{\sigma\} - d\{f\}^T \cdot \{P\}$$

or by using Eqs. (2.6)

$$(\delta)_e^T \cdot ([B]^T \{\sigma\} - [N]^T \{P\})$$

Equating the external work with the total internal work obtained by integrating over the volume of the element

$$(\delta)_e^T \{F\}_e = (\delta)_e^T \left( \int [B]^T \{\sigma\} d(vol) - \int [N]^T \{P\} d(vol) \right) \quad (2.7)$$

As this relation is valid for any value of the virtual displacement, equality of the multipliers must exist. On substitution of Eqs. (2.2) and (2.4), therefore

$$\begin{aligned} \{F\}_e &= \left( \int [B]^T [D] [B] d(vol) \right) \{\delta\}_e - \int [B]^T [D] \{\epsilon\}_o d(vol) \\ &+ \int [B]^T \{\sigma\}_o d(vol) - \int [N]^T \{P\} d(vol) \end{aligned} \quad (2.8)$$

the stiffness matrix is

$$[K] = \int [B]^T [D] [B] d(vol) \quad (2.9)$$

nodal forces due to distributed loads are

$$\{F\}_P = - \int [N]^T \{P\} d(vol) \quad (2.10)$$

and those due to initial strains are

$$\{F\}_{\epsilon o} = - \int [B]^T [D] \{\epsilon\}_o d(vol) \quad (2.11)$$

Due to initial stresses, present at the outset of the analysis, nodal

forces contributed are

$$\{F\}_{\sigma_0} = \int [B]^T \{\sigma\}_0 d(vol) \quad (2.12)$$

## 2.5 Non-linear material formulation

Whether the material behaviour is linear or non-linear, equilibrium condition between internal and external forces have to be satisfied. Thus, from Eq. (2.7)

$$\{F\}_e = \int [B]^T \{\sigma\} d(vol) - \int [N]^T \{P\} d(vol)$$

Assuming that no distributed loads exist or, if any, they have been distributed appropriately between the nodal points, the equilibrium equation then reduces to

$$\{F\}_e = \int [B]^T \{\sigma\} d(vol) \quad (2.13)$$

For a non-linear continuum it is, however, preferable to express the equilibrium equation in an incremental form. If we consider two sets of equilibrium conditions at two loads, displacements and straining conditions defined by  $\{F\}_e$ ,  $\{\delta\}_e$ ,  $\{\sigma\}$  and by  $\{F\}_e + d\{F\}_e$ ,  $\{\delta\}_e + d\{\delta\}_e$ ,  $\{\sigma\} + d\{\sigma\}$ , we should have

$$(\{F\}_e + d\{F\}_e) = \int [B]^T (\{\sigma\} + d\{\sigma\}) d(vol) \quad (2.14)$$

Subtracting Eq. (2.13) from Eq. (2.14), the equilibrium equation can be obtained as

$$d\{F\}_e = \int [B]^T d\{\sigma\} d(vol) \quad (2.15)$$

which expresses the equilibrium condition when strains and displacements are infinitesimal. If displacements are large the variation of matrix  $[B]$  must also be taken into account. Thus Eq. (2.13) may be rewritten as

$$(\{F\}_e + d\{F\}_e) = \int ([B]^T + d[B]^T) \cdot (\{\sigma\} + d\{\sigma\}) d(vol) \quad (2.16)$$

Simplifying Eq. (2.16) and neglecting second-order terms, leads to

$$d\{F\}_e = \int [B]^T d\{\sigma\} d(vol) + \int d[B]^T \{\sigma\} d(vol) \quad (2.17)$$

where matrix  $[B]$ , now dependent on  $\{\delta\}$ , can be conveniently expressed as

$$[B] = [B_0] + [B_L] \quad (2.18)$$

in which  $[B_0]$  is the same matrix as in small strain analysis and only  $[B_L]$  depends on the displacement. In general  $[B_L]$  is found to be a linear function of such displacements.

To proceed further, matrix  $d\{\sigma\}$  in Eq. (2.17) must be related to  $d\{\epsilon\}$  and thus to  $d\{\delta\}$ .

The general case of elastic-plastic deformation (in which both the elastic and plastic components of strain are finite) has been considered by Lee (55). He has shown that, in this case the usual assumption of small strain plasticity is not true; i.e. the total strain components cannot be resolved into a purely elastic and a purely plastic component. Thus

$$d\{\epsilon\} = \{\epsilon\}^E + d\{\epsilon\}^P, \quad (2.19)$$

is not valid and must be replaced by a much more complicated matrix relation. However, when elastic strains are relatively small, the elastic matrix in Lee's formulation reduces to a unit matrix, and Eq. (2.19) can be accepted as the governing equation. On the basis of that equation then, it will be shown that it is possible to express the increment of stress components in terms of the increment of strain components, and by a similar relation used in linear elasticity analysis. Thus

$$d\{\sigma\} = [D]^{EP} d\{\epsilon\} \quad (2.20)$$

where matrix  $[D]^{EP}$  is the elasto-plastic stress-strain matrix and will be derived later.

By substituting for  $d\{\epsilon\}$  from Eqs. (2.6), we have

$$d\{\sigma\} = [D]^{EP} [B] d\{\delta\}_e \quad (2.21)$$

Substituting Eqs. (2.18) and (2.21) in Eq. (2.17),

$$\begin{aligned} d\{F\}_e &= \left[ \int ([B]_o + [B]_L)^T [D]^{EP} ([B]_o + [B]_L) d(vol) \right] d\{\delta\}_e \\ &+ \int d([B]_o + [B]_L)^T \{\sigma\} d(vol) \end{aligned} \quad (2.22)$$

The second term on the right of Eq. (2.22) can be divided into one matrix that is dependent on the current displacement and one that is not. With some rearrangement, we obtain the element matrices

$$d\{F\}_e = ([K]_o + [K]_1 + [K]_2) d\{\delta\}_e \quad (2.23)$$

where  $[K]_0$  is the small-displacement stiffness matrix,  $[K]_1$  is the initial-displacement matrix, and  $[K]_2$  is the initial stress matrix.

Eq. (2.23) is immensely similar to Marcal's derivation (36) where no restriction is imposed on the magnitude of strains and displacements. It must be emphasized however that when large strains and displacements are to be considered the use of ordinary definitions of strain and stress are not legitimate. In this case it is generally recommended to carry out the formulation using Green's strain and Kirchoff stress.

For a wide class of problems when small strains and displacements are to be considered the use of a general and complicated formulation is not the best strategy. Such strategy may terminate in a complete failure due to the considerable computing time necessary to calculate the immaterial matrices involved (see reference (54)). Considering the nature of our problems, we therefore restrict ourselves to small strain plasticity and adopt Eq. (2.15) as the governing equation. However, with the adoption of this equation if relatively large strains are to be tackled, some refinement will be necessary in order to minimize the relative size of the non-linear terms dropped. This is conveniently achieved (as employed by Ref. (53)) by a systematic updating of the nodal coordinates and geometrical matrices within the increments of loading procedure. Attention is here drawn to the fact that if finite strains and displacements were to be considered the use of a universal formulation, similar to Eq. (2.23), would become imperative and unavoidable.

### 2.5.1 Derivation of the elastic-plastic stress-strain matrix $[D]^{EP}$

The incremental plasticity relations which are to be used are



those of Prandtl-Reuss obeying the Von-Mises yield criterion. To start with, some relevant relationships are briefly reviewed.

According to the Von-Mises criterion, yielding occurs when the effective stress  $\bar{\sigma}$  attains a critical magnitude, where  $\bar{\sigma}$  is given by

$$\bar{\sigma} = \sqrt{\frac{3}{2} \sigma'_{ij} \sigma'_{ij}} \quad (2.24)$$

in which  $\sigma'_{ij}$  is the deviatoric stress corresponding to stress component  $\sigma_{ij}$ .

Effective plastic strain increment  $d\bar{\epsilon}^P$  is defined as a combination of the plastic strain components

$$d\bar{\epsilon}^P = \sqrt{\frac{2}{3} d\epsilon_{ij}^P d\epsilon_{ij}^P} \quad (2.25)$$

in which  $d\epsilon_{ij}^P$  is the plastic component of strain  $d\epsilon_{ij}$ .

The relation between effective stress and effective strain is established by a uniaxial tension test such as shown in Fig. 2-2.

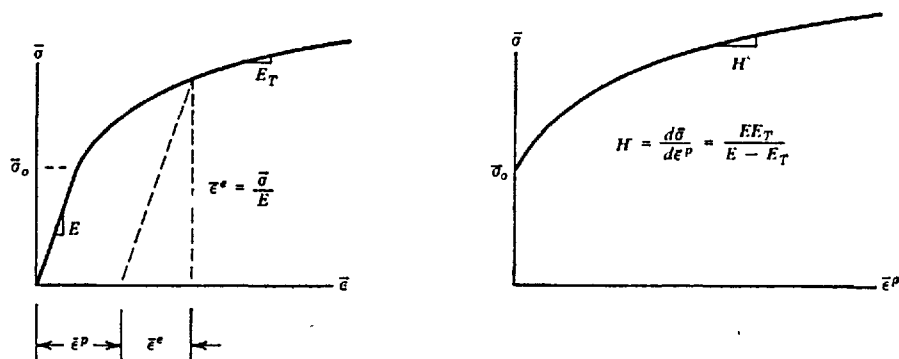


Fig. 2-2

where  $H$  is the slope of the effective stress-plastic strain curve at a particular level of effective stress. The relation between  $H$ ,

elastic modulus  $E$  and tangent modulus  $E_T$  is found by substitution of strain components into the relation

$$d\bar{\epsilon} = d\bar{\epsilon}^E + d\bar{\epsilon}^P$$

where  $d\bar{\epsilon} = \frac{d\bar{\sigma}}{E_T}$  ,  $d\bar{\epsilon}^E = \frac{d\bar{\sigma}}{E}$  and  $d\bar{\epsilon}^P = \frac{d\bar{\sigma}}{H}$  .

Increment of the effective stress will be required and in matrix language is given by

$$d\bar{\sigma} = \left\{ \frac{\sigma'}{\bar{\sigma}} \right\}^T d\{\sigma\} \quad (2.26)$$

where  $\left\{ \frac{\sigma'}{\bar{\sigma}} \right\} = \frac{3}{2\bar{\sigma}} \{ \sigma'_x \quad \sigma'_y \quad \sigma'_z \quad 2\tau_{xy} \quad 2\tau_{yz} \quad 2\tau_{zx} \}$  (2.27)

in which  $\sigma'_i = \sigma_i - \sigma_m$ , and  $\sigma_m$  is the hydrostatic stress.

Finally, the Prandtl-Reuss relations state that

$$d\{\epsilon\}^P = \left\{ \frac{\sigma'}{\bar{\sigma}} \right\} d\bar{\epsilon}^P \quad (2.28)$$

where this defines the plastic strain increments when, under a known state of stress, the effective plastic strain increment  $d\bar{\epsilon}^P$  occurs.

As previously stated, for relatively small strains and displacements, changes of strain can be assumed to be resolvable into elastic and plastic components, thus

$$d\{\epsilon\} = d\{\epsilon\}^E + d\{\epsilon\}^P \quad (2.19)$$

The elastic strain increments are related to stress increments by a symmetric matrix  $[D]^E$  as

$$d\{\sigma\} = [D]^E d\{\epsilon\}^E.$$

Substituting for  $d\{\epsilon\}^E$  from Eq. (2.19) leads to

$$d\{\sigma\} = [D]^E ( d\{\epsilon\} - d\{\epsilon\}^P ) \quad (2.29)$$

A relation that yields  $d\epsilon^{-P}$  from the strain increments  $d\{\epsilon\}$  is obtained by substituting Eq. (2.28) in Eq. (2.29) and multiplying both sides by  $\{\frac{\sigma'}{\sigma}\}^T$ , thus

$$\{\frac{\sigma'}{\sigma}\}^T d\{\sigma\} = \{\frac{\sigma'}{\sigma}\}^T [D]^E ( d\{\epsilon\} - \{\frac{\sigma'}{\sigma}\} d\epsilon^{-P} ) \quad (2.30)$$

considering that  $\{\frac{\sigma'}{\sigma}\}^T d\{\sigma\} = H d\epsilon^{-P}$ , the increment of effective strain  $d\epsilon^{-P}$  can be evaluated as

$$d\epsilon^{-P} = \frac{\{\frac{\sigma'}{\sigma}\} [D]^E}{H + \{\frac{\sigma'}{\sigma}\}^T [D] \{\frac{\sigma'}{\sigma}\}} d\{\epsilon\} = [W] d\{\epsilon\} \quad (2.31)$$

The incremental stress-strain relation, analogous to Hooke's law but valid beyond the proportional limit, is obtained by substitution of Eq. (2.31) into Eq. (2.28) and the result into Eq. (2.29). The relation is

$$d\{\sigma\} = ([D]^E - [D]^E \{\frac{\sigma'}{\sigma}\} [W]) d\{\epsilon\} = ([D]^E - [D]^P) d\{\epsilon\} = [D]^{EP} d\{\epsilon\} \quad (2.32)$$

Examination of the matrices involved shows that the plastic



Clearly, matrix  $[D]^{EP}$  is given by

$$[D]^{EP} = \frac{E}{1 + \nu} \left[ \begin{array}{cccccc}
 \frac{1-\nu}{1-2\nu} - \frac{\sigma'_x{}^2}{s} & & & & & \\
 \frac{\nu}{1-2\nu} - \frac{\sigma'_x \sigma'_y}{s} & \cdot & \frac{1-\nu}{1-2\nu} - \frac{\sigma'_y{}^2}{s} & & & \\
 \frac{\nu}{1-2\nu} - \frac{\sigma'_x \sigma'_z}{s} & \cdot & \frac{\nu}{1-2\nu} - \frac{\sigma'_y \sigma'_z}{s} & \cdot & \frac{1-\nu}{1-2\nu} - \frac{\sigma'_z{}^2}{s} & \\
 -\frac{\sigma'_x \tau_{xy}}{s} & \cdot & -\frac{\sigma'_y \tau_{xy}}{s} & \cdot & -\frac{\sigma'_z \tau_{xy}}{s} & \cdot & \frac{1}{2} - \frac{\tau_{xy}^2}{s} \\
 -\frac{\sigma'_x \tau_{yz}}{s} & \cdot & -\frac{\sigma'_y \tau_{yz}}{s} & \cdot & -\frac{\sigma'_z \tau_{yz}}{s} & \cdot & -\frac{\tau_{xy} \tau_{yz}}{s} & \cdot & \frac{1}{2} - \frac{\tau_{yz}^2}{s} \\
 -\frac{\sigma'_x \tau_{zx}}{s} & \cdot & -\frac{\sigma'_y \tau_{zx}}{s} & \cdot & -\frac{\sigma'_z \tau_{zx}}{s} & \cdot & -\frac{\tau_{xy} \tau_{zx}}{s} & \cdot & -\frac{\tau_{yz} \tau_{zx}}{s} & \cdot & \frac{1}{2} - \frac{\tau_{zx}^2}{s}
 \end{array} \right] \begin{array}{l} \\ \\ \\ \text{symmetric} \\ \\ \\ \end{array} \quad (2.34)$$

Equation (2.34) corresponds to the inverse of the complete stress-strain relations of Prandtl-Reuss. The original stress-strain relations have been reduced to a single equation (2.32), and it must be emphasized that the elastic compressibility as well as the strain-hardening characteristics of the material are incorporated in the matrix  $[D]^{EP}$ . Comparing  $[D]^{EP}$  with  $[D]^E$ , it can be seen that the diagonal elements of  $[D]^{EP}$  are definitely less than the corresponding diagonal elements of  $[D]^E$ . This amounts to an apparent decrease of rigidity due to plastic yielding. Attention is also drawn to the validity of Eq. (2.32) for elastic perfectly plastic materials, as nothing in the derivation becomes infinity if  $H=0$ .

## 2.6 Solution algorithms

Whether the continuum is linear or non-linear, equilibrium conditions between internal and external forces have to be satisfied. This is given by

$$d\{F\}_e = \int [B]^T d\{\sigma\} d(vol) \quad (2.13)$$

Any plasticity problem now involves the solution of the equilibrium equation together with incremental stress-strain relations. These relations may be written as

$$d\{\sigma\} = [D]^{EP} d\{\epsilon\} \quad (2.35)$$

$$d\{\sigma\} = [D]^E (d\{\epsilon\} - d\{\epsilon\}^P) \quad (2.36)$$

$$d\{\sigma\} = d\{\sigma\}^E - d\{\sigma\}^P \quad (2.37)$$

If we now substitute various incremental stress-strain relationships into equilibrium equation we can obtain several forms of incremental equilibrium equation.

### 2.6.1 Tangential stiffness method

Substituting the stress increment  $d\{\sigma\}$  from Eq. (2.35) into the equilibrium equation, leads to

$$d\{F\}_e = \int [B]^T [D]^{EP} d\{\epsilon\} d(vol)$$

but  $d\{\epsilon\} = [B] d\{\delta\}_e$ , therefore

$$d\{F\}_e = \left( \int [B]^T [D]^{EP} [B] d(vol) \right) d\{\delta\}_e = [K]_e^{EP} d\{\delta\}_e \quad (2.38)$$

Clearly for elastic elements,  $[D]^{EP}$  must be replaced by  $[D]^E$  before the integration is carried out. The elemental stiffness matrices can be assembled to form  $[K]$  of the whole body. The overall stiffness matrix  $[K]$  relates the nodal load-increment  $d\{F\}$  to the nodal displacement increment  $d\{\delta\}$ , as

$$d\{F\} = [K] d\{\delta\} \quad (2.39)$$

In solving Eq. (2.39) two algorithms have found wider application in the literature extending the finite element method to non-linear problems. These are proposed in the already mentioned works by Yamada (20) and by Marcal and King (14).

In Yamada's formulation, small load increments are prescribed, and they are adequately rated in order to exactly yield one, or a few,

of the remaining elastic elements in the continuum. The procedure is schematized in Fig. 2-3, for a set of three elements. In the first graph points A, B and C represent the original situation of the three elastic elements. An arbitrary load increment is then applied, and the elastic solution is obtained, bringing the three elements to A', B' and C', respectively. In general, none of the elements will exactly yield. However, if the load increment is multiplied by the rating factor  $r$ , the minimum being taken in respect to all elements, the state of stress and strain will be represented by A'', B'' and C'' exactly yielding. Note that during this multiplication process all the incremental variables must also be multiplied by this same factor (due to linear relationships existing between them). In the second graph, points A, B, C represent the situation achieved after the previous load increment. A similar procedure is again applied for some arbitrary load increment, the state of stress and strain being represented by A', B', C', with C' following tangent to the flow curve.

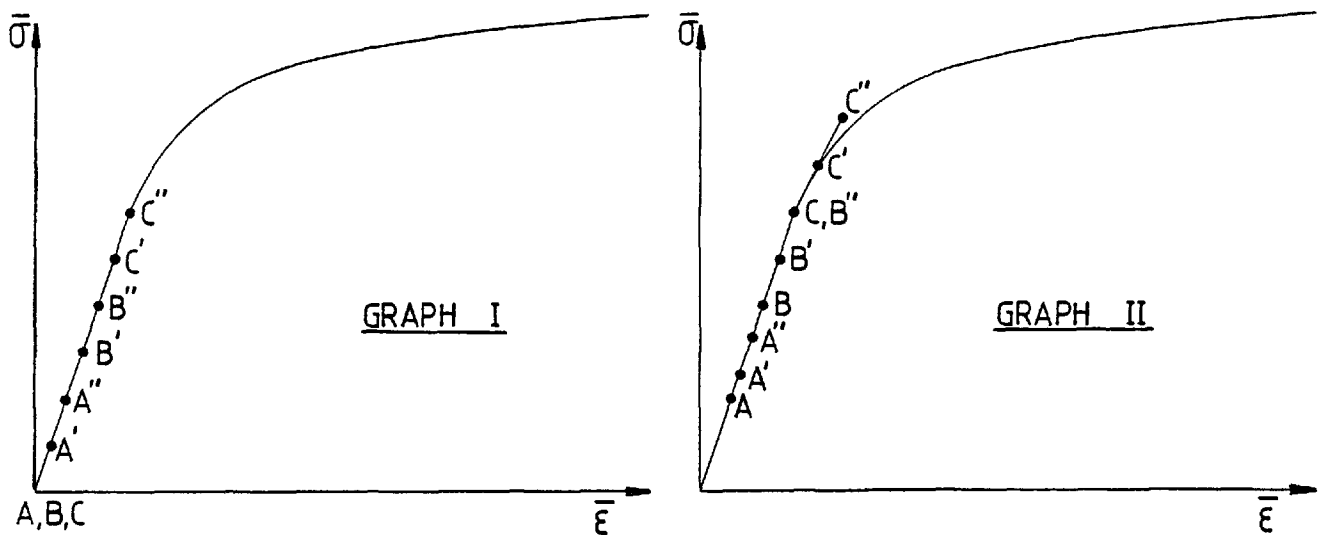


Fig. 2-3.



The rating factor  $r$  is again obtained, the minimum being taken with respect to all elements still in the elastic range, and the new situation corresponding to A'', B'', and C'', with B'' now yielding, are obtained. This procedure is repeated with at least one element yielding each time, until a desirable magnitude of deformation is attained.

Computational procedure for a typical increment of load is as follows:

- 1- Let us suppose that under loads  $\{F\}_A$ , the correct displacement  $\{\delta\}_A$  and structure tangent stiffness  $[K]_A^{EP}$  are known (see Fig. 2-4 for a single degree of freedom representation). Displacements produced by the next load increment are computed from equation (2.39)

$$d\{F\}_{AB} = \{F\}_B - \{F\}_A = [K]_A^{EP} d\{\delta\}_{AB}$$

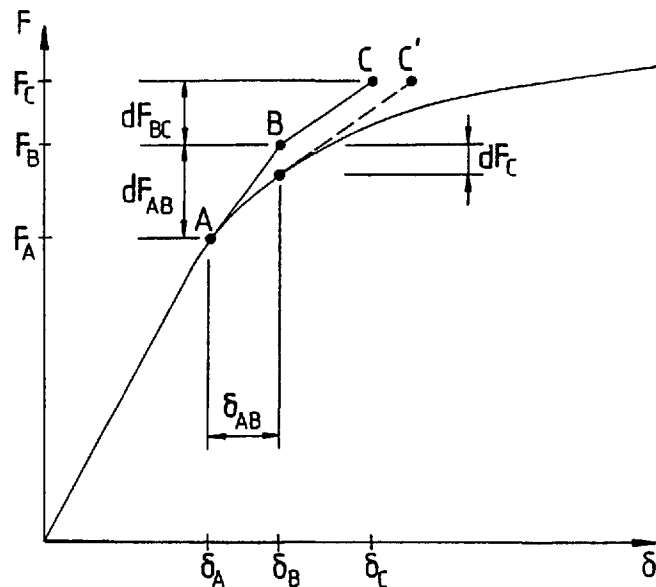


Fig. 2-4.

- 2- Displacements  $d\{\delta\}_e$  of an element are extracted from  $d\{\delta\}_{AB}$ .
- 3- For each sampling point within the element, increments of strain and stress are calculated by use of equations

$$d\{\epsilon\} = [B] d\{\delta\}_e \quad \text{from Eq. (2.2)}$$

$$d\bar{\epsilon}^P = [W]_A d\{\epsilon\} \quad \text{from Eq. (2.31)}$$

$$d\{\epsilon\}^P = \left\{ \frac{\sigma'}{\sigma} \right\} d\bar{\epsilon}^P \quad \text{from Eq. (2.28)}$$

$$d\{\sigma\} = [D]^E ( d\{\epsilon\} - d\{\epsilon\}^P ) \quad \text{from Eq. (2.29)}$$

Clearly, for elastic elements  $d\bar{\epsilon}^P$  must be set equal zero.

- 4- Sequence 3 is repeated over the sampling points within an element
- 5- Using the appropriate relationship for  $[D]^{EP}$ , the stiffness matrix for a yielded element is evaluated.
- 6- Sequence 5 is repeated for all the post yielded elements.
- 7- Finally, elements are assembled in the usual way. Thus the current structure stiffness matrix is produced, and another load increment  $d\{F\}_{BC}$  is applied.

During loading some of the elements may experience unloading, this is indicated by a negative  $d\bar{\epsilon}^P$  obtained from Eq. (2.31). For an unloaded element,  $d\bar{\epsilon}^P$  is set to zero and in the next load increment the stiffness matrix is based on elastic modulus  $[D]^E$  instead of on  $[D]^{EP}$ . If isotropic hardening is assumed, plastic action is resumed only when the effective stress exceeds its previous magnitude.

In the procedure outlined, increments of load were denoted by  $d\{F\}$  emphasizing small increments to be employed. However, if larger

increments are used a progressive drift from the actual response becomes unavoidable. Upon reaching B in Fig. 2-4, the computed displacement is too small, hence the resulting stresses are also too small and are not adequate to resist the applied load  $\{F\}_B$ . If a corrective load  $d\{F\}_C$  were added to the previous load increment, the computed displacement  $\{\delta\}_B$  would be larger and more nearly correct. The corrective load is the difference between the applied load and resistance produced by distorted elements. This resistance is evaluated from the  $\{\sigma\}_0$  term of Eq. (2.12), with  $\{\sigma\}_0$  now regarded as the total accumulated stress  $\{\sigma\}$  in the element. Therefore,

$$d\{F\}_C = \{F\}_B - \int [B]^T \{\sigma\} d(vol).$$

Correction load  $d\{F\}_C$  is then applied in the subsequent step. For instance, the equation for the next step from point B is (see Fig. 2-4)

$$d\{F\}_{BC} + d\{F\}_C = [K]_B^{EP} d\{\delta\}_{BC}'$$

Thus we arrive at point C' instead of the less correct point C. The procedure is the same as the incremental method with a one-step Newton-Raphson correction method. This explanation suggests that for still greater accuracy, at some computational expense, Newton-Raphson iteration may be applied within a load step  $d\{F\}_{AB}$  so that essentially zero  $d\{F\}_C$  exists at the beginning of the following step. Thus, within a step we analyse for the successive loads  $d\{F\}_{AB}$ ,  $d\{F\}_{C1}$ ,  $d\{F\}_{C2}$ , etc., updating strains, stresses and stiffnesses each time (Fig. 2-5).

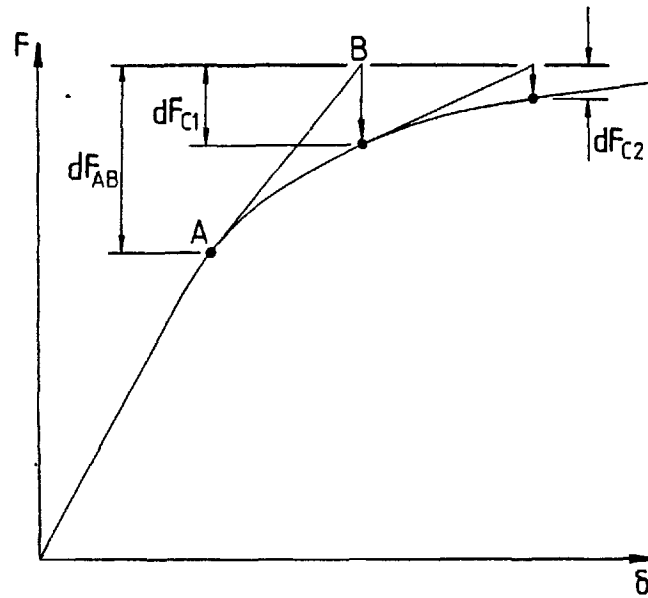


Fig. 2-5.

Marcal and King (14) prescribe large load increments, for which several elements are expected to yield. The procedure is shown schematically in Fig. 2-6, for one element only entering the plastic range in the load increment. Elements staying in the elastic range, or already inside the plastic range, offer no special problem. For the element under consideration, elastic loading brings the image of the stress-strain situation from A to B. Marcal uses the relative elastic strain increment

$$m = \frac{\bar{\epsilon}_O - \bar{\epsilon}_A}{\bar{\epsilon}_B - \bar{\epsilon}_A} \quad (2.40)$$

to modify the elastic matrix  $[D]^E$  as,

$$[D]^{EP} = [D]^E - (1-m) [D]^E \left\{ \frac{\sigma'}{\sigma} \right\} [W] \quad (2.41)$$

where  $\left\{ \frac{\sigma'}{\sigma} \right\}$  is based on stresses corresponding to point B. The

stiffnesses of the yielded elements are then modified and finally assembled. Actual analysis under the current load increment is now carried out, and stresses  $\Delta\{\sigma\} = [D]^{EP} \Delta\{\epsilon\}$  are computed using the most recent estimate of  $[D]^{EP}$ . The current state may now correspond to point C and the procedure is repeated until convergence is obtained. Convergence should be rapid because the transition zone is probably only a small portion of the structure. After convergence, calculation of plastic strains in Eqs. (2.31) and (2.29) must be based on  $(1-m) \Delta\{\epsilon\}$  instead of on the full increment  $\{\epsilon\}$ .

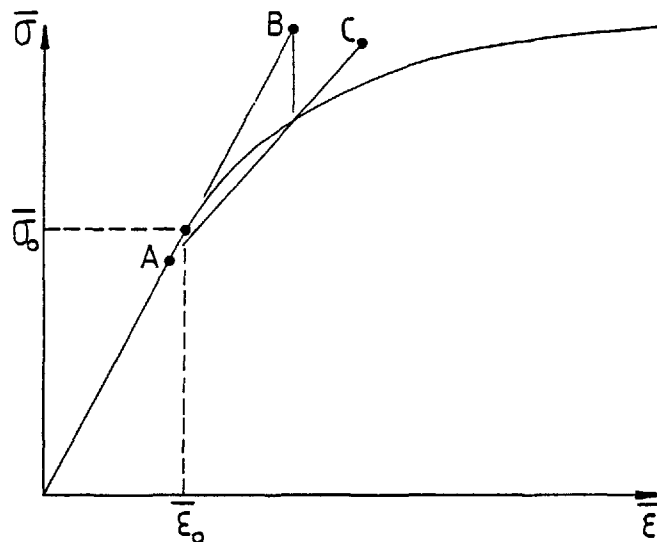


Fig. 2-6.

Comparing the two algorithms described, Yamada's procedure can be uneconomical because of the large number of load increments required to bring the elements into the plastic range. Marcal's, on the other hand, requires a small number of load increments, but everyone of them requires an additional iterative procedure, with a new stiffness matrix computed at each iteration.

### 2.6.1.1 Calculation of the rating factor

An elastic point with a given state of stresses  $\{\sigma\}$  is considered. An arbitrary increment of load is applied and stress increments,  $d\{\sigma\}$ , are calculated. By introduction of the rating factor the aim is to increase or decrease the load increment in such a way to bring the elastic point to the point of yielding.

Assume that the states of stresses before and after the load increment are represented by  $\{\sigma\}$  and  $\{\sigma\} + d\{\sigma\}$ , respectively. If 'r' is the rating factor then from Eq. (2.24), we should have

$$Y^2 = \frac{3}{2} (\sigma'_{ij} + r d\sigma'_{ij}) (\sigma'_{ij} + r d\sigma'_{ij})$$

where  $Y$  is the yield stress. On expansion, we have

$$\frac{2}{3} Y^2 = \sigma'_{ij} \sigma'_{ij} + 2r \sigma'_{ij} d\sigma'_{ij} + r^2 d\sigma'_{ij} d\sigma'_{ij}$$

Considering that  $\sigma'_{ij} \sigma'_{ij}$  is equal to the effective stress of the material before the load increment and rearranging of the above equation

$$r^2 d\sigma'_{ij} d\sigma'_{ij} + 2r \sigma'_{ij} d\sigma'_{ij} + \frac{2}{3} (\bar{\sigma}^2 - Y^2) = 0$$

in which  $\bar{\sigma}$  represents the previous magnitude of the material effective stress. The rating factor is finally expressed by

$$r = \frac{-\sigma'_{ij} \sigma'_{ij} + \sqrt{(\sigma'_{ij} \sigma'_{ij})^2 - \frac{2}{3}(\bar{\sigma}^2 - Y^2)(d\sigma'_{ij} d\sigma'_{ij})}}{d\sigma'_{ij} d\sigma'_{ij}} \quad (2.42)$$

In the computation if the rating factor found is greater than unity,

it is advisable to limit this parameter (e.g. by setting equal to unity) in order to avoid an unexpected increment of load.

### 2.6.2 Initial strain method

Another modification of Eq. (2.13) is based on the idea of modifying the right hand-side of the equation of equilibrium by treating the plastic strain in the same way as the thermal strains. This is achieved as follows:

From Eq. (2.36),  $d\{\sigma\}$  is substituted into the equilibrium Eq. (2.13), thus

$$d\{F\}_e = \int [B]^T [D]^E (d\{\epsilon\} - d\{\epsilon\}^P) d(vol)$$

$$\therefore d\{F\}_e = \int [B]^T [D]^E d\{\epsilon\} d(vol) - \int [B]^T [D]^E d\{\epsilon\}^P d(vol) \quad (2.43)$$

or in a compact form

$$d\{F\}_e = [K]_e^E d\{\delta\}_e - d\{P\}_e \quad \text{or} \quad [K]_e^E d\{\delta\}_e = d\{F\}_e + d\{P\}_e \quad (2.44)$$

where  $[K]_e^E = \int [B]^T [D]^E [B] d(vol)$  and  $d\{P\}_e = \int [B]^T [D]^E d\{\epsilon\}^P d(vol)$

$$(2.45)$$

It should be noted that, by using Eqs. (2.28) and (2.26),  $d\{\epsilon\}^P$  may be expressed in terms of  $d\{\sigma\}$ , thus

$$d\{\epsilon\}^P = \left\{ \frac{\sigma'}{\sigma} \right\} d\bar{\epsilon}^{-P} = \frac{1}{H} \left\{ \frac{\sigma'}{\sigma} \right\} \left\{ \frac{\sigma'}{\sigma} \right\}^T d\{\sigma\} \quad (2.46)$$

Clearly, solution of Eq. (2.46) is impossible if the material is

assumed elastic perfectly plastic (i.e.  $H=0$ ).

To obtain the overall stiffness matrix of the whole body, stiffness matrices of the elements, based on the elastic matrix  $[D]^E$ , are calculated and assembled. This leads to an equation similar to Eq. (2.44), thus

$$[K]^E d\{\delta\} = d\{F\} + d\{P\} \quad (2.47)$$

where  $d\{P\}$  are forces due to the increment of plastic strains.

Gallagher (8) and Argyris (56) have effectively used equation (2.47) in the analysis of non-linear problems. The essential difference from the tangential stiffness method is the evaluation of  $d\{P\}$  by iterations. As suggested by Argyris (56) the iteration starts with estimation of stress increment  $d\{\sigma\}_i$ , where the suffix  $i$  denotes the iteration number. The basic steps in this method are:

1- Assume the stress increments  $d\{\sigma\}_i$  (at least for plastic zones)

2- Compute  $d\{\epsilon\}_i^P = \frac{1}{H} \left\{ \frac{\sigma'}{\sigma} \right\} \left\{ \frac{\sigma'}{\sigma} \right\}^T d\{\sigma\}_i$

3- Compute  $d\{P\}$

4- Calculate  $d\{\delta\} = ([K]^E)^{-1} (d\{F\} + d\{P\})$

5- Calculate strain increments  $d\{\epsilon\}$

6- Calculate stress increments  $d\{\sigma\}_{i+1} = [D]^{EP} d\{\epsilon\}$

7- Repeat steps (2) to (6).



Here the iteration procedure has been developed for finding  $d\{\epsilon\}^P$  and the convergence is achieved when  $d\{\epsilon\}_{i+1}^P - d\{\epsilon\}_i^P$  is less than a reasonably small value.

For solution of Eq. (2.47),  $([K]^E)^{-1}$  is stored and not subsequently updated. The method is therefore not likely to be as costly as the tangential stiffness method. However, as the yielding of the material increases the number of iterations required are expected to increase rapidly.

### 2.6.3 Initial stress method

Due to the initial strain method not being applicable to ideally elastic-plastic material an alternative method called 'initial stress method' was introduced by Zienkiewicz, Valliappan and King (29). Here the equilibrium Eq. (2.13) is written as, from Eq. (2.37)

$$d\{F\}_e = \int [B]^T (d\{\sigma\}^E - d\{\sigma\}^P) d(vol)$$

$$\text{where } d\{\sigma\}^E = [D]^E d\{\epsilon\} \quad \text{and} \quad d\{\sigma\}^P = [D]^P d\{\epsilon\} \quad (2.48)$$

Thus

$$d\{F\}_e = \left( \int [B]^T [D]^E [B] d(vol) \right) d\{\delta\}_e - \int [B]^T d\{\sigma\}^P d(vol)$$

$$\text{or} \quad d\{F\}_e = [K]^E_e d\{\delta\}_e - d\{P\}_e$$

$$\text{in which } d\{P\}_e = \int [B]^T d\{\sigma\}^P d(vol) \quad (2.49)$$

As before, for the whole system, we may write

$$d\{F\} = [K]^E d\{\delta\} - d\{P\} \quad \text{or} \quad [K]^E d\{\delta\} = d\{F\} + d\{P\} \quad (2.50)$$

For a typical load increment, the method can be summarized in the following way:

The iteration cycle is started with the stresses known as  $\{\sigma\}_0$ .

- 1- In Eq. (2.50), assume  $d\{P\}=0$  and calculate the first displacement matrix from purely elastic analysis as given by

$$d\{\delta\}_0 = ([K]^E)^{-1} d\{F\}_n$$

where  $d\{F\}_n$  is the  $n$ th load increment.

- 2- Calculate  $d\{\sigma\}_0^E = [D]^E d\{\epsilon\}_0$ ,  $d\{\sigma\}_0^P = [D]^P d\{\epsilon\}_0$  and therefore  $d\{\sigma\}_0 = d\{\sigma\}_0^E - d\{\sigma\}_0^P$ . Find the total stress  $\{\sigma\}_1 = \{\sigma\}_0 + d\{\sigma\}_0$ .

- 3- From increments  $d\{\sigma\}_0^P$  calculate the initial loads  $d\{P\}_0$ .

- 4- Using Eq. (2.50), obtain the first corrective displacement matrix

$$d\{\delta\}_1 = ([K]^E)^{-1} (d\{F\}_n + d\{P\}_0).$$

- 5- Similar to step 2 obtain  $d\{\sigma\}_1^E$ ,  $d\{\sigma\}_1^P$  and thus  $\{\sigma\}_2$ .

- 6- Repeat steps 3 to 5 by the sequential substitution in various equations for displacement-, strain- and stress-increments and also initial load increments until convergence is achieved.

From the steps given above it is clear that this method is simple

and presents no problems for a cyclic loading case as the unloading proceeds on a purely elastic basis. However its preference over other methods such as the tangential stiffness method depends mainly on the rate of convergence. The initial stress method converges very rapidly in the beginning and becomes very slow near general yield.

## 2.7 Comparison of algorithms

It is evident from the theory outlined that as the plasticity relations are formulated incrementally, the iterative process must be applied strictly to small load increments. Within such increments, however, any of the three algorithms described can be applied.

In the earliest applications of the finite element process to plasticity the initial strain approach was favoured. However, this approach fails entirely if ideal non-strain-hardening plasticity is considered. In this case the strains cannot be uniquely determined for prescribed stress levels. In subsequent work the variable stiffness approach appears to have been favoured. The greatest advantage of the variable stiffness approach over the initial strain approach is its high rate of convergence. In fact, if the load increments are sufficiently small, no iterative procedure is needed, since mathematically the residuals will be considerably negligible. On the other hand the preference of the initial strain method over the variable stiffness method lies in its great potential economy due to the fact that the overall stiffness matrix need not to be updated within the process of loading. With regard to convergence, the initial stress method is identical to the initial strain method but the former is capable of handling non-strain-hardening plasticity.

## 2.8 Elements implemented in the computer programs

One of three types of elements were used in discretizing a deforming continuum under conditions of plane strain, each type being implemented in a computer program. The types of elements implemented were: constant strain triangle, quadrilateral (built up from four triangles) and quadrilateral (isoparametric). These elements mainly differ in the mesh pattern and also in the polynomial terms considered in the expansion of the shape function. The effect of using higher terms gives a considerable advantage resulting in the reduction of the total number of unknowns for a desired accuracy, and also a saving in the preparation of data.

In what follows, the fundamental features of these three types of elements are presented.

### 2.8.1 Constant strain triangle elements

Fig. 2-7 shows a typical triangular element. The element is widely used, owing perhaps to its simplicity and early widespread adoptions.

The displacements within the element are uniquely defined by a linear shape function of the form

$$\{f\} = [N] \{\delta\}_e \quad (2.51)$$

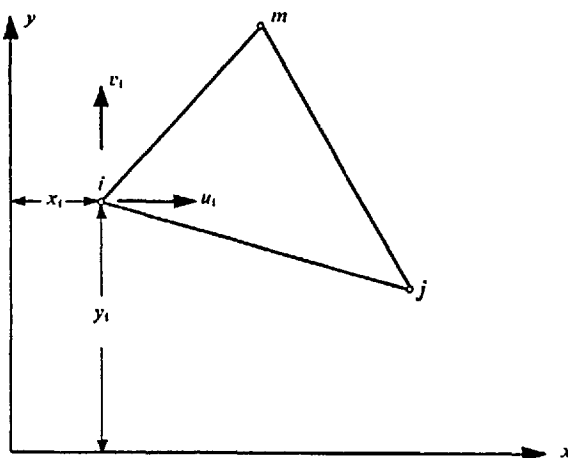


Fig. 2-7.

where the shape function is usually expressed as

$$[N] = [I N_i, I N_j, I N_m]$$

in which  $I$  is a two by two identity matrix and

$$N_i = (a_i + b_i x + c_i y) \quad (2.52)$$

$a_i$ ,  $b_i$  and  $c_i$  are determined by inserting the nodal coordinates and the corresponding nodal displacements into Eq. (2.51).

Strain-displacement matrix  $[B]$  is given by differentiation of matrix  $[N]$ , thus

$$[B] = \begin{bmatrix} \frac{\partial}{\partial x} & 0 \\ 0 & \frac{\partial}{\partial y} \\ \frac{\partial}{\partial y} & \frac{\partial}{\partial x} \end{bmatrix} [N] \quad (2.53)$$

Clearly, due to the linear shape function, matrix  $[B]$  is not a function of  $x$  or  $y$ . Thus, the elemental stiffness matrix reduces to

$$[K] = [B]^T [D] [B] t \Delta \quad (2.54)$$

in which,  $[D]$  may take either  $[D]^E$ ,  $[D]^P$  or  $[D]^{EP}$ , depending on the state of material,  $t$ =element thickness and  $\Delta$ =element area.

For plane strain elements matrices  $[D]^E$  and  $[D]^{EP}$  reduce to (from Eqs. (2.5) and (2.33) respectively),

$$[D]^E = \frac{E}{(1+\nu)(1-2\nu)} \begin{bmatrix} 1-\nu & & \text{symmetric} \\ \nu & 1-\nu & \\ 0 & 0 & 1-2\nu \end{bmatrix} \quad (2.55)$$

and

$$[D]^P = \frac{E}{1+\nu} \begin{bmatrix} \frac{\sigma'_x{}^2}{s} & & \text{symmetric} \\ \frac{\sigma'_x \sigma'_y}{s} & \frac{\sigma'_y{}^2}{s} & \\ \frac{\sigma'_x \tau_{xy}}{s} & \frac{\sigma'_y \tau_{xy}}{s} & \frac{\tau_{xy}^2}{s} \end{bmatrix} \quad (2.56)$$

where they have been obtained by deleting the three rows and three columns corresponding to  $d\epsilon_z = d\epsilon_{xz} = d\epsilon_{yz} = 0$ . The row corresponding to  $d\epsilon_z$  has been eliminated but to trace the third component of normal stress  $\sigma_z$ , in order to evaluate hydrostatic pressure required in Eq. (2.56), its increment must be separately included in the computational procedure. From Eq. (2.34), this is given by

$$d\sigma_z = \frac{E}{1+\nu} \left[ \left( \frac{\nu}{1-2\nu} - \frac{\sigma'_x \sigma'_z}{s} \right) d\epsilon_x + \left( \frac{\nu}{1-2\nu} - \frac{\sigma'_y \sigma'_z}{s} \right) d\epsilon_y - \left( \frac{\sigma'_z \tau_{xy}}{s} \right) d\epsilon_{xy} \right]$$

Of course, for elastic elements this reduces to

$$d\sigma_z = \frac{E}{1+\nu} \left[ \frac{\nu}{1-2\nu} d\epsilon_x + \frac{\nu}{1-2\nu} d\epsilon_y \right].$$

It is interesting to notice that in spite of  $d\epsilon_z=0$ , its components exist and are related by

$$d\epsilon_z^P + d\epsilon_z^E = d\epsilon_z = 0$$

or  $d\epsilon_z^P = -d\epsilon_z^E$ . That is the increment of plastic strain is compensated by the decrement of the elastic strain.

### 2.8.2 Quadrilateral elements (consisting of four constant strain triangles)

In order to improve accuracy and versatility, four constant strain triangles can be combined in such a way to produce a quadrilateral. By the combination of the triangular elements an additional degree of freedom for the combined element is introduced. This degree of freedom may be introduced to correct a specific defect of an element, or it may merely serve to improve accuracy by virtue of adding more terms to the assumed displacement field.

In modeling a plane structure it is often convenient to use quadrilateral elements of arbitrary shape. Input data to the program consists of quadrilateral elements and the computer program automatically divides the elements into component triangular elements and properly assembles stiffnesses of the component triangles. In effect each quadrilateral becomes a small structure built of four elements. Usually, the internal node is assigned coordinates (Fig. 2-8)

$$x_5 = \frac{x_1 + x_2 + x_3 + x_4}{4}, \quad y_5 = \frac{y_1 + y_2 + y_3 + y_4}{4}$$

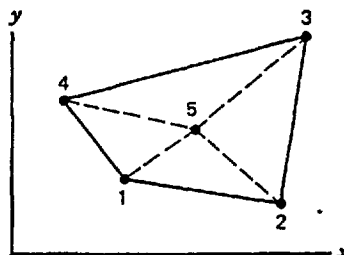


Fig. 2-8.

The stiffness matrix of a quadrilateral is 10 by 10. It is both convenient and efficient to eliminate the two internal degrees of freedom before assembling the elements. The element stiffness matrix is thus reduced to size 8 by 8. This process is performed before the solution of the complete system of equations on the elemental level prior to assembly. This process of elimination is widely used, and in some elements there may be several internal nodes to be eliminated. These nodes may appear anywhere in the nodal displacement array and may be eliminated in any order. However, the most common and easily described case is treated in the following, where all degrees of freedom to be eliminated are grouped at the end of the array.

Let us partition the element stiffness equation so that  $\{\delta_2\}$  represents the internal degrees of freedom to be eliminated.

$$\begin{bmatrix} K_{11} & K_{12} \\ K_{21} & K_{22} \end{bmatrix} \begin{Bmatrix} \delta_1 \\ \delta_2 \end{Bmatrix} = \begin{Bmatrix} F_1 \\ F_2 \end{Bmatrix} \quad (2.57)$$

in which the right hand-side matrix represents loads applied to the element nodes. To eliminate the internal nodes, we first solve for  $\{\delta_2\}$  in terms of  $\{\delta_1\}$

$$\{\delta_2\} = [K_{22}]^{-1} (\{F_2\} - [K_{21}] \{\delta_1\}) \quad (2.58)$$

then substitute this result into the other Eqs. (2.57) to get

$$([K_{11}] - [K_{12}] [K_{22}]^{-1} [K_{21}]) \{\delta_1\} = \{F_1\} - [K_{12}] [K_{22}]^{-1} \{F_2\} \quad (2.59)$$



The coefficient of  $\{\delta_1\}$  is the element stiffness matrix of a quadrilateral. The stiffness matrices are assembled and structural equations solved in the usual way, thus determining  $\{\delta_1\}$  for each element. As a final step in solution of equations the internal degree of freedom may be found by application of Eq. (2.58) to each element.

It must be noted that elimination and solution of equations are basically the same process. Both are processes in which unknowns are eliminated by substitution into the remaining equations. Indeed, if instead of using elimination we were to carry the internal degrees of freedom into the structural system of equations, exactly the same results would be obtained. However, if elimination is avoided, the array of structural equations becomes longer and has a greater bandwidth, and the numerical effort of solution can be expected to increase.

Usually, when these elements are employed the average value of stresses of four triangles, evaluated at the internal nodal point, is assigned as the value of stress of the quadrilateral element. It must be noted that such assignment will result in a reasonably smooth field of stress as the triangles are of the same areas.

### 2.8.3 Quadrilateral isoparametric elements

A typical quadrilateral isoparametric element is shown in Fig 2-9.

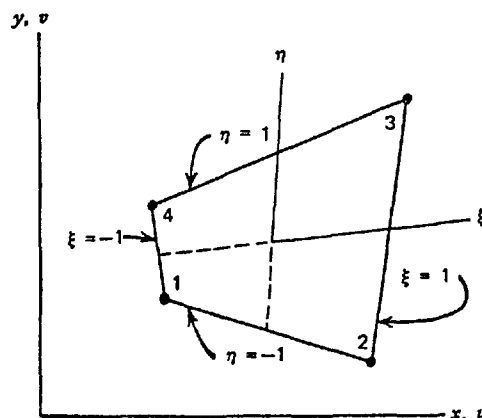


Fig. 2-9.

This group of elements are formulated using an intrinsic coordinate system  $\xi\eta$ , which is defined by element geometry and not by the element orientation in the global coordinate system  $xy$ . There is, of course, a relation between the two systems for each element of the structure. This relation is expressed by

$$\begin{Bmatrix} x \\ y \end{Bmatrix} = \begin{bmatrix} N_1 & 0 & N_2 & 0 & N_3 & 0 & N_4 & 0 \\ 0 & N_1 & 0 & N_2 & 0 & N_3 & 0 & N_4 \end{bmatrix} \begin{Bmatrix} x_1 \\ y_1 \\ x_2 \\ y_2 \\ x_3 \\ y_3 \\ x_4 \\ y_4 \end{Bmatrix} \quad (2.60)$$

where

$$N_1 = \frac{(1-\xi)(1-\eta)}{4}, \quad N_2 = \frac{(1+\xi)(1-\eta)}{4}$$

$$N_3 = \frac{(1+\xi)(1+\eta)}{4}, \quad N_4 = \frac{(1-\xi)(1+\eta)}{4}$$

This mapping relates a unit square in natural coordinates  $\xi\eta$  to a quadrilateral in  $xy$  coordinates whose size and shape are determined by eight nodal coordinates. The mapping is also an interpolation scheme that yields the coordinates of any point in the element when the corresponding  $\xi\eta$  coordinates are given.

Displacements within the element are defined by the same functions as used to define the element shape. This is merely a result of isoparametric element definition. Thus

$$\{f\} = [N] \{\delta\}_e \quad (2.61)$$

where  $[N]$  is the rectangular matrix of Eq. (2-60).

The element matrices are formulated according to the previous procedure for the triangular elements. However, the formulation is carried out in terms of isoparametric coordinates  $\xi_n$ , as follows:

From the previous Eqs. (2.60) and (2.61), we may re-write

$$\begin{aligned} x &= \sum_{i=1}^4 N_i x_i & y &= \sum_{i=1}^4 N_i y_i \\ u &= \sum_{i=1}^4 N_i u_i & v &= \sum_{i=1}^4 N_i v_i \end{aligned} \quad (2.62)$$

Relations between derivatives in the two coordinate systems are established by the chain rule of differentiation

$$\begin{Bmatrix} \frac{\partial u}{\partial \xi} \\ \frac{\partial u}{\partial \eta} \end{Bmatrix} = \begin{bmatrix} \frac{\partial x}{\partial \xi} & \frac{\partial y}{\partial \xi} \\ \frac{\partial x}{\partial \eta} & \frac{\partial y}{\partial \eta} \end{bmatrix} \begin{Bmatrix} \frac{\partial u}{\partial x} \\ \frac{\partial u}{\partial y} \end{Bmatrix} = [J] \begin{Bmatrix} \frac{\partial u}{\partial x} \\ \frac{\partial u}{\partial y} \end{Bmatrix} \quad (2.63)$$

where  $[J]$  is the Jacobian matrix. From Eqs. (2.62), matrix  $[J]$  is given by

$$[J] = \begin{bmatrix} \frac{\partial N_1}{\partial \xi} & \frac{\partial N_2}{\partial \xi} & \frac{\partial N_3}{\partial \xi} & \frac{\partial N_4}{\partial \xi} \\ \frac{\partial N_1}{\partial \eta} & \frac{\partial N_2}{\partial \eta} & \frac{\partial N_3}{\partial \eta} & \frac{\partial N_4}{\partial \eta} \end{bmatrix} \begin{bmatrix} x_1 & y_1 \\ x_2 & y_2 \\ x_3 & y_3 \\ x_4 & y_4 \end{bmatrix} \quad (2.64)$$

Using the inverse relation from Eq. (2.63), we may write

$$\begin{Bmatrix} \frac{\partial u}{\partial x} \\ \frac{\partial u}{\partial y} \\ \frac{\partial v}{\partial x} \\ \frac{\partial v}{\partial y} \end{Bmatrix} = \begin{bmatrix} [J]^{-1} & [0] \\ [0] & [J]^{-1} \end{bmatrix} \begin{Bmatrix} \frac{\partial u}{\partial \xi} \\ \frac{\partial u}{\partial \eta} \\ \frac{\partial v}{\partial \xi} \\ \frac{\partial v}{\partial \eta} \end{Bmatrix} \quad (2.65)$$

where  $[0]$  is a 2 by 2 matrix.

The strain-displacement relation may be written as

$$\{\epsilon\} = \begin{Bmatrix} \epsilon_x \\ \epsilon_y \\ \epsilon_{xy} \end{Bmatrix} = \begin{bmatrix} 1 & 0 & 0 & 0 \\ 0 & 0 & 0 & 1 \\ 0 & 1 & 1 & 0 \end{bmatrix} \begin{Bmatrix} \frac{\partial u}{\partial x} \\ \frac{\partial u}{\partial y} \\ \frac{\partial v}{\partial x} \\ \frac{\partial v}{\partial y} \end{Bmatrix} \quad (2.66)$$

and, from Eqs. (2.62)

$$\begin{Bmatrix} \frac{\partial u}{\partial \xi} \\ \frac{\partial u}{\partial \eta} \\ \frac{\partial v}{\partial \xi} \\ \frac{\partial v}{\partial \eta} \end{Bmatrix} = \begin{bmatrix} \frac{\partial N_i}{\partial \xi} & 0 \\ \frac{\partial N_i}{\partial \eta} & 0 \\ 0 & \frac{\partial N_i}{\partial \xi} \\ 0 & \frac{\partial N_i}{\partial \eta} \end{bmatrix}_{i=1} \quad \begin{bmatrix} \phantom{\frac{\partial N_i}{\partial \xi}} \\ \phantom{\frac{\partial N_i}{\partial \eta}} \\ \phantom{\frac{\partial N_i}{\partial \xi}} \\ \phantom{\frac{\partial N_i}{\partial \eta}} \end{bmatrix}_{i=2} \quad \begin{bmatrix} \phantom{\frac{\partial N_i}{\partial \xi}} \\ \phantom{\frac{\partial N_i}{\partial \eta}} \\ \phantom{\frac{\partial N_i}{\partial \xi}} \\ \phantom{\frac{\partial N_i}{\partial \eta}} \end{bmatrix}_{i=3} \quad \begin{bmatrix} \phantom{\frac{\partial N_i}{\partial \xi}} \\ \phantom{\frac{\partial N_i}{\partial \eta}} \\ \phantom{\frac{\partial N_i}{\partial \xi}} \\ \phantom{\frac{\partial N_i}{\partial \eta}} \end{bmatrix}_{i=4} \quad \begin{Bmatrix} u_1 \\ v_1 \\ u_2 \\ v_2 \\ u_3 \\ v_3 \\ u_4 \\ v_4 \end{Bmatrix} \quad (2.67)$$

Combination of Eqs. (2.65) through (2.67) yields the relation

$$\{\epsilon\} = [B] \{\delta\}_e.$$

Having established matrix  $[B]$  one may proceed to the integration of the expression  $[B]^T [D] [B]$ , where  $[D]$  may represent  $[D]^E$ ,  $[D]^P$  or  $[D]^{EP}$ , depending on the state of material.

For a typical integral the change of coordinates is

$$\int [B]^T [D] [B] d(vol) = \int_{-1}^{+1} \int_{-1}^{+1} [B]^T [D] [B] det[J] d\xi d\eta \quad (2.68)$$

where all matrices on the left hand-side of Eq. (2.68) are expressed in terms of  $x$  and  $y$ , whilst the ones on the right-side are expressed in terms of  $\xi$  and  $\eta$ . In general, the integration cannot be carried out explicitly because of the complexity of the expressions.

Although, it can be easily evaluated numerically by the Gaussian method.

For a one variable function, the integration is written as

$$I = \int_{-1}^{+1} f(\xi) d\xi = \sum_{i=1}^n H_i f(\xi_i)$$

that is, at each sampling point the product  $H_i f(\xi_i)$  is determined and the sum of these products for all the sampling points approximate to the integral,  $I$ .

The Gauss method locates the sampling points so that for a given number of points, greatest accuracy is obtained. Sampling points are located symmetrically with respect to the centre of the interval. Figure 2-10 shows the symmetrical positions and weighting coefficients for Gaussian integration.

The above procedure can be extended to evaluate a double integral. The most obvious way of obtaining the integral

$$I = \int_{-1}^{+1} \int_{-1}^{+1} f(\xi, \eta) d\xi d\eta$$

is to first evaluate the inner integral keeping  $n$  constant and then the outer integral. Thus

$$I = \sum_{j=1}^n H_j \int_{-1}^{+1} f(\xi_j, \eta) d\eta = \sum_{j=1}^n \sum_{i=1}^n H_j H_i f(\xi_j, \eta_i)$$

ABSCISSAE AND WEIGHT COEFFICIENTS OF THE GAUSSIAN QUADRATURE FORMULA

$$\int_{-1}^1 f(x) dx = \sum_{j=1}^n H_j f(a_j)$$

$\pm a$	$H$
$n = 1$ 0	2 00000 00000 00000
$n = 2$ 0 57735 02691 89626	1 00000 00000 00000
$n = 3$ 0 77459 66692 41483 0 00000 00000 00000	0 55555 55555 55556 0 88888 88888 88889
$n = 4$ 0 86113 63115 94053 0 33998 10435 84856	0 34785 48451 37454 0 65214 51548 62546
$n = 5$ 0 90617 98459 38664 0 53846 93101 05683 0 00000 00000 00000	0 23692 68850 56189 0 47862 86704 99366 0 56888 88888 88889
$n = 6$ 0 93246 95142 03152 0 66120 93864 66265 0 23861 91860 83197	0 17132 44921 79170 0 36076 15730 48139 0 46791 39345 72691

Fig. 2-10.

2.9 Conclusion

In the preceding chapter, the incremental methods for the prediction of elasto-plastic deformation of a continuum by the finite element method were presented and compared. Amongst the methods presented, the method of variable stiffness matrix was selected for future computer implementation, owing to its rapid rate of convergence although at the cost of slightly higher computing time.

The restrictions introduced are:

- a- Small deformations

- b- Absence of Bauschinger effect
- c- Isothermal deformation
- d- Isothropic material behaviour

Restriction 'd' could be easily lifted by abandoning the symmetry properties of the constitutive tensor. The final expressions obtained would not be applicable but alternative expressions could easily be produced. Clearly, using such a formulation would dramatically increase the computing time. Restriction 'c' and 'b' might also be removed without substantial difficulty in the derivation stage. Again one should expect the computing time to be substantially affected. Restriction 'a' is the most decisive one in the formulation. Should this one be lifted a substantially new formulation would be required and for that purpose Marcal's work (36) might prove to be of invaluable help.

CHAPTER 3  
THE COMPUTER PROGRAMS

3.1 Introduction

The computer programs presented in this thesis are based on an approach similar to that due to Yamada (20), described in the previous chapter. In the present approach, however, an instantaneous frame of reference is used to describe the incremental elasto-plastic deformation of the continuum. As previously described, this kind of strategy to some extent offsets the effect of omitting the non-linear terms and therefore strains of higher magnitude may be tackled within a certain degree of accuracy. Moreover, in the present approach, negative plastic strains are treated and considered to indicate the elastic unloading of the material.

The computer programs developed (written in Fortran IV) are mainly restricted to small strain plasticity. They can, however, be modified to perform a similar analysis on a large strain and large displacement formulation, such as derived by Marcal (36). The modifications, as Marcal believes, are minor and can be implemented easily in an available elastic-plastic computer program.

3.2 Computation procedure

The computer programs were developed on the following sequence of computations:

- 1- For the boundary condition imposed, nodal displacement and thus elastic strains, stresses and equivalent stresses ( $\bar{\sigma}$ ) within each element were calculated.
- 2- All elastic values were scaled up in order to induce yield in the

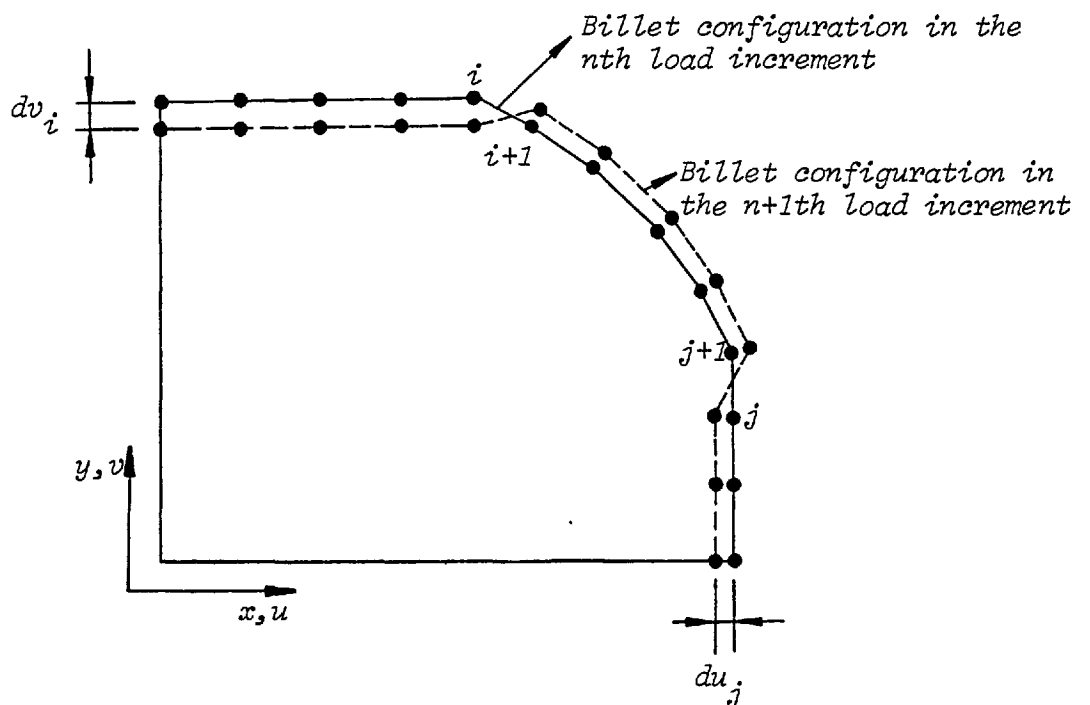


- element with the maximum equivalent stress. The rating factor was  $r = \frac{Y}{\bar{\sigma}_{max}}$ , where  $Y$  denotes the yield stress of the material under consideration and  $\bar{\sigma}_{max}$  is the maximum equivalent stress.
- 3- The nodal displacements and forces and also the element strains and stresses were multiplied by rating factor  $r$ .
  - 4- Matrix  $[D]$  and hence  $[K]$  were updated for the yielded elements.
  - 5- The overall stiffness matrix of the whole body was modified.
  - 6- The geometrical matrices were updated using the current nodal coordinates. Clearly, this is not a mandatory sequence at the beginning of the loading procedure.
  - 7- The instantaneous boundary conditions were read-in.
  - 8- The modified system of equations were solved and strain-, stress- and equivalent stress-increments within each element were calculated.
  - 9- The rating factor  $r$  was calculated for every element remaining in the elastic state.
  - 10- The minimum value of the rating factors was found and designated  $r_1$ . If  $r_1$  was larger than some prescribed value limiting the amount of deformation, then  $r_1$  was set equal to the prescribed value (this is explained further below).
  - 11- The nodal displacement- and force-increments and also the elemental strain- and stress-increments were multiplied by the latest value of the rating factor.
  - 12- Strain- and stress-increments for unloaded elements were recalculated.
  - 13- The nodal displacement- and force-increments and also the strain- and stress-increments were added to the previous displacements, forces, strains and stresses, respectively.
  - 14- Matrix  $[D]$  was updated for the yielded and unloaded elements.

- 15- The elemental stiffness matrices of all elements were updated.
- 16- The overall stiffness matrix of the whole body was modified.
- 17- Sequences 6 through 16 was repeated until a desirable deformation was attained.

Sequence 11 is explained further as follows:

There are circumstances for which the rating factor  $r_1$  may have to be reduced in order to avoid an undesirable increment of deformation. For instance, if the rating factor is found to be very large, it must be reduced to a prescribed value (e.g. by setting it equal to unity) in order to prevent the possibility of a large and unexpected amount of deformation severely influencing the accuracy of the calculation. As a further example, when a round billet is indented in a rectangular-shaped chamber, at some stage of deformation the rating factor must be set equal to a prescribed value in order to avoid any violation of the physical nature of the deformation (see the illustration)



It can be deduced from the illustration that in order to bring back the violating node (denoted by  $i+1$ ) to within the imposed upper boundary, we should have

$$y_i + v_i + r_2 dv_i = y_{i+1} + v_{i+1} + r_2 dv_{i+1}$$

where:

$r_2$  is the required rating factor

$y_i, y_{i+1}$  are the initial  $y$  coordinates of nodes  $i$  and  $i+1$

$v_i, v_{i+1}$  are the vertical displacements of nodes  $i$  and  $i+1$  at the end of the  $n$ th load increment

$dv_i, dv_{i+1}$  are the increments of  $v_i$  and  $v_{i+1}$  at the end of  $(n+1)$ th load increment

Rearranging the above equation gives

$$r_2 = - \frac{y_i - y_{i+1} + v_i - v_{i+1}}{dv_i - dv_{i+1}}$$

Similarly, to bring back the violating node (denoted by  $j+1$ ) to within the imposed boundary on the right, we should have

$$r_3 = - \frac{x_j - x_{j+1} + u_j - u_{j+1}}{du_j - du_{j+1}}$$

The minimum values of  $r_1, r_2$  and  $r_3$  determine the admissible rating factor.

### 3.3 Description of the programs

The computer programs presented, include one of each the three types of elements previously described. This avoids involving all three types of elements in a single cumbersome program. This kind of presentation not only simplifies the description of the programs but also gives a good estimation of the effort required to introduce a new type of element into an available computer program.

The general name of the program is 'EPFEAX', standing for Elastic-Plastic Finite Element Analysis. The symbol 'X' indicates the type of element implemented and may take the values 1, 2 or 3 for constant triangular, quadrilateral and quadrilateral isoparametric elements, respectively.

### 3.4 Analysis of the program EPFEA 1

This program was developed to analyse elasto-plastic deformation of a continuum by using constant strain triangular elements. The listing of the program and variables involved are presented in appendix A. The flow chart is shown in Fig. 3-1. As shown, the program can be roughly subdivided into seven main subroutines, in each of which specific operations are performed. The basic features of these subroutines are as follows:

#### 3.4.1 Subroutine GDATA

This routine concerns the entering of data, via punched cards. The data includes number of elements, number of nodes, nodal connections of the elements, material properties and many other specifying information. The data is subsequently used to compute additional but related data. Nodes are scanned, the nodal coordinates being scaled

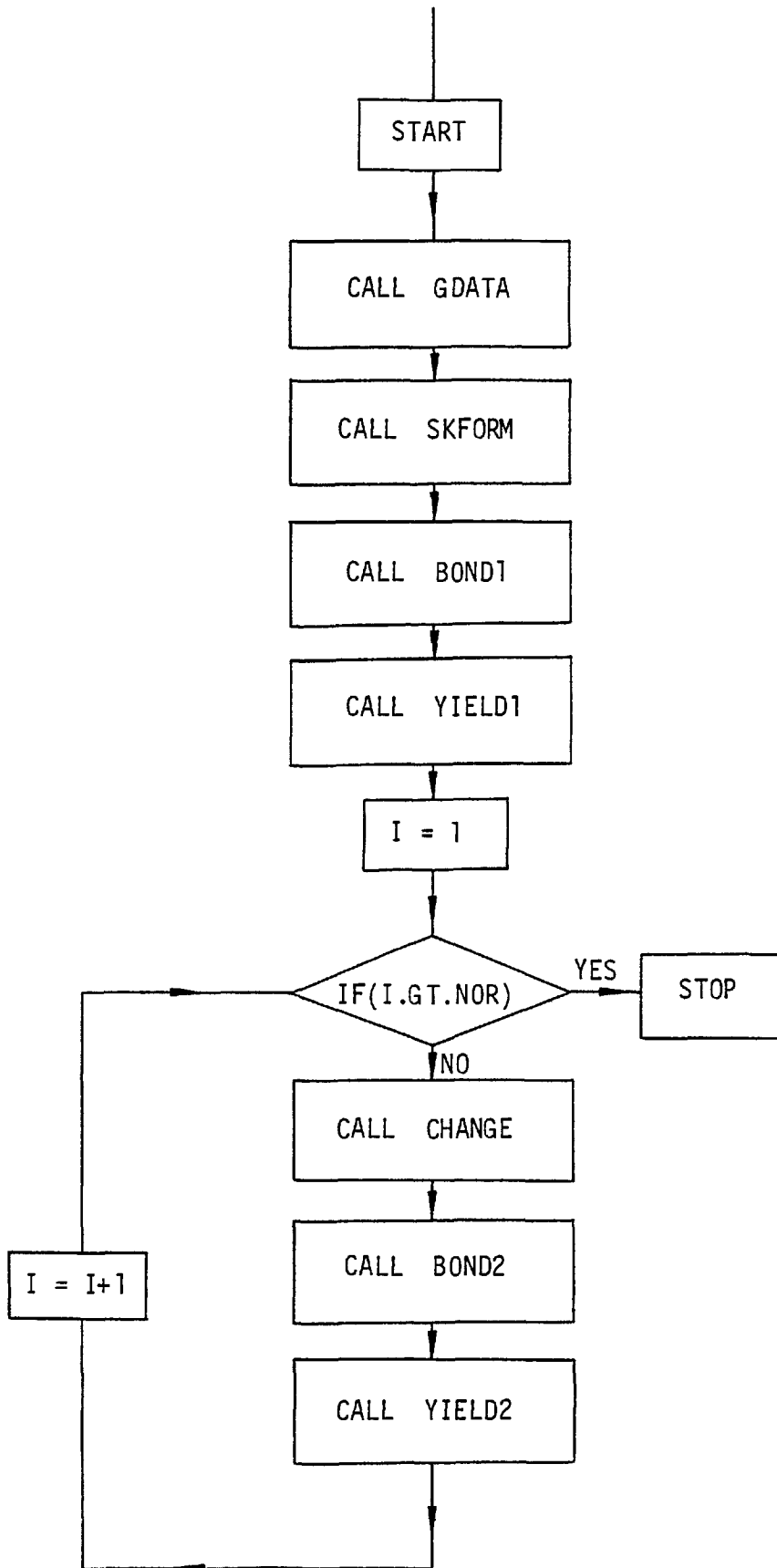


Fig. 3-1.

down. Elements are scanned and geometrical matrices related to the elements are computed. Finally, elemental elastic matrices are initialised.

### 3.4.2 Subroutine SKFORM

The general purpose of this routine is to create the elastic elemental stiffness matrices. All necessary data is transmitted to it from routine GDATA. The elements are scanned and the basic operations are:

- 1- To construct the strain-displacement matrix  $[B]$ .
- 2- To construct the stress-strain relationship  $[D]$ .
- 3- To multiply the transpose of  $[B]$  by  $[D]$  and then by  $[B]$ , i.e. obtaining the  $[B]^T [D] [B]$ .
- 4- To multiply the product matrix by the area of the element.
- 5- To add appropriately the elemental stiffness matrix to the overall stiffness matrix. This is achieved by an internal routine called SADD, which adds the elemental stiffness matrices in a banded form to the overall stiffness matrix.

### 3.4.3 Subroutine BOND 1

This routine prepares the initial boundary conditions by allocating integer values to a pointer vector NP which is then used to modify the system of equations prior to solving them. Boundary conditions are read-in as either '0' or '1' for each degree of freedom, with '0' denoting a prescribed force and '1' denoting a prescribed displacement. It is worth mentioning that the corresponding elements of vector NP due to the node  $i$  are  $2i-1$  and  $2i$  in the X and Y directions, respectively.

#### 3.4.4 Subroutine YIELD 1

Plastic deformation is initiated by a call made to this routine. The system of equations and boundary conditions created by the previous routines and transmitted to this subroutine are transferred to an internal routine called SOLVE. The routine SOLVE (or equation solver routine) modifies the system of equations prior to solving them. The modification procedure involves the multiplication of the appropriate diagonal term by a large number (e.g.  $10^{20}$ ) when a prescribed displacement is encountered and then modification of the corresponding load vector.

The system of equations are solved using the direct method of Gauss elimination, although the Gauss-Seidal iterative method is preferable for its ease of programming and also for its undeniable saving in computing time when using the optimum relaxation factor. In plasticity the relaxation factor must be successively redefined in order to take into account the decrease of rigidity of the system of equations. There is not a definite method of determining the relaxation factor and hence the convergence is neither likely to be achieved nor the time taken to be economical. Particularly when the system of equations becomes ill-conditioned owing to the bulk plastic yielding of the continuum.

Having obtained the nodal displacements, elements are scanned and using the appropriate relations, strains and hence stresses within the elements are calculated. The element with the maximum equivalent stress is determined and the rating factor  $r = \frac{Y}{\sigma_{max}}$  is calculated. The variables such as nodal forces and displacements and also elemental strains, stresses and equivalent stresses are then multiplied by the rating factor  $r$ . In the subsequent operation, the element with the

maximum equivalent stress is considered yielded and its stiffness matrix is calculated according to the appropriate elasto-plastic relationships. In EPFEA 1, however, a provision was made for some elements to be included amongst the yielded elements just prior to yielding. This allowance is advantageous for saving computing time. In the program, elements of  $\bar{\sigma} > 0.98 Y$  are considered to be plastic.

When an element yielded, the corresponding element of a status vector called NPI is set equal to 1. There-by, the status of the post-yield elements can be simply distinguished from the remaining elastic elements. At the end of this routine, the elemental stiffness matrices of the post-yield elements are deleted from the overall stiffness matrix and new values are substituted.

#### 3.4.5 Subroutine CHANGE

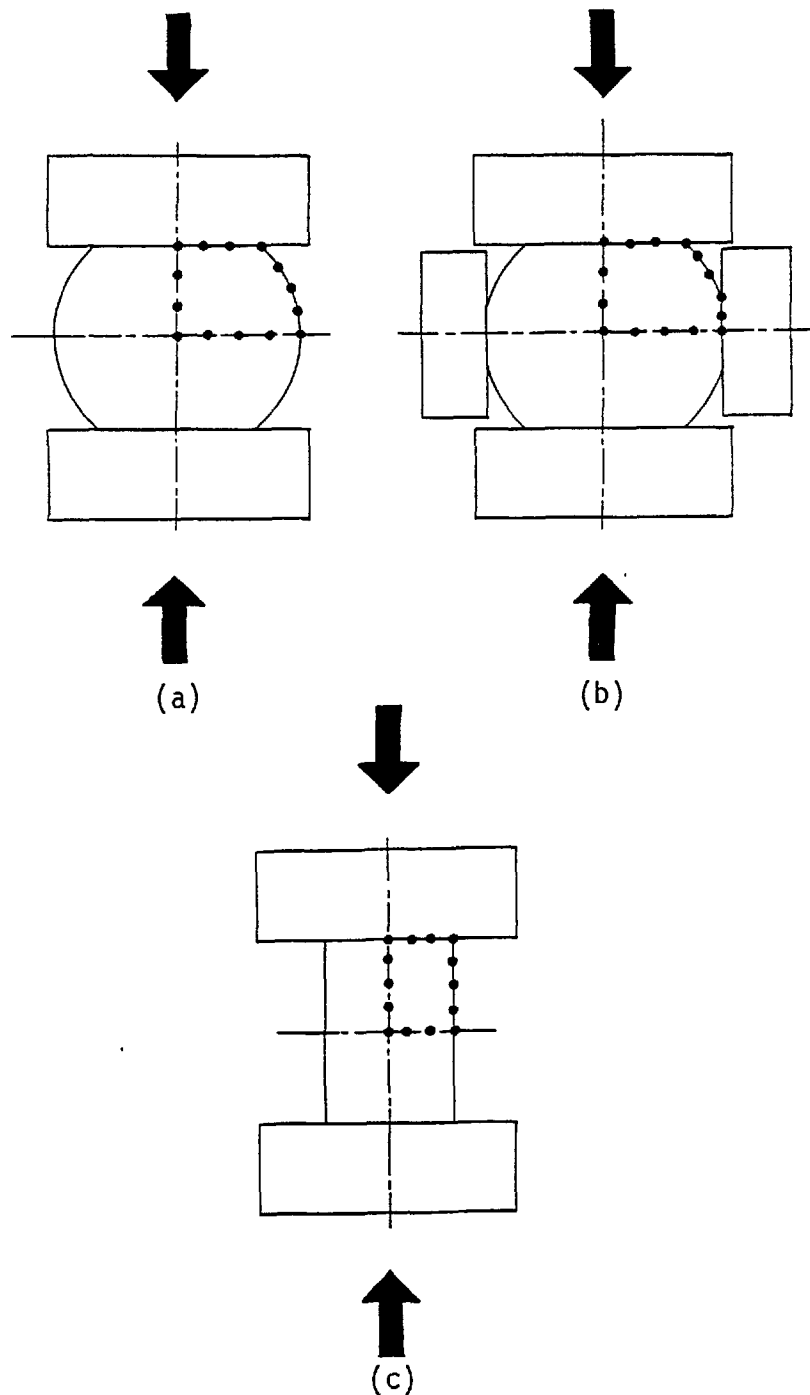
The geometry of the continuum is updated by a call made to this routine. Nodes are scanned and the initial nodal coordinates are added to the corresponding nodal displacements. Subsequently, elements are scanned and geometrical matrices related to the elements are recalculated.

#### 3.4.6 Subroutine BOND 2

The instantaneous boundary conditions are provided by a call made to this routine. This is a compulsory routine if the initial boundary conditions are to be redefined in order to deform the continuum in a particular manner. For instance, when a billet is indented between two approaching platens, the peripheral nodal points must be maintained below the surfaces of the platens in order to avoid violation of the physical nature of the process (see the illustration a). Alternatively,



if the billet is indented as shown in illustration b, the initial boundary conditions have to be appropriately redefined in order to prevent any of the peripheral nodes passing the imposed surfaces. Conversely, if during deformation the initial boundary conditions remain unchanged as shown in illustration c, then this routine can be either by-passed or eliminated altogether.



### 3.4.7 Subroutine YIELD 2

This important routine is successively called until a desirable magnitude of deformation is attained. Briefly, it performs the following operations:

- 1- The system of equations and instantaneous boundary conditions transmitted to this routine are passed to the routine SOLVE and the incremental variables are calculated.
- 2- Elements are scanned and the strain- and stress-increments are obtained.
- 3- The rating factors, for those elements remaining in the elastic state are obtained and the maximum is designated YP.
- 4- In the indentation of the round billet in a rectangular-shaped chamber, the peripheral nodes are scanned. If any of the nodes violate the imposed boundary, factors YP1 and YP2 are calculated as described in order to bring back the nodes within the specified boundary. The minimum value of YP, YP1 and YP2 is taken as the allowable rating factor.
- 5- The incremental variables such as displacement- and load-increments, etc. are multiplied by the recent value of the rating factor. Using the same allowance as before, elastic elements with  $\sigma > 0.98 Y$  are considered to be plastic.
- 6- Elements are scanned, the effective strain- and stress-increments being obtained. For the post-yield elements, the effective plastic strain increments are also calculated. If, any of the post-yield elements unloaded,  $d\bar{\epsilon}^P$  is set equal zero and on the basis of elastic matrices, the strain-, stress- and effective stress-increments are recalculated. The unloaded elements are considered elastic and their yield stresses are changed to their latest attained values of

effective stresses.

- 7- Nodes are scanned and the current nodal coordinates are added to the corresponding nodal displacement-increments.
- 8- Elements are scanned and the current elemental stresses, strains, effective stresses and effective plastic strains (for the post-yield elements) are obtained.
- 9- Depending on the recent state of elements the elemental stiffness matrices are recalculated, so modifying the overall stiffness matrix of the whole body.
- 10- Having applied a number of increments, the total forces applied by the platens and their contact widths with the billet and other required information are written on the tape for further processing.
- 11- Having obtained a particular amount of deformation, nodes are scanned and the average effective stresses and effective plastic strains of the elements associated with that particular node are calculated and printed out.

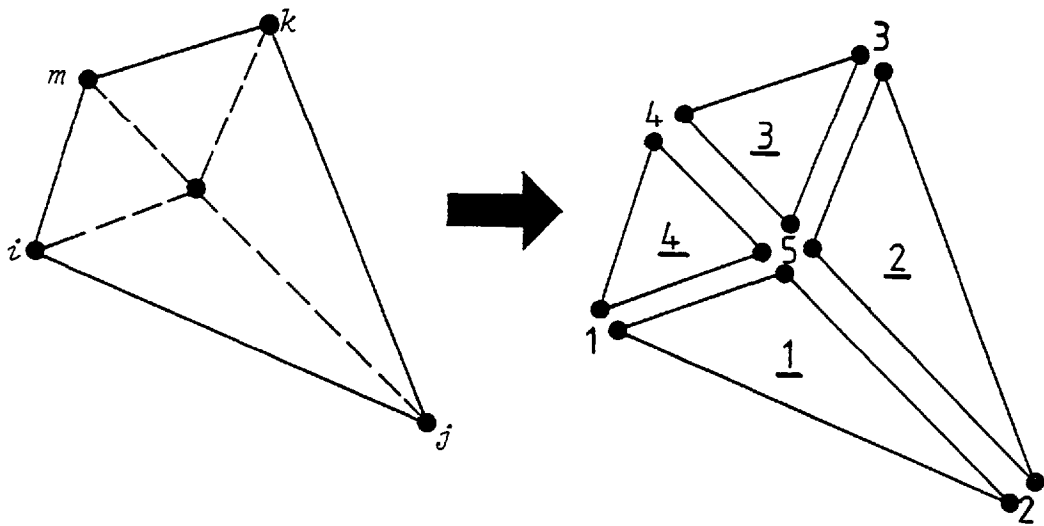
### 3.5 Analysis of the program EPFEA 2

This program was developed to analyse elasto-plastic deformation of a continuum by using quadrilateral elements. Although the structure of EPFEA 2 differs substantially from EPFEA 1 they both perform basically the same operations, since in EPFEA 2 each quadrilateral element is subdivided into four constant strain triangles. The general feature of this program is outlined below, the listing of the program including the variables used being shown in appendix B. It is worth mentioning that in the following, only substantial differences from EPFEA 1 are presented and discussed.

### 3.5.1 Subroutine GDATA

Elements are scanned, average nodal coordinates of the element under consideration being calculated and assigned as the coordinates of the internal node (see the illustration), i.e.

$$x_5 = \frac{x_1 + x_2 + x_3 + x_4}{4} \quad \text{and} \quad y_5 = \frac{y_1 + y_2 + y_3 + y_4}{4}$$



In the subsequent operation the element is subdivided in anticlockwise and according to the elemental node numbering. The subdivided element is node-numbered corresponding to the node numbering of the original element. Thus the internal node is designated the last node in the substructure comprising four triangles. As described, this has the effect of grouping all the degrees of freedom to be eliminated in the 9th and 10th rows of the substructure stiffness matrix. Having numbered the resulting four triangular elements, the geometrical matrices corresponding to the triangles are calculated.

### 3.5.2 Subroutine SKFORM

Elements are scanned and the stiffness matrices of the triangles, comprising the quadrilateral element under consideration, are calculated and assembled. Rows corresponding to the internal node are then eliminated obtaining the stiffness matrix of the quadrilateral element. In the usual way, the stiffness matrices of quadrilateral elements are assembled and thus the overall stiffness matrix of the whole body is built up.

### 3.5.3 Subroutine YIELD 1

A substantial change in this routine is the introduction of two additional vectors to resume the displacement of the internal nodes when required.

The system of equations are solved. Elements are scanned and using the appropriate relations the internal nodal displacements are calculated and stored. As usual, for the resulting triangles the strains; stresses and effective strains are calculated. Elements are scanned and if any of the comprising triangular elements are found to have yielded, the quadrilateral stiffness matrix is recalculated and substituted in the overall stiffness matrix of the whole body.

### 3.5.4 Subroutine YIELD 2

This routine functions basically on the same principle as YIELD 1. In YIELD 2, however, provision is made to treat the unloaded quadrilateral elements. Elements are scanned and if any of the comprising triangular elements are found to be unloaded, the elemental stiffness matrix is recalculated and substituted in the overall stiffness matrix of the whole body.

When a desirable magnitude of deformation is attained, the elements are scanned and average values of the effective plastic strains and also effective stresses of the comprising triangular elements are calculated and assigned as the mean values of the element under consideration.

### 3.6 Analysis of the program EPFEA 3

This program was developed to analyse elasto-plastic deformation of a continuum by using quadrilateral isoparametric elements. Although, in the present program only quadrilateral isoparametric elements were implemented, slight modifications would allow higher order elements such as quadratic or cubic isoparametric elements to be implemented also.

The flow chart of this program is essentially identical to that of EPFEA 1, although some additional routines have been introduced in order to perform appropriate operations (mostly now in the form of numerical integrations) attributed to the quadrilateral isoparametric elements. The listing of the program and variables involved are presented in appendix C.

The description of substantial changes, as compared with EPFEA 1, are as follows:

#### 3.6.1 Subroutine GDATA

To generate the element stiffness matrix a call is made to an internal routine called STIFF. In this routine the element stiffness matrix is initially set equal to zero. The Gaussian points (four, in the present case) within the element under consideration are then scanned and calls are made to routine SHAPE. Subsequently, stiffness

matrices corresponding to the Gaussian points are generated and assembled, forming the element stiffness matrix. In the usual way element stiffness matrices are assembled and the overall stiffness matrix of the whole body is built up.

It should be noted that routine SHAPE calculates the shape functions, derivatives of the shape functions and determinant of the Jacobian matrix, for a Gaussian point under consideration.

### 3.6.2 Subroutine YIELD 1

When the displacements are found, the Gaussian points are scanned. For the point under consideration a call is then made to routine SHAPE obtaining the shape functions. Strains are then calculated by multiplication of the shape functions and the corresponding element nodal displacements. Stresses and effective stresses are determined in the usual way.

Having obtained effective stresses, the Gaussian points are scanned and the point with the maximum effective stress and hence the rating factor, are determined. For any element in which one or more points have yielded, the element stiffness matrix is recalculated and substituted in the overall stiffness matrix.

It is of interest to note that quadrilateral isoparametric elements resemble quadrilateral elements if the four Gaussian points in the former are assumed to be representative of the four triangles involved in the latter. That is, irrespective of numerical integrations involved in the isoparametric elements, the two elements resemble each other in many respects when being implemented in a computer program.

CHAPTER 4  
EXPERIMENTAL WORK

4.1 Introduction

The first and main objective of the present work was to analyse the indentation process for the particular condition when the chamber and billet were respectively rectangular and circular in cross-section. The billet was assumed to undergo plane strain deformation. During the course of indentation the geometry of the billet cross-section was measured and recorded in the central region of the billet length. The loads applied to the different segments of the chamber were also measured and recorded. This study will be presented in the first part of the chapter.

The study of the maximum axial frictional force induced at the interface of the billet and chamber was the second objective of the present work. The billet was first indented, and then deformed by a pressure pad moving coaxially with the clamped billet, until slippage occurred. The maximum load applied to the pad was measured and recorded for various initial amounts of indentation and initial lengths of billet. This study will be considered in the second part of the chapter.



PART 1

STUDY OF THE INDENTATION PROCESS

4.2 Introduction

As described in section 1.6, in a friction actuated continuous extrusion process such as 'Context', the amount of indentation is determined by the minimum transverse distance that the segments have to travel in order to enter the tube which holds them together as they move towards the die. It is worth noting that in some friction actuated continuous extrusion processes such as 'Linex', the chamber segments are held together by means of guiding blocks which, nevertheless, in effect, constitute a tube. The following text therefore not only applies to a process such as 'Context' but also in principle to any other type of friction actuated continuous extrusion employing a similar mechanism to indent the billet. In such systems four different types of indentation can be distinguished, depending on the size of the billet relative to the chamber cross-section. These are shown in Fig. 4-1. In order for the segments to enter the tube for the cases shown in (a) and (c) the billet need only be indented by segments A and B. In (a), the billet does not make any contact with segments C and D during the course of indentation, which is in contrast to the case shown in illustration (b). In (c), the billet is in contact with segments C and D from the first moment of indentation. In (d), all four segments must indent the billet in order for them to enter the tube.

In the experimental work presented here, only the cases shown in (a) and (c) were considered. The deformation of the billet in these cases is entirely dependent on the transverse movement of segments

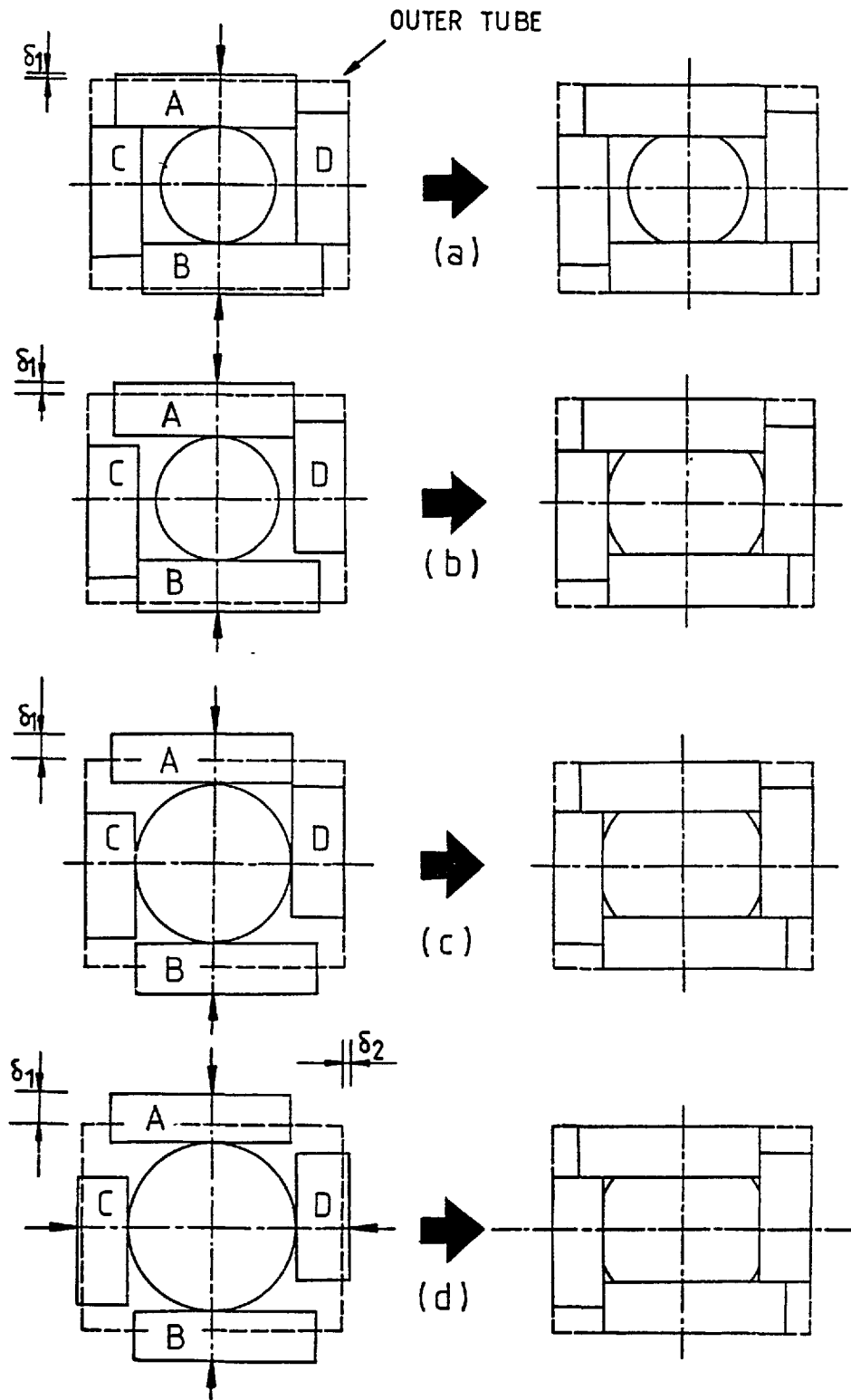


Fig. 4-1. Different modes of indentation.

A and B. In the rest of this work, those cases shown in illustrations (c) and (a) will simply be referred to respectively as indentation with and without side-restraint. The deformation of the billet for the cases shown in illustrations (b) and (d) is more complicated. In (b) it will be required to know the moment at which the billet makes contact with the segments C and D in order to define its state of deformation, and in (d) the transverse movement of these segments will also be required.

#### 4.3 Design considerations

As described in section 1.6, deformation of the billet during the course of indentation may reasonably be assumed to take place under conditions of plane strain and this was one of the major requirements considered in designing the test-rig. The main design requirements were as follows:

- 1- The chamber length in relation to the size of the chamber cross-section should be sufficiently large to ensure plane strain deformation.
- 2- Instrumentation should be provided for the instantaneous recording of loads applied to the chamber segments.

#### 4.4 Experimental set-up

The experimental set-up which served to indent the billet with and without side-restraint is shown in Fig. 4-2. The chamber was comprised mainly of segments A and B which were fixed to the upper and lower platens of a two pillar die-set. Segments C and D, fixed on blocks E and F, formed the other two sides of the chamber and were only employed for the case of indentation with side-restraint. The blocks

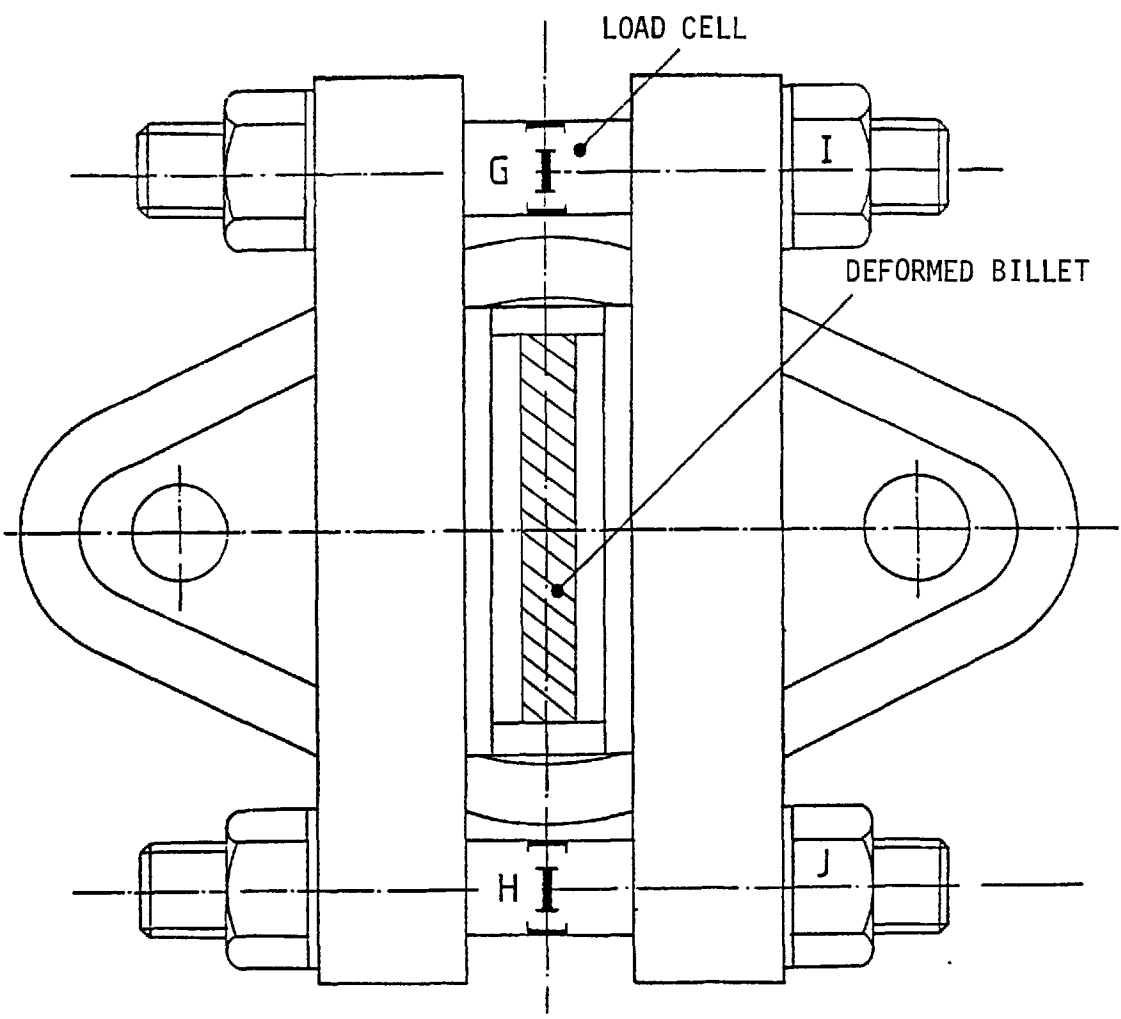
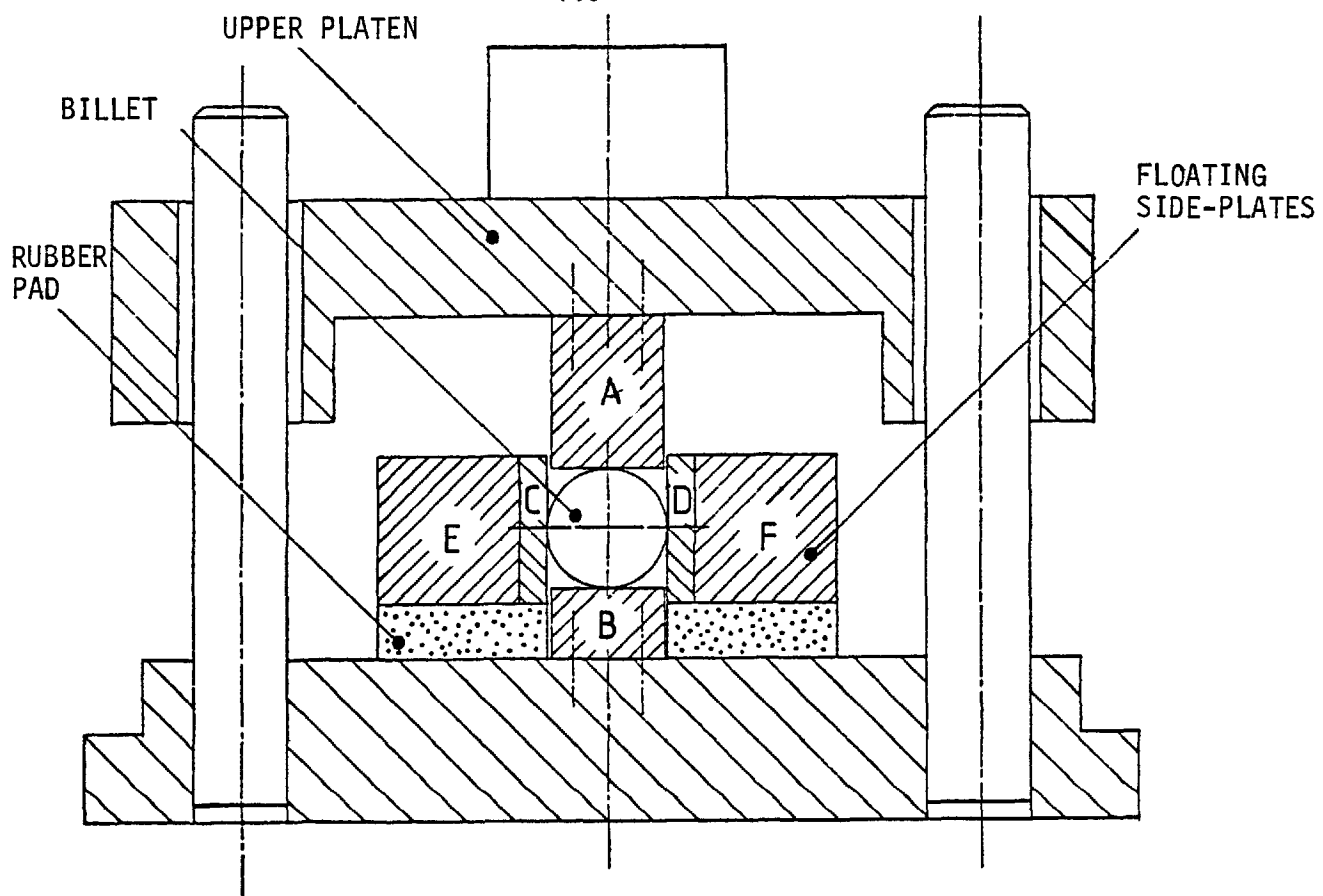


Fig. 4-2. Experimental set-up for billet indentation with and without side restraint.

E and F, at their two extreme ends, were connected together by means of rods G and H. These rods also served as load-cells in measuring the restraint forces applied to the billet by segments C and D.

In order to eliminate any lateral frictional forces which would be exerted on segments C and D, their supporting blocks E and F were designed to float on two rubber pads. Clearly, this provided the particular condition in which segments A and B would indent the billet at equal speed. The segments forming the chamber were made of EN24 steel and heat treated to 52 RC. After heat treatment the inside surfaces of the chamber were ground to C.L.A. of  $0.25 \mu\text{m}$  ( $10 \mu\text{in}$ ). The load-cells G and H were also made of EN24 steel but in annealed condition. Each of the load-cells were provided with four strain gauges forming a full Wheatstone bridge. Before calibration, the load-cells were subjected to alternate loading in order to stabilize the readings. The load-cells were finally calibrated under tension and the calibration curves are shown in Fig. 4-3.

The experiments were conducted on a 540 KN (120 000 Ib) Tinius-Olsen testing machine. Throughout the experiments the speed of the press-ram was maintained at  $1 \frac{\text{mm}}{\text{min}}$  ( $0.04 \frac{\text{in}}{\text{min}}$ ).

#### 4.5 Specimens

The cylindrical specimens were manufactured from commercially pure aluminium and lead. The aluminium specimens were machined from standard bars to diameter of 38.1 (1.5), 50.8 (2) and 63.5 mm (2.5 in) and to lengths of 130 and 190 mm.

To produce the lead billets, blocks of lead were melted and cast in the form of long cylinders. The lead specimens were then manufactured from these ingots to the same dimensions as those used in

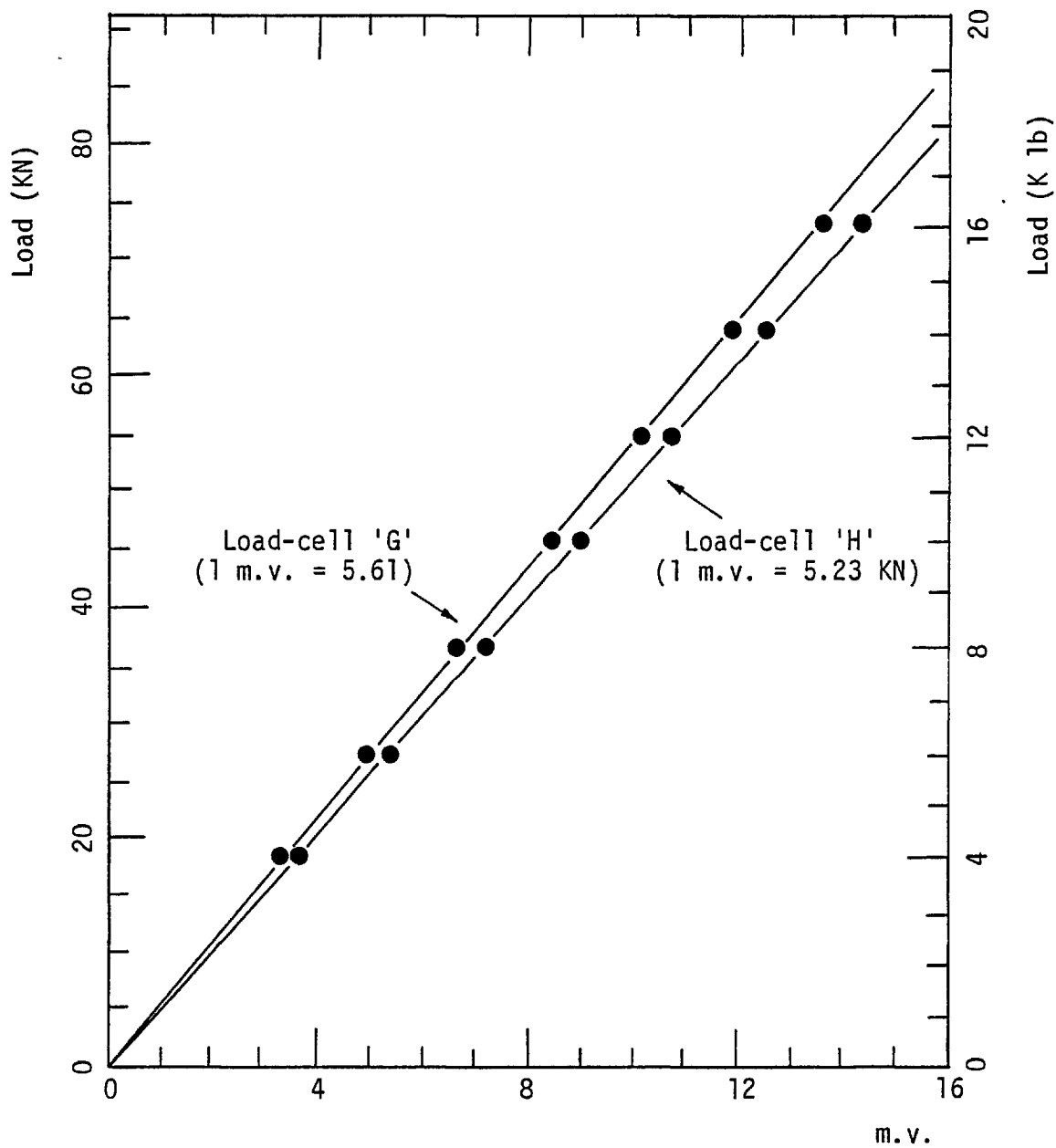


Fig. 4-3. Calibration curves for load-cells 'G' and 'H'.

the manufacturing of the aluminium specimens.

The aluminium and lead specimens were eventually annealed at 400 °C and 200 °C respectively for two hours.

#### 4.6 Instrumentation

##### 4.6.1 Data logger

A Solartron digital data recorder was used to measure and record strain or load with up to 100 analogue input signals. The inputs could be scanned in sequence at a speed which could be adjusted to various values between 10 samples per second and one per four seconds. A single channel could be selected and continually sampled or alternatively a number of channels.

The analogue signals were converted to digital form and their values could be observed on an in-line illuminated display unit. A high speed numeric printer was connected to the data logger from which the channel identity, polarity of the readings and digital voltage values could be printed out.

##### 4.6.2 Measurement of dimension and area

To measure the variables involved in the experiments a number of mechanical instruments were used. The instruments and measuring procedures employed were as follows:

- 1- A bench micrometer was used to measure the billet height, i.e. distance between segments A and B (see Fig. 4-2). The accuracy of the instrument was  $\pm 0.0025$  mm ( $\pm 0.0001$ ). The measurement was carried out when the billet was unloaded and removed from the chamber since the elastic recovery was assumed negligible in comparison with the extent of the plastic deformation.

- 2- A standard vernier was used in measuring the widths of the contact surfaces. The measurement was carried out at the central region of the billet length, where the deformation was most likely to be under conditions of plane strain.
- 3- A planimeter was used in measuring the areas of the contact surfaces. The accuracy of the instrument was  $\pm 1 \text{ mm}^2$ .

#### 4.6.3 Surface profile measurements

A Talysurf machine was used in measuring the roughness of a desired surface. Essentially, the instrument consists of a pick-up unit having a sharply pointed stylus which is transversed across the surface by means of a motorised driving unit.

The up and down movements of the stylus are converted into corresponding changes in an electric current which are amplified by means of a valve amplifier, and then used to control:

- 1- A graph recorder which provides a profile of the surface.
- 2- An average meter which shows the centre-line-average (C.L.A.) index of all irregularities coming within a standardised length of surface.

#### 4.7 Parameters defining the state of deformation

In order to pursue the state of deformation a number of parameters during the course of indentation were measured and recorded (see Fig. 4-4). The measured parameters in indentation of round billets without side-restraint were as follows:

- 1- H = height of billet
- 2-  $W_1$  = width of contact surface with the chamber top segment
- 3- D = diameter of billet



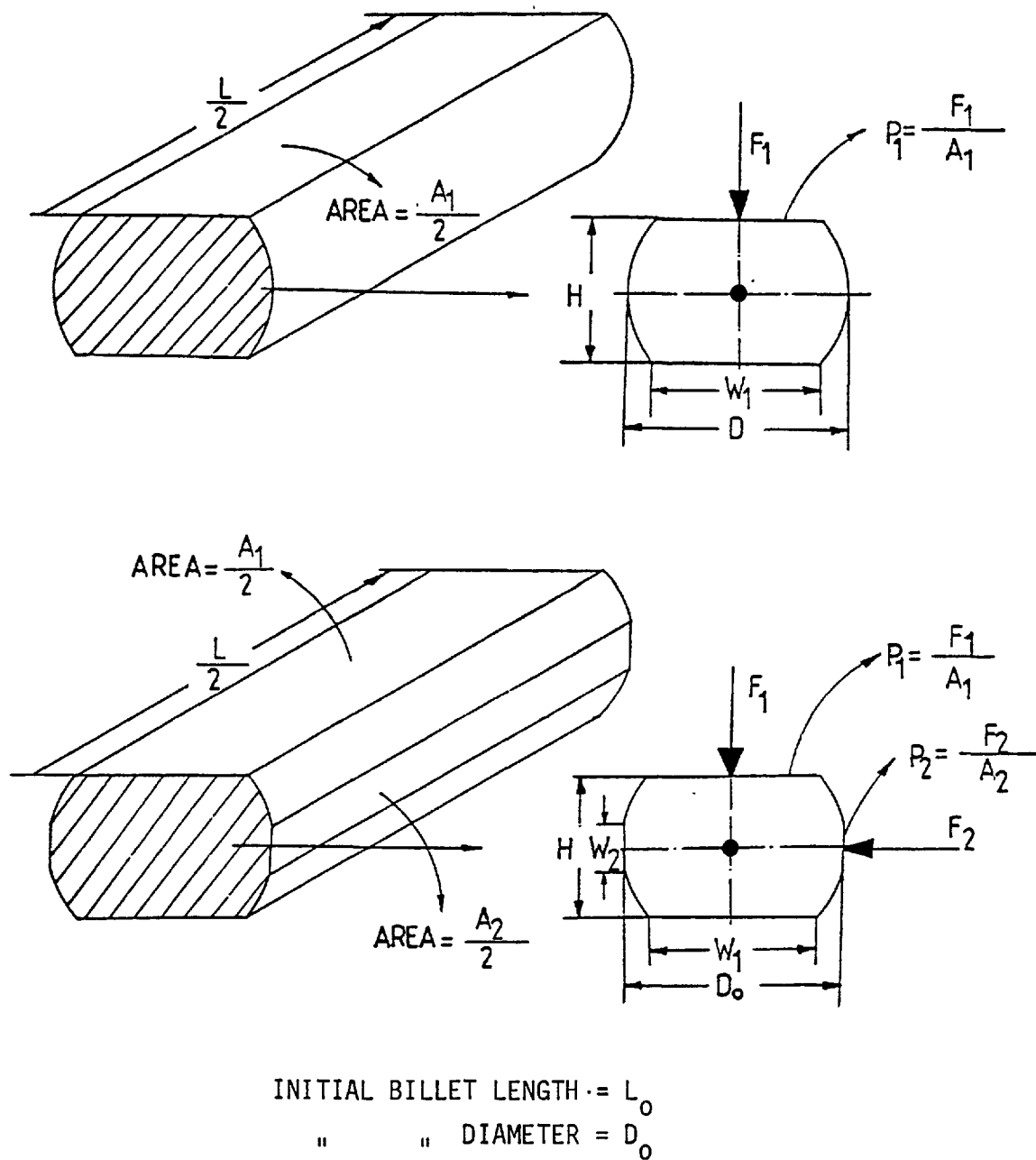


Fig. 4-4. Definition of various parameters in indentation of round billets with and without side restraint.

4-  $F_1$  = indenting force applied by the top segment, or vertical indenting force.

5-  $A_1$  = area of contact surface with the top segment.

In the indentation of round billets with side-restrain the parameters measured were as follows:

1-  $H$  = height of billet.

2-  $W_1, W_2$  = widths of contact surfaces with the top and side segments respectively.

3-  $F_1, F_2$  = indenting forces, applied by the top and side segments, or vertical and horizontal indenting forces respectively.

4-  $A_1, A_2$  = areas of contact surfaces with the top and side segments.

It is worth commenting that in theory, for plane strain deformation the parameters  $W_1, W_2, D, F_1$  and  $F_2$  are related linearly to the initial diameter of the billet, and also that the parameters  $F_1$  and  $F_2$  are related linearly to the length of the billet. The parameters used in representing the experimental data were as follows:

1-  $\frac{H_0 - H}{H_0}$  = amount of indentation.

2-  $\frac{W_1}{D_0}, \frac{W_2}{D_0}$  = widths of contact surfaces.

3-  $\frac{D - D_0}{D_0}$  = increase in the billet diameter.

4-  $\frac{F_1}{L_0 \times D_0}, \frac{F_2}{L_0 \times D_0}$  = vertical and horizontal indenting forces.

5-  $P_1 (= \frac{F_1}{A_1}), P_2 (= \frac{F_2}{A_2})$  = mean normal pressures applied by the top and side segments.

#### 4.8 Experimental procedure

An incremental procedure was employed for the indentation of the billets. Incremental loading was continued until a desirable amount of indentation was obtained or in some cases until the load required exceeded the capacity of the press.

For indentation of billets without side-restraint the side-segments from the die-set were removed. The experimental procedure was as follows (see Fig. 4-2 as required):

The billet was first symmetrically placed on the lower segment of the chamber. After applying an increment of load, the billet was unloaded and removed from the chamber and the required measurements were taken. The billet was then replaced in the die-set and then re-set for the next increment of load.

For indentation of billets with side-restraint the side-segments were inserted in the die-set. The experimental procedure was as follows:

The billet was placed on the lower segment of the chamber as before. The rubber pads, which were supporting segments C and D, were adjusted in height in order to level the axis of symmetry of the billet and those of the load-cells G and H. This was to eliminate any eccentric forces which would be applied to segments C and D. If these were to occur the bending moments induced could drastically affect the load-cell readings. Nuts I and J were then uniformly tightened until segments C and D embraced the billet without any slackness. The billet was then incrementally indented as before. At intervals, however, the billet was removed from the chamber by first retracting segments A and B. The residual forces applied to segments C and D were then recorded and finally by slackening nuts I and J the billet was removed

from the chamber for the required measurements. At the beginning of the next increment of load the reverse procedure was followed. Initially the billet was symmetrically placed between segments C and D and nuts I and J were tightened until reaching the same level of residual forces recorded by load-cells G and H. Finally, the billet which was clamped between segments C and D was symmetrically placed in the die-set between segments A and B.







The experiments were conducted on both dry and lubricated billets. Dry billets were prepared by cleaning with trichloroethylene, and leaving to dry completely before starting the experiments. Lubricated billets were prepared by coating the specimens with a thin film of molybdenum disulphide. During the course of the experiments no additional lubrication was provided.

#### 4.9 Experimental results and discussions

The results obtained from the indentation of round billets without and with side-restraint are shown in Figs. 4-6 to 4-13. The symbols used and the specification of the billets are shown in Fig. 4-5. In the results shown, the main parameter against which the other parameters were plotted was the amount of indentation,  $(H_0 - H)/H_0$ .

In Figs 4-6-A to 4-6-D the results obtained for the case of indentation of round billets without side-restraint are shown. The relationships between contact width  $W_1/D_0$  and the amount of indentation  $(H_0 - H)/H_0$  and also between  $(D - D_0)/D_0$  and  $(H_0 - H)/H_0$  are shown in Figs. 4-6-A and 4-6-B respectively. For billets of different sizes, the values of both  $W_1/D_0$  and  $(D - D_0)/D_0$  lie on unique curves when plotted against  $(H_0 - H)/H_0$ , as shown in Figs 4-6-A and 4-6-B (dotted lines). From the uniqueness of these curves it is concluded that these parameters are both

BILLETS SPECIFICATIONS

	$L_0$ (mm)	$D_0$ (mm) {in}
	- - - - - 130 - - - - -	- - - - - 38 {1.5}
	- - - - - 130 - - - - -	- - - - - 51 {2.0}
	- - - - - 130 - - - - -	- - - - - 64 {2.5}
	- - - - - 190 - - - - -	- - - - - 38 {1.5}
	- - - - - 190 - - - - -	- - - - - 51 {2.0}
	- - - - - 190 - - - - -	- - - - - 64 {2.5}

PUNCH LENGTH = 150 mm

IN THE CALCULATION OF  $\frac{F_0}{D_0 \times L_0}$  IF  $L_0 >$  PUNCH LENGTH, THE PUNCH LENGTH WAS INSERTED.

Fig. 4-5. Specifications of the billets used for experiments.

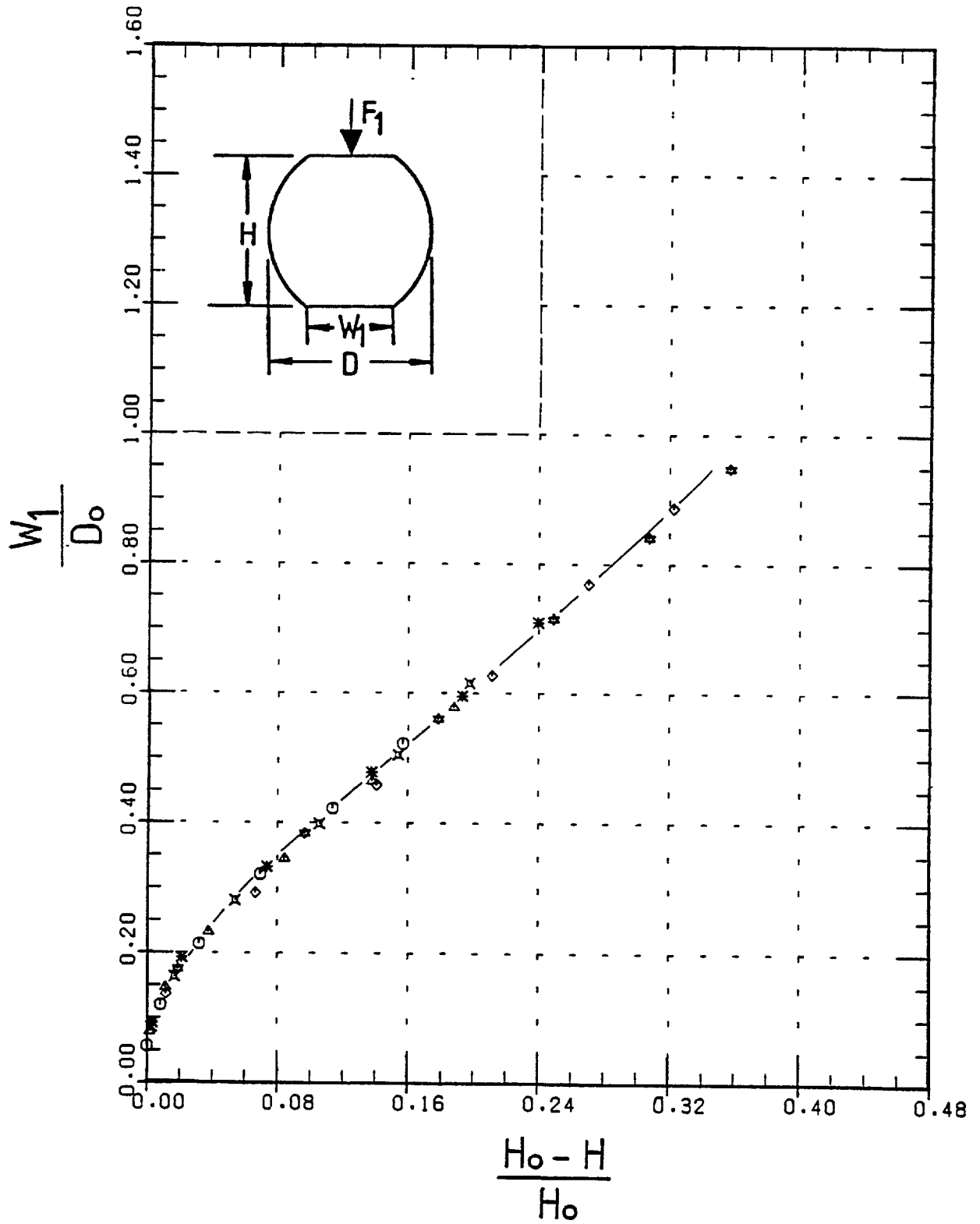


Fig. 4-6-A. Variation of contact width ' $W_1$ ' with height ' $H$ ' for commercially pure aluminium under dry condition.

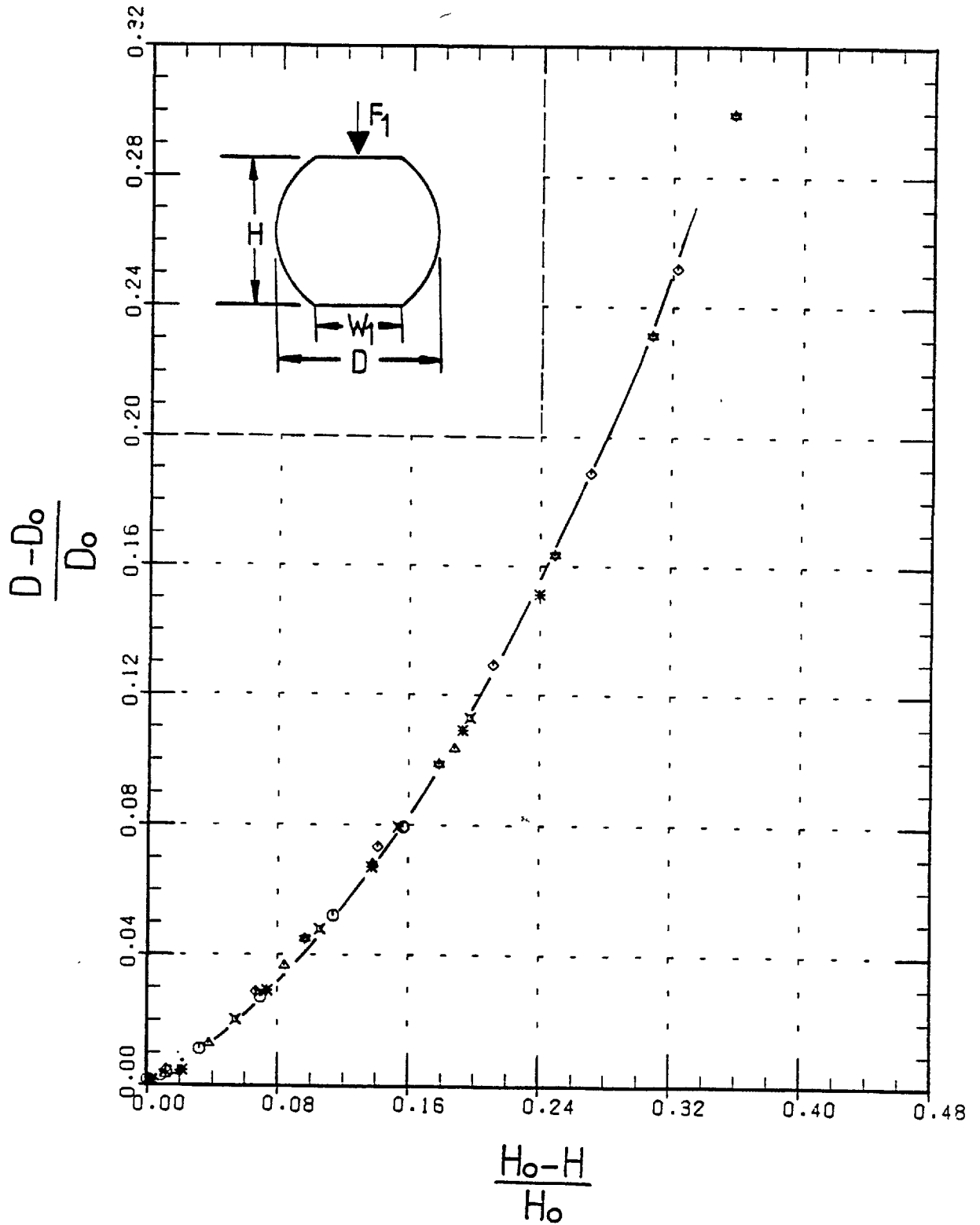


Fig. 4-6-B. Variation of diameter 'D' with height 'H' for commercially pure aluminium under dry condition.

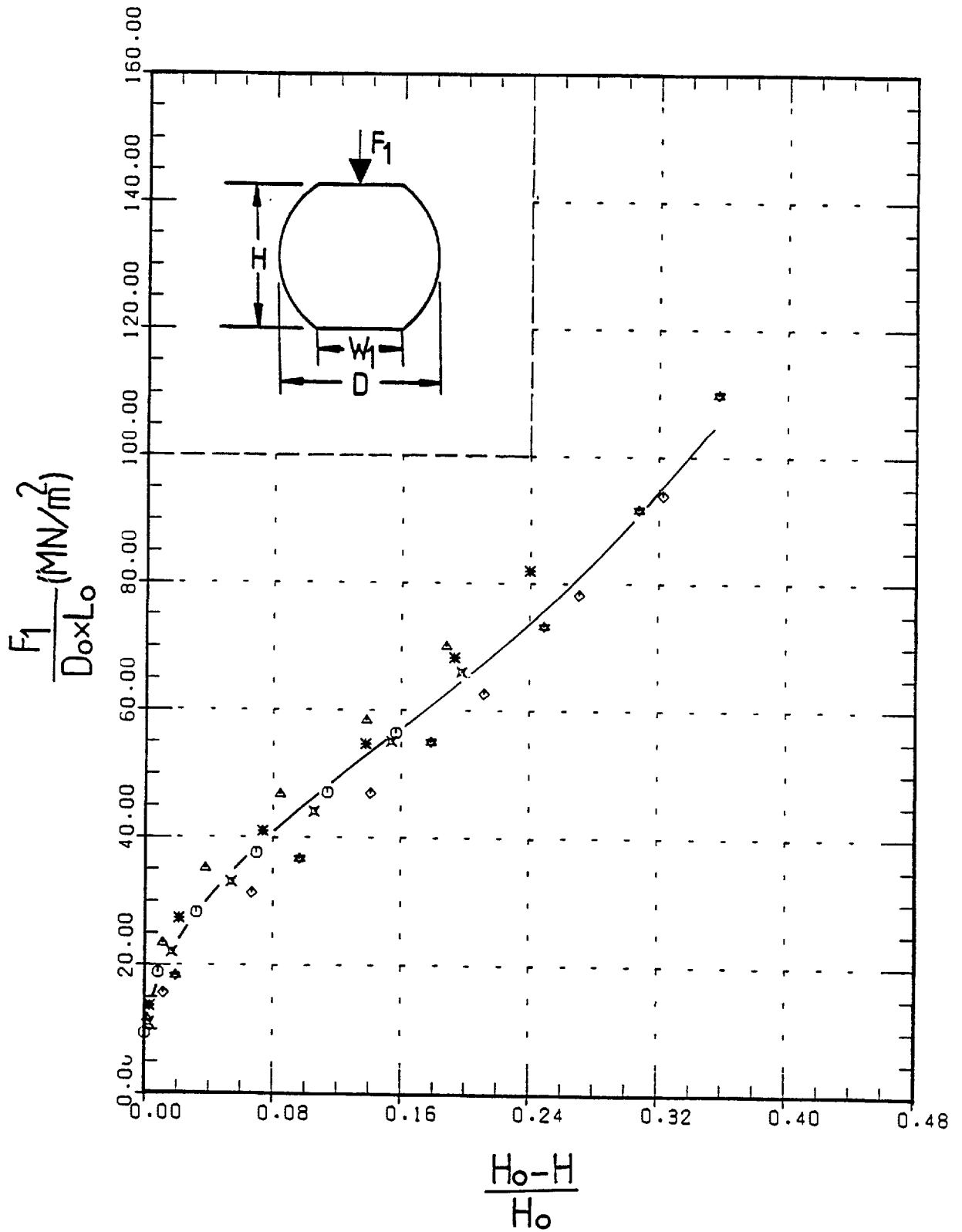


Fig. 4-6-C. Variation of indeting force ' $F_1$ ' with height ' $H$ ' for commercially pure aluminium under dry condition.



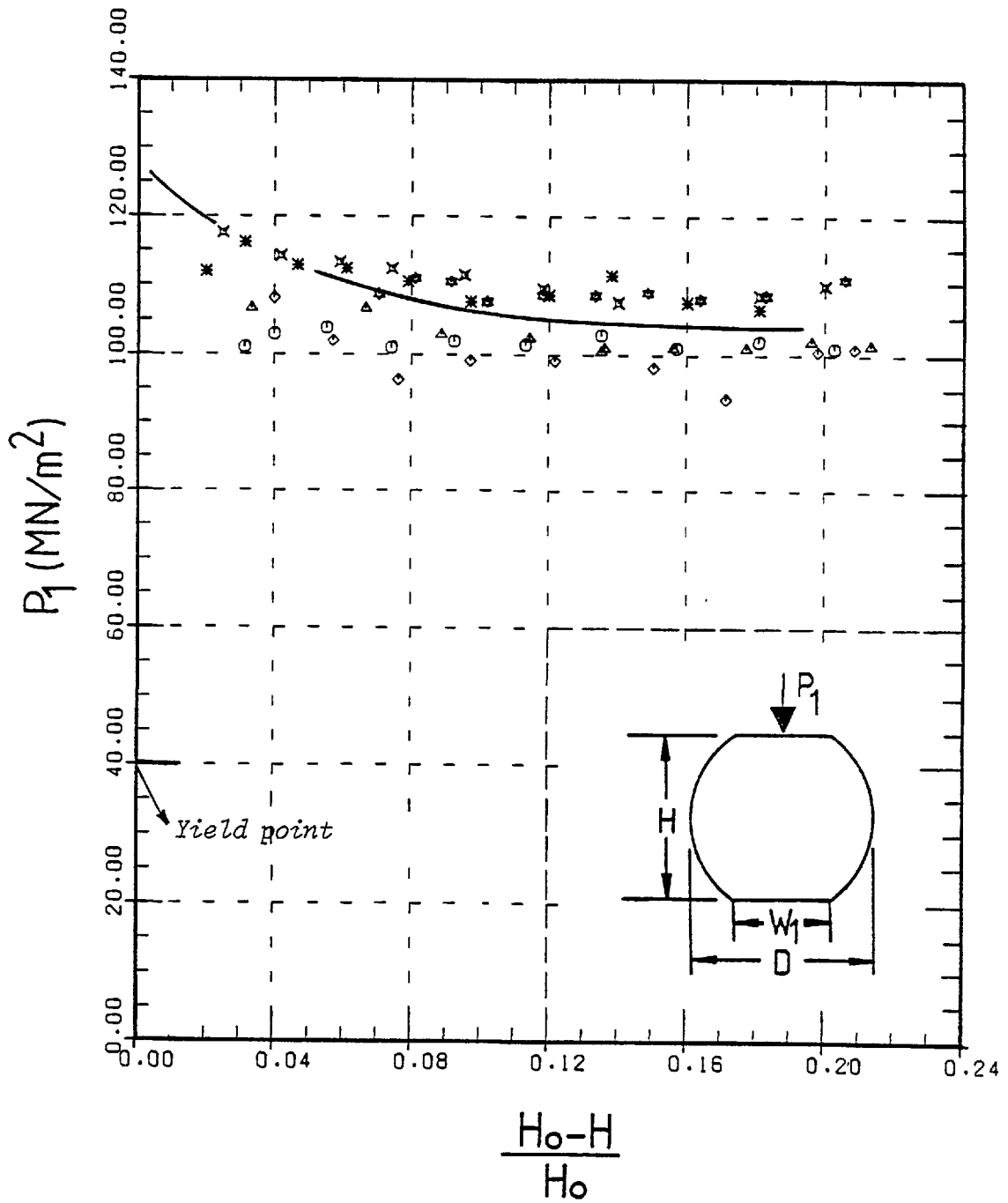


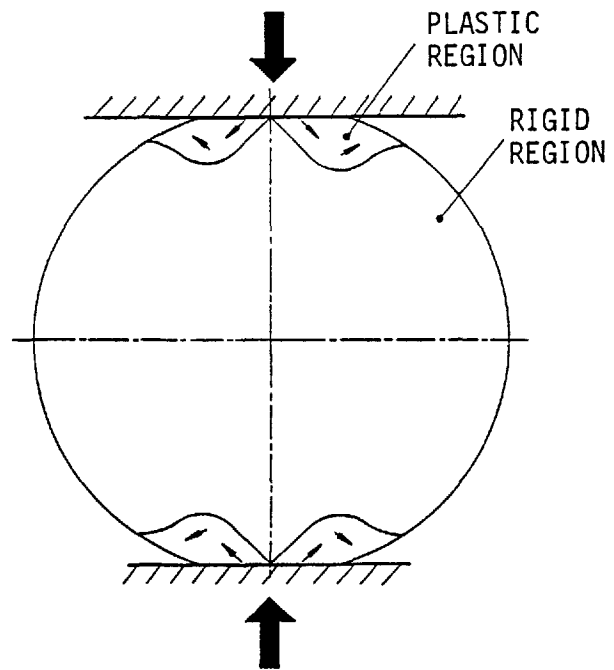
Fig. 4-6-D. Variation of mean normal pressure ' $P_1$ ' with height ' $H$ ' for commercially pure aluminium under dry condition.

related linearly to the initial diameter of the billets. This is consistent with the theoretical requirement for plane strain conditions. Furthermore it is also concluded that during the course of deformation the central region of the billet length was subject to conditions of plane strain.

By reference to the propagation of plastic deformation, as described in (57), it is possible to explain the behaviour of the parameters  $W_1/D_0$  and  $(D-D_0)/D_0$ . When the amount of indentation is sufficiently small, plastic deformation occurs most intensely in the proximity of the segments, as shown in the illustration below (this type of deformation is usually

referred to as mode I).

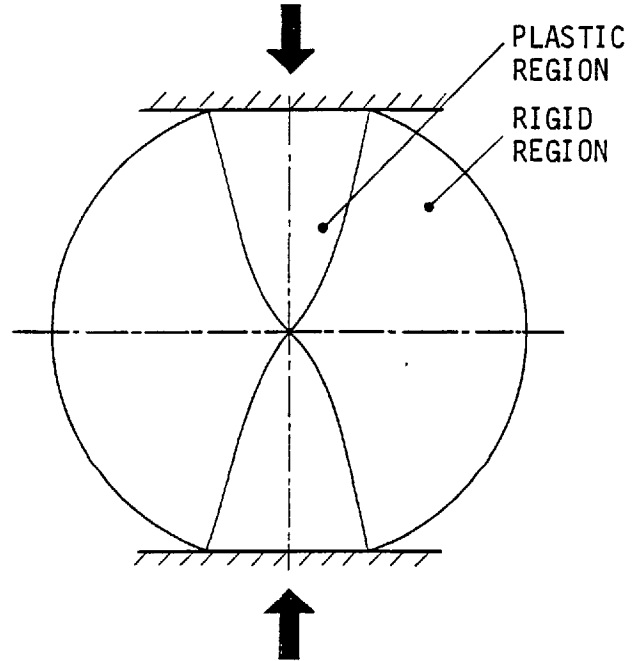
As illustrated, in this mode of deformation a portion of the free-surface is pushed out and hence accelerates contact between the billet and the segment-surface. Also, since the free-surface is tangential to the segment-surface, the



rate at which it makes contact with the latter is a maximum. This, together with the above fact accounts for the initial sudden rise in the curve shown in Fig. 4-6-A. Since during this period of indentation the diameter of the billet is subject to hardly any plastic deformation it sustains negligible deformation (as shown in Fig. 4-6-B). When the

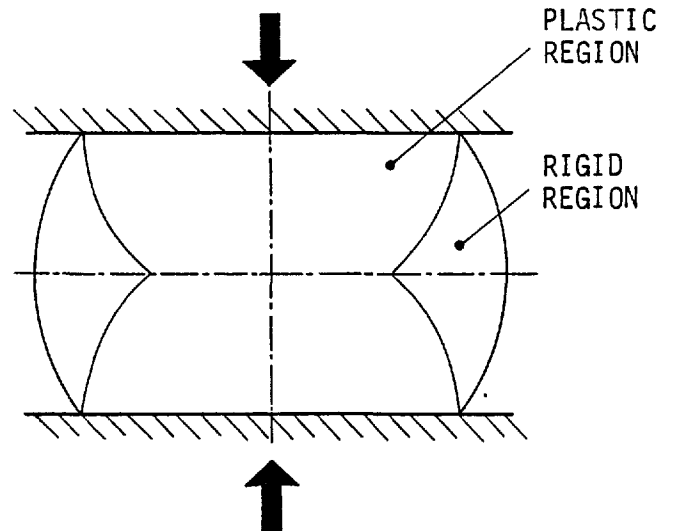
amount of indentation is increased beyond a critical value, a plastic region, as shown in the illustration below, develops in the material between the upper and lower segments (mode II deformation).

As shown, in this mode of deformation the sides of the billet move apart as rigid masses. During this period of indentation the contact width ' $W_1$ ' increases almost at a constant rate, whilst the rate of increase of diameter ' $D$ ' accelerates. When the amount



of indentation is increased beyond the critical value for which  $W_1 \geq H$ , the plastic deformation extends to the billet-sides as shown in the illustration below (mode III).

During this mode of deformation the contact width ' $W_1$ ' and diameter ' $D$ ' begin to increase rapidly. Clearly, when the height of the billet has been greatly decreased the contact width ' $W_1$ ' and diameter ' $D$ ' will increase drastically since any further decrease



in height will cause a large volume of material to be displaced outwards. The contact width ' $W_1$ ' and diameter ' $D$ ' will tend to infinity as the height of the billet is reduced to negligible values.

The relationship between the indenting force  $F_1/(L_0 \times D_0)$  and the amount of indentation  $(H_0 - H)/H_0$  is shown in Fig. 4-6-C. As it can be seen the results are to some extent dependent on the initial size of the billet. The dependence of the results on the billet size is due to the non-uniformity of deformation along the length of the billet, particularly near the ends. It is worth mentioning that billets of different diameters, which were cut from standard rods of different sizes, were found, from a hardness survey, to have slightly different mechanical properties. This explains the greater dependence of the results on the billet initial diameter rather than the billet initial length.

The indenting force curves, shown in Fig. 4-6-C, vary approximately in the same manner as the contact width curves shown in Fig. 4-6-A. The rate at which the indenting forces increase first rises rapidly, then remains constant, and finally increases considerably. These various rates come into effect as different modes of plastic deformation described above are developed in the billet cross-section.

The relationship between the normal pressure ' $P_1$ ' and the amount of indentation  $(H_0 - H)/H_0$  is shown in Fig. 4-6-D. As it can be seen, the results are markedly dependent on the billet size, and hence do not precisely represent the variation of pressure during plane strain indentation. Under conditions of plane strain, the variation of pressure will be represented by that obtained from the billet of greatest length and smallest diameter, since for this case deformation was least influenced by the end-effect. As it can be seen from Fig. 4-6-D, the pressure at first decreases, then remains constant, and finally increases. Similarly these various intervals correspond to

the regions when the various modes of deformation take effect.

The results obtained from the indentation of lubricated aluminium billets and dry lead billets without side-restraint are shown in Figs. 4-7 (A to C) and 4-8 (A to D) respectively. These show the same trend as those obtained from the indentation of dry aluminium billets shown in Fig. 4-6 (A to D) above. As can be seen, the results obtained from the indentation of dry lead billets are more scattered than the corresponding ones obtained from the indentation of dry aluminium billets. This can be attributed to the metallurgical defects developed during the casting of the lead billets. Examination of the indented lead billets revealed defects such as internal voids and inclusion of foreign metals.

The best curves fitted to those shown in Figs. 4-6, 4-7 and 4-8 are shown in Figs. 4-9 (A to C) for comparison. These results merely represent the trend of those narrow bands within which the previously presented curves fall and hence, for example, are not representative of any particular billet size. The relationship between the contact width  $W_1/D_0$  and the amount of indentation  $(H_0-H)/H_0$  is shown in Fig. 4-9-A. As it can be seen, the contact width for the case of lubricated billets falls slightly below that for the case of dry billets (in contrast to the theoretical prediction which will be presented in the next chapter). This erroneous trend is due to the violation of conditions of plane strain for the case of indentation of lubricated aluminium billets. Measurement of the longitudinal extension for the two cases of dry and lubricated aluminium billets indicated that the lubricated billets suffered comparatively higher axial extension. The contact widths  $W_1$  for the case of lead billets compared to those of aluminium billets with and without lubricant can be seen to show some discrepancy, as shown in

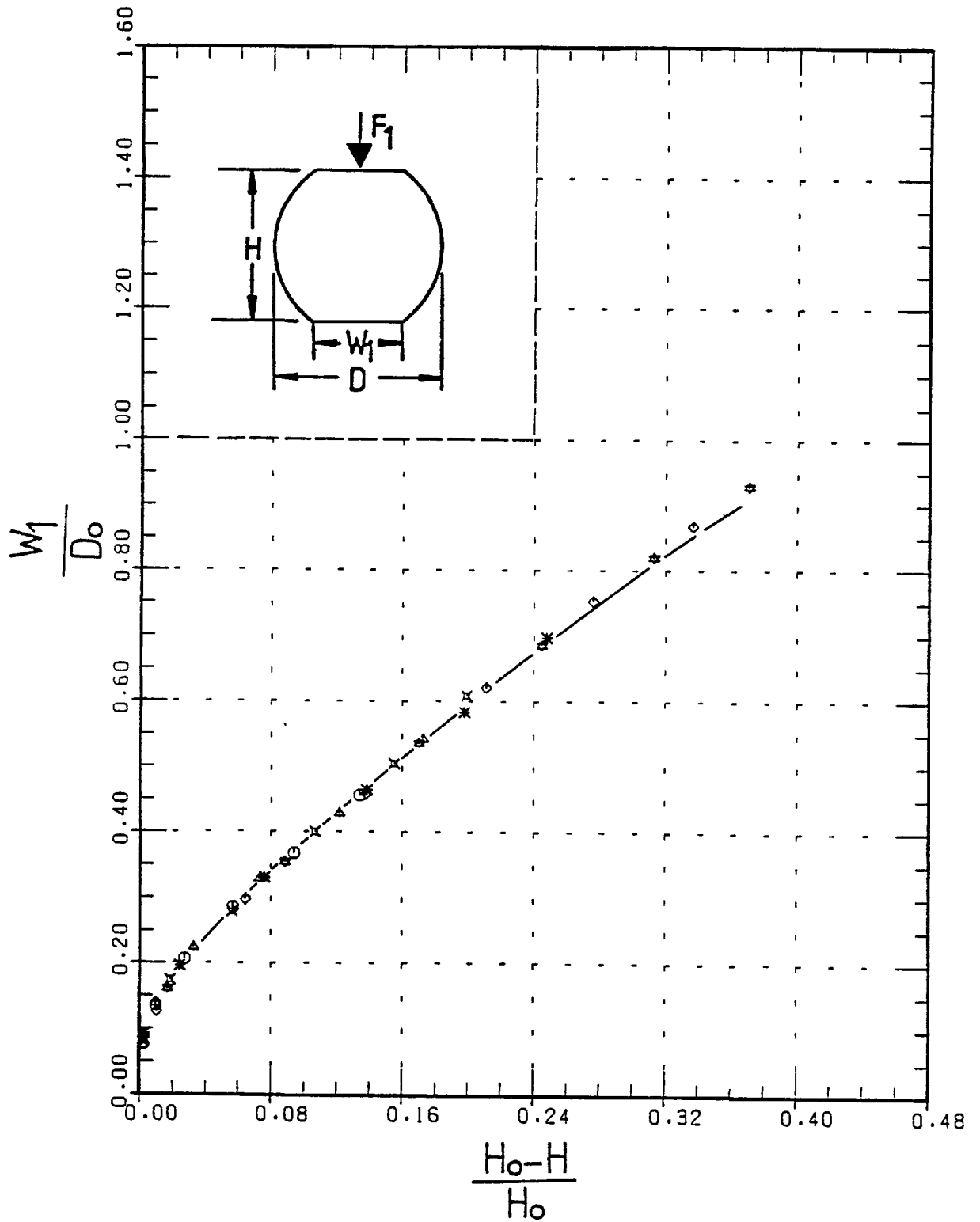


Fig. 4-7-A. Variation of contact width ' $W_1$ ' with height ' $H$ ' for commercially pure aluminium under lubricated condition.

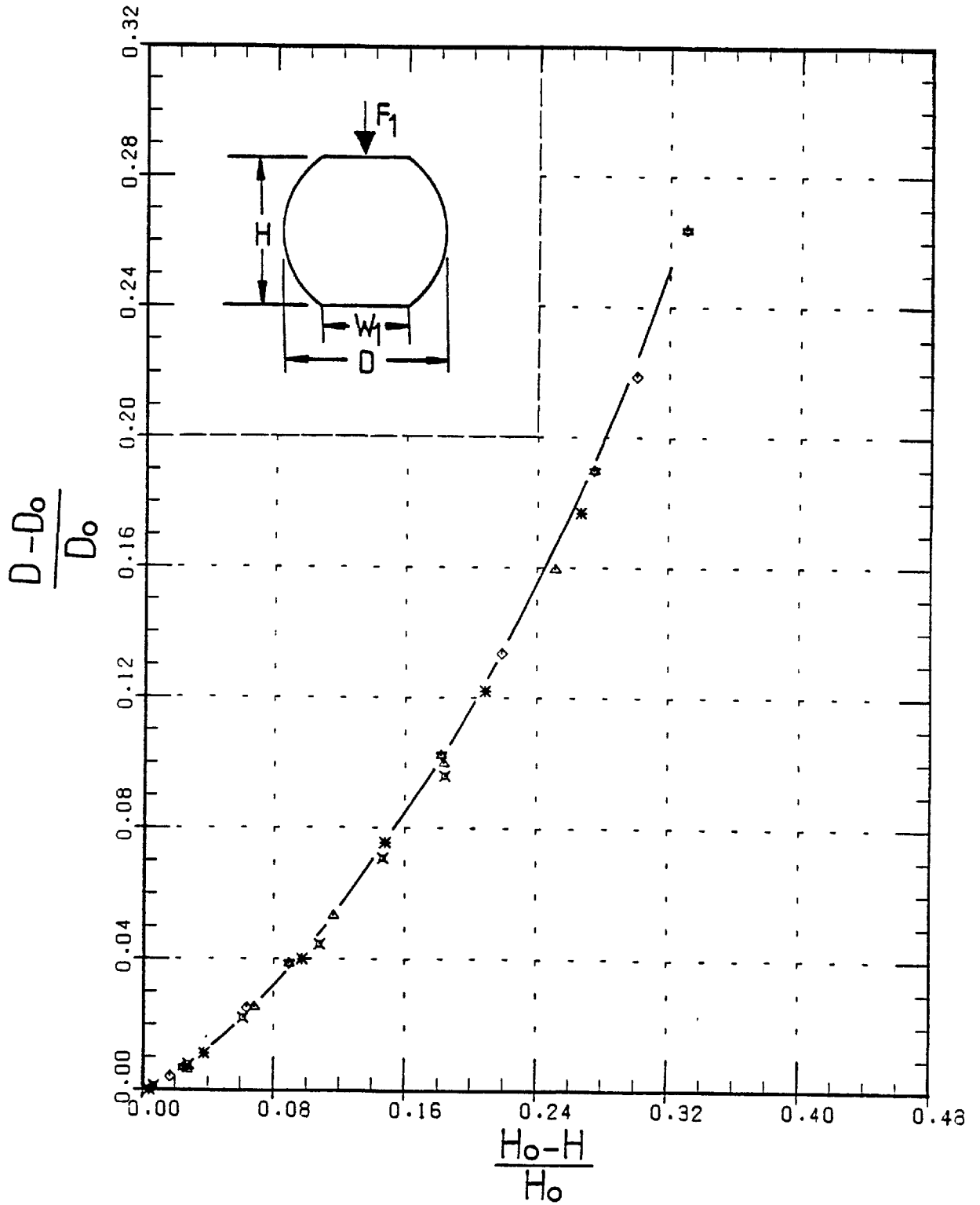


Fig. 4-7-B. Variation of diameter 'D' with height 'H' for commercially pure aluminium under lubricated condition.

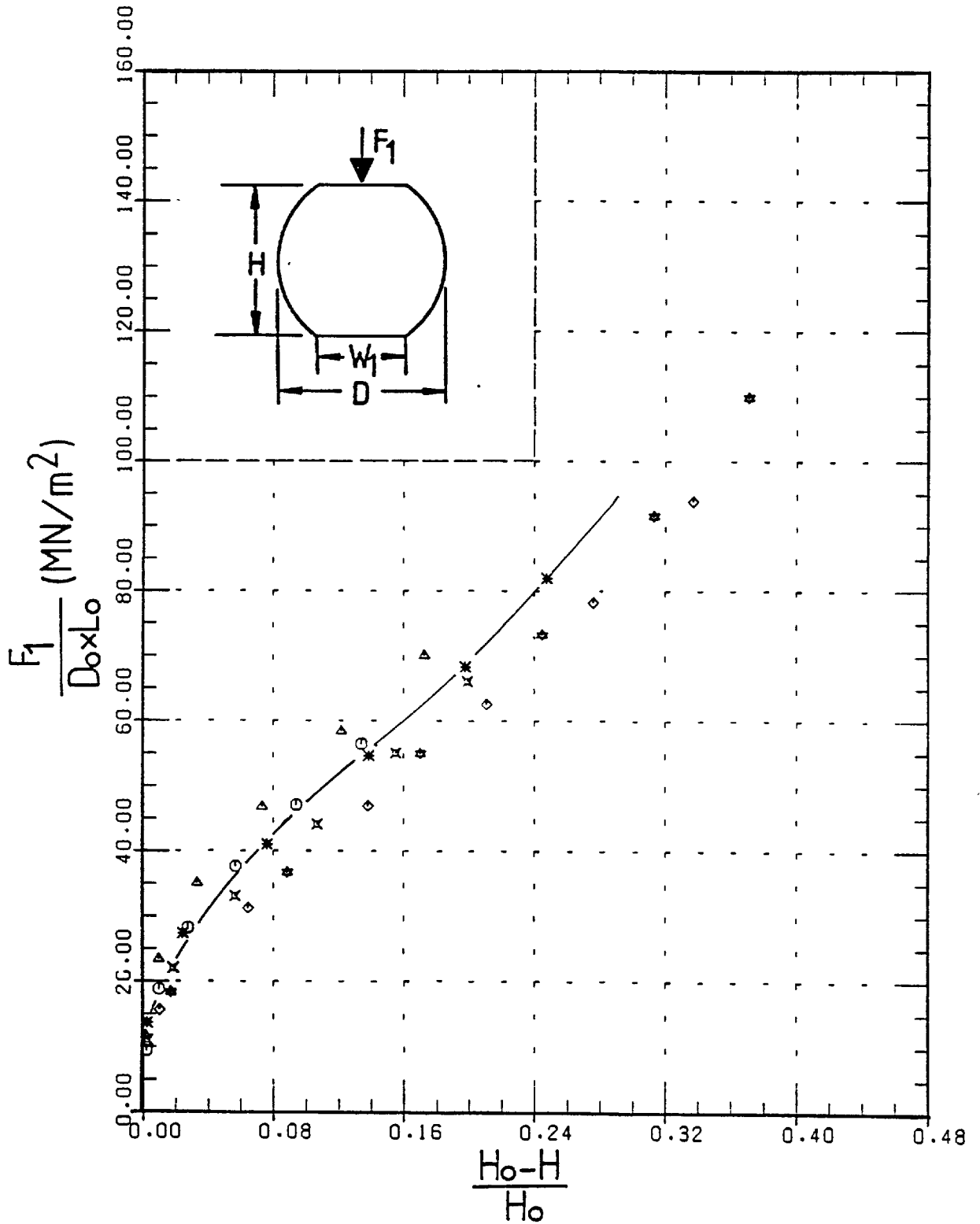


Fig. 4-7-C. Variation of indenting force ' $F_1$ ' with height ' $H$ ' for commercially pure aluminium under lubricated condition.



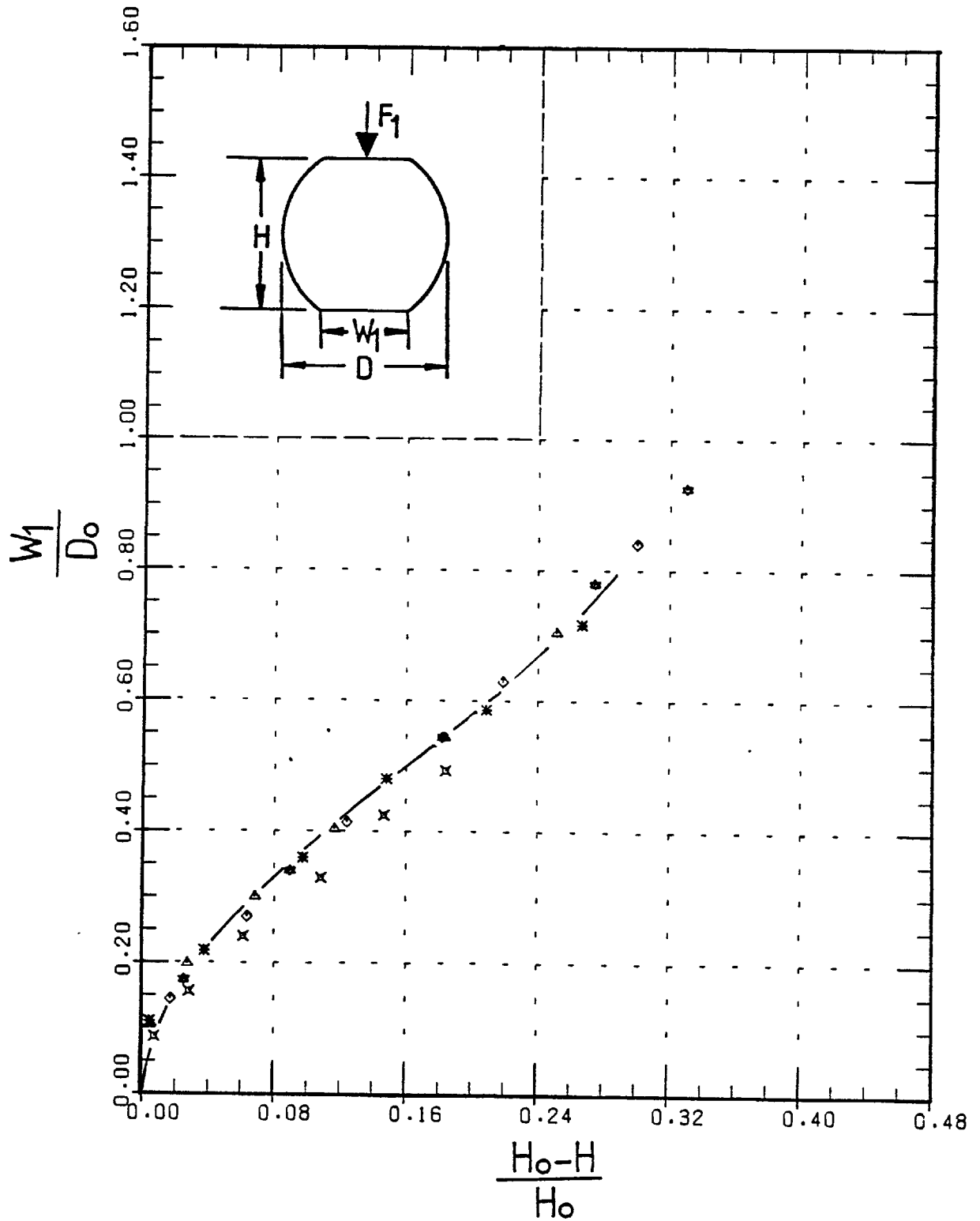


Fig. 4-8-A. Variation of contact width ' $W_1$ ' with height ' $H$ ' for commercially pure lead under dry condition.

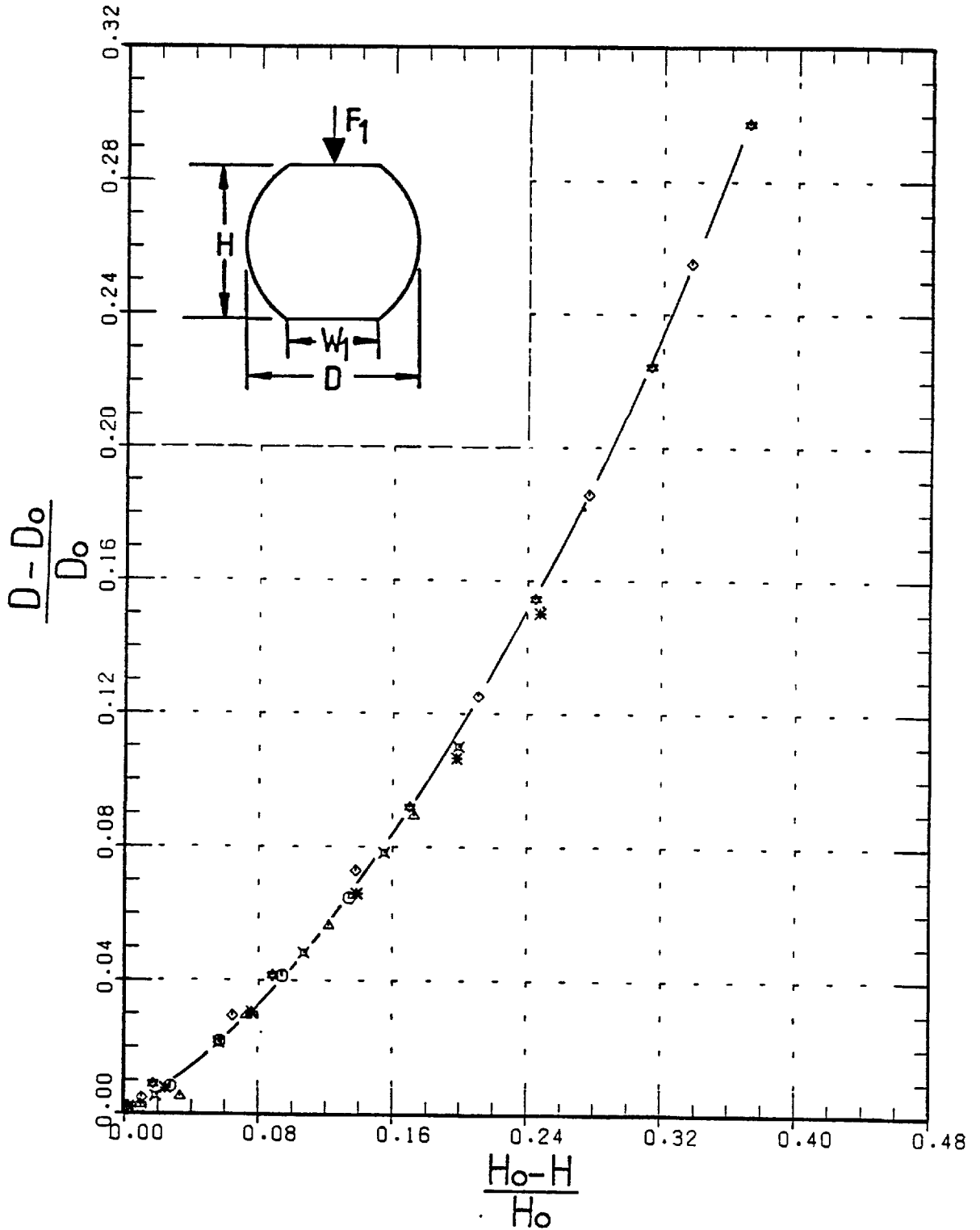


Fig. 4-8-B. Variation of diameter 'D' with height 'H' for commercially pure lead under dry condition.

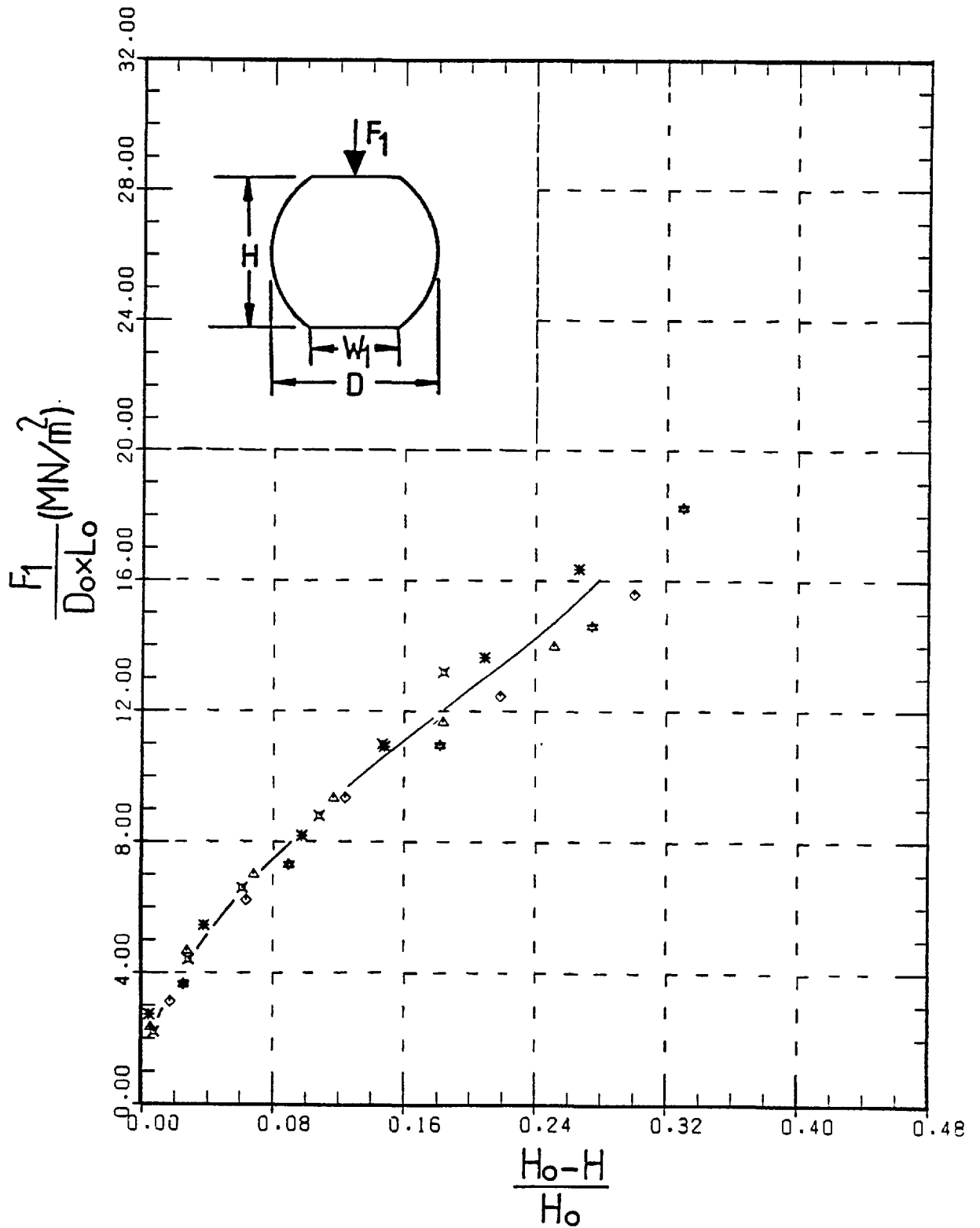


Fig. 4-8-C. Variation of indenting force ' $F_1$ ' with height ' $H$ ' for commercially pure lead under dry condition.

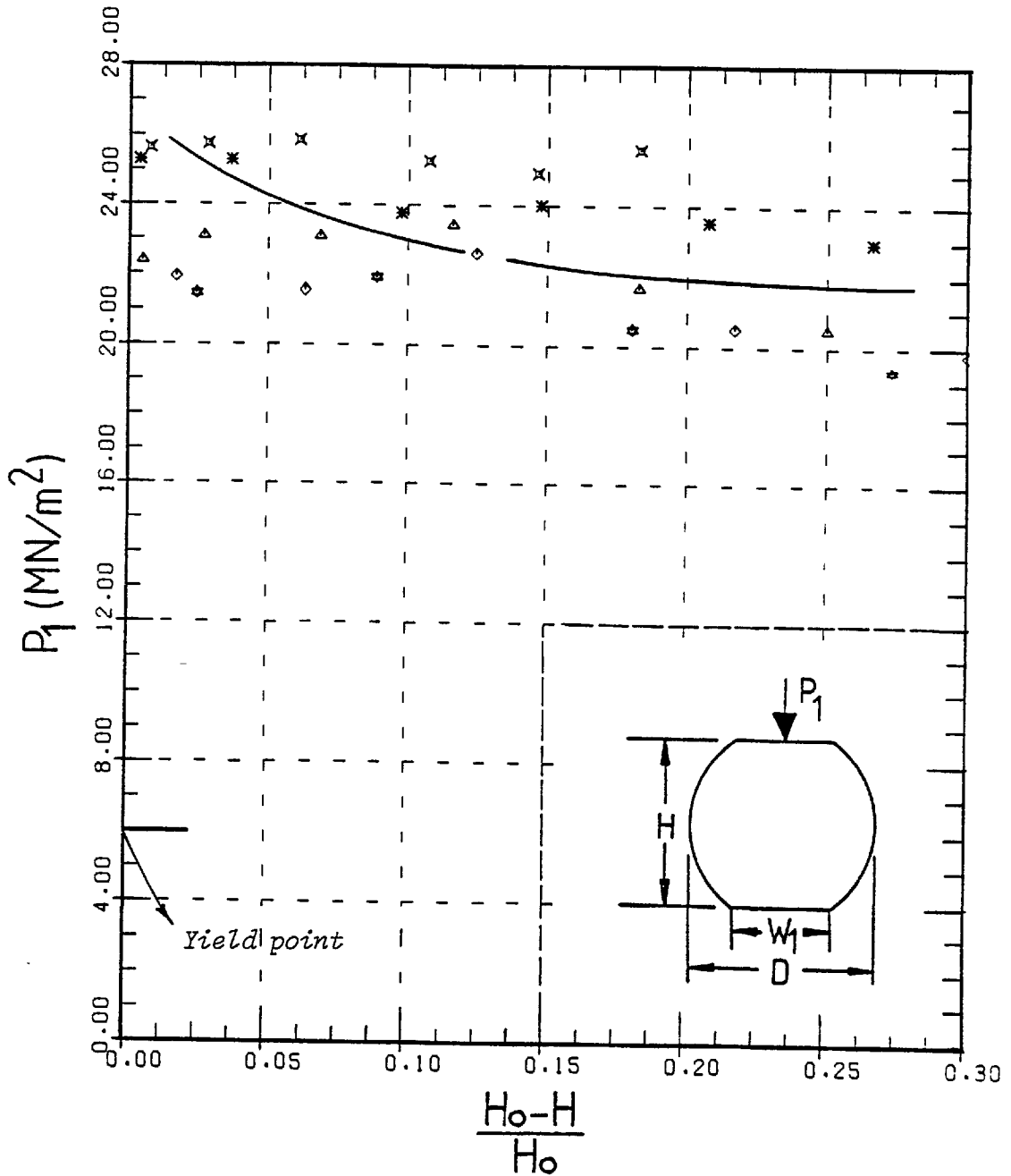


Fig. 4-8-D. Variation of mean normal pressure ' $P_1$ ' with height ' $H$ ' for commercially pure lead under dry condition.

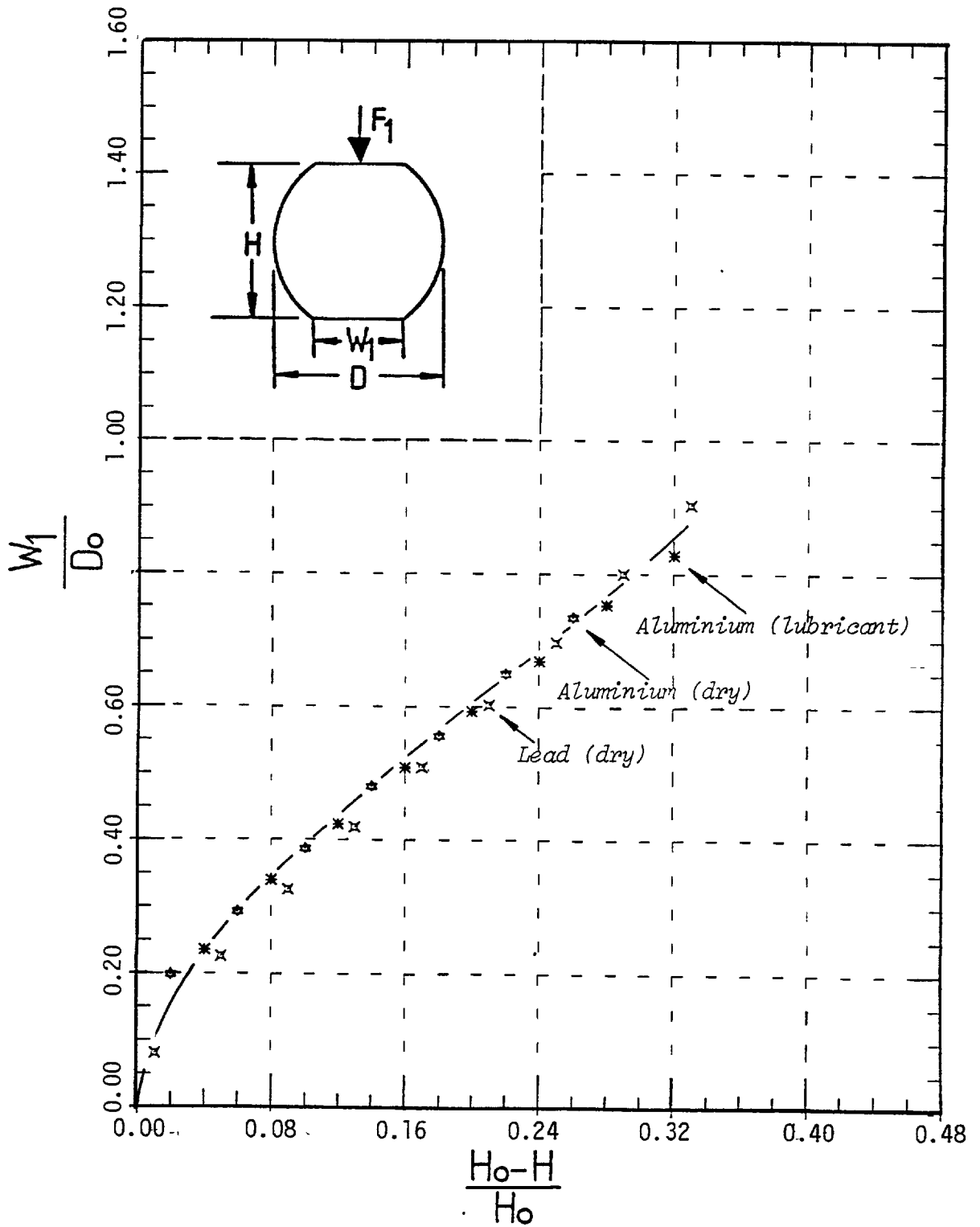


Fig. 4-9-A. Variation of contact width ' $W_1$ ' with height ' $H$ ' for commercially pure aluminium and lead for comparison.

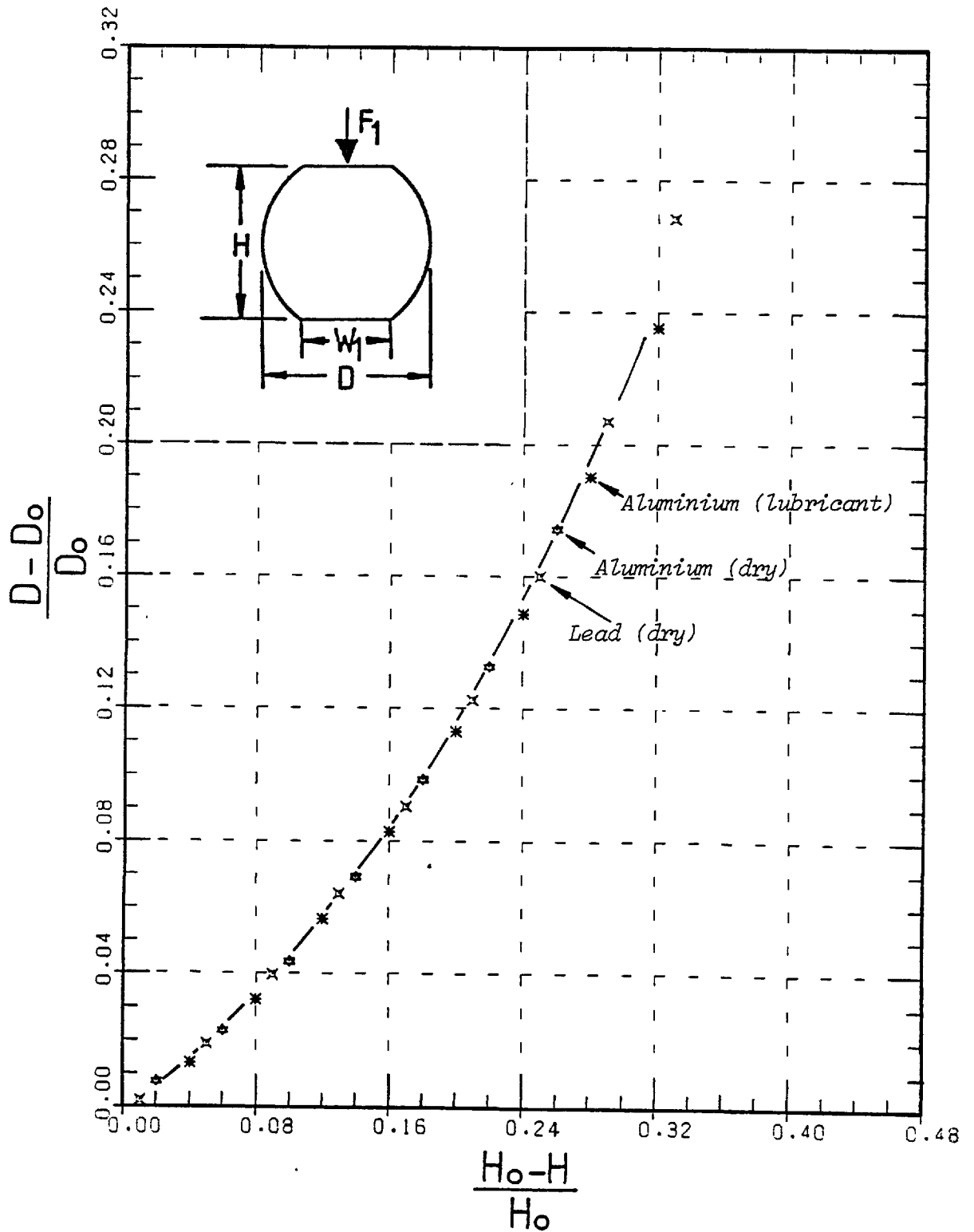


Fig. 4-9-B. Variation of diameter 'D' with height 'H' for commercially pure aluminium and lead for comparison.

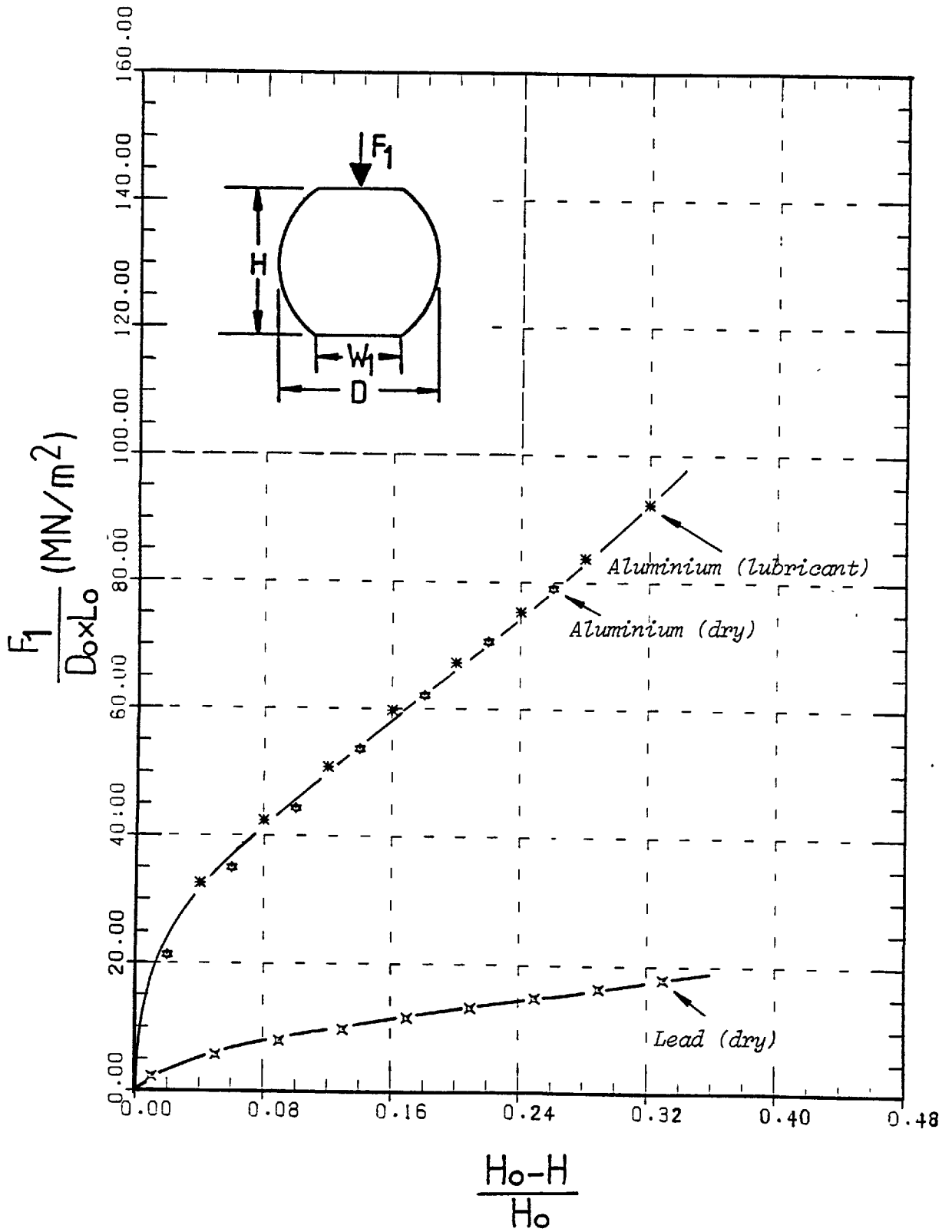


Fig. 4-9-C. Variation of indenting force ' $F_1$ ' with height ' $H$ ' for commercially pure aluminium and lead for comparison.

Fig. 4-9-A. This discrepancy may be attributed to the material properties of the lead and aluminium from which the billets were made. The extension in diameter,  $(D-D_0)/D_0$ , for the cases of dry and lubricated aluminium and also for dry lead billets are observed to be identical.

The relationship between the indenting force  $F_1/(L_0 \times D_0)$  and the amount of indentation is shown in Fig. 4-9-C. The curve for the case of dry aluminium slightly falls below that for lubricated aluminium (in contrast to the theoretical prediction which will be presented in the next chapter). As was previously described, this erroneous trend is due to the violation of conditions of plane strain whilst indenting the lubricated aluminium billets.

Figs. 4-10 (A to F) show the results for the case of indentation of dry aluminium billets with side-restraint. Despite the previous cases (in which the deformation was interrupted when the force required for indentation exceeded the press capacity) here the process was interrupted when it was observed that conditions of plane strain were drastically violated as indicated by excessive axial extension of the billet. The degree of violation of conditions of plane strain can be appreciated if the limiting values of the parameters  $H$ ,  $W_1$ ,  $W_2$ ,  $F_1$  and  $F_2$  (for which the billet is deformed into a rectangle) under plane strain conditions are obtained and compared with those of experiments. If the volume constancy assumption is adopted, then the limiting values of  $H$ ,  $W_1$  and  $W_2$  can be obtained by equating the cross-sectional area of the billet to that of the resulting rectangle (see the illustration below). Thus,

$$\frac{\pi}{4} D_0^2 = D_0 H \quad \therefore \quad H = \frac{\pi}{4} D_0$$



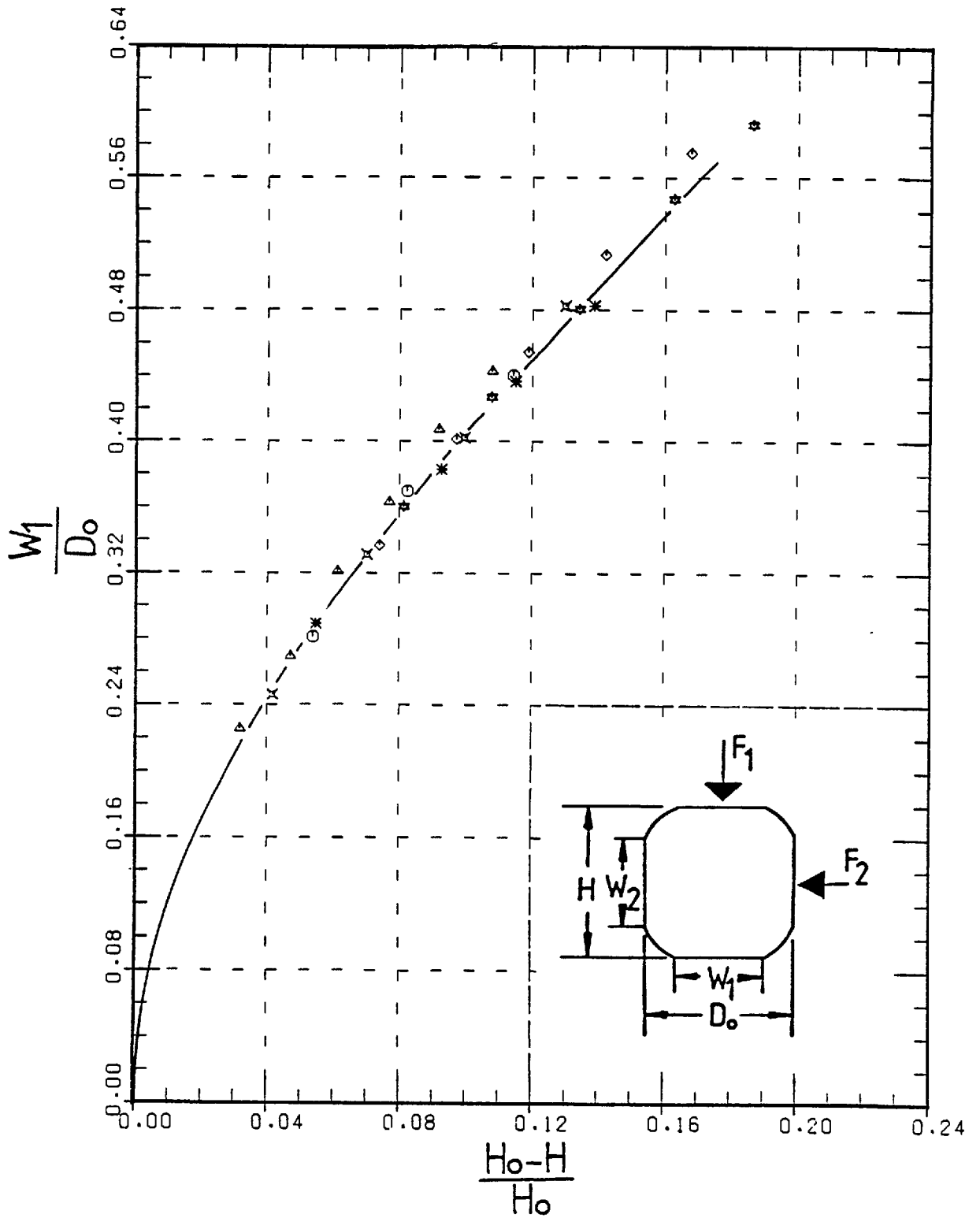


Fig. 4-10-A. Variation of contact width ' $W_1$ ' with height ' $H$ ' for commercially pure aluminium under dry condition.

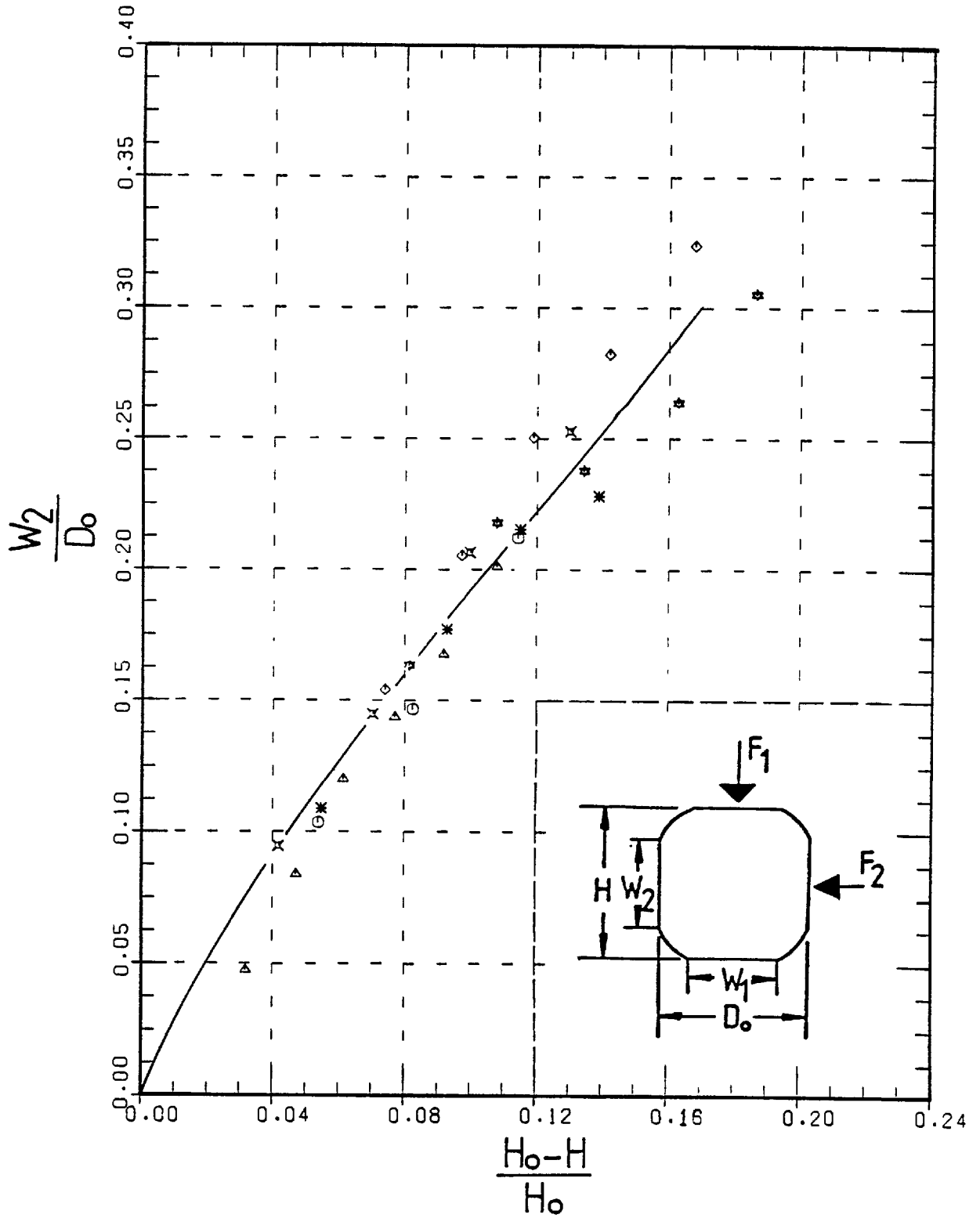


Fig. 4-10.B. Variation of contact width ' $W_2$ ' with height ' $H$ ' for commercially pure aluminium under dry condition.

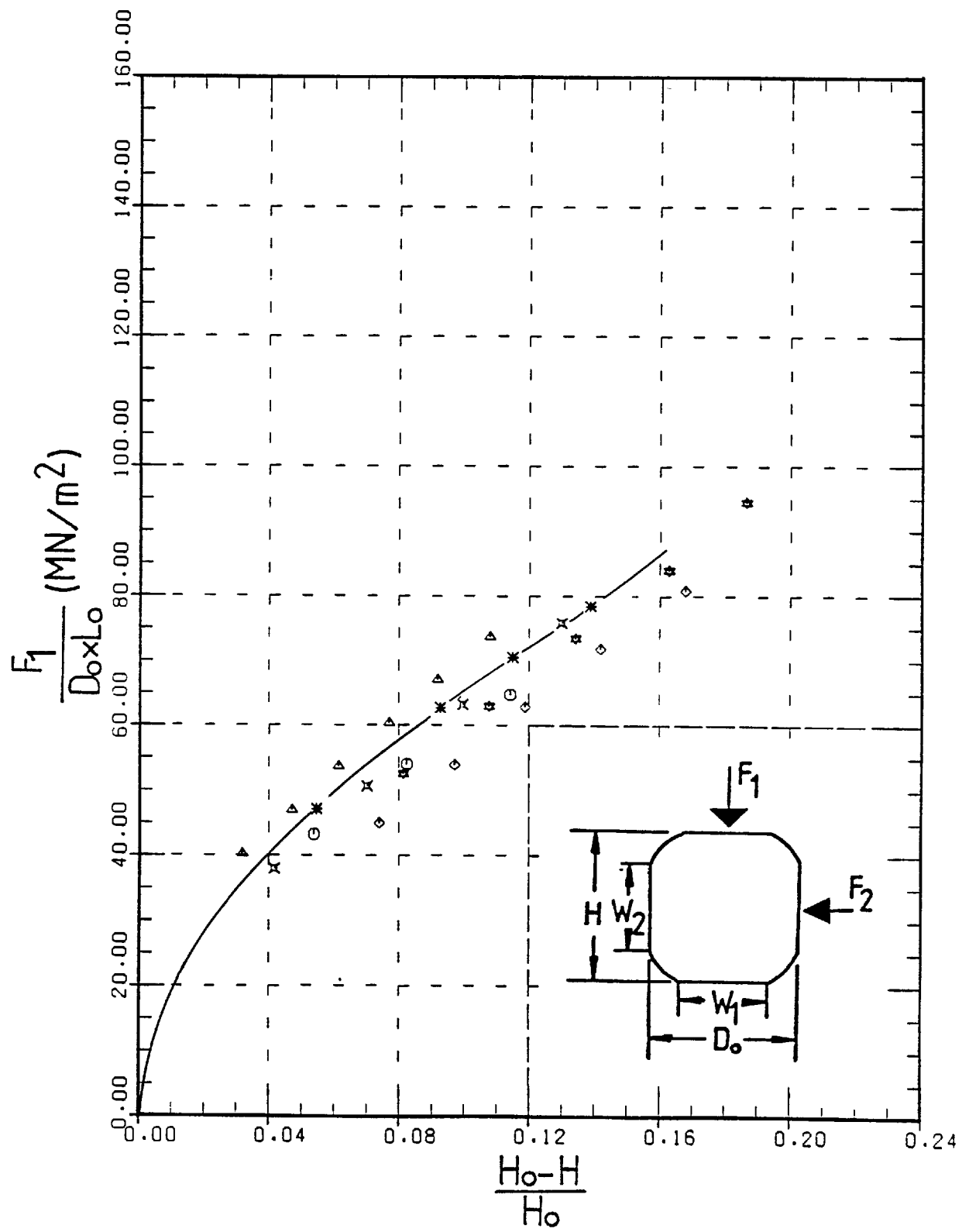


Fig. 4-10-C. Variation of indenting force 'F<sub>1</sub>' with height 'H' for commercially pure aluminium under dry condition.

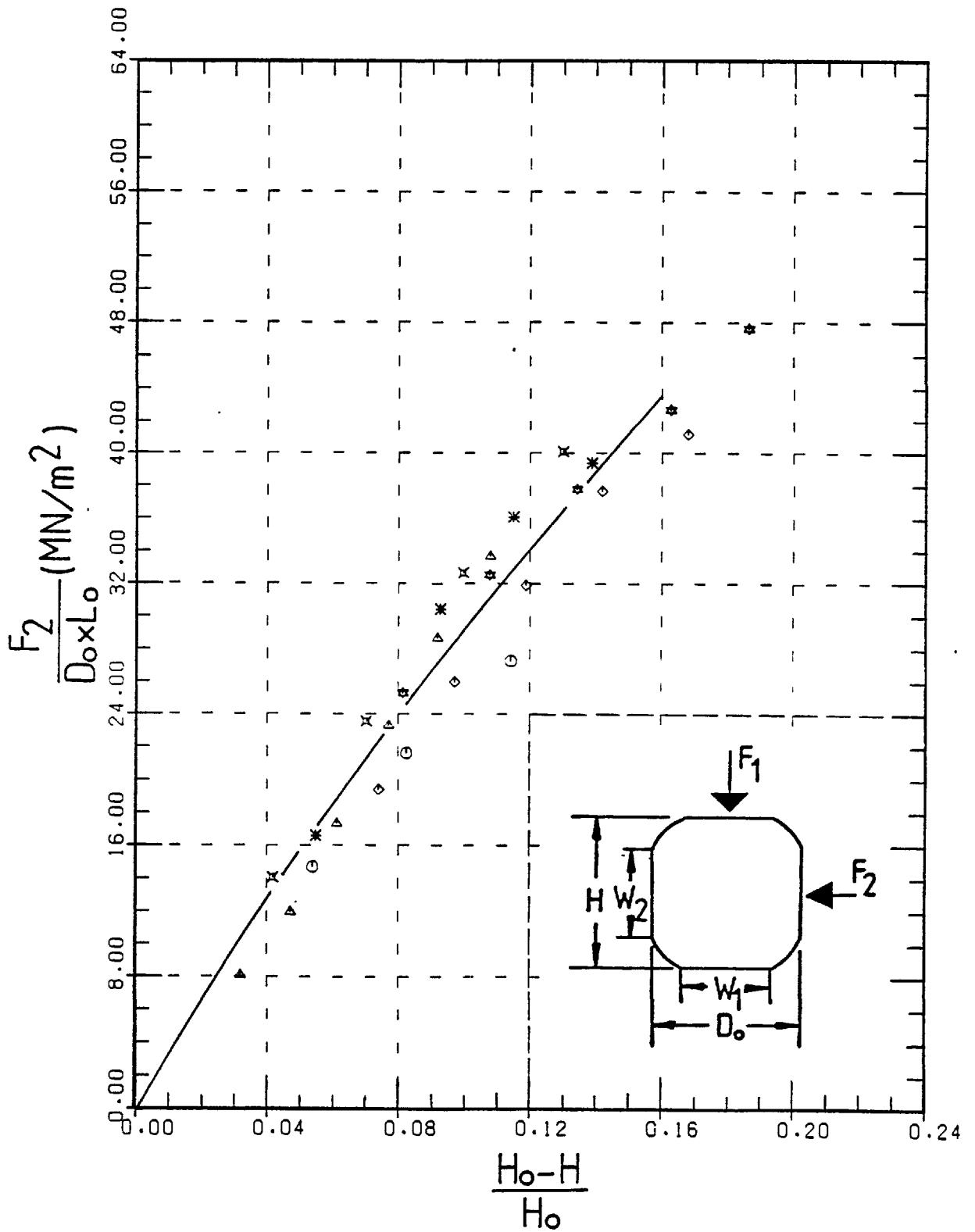


Fig. 4-10-D. Variation of indenting force ' $F_2$ ' with height ' $H$ ' for commercially pure aluminium under dry condition.

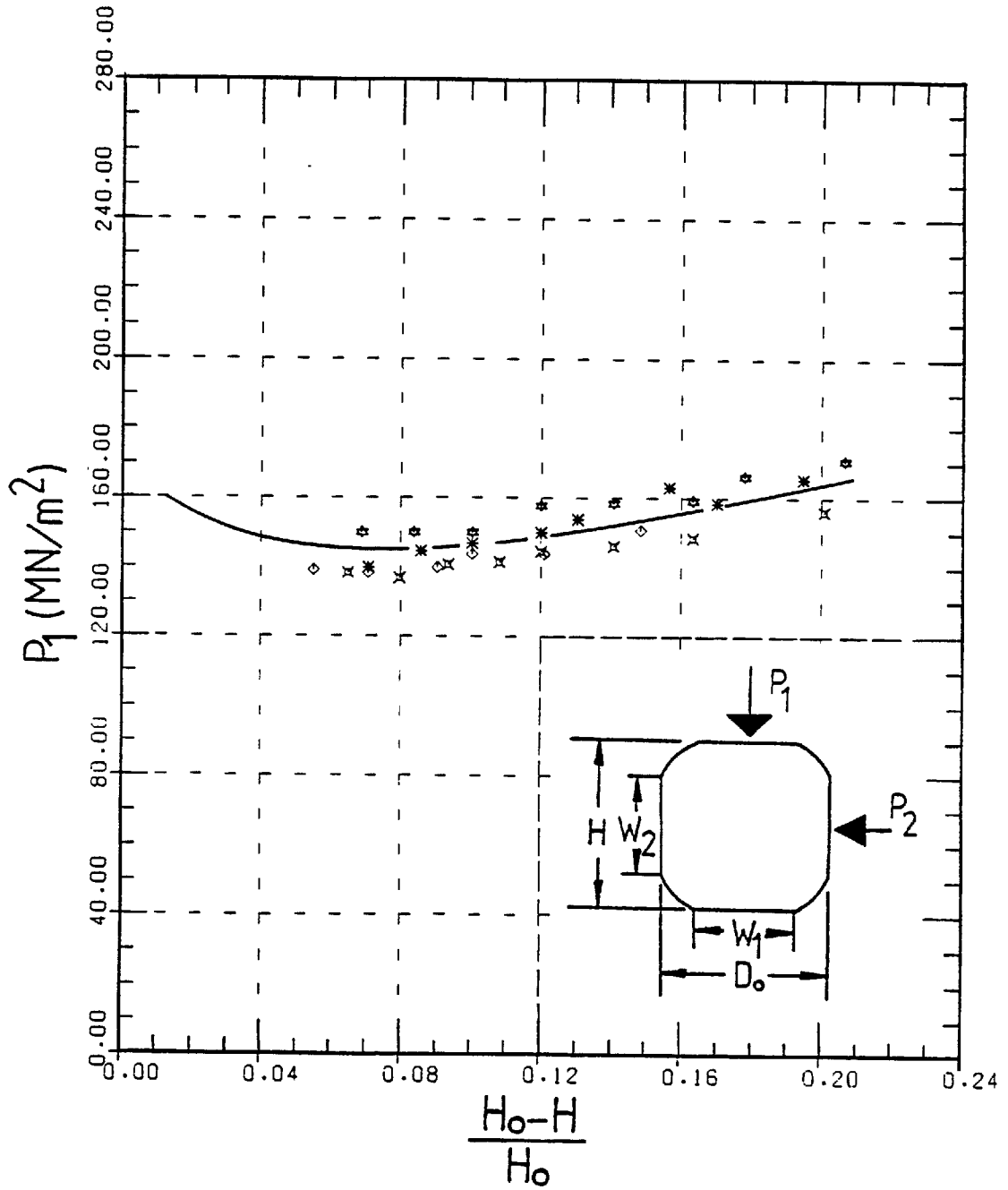


Fig. 4-10-E. Variation of mean normal pressure ' $P_1$ ' with height ' $H$ ' for commercially pure aluminium under dry condition.

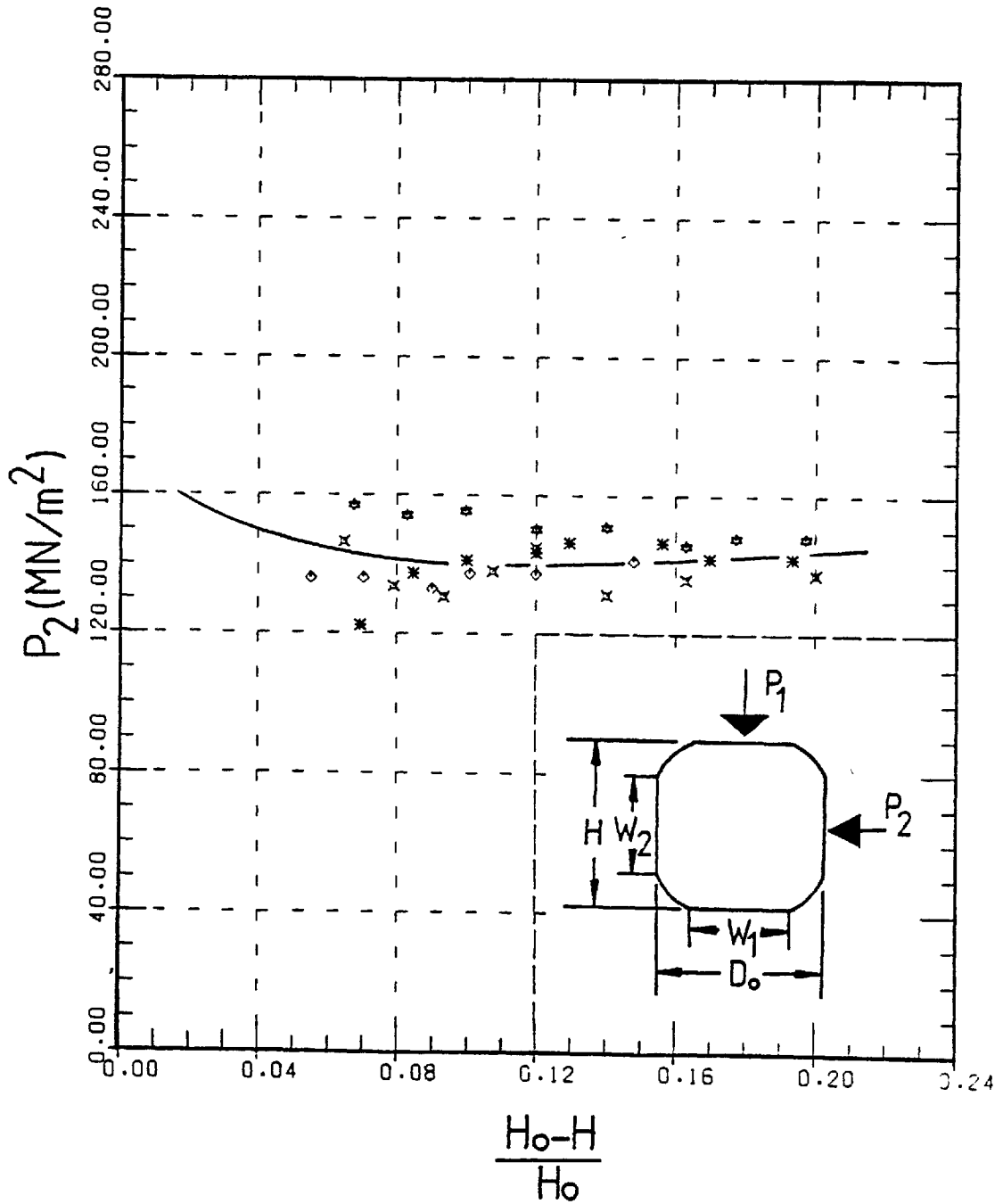


Fig. 4-10-F. Variation of mean normal pressure ' $P_2$ ' with height ' $H$ ' for commercially pure aluminium under dry condition.

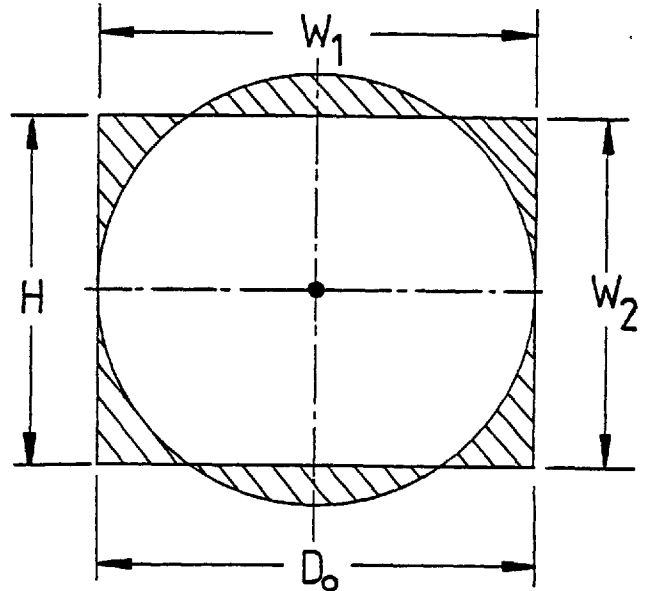
and also

$$W_1 = D_0, \quad W_2 = H = \frac{\pi}{4} D_0$$

The limiting values for  $(H_0 - H)/H_0$ ,  $W_1/D_0$  and  $W_2/D_0$  are

$$(H_0 - H)/H_0 = 1 - \frac{\pi}{4} = 0.215$$

$$W_1/D_0 = 1.00, \quad W_2/D_0 = \frac{\pi}{4} = 0.785$$



and, of course, the limiting values for the indenting forces  $F_1/(L_0 \times D_0)$  and  $F_2/(L_0 \times D_0)$  are both infinity. To assess the degree of violation of plane strain conditions, at  $(H_0 - H)/H_0 = 0.215$  the experimental findings for  $W_1/D_0$ ,  $W_2/D_0$ ,  $F_1/(L_0 \times D_0)$  and  $F_2/(L_0 \times D_0)$  can be obtained and compared with the theoretical values given above. A comparison such as this for the results shown in Figs. 4-10 (A to D) reveal that the billets did not exactly undergo plane strain deformation. As seen, in contrast to the previous cases, the results are noticeably scattered. The scatter of the results can be attributed to the shortcomings of the test-rig and the loading procedure employed. These shortcomings can be summarized as follows:

- 1- The length of the chamber in relation to the size of the chamber cross-section was not sufficiently large and as a result the billets did not exactly undergo plane strain deformation.
- 2- Rods G and H (which served to restrain the side-segments, see Fig. 4-2) undesirably deflected allowing the segments to move apart, despite the test-rig requirements. This movement (which varied

with the size of billet) had a greater effect on the indenting forces than on the contact widths.

- 3- In re-setting the billet after unloading, the loads recorded by the load-cells G and H (measured before the removal of the billet from segments C and D) could not be precisely attained. Thus the state of deformation at the beginning of the next step of load was slightly different from that of the preceding step.
- 4- During the unloading procedure, at intervals in which segment A (see Fig. 4-2 if needed) was first withdrawn, the billet underwent additional plastic deformation due to the remaining forces imparted by the side-segments. The amount of this plastic deformation varied depending on the size of the billet and the amount of indentation.

The variations of normal pressures ' $P_1$ ' and ' $P_2$ ' are shown in Figs. 4-10-E and 4-10-F respectively. As the amount of indentation increases both pressures ' $P_1$ ' and ' $P_2$ ' can each be seen to approach relatively constant values. This is in contrast to the theoretical predictions presented in the next chapter for which both pressures approach infinity as the amount of indentation approaches its limiting value of 0.215. This erroneous trend can again be contributed to the shortcomings of the test-rig. The test-rig used had limited ability to withstand high pressures which would have caused the side-segments to move apart drastically and also the billet to be extruded out from the open-ends of the chamber.

The results for the cases of lubricated aluminium and dry lead billets with side-restraint are shown in Fig. 4-11 (A to D) and 4-12 (A to F) respectively. The results in both cases show the same trend as those which were previously presented for the case of dry aluminium



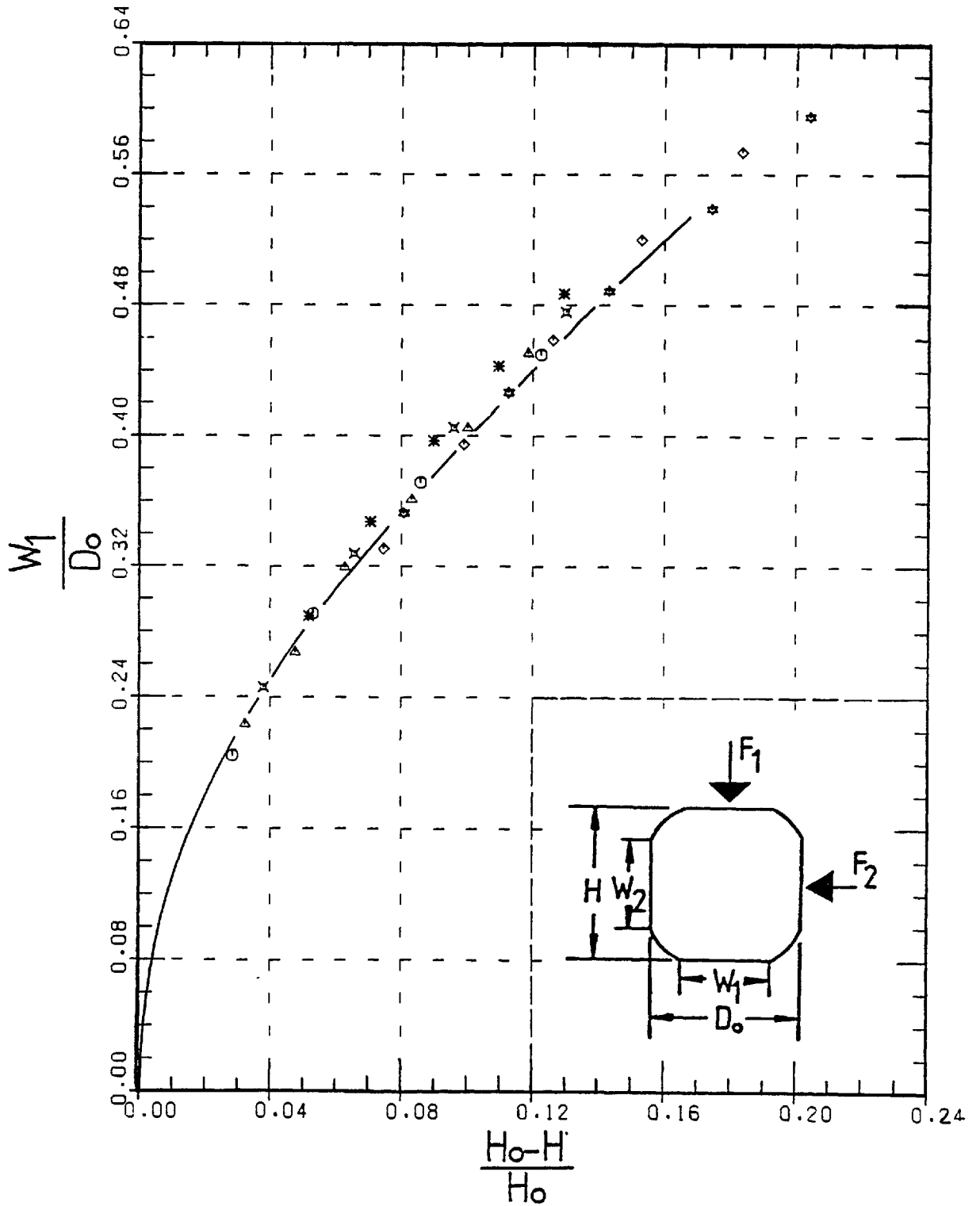


Fig. 4-11-A. Variation of contact width ' $W_1$ ' with height ' $H$ ' for commercially pure aluminium under lubricated condition.

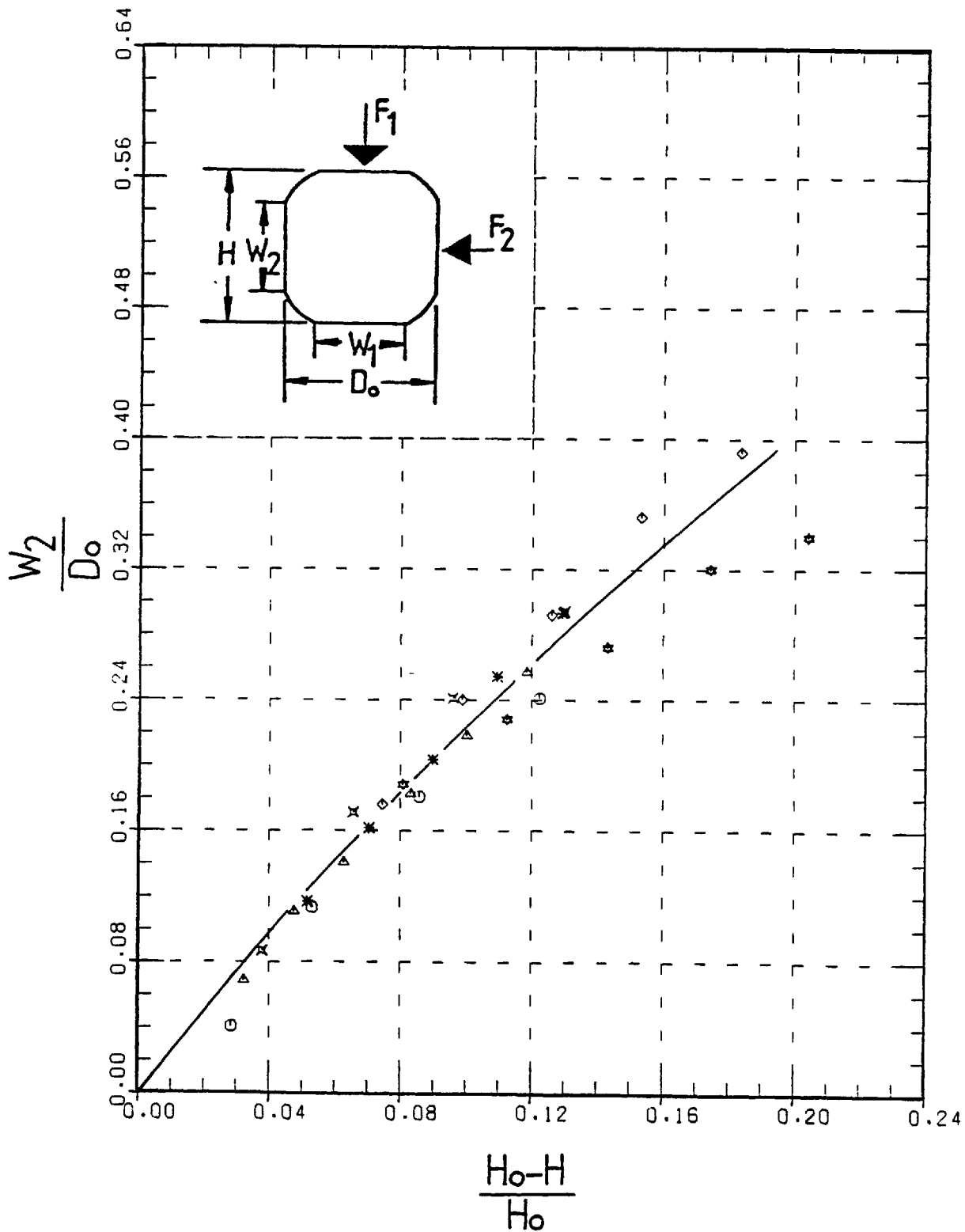


Fig. 4-11-B. Variation of contact width ' $W_2$ ' with height ' $H$ ' for commercially pure aluminium under lubricated condition.

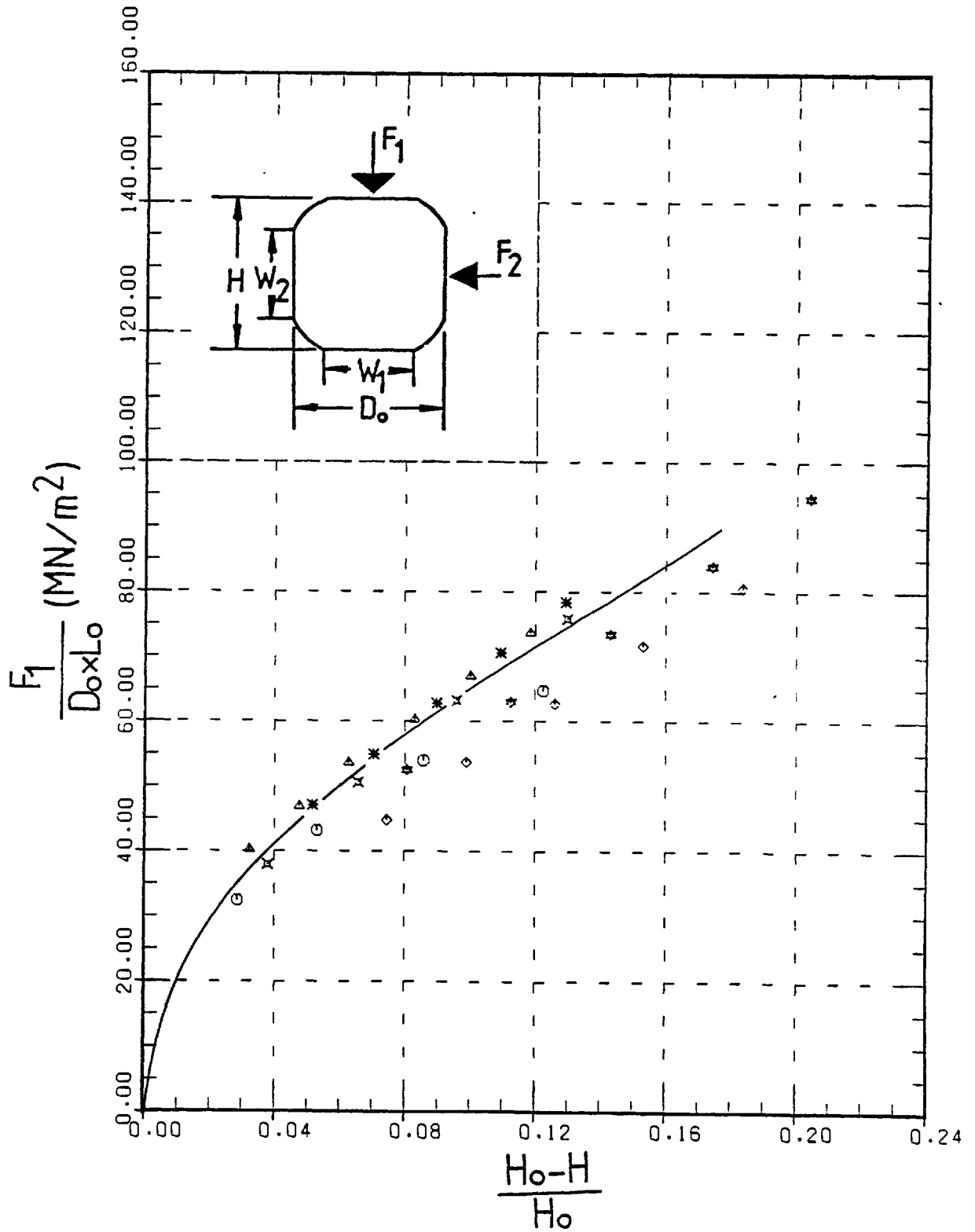


Fig. 4-11-C. Variation of indenting force ' $F_1$ ' with height ' $H$ ' for commercially pure aluminium under lubricated condition.

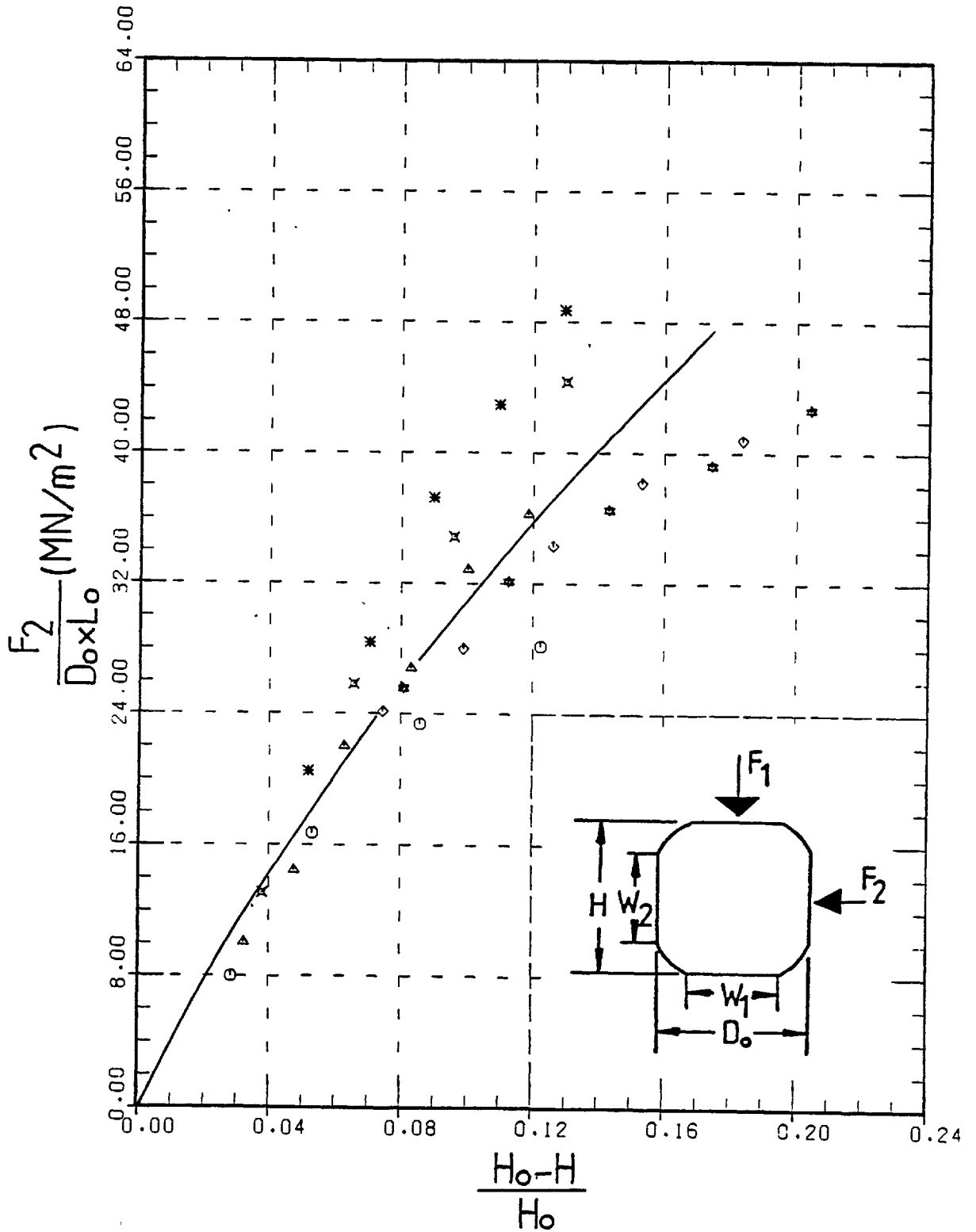


Fig. 4-11-D. Variation of indenting force ' $F_2$ ' with height ' $H$ ' for commercially pure aluminium under lubricated condition.

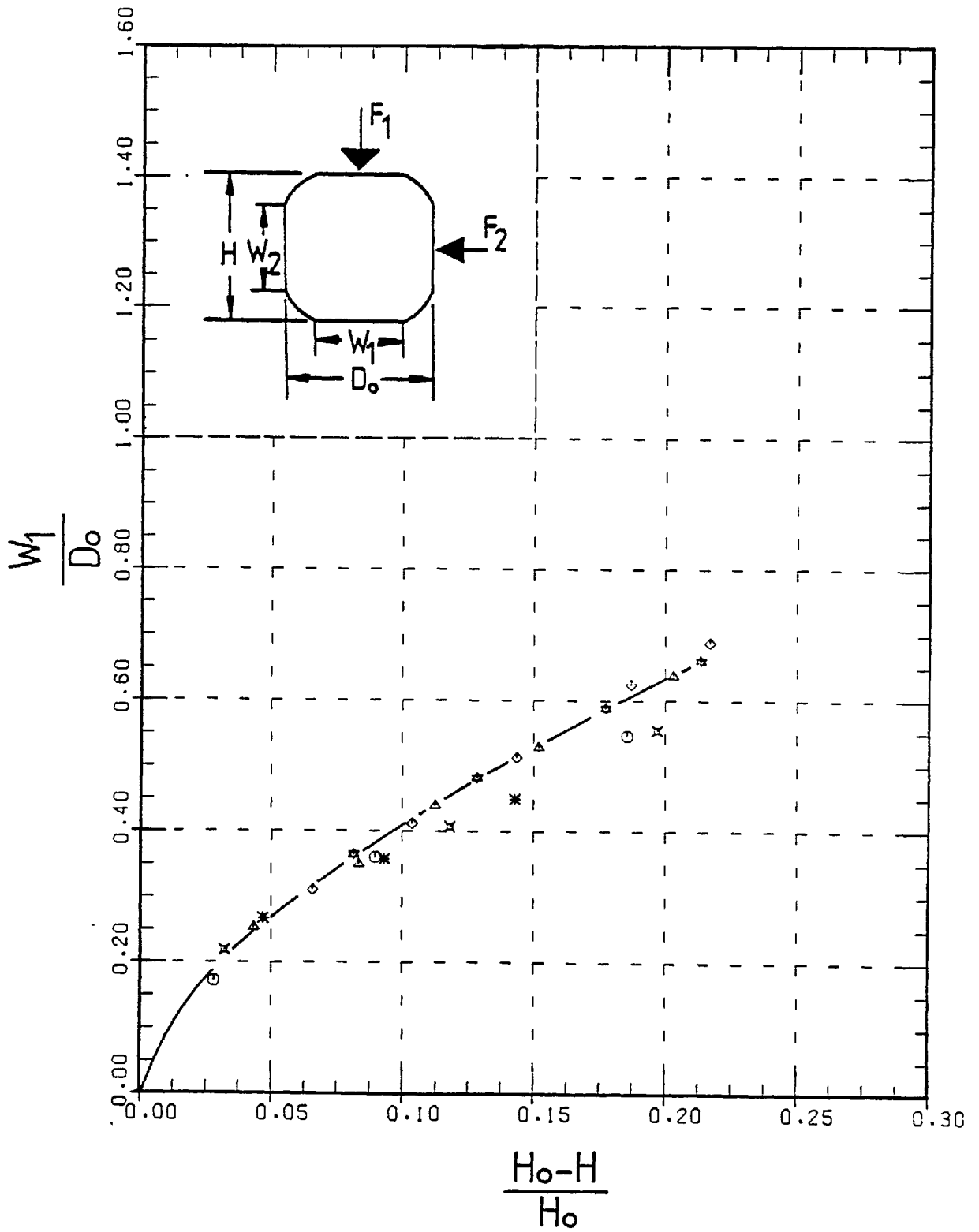


Fig. 4-12-A. Variation of contact width ' $W_1$ ' with height ' $H$ ' for commercially pure lead under dry condition.

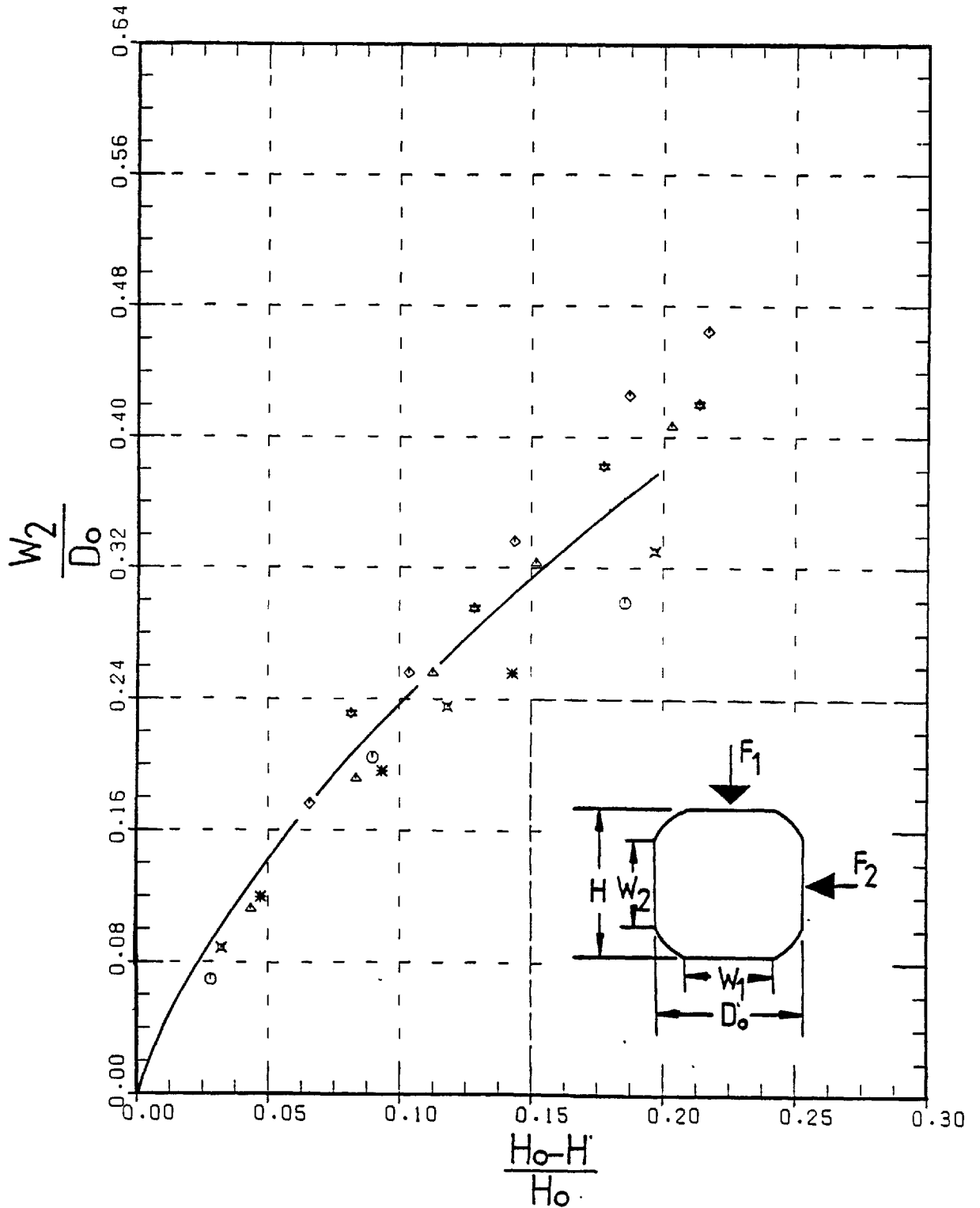


Fig.4-12-B. Variation of contact width ' $W_2$ ' with height ' $H$ ' for commercially pure lead under dry condition.

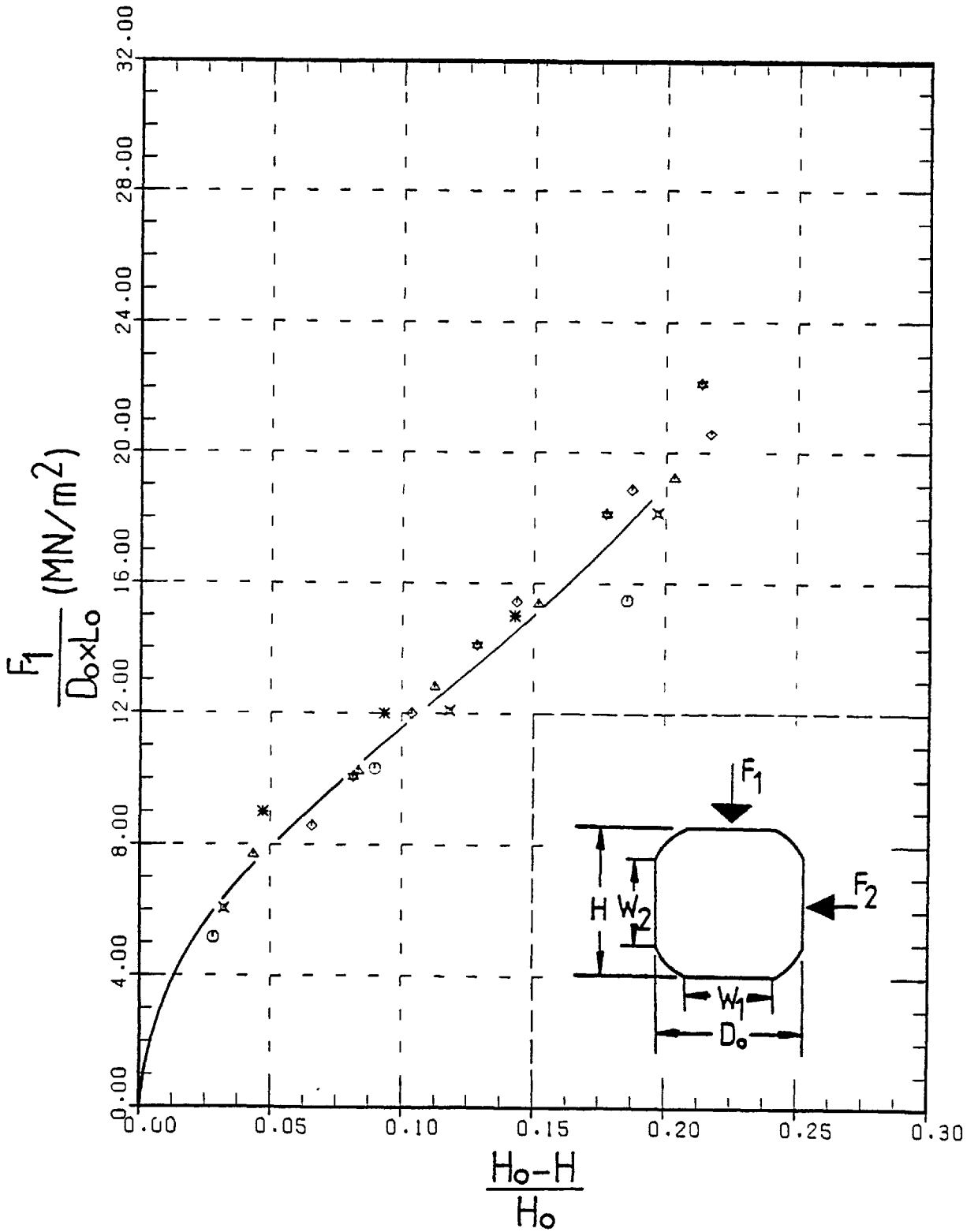


Fig. 4-12-C. Variation of indenting force ' $F_1$ ' with height ' $H$ ' for commercially pure lead under dry condition.

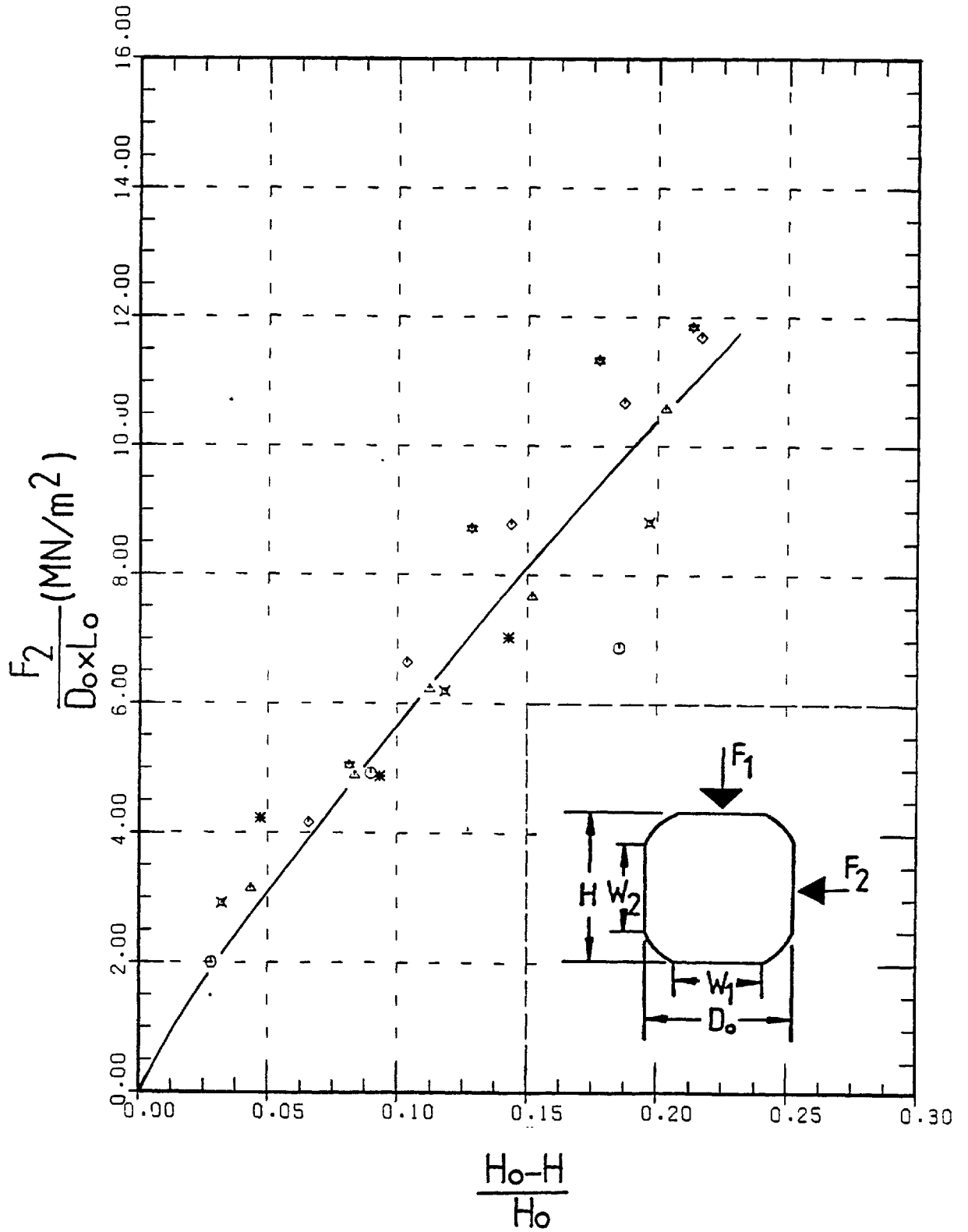


Fig. 4-12-D. Variation of indenting force 'F<sub>2</sub>' with height 'H' for commercially pure lead under dry condition.



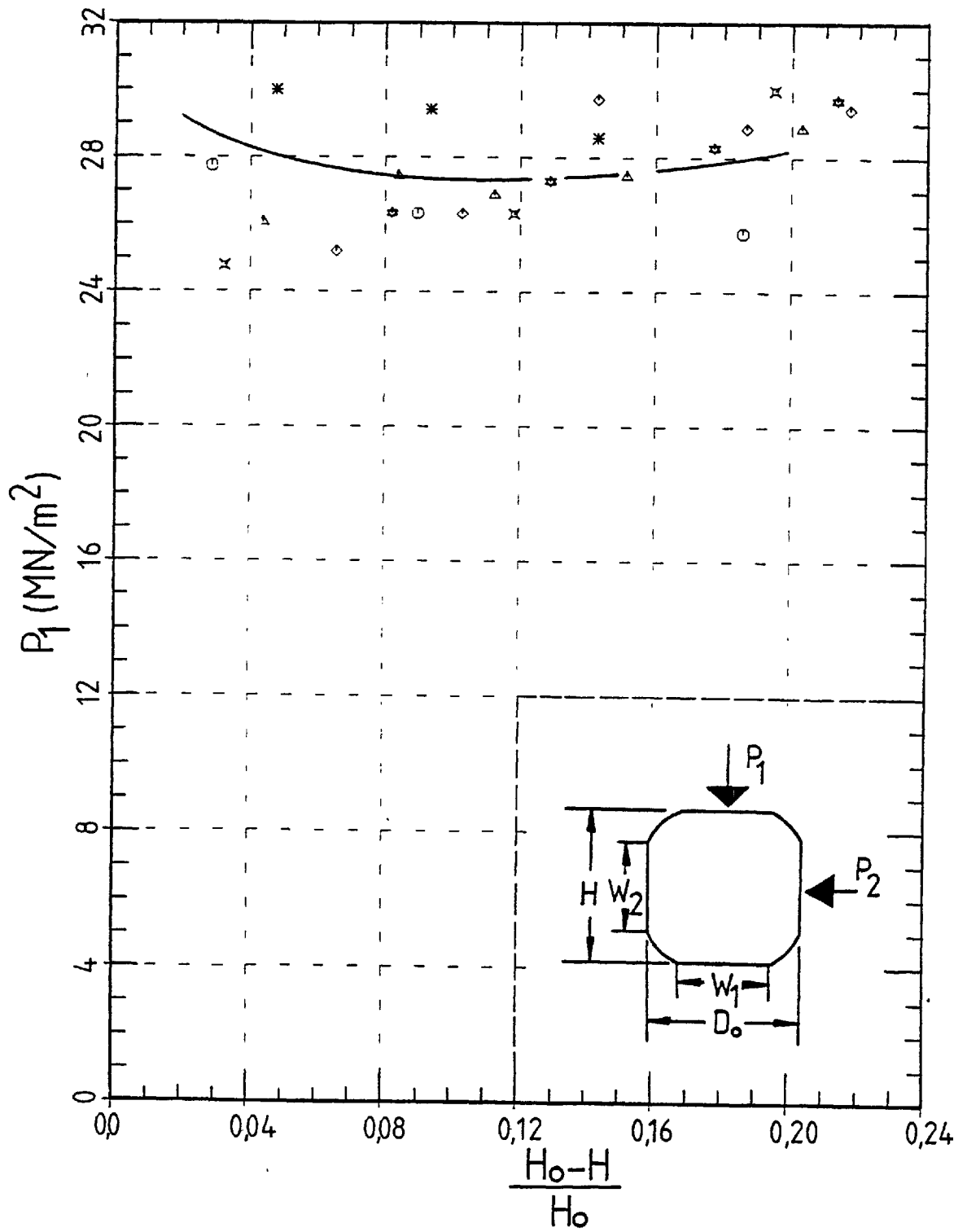


Fig. 4-12-E. Variation of mean normal pressure ' $P_1$ ' with height ' $H$ ' for commercially pure lead under dry condition.

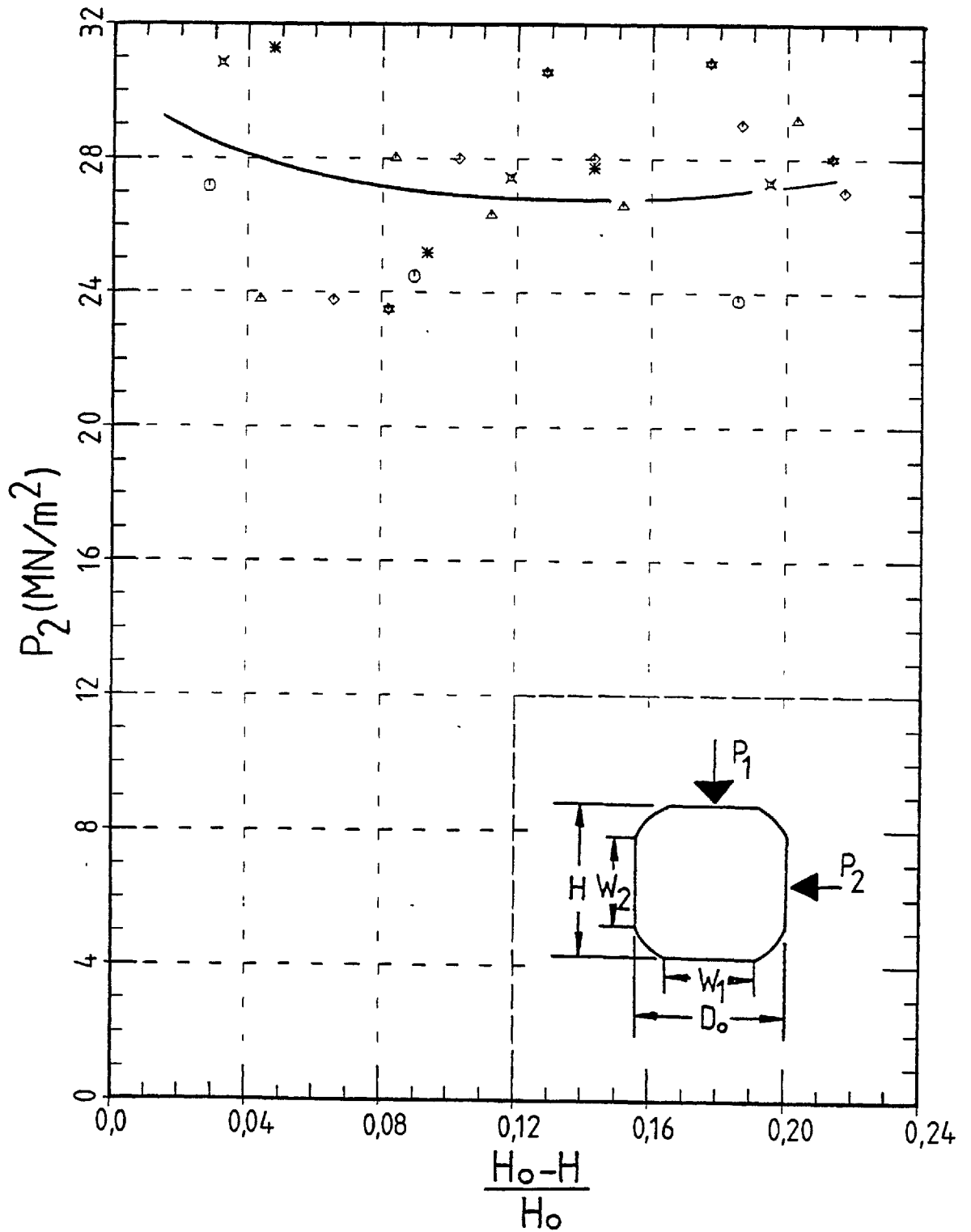


Fig. 4-12-F. Variation of mean normal pressure ' $P_2$ ' with height ' $H$ ' for commercially pure lead under dry condition.

billet with side-restraint, shown in Fig. 4-10 (A to F). At  $(H_0 - H)/H_0 = 0.215$ , from Figs. 4-12-A and 4-12-B, the values of  $W_1/D_0$  and  $W_2/D_0$  for the case of dry lead billets are found to be 0.70 and 0.40 respectively. Although these values are slightly higher than those for the case of dry aluminium billets, they are still far less than the limiting values of 1.00 and 0.785 for conditions of plane strain.

The best fitted curves to those shown in Figs. 4-10, 4-11 and 4-12 are shown in Figs. 4-13 (A to D) for comparison. These results merely represent the trend of those narrow bands within which the previously presented curves fall and hence, for instance, are not representative of any particular billet size. As it can be seen, in general, the results obtained for the cases of dry and lubricated aluminium billets and dry lead billets show the same trend. Attention is however drawn to the shortcomings of the test-rig and the loading procedure which caused the test-rig-response for the cases of dry and lubricated aluminium billets to be hardly distinguishable. In the case of lubricated billets the conditions of plane strain were violated to a greater extent than in the case of dry billets.

The following modifications could have brought to light the effect of lubricant more noticeably:

- 1- The test-rig could be modified, e.g. by providing V-shaped protrusions across the faces of the segments. If this were done the deformation of the billet in the longitudinal direction could be drastically reduced, if not stopped.
- 2- The loading procedure could also be altered, e.g. continuous instead of incremental. Clearly, if a continuous loading procedure is employed, for the dry condition the induced frictional forces and their effects will be greater, since in the incremental loading

procedure, the induced frictional forces are automatically released at intervals, irrespective of the experimental conditions (i.e. lubricated or dry).

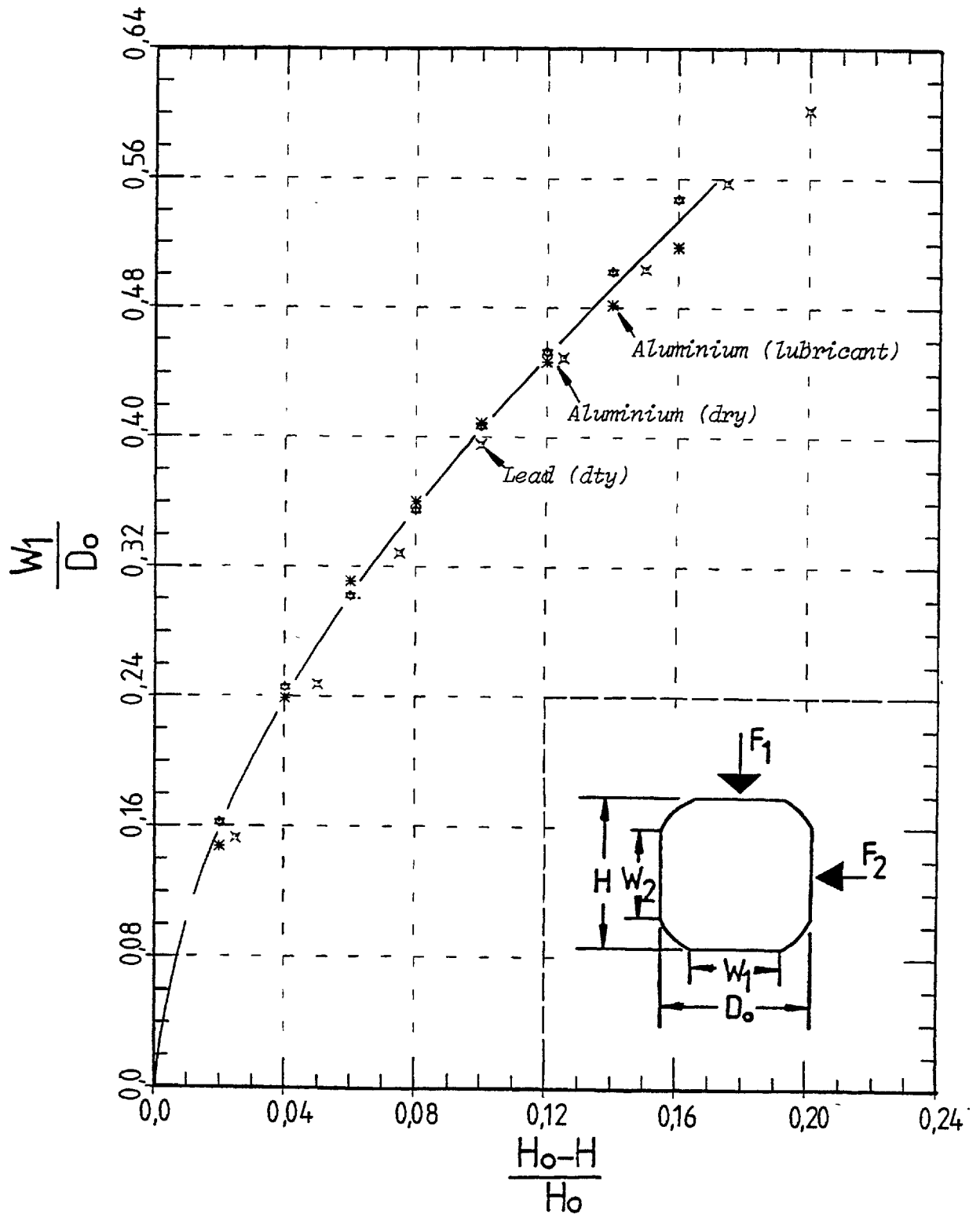


Fig. 4-13-A. Variation of contact width ' $W_1$ ' with height ' $H$ ' for commercially pure aluminium and lead for comparison.

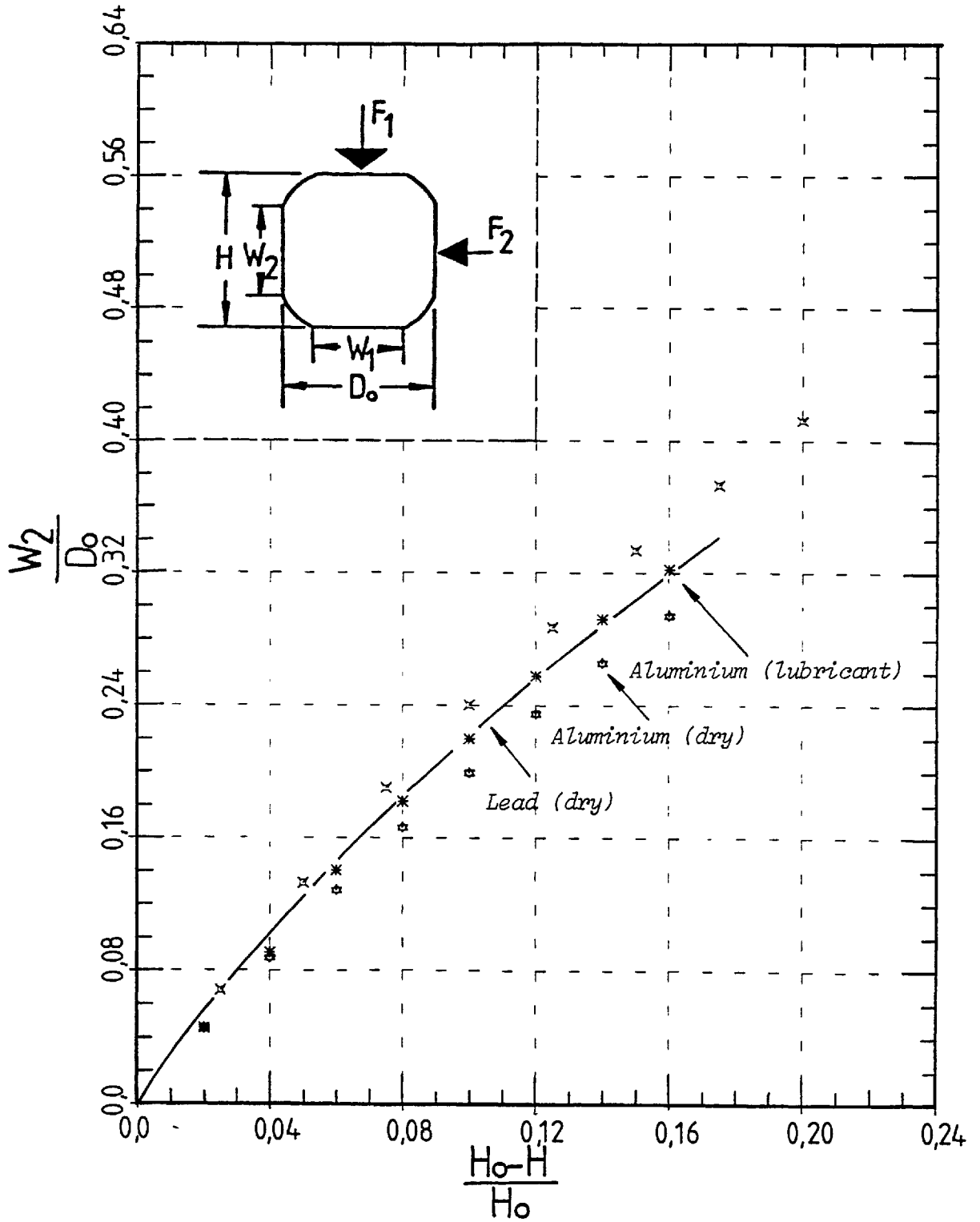


Fig. 4-13-B. Variation of contact width ' $W_2$ ' with height ' $H$ ' for commercially pure aluminium and lead for comparison.

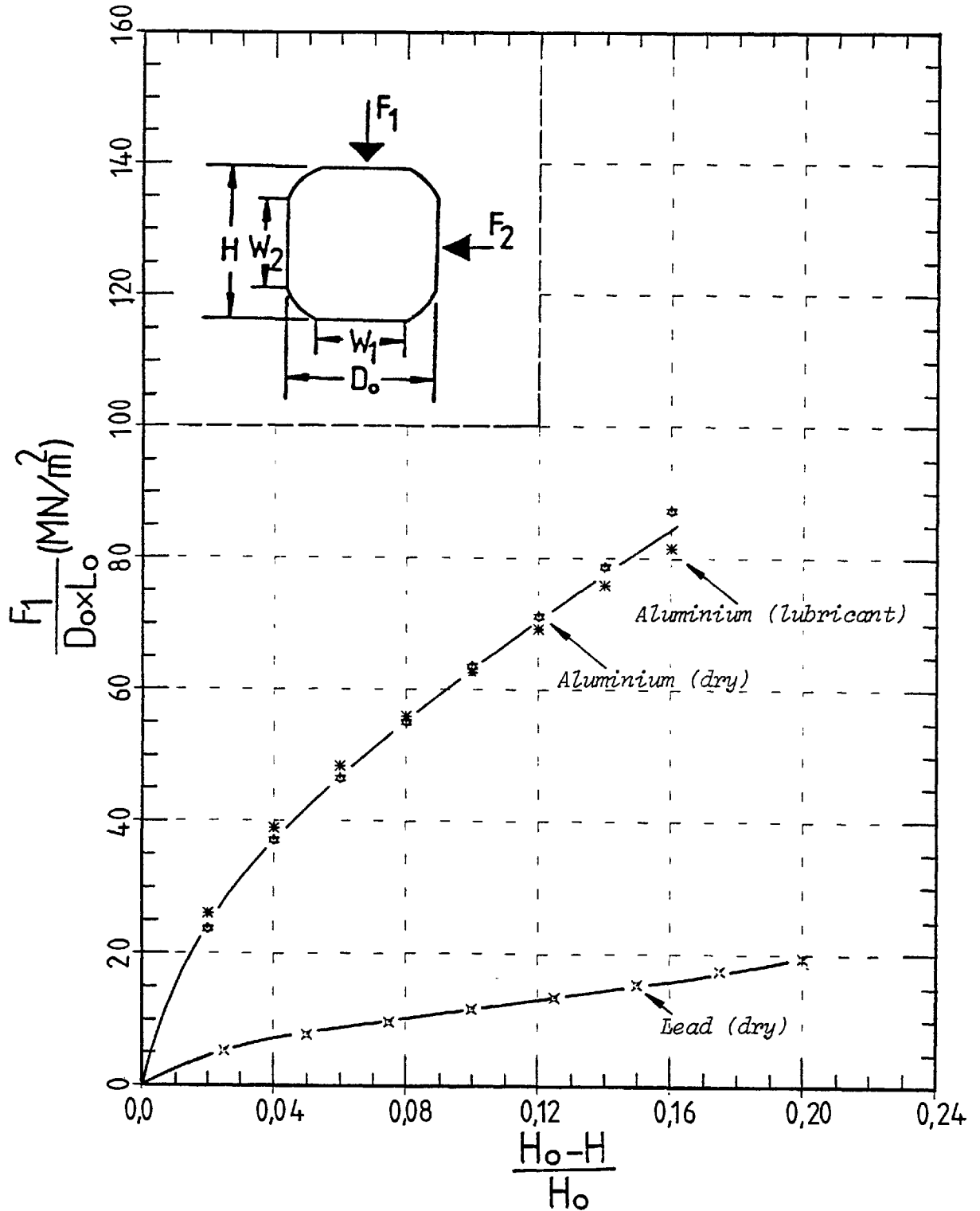


Fig. 4-13-C. Variation of indenting force 'F<sub>1</sub>' with height 'H' for commercially pure aluminium and lead for comparison.

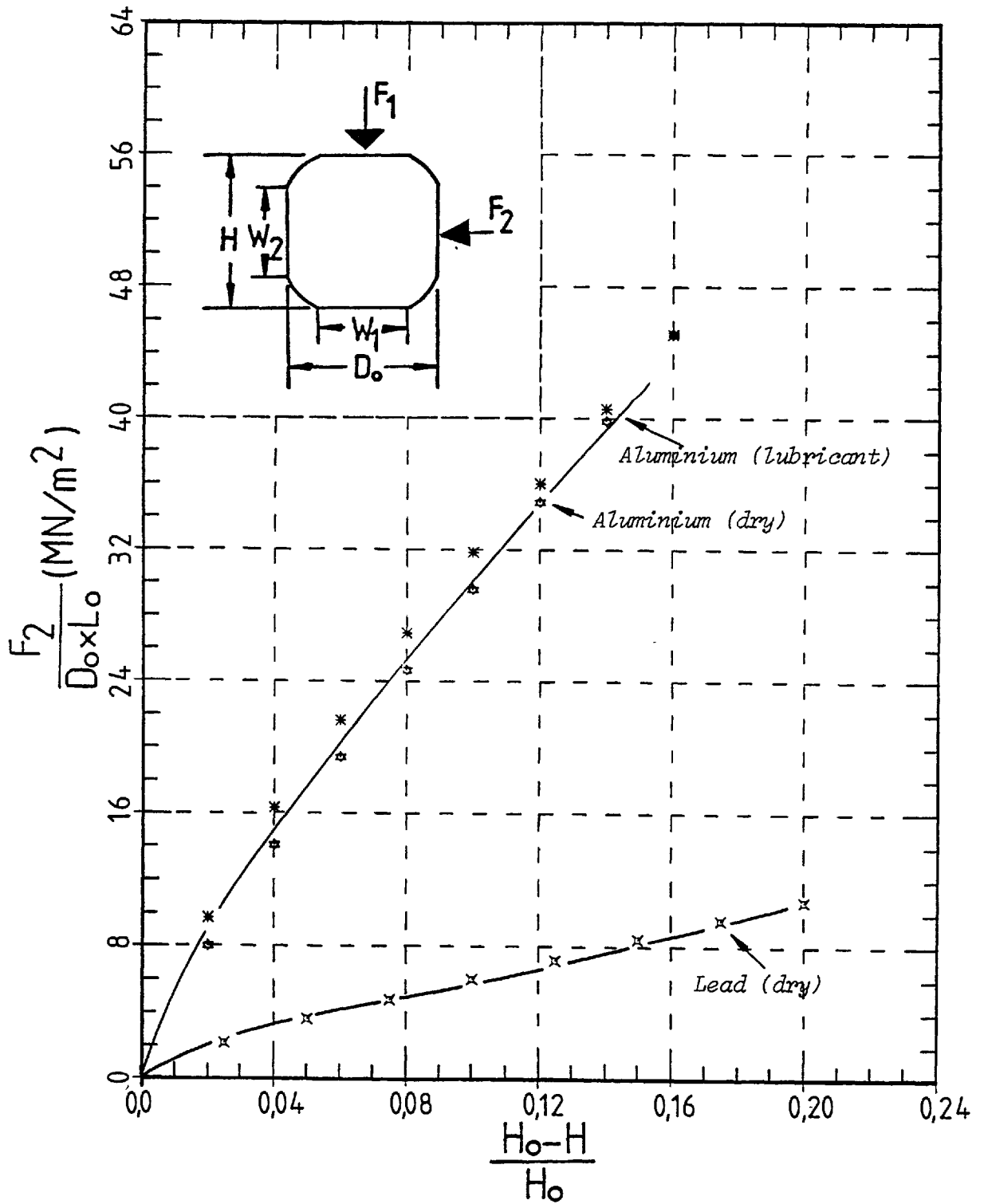


Fig. 4-13-D. Variation of indenting force ' $F_2$ ' with height ' $H$ ' for commercially pure aluminium and lead for comparison.



Part II

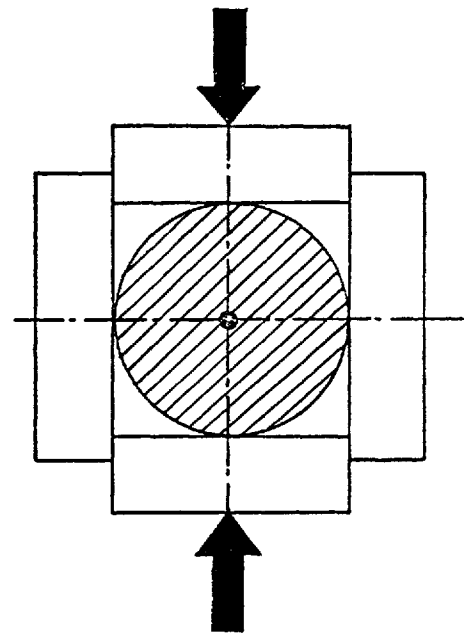
Study of the maximum drag-force induced at the interface  
of the billet and the chamber in Context continuous extrusion

4.10 Introduction

The present study was aimed at determining both practically and theoretically the maximum drag-force developed at the interface of the billet and chamber in a Context type extrusion machine. The indenting mechanism of the machine, consisting of four segments, was assumed to indent the billet in the direction indicated by the arrows as shown in illustration. The machine was also assumed to be fed by a round billet with its initial diameter precisely equal to the distance between its two stationary segments.

The practical model which was used to simulate such a Context machine is shown in Fig. 4-14 which, although simplified, still retained all the characteristics of the actual machine from the point of view of the billet.

Although in the actual machine the chamber and the clamped billet advance towards a stationary die, here a reverse order was employed in which the die advanced towards the billet clamped in the stationary chamber. Axial force was applied to the billet by a pressure pad simulating a die so that the pressure on the pad increased until the billet retreated into the chamber. The drag-force developed in the model used was dependent on three



parameters:

- i- Initial amount of indentation.
- ii- Initial length of billet.
- iii- Friction coefficient.

The 'initial amount of indentation' parameter affects both the interfacial area and the normal pressure between the billet and chamber. Any increase in this parameter will increase the contact widths ' $W_1$ ' and ' $W_2$ ' though the normal pressure may decrease or increase depending on the amount of indentation, see Figs. 4-12-E and 4-12-F. The 'initial length of billet' parameter merely affects the interfacial area and clearly the effect is linear if indentation of the billet is carried out under conditions of plane strain. The 'friction coefficient' parameter is undoubtedly the most important one since a slight decrease in this parameter could drastically decrease the drag-force developed.

#### 4.11 Design considerations

The main design requirements for the test-rig were as follows:

- 1- The billet, made of commercially pure lead, should be precisely 30 mm in diameter.
- 2- The chamber length should be at least 300 mm.
- 3- The experiments should be carried out on a Tinius-Olsen testing machine with a maximum capacity of 540 KN (120 000 lb).

#### 4.12 Experimental set-up

Fig. 4-14 shows the experimental test-rig, which for the sake of low cost and ease of machining was made from mild steel.

The chamber, comprising the four closely-fitted segments A, B, C and D, was vertical. The main indentors, segments A and B, were

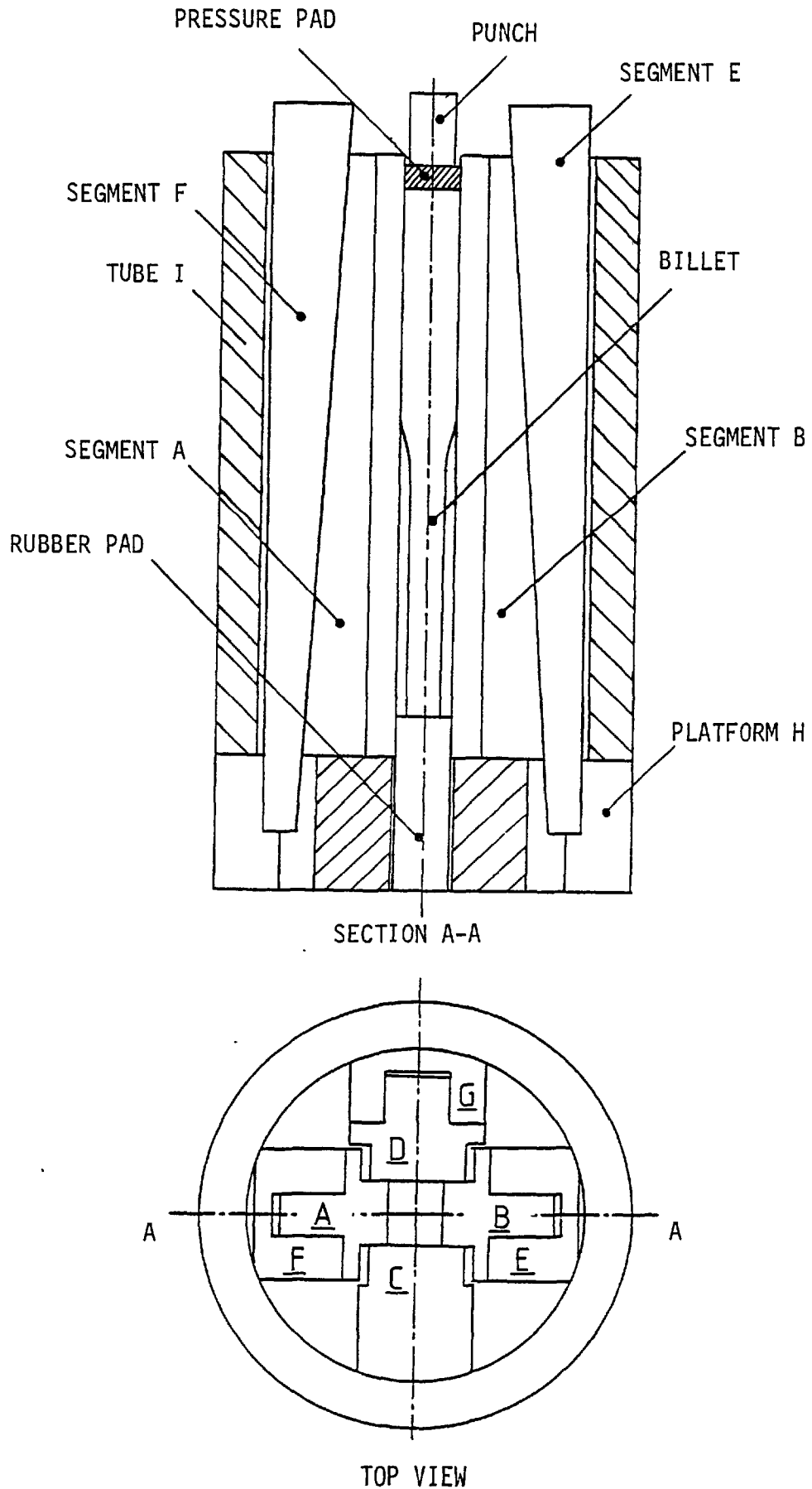


Fig. 4-14. Experimental set-up for indentation and axial deformation of round billets.

tapered on their outside faces and could be driven inwards by means of the wedges E and F. The wedge G was provided to facilitate adjustment to the stationary segment D. By adjustment to G any slackness in the mechanism could be eliminated, or by removing it, the billet could be ejected at the end of the process. The wedges and segment C were supported externally by the thick-walled tube I standing on the platform H. This platform, which held the segments in the vertical position, was provided with three locating cut-outs placed round the periphery at  $90^{\circ}$  intervals. These cut-outs matched accurately to slots machined along the vertical length of the segments, thereby maintaining the squareness of the chamber during the indentation process. The pressure pads allowed various settings between segments A and B but maintained a constant distance between segments C and D. The initial amount of indentation was determined by the dimensions of the pad in use.

The internal faces of the chamber were cross-ground and a roughness test indicated a C.L.A. of  $0.25 \mu\text{m}$  ( $10 \mu\text{in}$ ). The friction coefficient between the billet and the inside walls of the chamber was also determined by the ring-test suggested by Male and Cockcraft (58). The mean value of friction coefficient was found to be approximately equal to 0.2.

#### 4.13 Specimens

Billets made from commercially available pure lead were used for the trials. As the test-rig had a constant width of 30 mm, it was necessary for the billets to be made with a diameter of precisely 30 mm in order to fit the chamber. In the production of the billets, initially lead billets were cast in the form of long cylinders and then

machined until their oxidised and porous surface was completely removed. The machined cylinders were then extruded by conventional direct extrusion to produce straight rods of good surface finish of the specified diameter. The billets were cut from the extruded products into lengths of 210, 230 and 240 mm and annealed at 200 °C for two hours.

#### 4.14 Experimental procedure

Initially the segments of the chamber were placed in their precise positions inside the tube I on top of the platform H. The billet was then held vertically over the mouth of the chamber and lowered inside until it was resting on a cylindrical rubber pad placed at the bottom-end of the chamber, see Fig. 4-14. The ejecting wedge G was then pressed down until the segments fitted closely together. At this stage segments C and D precisely embraced the billet. Segments A and B were then adjusted by moving them inwards or outwards until the upper ends of the wedges E and F were levelled. The object of this was to indent the billet in a symmetrical manner. The pad was then placed in the mouth of the chamber and the wedges E and F were pressed down at a ram speed of 7.5 mm/min until the segments closely embraced the pressure pad. The speed of the ram was calculated such that segments A and B indented the billet with a relative speed of 0.05 mm/min, consistent with that used for the previous experiments presented in 'Part I'.

Finally axial load was applied to the pressure pad by the ram of the press at a ram speed of 0.05 mm/min, and continued at constant speed until the billet retracted into the chamber, at which point a sudden drop in the load was observed. After recording the maximum load attained,

the billet was unloaded by withdrawing the pad, and then withdrew from the chamber after first removing the wedges.

Prior to each experiment the billet and inside walls of the chamber were thoroughly cleaned with trichloroethylene. A thin film of molybdenum disulphide was then applied to the contact surfaces between the wedges and segments in order to decrease the load needed for indentation.

In what follows, a simple theoretical solution is first developed for a pattern of deformation the same as that imparted by the test-rig described above. The experimental and theoretical findings are then presented and compared.

#### 4.15 Theoretical solution

The gradual deformation of a billet inserted in the test-rig described above, is shown in Fig. 4-15. In the first stage of deformation (illustration b) the billet inserted in the chamber is indented. During indentation the billet suffers an axial extension depending on its initial length, friction coefficient and the amount of indentation. Amongst the parameters mentioned, the axial extension of the billet is highly dependent on the amount of indentation. When this is moderate the amount of extension in comparison with the initial length of the billet will be negligible. In the next stage of deformation, shown in illustration (c), the solid pad advances towards the billet which is clamped in the chamber and the billet is deformed axially. If the initial amount of indentation is sufficient, the drag-force developed between the billet and chamber will be negligible and the billet will retreat before receiving any major plastic deformation. For a moderate amount of indentation,

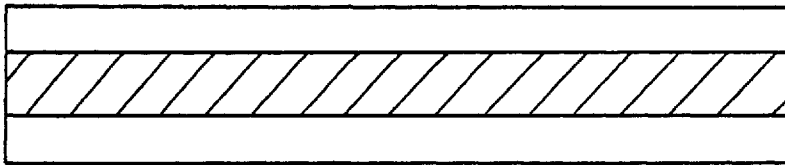
however, the drag-force developed is higher and thus the billet will upset into the chamber before it retreats. The advancing of the pressure pad causes a deformation along the billet which from the geometrical point of view can be divided into three regions as shown in illustration (c). In region '1', the geometry of the billet remains almost constant despite the axial stress which slightly increases along the billet towards the pad. In region '2' an abrupt change in the cross-section occurs and the axial stress increases, but not noticeably, since the billet is not yet fully deformed in the chamber. In region '3', the billet completely fills the chamber cross-section and the axial stress increases drastically.

The lengths of the regions mentioned above are dependent on the amount of advance of the pressure pad into the chamber. At the beginning of the process when the pad starts to advance, the length of region '1' is at its maximum whilst the lengths of the other two regions (i.e. regions '2' and '3') are zero. Provided, of course, that the billet does not retreat, regions '2' and '3' appear as the pad advances, and cause the length of region '1' to be shortened. Further advance of the die causes a further increase in the lengths of regions '2' and '3' and also a further decrease in the length of region '1'. The advance of the pad will continue until the length of region '1' is shortened to a critical value, indicated by ' $X_{min}$ ' shown in illustration (d). At this point the axial force existing at the intersection of regions '1' and '2' exceeds the drag-force supplied by the contact surfaces of this region and thus the billet will retreat.

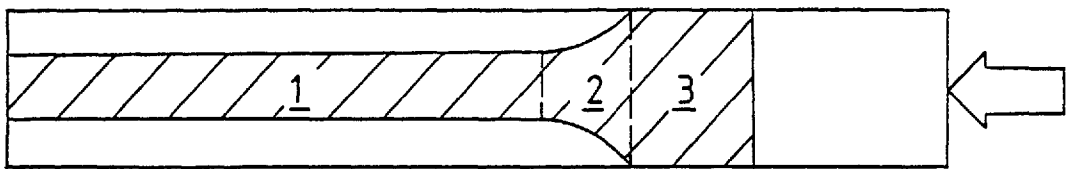
To determine the maximum drag-force induced at the billet and chamber interface, the lengths of the regions mentioned must first be determined. As there are a great number of unknowns involved it will



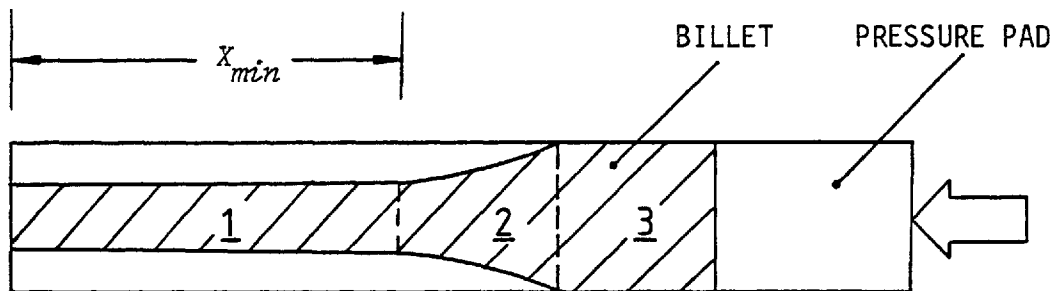
(a)



(b)



(c)



(d)

Fig. 4-15. Progressive plastic deformation of billet during indentation and axial deformation.



be complicated, although possibly feasible, to develop a general solution. The strategy which is followed here is to eliminate some of the unknowns involved by making some simplifying assumptions.

It will be assumed that:

- 1- The Tresca Criterion holds.
- 2- The billet material, i.e. lead, is rigid and perfectly plastic.
- 3- During indentation of the billet, the axial extension in comparison with the billet length is negligible.
- 4- The plastic deformation in region '1' during the advancing of the pressure pad is negligible (i.e. the billet cross-section in this region remains constant as the pad advances into the chamber).
- 5- In region '1', the normal pressures acting at the interface of the billet with the sides of the chamber are equal in value and remain constant throughout the indentation process, i.e.  $P_1 = P_2 = \text{constant}$ . This is a reliable assumption when the amount of indentation is moderate (see Figs. 4-12-E and 4-12-F).
- 6- Region '2' is eliminated by extending regions '1' and '3' towards each other (see Fig. 4-16). This is a vital assumption since along this region neither the cross-section variations nor the interfacial pressure variations are known.
- 7- In region '3', the interfacial pressure at any plane perpendicular to the billet axis is uniform.
- 8- The normal stresses acting at the perpendicular faces of the billet are principal stresses.

By referring to Fig. 4-16 and using the Tresca Criterion, the axial pressures at sections 'A' and 'B' (i.e.  $\bar{P}_A$  and  $\bar{P}_B$ ) can be expressed in terms of their normal interfacial pressures  $P_A$  and  $P_B$ . Thus

Transient zone shown in dotted line

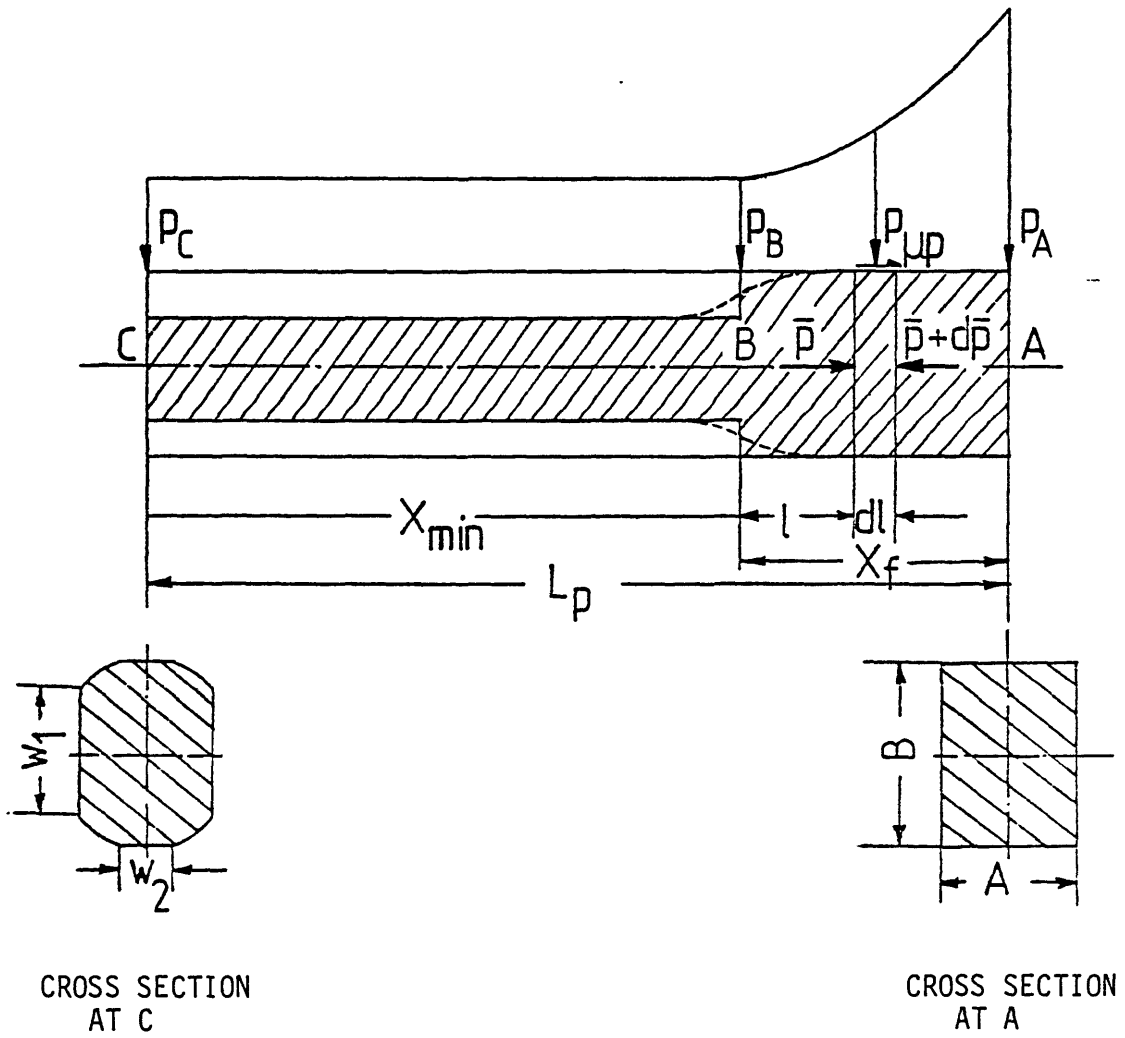


Fig. 4-16. Pattern of deformation at the instant of retreat.

$$\bar{P}_A - P_A = Y \quad \therefore \quad \bar{P}_A = P_A + Y \quad (4.1)$$

in which 'Y' is the yield stress of the material. Similarly at section 'B'

$$\bar{P}_B - P_B = Y \quad \therefore \quad \bar{P}_B = P_B + Y \quad (4.2)$$

Noting that  $P_B = P_C$  and by defining  $\alpha = \frac{P_C}{Y}$ ,  $\bar{P}_B$  can be expressed as

$$\bar{P}_B = Y(\alpha + 1) \quad (4.3)$$

As the billet is on the point of sliding, the equilibrium equation for region '1' becomes

$$ab \bar{P}_B = 2\mu(W_1 + W_2) X_{min} P_C \quad \therefore \quad X_{min} = \frac{ab \bar{P}_B}{2\mu(W_1 + W_2) P_C} \quad (4.4)$$

where  $X_{min}$  and  $\mu$  are the length of region '1' and the friction coefficient respectively. Substituting  $\bar{P}_B$  from Eq. (4.3) leads to

$$X_{min} = \frac{ab(\alpha + 1)}{2\mu(W_1 + W_2) \alpha} \quad (4.5)$$

In region '3', the equilibrium equation, for an infinitesimal element of length 'dl' becomes

$$ab d\bar{P} = 2(\alpha + b) \mu P dl \quad (4.6)$$

but from the Tresca Criterion

$$\bar{P} - P = Y \quad \therefore \quad P = \bar{P} - Y \quad (4.7)$$

Substituting Eq. (4.7) into Eq. (4.6) leads to

$$ab \, d\bar{P} = 2\mu(\alpha + b)(\bar{P} - Y) \, d\bar{l} \quad \therefore \quad \frac{d\bar{P}}{\bar{P} - Y} = \frac{2\mu(\alpha + b)}{ab} \, d\bar{l} \quad (4.8)$$

Integrating equation (4.8) between  $\bar{P} = \bar{P}_B$  at  $\bar{l} = 0$  and  $\bar{P} = \bar{P}$  at  $\bar{l} = \bar{l}$ , gives

$$\int_{\bar{P}_B}^{\bar{P}} \frac{d\bar{P}}{\bar{P} - Y} = \frac{2\mu(\alpha + b)}{ab} \int_0^{\bar{l}} d\bar{l} \quad (4.9)$$

Integrating Eq. (4.9) and inserting  $\bar{P}_B$  from Eq. (4.3)

$$\bar{P} = Y \left\{ 1 + \alpha \exp \left[ \frac{2\mu(\alpha + b)}{ab} \bar{l} \right] \right\} \quad (4.10)$$

and from Eq. (4.7)

$$P = \alpha Y \exp \left[ \frac{2\mu(\alpha + b)}{ab} \bar{l} \right] \quad (4.11)$$

The variation of the shear stress, in region '3', can be found by substituting  $P$  from Eq. (4.11) into the relation  $\tau = \mu P$ , thus

$$\tau = \mu \alpha Y \exp \left[ \frac{2\mu(\alpha + b)}{ab} \bar{l} \right] \quad (4.12)$$

Clearly, the shear stress can not exceed the shear yield stress of the material (i.e.  $k = \frac{Y}{2}$ ), thus

$$\frac{Y}{2} = \mu \alpha Y \exp \left[ \frac{2\mu(\alpha + b)}{ab} \bar{l}_{Cr} \right] \quad (4.13)$$

in which  $l_{Cr}$  is the critical value of  $l$  for which the shear stress reaches its maximum value of  $k$ . From Eq. (4.13),  $l_{Cr}$  can be calculated as

$$l_{Cr} = \frac{-ab \ln(2\mu\alpha)}{2\mu(a+b)} \quad (4.14)$$

The normal pressure  $P_{Cr}$  and the axial pressure  $\bar{P}_{Cr}$ , at this critical value of  $l_{Cr}$ , are given by

$$P_{Cr} = \frac{\tau}{\mu} = \frac{Y}{2\mu} \quad (4.15)$$

and

$$\bar{P}_{Cr} = Y\left(1 + \frac{1}{2\mu}\right) \quad (4.16)$$

The shear stress, for the values of  $l$  exceeding  $l_{Cr}$ , is no longer proportional to the normal stress. For  $l > l_{Cr}$  the shear stress remains constant and equal to  $k (= \frac{Y}{2})$ . The equilibrium equation for  $l > l_{Cr}$  becomes

$$ab \, d\bar{P} = 2(a+b) \frac{Y}{2} \, dl \quad (4.17)$$

where  $\mu P$  in equation (4.6) has been replaced by  $\frac{Y}{2}$ . Integrating Eq. (4.17) between  $\bar{P}_{Cr}$  at  $l_{Cr}$  and  $\bar{P}$  at  $l$

$$\int_{\bar{P}_{Cr}}^{\bar{P}} ab \, d\bar{P} = 2(a+b) \frac{Y}{2} \int_{l_{Cr}}^l dl \quad (4.18)$$

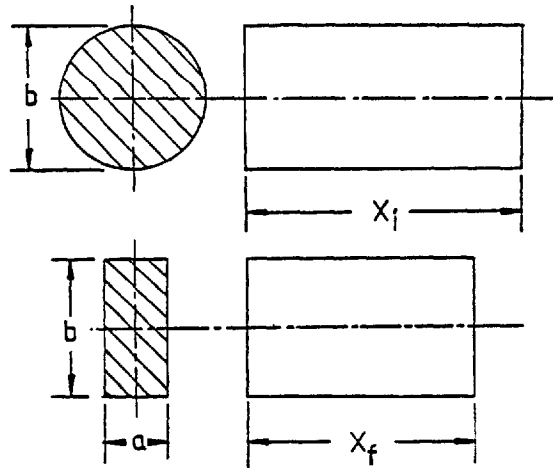
Simplifying and then substituting  $\bar{P}_{Cr}$  from Eq. (4.16) gives

$$\bar{P} = Y \left[ 1 + \frac{1}{2\mu} + \frac{(a+b)(l - l_{Cr})}{ab} \right] \quad (4.19)$$

It is worth mentioning that for  $l \leq l_{Cr}$  the axial pressure  $\bar{P}$  varies exponentially whilst for  $l > l_{Cr}$  it varies linearly with respect to  $l$ .

The length ' $X_f$ ' of region '3' can be expressed in terms of its undeformed length ' $X_i$ ' from the volume constancy assumption (see the illustration below), thus

$$\frac{\pi}{4} b^2 X_i = ab X_f \quad \therefore \quad X_f = \frac{\pi b}{4a} X_i \quad (4.20)$$



To determine the maximum end-pressure, or the maximum drag-force developed between the billet and the chamber, Eqs. (4.5), (4.10), (4.19) and (4.20) can be solved as follows:

- 1- By solving Eq. (4.5), the length ' $X_{min}$ ' of region '1' is calculated.
- 2- If the initial length of the billet is shorter than ' $X_{min}$ ', the billet will retreat before the appearance of region '3'. However, if the billet length is greater than ' $X_{min}$ ', there will exist a fully filled region (i.e. region '3'). The length, ' $X_f$ ', of this region is then calculated from Eq. (4.20).
- 3- The maximum end-pressure ' $\bar{P}_A$ ' is finally calculated from Eqs. (4.10) or (4.19) depending on the length of region '3'.

The maximum end-pressure can alternatively be determined from the graphical representation of Eqs. (4.5), (4.10), (4.19) and (4.20). The graphical representations for these equations are shown in Figs. 4-18 to 4-22. In the computation of these graphs, the following assumptions were made:

- 1- The width of the chamber, ' $b$ ', was assumed to be 30 mm.
- 2- The pressure ' $P_C$ ' was assumed constant and equal to  $27 \text{ MN/m}^2$ . This was approximated from Figs. 4-12-E and 4-12-F presented in 'Part I'.
- 3- The yield stress of the material, for an effective strain taken as 0.4, was found to be  $19 \text{ MN/m}^2$  (see Fig. 4-17). The value taken for effective strain was quite arbitrary and any other values could have been taken.
- 4- For the variations of ' $W_1$ ' and ' $W_2$ ' in Eq. (4.5), theoretical values were inserted. These values were in their analytical forms and will be presented in the next chapter. Alternatively the experimental findings, presented in 'Part I' could have been used, but since these were in graphical form, implementation would have more difficult.

In what follows, some numerical examples are given to clarify the procedure of determining the maximum end-pressure by using the graphs illustrated in Figs. 4-18 to 4-22.

#### Example 1

Assuming that  $\mu = 0.2$ , the initial length of the billet  $L_0 = 200 \text{ mm}$  and the amount of indentation  $(H_0 - H)/H_0 = 0.04$ .

From Fig. 4-18, the length ' $X_{min}$ ' of region '1' is determined as  $X_{min} = 300 \text{ mm}$ . Since  $X_{min} > L_0$ , then the length ' $X_z$ ' of region '3'

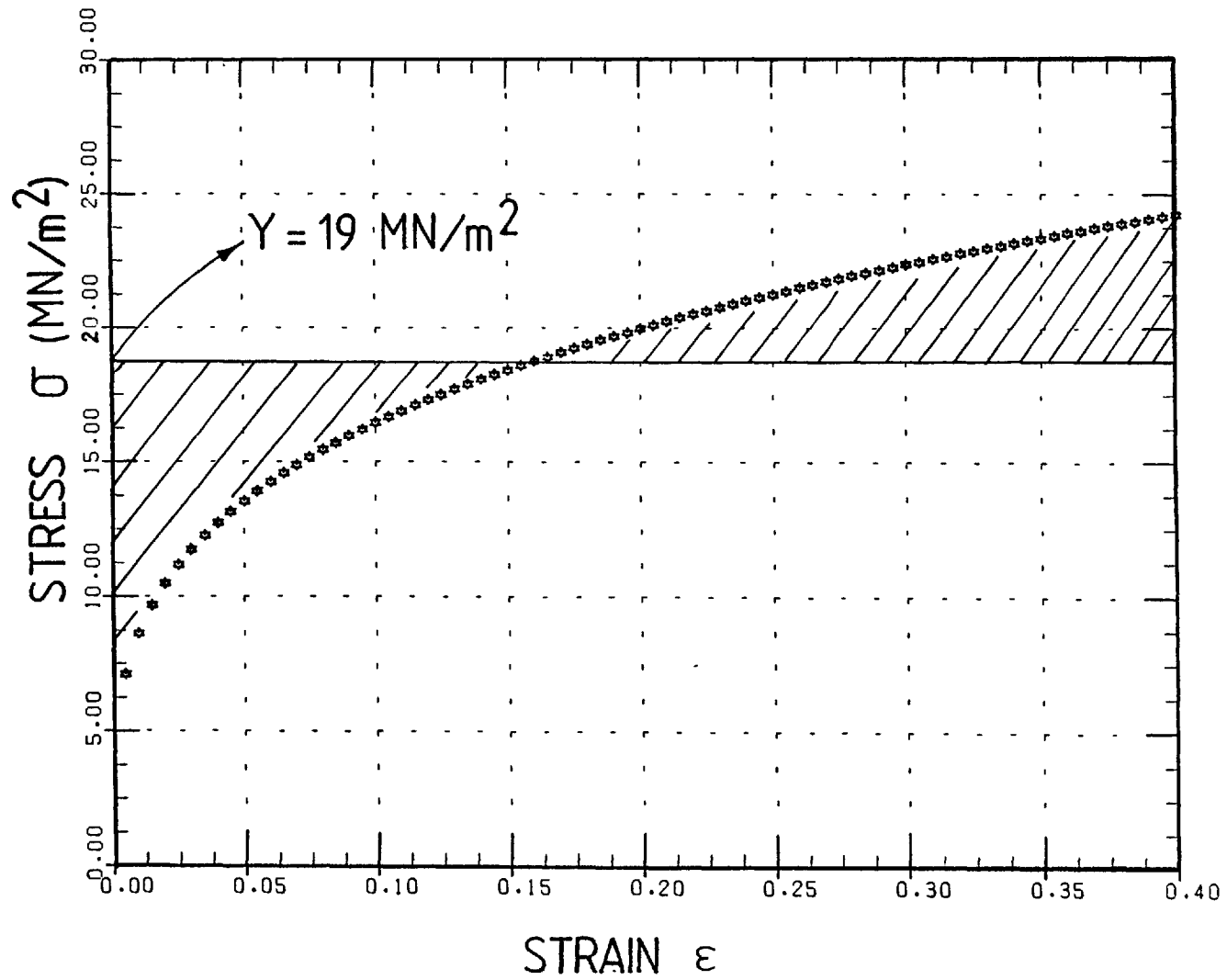


Fig. 4-17. Stress-strain diagram for lead



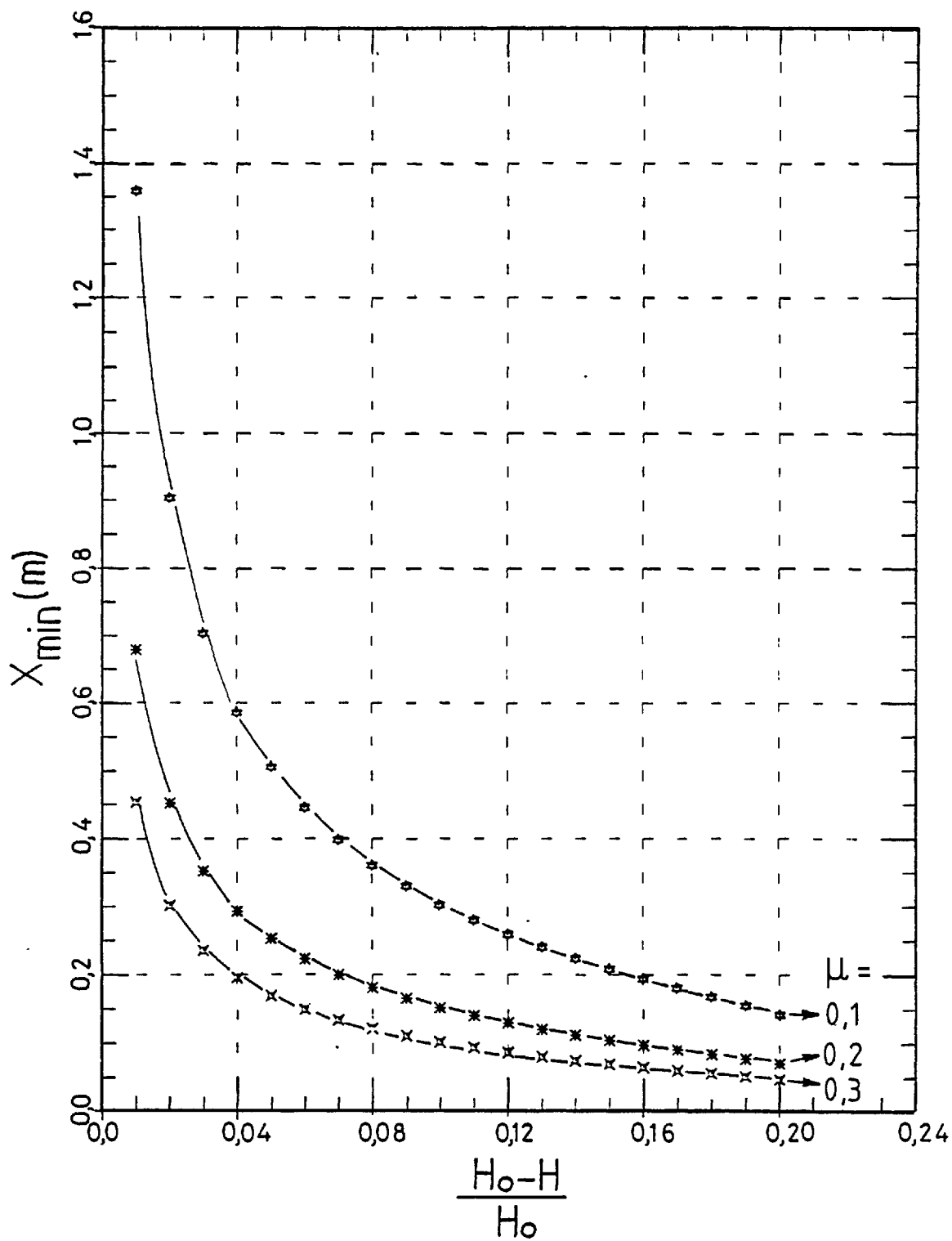


Fig. 4-18. Variation of minimum length ' $X_{min}$ ' with amount of indentation ' $(H_0 - H)/H_0$ ' .

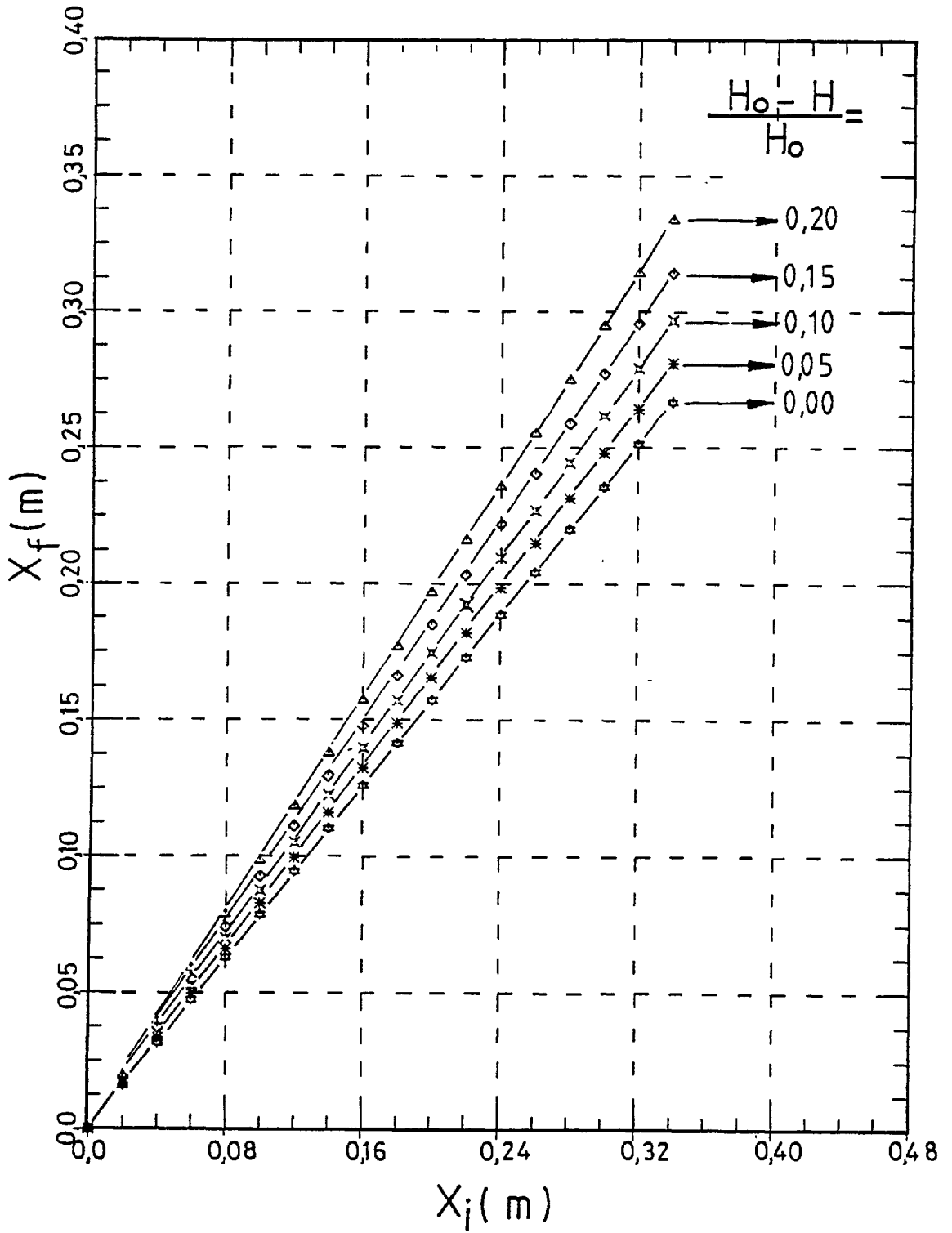


Fig. 4-19. Variation of deformed length ' $X_f$ ' with undeformed length ' $X_i$ ' .

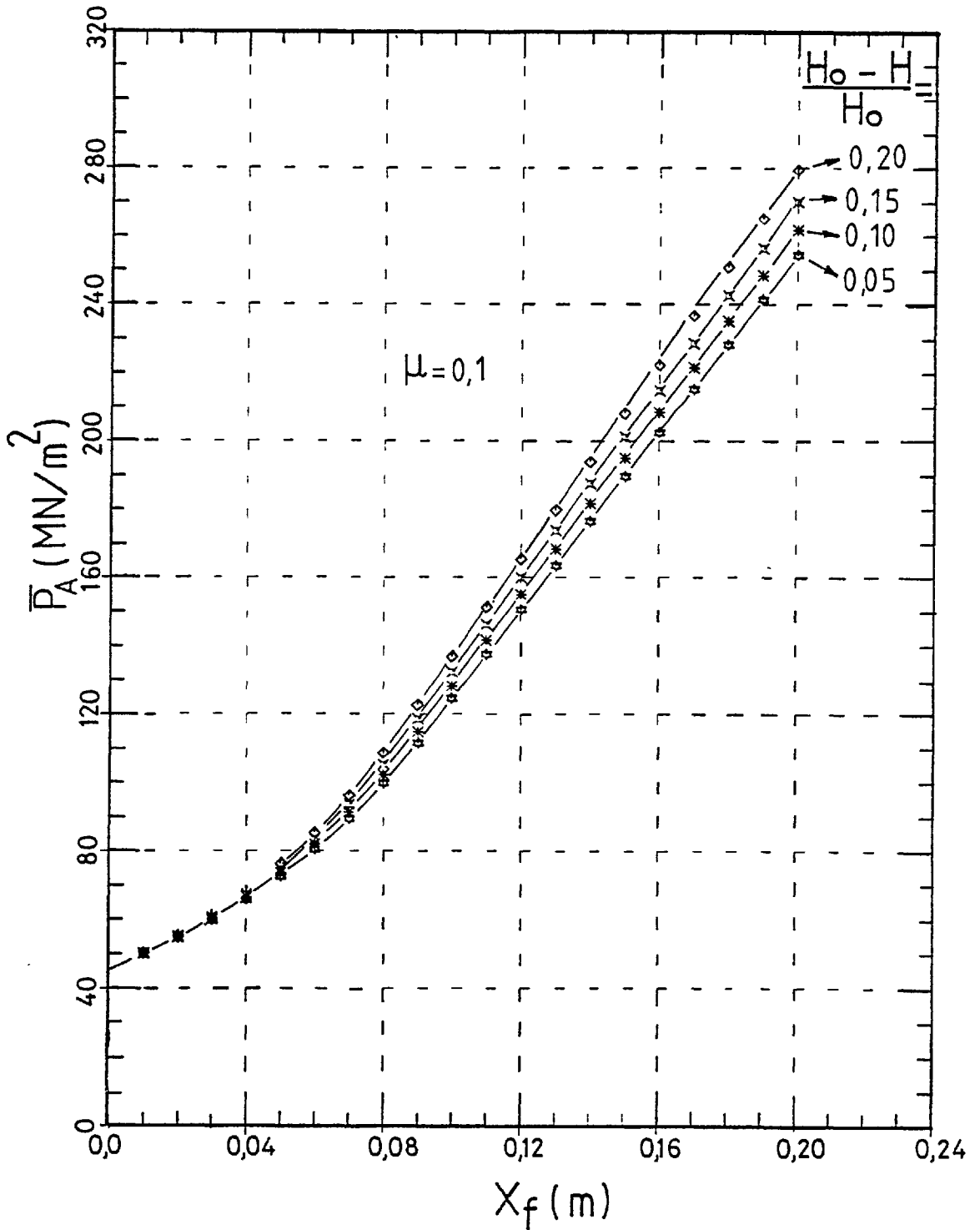


Fig. 4-20. Variation of maximum end-pressure ' $P_A$ ' with length of region (3), ' $X_f$ '. Coefficient of friction  $\mu=0.1$ .

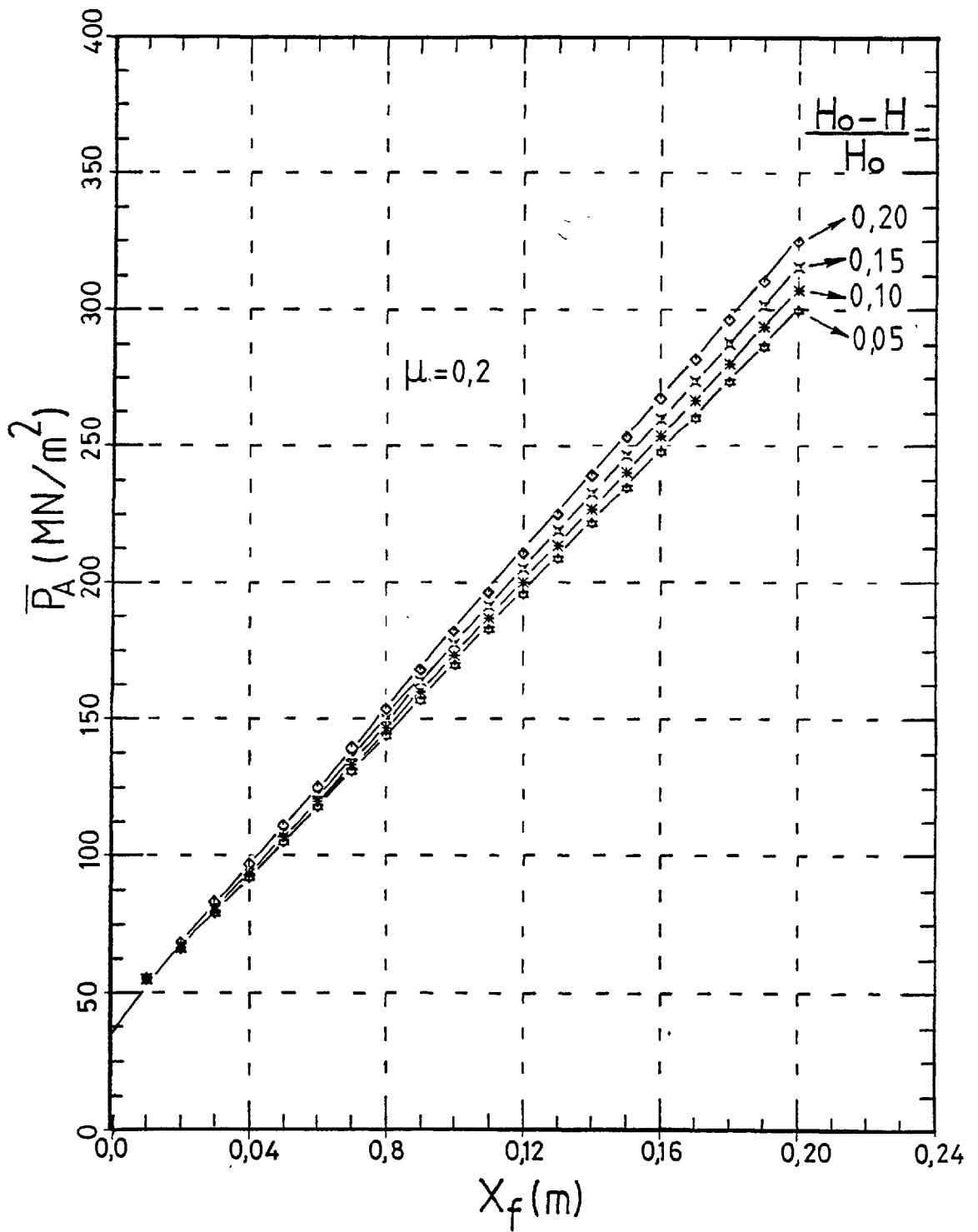


Fig. 4-21. Variation of maximum end-pressure ' $P_A$ ' with length of region (3), ' $X_f$ '. Coefficient of friction  $\mu=0.2$ .

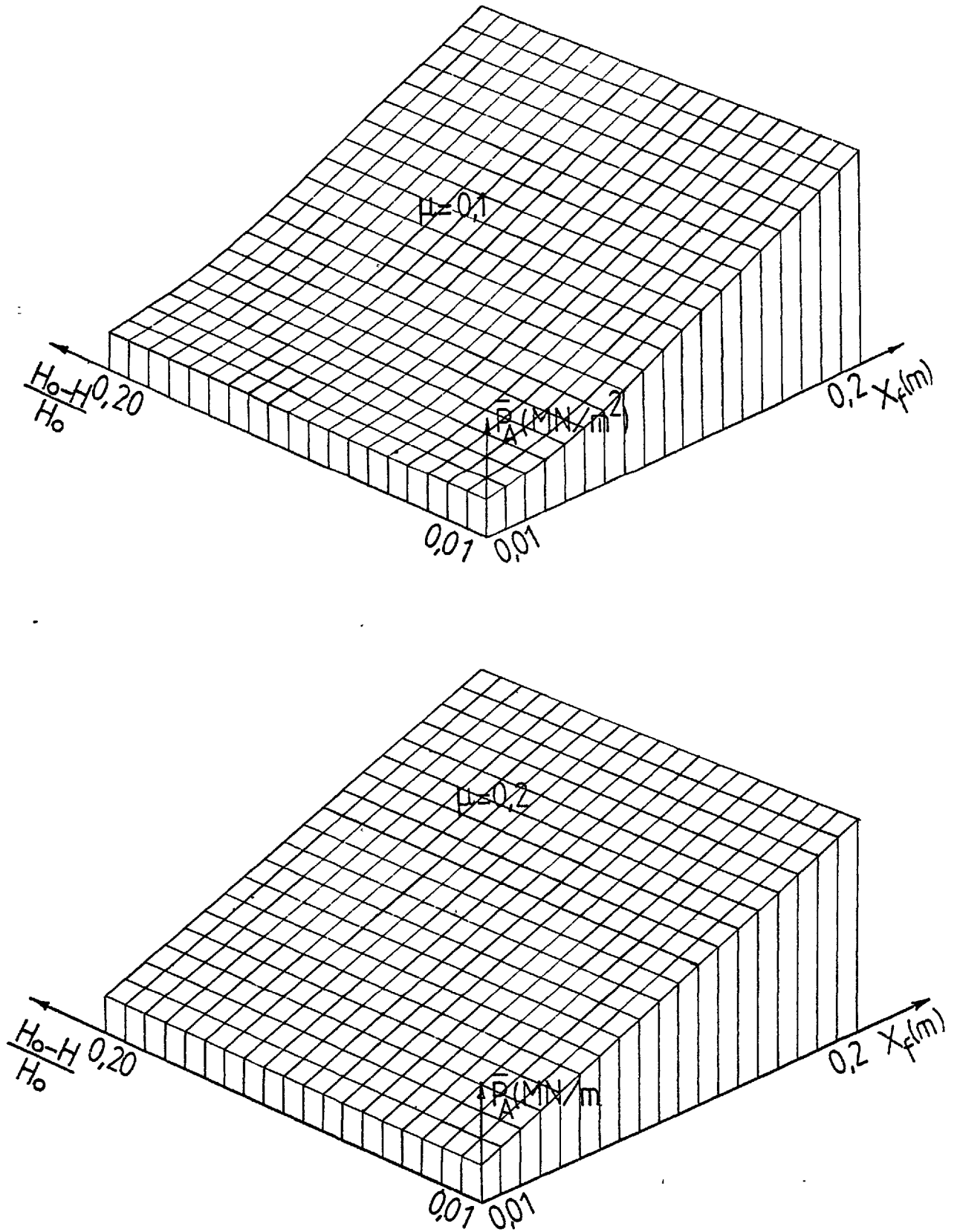


Fig. 4-22. Variation of maximum end-pressure ' $P_A$ ' with amount of indentation ' $(H_0 - H)/H_0$ ' and length of region (3), ' $X_f$ ' .

becomes  $X_i = X_f = 0$ .

From Fig. 4-21 the maximum end-pressure is obtained and found to be  $\bar{P}_A = 40 \text{ MN/m}^2$ .

### Example 2

Assuming that  $\mu = 0.2$ , the initial length of the billet  $L_o = 200 \text{ mm}$  and the amount of indentation  $(H_o - H)/H_o = 0.15$ .

From Fig. 4-18, the length of region '1', is determined as  $X_{min} = 100 \text{ mm}$ . Since  $X_{min} < L_o$ , then

$$X_i = L_o - X_{min} = 200 - 100 = 100 \text{ mm}$$

From Fig. 4-19, the length of region '3' can be calculated, thus  $X_f = 92.5 \text{ mm}$ .

Finally, from Fig. 4-21, the maximum end-pressure is obtained and is given by  $\bar{P}_A = 170 \text{ MN/m}^2$ .

### 4.16 Experimental and theoretical results and discussions

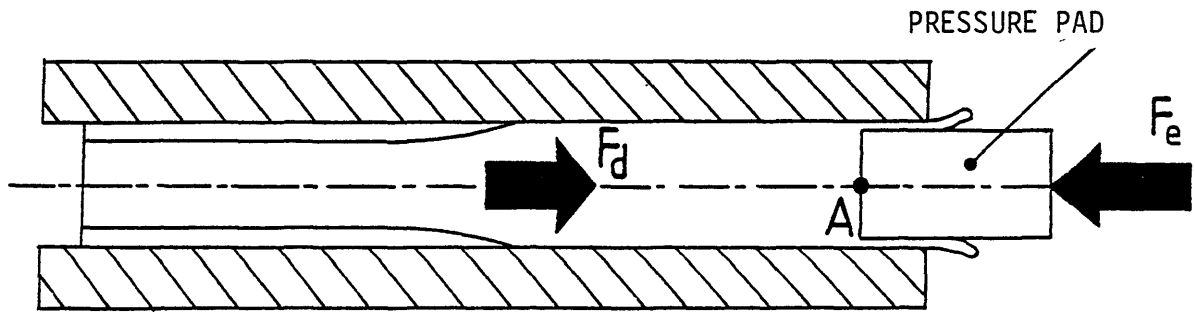
Due to the non-uniform distortion of the chamber, which caused the amount of indentation to vary along the billet and relatively large gaps to be created between the pad and segments, the following refinements in computing the experimental results were introduced:

- 1- The maximum pressure,  $\bar{P}_A$ , applied to the pad-face was obtained by dividing the maximum end-load by the cross-sectional area of the billet, rather than by the pressure pad cross-section which was slightly smaller. The slight overestimation of the maximum drag-force ' $F_d$ ', through the measurement of the end-load ' $F_e$ ', was therefore to some extent offset (see the illustration below). That

is

$$\bar{P}_A = \frac{F_d}{\text{Cross-sectional area of the pad at A}}$$

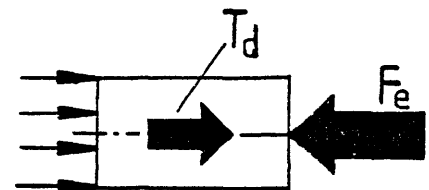
$$\approx \frac{F_e}{\text{Cross-sectional area of the billet at A}}$$



$F_e$  = maximum end-load

$F_d$  = maximum drag-force

$T_d$  = drag-force applied to the die by the extruded metal



2- In the measurement of the amounts of indentation, the mean values at the top- and bottom-ends of the billet were calculated and assigned to be the amount of indentation imparted.

In computing the theoretical predictions the friction coefficient was assumed to be 0.2. For a given length and an amount of indentation, the maximum pressure was determined from the graphs shown in Figs. 4-18, 4-19 and 4-21.

The experimental and theoretical findings of the maximum pressure developed on the pad-face are shown in Fig. 4-23. As can be seen, within the considered range of indentation, both the experimental and theoretical findings vary almost linearly with respect to the amount of

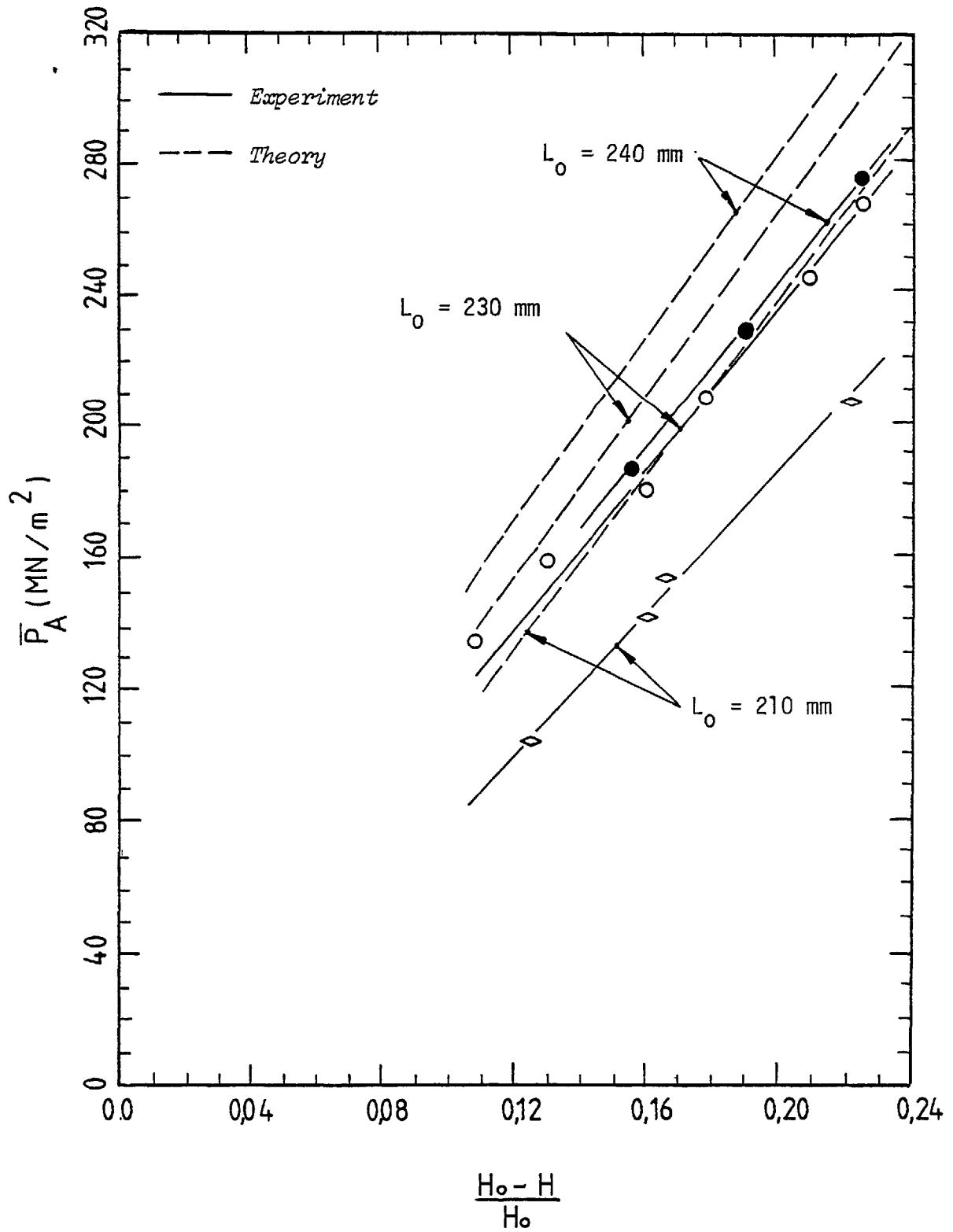
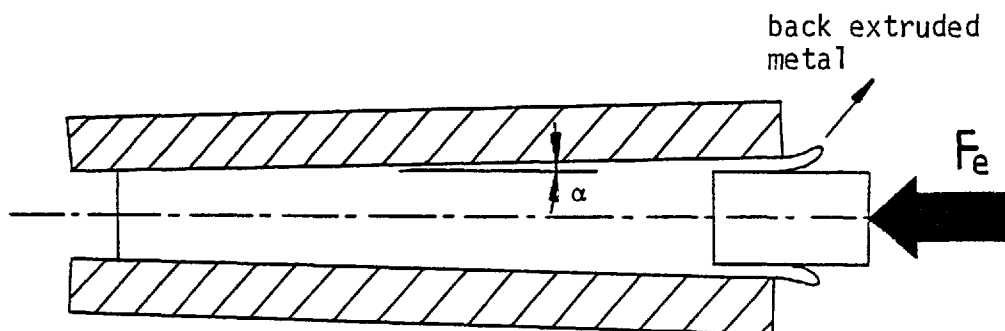


Fig. 4-23. Comparison of experimental and theoretical data.



indentation. When the amount of indentation is moderate, the experimental and theoretical curves are in good agreement. However, as the amount of indentation increases, particularly towards large values, the experimental curves deviate from those obtained theoretically. The deviation can be attributed to the shortcomings of the test-rig and to the numerous assumptions used in the theoretical solution. The following shortcomings whilst conducting the experiments were observed:

- 1- The conditions of plane strain during indentation of the billet were violated. In Fig. 4-23 a value of 0.225 for the amount of indentation is reported. As it was previously explained in 'Part I', if the indentation process had been subject to plane strain conditions the limiting value of 0.215 could not have been exceeded.
- 2- The chamber distorted in a non-uniform manner due to the high pressure induced at the top-end of the test-rig. Therefore the maximum drag-force, which in the theoretical solution was assumed to be dependent only on the frictional forces induced at the billet and chamber interface, was also dependent on the slight angle formed between the segments and the billet axis (see the illustration below).



- 3- The back extrusion of the billet into the gaps formed between the pad and chamber, created an additional drag-force, causing the measured end-load to be slightly higher than the actual drag-force developed between the billet and chamber.

The following assumptions in the theoretical solution may also have contributed to the deviation observed between the theoretical and experimental findings:

- 1- The billet material was assumed to be a rigid, perfectly plastic material. This can be regarded as a relatively unrealistic assumption since the billet material (even though lead) work-hardens depending on the extent of plastic deformation.
- 2- In the physical model, only regions '1' and '3' were assumed to exist along the billet. The elimination of region '2', by extending regions '1' and '3' towards each other, clearly increased the length of region '3' and thus the maximum pressure developed on the pad-face.
- 3- The principal planes were assumed to coincide with the internal faces of the segments. This, in practice, would certainly not occur since the frictional forces existing on the segment faces would cause the principal planes to rotate.
- 4- The contact widths ' $w_1$ ' and ' $w_2$ ' were assumed to be related to the amount of indentation by formulae based on the volume constancy assumption. In the next chapter it will be shown that such formulae predict variations for ' $w_1$ ' and ' $w_2$ ' which are slightly higher than those obtained by experiment. Had the experimental variations of ' $w_1$ ' and ' $w_2$ ' been substituted in Eq. (4.5), a longer length for region '1' would have been obtained, resulting in a decrease in the length of region '3' and in turn, a decrease in the maximum pressure

developed on the pad-face.

#### 4.17 Conclusions and further work

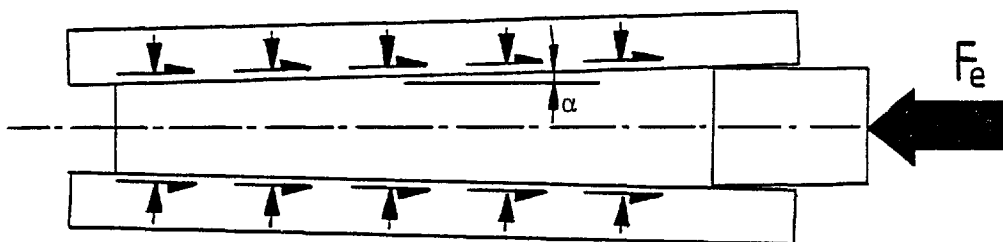
From the experimental and theoretical predictions the following conclusions can be drawn:

- 1- The magnitude of the drag-force developed between the billet and chamber was considerable when both the length of the billet and the initial amount of indentation were moderate. This automatically implies the possibility of achieving very large extrusion ratios through the process of Context.
- 2- The theoretical solution, based on a simple and straight-forward approach and using many simplifying assumptions, could well predict within a certain degree of accuracy the maximum pressure developed on the pad-face. The discrepancies, particularly at high amounts of indentation, will diminish even further if some of the assumptions are removed.

For any further work it is suggested:

- 1- To avoid the back extrusion of the billet in the gaps formed between the pad and segments. The back extrusion could be avoided, or at least minimised, either: i) by reinforcing the outer tube, in which case the segments will be restrained from excessive movements, or ii) by introducing a V-ring device, such as that used in direct conventional extrusion, to stop the flow of fluid between the punch and the container on the perimeter of the punch-tip, or of course by a combination of both i and ii. The drag-force developed between the billet and chamber can be determined more accurately if back extrusion of the billet is avoided.
- 2- To avoid the non-uniform distortion of the outer tube by

proportionately reinforcing it where distortion is higher. If this is done the drag-force will only be dependent on the frictional forces developed between the billet and the chamber. In the experiments carried out, the drag-force was not only dependent on the frictional forces developed but also on the slight unknown angle formed between the segment and the billet axis (see the illustration below).



- 3- To modify the test-rig by reinforcing the outer tube and the segments, or to design an entirely new test-rig in order to carry out similar experiments on billets with higher yield stress, such as aluminium, copper or mild steel.
- 4- A heating facility can be provided for the test-rig, e.g. by inserting heating coils around the outer-tube to enable experiments to be carried out at elevated temperatures.

## CHAPTER 5

### Results and discussions

#### 5.1 Introduction

In the present work the computer program presented in 'Chapter 3', section 3.5 was applied to a number of indentation processes. In the processes analysed, the effects on the deformation of the billet were studied when varying the shape of the billet, mechanical properties of the billet, configuration of the chamber, mode of indentation and boundary conditions. The processes analysed can conveniently be divided into the following cases (see Fig. 5-1 for illustrations):

Case (a) The chamber was assumed rectangular and comprised four platens. The moving platens were driven at equal speed in the direction indicated by the arrows in order to indent an initially round billet. During deformation the billet was assumed to be deformed by the vertical platens only.

Case (b) The chamber was assumed rectangular and comprised four platens, the moving platens being driven at equal speed to indent an initially round billet as above. In this case, the initial diameter of the billet was assumed to be equal to the distance between the stationary platens. In contrast to case (a), the stationary platens also contributed to the deformation of the billet.

Case (c) The chamber was assumed rectangular and comprised four platens, and all four platens were driven at equal speed in the direction indicated by the arrows to indent an initially round billet. In this case, all four platens equally contributed to the

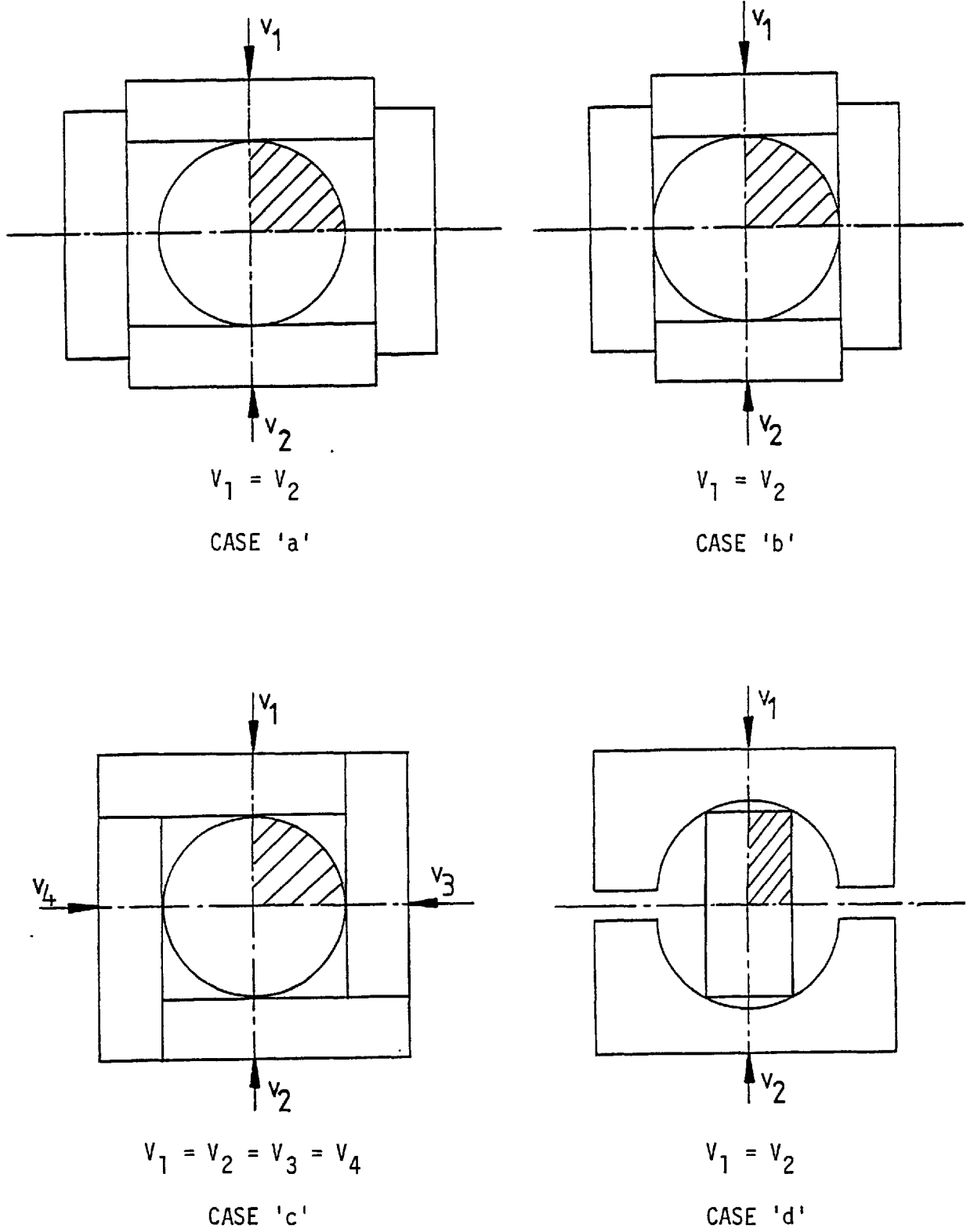


Fig. 5-1. Various kind of indentation analysed.

deformation of the billet.

Case (d) The chamber was circular and comprised two similar platens. The moving platens were driven inwards at equal speed to indent a billet with an initially rectangular cross-section. The indentation was continued until the platens were brought together.

For the analysis of these cases some prior investigations on the presented computer programs in 'Chapter 3' were conducted. From the preliminary computer runs the following conclusions were drawn:

- 1- In terms of computing time the program 'EPFEA2' was, for the same degree of accuracy, more economical than 'EPFEA1'.
- 2- The program 'EPFEA3' was, for the same number of elements, more demanding in terms of computer time than 'EPFEA2'. However, the results from 'EPFEA3' were found to be slightly more accurate than those from 'EPFEA2'.

For the analysis of the cases (a) to (d) mentioned above, the computer program 'EPFEA2', using quadrilateral elements, was used. The choice of program 'EPFEA2' was based on a compromise of the two factors of economy and accuracy.

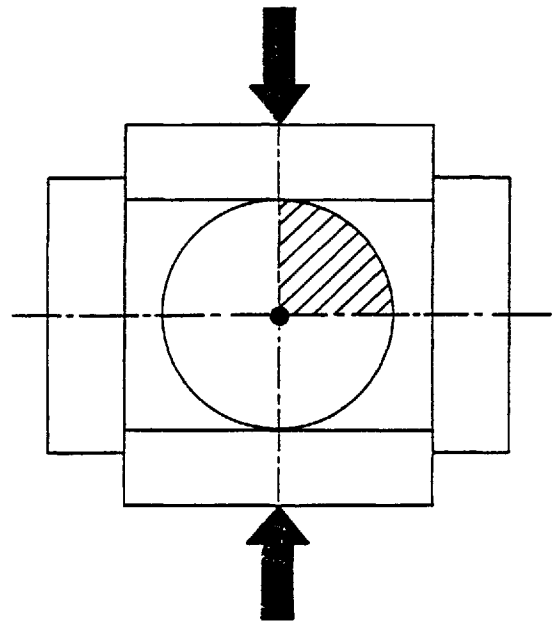
In what follows, the theoretical predictions for cases (a) to (d) for load versus displacement, current configuration of the billet, distribution of velocity, distribution of effective strain, etc., are presented and discussed. The theoretical predictions are then compared with the relevant experimental results where these are available. Although the theoretical prediction were in the main obtained from the finite element method, in some cases other methods of analysis were also used. In cases (a), (b) and (c), for instance, the current configuration of the billet was also obtained from the volume constancy assumption.

In cases (a) and (b), the mean normal pressure applied by the vertical platens was also determined respectively from the theories of slip-line field and upper-bound.

## 5.2 A study of case (a)

As described in section 5.1, the chamber was assumed to be rectangular and comprised four platens (see the illustration below).

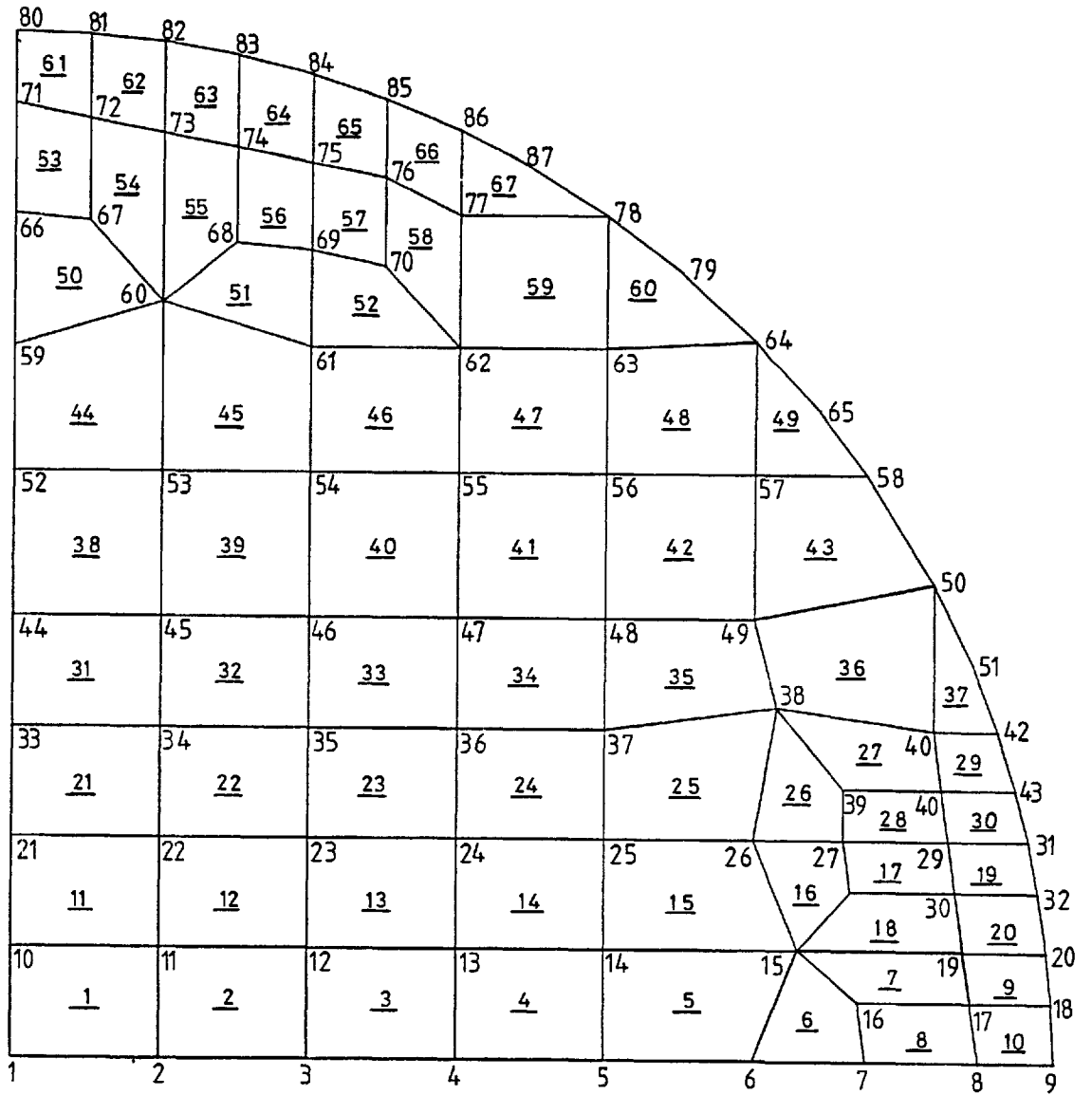
The moving platens were driven at equal speed in the direction indicated by the arrows to indent an initially round billet. The diameter of the billet was assumed smaller than the distance between the stationary platens, such that during indentation it would not come into contact with these platens.



In the computation, only one quarter of the billet cross-section was considered owing to the symmetry of the deformation. The mesh configuration (which was also used in cases 'b' and 'c') was comprised of 67 quadrilateral elements and 87 nodal points, see Fig. 5-2. As it can be seen in Fig. 5-2, finer divisions were provided in the regions where contacts were to occur since here the stresses produced in the billet were higher. Although the elements were numbered arbitrarily, the nodal points were numbered in such a way as to minimize the bandwidth of the overall stiffness matrix. The mesh used had a bandwidth of 34.

The stress-strain characteristics of commercially pure aluminium





67 quadrilateral elements  
87 nodal points

Fig. 5-2. Finite element mesh for a billet with round cross-section (quarter of cross-section shown).

and lead, shown in Figs. 5-3 and 5-4, were obtained from uniaxial compression tests. For the computer analysis, the stress-strain curve of the material was approximated by two straight lines. The material properties used in the computation were as follows:

For aluminium

$$E = 0.07 \times 10^6 \text{ MN/m}^2 \qquad \nu = 0.345$$

$$\bar{\sigma} = Y_0 + H_0 (\bar{\epsilon}_P) \qquad \text{for} \qquad 0.1 \geq \bar{\epsilon}_P \geq 0$$

$$\bar{\sigma} = Y_1 + H_0 (\bar{\epsilon}_P) \qquad \text{for} \qquad \bar{\epsilon}_P > 0.1$$

where  $Y_0 = 40 \text{ MN/m}^2$   $H_0 = 500 \text{ MN/m}^2$

$$Y_1 = 90 \text{ MN/m}^2 \qquad H_1 = 75 \text{ MN/m}^2$$

For lead

$$E = 0.01 \times 10^6 \text{ MN/m}^2 \qquad \nu = 0.431$$

$$\bar{\sigma} = Y_0 + H_0 (\bar{\epsilon}_P) \qquad \text{for} \qquad 0.05 \geq \bar{\epsilon}_P \geq 0$$

$$\bar{\sigma} = Y_1 + H_0 (\bar{\epsilon}_P) \qquad \text{for} \qquad \bar{\epsilon}_P > 0.05$$

where  $Y_0 = 6 \text{ MN/m}^2$   $H_0 = 180 \text{ MN/m}^2$

$$Y_1 = 15 \text{ MN/m}^2 \qquad H_1 = 26 \text{ MN/m}^2$$

The following parameters were calculated and recorded during the computation (see also the illustration below):

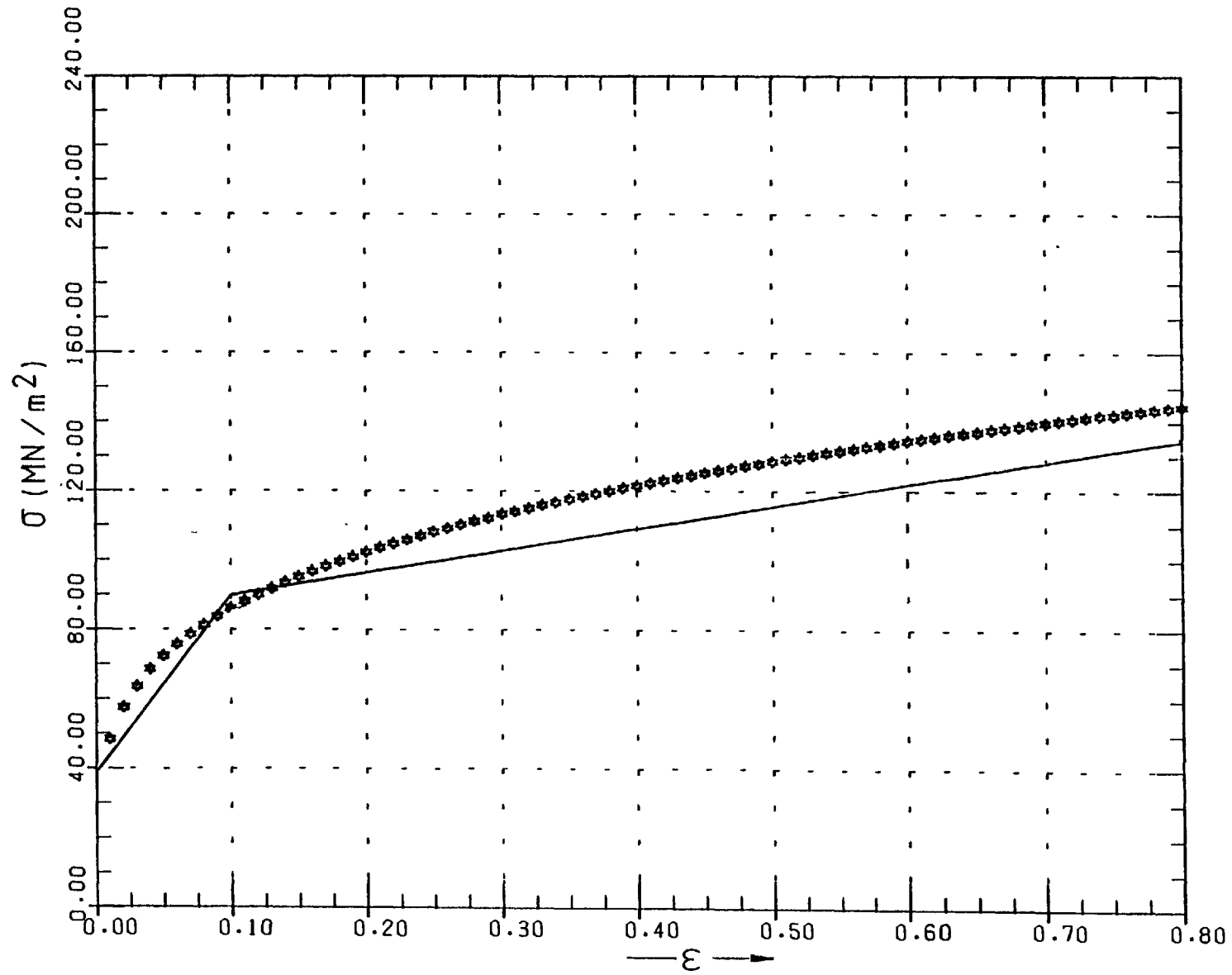


Fig. 5-3. Stress-strain curve for computer analysis of plane-strain indentation for commercially pure aluminium.

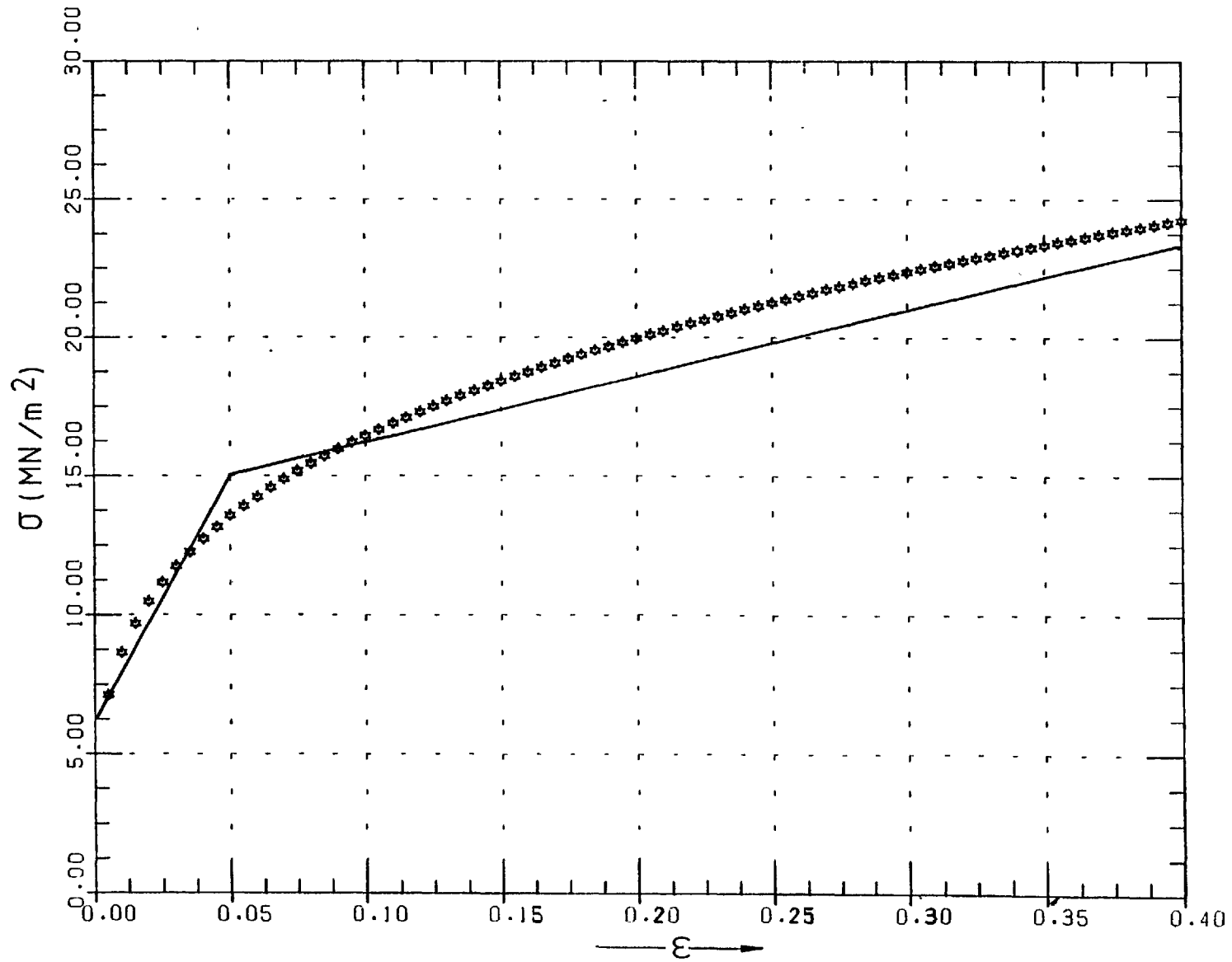


Fig. 5-4. Stress-strain curve for computer analysis of plane-strain indentation for commercially pure lead.

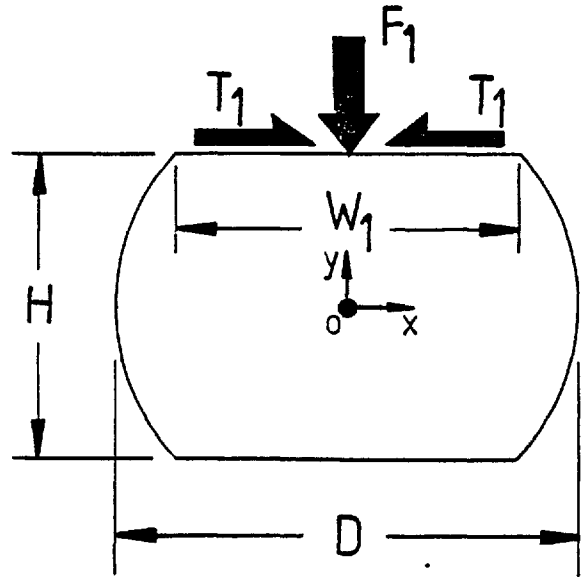
1-  $\frac{H_0 - H}{H_0}$  = amount of indentation.

2-  $\frac{W_1}{D_0}$  = non-dimensional width of the flat.

3-  $\frac{D - D_0}{D_0}$  = amount of increase in diameter 'D'.

4-  $\frac{F_1}{L_0 \times D_0}$  = indenting force in the y direction.

5-  $\frac{T_1}{L_0 \times D_0}$  = frictional force at billet/chamber interface in the x direction.



where  $D_0 = H_0$  = the initial diameter of the billet.

$L_0$  = the initial length of the billet.

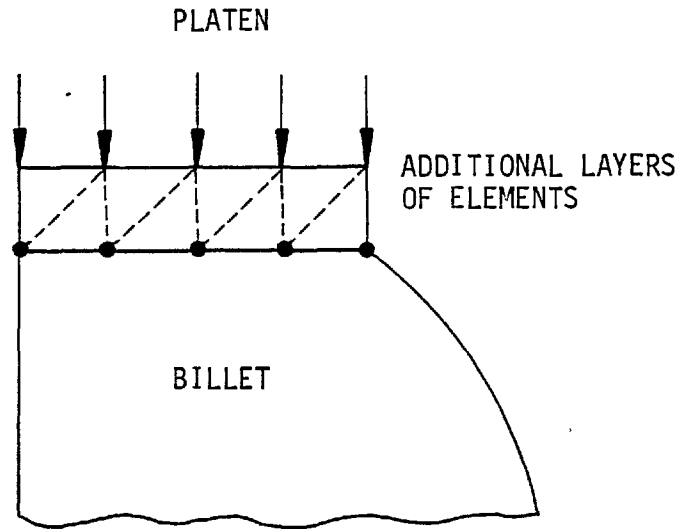
$D_0$  and  $L_0$  were arbitrarily taken as 20 and 10 mm respectively.

In the computation two types of boundary conditions were considered. In one type, nodal points in contact with the platen were permitted to move freely along the surface of the platen. In practice this condition prevails when the platens, in a well lubricated process, have a smooth surface. In the other type of condition, nodal points in contact with the platen were not permitted to move along the surface of the platen at all. In practice this condition prevails when the platens have a rough surface and is sometimes referred to as complete sticking. Although in the present study only these limiting boundary conditions (i.e. frictionless and complete sticking) were considered, any other types of friction

condition could also be considered by the technique outlined in (59). In that technique, a layer of elements is considered to exist between the contact area and the surface

of the platen as shown in the illustration. The properties of the layer are usually specified in the following way, using an interface factor

' $m$ ';  $\sigma_{YL} = m\sigma_{Yb}$ ,  $E_L = mE_b$ ,  
 $H'_L = mH'_b$ . Where  $\sigma_{Yb}$ ,  $E_b$  and  
 $H'_b$  are the material properties of the billet and  $\sigma_{YL}$ ,  $E_L$  and  
 $H'_L$  are those of the layer.



Various conditions of friction are imposed by the interface factor  $m$ ; with  $m=0$  there is no influence of the layer and with  $m=1$  influence of the layer is greatest (i.e. infinite stiffness). Although not considered here, the technique is easily adoptable without requiring major changes, to the formulation presented in Chapter 2.

### 5.2.1 Results obtained by the finite element method

The computed results using the material properties of aluminium are shown in Figs. 5-5-A to 5-5-D.

The relationship between the contact width  $W_1/D_0$  and the amount of indentation  $(H_0-H)/H_0$  is shown in Fig. 5-5-A. The reason for the steps in the calculated curve is due to the discrete manner in which the billet cross-section was divided into elements. Clearly, the continuity of the curve will increase by decreasing the element sizes along the free-surface. By decreasing these element sizes the consecutive nodes

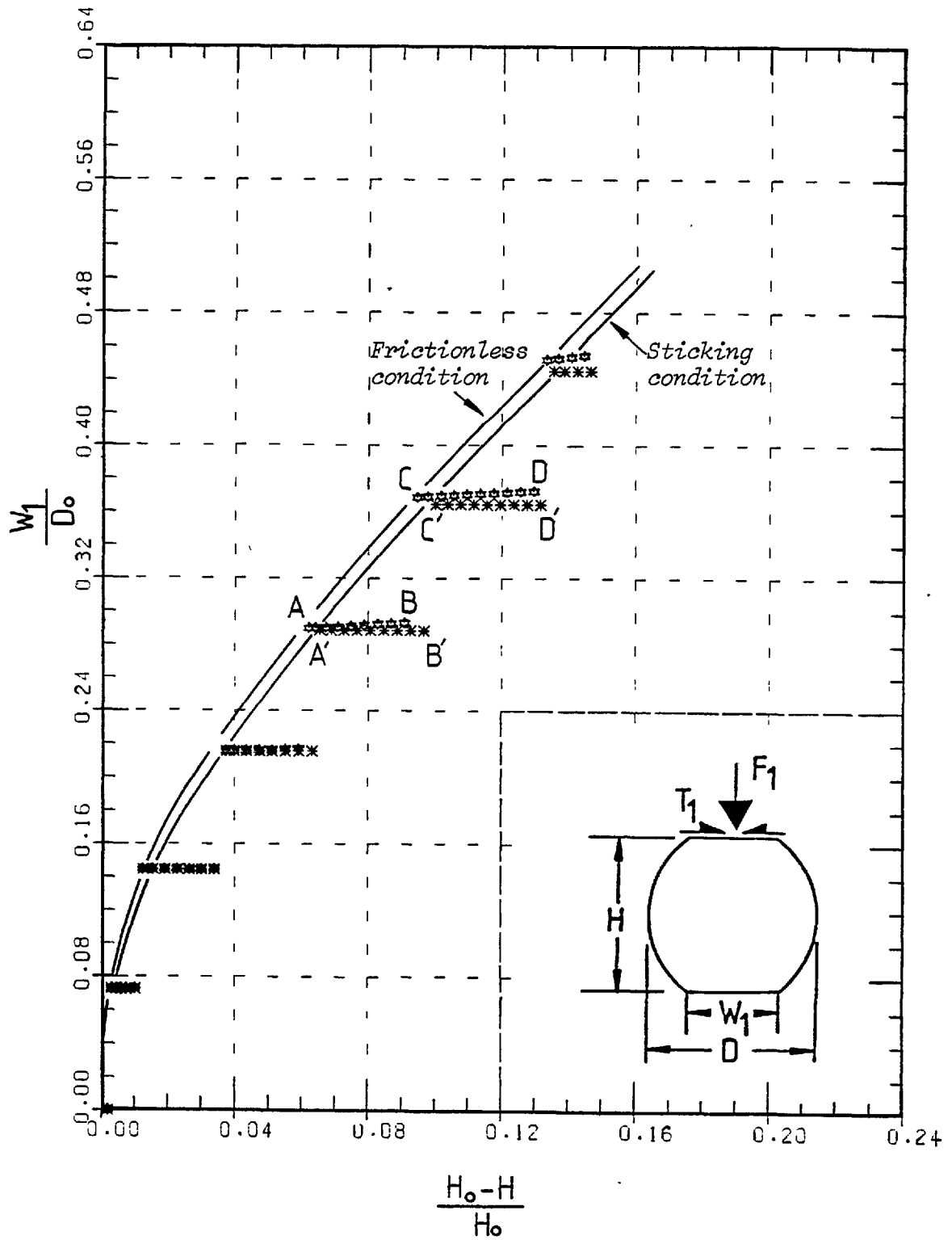


Fig. 5-5-A. Variation of contact width ' $W_1$ ' with height ' $H$ ' for commercially pure aluminium obtained by the finite element method.

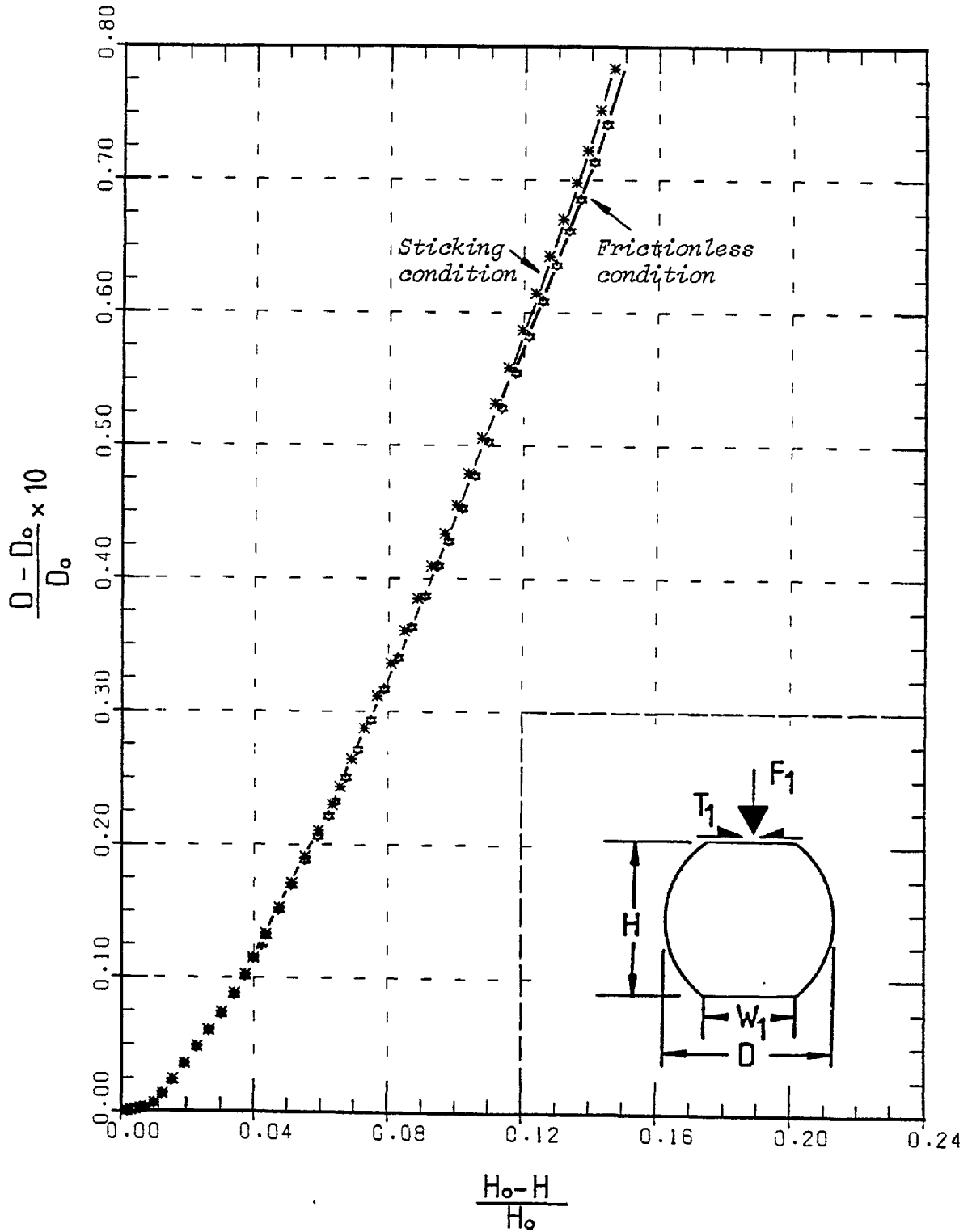


Fig. 5-5-B. Variation of diameter 'D' with height 'H' for commercially pure aluminium obtained by the finite element method.



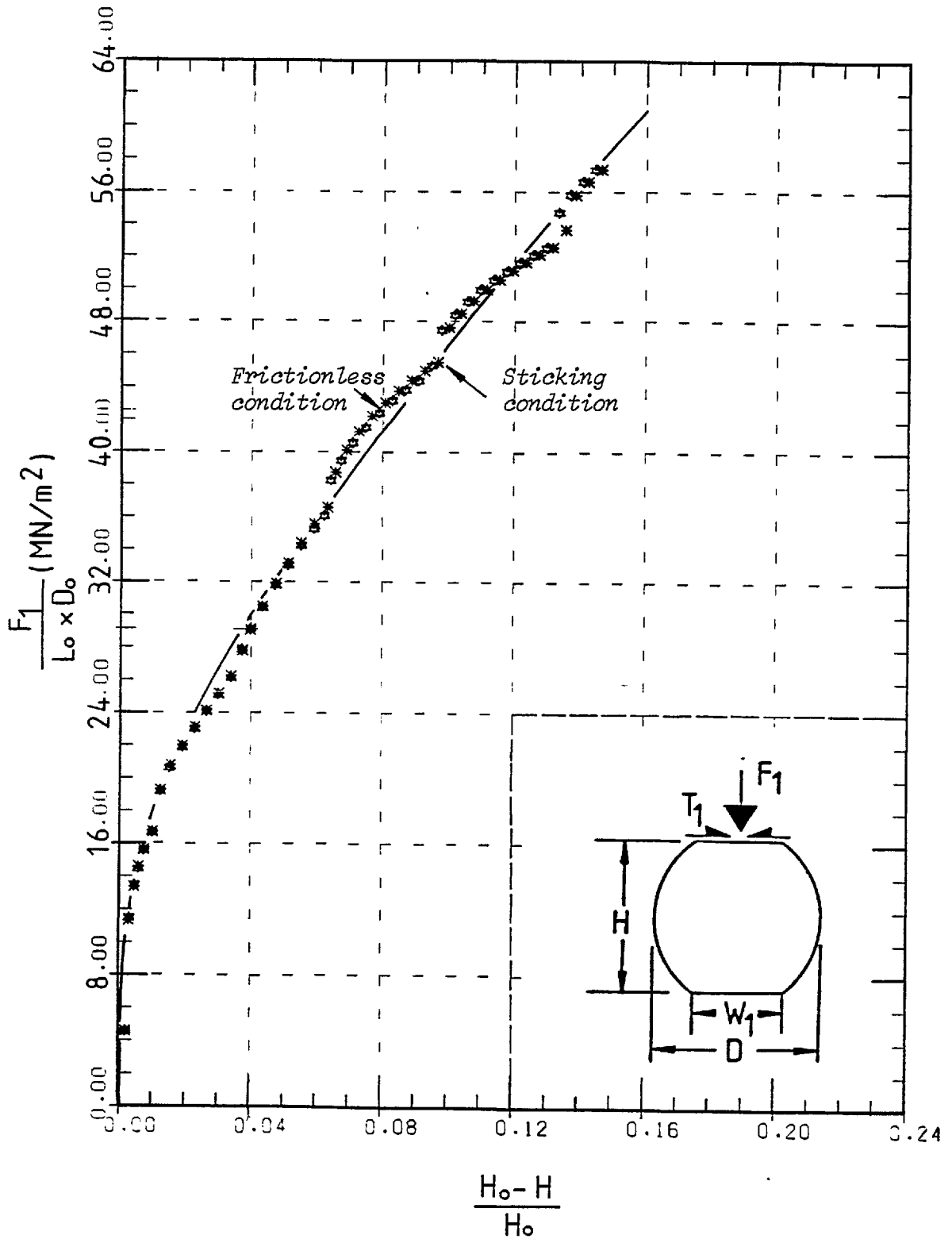


Fig. 5-5-C. Variation of indenter force ' $F_1$ ' with height ' $H$ ' for commercially pure aluminium obtained by the finite element method.

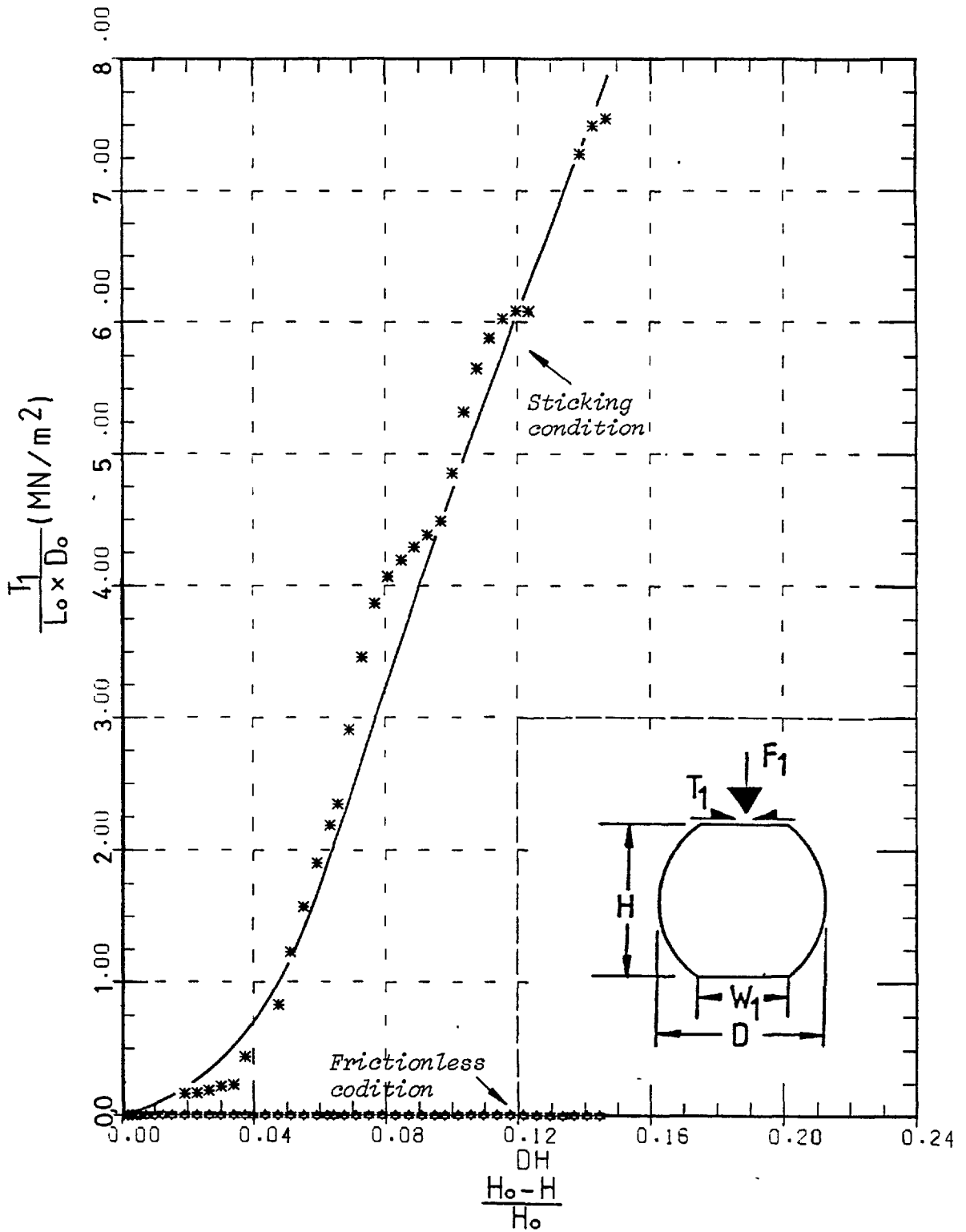


Fig. 5-5-D. Variation of interfacial frictional force ' $T_1$ ' with height ' $H$ ' for commercially pure aluminium obtained by the finite element method.

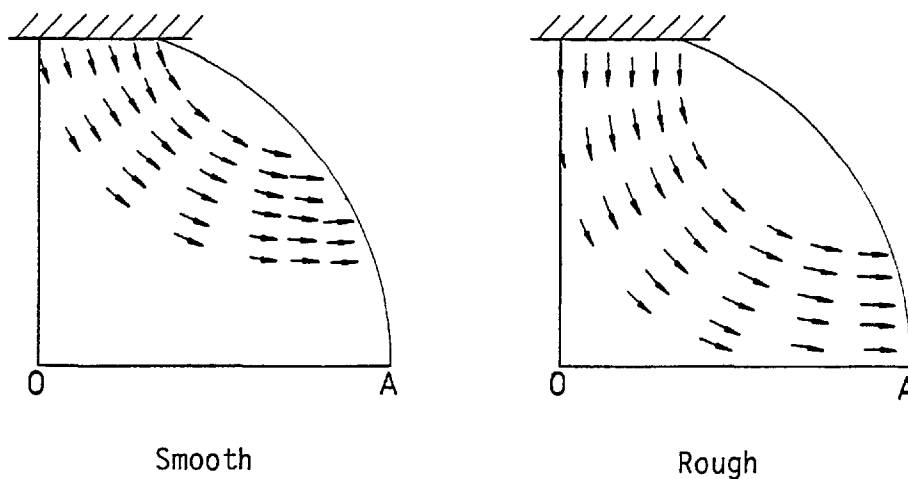
along the free-surface will be closer, and thus increments in contact width will be smaller whenever a nodal point comes into contact with the platen.

In the finite element model of the billet, deformation was produced by the displacement of those nodal points lying on the line of contact with the top platen. The contact width therefore changes in a stepwise manner whenever a new node makes contact with the top platen. In Fig. 5-5-A, the lines such as AB represent the period through which the number of nodes which take part in the deformation remains constant. At a point B where a new node contacts the platen, another line, CD is started. If the platen is assumed to be smooth, on moving from A to B, the contact width increases by an amount depending on the tendency of the contact nodes to move along the platen surface. The greater this tendency is, the higher will be the frictional force when the platen is partially or completely rough.

As described above, the discontinuity of the curves shown in Fig. 5-5-A is due to the finite size of the elements along the free-surface. Clearly, if the elements were of infinitesimal size, then the continuous curves illustrated would have been obtained. These continuous curves pass through points  $\dots, A, C, \dots$  or  $\dots A', C', \dots$  depending on the roughness of the platens. As expected, the contact width  $W_1$  for a particular height  $H$  is larger for the frictionless case than for a perfectly rough platen.

The relationship between  $(D-D_0)/D_0$  and the amount of indentation is shown in Fig. 5-5-B. At first, the curve rises very slowly, and this rise corresponds to that interval through which plastic deformation occurs entirely in the material close to the top platen. The curve later rises rapidly when plastic deformation propagates through the

material between the platens. The effect of friction, particularly at high amounts of indentation, is clearly shown by the slight rise in the curve. The effect of friction on the variation of billet diameter 'D' can be explained by revealing the pattern of deformation through the billet cross-section. The flow patterns established by a smooth and a rough platen are shown in the illustrations.



A smooth platen establishes a shallow stream of metal flow which is immediately diverted away from the axis of the platens. However, a rough platen establishes a deeper flow which is diverted midway between the platens. Clearly the diameter of the billet 'D' ( $=2 \times \overline{OA}$ ) sustains higher deformation when the metal flow is deeper.

The relationship between the indenting force  $F_1 / (L_0 \times D_0)$  and the amount of indentation  $(H_0 - H) / H_0$  is shown in Fig. 5-5-C. The effect of friction on the indenting force  $F_1$  is negligible, despite a rather significant frictional force induced at the interface of the billet and platen, see Fig. 5-5-D. The negligible effect of friction on the indenting force is perhaps due to the fact that the effect of a deeper flow established by a rough platen offsets the effect of larger contact

width obtained for a smooth platen. It is quite clear that a higher indenting force will be required if a deeper flow of metal is to be established, or if a billet with a greater contact width is to be indented.

The manner in which the original mesh, shown in Fig. 5-2 was distorted after an average amount of indentation of 0.145 is shown in Fig. 5-7. The distorted mesh for smooth platens is shown in Fig. 5-7-A. Comparing this with the original mesh it becomes clear that angular distortion, and hence shear strain and shear stress within those elements adjoining the platen, increases in moving outwards along the contact width. The elements with the highest angular distortions, the marked elements, are those positioned between the centre of the billet and the edge of the contact width. As will be discussed later in the application of the slip-line theory, one of the velocity discontinuities in the slip-line field passes through these (the marked) elements with highest angular distortion. The unmarked elements, particularly those positioned on the right hand-side of those marked, are either distorted slightly or not at all. The distorted mesh for completely rough platens is shown in Fig. 5-7-B. In general, the distortion of the elements is identical to that shown in Fig. 5-7-A for a smooth platen, except that the elements adjoining the platen are slightly less distorted than those in Fig. 5-7-A.

The flow patterns for the indentation of a round billet by a smooth and a rough platen are shown in Figs. 5-8 and 5-9 respectively. In the computation the velocity of the platen was assumed to be -1. In Fig. 5-8, the flow field established by a smooth platen is shown. The speed of the metal particles increases slightly above the speed of the platen in moving outwards along the contact width. Along the

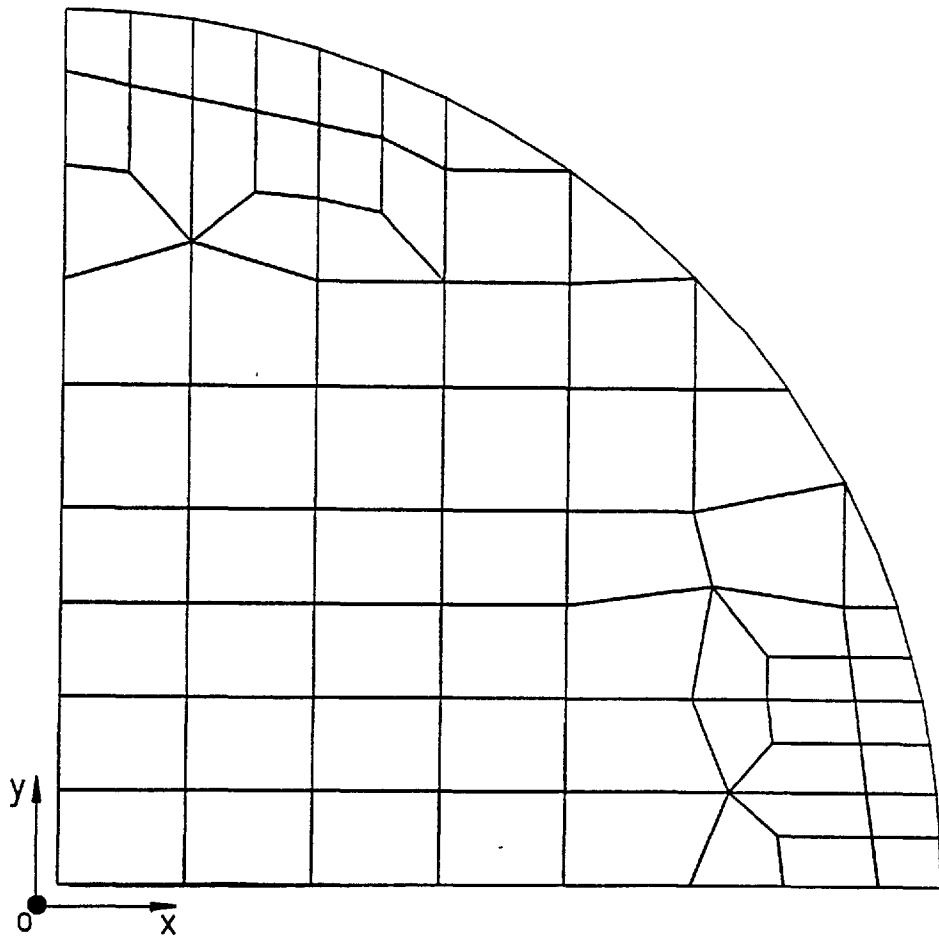


Fig. 5-6. Original finite element mesh.

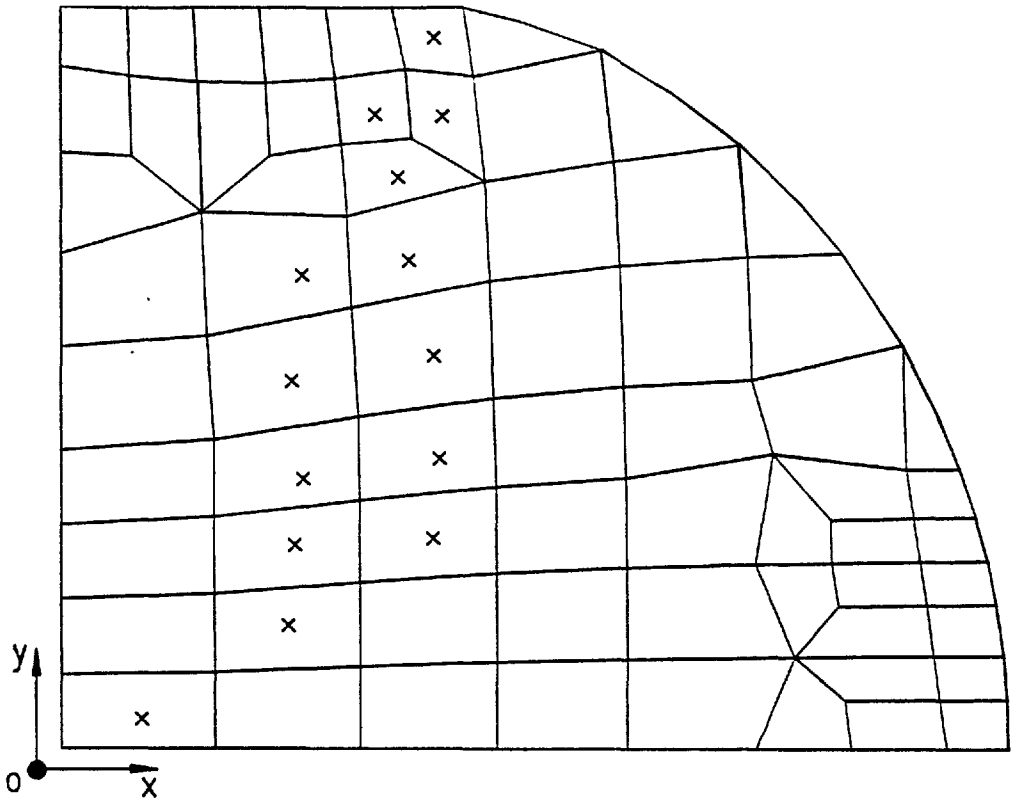


Fig. 5-7-A. Deformation of original mesh in frictionless condition at  $(H_0 - H)/H_0 = 0.145$ .

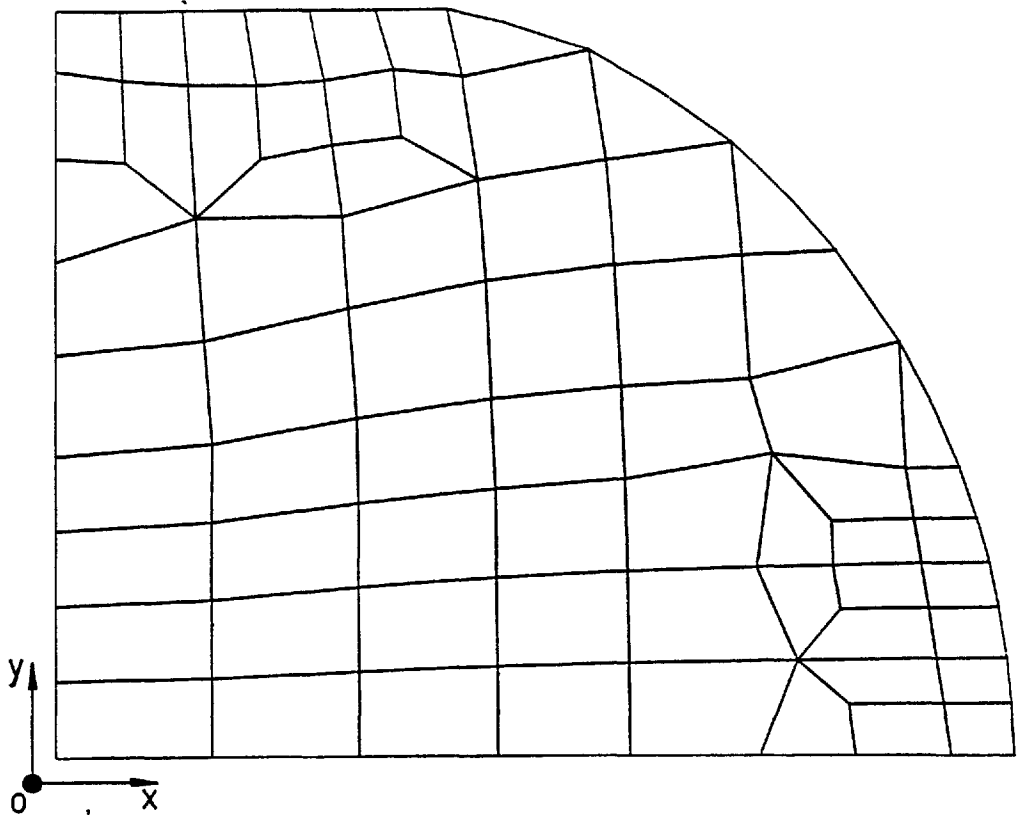
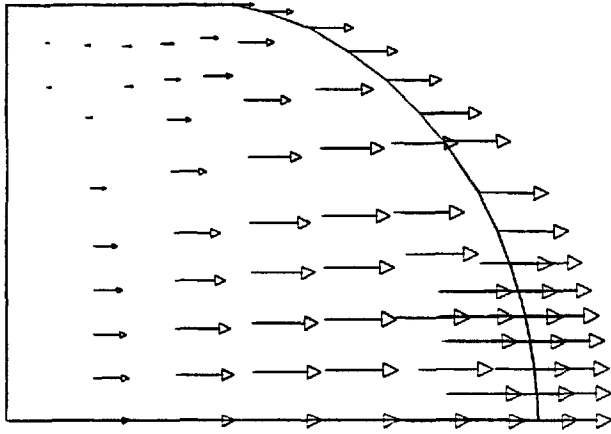
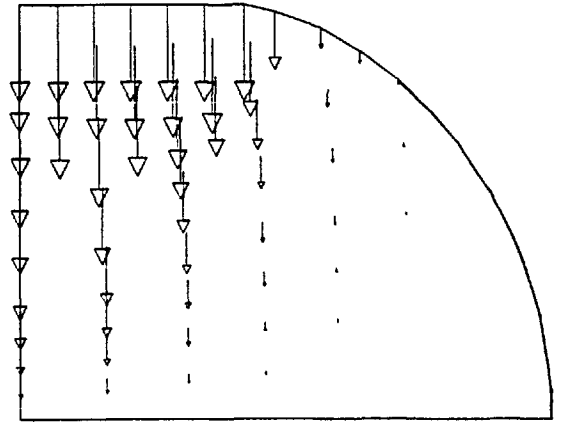


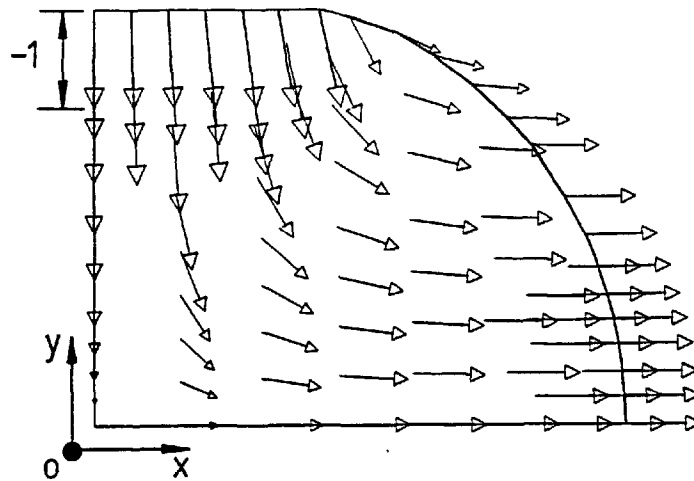
Fig. 5-7-B. Deformation of original mesh in sticking condition at  $(H_0 - H)/H_0 = 0.145$ .



Components of velocity vectors in the x direction



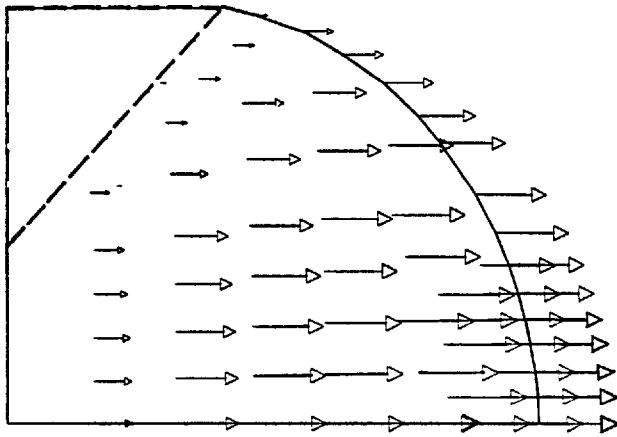
Components of velocity vectors in the y direction



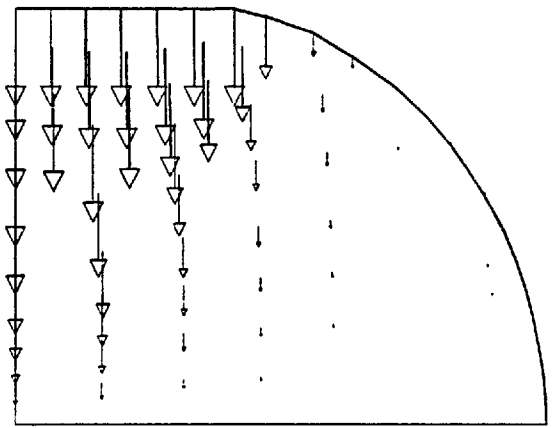
Absolute velocity vectors

Fig. 5-8. Flow pattern at  $(H_0-H)/H_0=0.145$  in frictionless condition, velocity of the platen being -1.

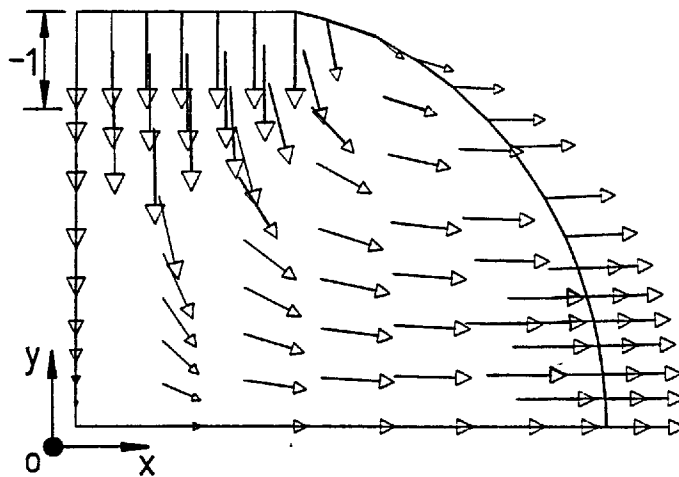




Components of velocity vectors in the x direction



Components of velocity vectors in the y direction



Absolute velocity vectors

Fig. 5-9. Flow pattern at  $(H_0 - H)/H_0 = 0.145$  in sticking condition, velocity of the platen being -1.

free-surface the velocity vectors are in general in the x direction. The speed along the free-surface first increases, and later becomes uniform, particularly near the right bottom corner. The flow field established by a rough platen is shown in Fig. 5-9. The major effect of friction on the flow pattern is perhaps the appearance of a rigid region near the top platen which is shown in dotted lines. All the particles within this region move in the y direction and with the same speed as the platen.

The distribution of effective strains for the case when the billet is indented by a smooth platen is shown in Fig. 5-10-A. The largest effective strains occur at the billet centre and near the edge of the contact surface. In the neighborhood of the platen the effective strain increases towards the free-arc of the billet. Half-way between the platens the effective strain decreases towards the free-arc and it becomes zero-near the billet surface. In this field the least strained region is positioned just beneath the surface of the billet. Comparing Figs. 5-10-A and 5-10-B it becomes clear that the effect of friction on the distribution of effective strain is negligible.

### 5.2.2 Results obtained from volume constancy

The current configuration of the billet can be determined from volume constancy by assuming the behaviour of the free-surface of the billet. Perhaps the simplest assumption (which is almost in agreement with the flow fields shown in Figs 5-8 and 5-9 obtained by the finite element method) is that the free-surface will remain undeformed during the course of indentation. As the deformation is symmetrical with respect to the x axis (see the illustration below) it is concluded that during such deformation the centre of the free-surface will remain on this

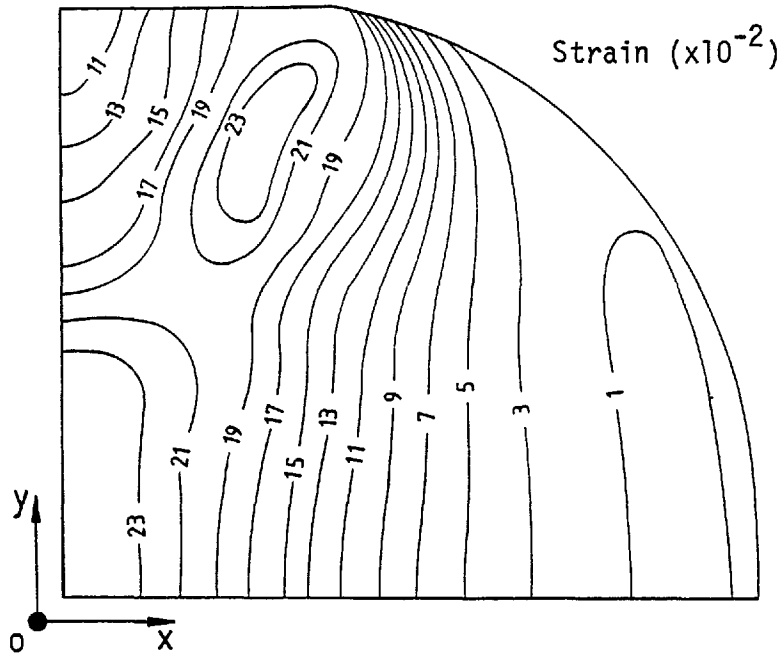


Fig. 5-10-A. Distribution of effective strain at  $(H_0-H)/H_0=0.145$  in frictionless condition.

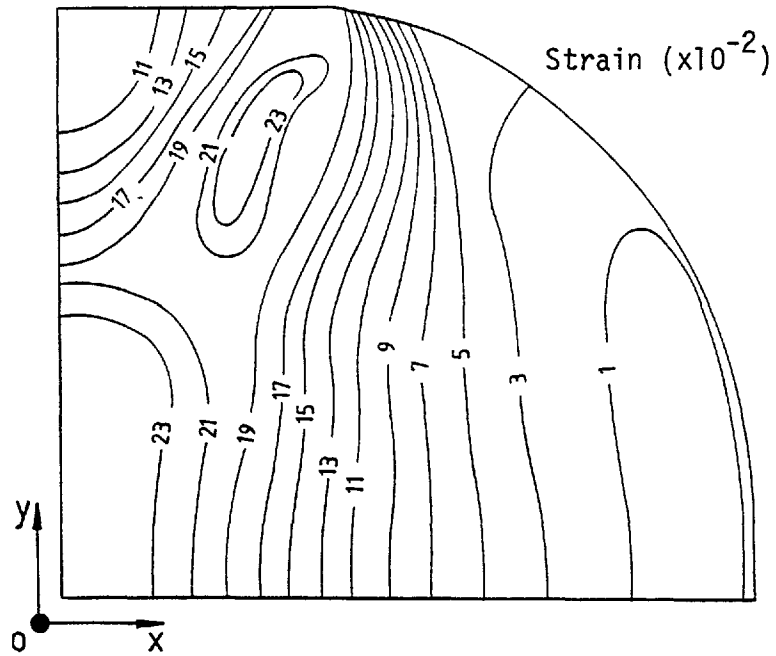
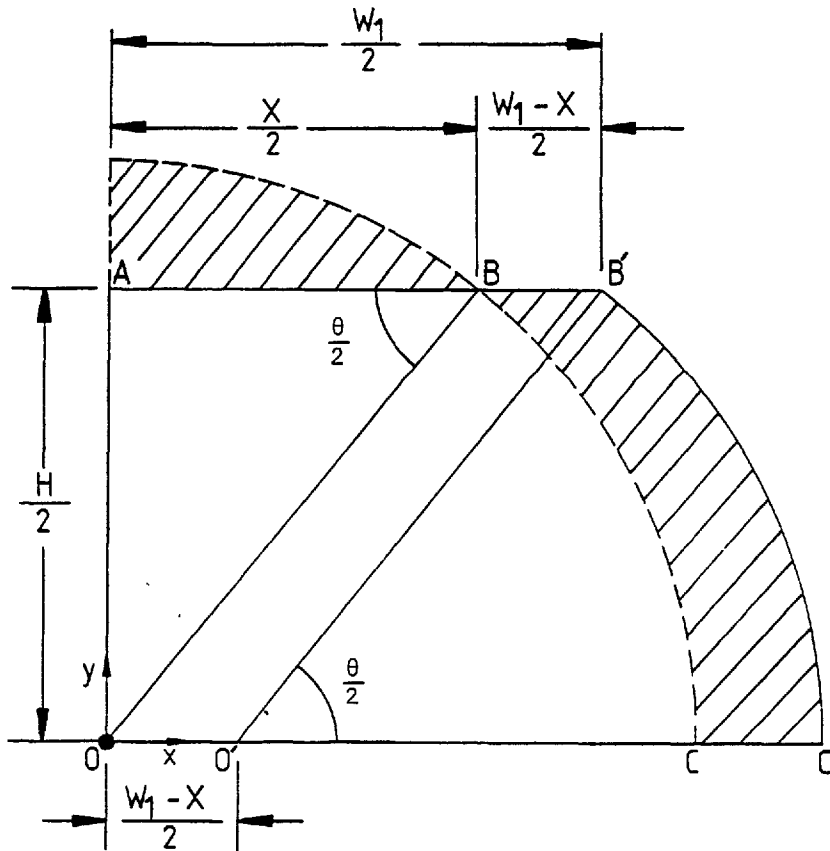


Fig. 5-10-B. Distribution of effective strain at  $(H_0-H)/H_0=0.145$  in sticking condition.

axis of symmetry. The original and final cross-sections of the billet are shown in the illustration.



As it was assumed that the free-surface will remain undeformed, every point lying on this surface will move by the same amount as the centre of the surface itself. The new position of the centre of the free-surface can therefore be determined by drawing the line  $B'O'$  parallel to  $BO$ . If the initial radius of the billet is  $R_0$ , then from volume constancy

$$\frac{1}{4} \pi R_0^2 = \frac{1}{2} R_0^2 \left(\frac{\theta}{2}\right) + \frac{1}{2} \frac{H}{2} \left(\frac{2W_1 - H}{2}\right)$$

where the first and second terms are the areas of the sector  $O'B'C'$  and the trapezoid  $OAB'C'$ , respectively.

On simplifying the above equation

$$H W_1 = R_o^2 \left[ \frac{1}{4} \pi - \left( \theta - \frac{H X}{2R_o^2} \right) \right] \quad (5.1)$$

but 
$$H = 2R_o \sin\left(\frac{\theta}{2}\right) \quad (5.2)$$

and also 
$$X = 2R_o \cos\left(\frac{\theta}{2}\right) \quad (5.3)$$

Substituting Eqs. (5.2) and (5.3) in Eq. (5.1) yields

$$H W_1 = R_o^2 \left[ \frac{1}{4} \pi - (\theta - \sin \theta) \right]$$

or 
$$W_1 = \frac{R_o^2}{H} \left[ \frac{1}{4} \pi - (\theta - \cos \theta) \right] \quad (5.4)$$

where 
$$\theta = 2 \sin^{-1}\left(\frac{H}{R_o}\right) \quad (5.5)$$

By solving Eqs. (5.4) and (5.5), the contact width ' $W_1$ ' is determined. Having determined ' $W_1$ ', from Eq. (5.3) and using  $D = D_o + W_1 - X$ , the values of ' $X$ ' and ' $D$ ' can also be determined. These values may then be used to compute  $W_1/D_o$ ,  $X/D_o$  and  $(D-D_o)/D_o$ . The computed results are shown in Figs. 5-11 and 5-12. The relationships between  $W_1/D_o$  and  $(H_o-H)/H_o$  and also between  $X/D_o$  and  $(H_o-H)/H_o$  are shown in Fig. 5-11. The difference between the two curves represents that portion of contact width which has been produced by the displaced material. As shown the contribution of this portion to the contact width increases as the amount of indentation increases. When the billet

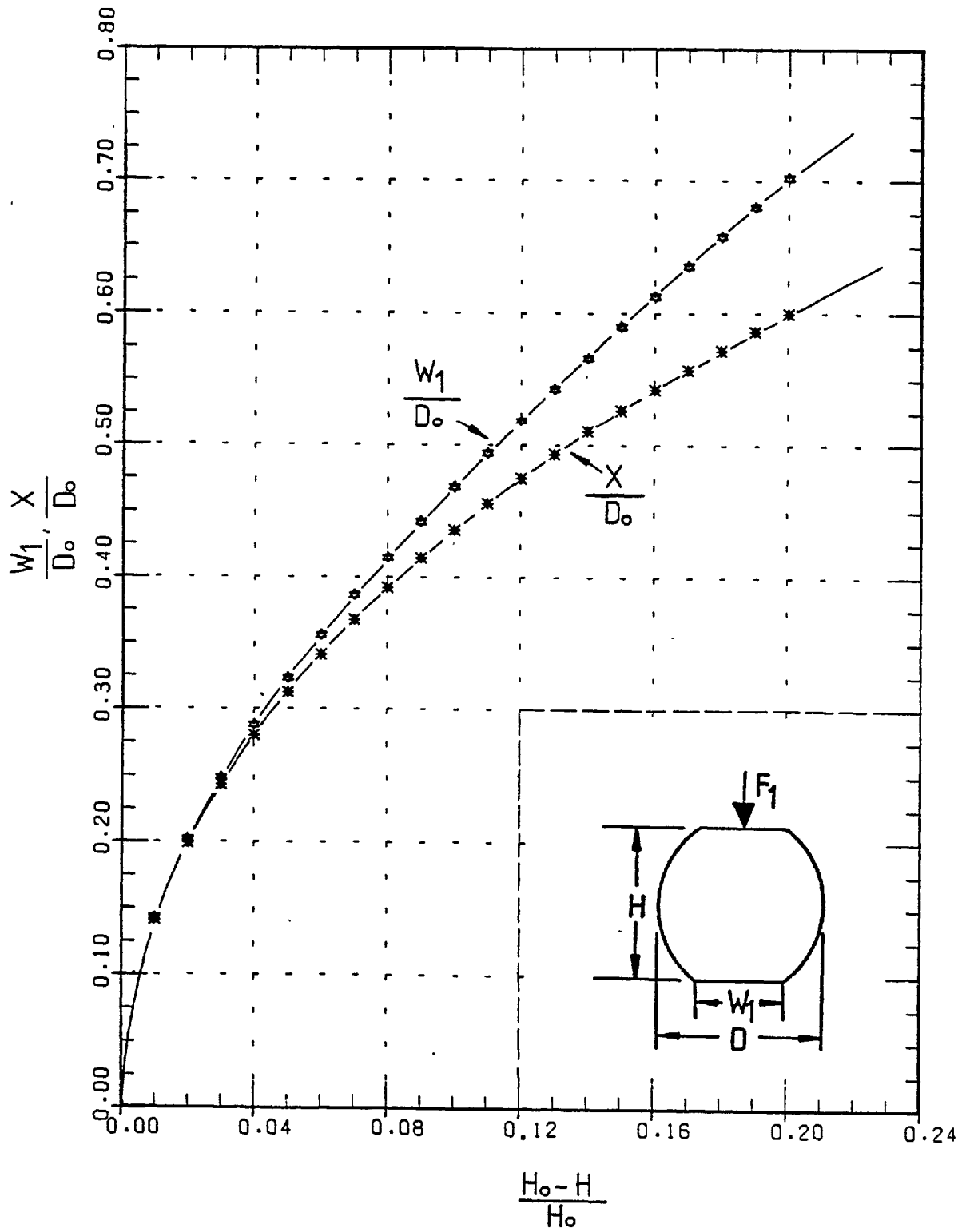


Fig. 5-11. Variations of contact width ' $W_1$ ' and of parameter ' $X$ ' with height ' $H$ ' obtained by the volume constancy assumption.

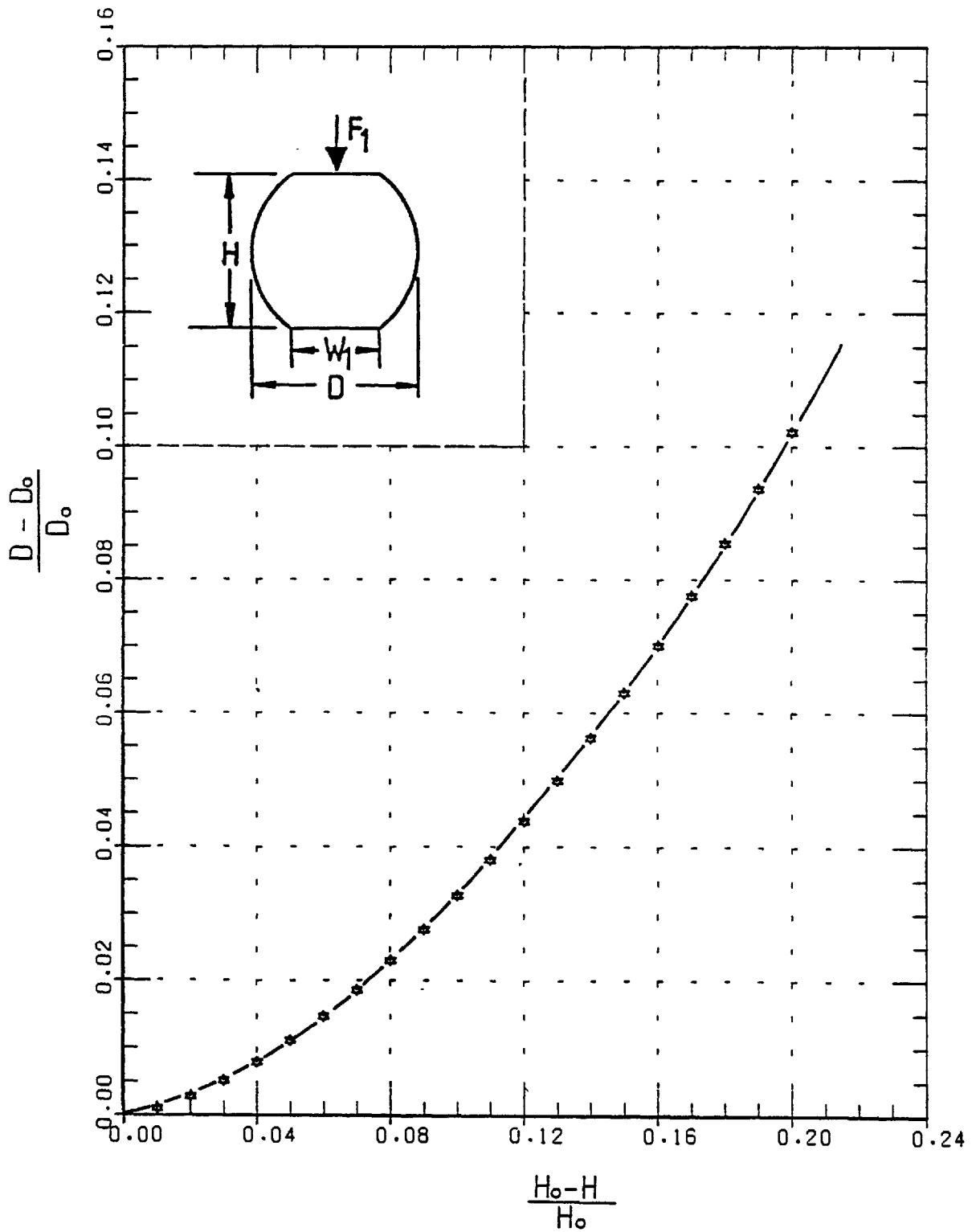


Fig. 5-12. Variation of diameter 'D' with height 'H' obtained by the volume constancy assumption.

is highly indented the contact width will increase drastically, since any small movement of the platen causes a large volume of material to be displaced.

By applying Eq. (5.4), the current configuration of the billet during the course of indentation can be determined. To substantiate the assumption that the free-surface of the billet during indentation remains undeformed, the current billet configuration determined from Eq. (5.4) can be compared with the corresponding one obtained from experiment.

In an experiment which was conducted, a number of points were selected on the periphery of a section situated at the central region of the billet. The billet was incrementally indented and the current positions of the selected points were measured and recorded. The theoretical predictions together with the current positions of the experimental points during the course of indentation are shown in Fig. 5-13. At the beginning of the indentation process the current positions of the experiment points well coincide with the surface predicted from volume constancy. Later, however, the experimental points, particularly those near the contact with the platen, deviate from the predicted surface. At all stages of deformation the experimental points define an area which is slightly smaller than that defined by the theoretical solid line. The discrepancy observed, particularly when the amount of indentation is high, is due to the slight violation of plane strain conditions in the experiments and also to some plastic deformation of the free-surface occurring during the course of indentation. It is worth noting that the movement of the free-surface obtained by experiment is in agreement with that obtained from the finite element method, see Figs. 5-8 and 5-9. There the upper



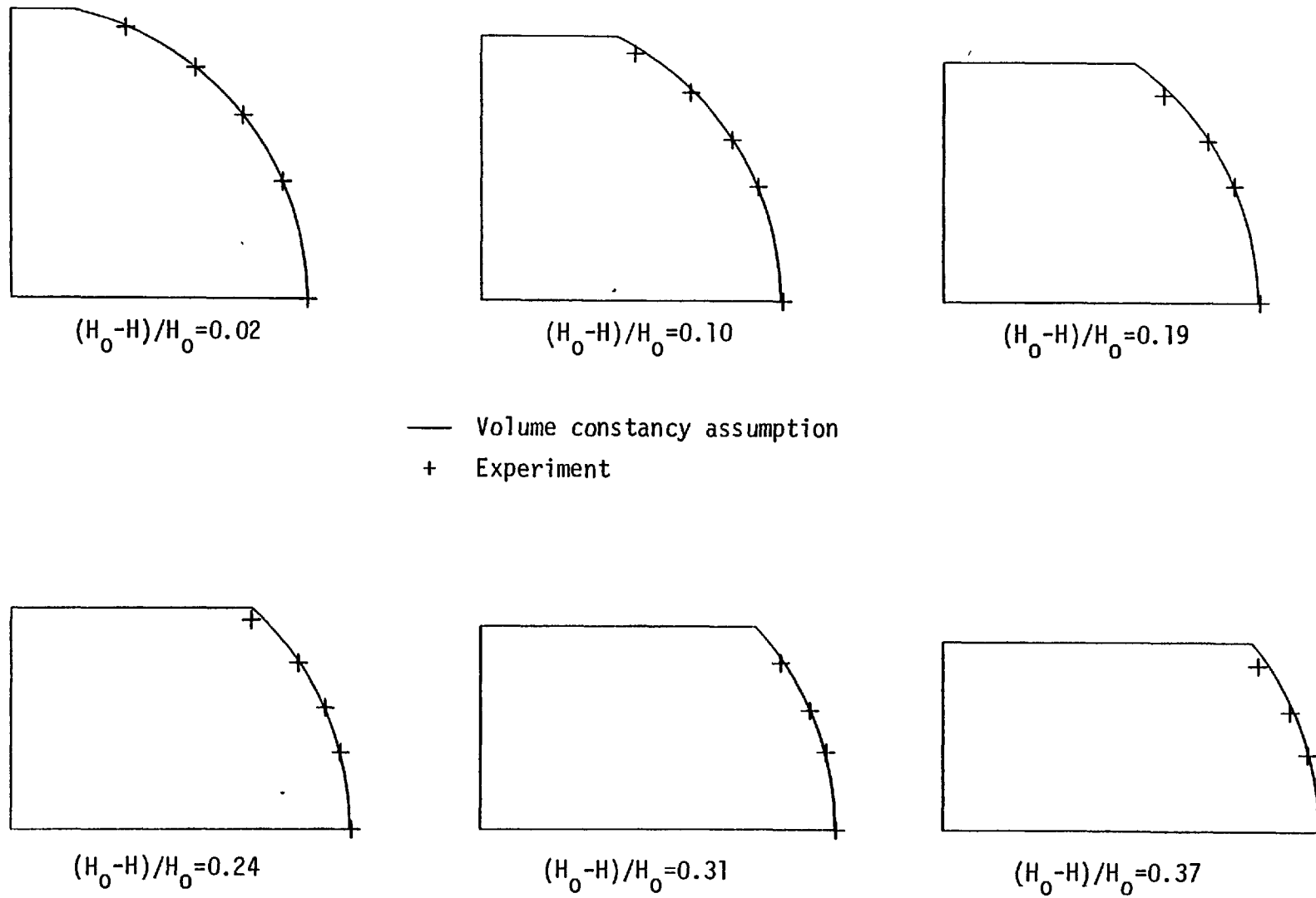


Fig. 5-13. Comparison of billet configurations obtained by the volume constancy assumption and experiment at various heights, 'H'.

part of the free-surface moves more slowly than the lower part.

### 5.2.3 Results obtained from slip-line theory

In a well lubricated process, in which the interfacial frictional forces are absent, the indenting force ' $F_1$ ' during the course of indentation can be determined by applying the slip-line theory. In the problem of billet indentation three types of deformation must be distinguished depending on the amount of indentation. When the amount of indentation is sufficiently small plastic deformation occurs only in the material adjacent to the platen. The well-known slip-line field (usually referred to as type I) for this kind of deformation is shown in Fig. 5-14. Here, since the process is assumed to be frictionless, the slip-lines meet the surface of the platen at  $45^\circ$ . Due to the absence of shear stress on the free-surface the slip-lines also meet the free-surface of the billet at  $45^\circ$ . The indenting force ' $F_1$ ' can be determined as follows:

Using Hencky's equation along  $\alpha$ -line CBA

$$P_A - P_C = 2k \phi_{AC} \quad \therefore \quad P_C = P_A - 2k \phi_{AC}$$

but  $P_A = -k$  and  $\phi_{AC} = \phi_A - \phi_C = \frac{\pi}{2} - \psi$ . Thus

$$P_C = -k - 2k \left( \frac{\pi}{2} - \psi \right).$$

For the  $y$  direction, the equilibrium equation for the infinitesimal element DCE becomes

$$dF_1 + P_C d\omega - k d\omega = 0$$

On substituting for  $P_C$  and integrating along the contact width

$$\int_0^{W_1} dF_1 + 2 \int_0^{\frac{W_1}{2}} [-k - 2k(\frac{\pi}{2} - \psi)] d\omega - 2 \int_0^{\frac{W_1}{2}} k d\omega = 0$$

or after simplification

$$F_1 = 2k W_1 + 2k \frac{\pi}{2} W_1 - 2k \int_0^{\frac{W_1}{2}} \psi d\omega \quad (5.6)$$

The indenting force  $F_1$  is normally expressed in terms of mean normal pressure  $P_1$ . Thus, from  $F_1 = P_1 W_1$

$$P_1 W_1 = 2k W_1 + 2k \frac{\pi}{2} W_1 - 2k \int_0^{\frac{W_1}{2}} \psi d\omega$$

or

$$\frac{P_1}{2k} = 1 + \frac{\pi}{2} - \frac{1}{W_1} \int_0^{\frac{W_1}{2}} \psi d\omega \quad (5.7)$$

in which the integral must be evaluated along the free-surface of the billet as shown in Fig. 5-14. This solution is valid up to the point at which the stress field due to the upper platen begins to influence the stress field due the lower platen. Plastic deformation then occurs in the material between the platens, and the ends of the billet move apart as rigid masses. The well-known slip-line (referred to as type II) for this kind of deformation is shown in Fig. 5-15. Here again the slip-lines meet the surface of the top platen at  $45^\circ$ . Due to the absence of shear stress along the horizontal axis of the billet, the slip-lines also meet this axis at  $45^\circ$ . The indenting force ' $F_1$ ' can be determined as follows:

Using Hencky's equation for  $\beta$ -line OB, the pressure P can be expressed as

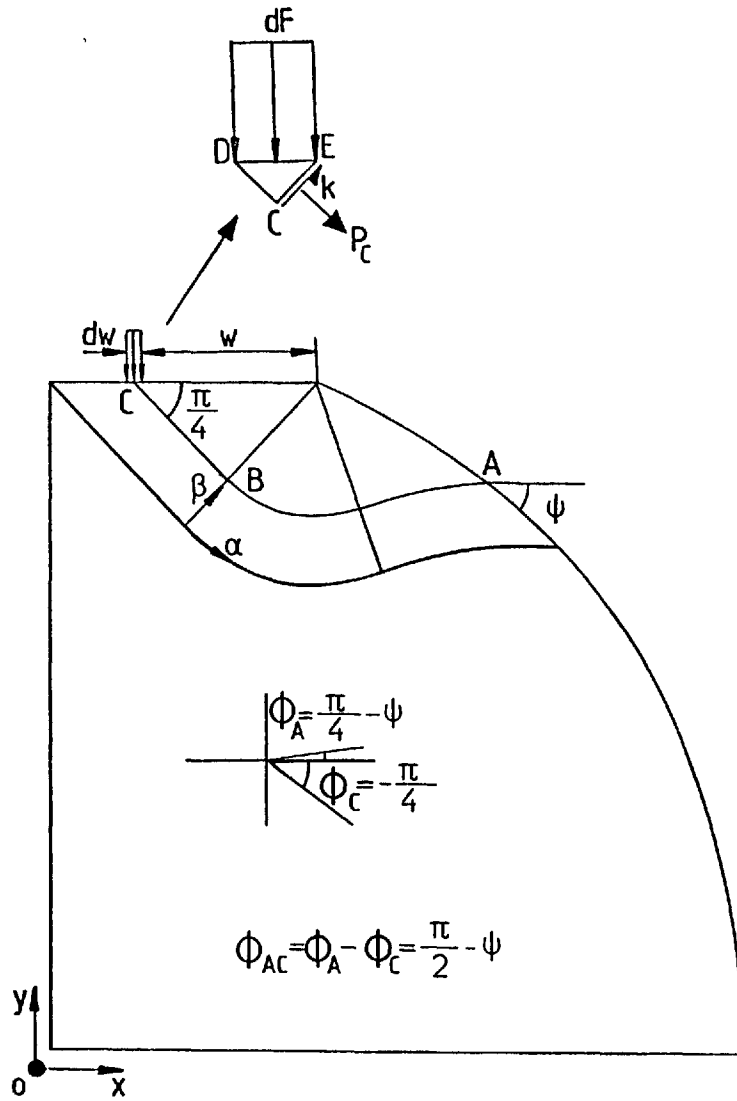


Fig. 5-14. Slip line field when  $(H_0 - H)/H_0$  is sufficiently small (type I).

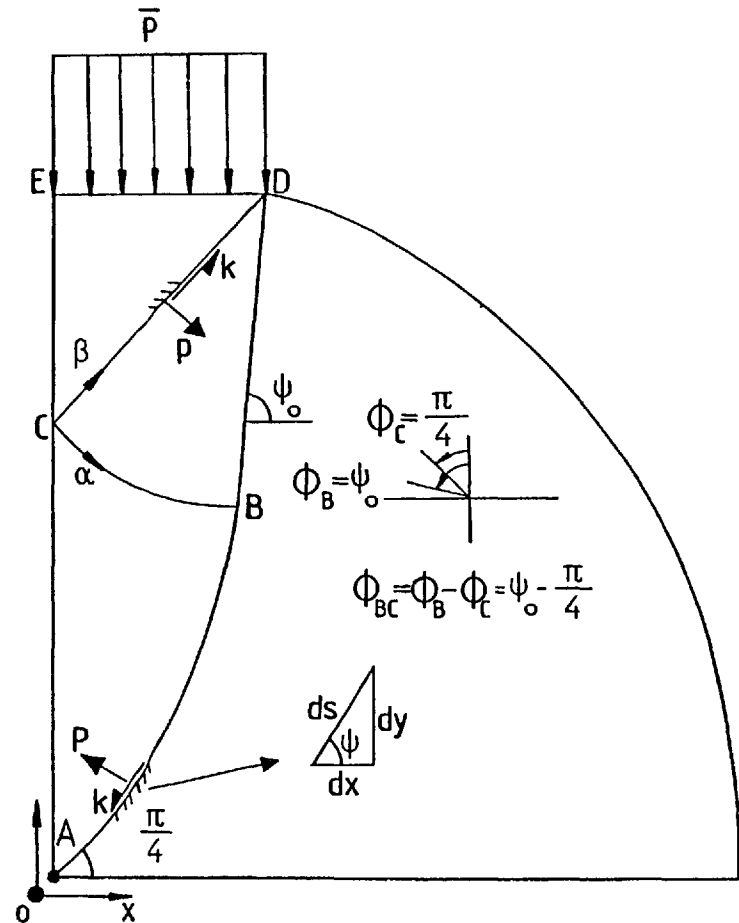


Fig. 5-15. Slip line field when  $(H_0 - H)/H_0$  is moderate (type II).

$$P = C - 2k \psi \quad (5.8)$$

where the unknown 'C' can be determined from the equilibrium equation of the rigid region in the x direction, thus

$$2 \int_{\frac{\pi}{4}}^{\psi_0} (C - 2k \psi) \sin \psi \, ds + 2 \int_{\frac{\pi}{4}}^{\psi_0} k \cos \psi \, ds = 0$$

from which 'C' is determined as

$$C = \frac{4k}{H} \int_{\frac{\pi}{4}}^{\psi_0} \psi \sin \psi \, ds - \frac{k W_1}{H} \quad (5.9)$$

From Eqs. (5.8) and (5.9), the pressure ' $P_B$ ' at B is given by

$$P_B = \frac{4k}{H} \int_{\frac{\pi}{4}}^{\psi_0} \psi \sin \psi \, ds - \frac{k W_1}{H} - 2k \psi_0 \quad (5.10)$$

On moving from B to C, Hencky's equation becomes

$$P_B - P_C = 2k(\psi_0 - \frac{\pi}{4})$$

from which  $P_C$  can be calculated by substituting for  $P_B$  from Eq. (5.10).

Thus

$$P_C = \frac{4k}{H} \int_{\frac{\pi}{4}}^{\psi_0} \psi \sin \psi \, ds - \frac{k W_1}{H} - 4k \psi_0 + 2k \frac{\pi}{4} \quad (5.11)$$

The indenting force  $F_1$  can be determined from the equilibrium equation of element CDE in the y direction, thus

$$\frac{F_1}{2} + P_C \frac{W_1}{2} - k \frac{W_1}{2} = 0$$

by inserting  $P_C$  from Eq. (5.11), the indenting force  $F_1$  becomes

$$F_1 = W_1 \left[ k \left( 1 + \frac{W_1}{H} \right) - 2k \frac{\pi}{4} + 4k \psi_0 - \frac{4k}{H} \int_{\frac{\pi}{4}}^{\psi_0} \psi \sin \psi \, ds \right] \quad (5.12)$$

Also, the mean normal pressure can be determined from  $F_1 = P_1 W_1$ , thus

$$P_1 W_1 = W_1 \left[ k \left( 1 + \frac{W_1}{H} \right) - 2k \frac{\pi}{4} + 4k \psi_0 - \frac{4k}{H} \int_{\frac{\pi}{4}}^{\psi_0} \psi \sin \psi \, ds \right]$$

or

$$\frac{P_1}{2k} = \frac{1}{2} \left( 1 + \frac{W_1}{H} \right) - \frac{\pi}{4} + 2\psi_0 - \frac{2}{H} \int_{\frac{\pi}{4}}^{\psi_0} \psi \sin \psi \, ds \quad (5.13)$$

where the integral must be evaluated along the line ABD. This solution is valid up to the point at which the contact width ' $W_1$ ' of the billet becomes equal to its height 'H'. At this point the apex, C, of the triangle EDC will coincide with the billet centre and thus the sector DBC will vanish completely. Plastic deformation then propagates through the rigid-ends of the billet, and the slip-line field (referred to as type III) changes shape slightly depending on the ratio  $W_1/H$ . In practice, this type of deformation is seldom encountered and will not be discussed here. Reference is made to a paper by Kobayashi (57) in which a study is also made of type III deformation, for the case when ' $W_1$ ' exceeds H.

When  $W_1 \leq H$ , depending on the amount of indentation, the indenting pressure ' $P_1$ ' is either given by Eq. (5.7) or Eq. (5.13). The variations of mean normal pressure ' $P_1$ ', shown in Fig. 5-16, were computed on the following basis:

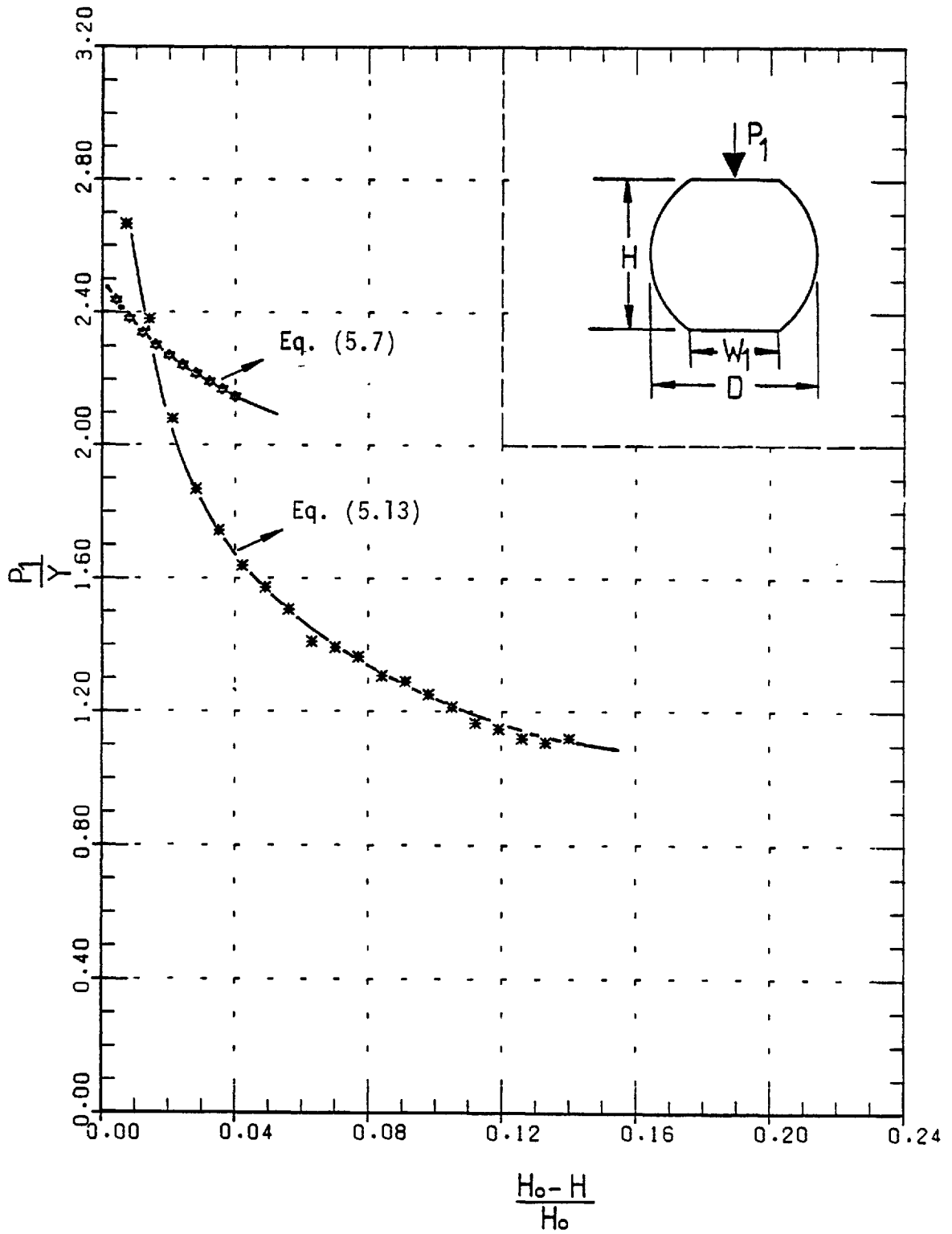


Fig. 5-16. Variation of mean normal pressure ' $P_1$ ' obtained by the slip-line field theory.

### Type I deformation

- 1- Within a narrow range,  $H \leq 0.96 H_0$ , the height  $H$  of the billet was incrementally decreased and using Fig. 5-11 the contact width ' $W_1$ ' was obtained.
- 2- A slip-line field similar to that shown in Fig. 5-14 was then graphically constructed and using Eq. (5.7) the pressure ' $P_1$ ' was calculated and steps 1 to 2 were repeated over the whole range.

### Type II deformation

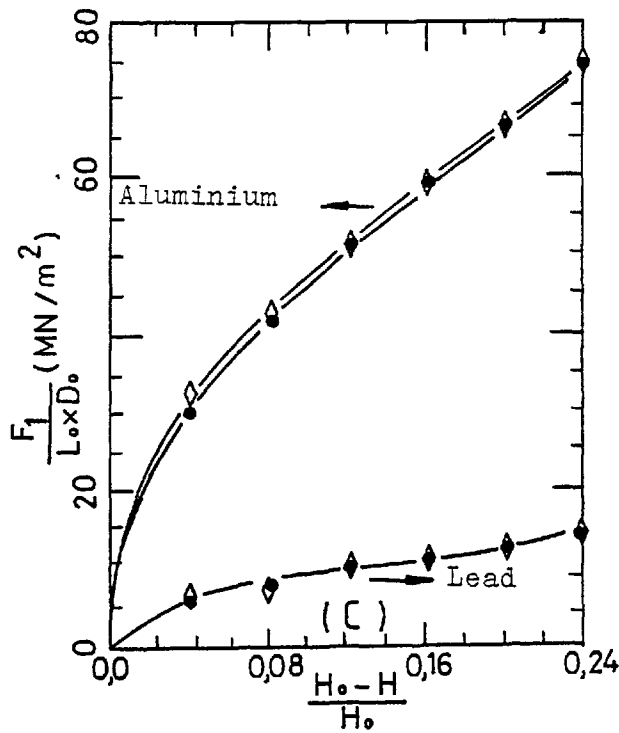
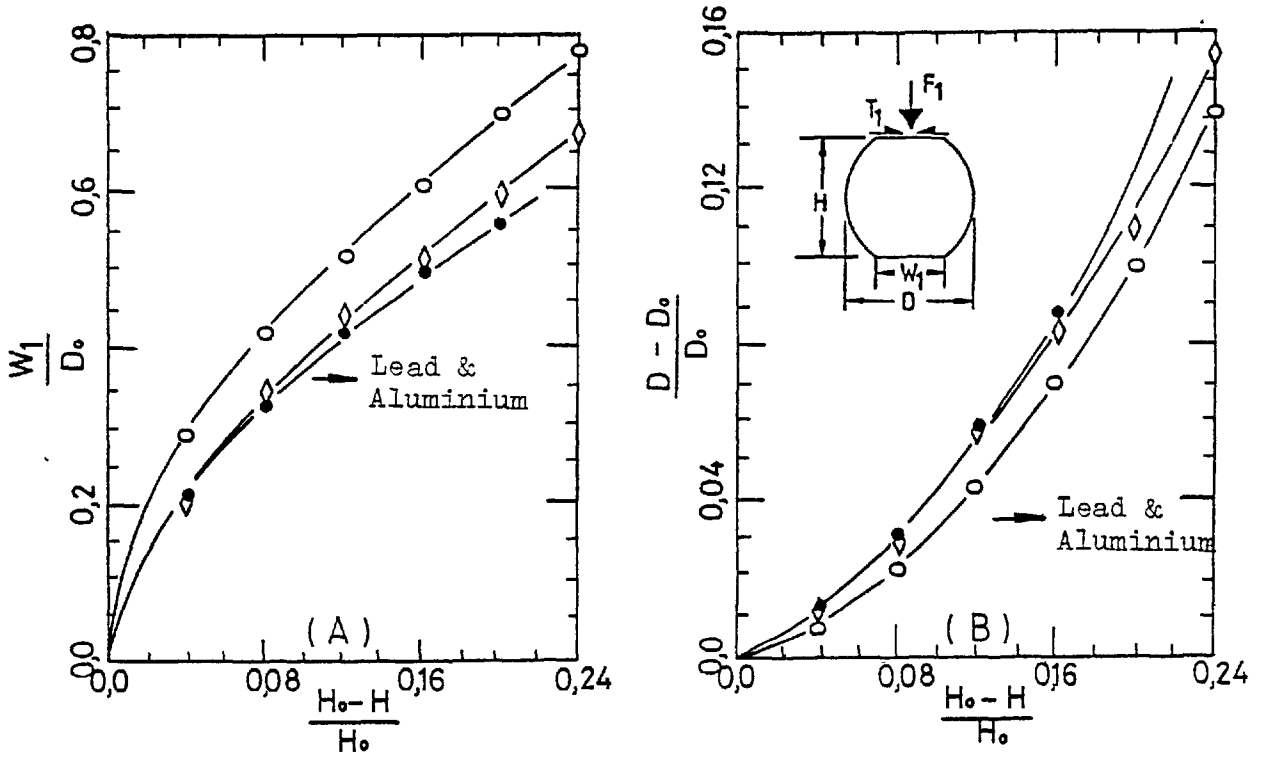
- 1- Within a wide range, but still  $H \geq W_1$ , the height  $H$  of the billet was incrementally decreased and using Fig. 5-11 the contact width ' $W_1$ ' was obtained.
- 2- A slip-line field similar to that shown in Fig. 5-15 was then graphically constructed and using Eq. (5.13) the pressure ' $P_1$ ' was calculated and steps 1 to 2 were repeated over the whole range.

In Fig. 5-16, the intersection of the two curves indicates the amount of indentation at which the type I slip-line field changes into type II. Clearly, below the intersecting point, a type II slip-line field cannot exist since a pressure higher than that for type I would be required to maintain it. For the same reason, above the intersecting point, a type I slip-line field cannot exist.

#### 5.2.4 Comparison of the results

The best curves fitted to the experimental and theoretical results are shown in Fig. 5-17. In the construction of these curves slight discrepancies, e.g. due to friction, were neglected and the curves shown merely represent the general trend of those narrow bands within which





- VOLUME CONSTANCY ASSUMPTION
- ◇ FINITE ELEMENT METHOD
- EXPERIMENT

Fig. 5-26. Comparison of experimental and theoretical data.

the experimental and theoretical curves fall.

The relationship between the contact width  $W_1/D_0$  and the amount of indentation  $(H_0-H)/H_0$  are shown in Fig. 5-17-A. At the beginning the experimental curve is in good agreement with the curve obtained by the finite element method. As the amount of indentation increases, however, the former slightly deviates from the latter. The deviation observed is due to some discrepancies with regard to the material stress-strain curve used in the computation. The curve obtained from volume constancy deviates slightly from those obtained by experiment and the finite element method. The deviation is due to the rather unrealistic assumed behaviour of the free-surface used in the former theoretical method. There, with the assumption that the free-surface would remain undeformed, it was concluded that all the particles along the free-arc would move at an equal speed. It was previously shown in section 5.2.2 that in reality the particles positioned in the lower part of the free-arc move much faster than those in the upper part as shown in Fig. 5-13.

The relationship between the amount of increase in the billet diameter  $(D-D_0)/D_0$  and the amount of indentation  $(H_0-H)/H_0$  is shown in Fig. 5-17-B. In general the experimental curve and the curve obtained by the finite element method are in good agreement. The curve obtained from the volume constancy assumption deviates, particularly at large amounts of indentation, both from the curves obtained by experiment and by the finite element method.

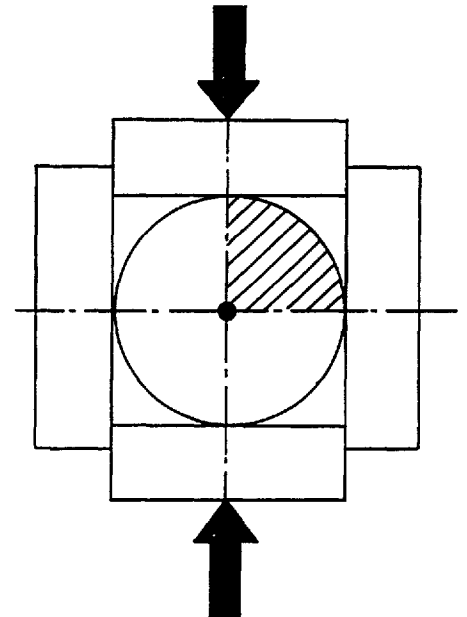
The relationship between the indenting force  $F_1/(L_0 \times D_0)$  and the amount of indentation  $(H_0-H)/H_0$  is shown in Fig. 5-17-C. The theoretical and experimental curves are seen to be in good agreement. The slight deviation of the results is due to some discrepancies with

regard to the material stress-strain curve used in the computation and also to the lack of complete specification of experimental conditions.

### 5.3 A study of case (b)

As described in section 5.1, in this case the chamber was rectangular in shape and comprised four platens (see the illustration below). The moving platens were driven in the direction indicated by the arrows at equal speed to indent an initially round billet. The diameter of the billet in this case was assumed to be precisely equal to the distance between the stationary platens.

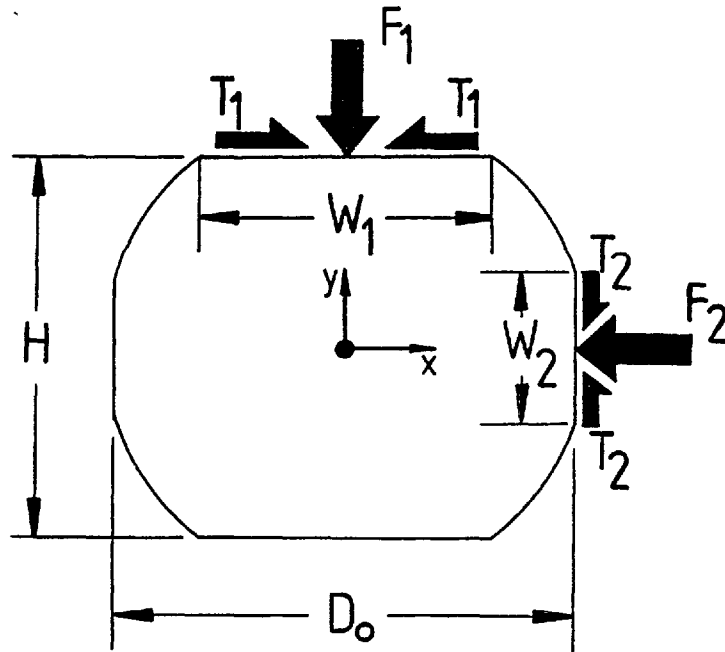
As before in section 5.2, owing to the symmetry of deformation only one quarter of the billet cross-section was considered in the computation. The finite element mesh was the same as that used in case (a), see Fig. 5-2. The computation was carried out using the material properties of commercially pure aluminium and lead. The stress-strain characteristics were those previously used in case (a), see Figs. 5-3 and 5-4.



To pursue the history of deformation the following parameters were calculated and recorded (see also the illustration below):

$$1- \frac{H_0 - H}{H_0} = \text{amount of indentation}$$

- 2-  $\frac{W_1}{D_0}$  and  $\frac{W_2}{D_0}$  = non-dimensional widths of the flats
- 3-  $\frac{F_1}{L_0 \times D_0}$  and  $\frac{F_2}{L_0 \times D_0}$  = indenting forces
- 4-  $\frac{T_1}{L_0 \times D_0}$  and  $\frac{T_2}{L_0 \times D_0}$  = frictional forces at billet/chamber interface



As in case (a), two types of boundary conditions were considered in the computation. In one type, nodal points in contact with the platens were permitted to move freely along the platen surfaces and in the another type such nodal points were not permitted to move at all. As described before, in practice, the former condition prevails when the platens, in a well lubricated process, have smooth surfaces. The latter condition, which is sometimes referred to as 'complete sticking condition', prevails when the platens have rough surfaces.

### 5.3.1 Results obtained by the finite element method

The computed results using the material properties of aluminium are shown in Figs. 5-18-A to 5-18-F. As was previously mentioned the discontinuity of the results is due to the finite sizes of elements along the free-surface of the billet.

The relationships between  $W_1/D_0$  and  $(H_0-H)/H_0$  and also between  $W_2/D_0$  and  $(H_0-H)/H_0$  are shown in Figs. 5-18-A and 5-18-B. The effect of friction on the results, particularly when the amount of indentation is large, is quite clear. Friction has the effect of decreasing the contact width  $W_1/D_0$  but increasing the contact width  $W_2/D_0$ . The effect of friction on the contact width curves can be considered as being due to its direct and indirect effects. The direct effect of friction is concerned with the prevention of extension or contraction of the contact width. This effect is important if the contact widths sustain a great extension or contraction during indentation between smooth platens, since such extension or contraction will be completely prevented during indentation between rough platens. The indirect effect of friction is concerned with the additional deformation of the free-surface due to friction, which may accelerate or decelerate the rate at which the free-surface comes into contact with the surface of the platen.

It follows from the above argument that the difference in the values of contact width  $W_1/D_0$  at points such as A and B, see Fig. 5-18-A, is a measure of the direct effect of friction. As the amount of indentation increases the direct effect of friction becomes markedly more important. Conversely, the direct effect of friction on the contact width  $W_2/D_0$  is negligible (i.e.  $W_2$  at B  $\approx$   $W_2$  at A), see Fig. 5-18-B. Thus friction, which causes some discrepancies between the two-curves shown in Fig. 5-18-B, has only an indirect effect on the contact width  $W_2/D_0$ .

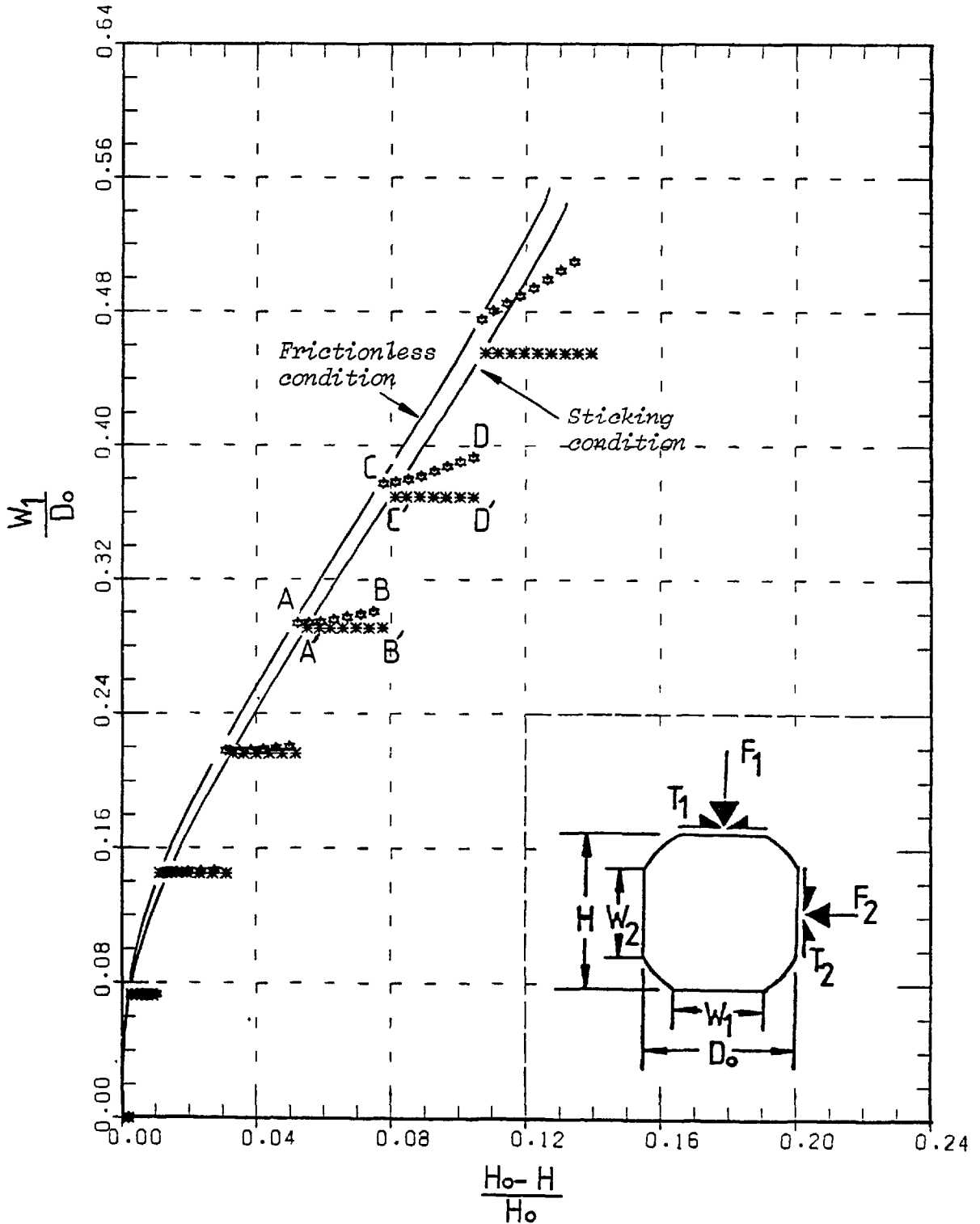


Fig. 5-18-A. Variation of contact width ' $W_1$ ' with height ' $H$ ' for commercially pure aluminium obtained by the finite element method.

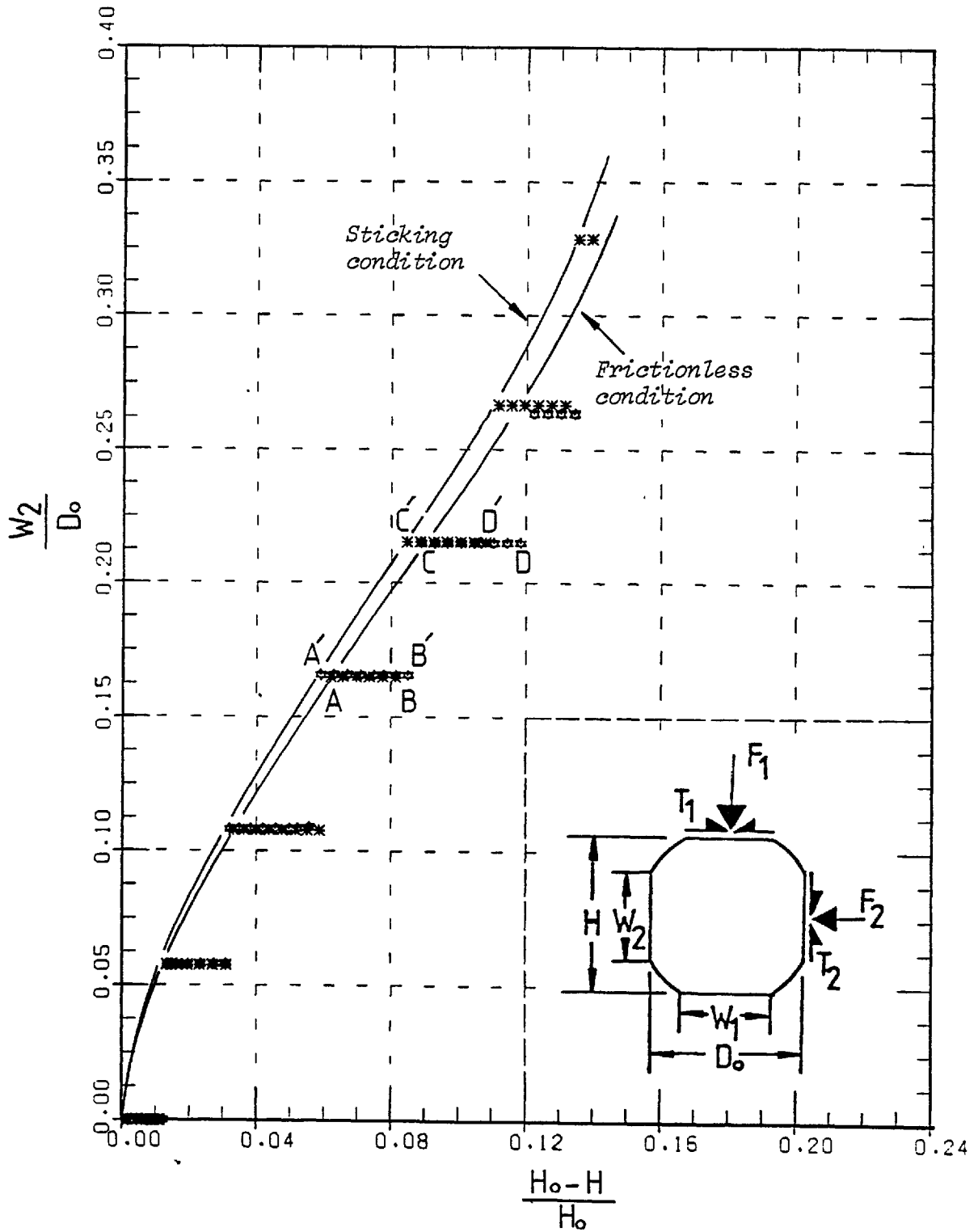


Fig. 5-18-B. Variation of contact width ' $W_2$ ' with height ' $H$ ' for commercially pure aluminium obtained by the finite element method.

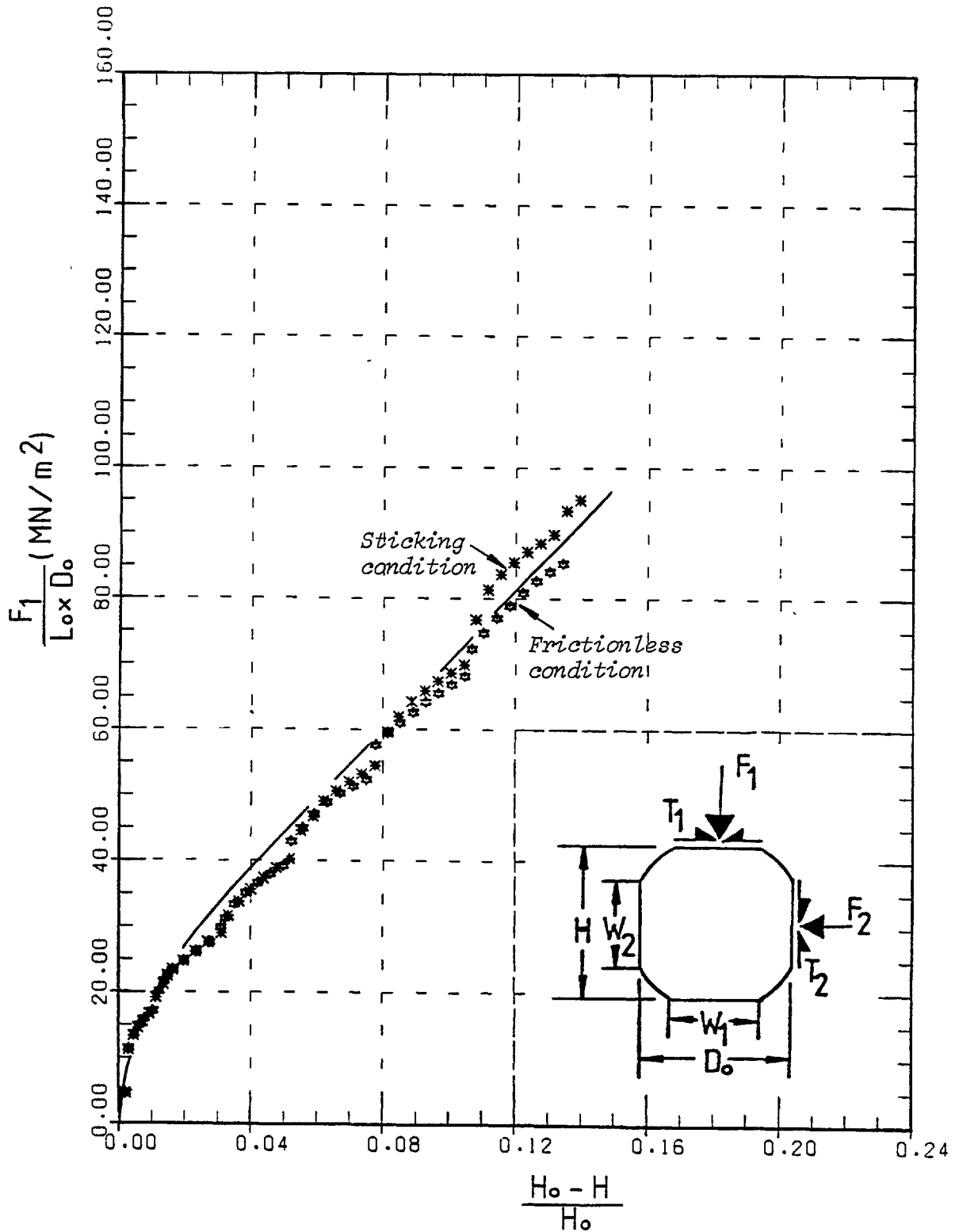


Fig. 5-18-C. Variation of indenting force ' $F_1$ ' with height ' $H$ ' for commercially pure aluminium obtained by the finite element method.



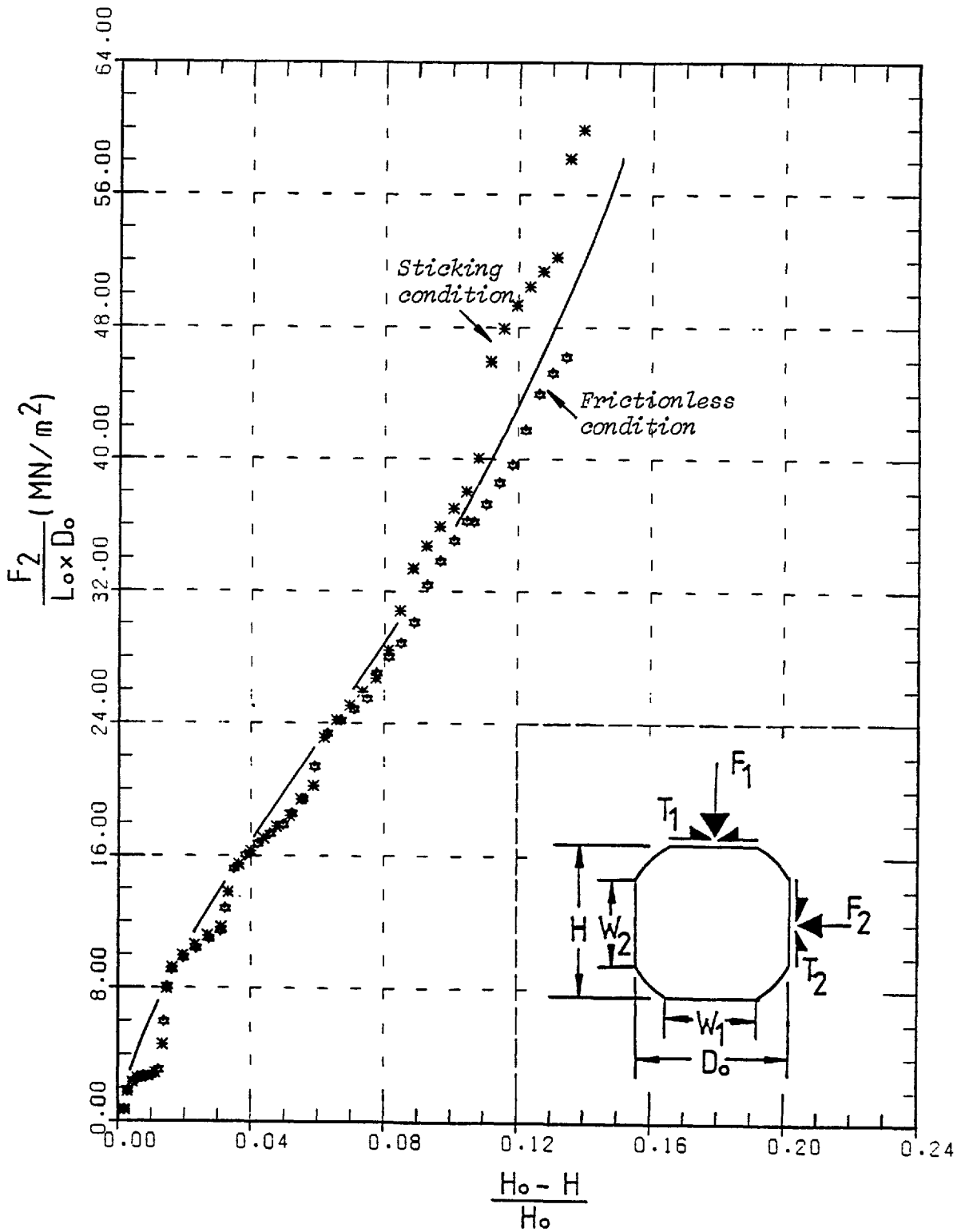


Fig. 5-18-D. Variation of indenting force ' $F_2$ ' with height ' $H$ ' for commercially pure aluminium obtained by the finite element method.

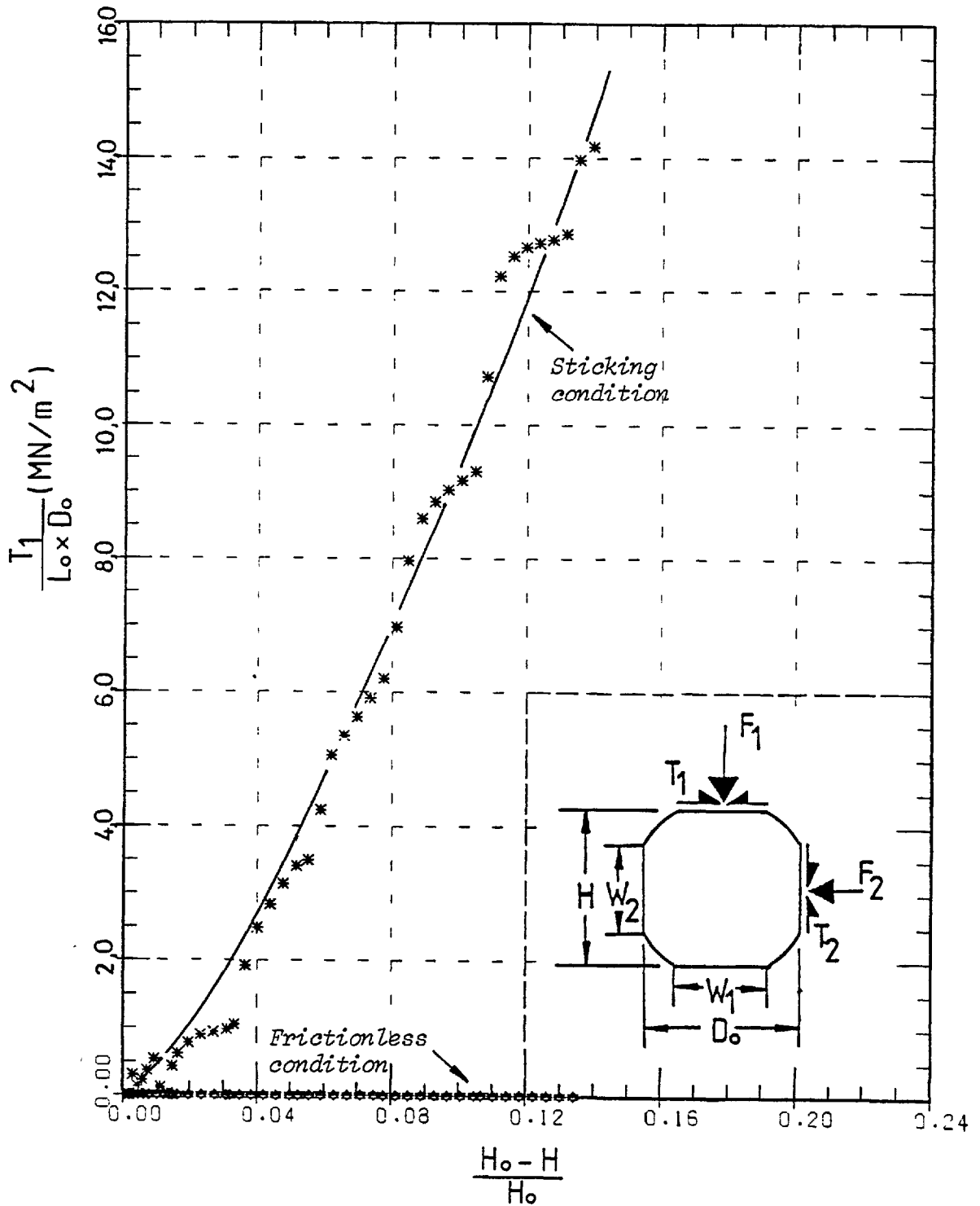


Fig. 5-18-E. Variation of interfacial frictional force ' $T_1$ ' with height ' $H$ ' for commercially pure aluminium obtained by the finite element method.

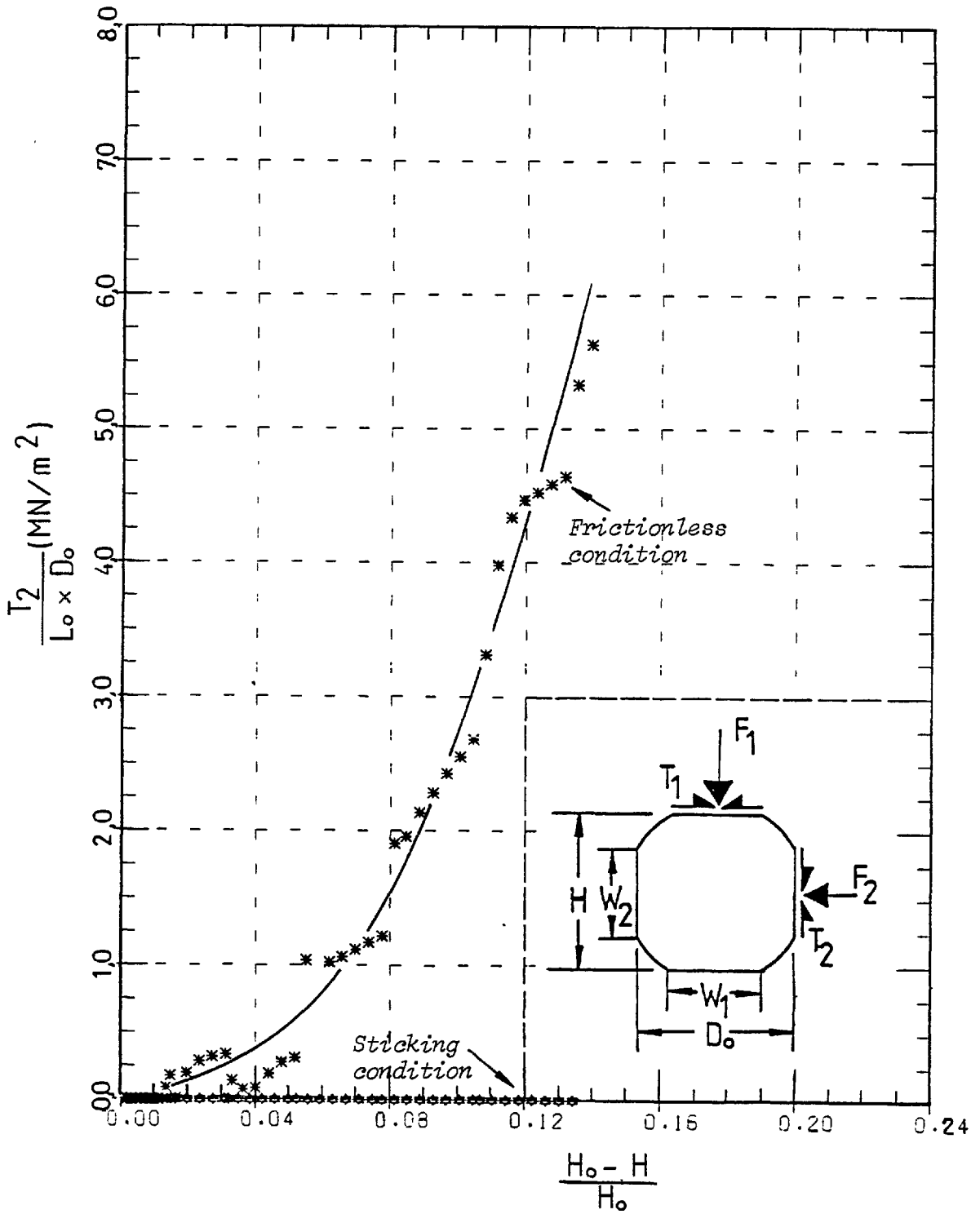


Fig. 5-18-F. Variation of interfacial frictional force ' $T_2$ ' with height ' $H$ ' for commercially pure aluminium obtained by the finite element method.

The relationships between the indenting forces and the amount of indentation are shown in Figs. 5-18-C and 5-18-D. As seen, the effect of friction on the indenting forces is negligible when the amount of indentation is less than 0.08. For amounts of indentation greater than 0.08, friction takes effect and the indenting forces obtained for rough platens become considerably greater than those obtained for smooth platens. The relationships between the frictional force  $T_1/(L_0 \times D_0)$  and the amount of indentation  $(H_0 - H)/H_0$  and also between the frictional force  $T_2/(L_0 \times D_0)$  and the amount of indentation  $(H_0 - H)/H_0$  are shown in Figs. 5-18-E and 5-18-F. As the amount of indentation increases the curves of frictional forces rise markedly. It is worth mentioning that the discontinuity of the curves is due to the finite sizes of elements positioned along the free-surface of the billet.

The manner in which the original finite element mesh (shown in Fig. 5-2) was distorted after receiving an indentation of nearly 0.14 is shown in Fig. 5-19. The distorted mesh, for the case when the billet was indented between smooth platens, is shown in Fig. 5-19-A. Comparing this with the original mesh, it becomes clear that elements beneath the top platen and the stationary platen on the right are those with maximum angular distortions. The least distorted elements are those positioned along the free-surface and the diameters of the billet in the x and y directions. Other elements within the mesh, particularly those positioned near the moving platen, are noticeably distorted. The distorted mesh for the case when the billet was indented between rough platens, is shown in Fig. 5-19-B. Comparing this with the original mesh, it becomes clear that the angular distortions of elements adjoining the moving platen and the stationary platen are less than those of the

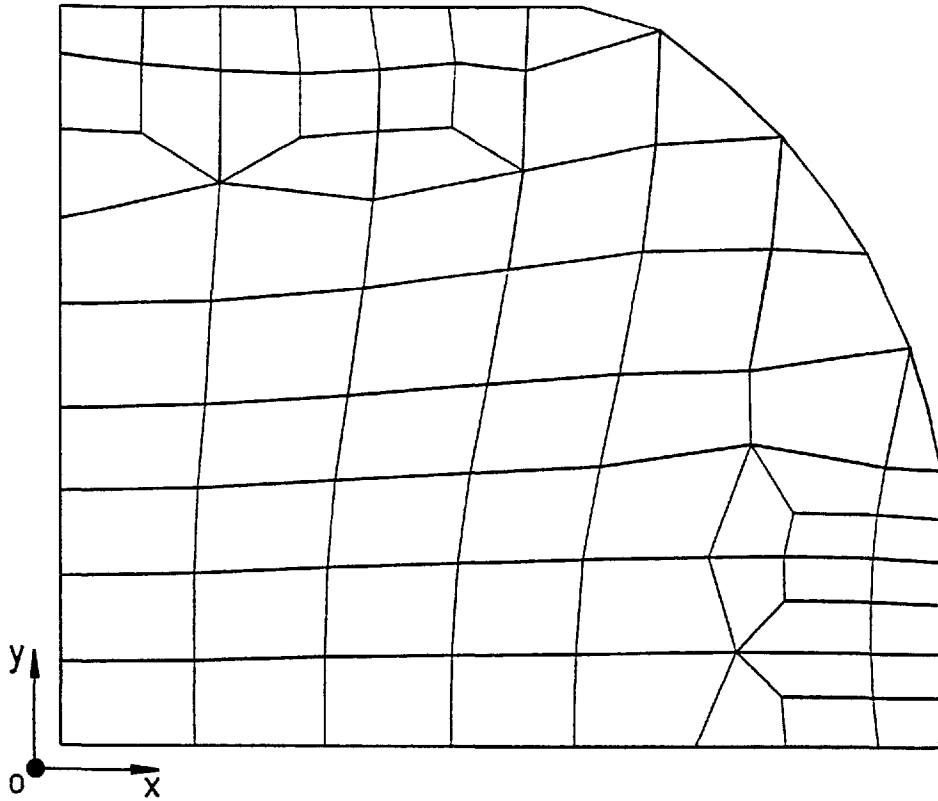


Fig.5-19-A. Deformation of original mesh at  $(H_0 - H)/H_0 = 0.135$  in frictionless condition.

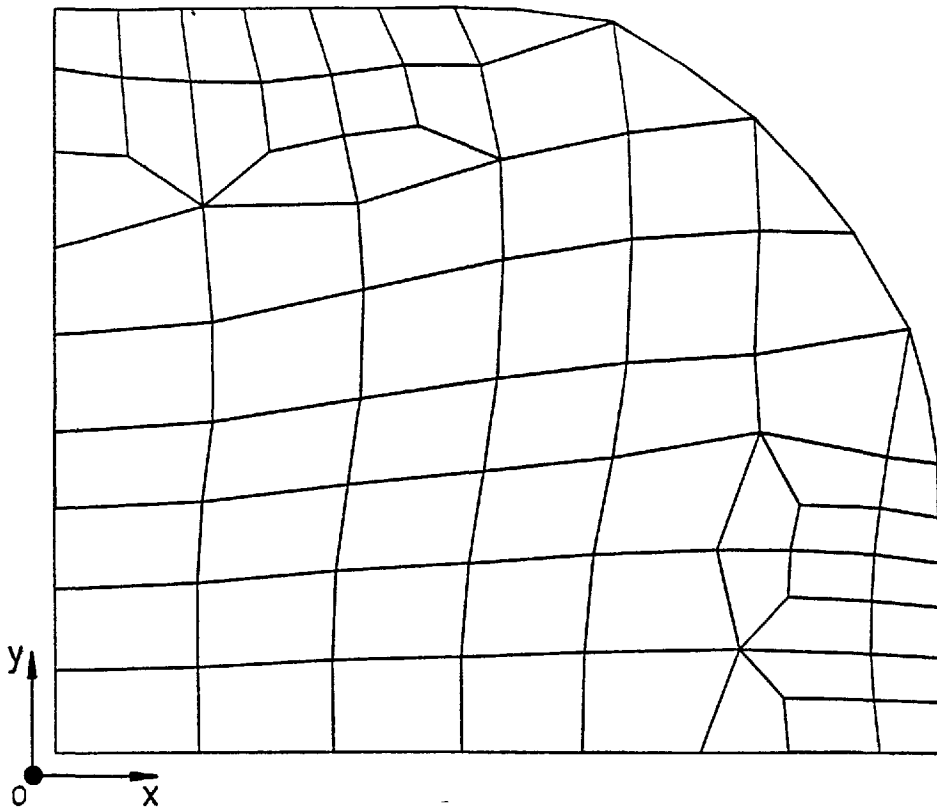
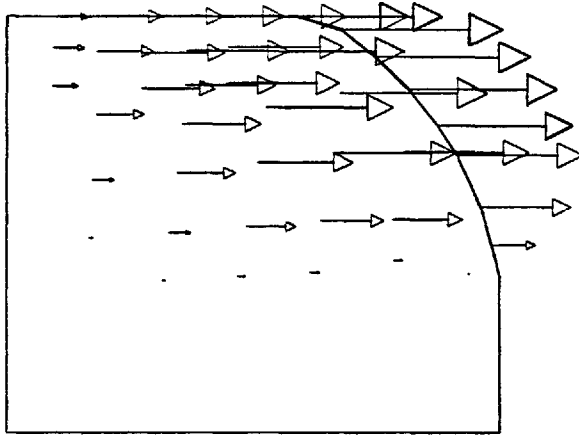


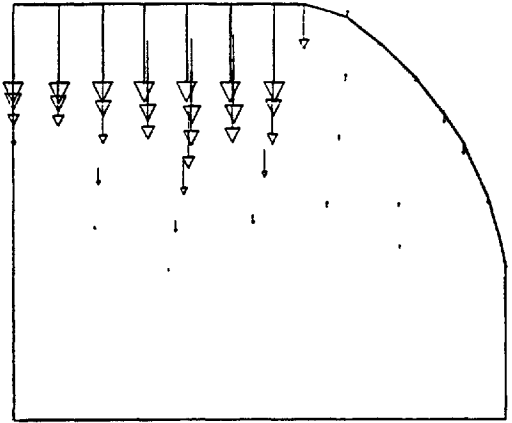
Fig. 5-19-B. Deformation of original mesh at  $(H_0 - H)/H_0 = 0.14$  in sticking condition.

corresponding elements in the previous mesh shown in Fig. 5-19-A. Thus, friction has the effect of decreasing the angular distortion of these elements and in turn their shear strains. In Fig. 5-19-B the least distorted elements are those positioned along the free-surface and the diameters of the billet in the x and y directions. Other elements within the mesh, particularly those positioned near the moving platen are distorted noticeably and more than the corresponding elements in Fig. 5-19-A. Hence, friction has the effect of increasing the distortion of these elements.

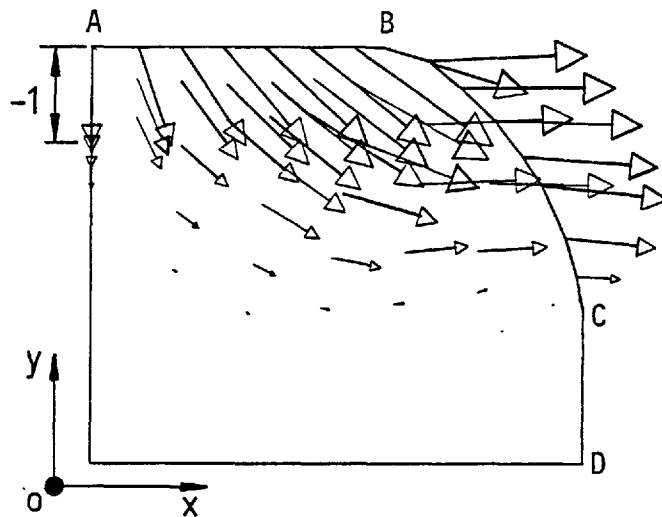
The flow fields for indentation of a round billet between smooth and rough platens are shown in Figs. 5-20 and 5-21 respectively. In the computation the velocity of the top platen was assumed to be -1. In Fig. 5-20, the flow field established by smooth platens is shown. It can be seen that in moving outwards the speed of metal particles along the contact width AB increases rather noticeably above the reference speed of the top platen. Along the free-arc the particle-speed is generally in the x direction. The speed along the free-arc, in moving from C to B, rapidly increases and then, over most of the free-surface becomes almost uniform. In this flow field the existence of a dead zone between the stationary platen and the diameter of the billet in the y direction is quite clear. In Fig. 5-21 the flow field established by rough platens is shown, where all the particles in contact with the moving platen move with the same speed as that of the platen. Along the free-arc the speed of the particles, despite the previous field, is not only in the x direction but also in the y direction. Comparing the flow fields shown in Figs. 5-20 and 5-21, the establishment of an entirely different flow field when friction comes into effect is quite clear. In Fig. 5-21 the metal flows in a deep pattern affecting almost



Components of velocity vectors in the x direction

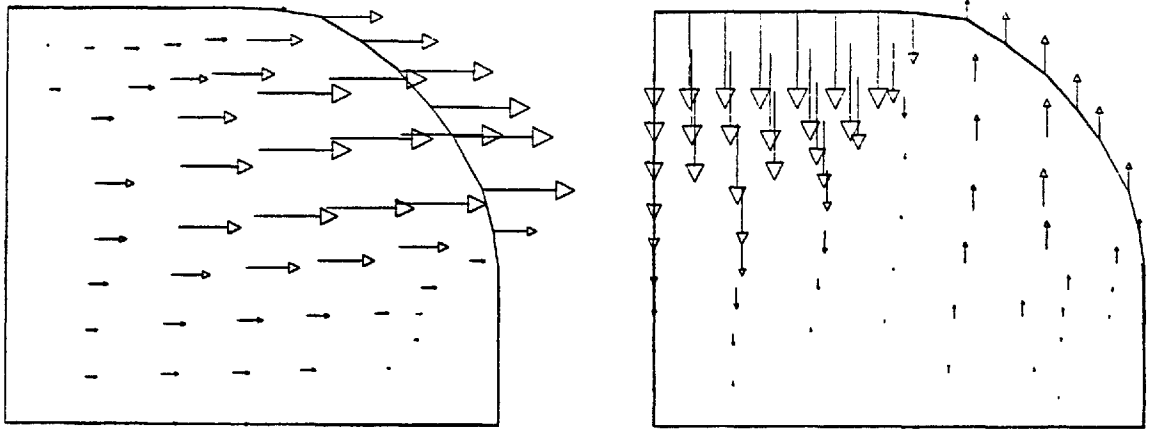


Components of velocity vectors in the y direction



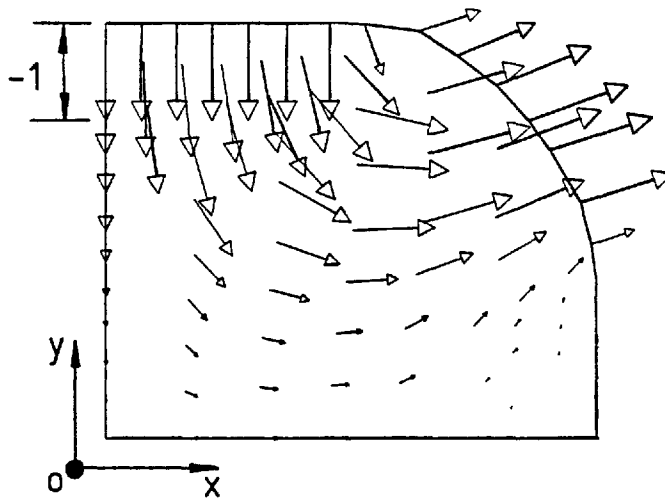
Absolute velocity vectors

Fig. 5-20. Flow pattern at  $(H_0 - H)/H_0 = 0.135$  in frictionless condition, velocity of the top platen being -1.



Components of velocity vectors in the x direction

Components of velocity vectors in the y direction



Absolute velocity vectors

Fig. 5-21. Flow pattern at  $(H_0 - H)/H_0 = 0.14$  in sticking condition, velocity of the top platen being -1.



the entire volume of the billet, in contrast to that shown in Fig. 5-20 in which the metal flows in a shallow pattern with a significant portion of the billet material remaining stationary.

The distribution of effective strains for the case when the billet was indented by smooth platens is shown in Fig. 5-22-A. The largest effective strains occur close to the moving platen. The least strained regions are those positioned beneath the free-surface and along the diameter of the billet in the x direction. Comparing this with Fig. 5-10-A, it is seen how the constant strain lines change direction when the flow of metal in the x direction is prevented by adding a stationary smooth platen on the right. In Fig. 5-10-A the contours are directed towards the y direction whilst in Fig. 5-22-A they are approximately towards the x direction. It is an interesting matter to observe how the adding of the stationary platen prevents the straining of the billet centre. In Fig. 5-10-A the centre of the billet is one of the most strained regions whilst in Fig. 5-22-A one of the least. The distribution of effective strains for the case when the billet is indented by rough platens is shown in Fig. 5-22-B. The region with the maximum effective strain is that adjoining the moving platen. As in Fig. 5-22-A, the least strained regions are those positioned beneath the free-surface and along the diameter of the billet in the x direction. Comparing this with Fig. 5-22-A, it is observed that the constant strain lines, particularly those adjacent to the platens, change considerably when friction comes into effect.

### 5.3.2 Results obtained from volume constancy

If the behaviour of the free-surface during the course of indentation is known, the current configuration of the billet can be determined from

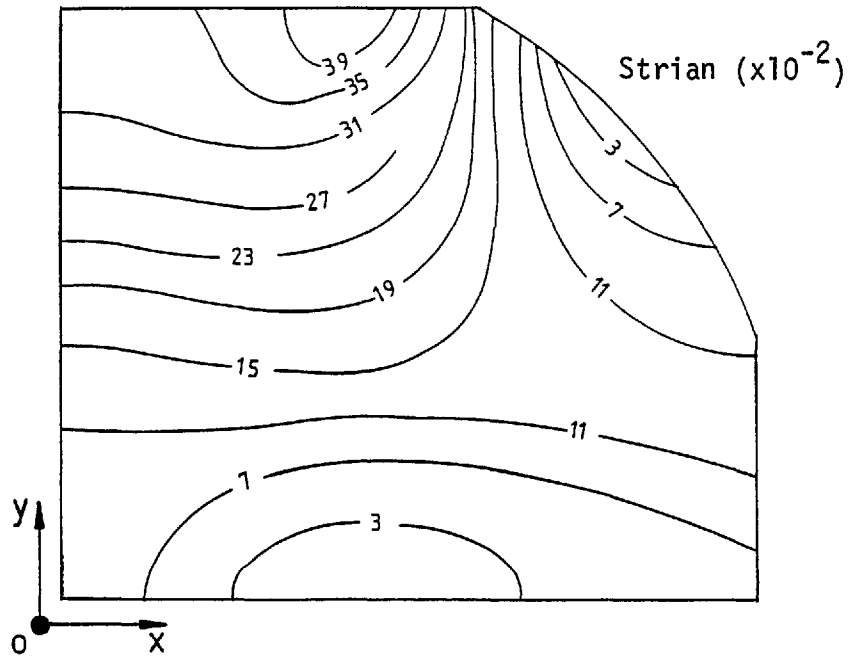


Fig. 5-22-A. Distribution of effective strain at  $(H_0 - H)/H_0 = 0.135$  in frictionless condition.

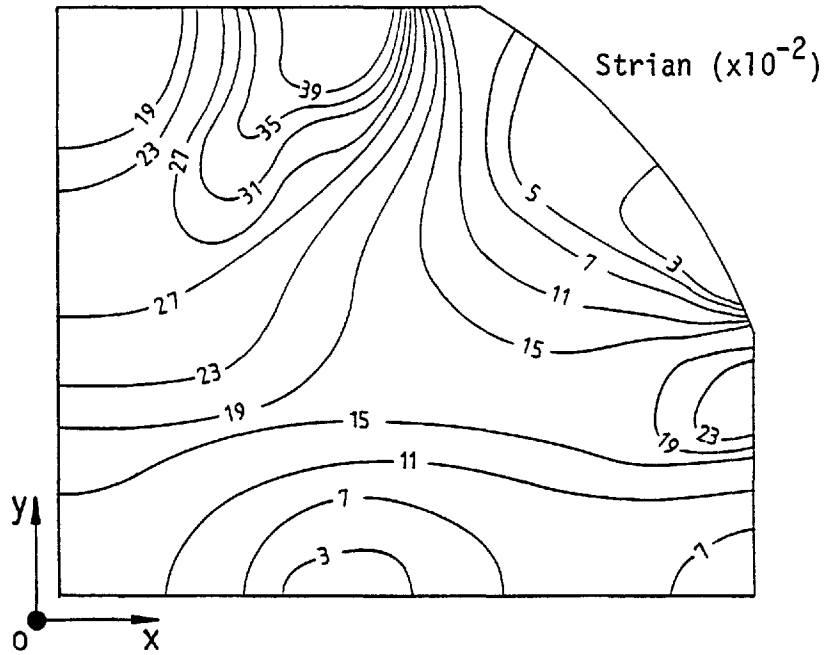


Fig. 5-22-B. Distribution of effective strain at  $(H_0 - H)/H_0 = 0.14$  in sticking condition.

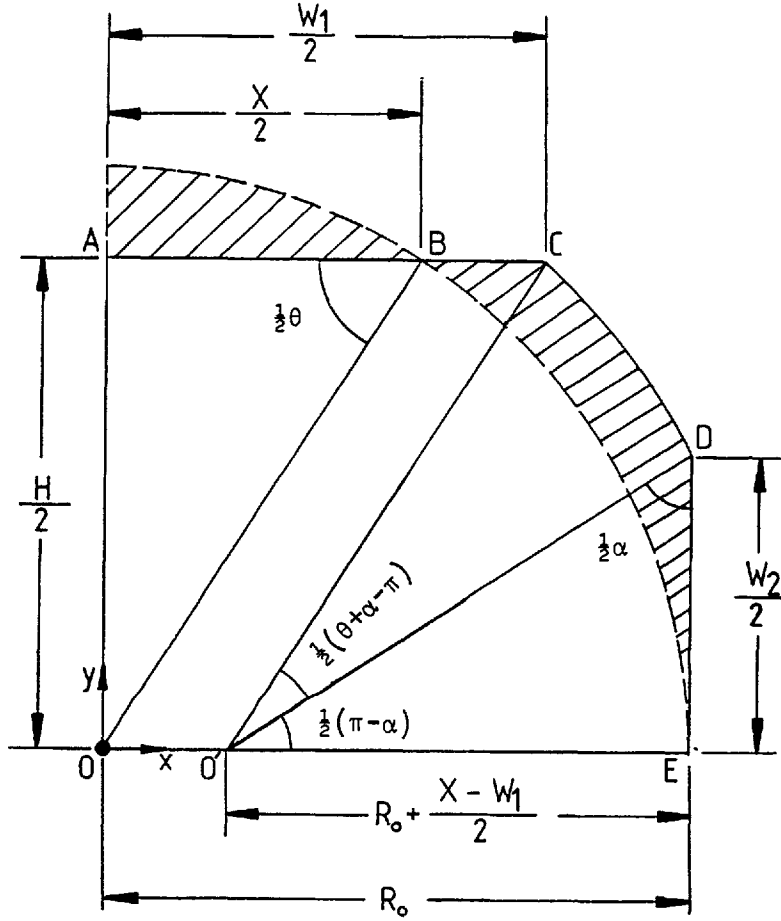
volume constancy.

As previously shown in section 5.3.1, from the results obtained by the finite element method, the behaviour of the free-surface in this kind of indentation is highly dependent on the surface condition of the platen. Fig. 5-21 shows that in the flow field established by rough platens the free-surface of the billet moves in a changing direction, although the velocity vectors along this surface are approximately parallel and equal in magnitude. In the flow field established by smooth platens, however, the free-surface generally moves uniformly and only in the x direction, see Fig. 5-20.

In what follows, the volume constancy assumption is applied to an indentation problem in which the platens are smooth. In accordance with the flow field shown in Fig. 5-20 it is assumed that the free-surface of the billet during the course of indentation will move uniformly and only in the x direction. For such an assumed behaviour of the free-surface it is quite clear that the centre of curvature of the free-surface during deformation will remain on the horizontal axis of symmetry of the billet. The original and distorted configurations of the billet are shown in the illustration below. As before, the centre of the free-surface in the deformed state can be determined by drawing CO' parallel to BO. If the initial radius of the billet is called  $R_0$ , from volume constancy

$$\frac{1}{4} \pi R_0^2 = \frac{1}{2} R_0^2 \left( \frac{\theta + \alpha - \pi}{2} \right) + \frac{1}{2} \frac{H}{2} \left( \frac{2W_1 - X}{2} \right) + \frac{1}{2} R_0 \left( R_0 + \frac{X - W_1}{2} \right) \sin\left(\frac{\pi - \alpha}{2}\right)$$

where the first, second and third terms on the right are the areas of



the sector O'DC, the trapezoid OO'CA and the triangle O'ED respectively. Simplifying the above equation, the contact width ' $W_1$ ' can be determined by

$$W_1 = \frac{R_o^2}{H - R_o \sin(\frac{\pi - \alpha}{2})} \left\{ \frac{\pi}{4} - \left\{ (\theta + \alpha - \pi) - \left\{ \sin \theta - 2 \left[ 1 + \cos\left(\frac{\theta}{2}\right) \right] \sin\left(\frac{\pi - \alpha}{2}\right) \right\} \right\} \right\} \quad (5.14)$$

in which  $W_1$ ,  $\theta$  and  $\alpha$  are unknowns. From triangles O'ED and OAB it can also be written

$$\sin\left(\frac{\alpha}{2}\right) = \frac{O'E}{O'D} = \frac{R_o + \frac{X - W_1}{2}}{R_o} = 1 + \frac{X}{2R_o} - \frac{W_1}{2R_o} \quad (5.15)$$

$$\cos\left(\frac{\theta}{2}\right) = \frac{X}{2R_o} \quad (5.16)$$

$$\cos\left(\frac{\theta}{2}\right) = \frac{H}{2R_0} \quad (5.17)$$

Substituting Eq. (5.16) into Eq. (5.15) leads to

$$\sin\left(\frac{\alpha}{2}\right) = 1 + \cos\left(\frac{\theta}{2}\right) - \frac{W_1}{2R_0} \quad (5.18)$$

By solving Eqs. (5.14), (5.17) and (5.18), the contact width ' $W_1$ ' was computed. The method of computation used was as follows:

- 1- For a given height 'H', from Eq. (5.17), ' $\theta$ ' was calculated.
- 2- As a first approximation, ' $W_1$ ' was set equal to 'X'.
- 3- From Eq. (5.15), ' $\alpha$ ' was calculated.
- 4- By inserting ' $\alpha$ ' and ' $\theta$ ' into Eq. (5.14), a more correct value for ' $W_1$ ' was calculated.
- 5- Steps 3 to 4 were repeated until convergence was achieved. Having calculated the correct values of ' $W_1$ ' and ' $\alpha$ ', the value of ' $W_2$ ' was calculated from triangle O'ED. Thus

$$W_2 = 2 \overline{O'D} \cos\left(\frac{\alpha}{2}\right) = 2R_0 \cos\left(\frac{\alpha}{2}\right) \quad (5.19)$$

The relationships between the computed  $W_1/D_0$  and  $(H_0-H)/H_0$  and also between the computed  $W_2/D_0$  and  $(H_0-H)/H_0$  are shown in Fig. 5-23. The contact width  $W_1/D_0$  increases rapidly at first then almost linearly, and finally increases markedly, reaching its maximum value of unity as the amount of indentation approaches the limiting value of 0.215. The contact width  $W_2/D_0$  increases linearly at first and then increases markedly, reaching its maximum value of 0.875 as the amount of indentation approaches the limiting value of 0.215.

By using Eq. (5.14), the current configuration of the billet can

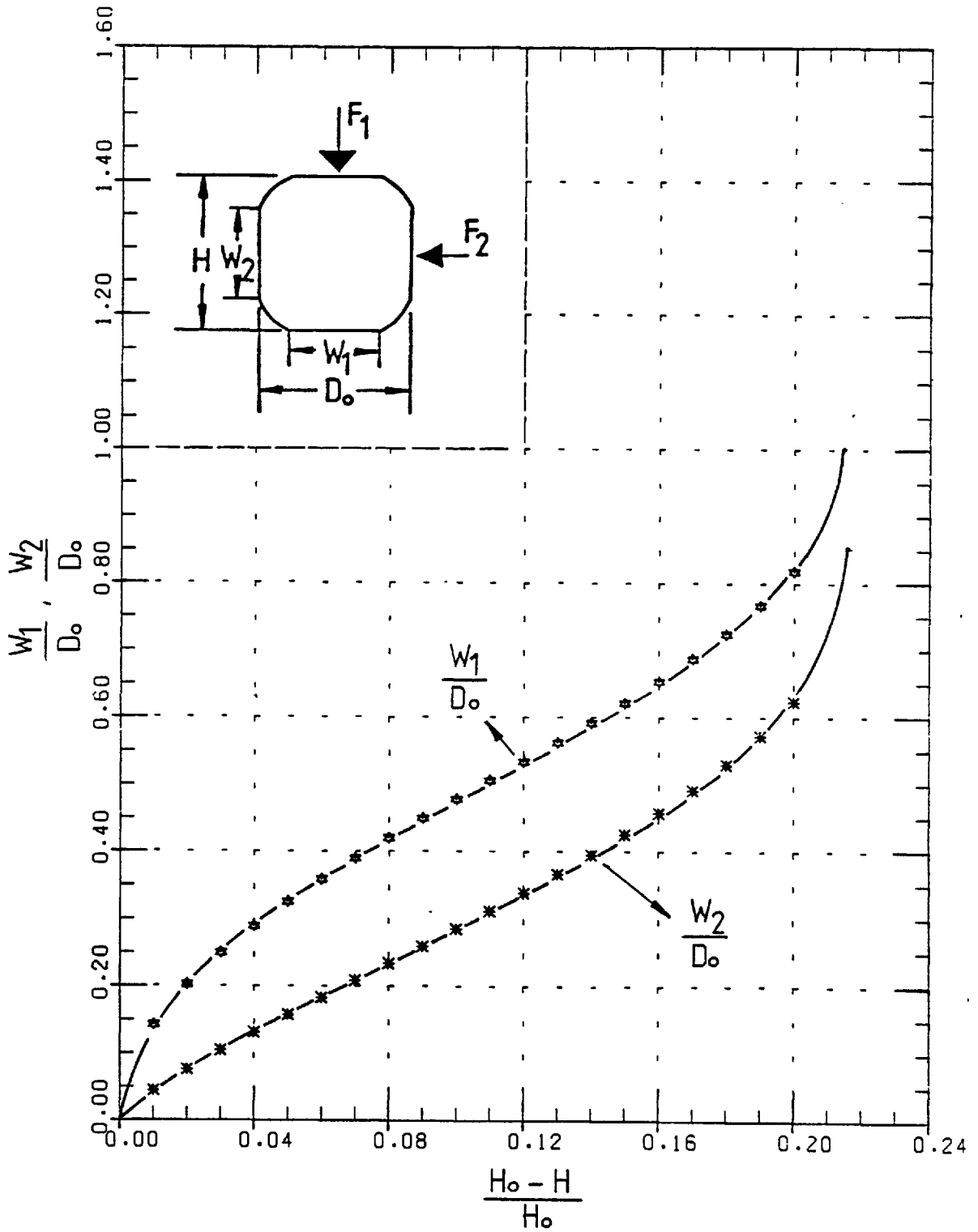
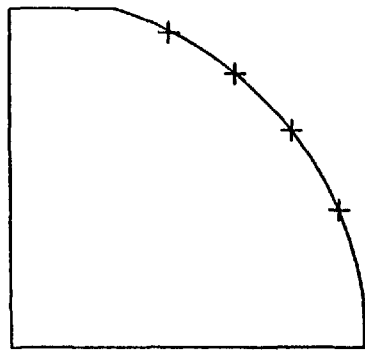


Fig. 5-23. Variations of contact widths ' $W_1$ ' and of ' $W_2$ ' with height ' $H$ ' obtained by the volume constancy assumption.

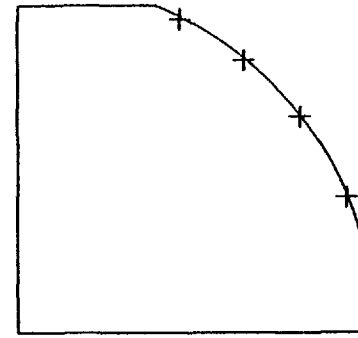
be obtained. To substantiate the assumed behaviour of the free-surface the current configuration of the billet can be compared with the actual one obtained from experiment. In the experiment a number of points were selected on the periphery of a section positioned at the central region of the billet. The billet was incrementally indented and the current positions of the selected points were measured and recorded. The theoretical predictions together with the current positions of the experimental points during the course of indentation are shown in Fig. 5-24. At the beginning of indentation the current positions of the experimental points coincide well with the surface predicted from volume constancy. Later, however, the experimental points, particularly those near the edge of the top contact surface, deviate from the theoretical surface. At all stages, particularly those for which the amount of indentation is high, the experimental points define an area smaller than that defined by the theoretical solid line. The discrepancy observed is due to the violation of plane strain conditions in the experiments.

### 5.3.3 Results obtained by the upper-bound theorem

In a well lubricated indentation process, for which the current configuration of the billet was just obtained, the indenting force ' $F_1$ ' was determined by applying the upper-bound theorem. The velocity field used, which was in reasonable agreement with the flow field shown in Fig. 5-20 obtained by the finite element method, consisted of three regions as shown in the illustration below. The velocities within the regions were assumed to vary as follows:

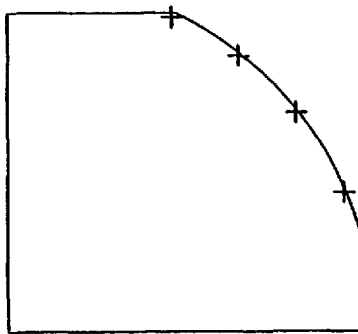


$$(H_0 - H)/H_0 = 0.044$$

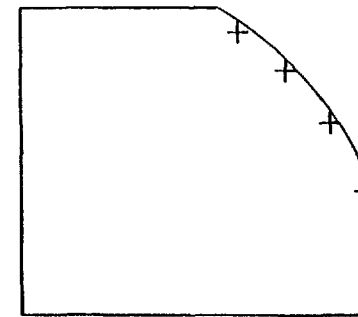


$$(H_0 - H)/H_0 = 0.078$$

— Volume constancy assumption  
 + Experiment



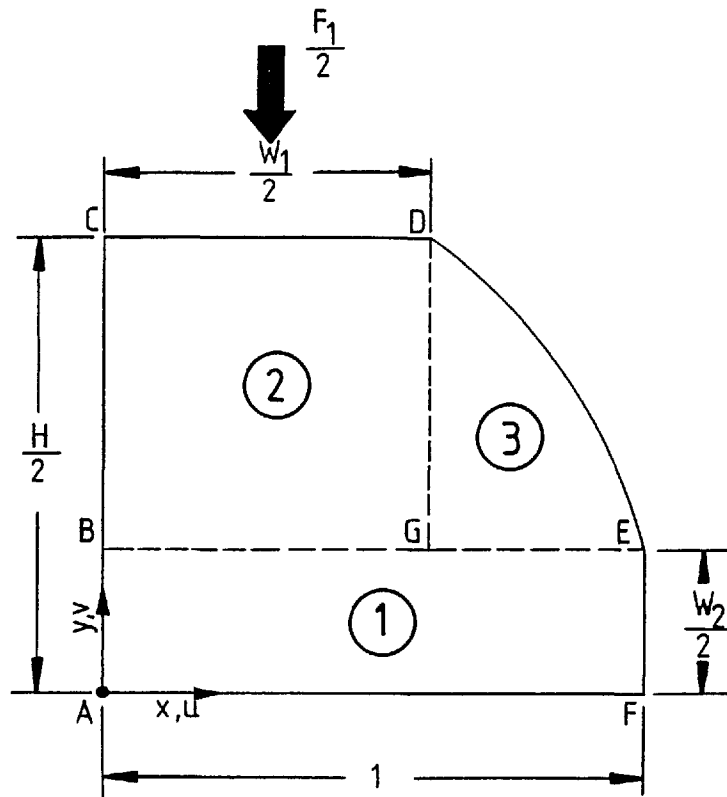
$$(H_0 - H)/H_0 = 0.10$$



$$(H_0 - H)/H_0 = 0.13$$

Fig. 5-24. Comparison of billet configurations obtained by the volume constancy assumption and experiment at various heights, 'H'.





Region 1

$$U_1 = V_1 = 0$$

which was assumed to be a dead zone.

Region 2

$$U_2 = \frac{2x}{H-W_2} \text{ and } V_2 = \frac{2y-W_2}{H-W_2}$$

where the velocity components  $U_2$  and  $V_2$  were assumed to vary by the given linear functions. The velocity of the top platen was assumed to be -1.

Region 3

$$U_3 = \frac{W_1}{H-W_2} \text{ and } V_3 = 0$$

where this region was assumed rigid. It is worth mentioning that the assumed velocity components will satisfy the mass conservation law at any point within any of the regions or on the boundary of any two adjacent regions. An upper bound to the indenting force ' $F_1$ ' is given by

$$\frac{1}{2} F_1 \cdot 1 = \overset{\circ}{E}_{11} + \overset{\circ}{E}_{12} + \overset{\circ}{E}_{22} + \overset{\circ}{E}_{23} + \overset{\circ}{E}_{33} + \overset{\circ}{E}_{31} \quad (5.20)$$

where the term on the left is the rate at which work is done by the platen force equal to half ' $F_1$ ', and the terms on the right are

$$\left\{ \begin{array}{l} \overset{\circ}{E}_{ij} = \text{rate of dissipated energy within region } i \text{ (when } i=j) \\ \overset{\circ}{E}_{ij} = \text{rate of dissipated energy at the boundary (when } i \neq j) \\ \text{between regions } i \text{ and } j \end{array} \right.$$

Clearly in Eq. (5.20), energy dissipation rates  $\overset{\circ}{E}_{11}$  and  $\overset{\circ}{E}_{33}$  will vanish since regions 1 and 3 were assumed rigid masses. The energy dissipation rate  $\overset{\circ}{E}_{22}$  is given by

$$\overset{\circ}{E}_{22} = \int Y \overset{\circ}{\epsilon}_2 dV$$

where the effective strain rate  $\overset{\circ}{\epsilon}_2$  is determined from

$$\overset{\circ}{\epsilon}_2 = \sqrt{\frac{2}{3} \left( \overset{\circ}{\epsilon}_x^2 + \overset{\circ}{\epsilon}_y^2 + \overset{\circ}{\epsilon}_{xy}^2 \right)}$$

in which

$$\frac{\partial U_2}{\partial x} = \frac{2}{H-W_2} \quad , \quad \frac{\partial V_2}{\partial y} = \frac{-2}{H-W_2}$$

and also 
$$\frac{\partial U_2}{\partial y} + \frac{\partial V_2}{\partial x} = 0.$$

Thus

$$\frac{\partial U_2}{\partial x} = \sqrt{4/3} \left( \frac{2}{H-W_2} \right)^2 = \frac{4}{\sqrt{3} (H-W_2)}$$

and hence the energy dissipation rate in region 2 is

$$\dot{E}_{22} = \int Y \frac{\partial U_2}{\partial x} dV = Y \frac{4}{\sqrt{3} (H-W_2)} \frac{W_1 (H-W_2)}{4} = \frac{Y W_1}{\sqrt{3}}$$

The energy dissipation rates at the boundaries of the regions are

$$\dot{E}_{21} = \frac{Y}{2} \int_0^{W_1/2} \frac{2x}{H-W_2} dx = \frac{Y W_1^2}{8(H-W_2)}$$

$$\dot{E}_{31} = \frac{Y}{2} \int_{W_1/2}^1 \frac{W_1}{H-W_2} dx = \frac{Y (H-W_2)}{8}$$

$$\dot{E}_{23} = \frac{Y}{2} \int_{W_2/2}^{H/2} \frac{2y-W_2}{H-W_2} dy = \frac{Y (H-W_2)}{8}$$

Substituting the energy dissipation rates in Eq. (5.20) leads to

$$F_1 = W_1 Y \left[ \frac{2}{\sqrt{3}} + \frac{H-W_2}{4W_1} + \frac{4-W_1}{4(H-W_2)} \right] \quad (5.21)$$

The mean normal pressure 'P<sub>1</sub>' applied by the top platen can be determined from  $F_1 = P_1 W_1$ , thus

$$P_1 = Y \left[ \frac{2}{\sqrt{3}} + \frac{H-W_2}{4W_1} + \frac{4-W_1}{4(H-W_2)} \right]$$

or 
$$\frac{P_1}{Y} = \frac{2}{\sqrt{3}} + \frac{H-W_2}{4W_1} + \frac{4-W_1}{4(H-W_2)} \quad (5.22)$$

The variation of pressure ' $P_1$ ' during the course of indentation can be computed by inserting the variations of ' $W_1$ ' and ' $W_2$ ' in terms of ' $H$ '. These variations, which were already found from volume constancy, are shown in Fig. 5-23. The computed variation of pressure ' $P_1$ ' is shown in Fig. 5-25. The pressure at first decreases rapidly, then after reaching a minimum, increases markedly as the amount of indentation approaches the limiting value of 0.215. The predicted pressure at the early period of indentation is unrealistic since then plastic deformation occurs only in regions adjacent to the platens, which is not reflected by the assumed velocity field.

#### 5.3.4 Comparison of the results

The best curves fitted to the experimental and theoretical results are shown in Fig. 5-26. As before the curves shown merely represent the trend of those narrow bands within which the experimental and theoretical curves fall. The theoretical results presented here are those obtained for smooth platens, since this was the approximate condition during the experiments.

The relationships between the contact width  $W_1/D_0$  and the amount of indentation  $(H_0-H)/H_0$  and also between the contact width  $W_2/D_0$  and the amount of indentation are shown in Figs. 5-26-A and 5-26-B respectively. At the beginning, the experimental curves are in good agreement with those obtained by the finite element method. As the amount of indentation increases, however, the finite element curves deviate from those obtained by experiments. The deviation observed is due to some discrepancies with regard to the material stress-strain

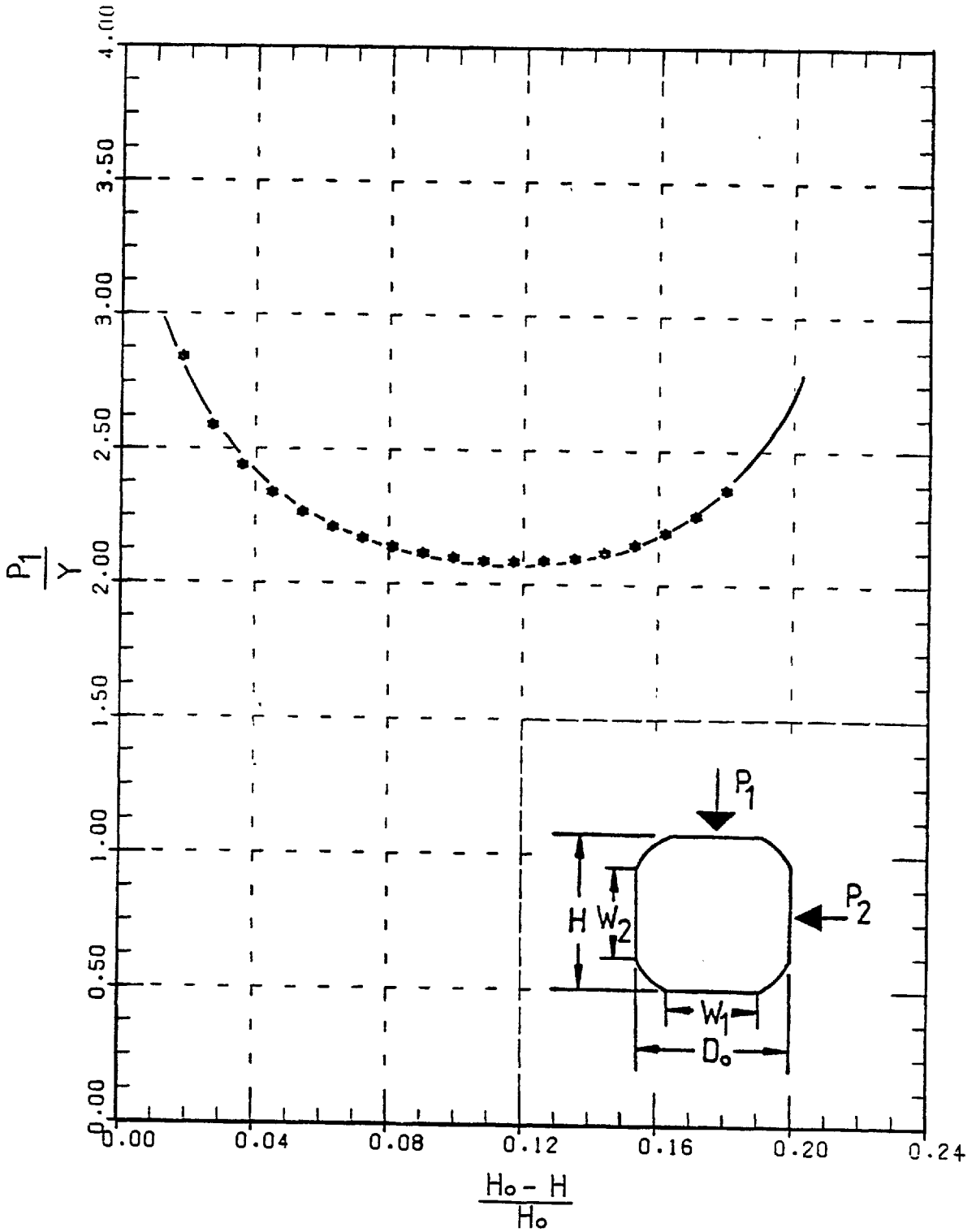


Fig. 5-25. Variation of mean normal pressure ' $P_1$ ' with height ' $H$ ' obtained by the upper bound theory.

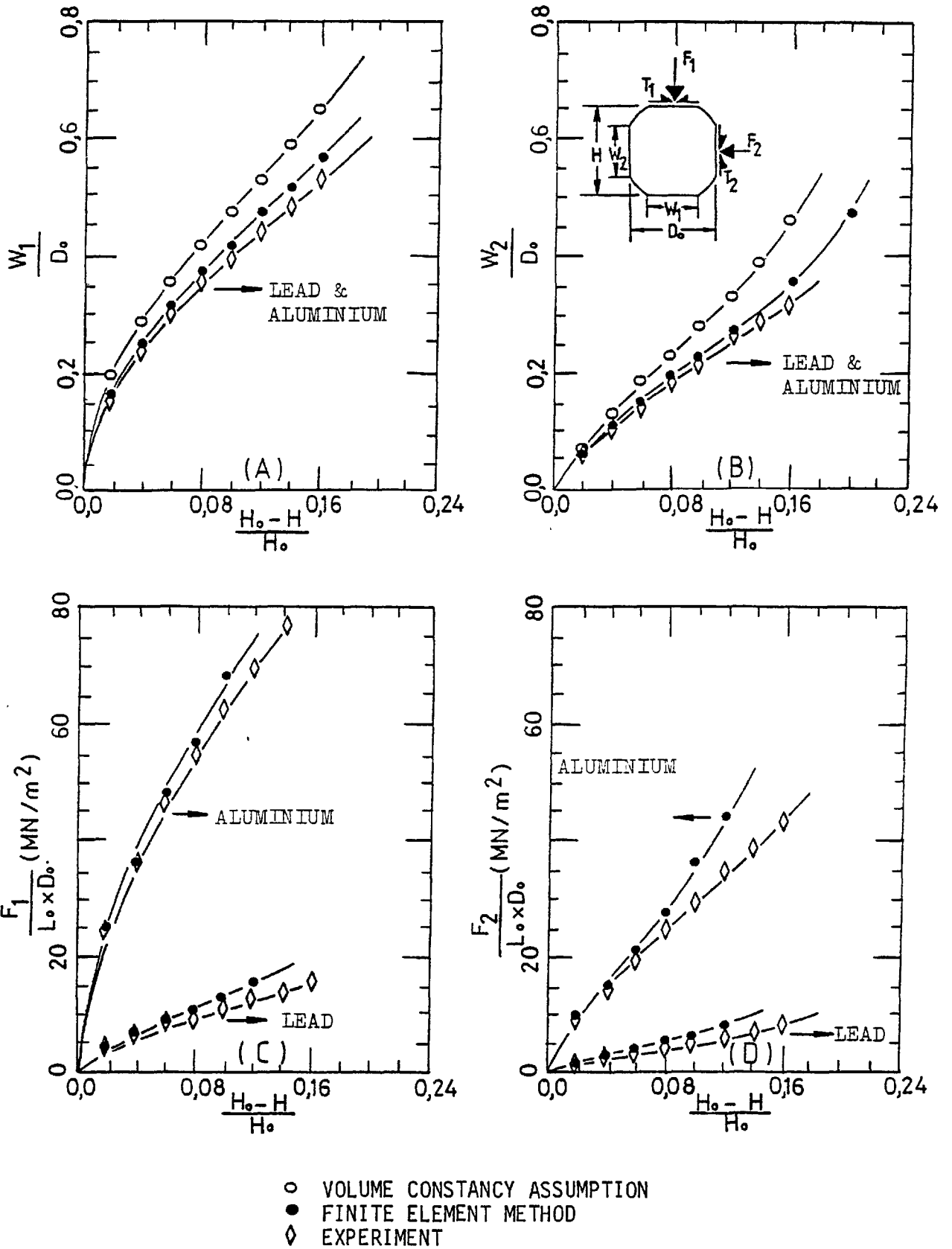
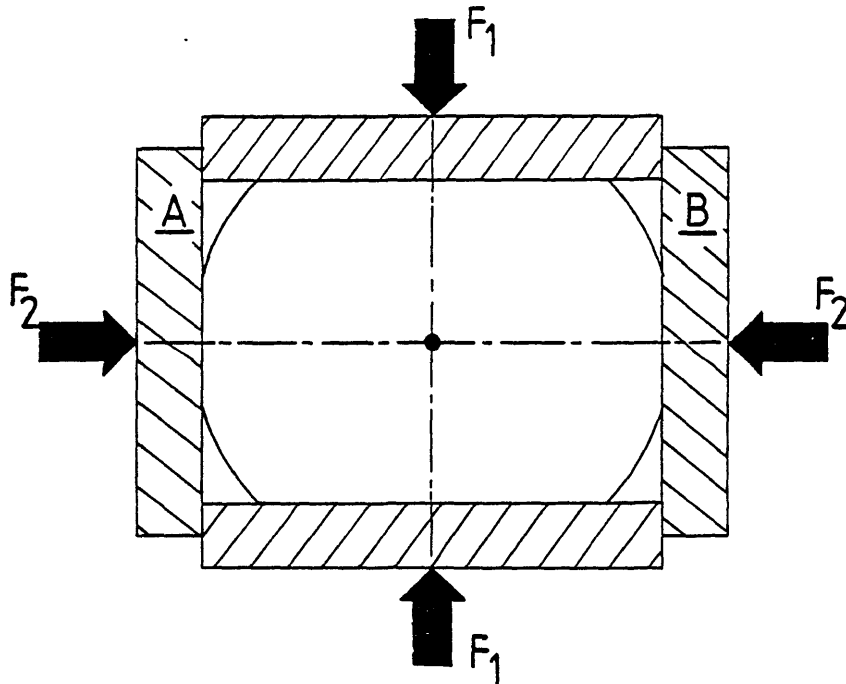


Fig. 5-26. Comparison of experimental and theoretical data.

used in the computation, and also because plane strain conditions were not strictly maintained during the experiment, particularly at large amounts of indentation. The curves obtained from volume constancy noticeably deviate from those obtained by experiment and by the finite element method. The higher predictions from volume constancy are due to the slightly unrealistic assumed behaviour of the free-surface which was used in this method, where it was assumed that all particles along the free-surface would move at the same speed in the x direction. As previously shown in section 5.3.2, this is in conflict with the actual movement of the free-surface obtained from experiment, particularly at large amounts of indentation, see Fig. 5-24.

The relationship between the indenting force  $F_1/(L_0 \times D_0)$  and the amount of indentation  $(H_0 - H)/H_0$  and also between the indenting force  $F_2/(L_0 \times D_0)$  and the amount of indentation  $(H_0 - H)/H_0$  are shown in Fig. 5-26-D. It can be seen that at small values of  $(H_0 - H)/H_0$  the theoretical results appear to be in good agreement with those obtained by experiment. As  $(H_0 - H)/H_0$  increases, however, deviation between these two sets of results becomes noticeable and is mainly due to some discrepancy with regard to the boundary conditions used in the computation. In the computation the deformation was considered under conditions of plane strain, contrary to the experimental conditions. As was previously argued in chapter 4, the conditions of plane strain were violated during the experiments, particularly at large amounts of indentation. Furthermore, the distance between platens A and B (see the illustration), used in the computation was considered constant during the course of indentation despite the fact that during the experiments the platens moved apart slightly. Clearly, if in the experiments the outward movement of platens A and B had been prevented, then greater

forces would have been sensed by all the platens and particularly by A and B. This explanation justifies the significant differences observed between the theoretical and experimental curves for the indenting force ' $F_2$ '.



#### 5.3.5 Supplementary computer runs

For this kind of indentation, some additional computer runs were performed to clarify the following two problems:

- I- The effect of different approximations of the actual stress-strain curve of the material on the computed results.
- II- The variations of the mean normal stress and mean shear stress at the interface of the billet and platens.

In what follows the computational results for these two problems are presented.

##### 5.3.5.1 Problem 'I'

The computation was carried out using the material properties of



of commercially pure aluminium and assuming no friction at the interface of the billet and platens. For the computation, two alternative linear approximations for the actual stress-strain curve of the material were used as shown in Fig. 5-27. The numerical values used for the two-straight-line approximation to the stress-strain curve were the same as those used before in case (a), section 5.2. For the single-straight-line approximation the numerical values used were as follows:

$$\bar{\sigma} = Y_0 + H_0 (\bar{\epsilon}_P)$$

where  $Y_0 = 90 \text{ MN/m}^2$  and  $H_0 = 78 \text{ MN/m}^2$ .

The computed results using the two different approximations of the material actual stress-strain curve are shown in Figs. 5-28-A to 5-28-D. The relationships between  $F_1/(L_0 \times D_0)$  and  $(H_0 - H)/H_0$  and also between  $F_2/(L_0 \times D_0)$  and  $(H_0 - H)/H_0$  are shown in Figs. 5-28-A and 5-28-B respectively. As previously described in section 5.2 the discontinuity of the curves is due to the finite sizes of elements along the free-surface of the billet. It is seen that the curves tend to become more continuous when the stress-strain curve is approximated in a more continuous manner (i.e. by approximations employing a greater number of straight lines). At low values of  $(H_0 - H)/H_0$  the indenting forces obtained by using the single-straight-line approximation are considerably larger than those obtained by using the two-straight-line approximation. This is because at small strains a much higher yield stress was used for the former approximation. At higher values of  $(H_0 - H)/H_0$  the indenting forces begin to converge. This occurs when the significant initial discrepancy between the two approximations of the actual stress-strain curve disappears at large plastic deformations. It is thus clear that

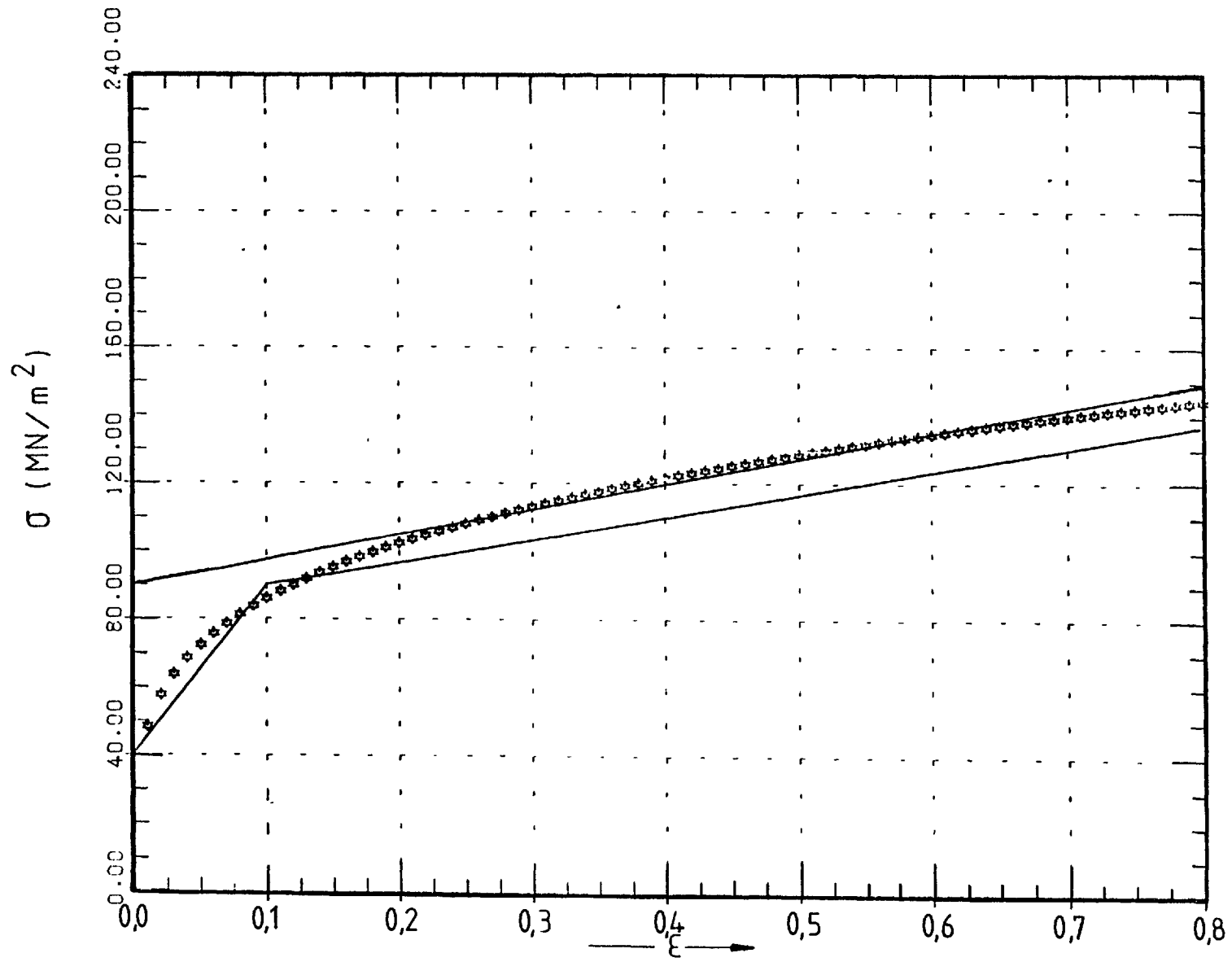


Fig. 5-27. Stress-strain curves for computer analysis for commercially pure aluminium.

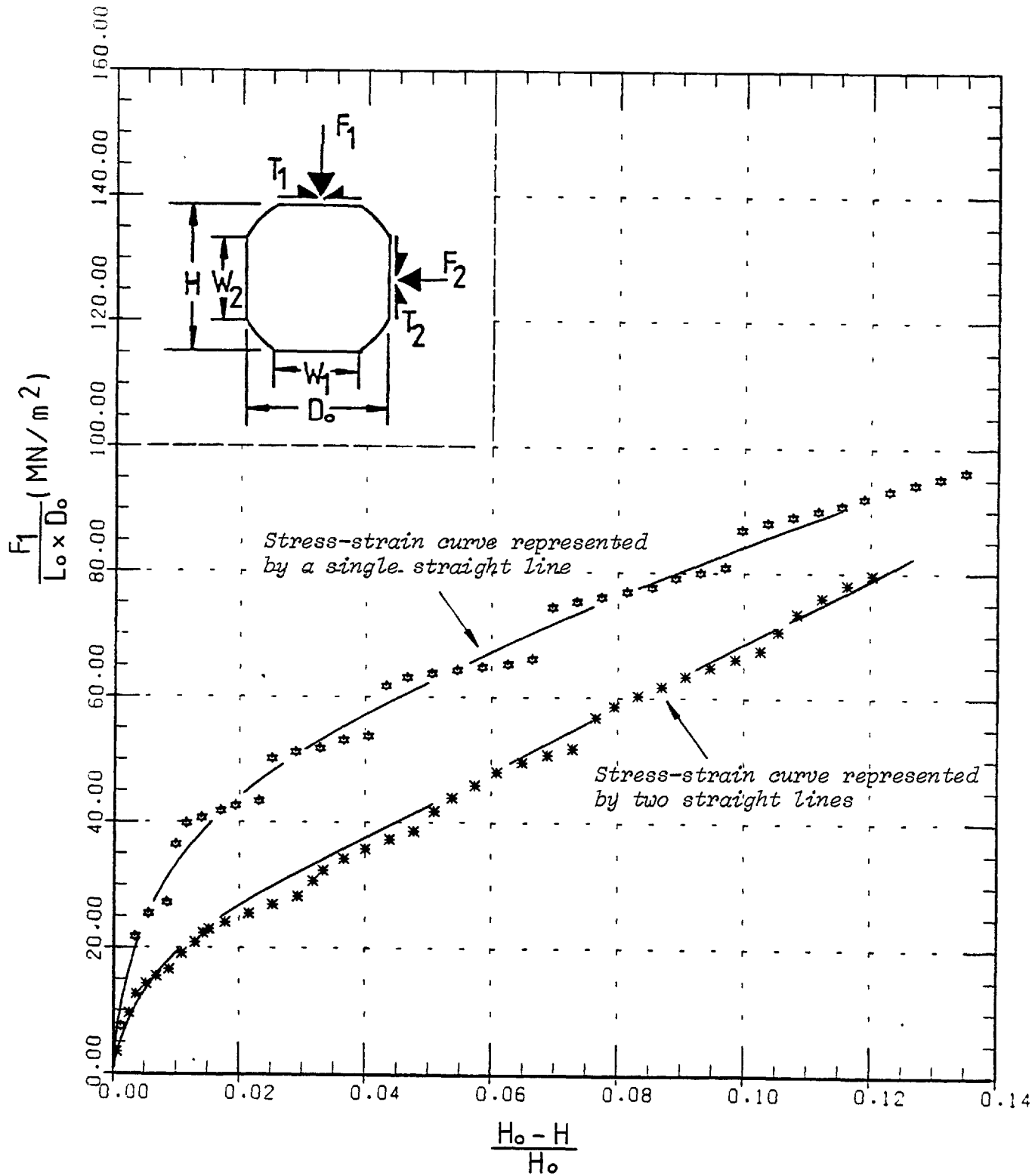


Fig. 5-28-A. Variations of indenting force ' $F_1$ ' with height ' $H$ ' for two different stress-strain curves approximating the commercially pure aluminium stress-strain curve.

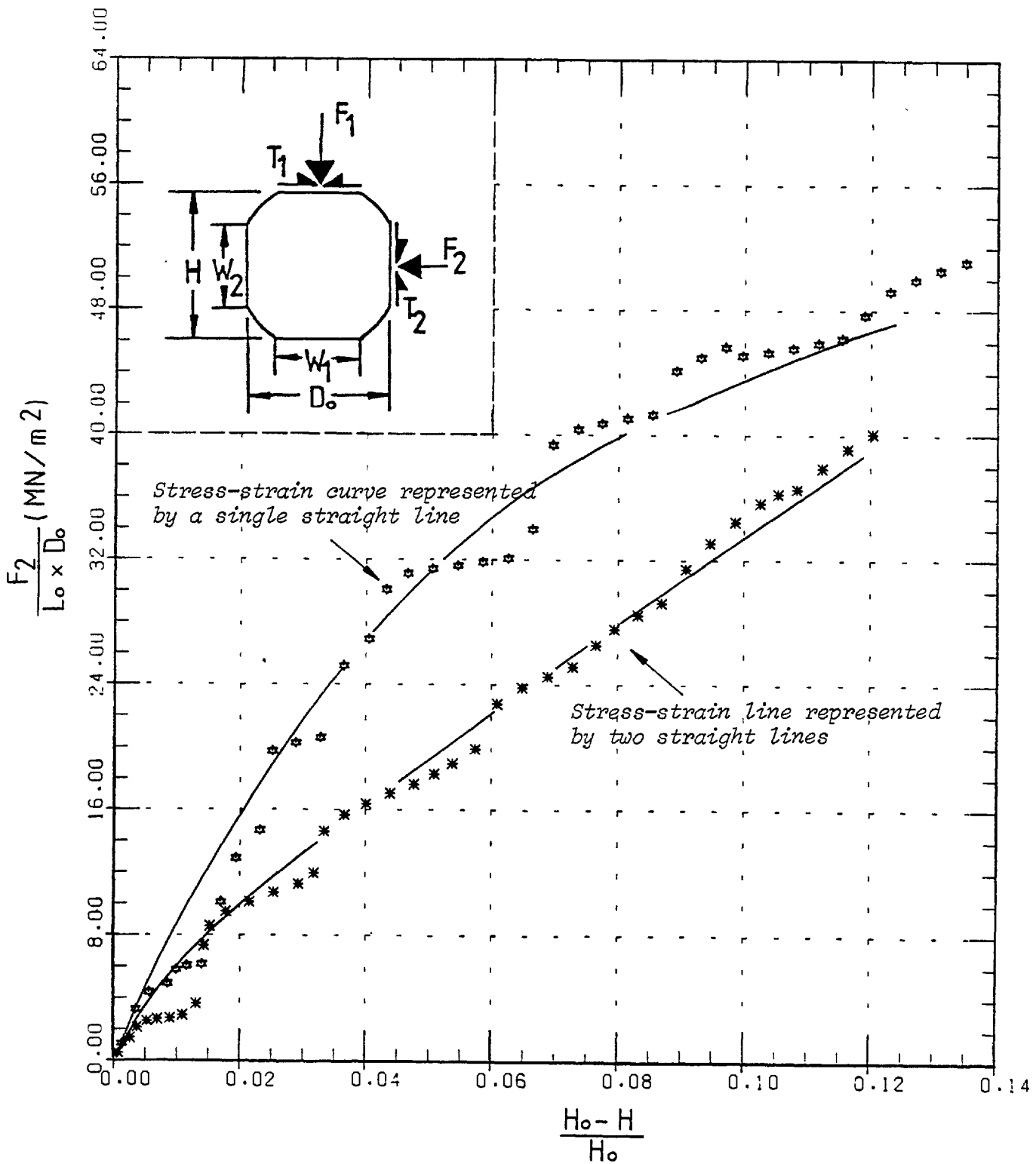


Fig. 5-28-B. Variations of indenting force ' $F_2$ ' with height ' $H$ ' for two different stress-strain curves approximating the commercially pure aluminium stress-strain curve.

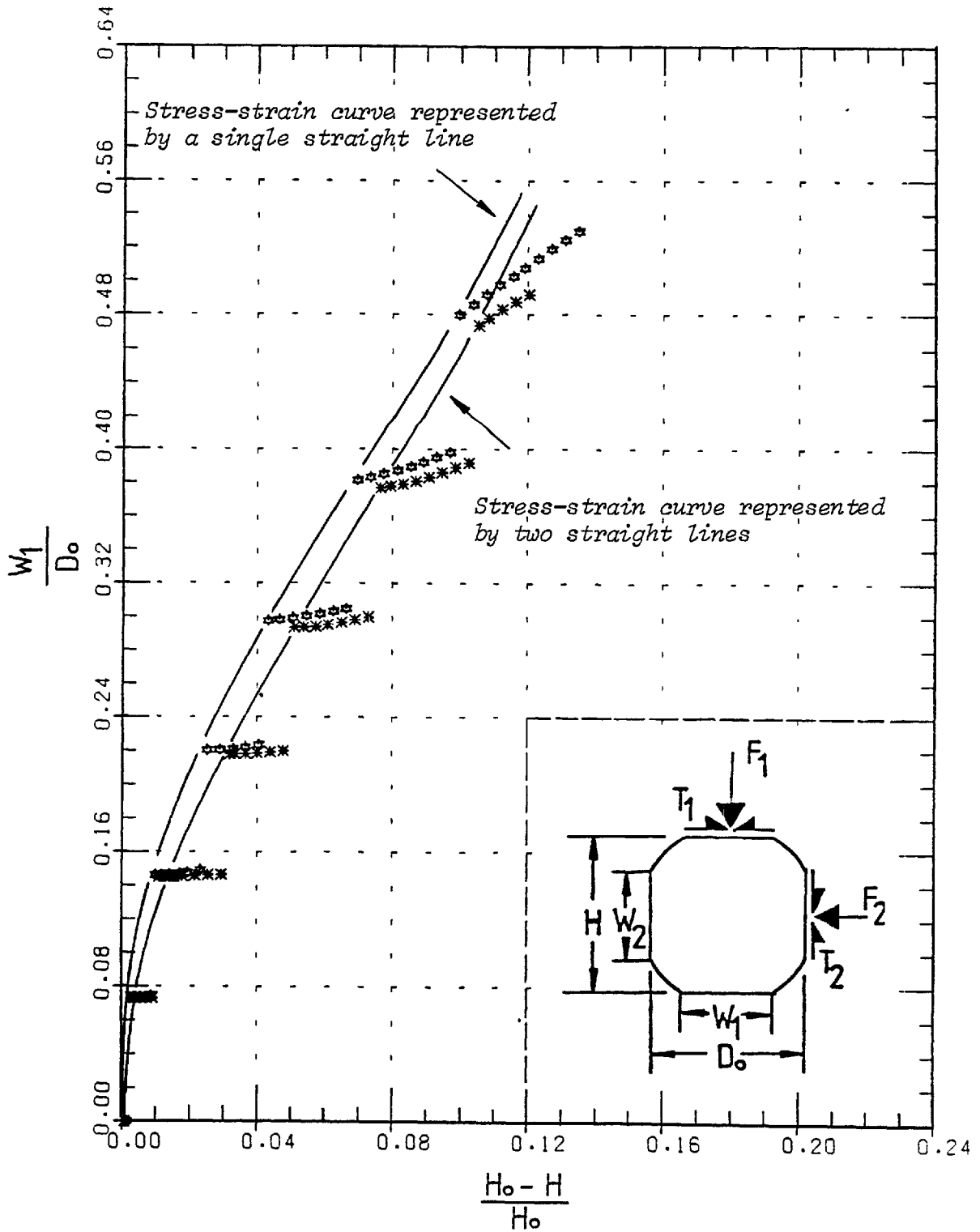


Fig. 5-28-C. Variations of contact width ' $W_1$ ' with height ' $H$ ', for two different stress-strain curves approximating the commercially pure aluminium stress-strain curve.

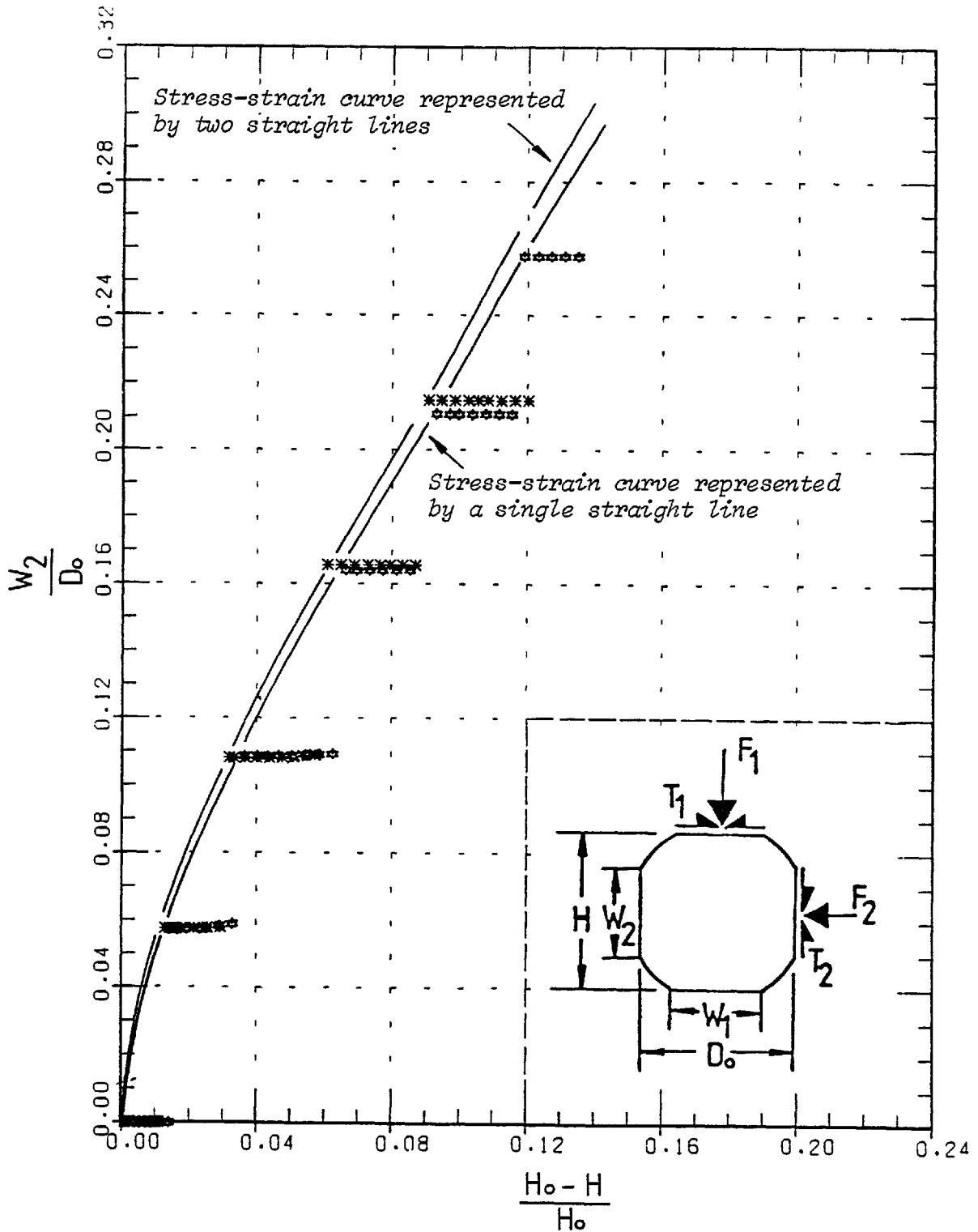


Fig. 5-28-C. Variations of contact width ' $W_2$ ' with height ' $H$ ' for two different stress-strain curves approximating the commercially pure aluminium stress-strain curve.

at large plastic deformations approximately the same results can be obtained from either a simple or a higher order approximation of the stress-strain curve. It is quite clear from the computation procedure that the rate at which deformation is imparted to the billet will increase if the stress-strain curve is a simple one. Clearly, the higher the rate of deformation, the less is the cost of computation. It is worth remembering that within the increments of displacement, the prescribed displacements must be decreased appropriately in order to allow the elements to pass one by one through the sharp corners of the assumed stress-strain curve. For a higher order curve (i.e. with a higher number of straight lines) a higher number of sharp corners must be passed, thus increasing computing time.

#### 5.3.5.2 Problem II

The computation was carried out using the material properties of lead and assuming two types of boundary conditions. In one type the platens were assumed smooth and thus there is no shear stress induced at the interface of the billet and the platens. In another type of boundary conditions the platens were assumed rough and the contact nodes were restrained from any movement along the platen surfaces. The computation was continued until a large amount of indentation of nearly 0.20 was achieved. It is worth mentioning that in all the problems analysed so far, due to the high cost of computation the billets were not indented by an amount greater than 0.14.

The computed results are shown in Figs. 5-29-A to 5-29-J. The best fitted curves which were subsequently used in the calculation of mean normal stress and mean shear stress, acting at the interface of the billet and the platens, are those shown in dotted lines. The

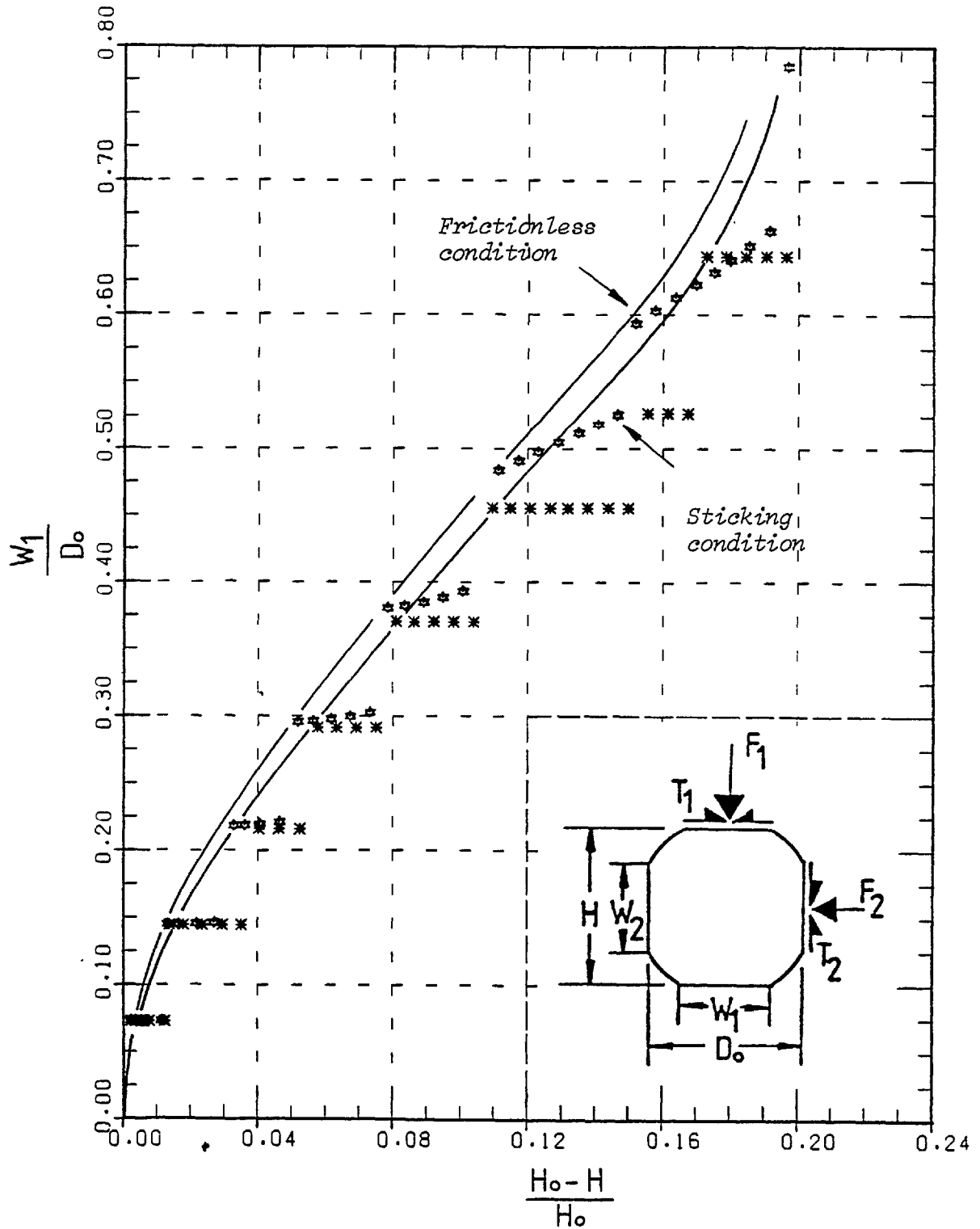


Fig. 5-29-A. Variation of contact width ' $W_1$ ' with height ' $H$ ' for commercially pure lead obtained by the finite element method.



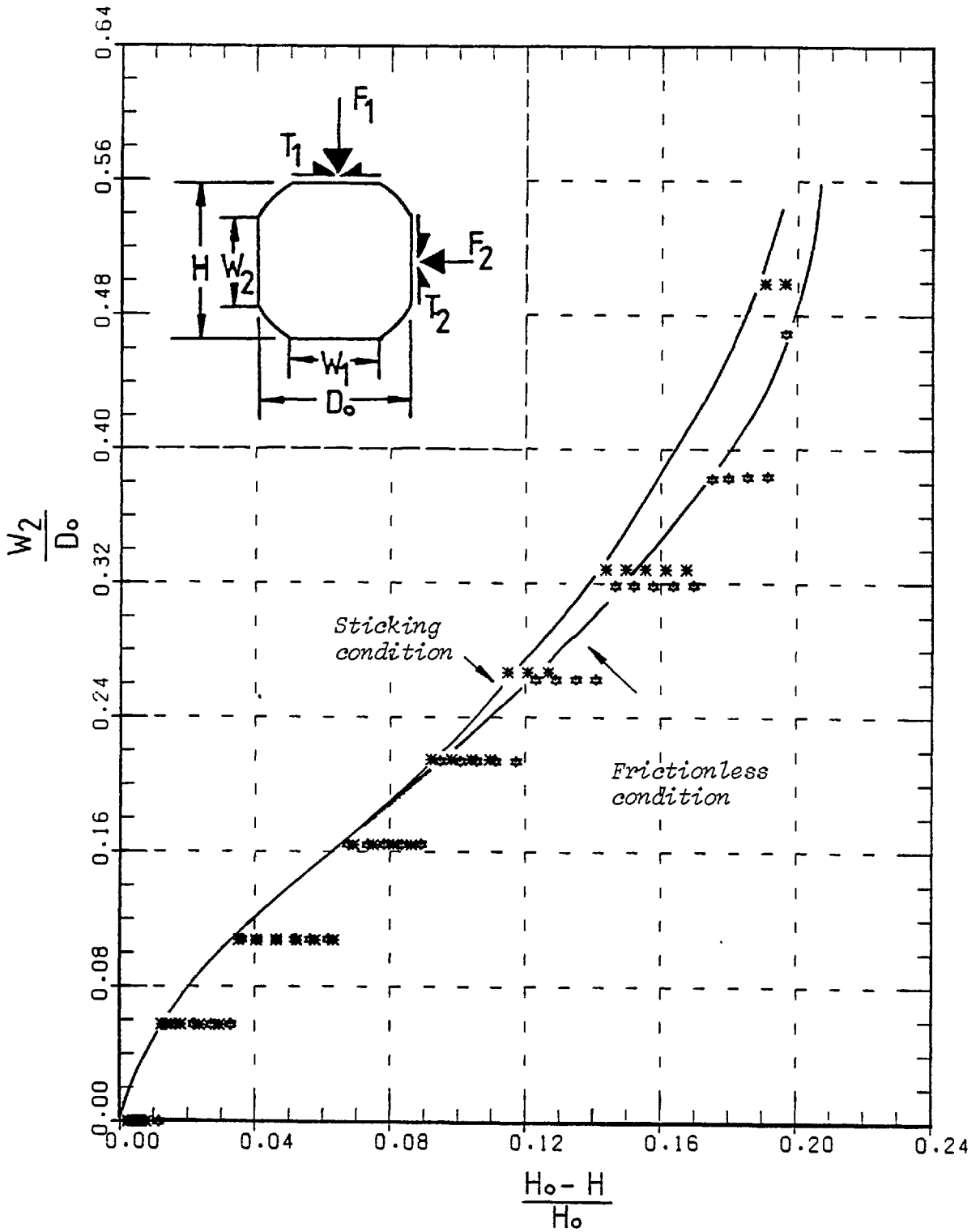


Fig. 5-29-B. Variation of contact width ' $W_2$ ' with height ' $H$ ' for commercially pure lead obtained by the finite element method.

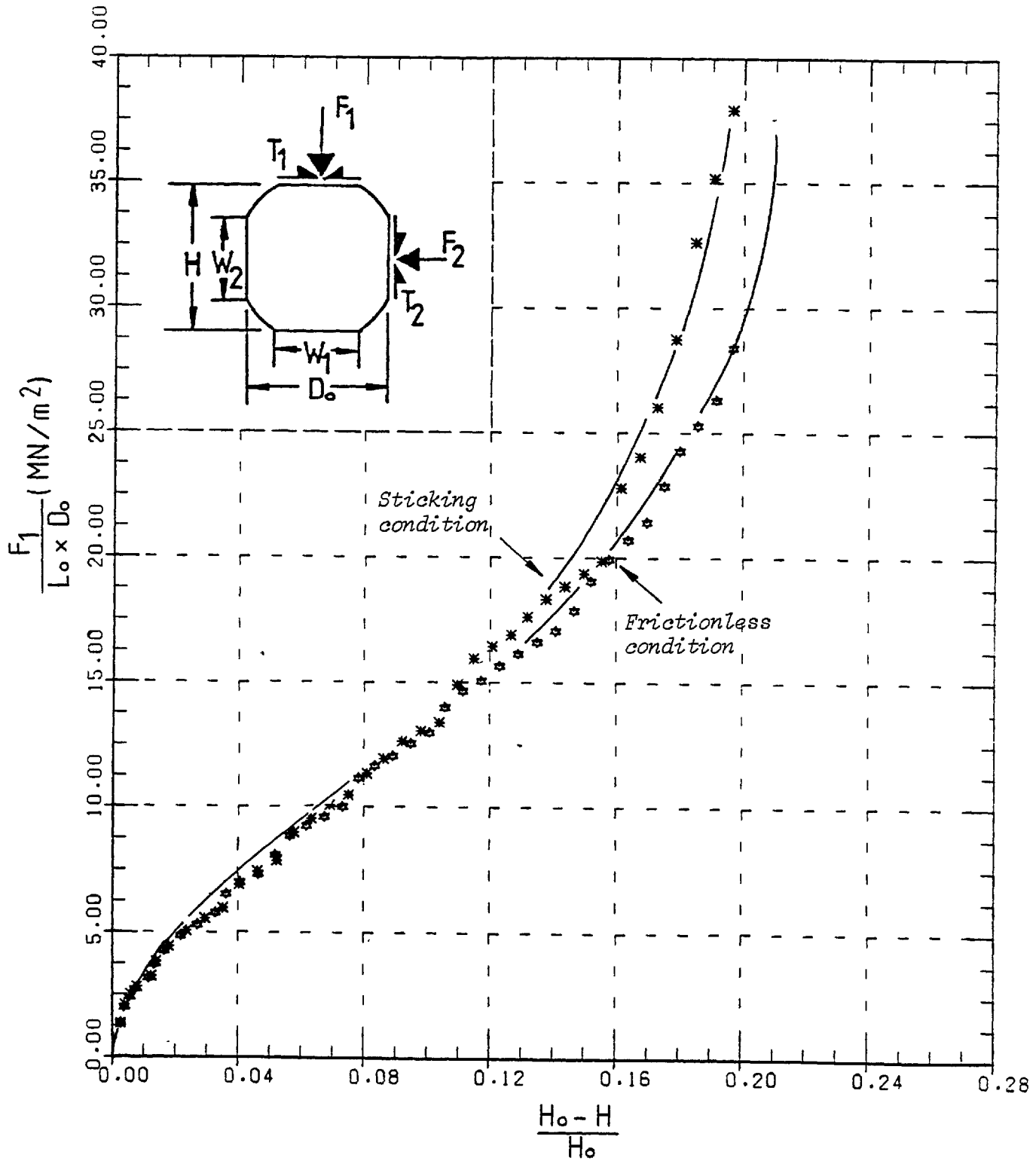


Fig. 5-29-C. Variation of indenting force ' $F_1$ ' with height ' $H$ ' for commercially pure lead obtained by the finite element method.

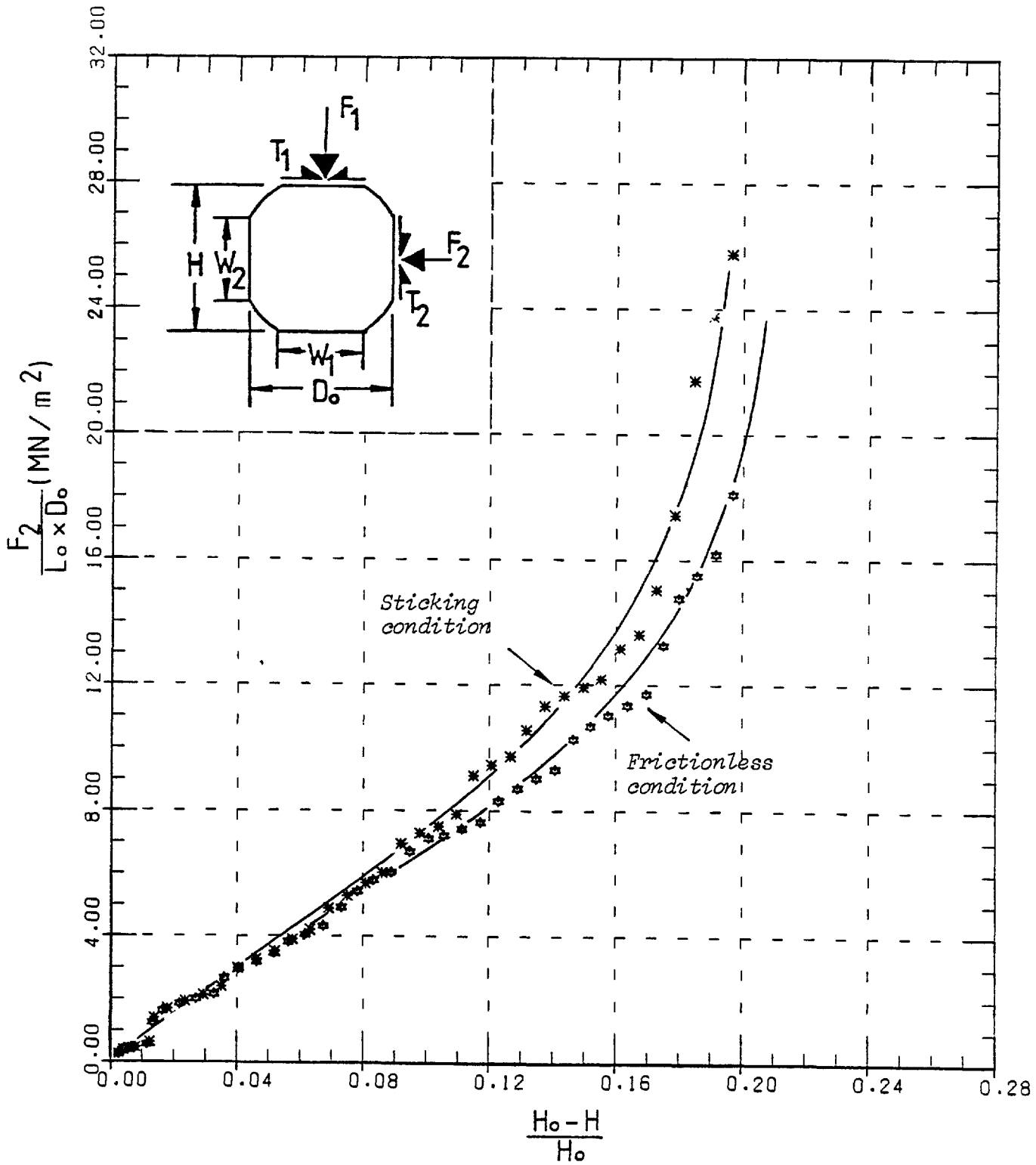


Fig. 5-29-D. Variation of indenting force ' $F_2$ ' with height ' $H$ ' for commercially pure lead obtained by the finite element method.

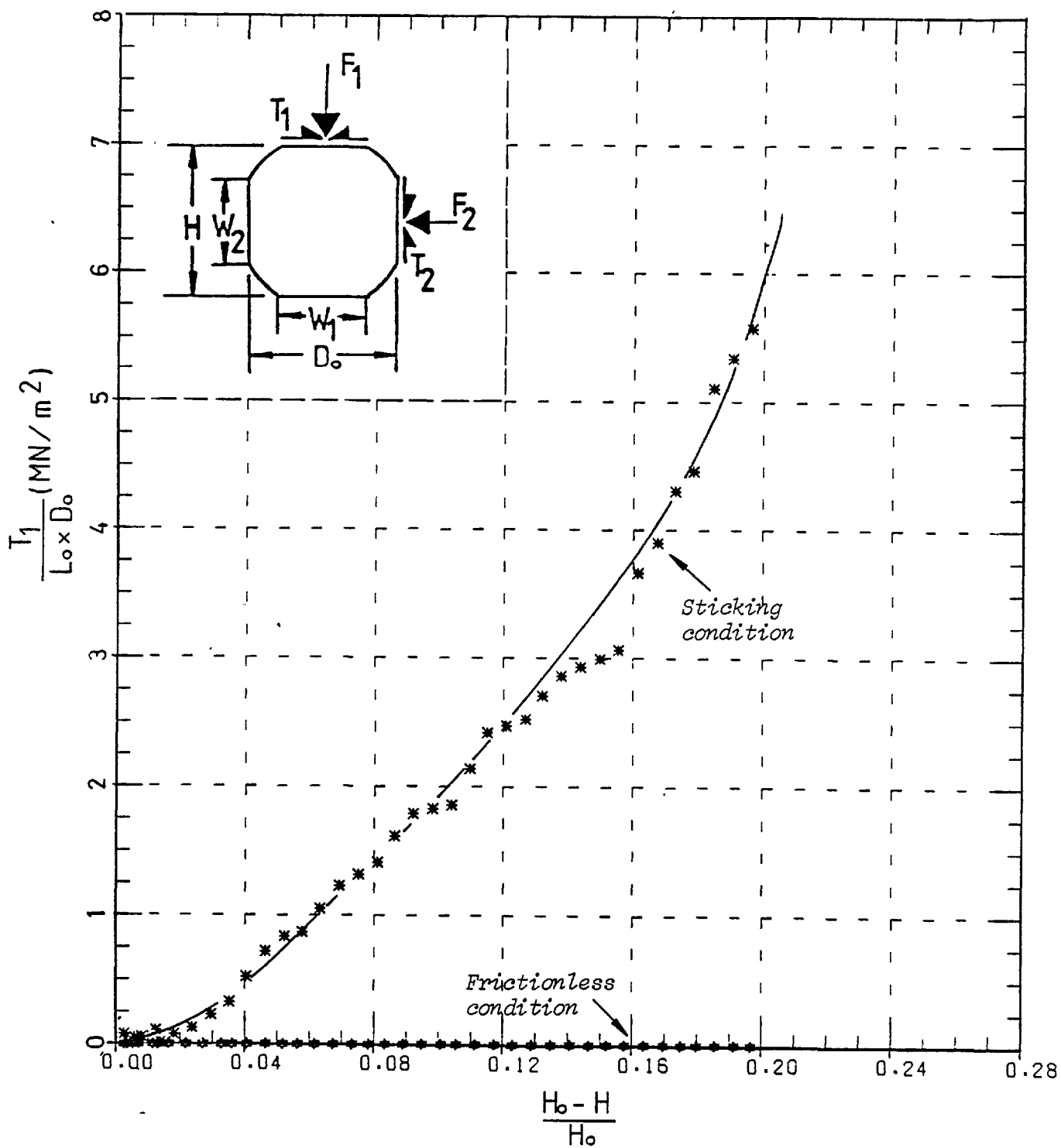


Fig. 5-29-A. Variation of interfacial frictional force ' $T_1$ ' with height ' $H$ ' for commercially pure lead obtained by the finite element method.

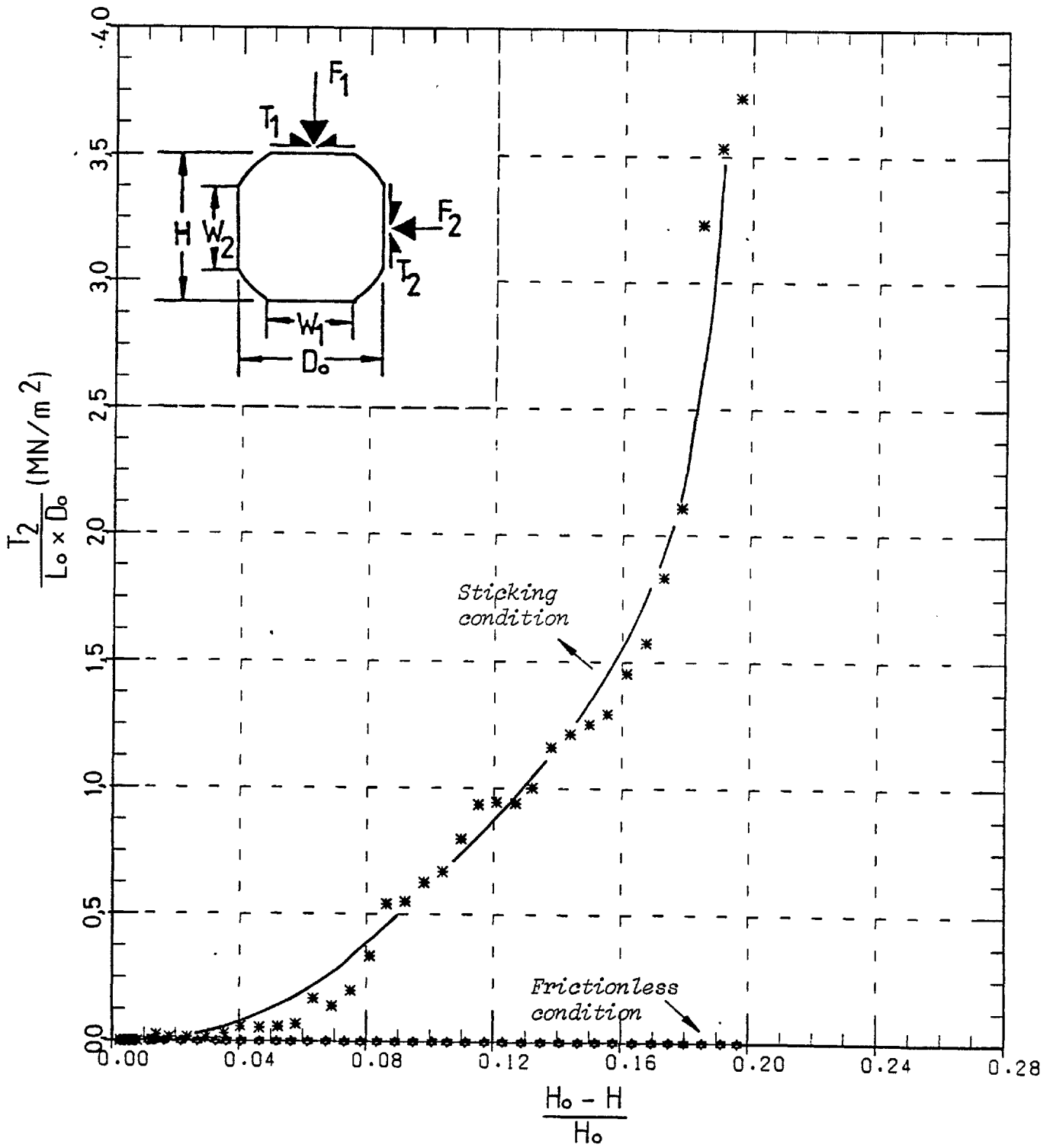


Fig. 5-29-F. Variation of interfacial frictional force ' $T_2$ ' with height ' $H$ ' for commercially pure lead obtained by the finite element method.

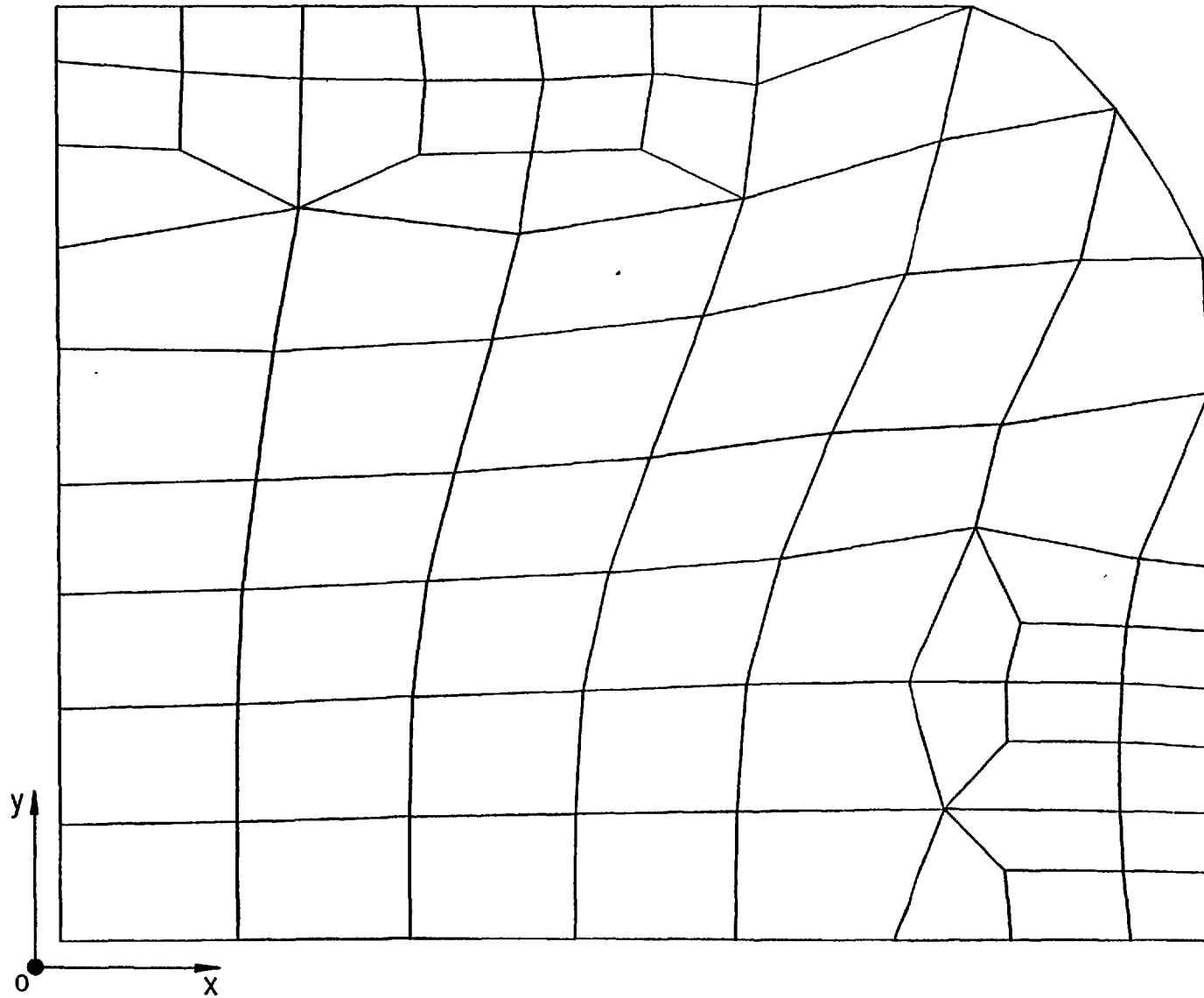


Fig. 5-29-G. Deformation of original mesh at  $(H_0 - H)/H_0 = 0.20$  in frictionless condition.

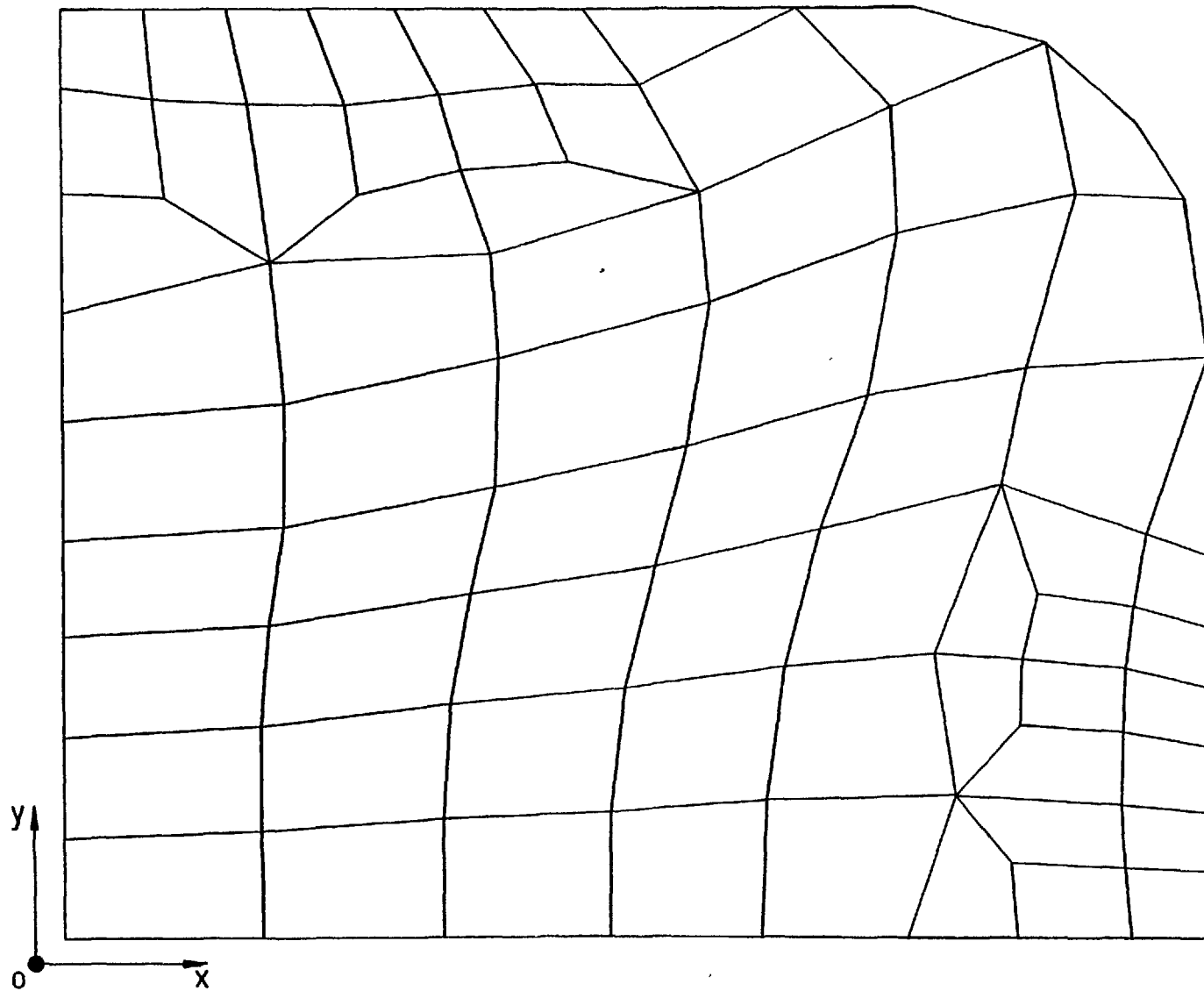


Fig. 5-29-H. Deformation of original mesh at  $(H_0 - H)/H_0 = 0.20$  in sticking condition.

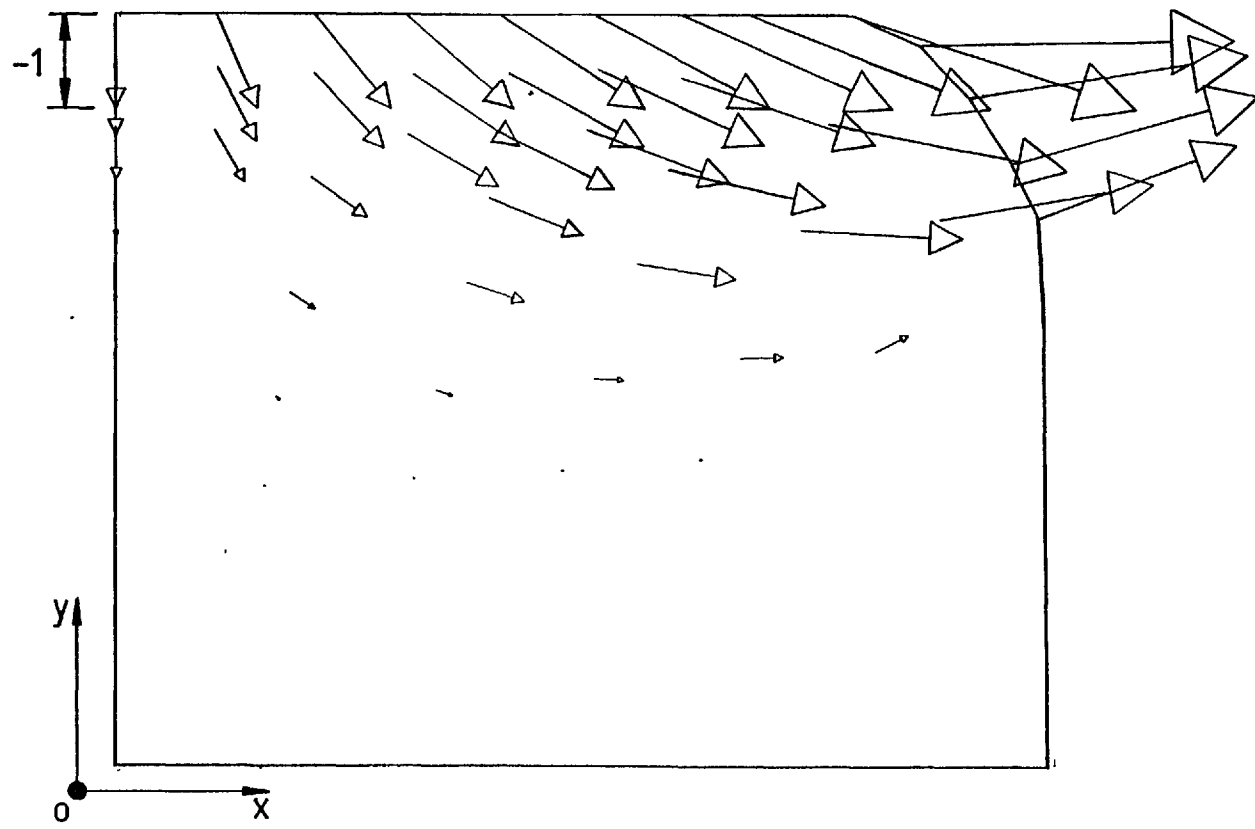


Fig. 5-29-1. Flow pattern at  $(H_0 - H)/H_0 = 0.20$  in frictionless condition, velocity of the top platen being -1.



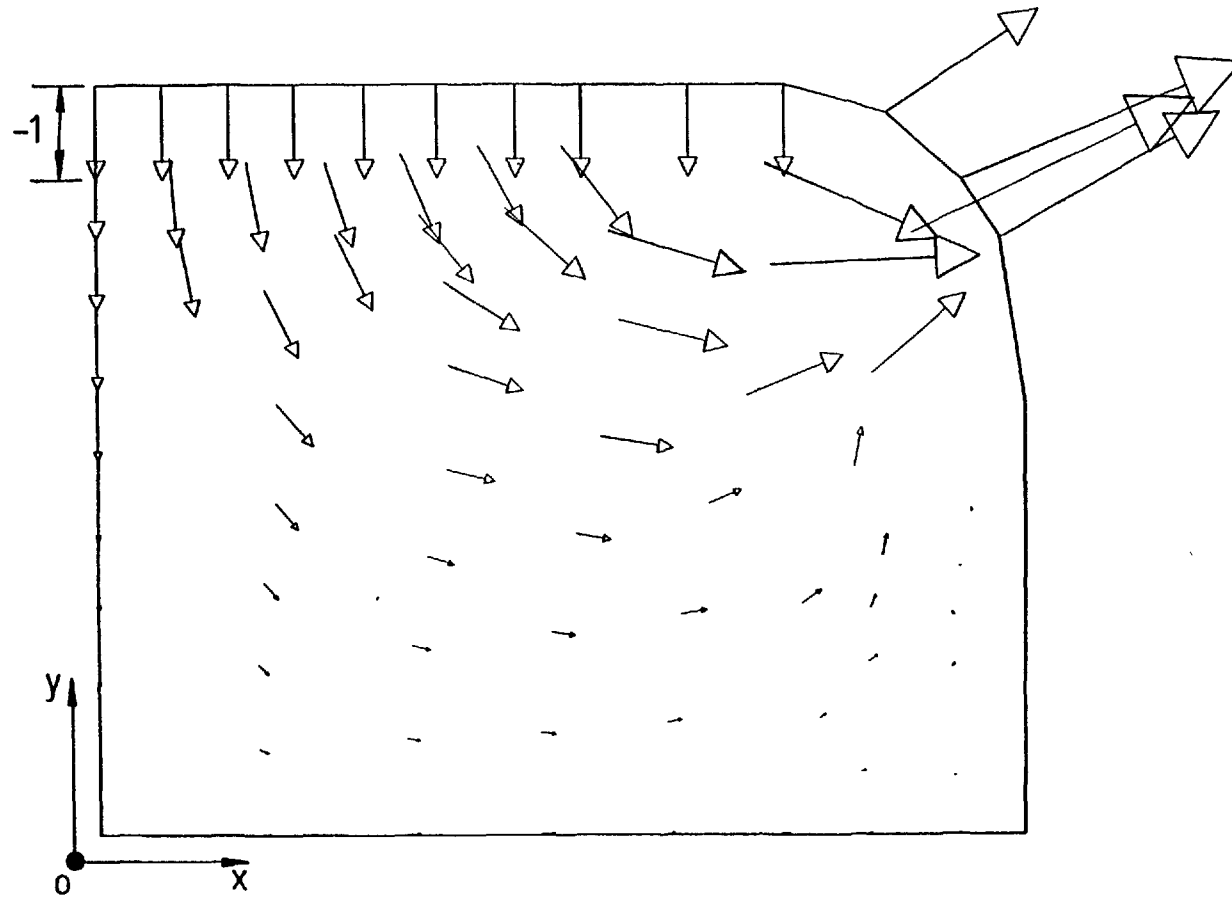
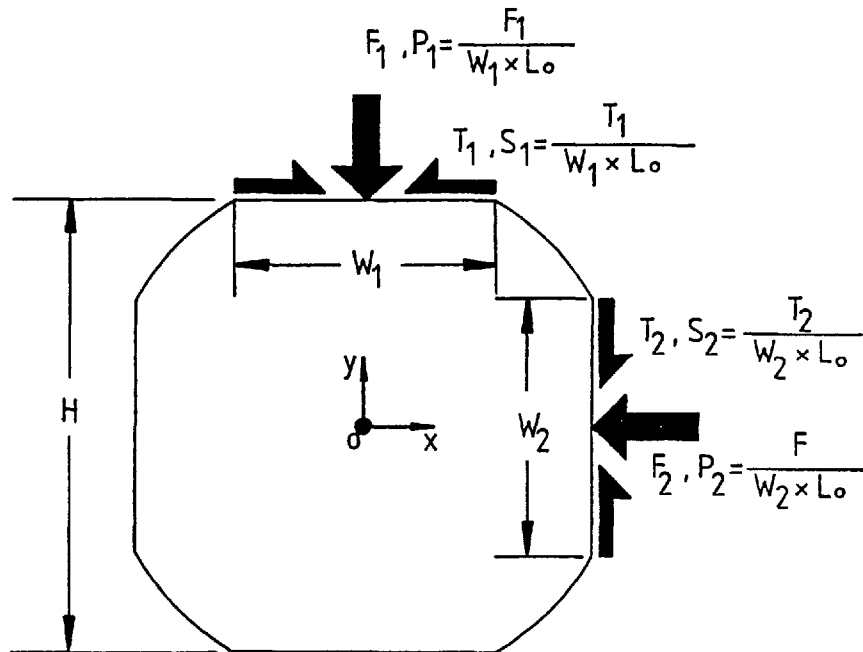


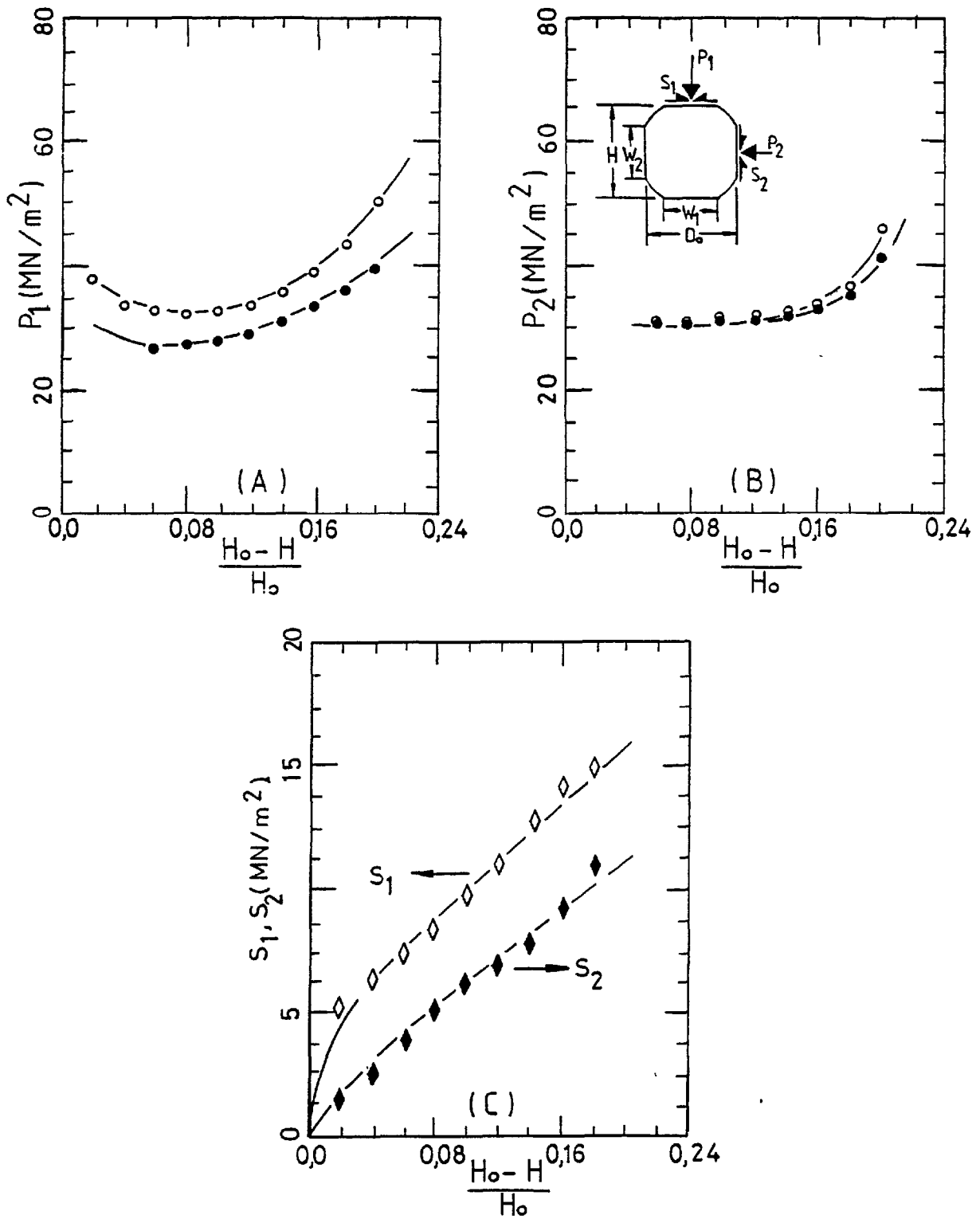
Fig. 5-29-J. Flow pattern at  $(H_0 - H)/H_0 = 0.20$  in sticking condition, velocity of the top platen being -1.

calculated mean normal stress and mean shear stresses are shown in Fig. 5-30 (for definition of the stresses used see the illustration below).



The relationship between the mean normal stress ' $P_1$ ' and the amount of indentation  $(H_0 - H)/H_0$  is shown in Fig. 5-30-A. As seen the curve decreases to a minimum and then increases towards infinity as the amount of indentation approaches the limiting value of 0.215. The effect of friction, which in general displaces the whole curve upwards can clearly be seen. It is worth noting that the general trend of the curve for the case without friction is in good agreement with that obtained from the upper-bound theorem, see Fig. 5-25.

The relationship between the mean normal pressure ' $P_2$ ' and the amount of indentation  $(H_0 - H)/H_0$  is shown in Fig. 5-30-B. As seen the curve first decreases, then remains constant over a relatively long period of indentation, and finally increases towards infinity as the



○ ◇ ◆ Sticking boundary condition  
 ● Frictionless boundary condition

Fig. 5-30. Variations of normal and shear stresses predicted by the finite element method for commercially pure lead.

amount of indentation approaches the limiting value of 0.215. The effect of friction on the curve over the first period of indentation is not significant, but at high amounts of indentation friction takes effect and displaces the curve slightly.

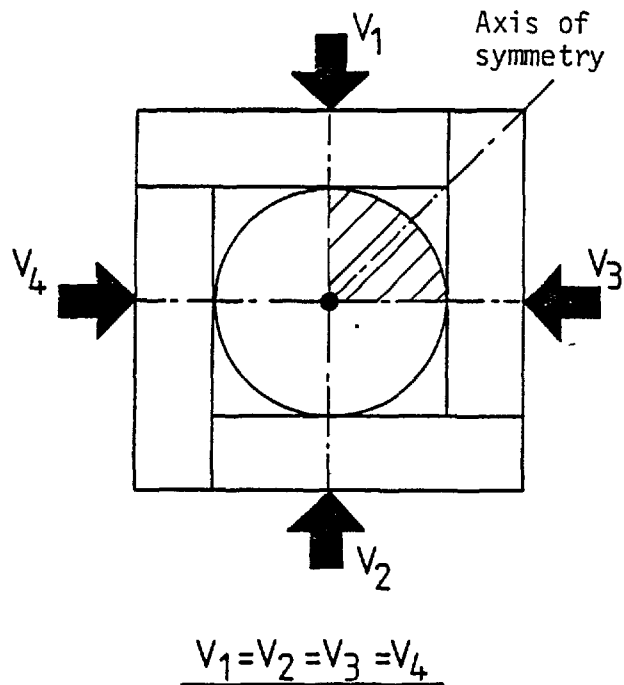
The relationships between the shear stress ' $S_1$ ' and the amount of indentation  $(H_0-H)/H_0$  and also between the shear stress ' $S_2$ ' and the amount of indentation  $(H_0-H)/H_0$  are shown in Fig. 5-30-C. The shear stress ' $S_1$ ' first rises rapidly and then increases at a constant rate. In general, the shear stress ' $S_2$ ' increases at a constant rate and nearly equal to the rate of the shear stress ' $S_1$ '.

#### 5.4 A study of case (c)

As was previously described in section 5.1, in this case the chamber was comprised of four platens (see the illustration below).

the moving platens  
being driven in the  
directions indicated by  
the arrows to indent an  
initially round billet.

As before, in the  
computation only one  
quarter of the billet  
cross-section was  
considered. Although  
in this case, due to  
the symmetry of  
deformation, one  
eighth of the cross-



section could also have been used, but at the expense of generating a new mesh entirely different from that shown in Fig. 5-2. The computation was carried out using the material properties of lead, the stress-strain curve was that previously used in case (a), section 5.2.

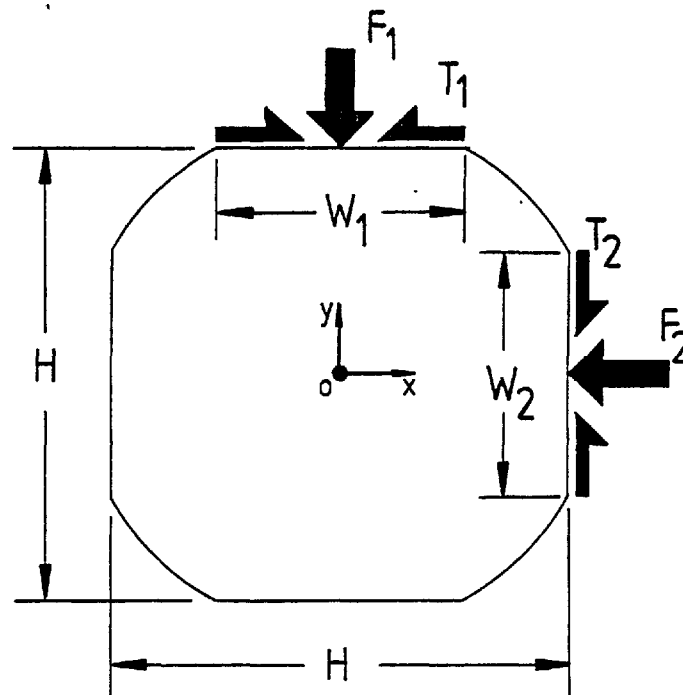
To persue the history of deformation the following parameters were computed and recorded (see also the illustration below):

1-  $\frac{H_0 - H}{H_0}$  = amount of indentation.

2-  $\frac{W_1}{D_0}$  and  $\frac{W_2}{D_0}$  = non-dimensional widths of the flats.

3-  $\frac{F_1}{L_0 \times D_0}$  and  $\frac{F_2}{L_0 \times D_0}$  = indenting forces.

4-  $\frac{T_1}{L_0 \times D_0}$  and  $\frac{T_2}{L_0 \times D_0}$  = frictional forces at billet/chamber interface.



where  $D_0 = H_0$  = initial diameter of the billet and  $L_0$  = initial length

of the billet.

Although the parameters  $W_1$ ,  $F_1$  and  $T_1$  were theoretically sufficient to describe the billet deformation, the parameters  $W_2$ ,  $F_2$  and  $T_2$  were also computed and recorded. Clearly any discrepancy in the symmetric parameter (e.g. in  $W_1$  and  $W_2$ ) will be due to the non-symmetric nature of the mesh. The discrepancy in the results obtained thus provides a means of studying the effect of mesh pattern.

As before in the computation two types of boundary conditions were considered. In one type, the billet was indented by smooth platens, and the nodes in contact with them were permitted to move freely along the surface of the platens. In the other type of the boundary condition the billet was indented by rough platens and the contact nodes were restrained from moving.

#### 5.4.1 Results obtained by the finite element method

The computed results using the material properties of lead are shown in Figs. 5-31-A to 5-31-F. The relationship between the contact width  $W_1/D_0$  and the amount of indentation is shown in Fig. 5-31-A. The curve shows the same trend as that obtained in case (b), Fig. 5-29-A, in which the platens positioned on the sides of the billet remained stationary during the course of indentation. The effect of friction on the curve is quite clear. Friction in general is seen to displace the whole curve upwards particularly when the amount of indentation is large.

The relationship between the contact width  $W_2/D_0$  and the amount of indentation is shown in Fig. 5-31-B. It was previously argued that that due to the symmetry of deformation the contact widths ' $W_1$ ' and ' $W_2$ ' should theoretically be equal, and that any discrepancy in ' $W_1$ ' and ' $W_2$ ' would be accounted for the non-symmetric nature of the mesh used.

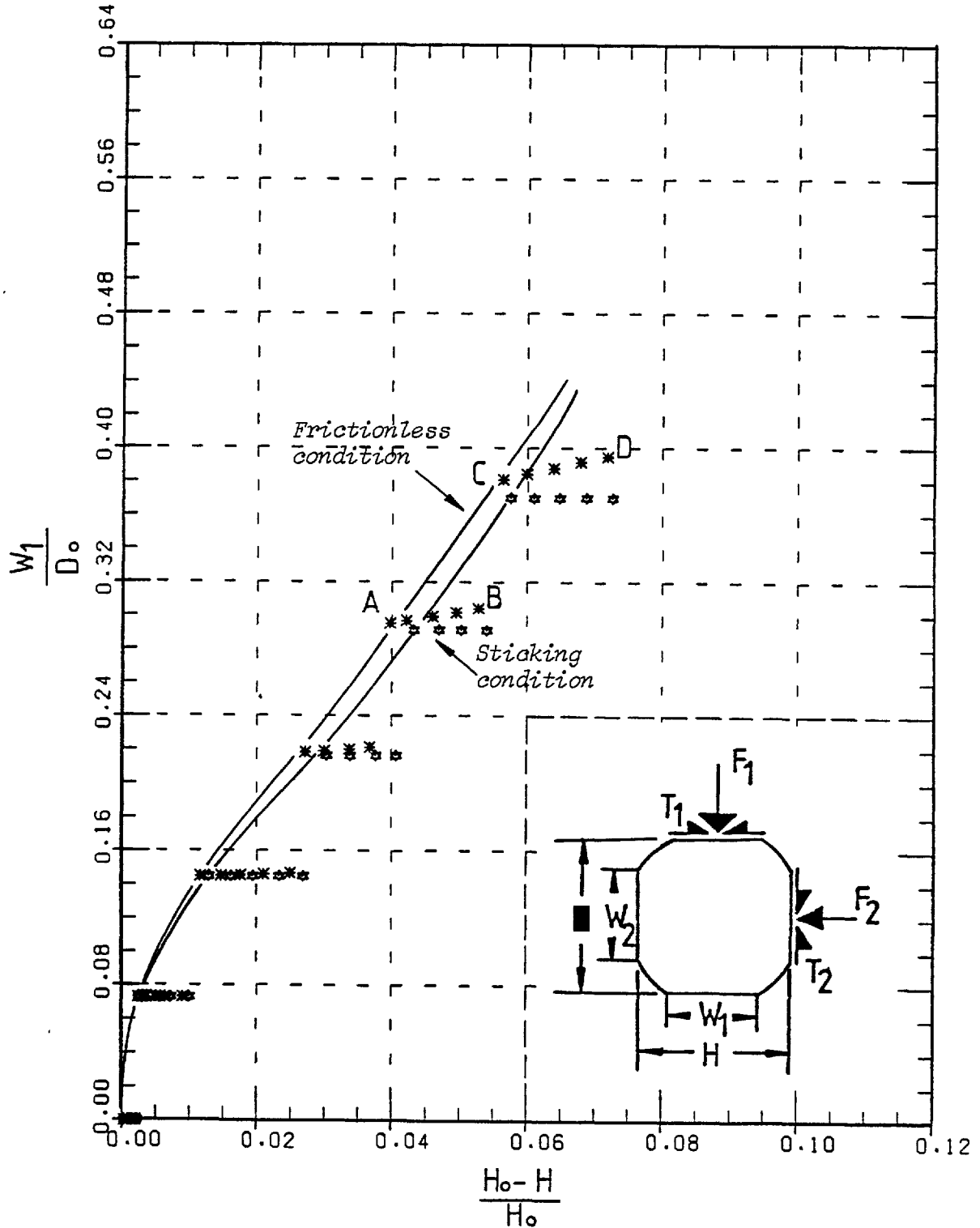


Fig. 5-31-A. Variation of contact width ' $W_1$ ' with height ' $H$ ' for commercially pure lead obtained by the finite element method.

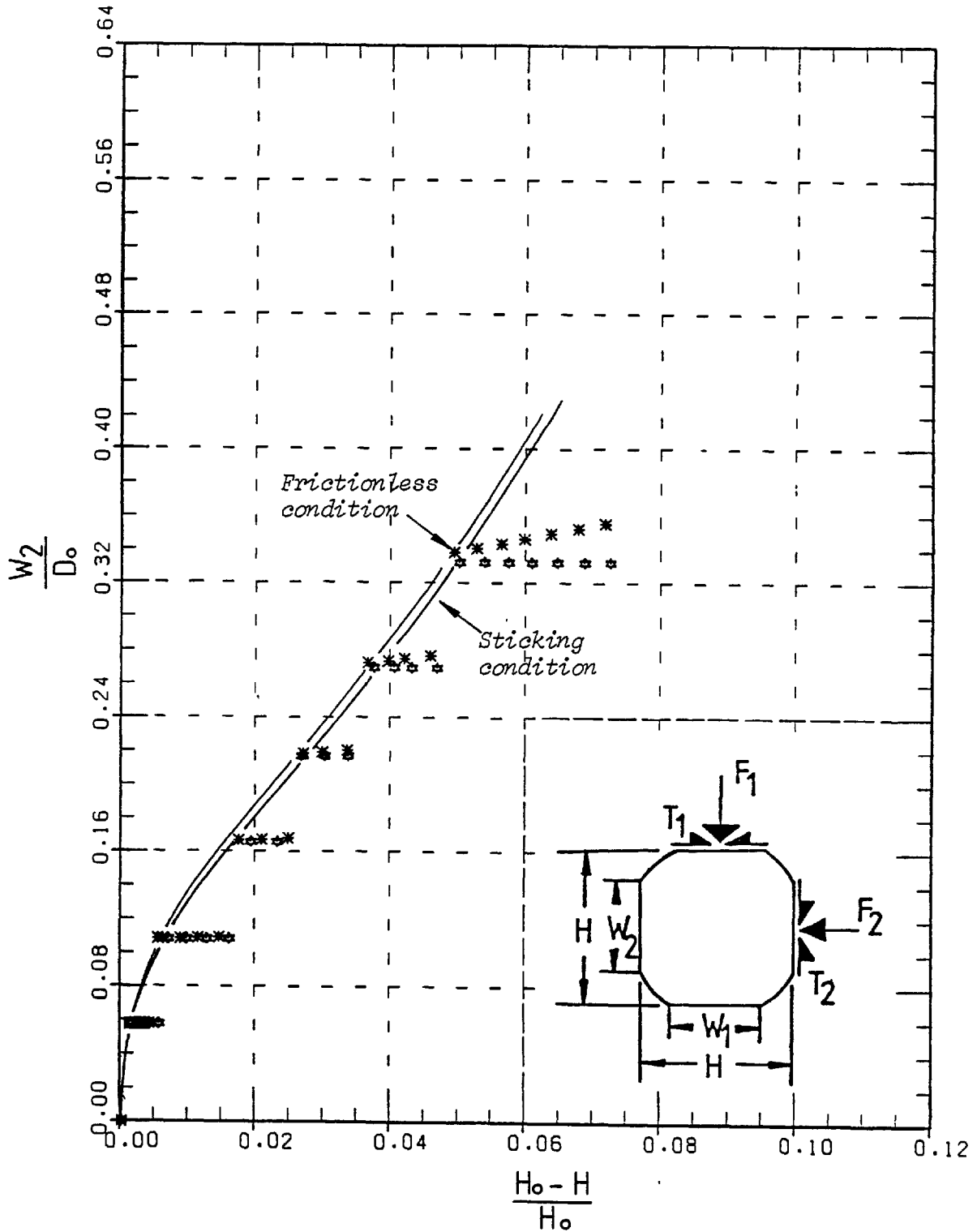


Fig. 5-31-B. Variation of contact width ' $W_2$ ' with height ' $H$ ' for commercially pure lead obtained by the finite element method.



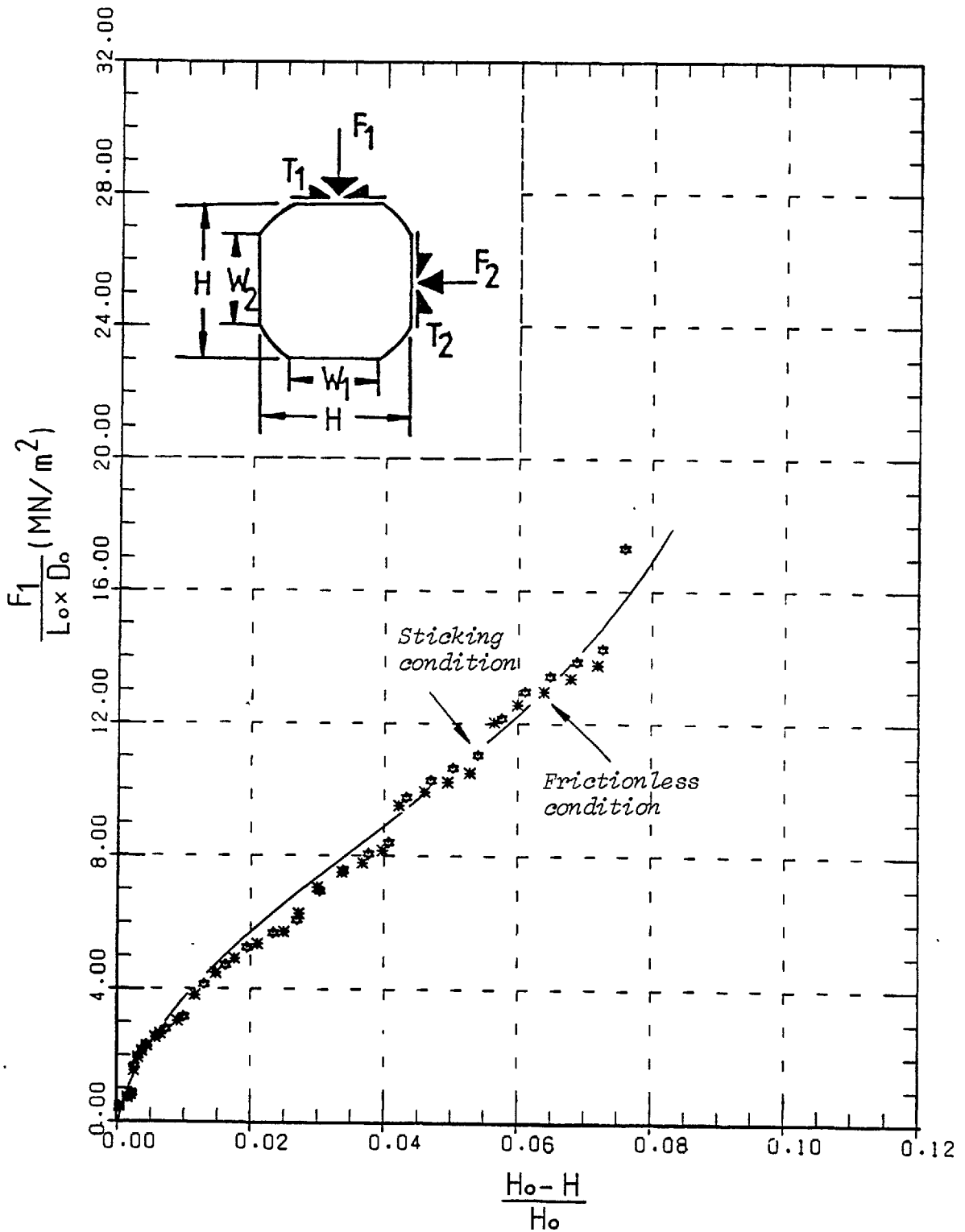


Fig. 5-31-C. Variation of indenting force ' $F_1$ ' with height ' $H$ ' for commercially pure lead obtained by the finite element.

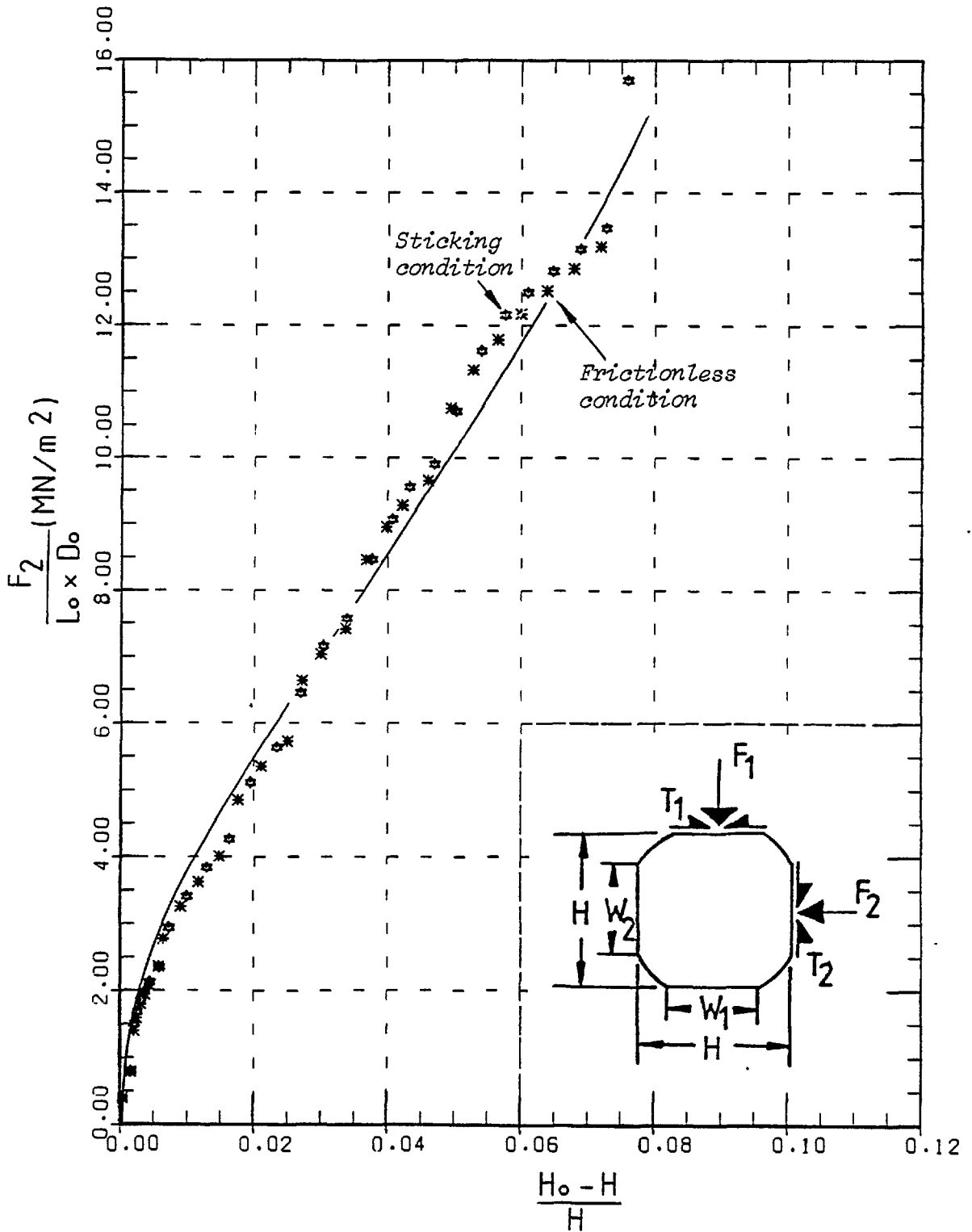


Fig. 5-31-D. Variation of indenting force 'F<sub>2</sub>' with height 'H' for commercially pure lead obtained by the finite element method.

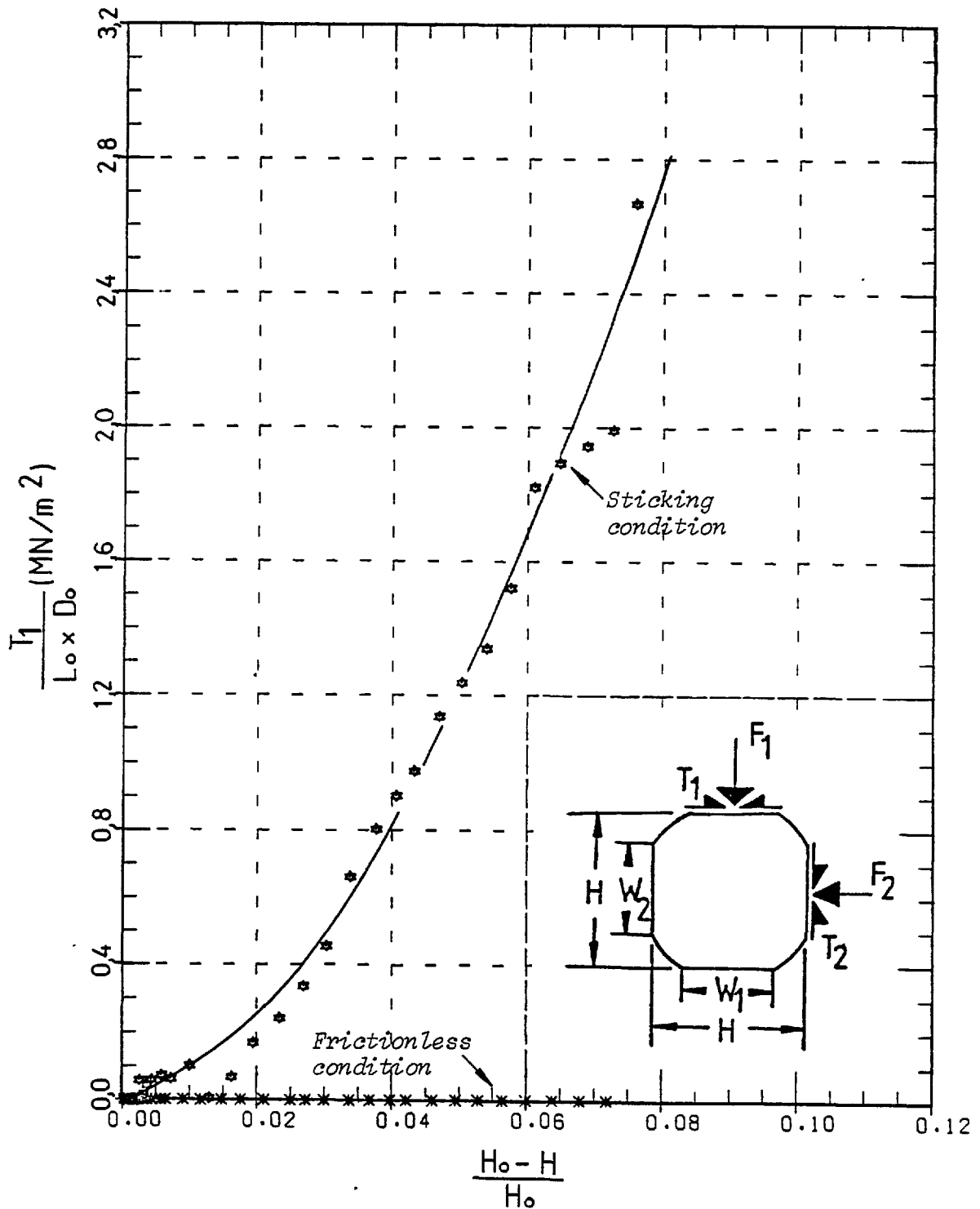


Fig. 5-31-E. Variation of interfacial frictional force ' $T_1$ ' with height ' $H$ ' for commercially pure lead obtained by the finite element method.

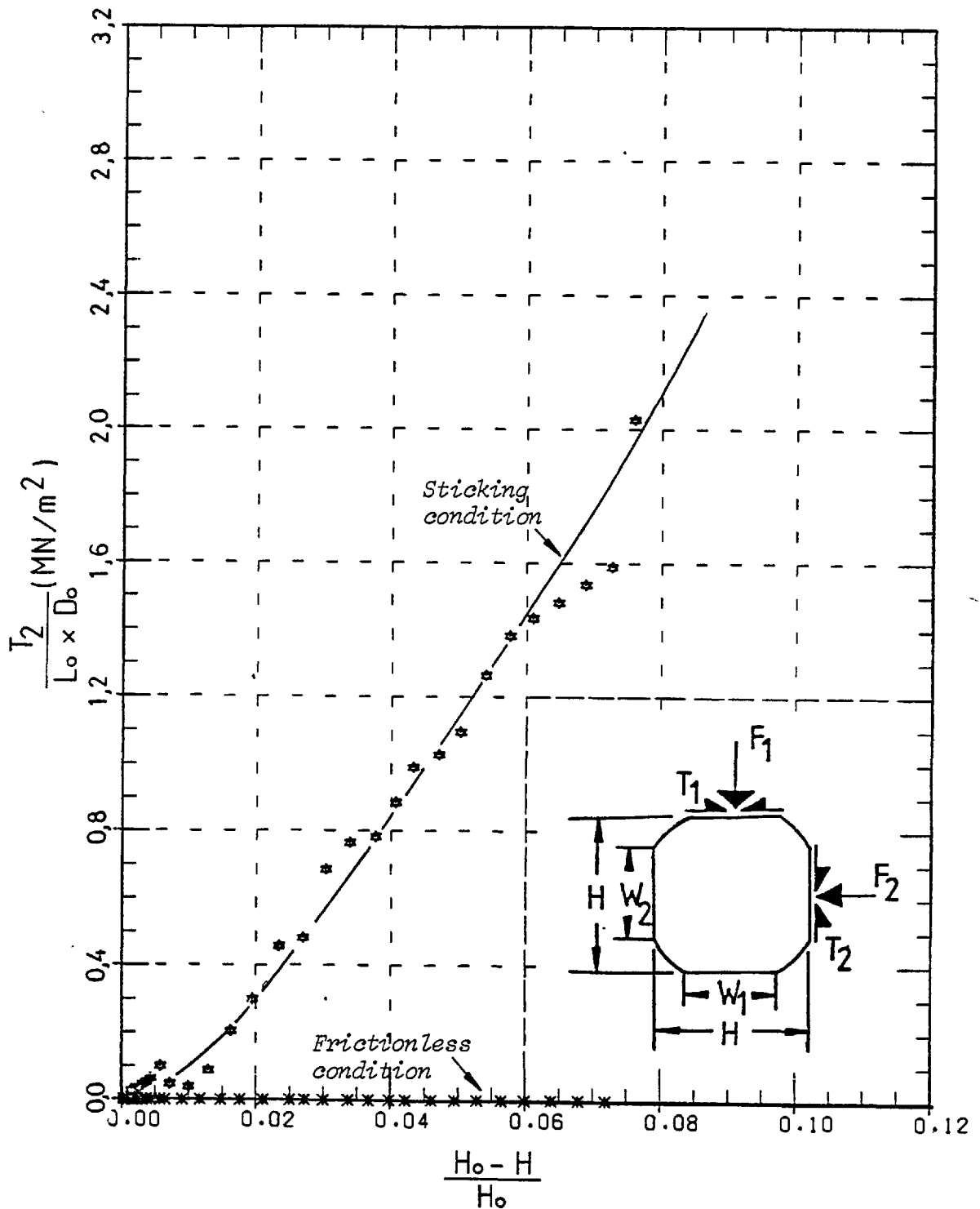
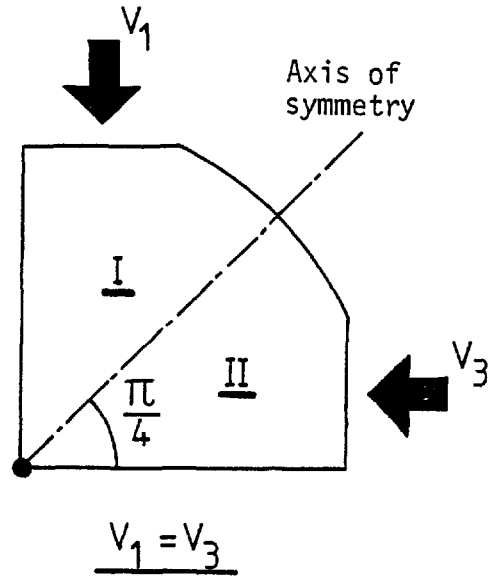


Fig. 5-31-F. Variation of interfacial frictional force ' $T_2$ ' with height ' $H$ ' for commercially pure lead obtained by the finite element method.

Comparing Figs. 5-31-A and 5-31-B, the discrepancy in the contact widths ' $W_1$ ' and ' $W_2$ ' is negligible. It is worth mentioning that the finite element mesh was not drastically non-symmetric with respect to the axis of symmetry shown in the illustration, see the finite element mesh in Fig. 5-2. The discrepancy in ' $W_1$ ' and ' $W_2$ ' would have been noticeable if the two halves (I and II) had been provided with entirely non-symmetric mesh.



The relationship between the indenting force  $F_1/(L_0 \times D_0)$  and the amount of indentation is shown in

Fig. 5-31-C. As seen the curve shows the same trend as that obtained in case (b), Fig. 5-29-C, in which the platens positioned on the sides of the billet remained stationary during the course of indentation. The effect of friction on the curve, over the considered range, is not significant particularly when the amount of indentation is less than 0.04.

The manner in which the original finite element mesh, shown in Fig. 5-2, was distorted after receiving 0.07 amount of indentation is shown in Fig. 5-32. The distorted mesh for the case when the platens were smooth is shown in Fig. 5-32-A. Comparing this with the original mesh it is clear that the elements adjoining the platens are those with maximum angular distortions. The least distorted elements are

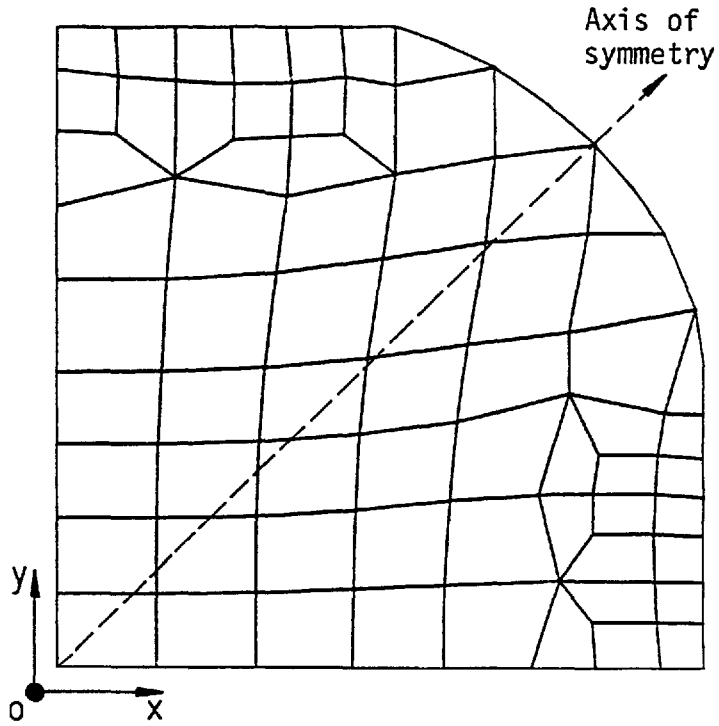


Fig. 5-32-A. Deformation of original mesh at  $(H_0-H)/H_0=0.07$  in frictionless condition.

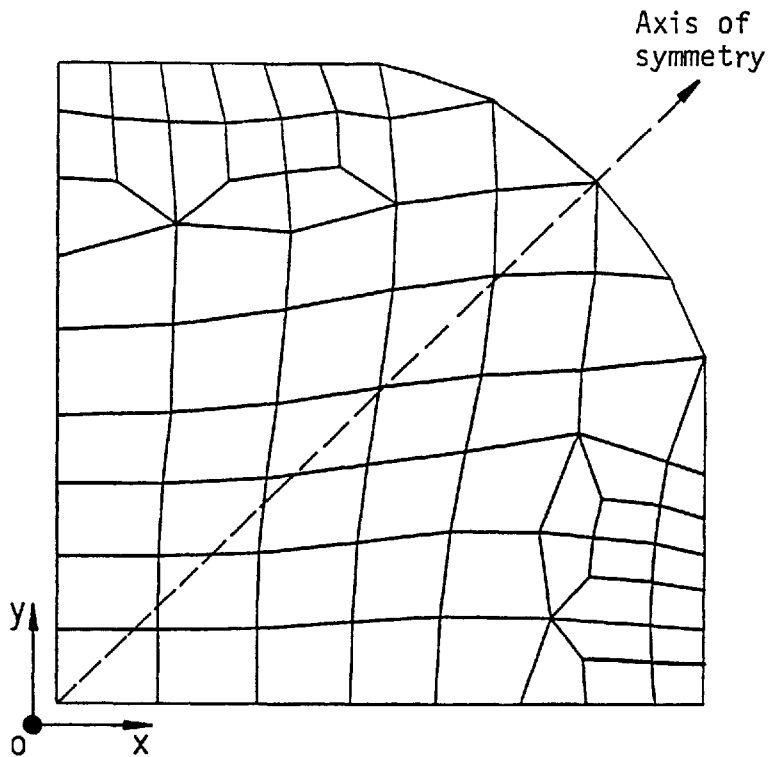
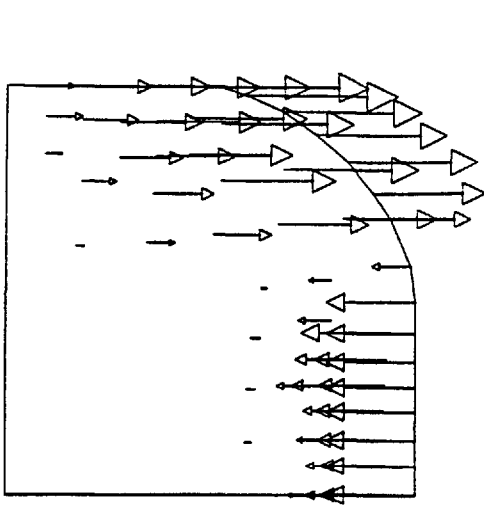


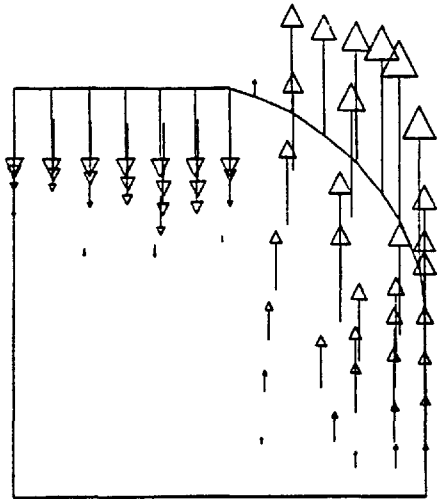
Fig. 5-32-B. Deformation of original mesh at  $(H_0-H)/H_0=0.07$  in sticking condition.

those positioned along the free-surface and the diameters of the billet in the x and y directions. The distorted mesh for the case when the platens were rough is shown in Fig. 5-32-B. Comparing this with the original mesh it is quite clear that the angular distortions of the elements adjoining the platens are not as high as those of the corresponding elements in the previous mesh shown in Fig. 5-32-A. Thus friction has the effect of decreasing the angular distortions of these elements and in turn their shear strains. In Fig. 5-32-B, the least distorted elements are the same as those in Fig. 5-32-A. Elements within the mesh, particularly those positioned along the axis of symmetry, are distorted rather noticeably and more than the corresponding elements in the previous mesh shown in Fig. 5-32-A. Thus friction has the effect of increasing the distortion of these elements.

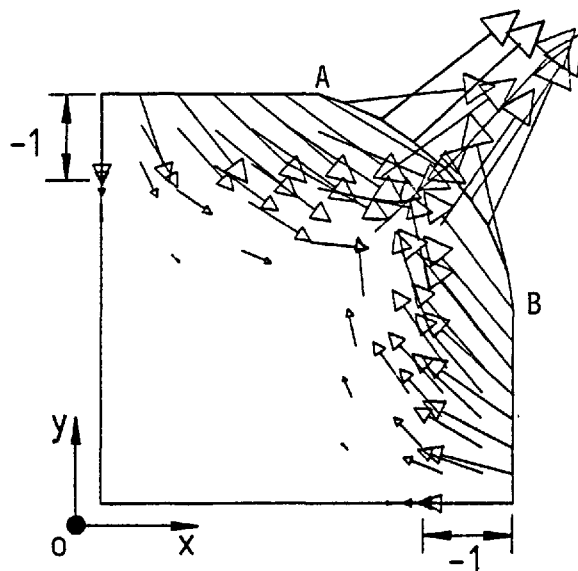
The flow fields for indentation of a round billet between smooth and rough platens are shown in Figs. 5-33 and 5-34 respectively. In the computation the speed of the platen were both assumed to be -1. The flow field for the case of indentation with smooth platens is shown in Fig. 5-33. The absolute velocity of metal particles in moving outwards along the contact widths increases well above the reference velocity of the platens. Comparing this with the flow field shown in Fig. 5-20, for which the platens positioned on the sides of the billet remained stationary, it is observed how the movement of the free-surface changes when the stationary platens are also driven with the same speed as the other two, operating in the y direction. Along the free-surface, moving from A to B, the velocity vectors first change direction abruptly and then become almost parallel at the middle. The flow of metal is seen to be confined to the regions near to the platens, and to quickly divert towards the free-surface of the billet. In this field the



Components of velocity vectors  
in the x direction



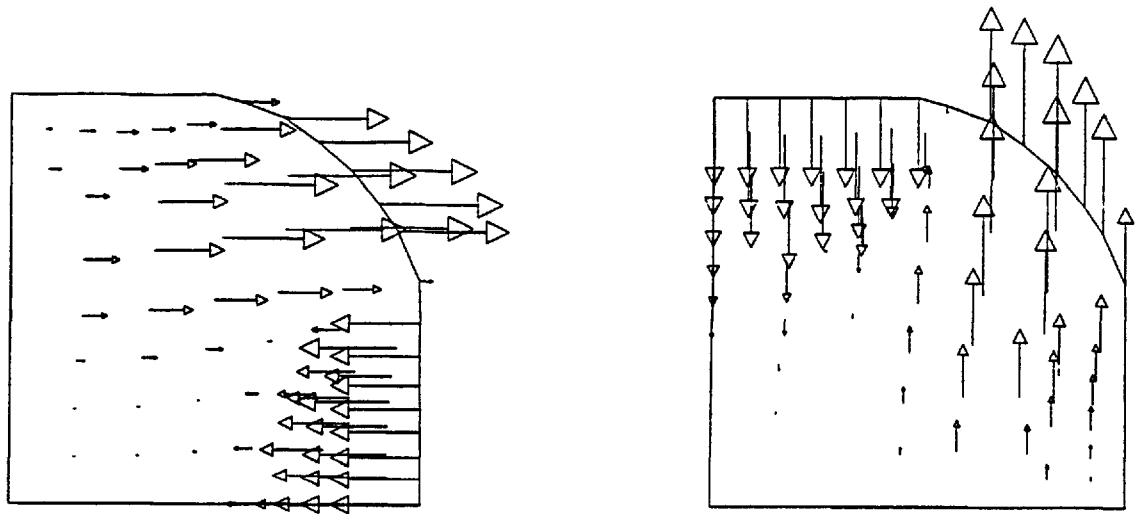
Components of velocity vectors  
in the y direction



Absolute velocity  
vectors

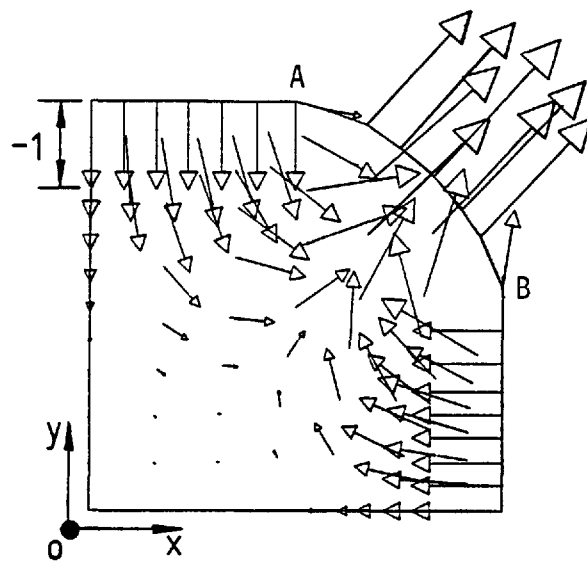
Fig. 5-33. Flow pattern at  $(H_0 - H)/H_0 = 0.07$  in frictionless condition, velocity of platens being -1.





Components of velocity vectors  
in the x direction

Components of velocity vectors  
in the y direction



Absolute velocity vectors

Fig. 5-34. Flow pattern at  $(H_0 - H)/H_0 = 0.07$  in sticking condition, velocity of platens being -1.

existence of a large dead zone in the central region of the billet cross-section is quite clearly seen. The flow field established by rough platens is shown in Fig. 5-34. The velocity vectors along the free-surface, moving from A to B, change direction abruptly and become parallel over the most part of the free-surface. A major part of the free-surface seems to be moving outwards with an almost uniform speed. Contrary to the previous case shown in Fig. 5-33, in this field the metal flow at first penetrates deeply into the billet cross-section and then diverts towards the free-surface of the billet. As in the previous field, a dead zone in the central region exists but is considerably smaller in size.

The distribution of effective strains for the case when the billet was indented by smooth platens is shown in Fig. 5-35-A.

Regions with the largest strains adjoin the platens. The least strained regions are positioned beneath the free-surface and near the centre of the billet. Comparing this with Fig. 5-22-A, it becomes clear how the constant strain lines change when the stationary platens are also driven with the same speed as the other two operating in the y direction. The distribution of effective strains for the case when the billet was indented between rough platens is shown in Fig. 5-35-B. Regions with the largest strains are those positioned beneath the platens. As before, regions beneath the free-surface and near the billet centre are the least strained regions. Comparing this with Fig. 5-35-A, the only substantial effect of friction seems to be the change in the constant strain lines adjoining the platens.

#### 5.4.2 Results obtained from volume constancy

To obtain the current configuration of the billet from volume

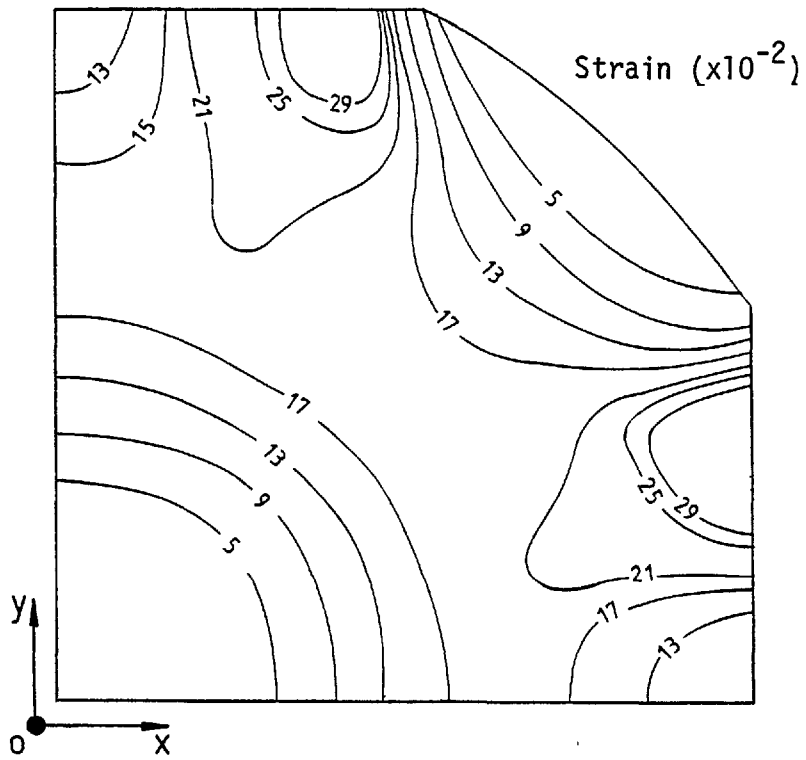


Fig. 5-35-A. Distribution of effective strain at  $(H_0 - H)/H_0 = 0.07$  in frictional condition.

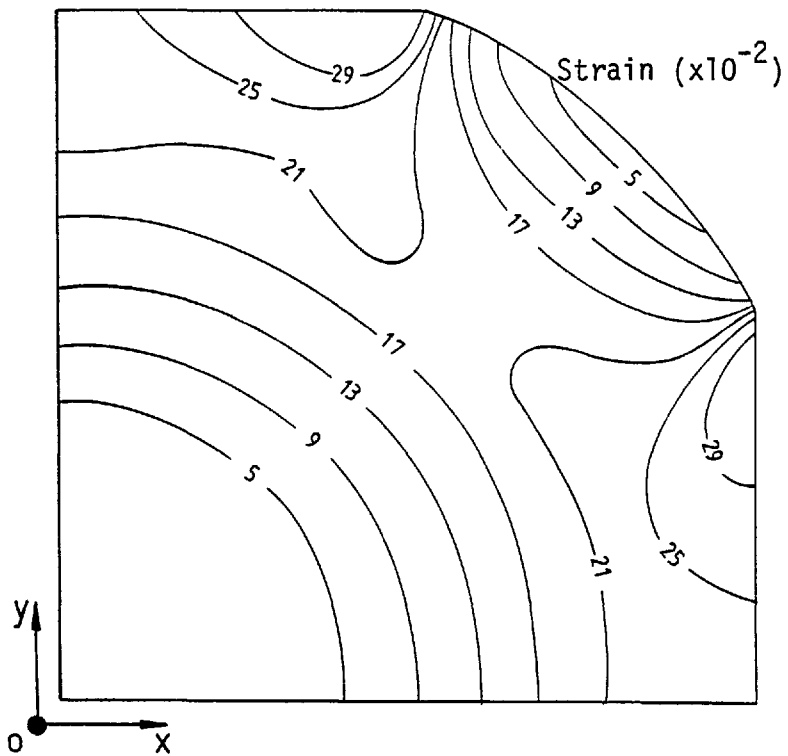


Fig. 5-35-B. Distribution of effective strain at  $(H_0 - H)/H_0 = 0.07$  in sticking condition.

constancy the behaviour of the free-surface must first be known. As it was previously argued in the results obtained by the finite element method the behaviour of the free-surface in this kind of indentation is highly dependent on the surface condition of the platens. When the billet is indented by smooth platens the velocity vectors along this surface, though almost equal in value, change direction abruptly, see Fig. 5-33. By contrast, when the billet is indented by rough platens the behaviour of the free-surface is approximately known since the velocity vectors along this surface are in general parallel and equal in value, see Fig. 5-34.

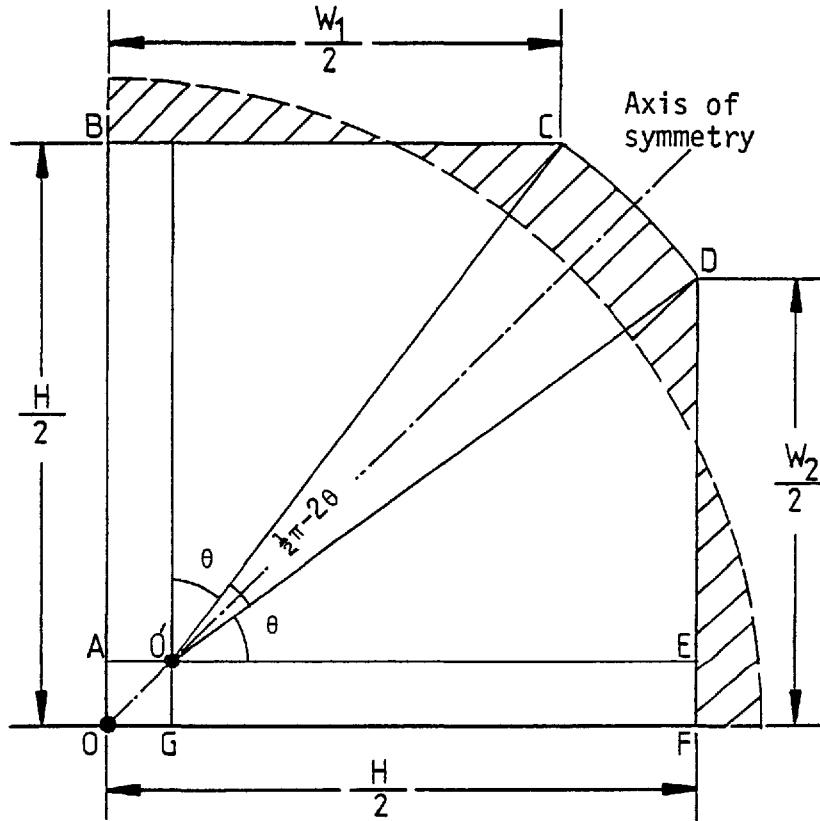
In the following, the volume constancy is applied to an indentation problem in which the platens are rough. In accordance with the flow field shown in Fig. 5-34, it is assumed that the free-surface of the billet during the course of indentation will be displaced outwards. This, of course, requires the radius of curvature of the free-surface to remain constant. For such an assumed behaviour of the free-surface it is quite clear that during indentation the centre of curvature of the free-surface will remain on the axis of symmetry of the two halves. The undistorted and distorted configurations of the billet are shown in the illustration below,  $O'$  being the centre of the free-surface in the distorted state.

If the radius of the billet is called  $R_0$ , then from volume constancy

$$\frac{1}{4} \pi R_0^2 = \frac{1}{2} \overline{AB} (\overline{BC} + \overline{AO'}) + \overline{OA} \cdot \overline{OG} + \frac{1}{2} \overline{GF} (\overline{FD} + \overline{GO'})$$

$$+ \frac{1}{2} R_0^2 \left( \frac{\pi}{2} - 2\theta \right)$$

where the last term on the right is the area of sector  $O'CD$ . Considering



the symmetry of deformation the above equation can be written as

$$\frac{1}{4} \pi R_o^2 = \overline{AB} (\overline{BC} + \overline{AO'}) + \overline{OA}^2 + \frac{1}{2} R_o^2 \left( \frac{\pi}{2} - 2\theta \right)$$

but  $\overline{AB} = R_o \cos \theta$ ,  $\overline{BC} = \frac{1}{2} W_1$  and  $\overline{OA} = \frac{1}{2} H - R_o \cos \theta$ . Thus

$$\begin{aligned} \frac{1}{4} \pi R_o^2 &= R_o \cos \theta \left( \frac{1}{2} W_1 + \frac{1}{2} H - R_o \cos \theta \right) + \left( \frac{1}{2} H - R_o \cos \theta \right)^2 \\ &+ \frac{1}{2} R_o^2 \left( \frac{\pi}{2} - 2\theta \right) \end{aligned}$$

From which the contact width ' $W_1$ ' can be determined by

$$W_1 = \frac{2R_o^2 \theta - (H - 2R_o \cos \theta)^2}{R_o \cos \theta} + 2R_o \cos \theta - H \quad (5.23)$$

The angle ' $\theta$ ' can be expressed in terms of ' $W_1$ ' and ' $H$ '. From triangle O'ED

$$\tan \theta = \frac{\overline{DE}}{\overline{OE}} = \frac{W_1 - H + 2R_o \cos \theta}{2R_o \cos \theta}$$

or 
$$\theta = \tan^{-1} \left[ \frac{W_1 - H + 2R_o \cos \theta}{2R_o \cos \theta} \right] \quad (5.24)$$

By solving Eqs. (5.23) and (5.24), the contact width ' $W_1$ ' was computed. The method of computation used was as follows:

- 1- For a given ' $H$ ', ' $\theta$ ' was assumed equal to zero.
- 2- From Eq. (5.23), ' $W_1$ ' was calculated.
- 3- By substituting for ' $W_1$ ', ' $\theta$ ' and ' $H$ ' in Eq. (5.24), a more correct value for ' $\theta$ ' was calculated.
- 4- Steps 2 to 3 was repeated until convergence was achieved.

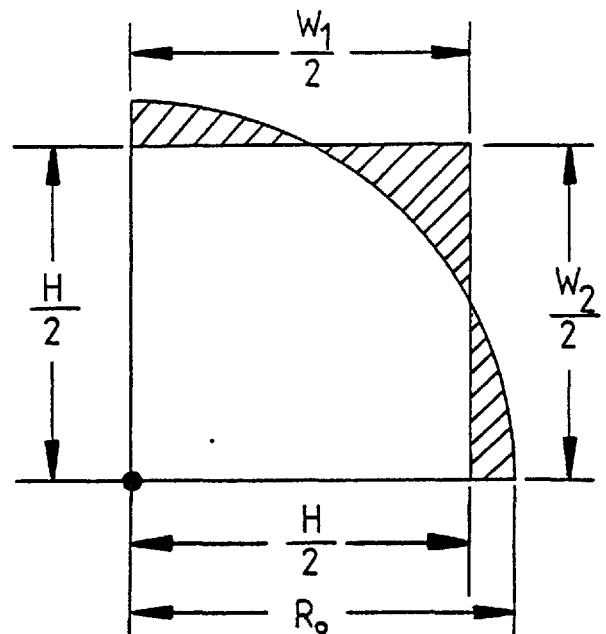
It is worth noting that the height ' $H$ ' cannot be smaller than a critical value at which the initial quadrant is fully converted into a square. If the initial diameter of the billet and the side of the square are assumed  $R_o$  and  $\frac{1}{2}H$  respectively, it can be written (see also the illustration):

$$\frac{1}{4}\pi R_o^2 = \left(\frac{1}{2}H\right)^2 \quad \therefore \quad H = R_o \sqrt{\pi}$$

Thus

$$(H_o - H)/H_o = \frac{2 - \sqrt{\pi}}{2} = 0.11,$$

$$W_1/D_o = W_2/D_o = \frac{\sqrt{\pi}}{2} = 0.89$$



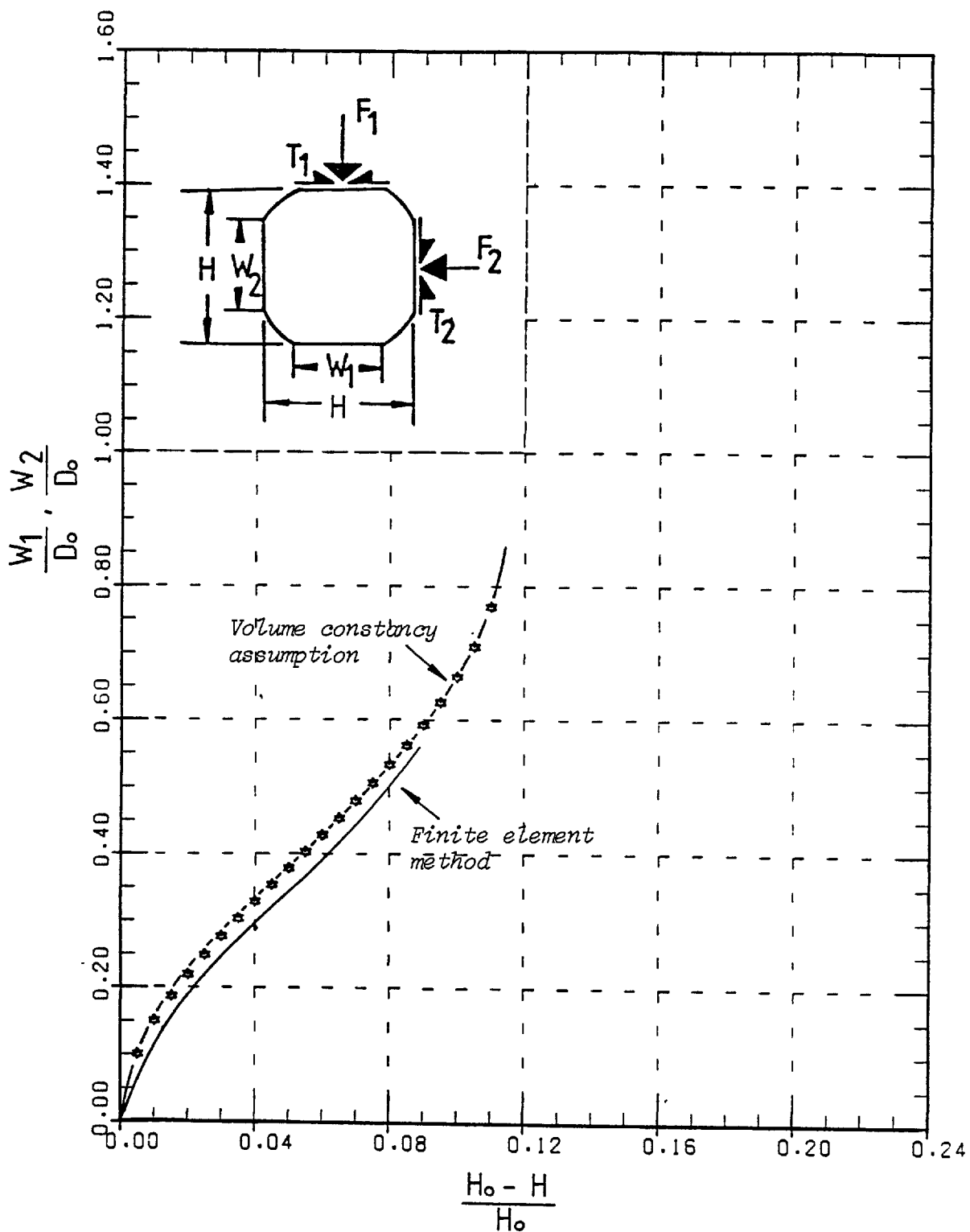
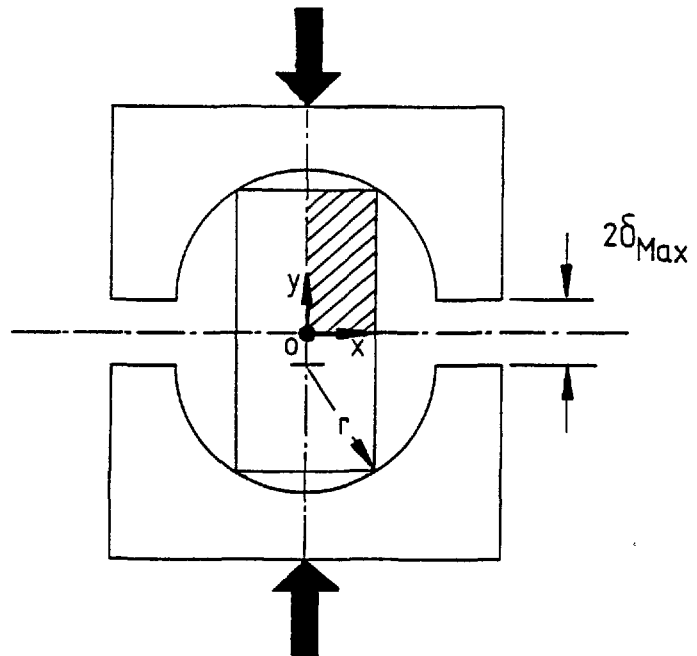


Fig. 5-36. Variations of contact width ' $W_1$ ' and of ' $W_2$ ' with height ' $H$ ' obtained by the finite element method and volume constancy assumption.

The computed results are shown in Fig. 5-36. The slope of the curve first decreases, then remains almost constant, and finally increases markedly as the amount of indentation approaches the limiting value of 0.11. The curve obtained from volume constancy appears in good agreement with that obtained by the finite element method. The slight discrepancy observed is due to the assumed behaviour of the free-surface which was not fully in agreement with that obtained by the finite element method.

### 5.5 A study of case (d)

As was previously described in section 5.1, in this case the chamber was comprised of two circular-shaped platens (see the illustration below), the moving platens being driven in the direction indicated by the arrows to indent a billet with an initially rectangular cross-section.



In the computation, due to the symmetry of deformation, only one quarter of the billet cross-section was considered. The finite element mesh comprised of 80 elements and 99 nodal points and is shown in Fig. 5-37. Due to the high extent of plastic deformation near the contact corner, finer divisions were provided in the nearby



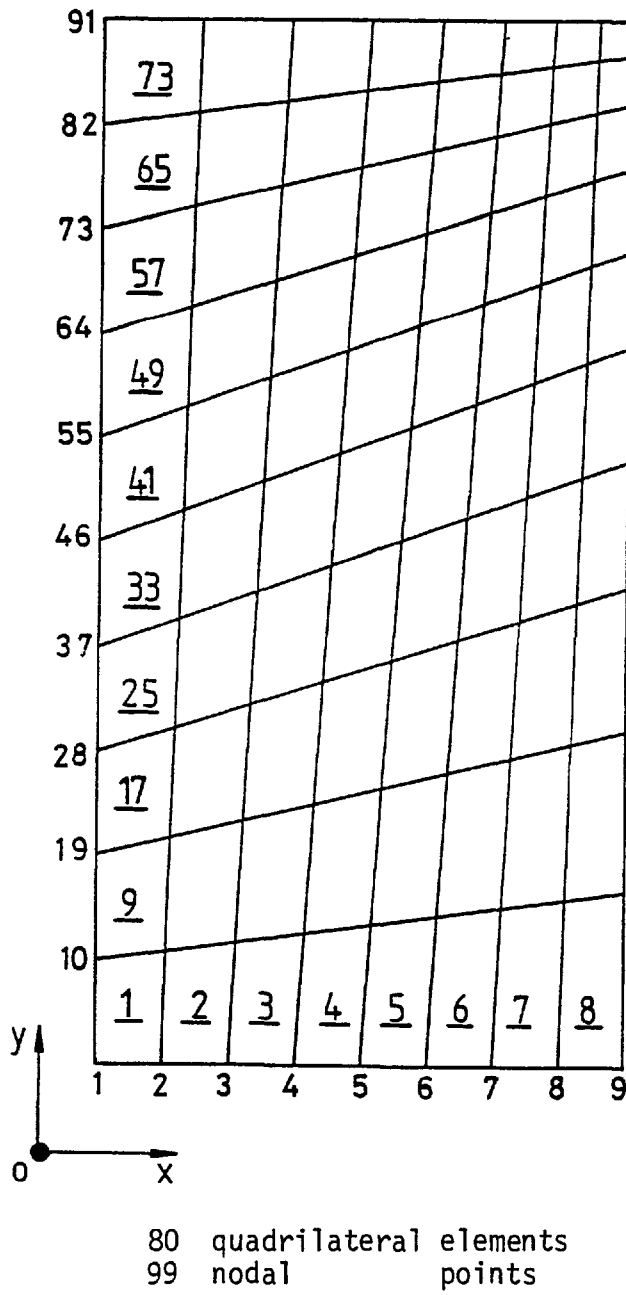
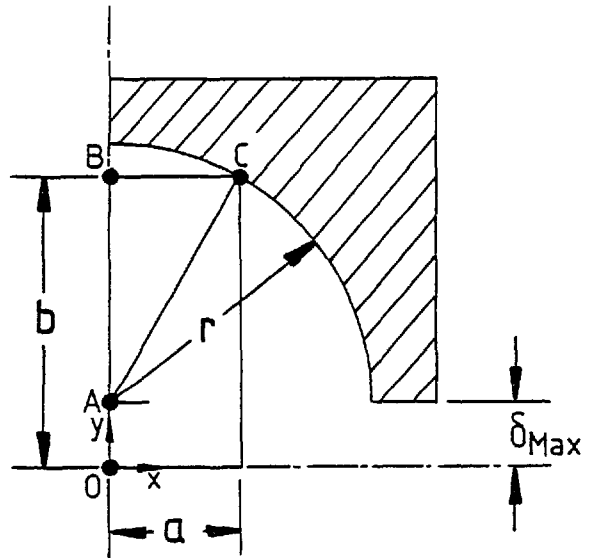


Fig. 5-37. Finite element mesh for a billet with rectangular cross-section (quarter of cross-section shown).

region. The computation was carried out using the material properties of aluminium and assuming complete sticking conditions at the interface of the billet and platens. The geometrical specifications of the billet used in the computation were as follows (see also the illustration below):

<u>Case I</u>	<u>Case II</u>
$a = 5 \text{ mm}$	$a = 10 \text{ mm}$
$b = 22 \text{ mm}$	$b = 20 \text{ mm}$
$r = 20 \text{ mm}$	$r = 20 \text{ mm}$



The maximum amounts of indentation  $\delta_{max}$ , for which the platens are brought together, were determined from

$$\delta_{max} = \overline{OA} = \overline{OB} - \overline{AB}$$

where  $\overline{OB} = b$  and  $\overline{AB} = \sqrt{\overline{AC}^2 - \overline{BC}^2} = \sqrt{r^2 - a^2}$

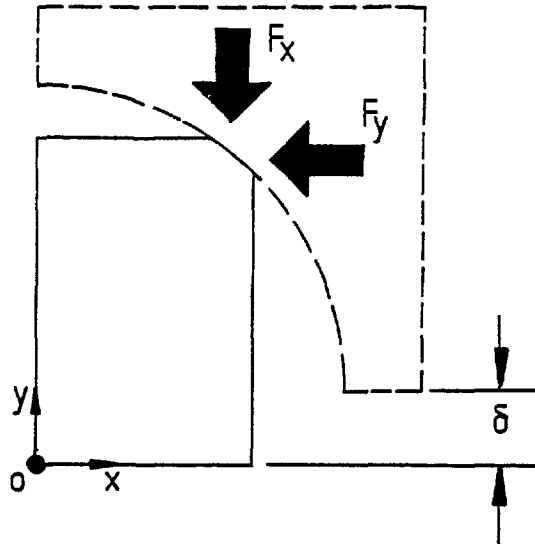
The maximum amounts of indentation in cases I and II were 2.64 and 2.68 mm respectively.

To pursue the history of deformation the following parameters were calculated and recorded (see also the illustration below):

1-  $\delta$  = amount of indentation

2-  $\frac{F_x}{L_0}$  and  $\frac{F_y}{L_0}$  = components of indenting force in the x and y directions

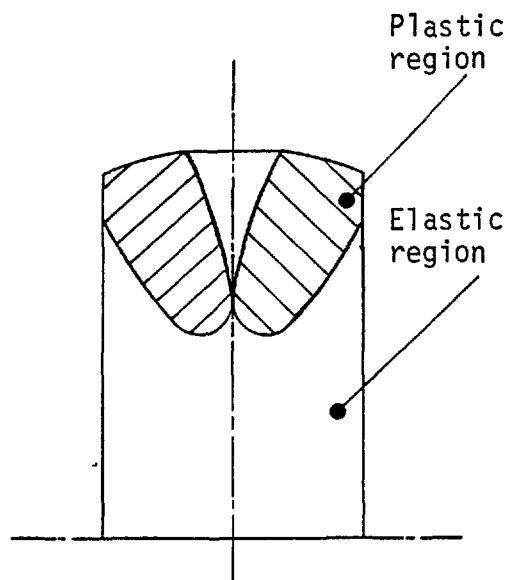
where  $L_0$  is the initial length of the billet.



### 5.5.1 Results obtained from the finite element method

The computed results are shown in Figs. 5-38 and 5-39. The relationship between the vertical component of indenting force  $F_y/L_0$ , and the amount of indentation is shown in Fig. 5-38. The initial size of the billet can be seen to have a marked effect on the manner in which the load-displacement curve varies. In case I, the curve remains almost unaffected whenever a nodal point comes into contact with the platen. In this curve, A is the point at which plastic regions (which are first nucleated at the top two contact points) begin to merge as shown in the illustration.

Point B is when the plastic regions fully merge, which occurs when the material comes into complete contact with the platen. In case II, the curve rises markedly whenever a nodal point comes into contact with the platen.



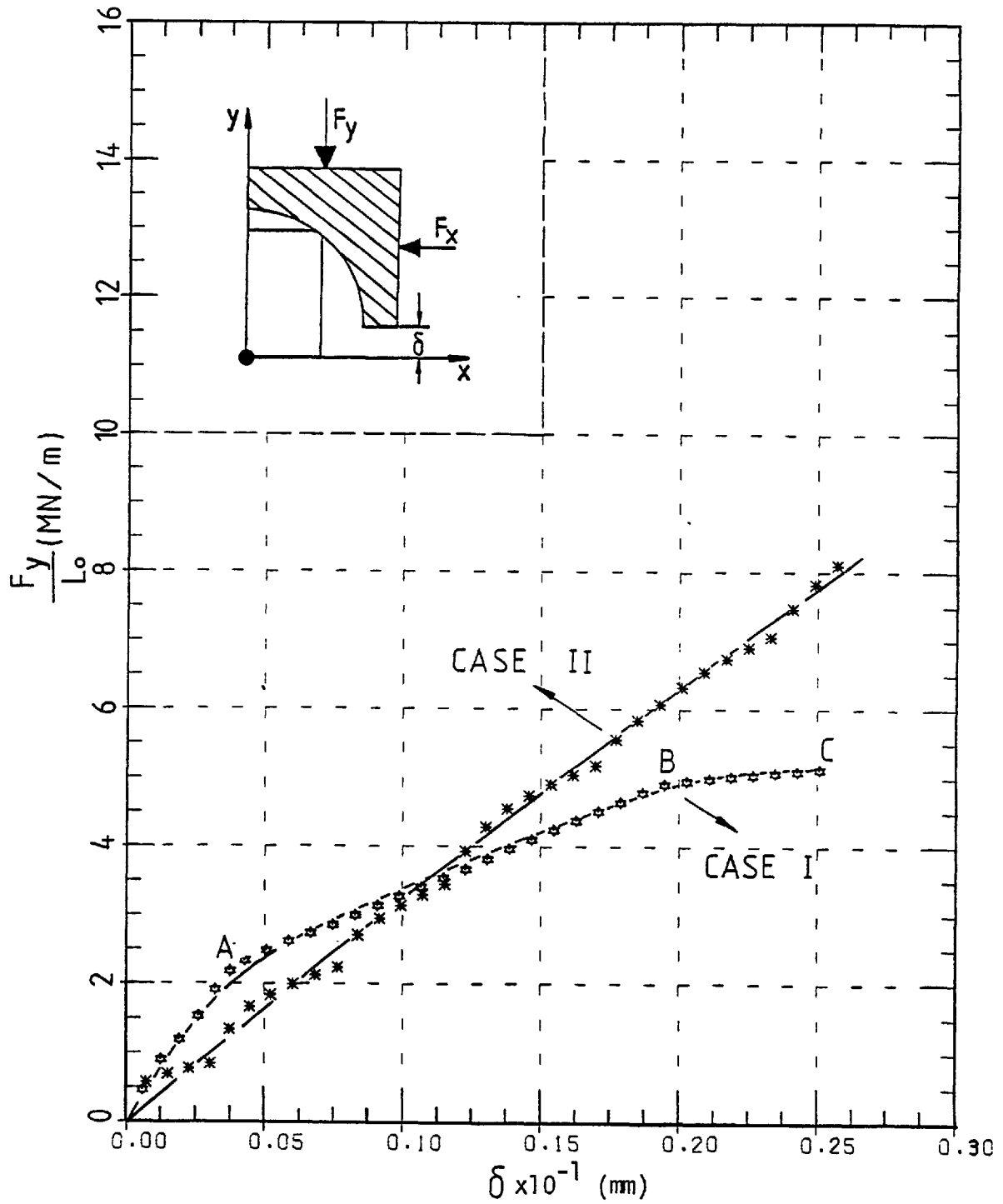


Fig. 5-38. Variations of indenting force ' $F_y$ ' with movement ' $\delta$ ' for commercially pure aluminium obtained by the finite element method.

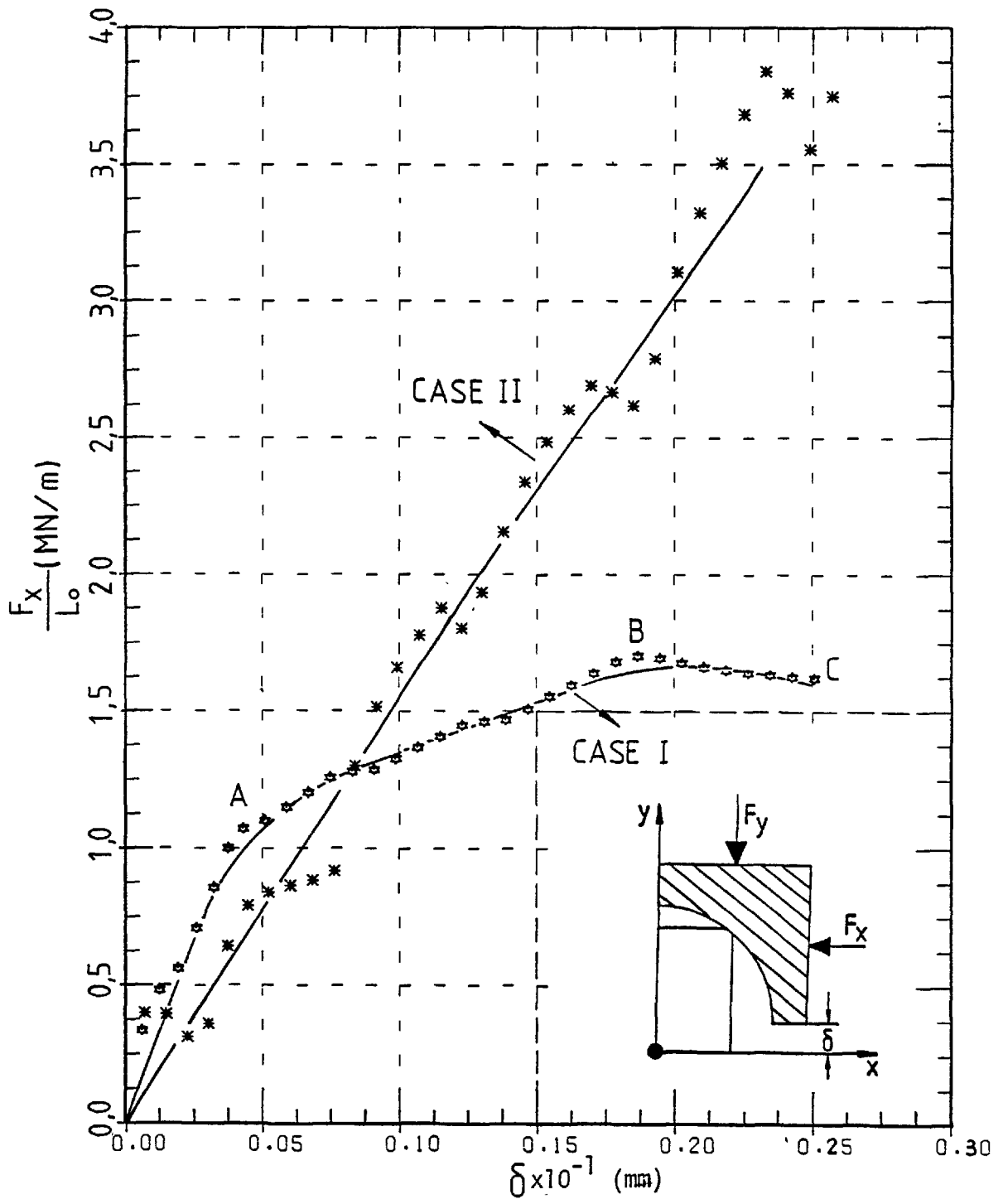
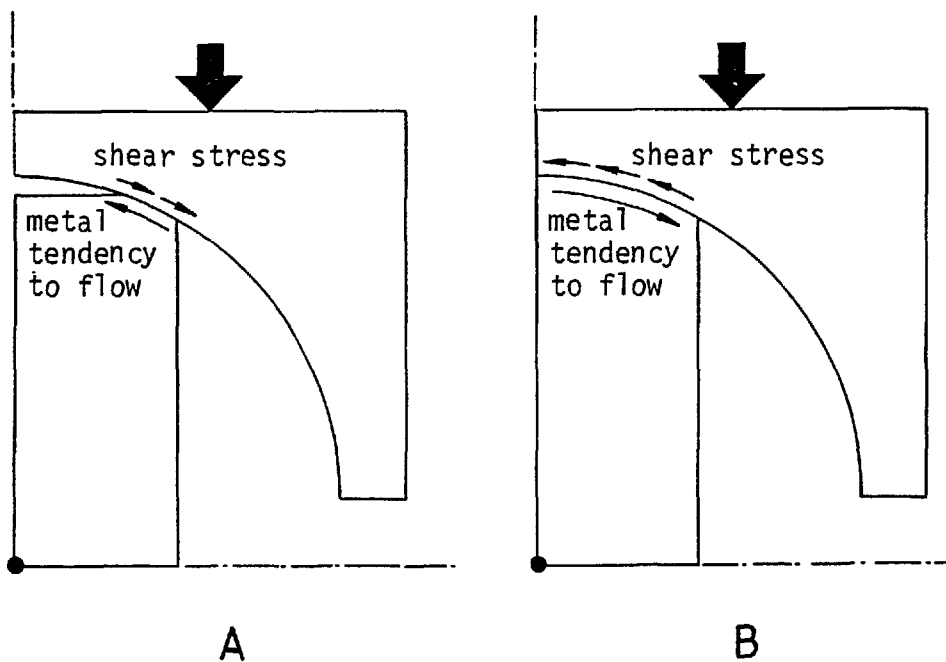


Fig. 5-39. Variation of indenting force ' $F_x$ ' with movement ' $\delta$ ' for commercially pure aluminium obtained by the finite element method.

In this curve points such as A and B do not exist, since the two plastic regions never merge and the uninterrupted interface between the billet material and platen, which signifies case I, is absent. This is because the billet width in this case was twice as large as that in case I.

The relationship between the indenting force  $F_x/L_0$  and the amount of indentation is shown in Fig. 5-39.

In case I the curve almost remains unaffected whenever a nodal point comes into contact with the platen. In this curve, point A represents the point when the two plastic regions begin to merge, and point B, when this merging is complete. Immediately after point B the curve is seen to drop slightly. The drop is perhaps due to the reversing of interfacial shear stresses when the billet top surface entirely comes into contact with the platen (see the illustration A and B).



The manner in which the original finite element mesh was distorted

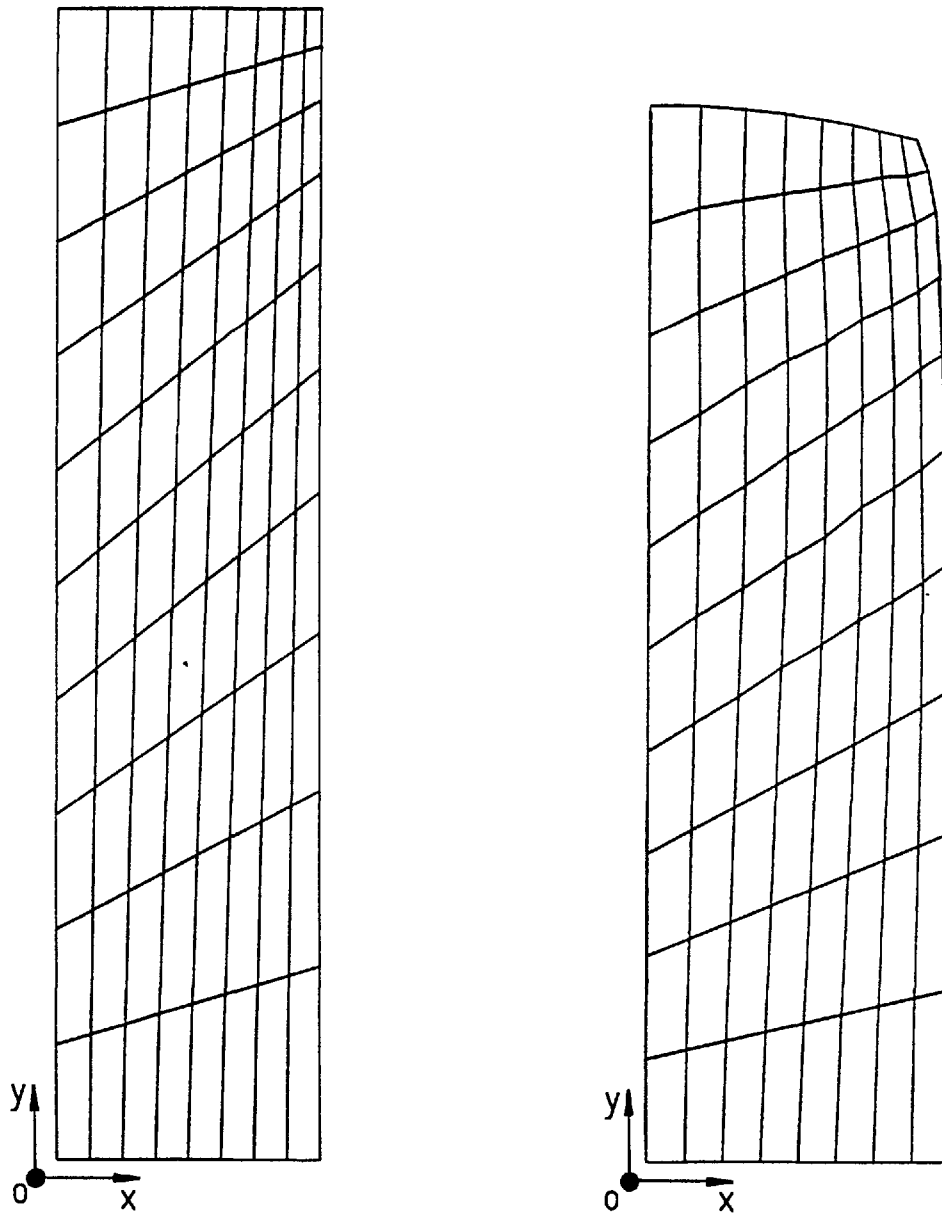
is shown in Figs. 5-40 and 5-41. In case I, the distortion of the billet top surface into a circular shape is quite clearly seen. In this case elements with maximum angular distortions are those positioned near the top right corner. In case II, only a part of the billet top surface is seen to have been deformed into the shape of the platen, the rest remaining almost undeformed. In this case the angular distortions of the elements positioned near the top right corner are extremely high. Here only part of the billet free-surface has come in contact with the platen.

The flow fields for this kind of indentation are shown in Fig. 5-42. In the computation the velocity of the platen was assumed to be -1. The flow fields are self-explanatory. The only matter of interest is the rather unusual movements of some particles within the circle shown in dotted lines. Here the velocity vectors are slightly diverted to the left.

The distributions of effective strain for cases I and II are shown in Fig. 5-43. In case I almost the entire cross-section of the billet has undergone a large amount of plastic deformation. The region with the largest effective strains is that positioned near the right top corner. The least strained region is positioned near the top left corner of the billet cross-section. In case II only a small part of the billet cross-section has undergone plastic deformation markedly. In this case the region positioned near the top right corner is considerably more strained than the corresponding one in case I.

### 5.5.2 Upper-bound solution

Although not reviewed here, an upper-bound solution to this kind of billet indentation has been presented by Chitkara and Johnson (60),



CASE (I)

Fig. 5-40. Original and distorted finite element mesh at  $\delta=2.64$  mm in case I.



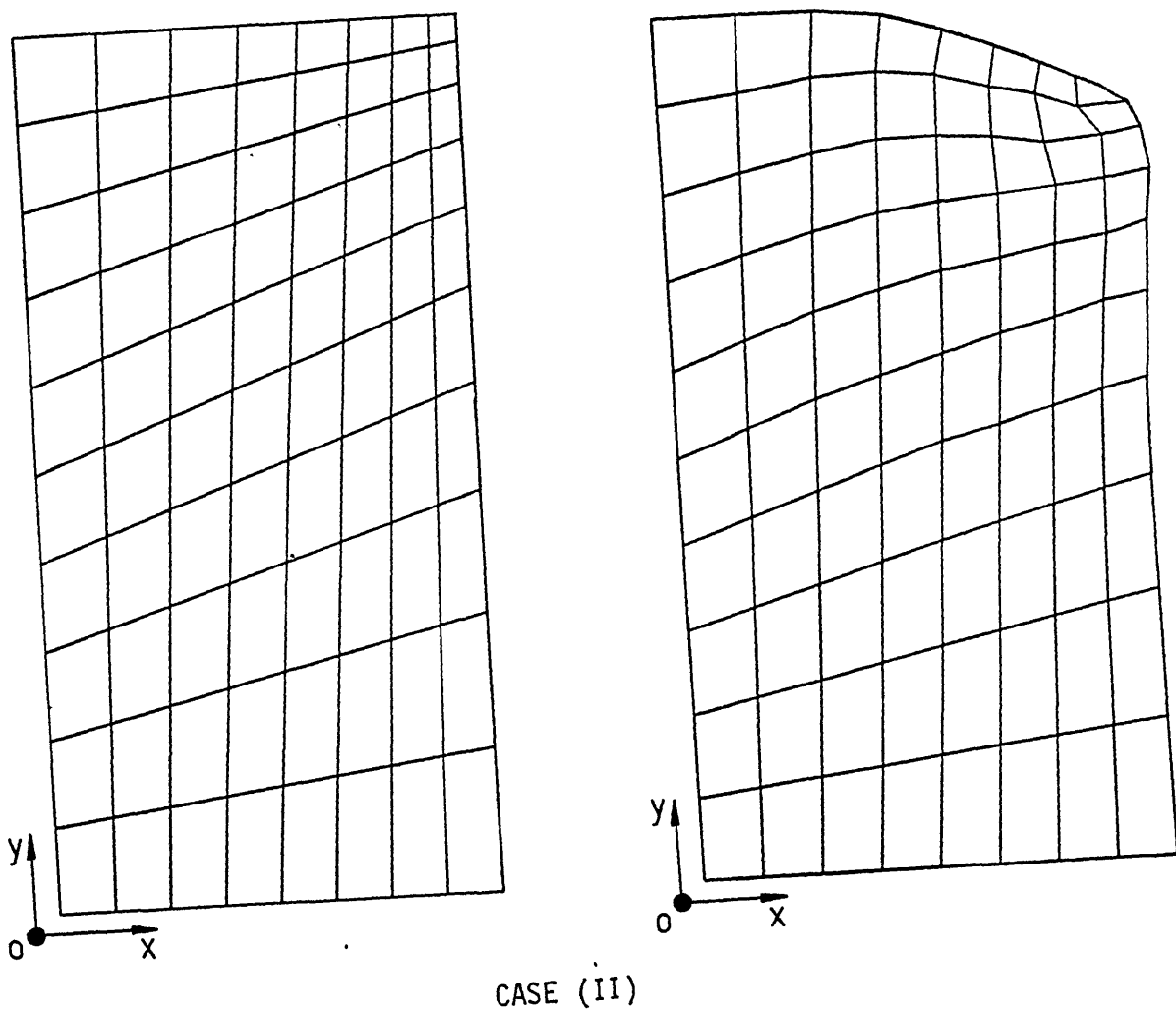


Fig. 5-41. Original and distorted finite element mesh at  $\delta=2.68$  mm in case II.

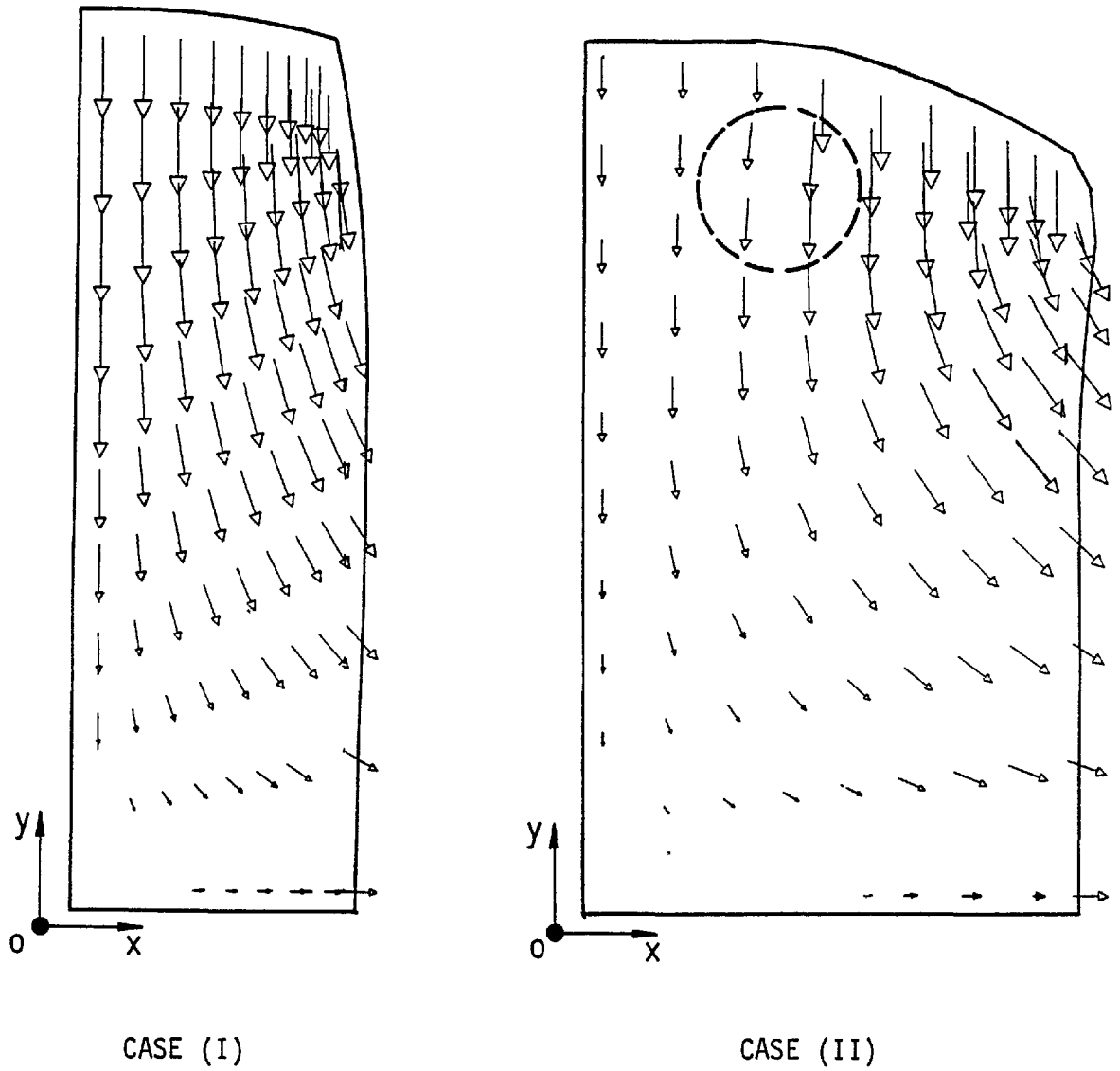


Fig. 5-42. Flow pattern at  $\delta=2.64$  mm in case I and at  $\delta=2.68$  mm in case II, velocity of the platen being -1.

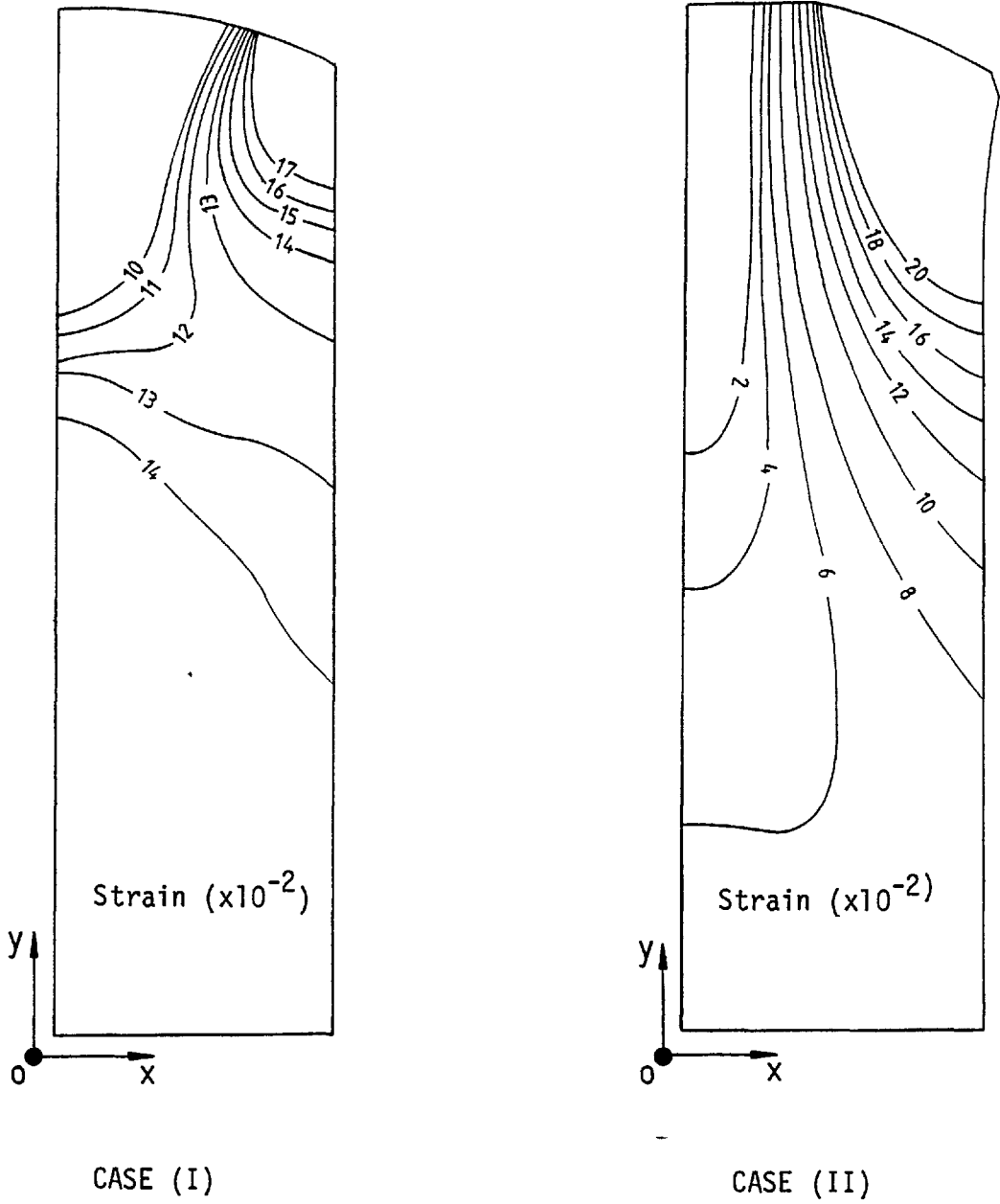


Fig. 5-43. Distribution of effective strain at  $\delta=2.64$  mm in case I and at  $\delta=2.68$  mm in case II.

where an assumed deformation flow field is used to predict the billet current configuration as well as the pressure required for indentation during the course of indentation.

## 5.6 Conclusions

The finite element method is a convincing and powerful tool for the solution of elasto-plastic problems. The method removes many restrictions imposed by other methods and offers the possibility of obtaining information that the other methods cannot provide.

The method of finite element is applicable to problems with complex geometry and easily takes into account the actual material properties. The method can reveal many features such as the load-displacement curve, continuum current configuration, distribution of velocity, distributions of stress and strain, and many others. However, questions will still remain with regard to the accuracy of the solutions and the efficiency of the computation.

The following conclusions can also be drawn:

- 1- Although the finite element formulation, presented in chapter two, was developed for small strains and displacements, the predicted results showed reasonably good agreement with the experiments even when strains and displacements were both rather noticeable.
- 2- The updating of nodal coordinates prove to be imperative when the theory of small strain and displacement are to be used for strain and displacement of a higher order.
- 3- The quadrilateral elements proved to be remarkably efficient in the analysis of two-dimensional problems.
- 4- The solution times for those problems studied indicated that the finite element method was rather expensive. The solution times may

however be reduced if a smaller number of higher order elements are used. In terms of the CDC 6400 computer units, the computation cost for the problems studied was 4000.

- 5- Simpler techniques of analysis in the field of metal working such as slip-line or upper-bound can easily provide realistic solutions and although not as accurate as those obtained by the finite element technique, their extreme low computation cost and implementation simplicity should not be disregarded if these simple techniques are to be compared with the finite element method.
- 6- Flow fields obtained by the finite element technique can be used to provide extremely reliable flow fields for later use in the upper bound technique.

APPENDIX 'A'

LISTING OF THE COMPUTER  
PROGRAM EPFEA 1  
USING TRIANGULAR ELEMENTS

NOMENCLATURE

Variable	Place in labelled common	Definition
NE	C1	Number of elements
NN	"	Number of nodes
NB	"	Band width of the overall stiffness matrix
NEQ	"	Number of equations
X,Y	"	Coordinates of nodal points
NI,NJ,NK	"	Nodal connection of elements
AI,AJ,AK, BI,BJ,BK	"	Local coordinates of elements
AREA	"	Area of elements
NP	"	Pointer vector for imposing boundary conditions
NP1, NP2	"	Pointer vectors for indicating state of elements
NX,NY	"	Peripheral nodal points matrices, due to the side and upper segments
EP	"	Stress-strain matrix of elements
E1	"	Modulus of elasticity
XU	"	Poisson's ratio
H	"	Tangent modulus
G	"	Shear modulus of elasticity
NOR	"	Number of load increments
SK	C2	Overall stiffness matrix
SKET	"	
DST	C3	Strain increment of elements
SS	"	Stress of elements
DSS	"	Stress-increment of elements
TSTP	C3	Effective plastic strain of elements
DTSTP	"	Effective plastic strain-increment of elements
TSS	"	Effective stress of elements
DTSS	"	Effective stress-increment of elements
TSS0	C4	Yield strength of elements

SSZ	"	Stress of elements in the z-direction
DSSZ	"	Stress-increment of elements in the z-direction
EPZ	"	Stress-strain matrix in the z-direction

Local Variable	Place in Subroutine	Definition
D	GDATA	Elastic material matrix
SKE	SKFORM	Element stiffness matrix
ST	YIELD 1.	Strain of elements
TST	"	Effective strain of elements

Variables of main program	Definition
U	Displacement of nodal points
F	Force of nodal points
DU	Displacement-increment of nodal points
DF	Force-increment of nodal points



PROGRAM 'EPFEA1'  
\*\*\*\*\*

```
C*****
C***** MAIN PROGRAM *****
C***** ELASTIC-PLASTIC FINITE ELEMENT ANALYSIS *****
C***** WRITTEN BY ALI NAJAFI-SANI IN THE FIRST SEMESTER OF 1978 *****
C***** DEVELOPED FOR TRIANGULAR ELEMENTS. *****
C*****
PROGRAM EPFEA1(INPUT,OUTPUT,TAPE5=INPUT,TAPE6=OUTPUT,TAPE1=113B,
*TAPE2=113B)
DIMENSION U(230),DU(230),F(230),DF(230),D(3,3)
COMMON /C1/ NE,NN,NB,NEQ,X(115),Y(115),NI(162),NJ(162),NK(162),AI(
*162),AJ(162),AK(162),BI(162),BJ(162),BK(162),AREA(162),NP(230),NP1
*(162),NP2(162),NX(30),NY(30),EP(3,3,162),B(3,6)
*,E1,XU,H,G,NOR
COMMON /C2/ SK(230,40),SKET(6,6,162)
COMMON /C3/ DST(3,162),SS(3,162),DSS(3,162),TSTP(162),DTSTP(162),T
*SS(162),DTSS(162)
COMMON /C4/ TSSO(162),SSZ(162),DSSZ(162),EPZ(3,162)
COMMON/C5/KS,LS
C*****
C***** INPUT OF DATA *****
CALL GDATA(D)
C*****
C***** GENERATION AND ASSEMBLY OF STIFFNESS MATRICES *****
CALL SKFORM(D)
C*****
C***** INPUT OF INITIAL BOUNDARY CONDITIONS *****
CALL BOND1(U,F)
C*****
C***** INITIATION OF PLASTIC DEFORMATION *****
CALL YIELD1(U,F,DU,DF,D)
NOR=1500
C*****
C***** INITIATION OF LOAD INCREMENTS *****
DO 1 I=1,NOR
C*****
C***** UPDATE OF GEOMETRICAL MATRICES *****
CALL CHANGE(D,U)
C*****
C***** INPUT OF INSTANTANEOUS BOUNDARY CONDITIONS *****
CALL BOND2(I,U,F,DU,DF)
C*****
C***** INITIATION OF INCREMENTAL PLASTIC DEFORMATION *****
CALL YIELD2(U,F,DU,DF,D,I)
1 CONTINUE
REWIND 1
REWIND 2
STOP
END
SUBROUTINE GDATA(D)
```

```
COMMON /C1/ NE,NN,NB,NEQ,X(115),Y(115),NI(162),NJ(162),NK(162),AI(
*162),AJ(162),AK(162),BI(162),BJ(162),BK(162),AREA(162),NP(230),NP1
*(162),NP2(162),NX(30),NY(30),EP(3,3,162),B(3,6)
*,E1,XU,H,G,NOR
COMMON /C2/ SK(230,40),SKET(6,6,162)
COMMON /C3/ DST(3,162),SS(3,162),DSS(3,162),TSTP(162),DTSTP(162),T
*SS(162),DTSS(162)
COMMON /C4/ TSSO(162),SSZ(162),DSSZ(162),EPZ(3,162)
DIMENSION D(3,3)
DATA NP/230*0/,NP1/162*1/,NP2/162*0/,NE/162/,NN/115/,NB/40/,NEQ/23
*0/
DATA NY/115,114,113,112,111,110,109,108,107,106,105,104,103,101,10
*0,99,98,90,89,88,87,80,79,78,77,67,66,65,64,50/
DATA NX/70,57,58,59,60,43,44,35,36,23,24,14,12,6,2,1,5,11,20,21,33
*,34,49,50,64,65,66,67,77,78/
WRITE(6,1)
1  FORMAT(////////,1X,28HINDENTATION OF ROUND BILLETS,/,30(1H*))
   READ(5,3)((M,NI(M),NJ(M),NK(M)),I=1,NE)
3  FORMAT(4I5)
   READ(5,2)((M,X(M),Y(M)),I=1,NN)
2  FORMAT(I3,2F10.6)
C***** EVALUATION OF THE PERIPHERAL NODAL COORDINATES *****
R=18.0
DO 22 N=1,NN
IF(Y(N).EQ.1.0) Y(N)=SQRT(R**2-X(N)**2)
IF(X(N).EQ.1.0) X(N)=SQRT(R**2-Y(N)**2)
22 CONTINUE
SC=Y(NY(1))
DO 12 K=1,NN
X(K)=X(K)/SC
Y(K)=Y(K)/SC
12 CONTINUE
E1=0.7E06 $ XU=0.345 $ H=0.86E03
G=E1/2.0/(1.0+XU)
DO 5 N=1,NE
I=NI(N)
J=NJ(N)
K=NK(N)
AI(N)=X(K)-X(J)
AJ(N)=X(I)-X(K)
AK(N)=X(J)-X(I)
BI(N)=Y(J)-Y(K)
BJ(N)=Y(K)-Y(I)
BK(N)=Y(I)-Y(J)
AREA(N)=0.5*(AK(N)*BJ(N)-AJ(N)*BK(N))
IF(AREA(N).GT.0.0) GO TO 5
WRITE(6,6) N
6  FORMAT(1X,I5,26HELEMENT WITH NEGATIVE AREA)
   STOP
5  CONTINUE
   WRITE(6,7)
7  FORMAT(///,2X,2HNO,24X,1HX,24X,1HY,/,60(1H*),//)
   WRITE(6,8)((I,X(I),Y(I)),I=1,NN)
8  FORMAT(1X,I3,10X,E15.5,10X,E15.5)
   WRITE(6,9)
9  FORMAT(//,2X,2HNO,9X,1HI,9X,1HJ,9X,1HK,16X,4HAREA,/,60(1H*),//)
```

```
WRITE(6, 10)(I, NI(I), NJ(I), NK(I), AREA(I), I=1, NE)
10  FORMAT(1X, I3, 7X, I3, 7X, I3, 7X, I3, 5X, E15.5)
    FACT=E1*(1.0-XU)/(1.0+XU)/(1.0-2.0*XU)
    D(1, 1)=FACT
    D(2, 2)=FACT
    D(1, 2)=FACT*XU/(1.0-XU)
    D(2, 1)=D(1, 2)
    D(1, 3)=0.0
    D(3, 1)=0.0
    D(2, 3)=0.0
    D(3, 2)=0.0
    D(3, 3)=E1/2.0/(1.0+XU)
    DO 11 N=1, NE
    EPZ(1, N)=D(1, 2)
    EPZ(2, N)=D(1, 2)
    EPZ(3, N)=0.0
    DO 11 K=1, 3
    DO 11 M=1, 3
11  EP(K, M, N)=D(K, M)
    RETURN
    END
    SUBROUTINE SKFORM(D)
    DIMENSION SKE(6, 6), D(3, 3), W4(3, 6), W5(3, 6), W6(6, 3)
    COMMON /C1/ NE, NN, NB, NEQ, X(115), Y(115), NI(162), NJ(162), NK(162), AI(
*162), AJ(162), AK(162), BI(162), BJ(162), BK(162), AREA(162), NP(230), NP1
*(162), NP2(162), NX(30), NY(30), EP(3, 3, 162), B(3, 6)
*, E1, XU, H, G, NOR
    COMMON /C2/ SK(230, 40), SKET(6, 6, 162)
    COMMON /C3/ DST(3, 162), SS(3, 162), DSS(3, 162), TSTP(162), DTSTP(162), T
*SS(162), DTSS(162)
    DO 4 I=1, NEQ
    DO 4 J=1, NB
4  SK(I, J)=0.0
    DO 2 I=1, 2
    DO 2 J=1, 6
2  B(I, J)=0.0
    DO 1 N=1, NE
    B(1, 1)=BI(N)
    B(1, 3)=BJ(N)
    B(1, 5)=BK(N)
    B(2, 2)=AI(N)
    B(2, 4)=AJ(N)
    B(2, 6)=AK(N)
    B(3, 1)=AI(N)
    B(3, 2)=BI(N)
    B(3, 3)=AJ(N)
    B(3, 4)=BJ(N)
    B(3, 5)=AK(N)
    B(3, 6)=BK(N)
    CALL MULT1(D, B, W5, 3, 3, 6)
    TT=4.0*AREA(N)
    DO 5 K=1, 6
    DO 5 M=K, 6
    SKE(K, M)=0.0
    DO 6 L=1, 3
6  SKE(K, M)=SKE(K, M)+B(L, K)*W5(L, M)
    SKE(K, M)=SKE(K, M)/TT
```

```

      SKET(K,M,N)=SKE(K,M)
5     CONTINUE
      CALL SADD(N,SKE)
1     CONTINUE
      RETURN
      END
      SUBROUTINE BOND1(U,F)
      DIMENSION U(230),F(230)
      COMMON /C1/ NE,NN,NB,NEQ,X(115),Y(115),NI(162),NJ(162),NK(162),AI(
*162),AJ(162),AK(162),BI(162),BJ(162),BK(162),AREA(162),NP(230),NP1
*(162),NP2(162),NX(30),NY(30),EP(3,3,162),B(3,6)
*,E1,XU,H,G,NOR
      ND=5
      NP(230)=1
      NP(229)=1
      NP(203)=1
      NP(181)=1
      NP(161)=1
      NP(141)=1
      NP(107)=1
      NP(137)=1
      NP(135)=1
      NP(136)=1
      NP(102)=1
      NP(74)=1
      NP(50)=1
      NP(52)=1
      NP(76)=1
      NP(106)=1
      NP(139)=1
      NP(140)=1
      DO 1 I=1,NEQ
      U(I)=0.0
1     F(I)=0.0
      KK=2*NY(1)
      U(KK)=- (Y(NY(1))-Y(NY(2)))/FLOAT(ND)
      RETURN
      END
      SUBROUTINE YIELD1(U,F,DU,DF,D)
      DIMENSION D(3,3),SSD(1,3),TSSD(3,1),W1(1,1),W2(1,3),W3(3,1),W4(3,3
*) ,W5(3,6),W6(6,3),SKEO(6,6),SKE(6,6),ST(3,162),TST(162)
      DIMENSION U(230),DU(230),F(230),DF(230)
      COMMON /C1/ NE,NN,NB,NEQ,X(115),Y(115),NI(162),NJ(162),NK(162),AI(
*162),AJ(162),AK(162),BI(162),BJ(162),BK(162),AREA(162),NP(230),NP1
*(162),NP2(162),NX(30),NY(30),EP(3,3,162),B(3,6)
*,E1,XU,H,G,NOR
      COMMON /C2/ SK(230,40),SKET(6,6,162)
      COMMON /C3/ DST(3,162),SS(3,162),DSS(3,162),TSTP(162),DTSTP(162),T
*SS(162),DTSS(162)
      COMMON /C4/ TSSO(162),SSZ(162),DSSZ(162),EPZ(3,162)
      H=0.86E03 $ YSR=500.0
      YS=400.0
      DO 300 I=1,NE
300   TSSO(I)=YSR
C*****
C***** SOLVE OF THE SYSTEM OF EQUATIONS *****
      CALL SOLVE(U,F)
```

```

C***** EVALUATION OF THE RATING FACTOR YP *****
  BIG=0.0
  DO 1 N=1,NE
    I=NI(N)
    J=NJ(N)
    K=NK(N)
    ST(1,N)=0.5*(BI(N)*U(2*I-1)+BJ(N)*U(2*J-1)+BK(N)*U(2*K-1))/AREA(N)
    ST(2,N)=0.5*(AI(N)*U(2*I)+AJ(N)*U(2*J)+AK(N)*U(2*K))/AREA(N)
    ST(3,N)=0.5*(AI(N)*U(2*I-1)+BI(N)*U(2*I)+AJ(N)*U(2*J-1)+BJ(N)*U(2*
  *J)+AK(N)*U(2*K-1)+BK(N)*U(2*K))/AREA(N)
    SS(1,N)=D(1,1)*ST(1,N)+D(1,2)*ST(2,N)+D(1,3)*ST(3,N)
    SS(2,N)=D(2,1)*ST(1,N)+D(2,2)*ST(2,N)+D(2,3)*ST(3,N)
    SS(3,N)=D(3,1)*ST(1,N)+D(3,2)*ST(2,N)+D(3,3)*ST(3,N)
    SSZ(N)=EPZ(1,N)*ST(1,N)+EPZ(2,N)*ST(2,N)+EPZ(3,N)*ST(3,N)
    TSS(N)=SQRT((SS(1,N)-SS(2,N))**2+(SS(1,N)-SSZ(N))**2+(SS(2,N)-SSZ(
  *N))**2+6.0*SS(3,N)**2)/SQRT(2.0)
    TST(N)=TSS(N)/E1
    IF(BIG.LT.TSS(N)) BIG=TSS(N)
1  CONTINUE
    YP=TSSO(1)/BIG
    IF(Y(NY(1))+U(2*NY(1)).GT.Y(NY(2))+U(2*NY(2))) GO TO 38
    YP1=(Y(NY(1))-Y(NY(2)))/(U(2*NY(2))-U(2*NY(1)))
    IF(YP1.LT.YP) YP=YP1
38  IF(NP(2*NX(1)-1).EQ.0) GO TO 39
    IF(X(NX(1)).GT.X(NX(2))+U(2*NX(2)-1)) GO TO 39
    YP1=(X(NX(1))-X(NX(2)))/U(2*NX(2)-1)
    IF(YP1.LT.YP) YP=YP1
39  TT=0.0
    DO 2 N=1,NE
      ST(1,N)=YP*ST(1,N)
      ST(2,N)=YP*ST(2,N)
      ST(3,N)=YP*ST(3,N)
      SS(1,N)=YP*SS(1,N)
      SS(2,N)=YP*SS(2,N)
      SS(3,N)=YP*SS(3,N)
      SSZ(N)=SSZ(N)*YP
      TST(N)=YP*TST(N)
      TSS(N)=YP*TSS(N)
      IF(TSS(N)/TSSO(1).GE.0.995) NP2(N)=1
      IF(NP2(N).EQ.1) NP1(N)=0
2  CONTINUE
    DO 6 I=1,NEQ
      DU(I)=0.0
      DF(I)=0.0
      U(I)=YP*U(I)
6  F(I)=YP*F(I)
    WRITE(6,10000)
10000 FORMAT(//,2X,2HNO,23X,2HUX,23X,2HUY,23X,2HFX,23X,2HFY,/,120(1H*),/
  */)
    L=0
    DO 20000 N=1,NEQ,2
      L=L+1
      X1=U(N)
      X2=U(N+1)
      Y1=F(N)
      Y2=F(N+1)
      WRITE(6,30000)L,X1,X2,Y1,Y2

```

```
30000 FORMAT(1X, I3, 10X, 4(E15.5, 10X))
20000 CONTINUE
      DO 100 K=1, NE
      DTSTP(K)=0.0
      TSTP(K)=0.0
100   CONTINUE
      A=E1/(1.0+XU)
      B1=(1.0-XU)/(1.0-2.0*XU)
      C=XU/(1.0-2.0*XU)
      DO 14 N=1, NE
      IF(NP2(N).EQ.0) GO TO 14
      S=2.0/3.0*TSS(N)*TSS(N)*(1.0+H/3.0/G)
      SM=(SS(1,N)+SS(2,N)+SSZ(N))/3.0
      S1=SS(1,N)-SM
      S2=SS(2,N)-SM
      S3=SS(3,N)
      S4=SSZ(N)-SM
      EP(1,1,N)=A*(B1-S1*S1/S)
      EP(2,1,N)=A*(C-S1*S2/S)
      EP(2,2,N)=A*(B1-S2*S2/S)
      EP(3,1,N)=-A*S1*S3/S
      EP(3,2,N)=-A*S2*S3/S
      EP(3,3,N)=A*(0.5-S3*S3/S)
      EP(1,2,N)=EP(2,1,N)
      EP(1,3,N)=EP(3,1,N)
      EP(2,3,N)=EP(3,2,N)
      EPZ(1,N)=A*(C-S1*S4/S)
      EPZ(2,N)=A*(C-S2*S4/S)
      EPZ(3,N)=-A*S3*S4/S
      DO 8 K=1, 3
      DO 8 M=1, 3
8     W4(K,M)=EP(K,M,N)
      B(1,1)=BI(N)
      B(1,3)=BJ(N)
      B(1,5)=BK(N)
      B(2,2)=AI(N)
      B(2,4)=AJ(N)
      B(2,6)=AK(N)
      B(3,1)=AI(N)
      B(3,2)=BI(N)
      B(3,3)=AJ(N)
      B(3,4)=BJ(N)
      B(3,5)=AK(N)
      B(3,6)=BK(N)
      CALL MULT1(W4,B,W5,3,3,6)
      TT=4.0*AREA(N)
      DO 10 K=1, 6
      DO 10 M=K, 6
      SKE(K,M)=0.0
      DO 161 L=1, 3
161   SKE(K,M)=SKE(K,M)+B(L,K)*W5(L,M)
      SKE(K,M)=SKE(K,M)/TT-SKET(K,M,N)
      SKET(K,M,N)=SKET(K,M,N)+SKE(K,M)
10    CONTINUE
      CALL SADD(N,SKE)
14    CONTINUE
      RETURN
```

```
END
SUBROUTINE CHANGE(D,U)
DIMENSION D(3,3),U(230)
COMMON /C1/ NE,NN,NB,NEQ,X(115),Y(115),NI(162),NJ(162),NK(162),AI(
*162),AJ(162),AK(162),BI(162),BJ(162),BK(162),AREA(162),NP(230),NP1
*(162),NP2(162),NX(30),NY(30),EP(3,3,162),B(3,6)
*,E1,XU,H,G,NOR
DO 5 N=1,NE
IF(NP2(N).NE.1) GO TO 5
I=NI(N)
J=NJ(N)
K=NK(N)
AI(N)=(X(K)+U(2*K-1))-(X(J)+U(2*J-1))
AJ(N)=(X(I)+U(2*I-1))-(X(K)+U(2*K-1))
AK(N)=(X(J)+U(2*J-1))-(X(I)+U(2*I-1))
BI(N)=(Y(J)+U(2*J))-(Y(K)+U(2*K))
BJ(N)=(Y(K)+U(2*K))-(Y(I)+U(2*I))
BK(N)=(Y(I)+U(2*I))-(Y(J)+U(2*J))
AREA(N)=0.5*(AK(N)*BJ(N)-AJ(N)*BK(N))
5 CONTINUE
RETURN
END
SUBROUTINE BOND2(IO,U,F,DU,DF)
DIMENSION U(230),DU(230),F(230),DF(230)
COMMON /C1/ NE,NN,NB,NEQ,X(115),Y(115),NI(162),NJ(162),NK(162),AI(
*162),AJ(162),AK(162),BI(162),BJ(162),BK(162),AREA(162),NP(230),NP1
*(162),NP2(162),NX(30),NY(30),EP(3,3,162),B(3,6)
*,E1,XU,H,G,NOR
COMMON/C5/KS,LS
IF(IO.NE.1)GO TO 1
KS=1
LS=1
1 DELTA=0.0002
DO 10 KK=1,30
DI=Y(NY(1))+U(2*NY(1))-Y(NY(KK))-U(2*NY(KK))
IF(DI.LT.0.00000001) KS=KK
IF(DI.LT.0.00000001) DU(2*NY(KK))=-DELTA
IF(DI.LT.0.00000001) NP(2*NY(KK))=1
10 CONTINUE
IF(NP(2*NX(1)-1).EQ.0) GO TO 7
DO 20 KK=1,30
DI=X(NX(1))-X(NX(KK))-U(2*NX(KK)-1)
IF(DI.LT.0.00000001) LS=KK
IF(DI.LT.0.00000001) DU(2*NX(KK)-1)=0.0
IF(DI.LT.0.00000001) NP(2*NX(KK)-1)=1
20 CONTINUE
7 RETURN
END
SUBROUTINE YIELD2(U,F,DU,DF,D,IO)
DIMENSION U(230),DU(230),F(230),DF(230)
DIMENSION D(3,3),SSD(1,3),TSSD(3,1),W1(1,1),W2(1,3),W3(3,1),W4(3,3
*),W5(3,6),W6(6,3),SKEO(6,6),SKE(6,6),ST(3,162),TST(162)
COMMON /C1/ NE,NN,NB,NEQ,X(115),Y(115),NI(162),NJ(162),NK(162),AI(
*162),AJ(162),AK(162),BI(162),BJ(162),BK(162),AREA(162),NP(230),NP1
*(162),NP2(162),NX(30),NY(30),EP(3,3,162),B(3,6)
*,E1,XU,H,G,NOR
COMMON /C2/ SK(230,40),SKET(6,6,162)
```

```
COMMON /C3/ DST(3,162),SS(3,162),DSS(3,162),TSTP(162),DTSTP(162),T
*SS(162),DTSS(162)
COMMON /C4/ TSSO(162),SSZ(162),DSSZ(162),EPZ(3,162)
COMMON /C5/KS,LS
YP=1000.0
CALL SOLVE(DU,DF)
DO 1 N=1,NE
I=NI(N)
J=NJ(N)
K=NK(N)
DST(1,N)=0.5*(BI(N)*DU(2*I-1)+BJ(N)*DU(2*J-1)+BK(N)*DU(2*K-1))/ARE
*A(N)
DST(2,N)=0.5*(AI(N)*DU(2*I)+AJ(N)*DU(2*J)+AK(N)*DU(2*K))/AREA(N)
DST(3,N)=0.5*(AI(N)*DU(2*I-1)+BI(N)*DU(2*I)+AJ(N)*DU(2*J-1)+BJ(N)*
*DU(2*J)+AK(N)*DU(2*K-1)+BK(N)*DU(2*K))/AREA(N)
DSS(1,N)=EP(1,1,N)*DST(1,N)+EP(1,2,N)*DST(2,N)+EP(1,3,N)*DST(3,N)
DSS(2,N)=EP(2,1,N)*DST(1,N)+EP(2,2,N)*DST(2,N)+EP(2,3,N)*DST(3,N)
DSS(3,N)=EP(3,1,N)*DST(1,N)+EP(3,2,N)*DST(2,N)+EP(3,3,N)*DST(3,N)
DSSZ(N)=EPZ(1,N)*DST(1,N)+EPZ(2,N)*DST(2,N)+EPZ(3,N)*DST(3,N)
IF(NP2(N).EQ.1) GO TO 1
TT=SQRT((SS(1,N)+DSS(1,N)-SS(2,N)-DSS(2,N))**2+(SS(1,N)+DSS(1,N)-S
*SZ(N)-DSSZ(N))**2+(SS(2,N)+DSS(2,N)-SSZ(N)-DSSZ(N))**2+6.0*(SS(3,N
*)+DSS(3,N))**2)/SQRT(2.0)-TSS(N)
IF(TT.LT.0.0) GO TO 1
A=(DSS(1,N)-DSS(2,N))**2+(DSS(1,N)-DSSZ(N))**2+(DSS(2,N)-DSSZ(N))
**2+6.0*DSS(3,N)**2
B1=DSS(3,N)*SS(3,N)*6.0+(DSS(1,N)-DSS(2,N))*(SS(1,N)-SS(2,N))+DSS
*(1,N)-DSSZ(N))*(SS(1,N)-SSZ(N))+DSS(2,N)-DSSZ(N))*(SS(2,N)-SSZ(N)
*)
C=2.0*(TSS(N)**2-TSSO(N)**2)
BIG=(-B1+SQRT(B1**2-A*C))/A
IF(BIG.LT.YP) YP=BIG
1 CONTINUE
KKU=1
IF(YP.LT.0.0) WRITE(6,103) KKU
103 FORMAT(10X,I10,///)
IF(YP.LT.0.0) STOP
IF(YP.GT.1.0) YP=1.0
DO 180 KK=2,30
IF(NP(2*NY(KK)).EQ.1) GO TO 180
IF((Y(NY(1))+U(2*NY(1))+DU(2*NY(1))).GT.(Y(NY(KK))+U(2*NY(KK))+DU(
*2*NY(KK)))) GO TO 180
YP1=(Y(NY(1))+U(2*NY(1))-Y(NY(KK))-U(2*NY(KK)))/(DU(2*NY(KK))-DU(2
**NY(1)))
IF(YP1.GT.0.0.AND.YP1.LT.YP) YP=YP1
180 CONTINUE
IF(NP(2*NX(1)-1).EQ.0) GO TO 39
DO 190 KK=2,30
IF(NP(2*NX(KK)-1).EQ.1) GO TO 190
IF(X(NX(1)).GT.(X(NX(KK))+U(2*NX(KK)-1)+DU(2*NX(KK)-1)))GO TO 190
YP1=(X(NX(1))-X(NX(KK))-U(2*NX(KK)-1))/DU(2*NX(KK)-1)
IF(YP1.GT.0.0.AND.YP1.LT.YP) YP=YP1
190 CONTINUE
39 TT=0.0
DO 2 N=1,NE
DST(1,N)=DST(1,N)*YP
DST(2,N)=DST(2,N)*YP
```



```
DST(3,N)=DST(3,N)*YP
DSS(1,N)=DSS(1,N)*YP
DSS(2,N)=DSS(2,N)*YP
DSS(3,N)=DSS(3,N)*YP
DSSZ(N)=DSSZ(N)*YP
2  CONTINUE
   DO 3 N=1,NE
4  DTSS(N)=SQRT((SS(1,N)+DSS(1,N)-SS(2,N)-DSS(2,N))**2+(SS(1,N)+DSS(1
*,N)-SSZ(N)-DSSZ(N))**2+(SS(2,N)+DSS(2,N)-SSZ(N)-DSSZ(N))**2+6.0*(S
*S(3,N)+DSS(3,N))**2)/SQRT(2.0)-TSS(N)
   IF(NP2(N).EQ.0) GO TO 5
   IF(DTSS(N).GE.0.0) GO TO 6
   TSSO(N)=TSS(N)
   NP2(N)=0
   NP1(N)=1
   DO 15 K=1,3
15  DSS(K,N)=D(K,1)*DST(1,N)+D(K,2)*DST(2,N)+D(K,3)*DST(3,N)
   DSSZ(N)=D(1,2)*DST(1,N)+D(1,2)*DST(2,N)
   GO TO 4
6  DTSTP(N)=DTSS(N)/H
   GO TO 3
5  DTSTP(N)=0.0
3  CONTINUE
   DO 90 N=1,NEQ
   U(N)=U(N)+YP*DU(N)
90  F(N)=F(N)+YP*DF(N)
   DO 11 N=1,NE
   TSS(N)=TSS(N)+DTSS(N)
   TSTP(N)=TSTP(N)+DTSTP(N)
   SSZ(N)=SSZ(N)+DSSZ(N)
   DO 110 K=1,3
   SS(K,N)=SS(K,N)+DSS(K,N)
110 CONTINUE
11  CONTINUE
   A=E1/(1.0+XU)
   B1=(1.0-XU)/(1.0-2.0*XU)
   C=XU/(1.0-2.0*XU)
   DO 12 N=1,NE
   IF(NP2(N).EQ.1) GO TO 14
   IF(TSS(N)/TSSO(N).GE.0.995) NP2(N)=1
   IF(NP2(N).EQ.1) NP1(N)=0
   IF(NP2(N).EQ.1) GO TO 14
   IF(DTSS(N).GE.0.0) GO TO 12
   EPZ(1,N)=D(1,2)
   EPZ(2,N)=D(1,2)
   EPZ(3,N)=0.0
   DO 13 K=1,3
   DO 13 M=1,3
   EP(K,M,N)=D(K,M)
13  W4(K,M)=D(K,M)
   GO TO 19
14  S=2.0/3.0*TSS(N)*TSS(N)*(1.0+H/3.0/G)
   SM=(SS(1,N)+SS(2,N)+SSZ(N))/3.0
   S1=SS(1,N)-SM
   S2=SS(2,N)-SM
   S3=SS(3,N)
   S4=SSZ(N)-SM
```

```
EP(1, 1, N)=A*(B1-S1*S1/S)
EP(2, 1, N)=A*(C-S1*S2/S)
EP(2, 2, N)=A*(B1-S2*S2/S)
EP(3, 1, N)=-A*S1*S3/S
EP(3, 2, N)=-A*S2*S3/S
EP(3, 3, N)=A*(0.5-S3*S3/S)
EP(1, 2, N)=EP(2, 1, N)
EP(1, 3, N)=EP(3, 1, N)
EP(2, 3, N)=EP(3, 2, N)
EPZ(1, N)=A*(C-S1*S4/S)
EPZ(2, N)=A*(C-S2*S4/S)
EPZ(3, N)=-A*S3*S4/S
DO 16 K=1, 3
DO 16 M=1, 3
16 W4(K, M)=EP(K, M, N)
19 TT=0.0
B(1, 1) =BI(N)
B(1, 3) =BJ(N)
B(1, 5)=BK(N)
B(2, 2)=AI(N)
B(2, 4)=AJ(N)
B(2, 6)=AK(N)
B(3, 1)=AI(N)
B(3, 2)=BI(N)
B(3, 3)=AJ(N)
B(3, 4)=BJ(N)
B(3, 5)=AK(N)
B(3, 6)=BK(N)
CALL MULT1(W4; B, W5, 3, 3, 6)
TT=4.0*AREA(N)
DO 17 K=1, 6
DO 17 M=K, 6
SKE(K, M)=0.0
DO 170 L=1, 3
170 SKE(K, M)=SKE(K, M)+B(L, K)*W5(L, M)
SKE(K, M)=SKE(K, M)/TT-SKET(K, M, N)
SKET(K, M, N)=SKET(K, M, N)+SKE(K, M)
17 CONTINUE
CALL SADD(N, SKE)
12 CONTINUE
IF(MOD(I0, 10).NE.0) GO TO 80
SUM1=ABS(U(2*NY(1)))
SUM6=ABS(U(2*NX(1)-1))
SUM2=0.0
SUM20=0.0
SUM3=0.0
SUM30=0.0
DO 220 KK=1, 30
SUM2=SUM2+F(2*NY(KK))
IF(KK.EQ.1) GO TO 212
SUM20=SUM20+F(2*NY(KK)-1)
SUM30=SUM30+F(2*NX(KK))
212 TT=0.0
220 SUM3=SUM3+F(2*NX(KK)-1)
SUM2=ABS(SUM2)
SUM3=ABS(SUM3)
SUM20=ABS(SUM20)
```

```
SUM30=ABS(SUM30)
SUM4=X(NY(KS))+U(2*NY(KS)-1)
SUM5=Y(NX(LS))+U(2*NX(LS))
WRITE(1,230) SUM1,SUM2,SUM3,SUM4,SUM5,SUM6,SUM20,SUM30
230  FORMAT(8(E12.5))
80   TT=0.0
     IF(MOD(I0,20).NE.0) GO TO 330
     WRITE(6,26)I0
26   FORMAT(/,1X,13HLOADING STEP=,I4)
     WRITE(6,4000)
4000 FORMAT(/,50X,13HPLASTIC ZONES,/,120(1H*))
     WRITE(6,4001)((N,NP2(N)),N=1,NE)
4001 FORMAT(7(I4,4X,I2,8X))
     WRITE(6,1990)
1990 FORMAT(/)
     WRITE(6,10000)
10000 FORMAT(2X,2HNO,16X,2HUX,16X,2HUY,16X,2HFX,16X,2HFX,16X,2HFX,16X,2HFX,13X,5HDTSTP,14X
*,4HTSTP,15X,3HTSS,/,130(1H*))
     DO 41 I=1,NN
     NO=0
     SUM1=0.0
     SUM2=0.0
     SUM3=0.0
     DO 42 N=1,NE
     IF(NI(N).EQ.I) GO TO 43
     IF(NJ(N).EQ.I) GO TO 43
     IF(NK(N).EQ.I) GO TO 43
     GO TO 42
43   NO=NO+1
     SUM1=SUM1+TSS(N)
     SUM2=SUM2+TSTP(N)
     SUM3=SUM3+DTSTP(N)
42   CONTINUE
     SUM1=SUM1/FLOAT(NO)
     SUM2=SUM2/FLOAT(NO)
     SUM3=SUM3/FLOAT(NO)
     X1=U(2*I-1)
     X2=U(2*I)
     Y1=F(2*I-1)
     Y2=F(2*I)
     WRITE(6,32)(I,X1,X2,Y1,Y2,SUM3,SUM2,SUM1)
32   FORMAT(I4,7(6X,E12.5))
41   CONTINUE
330  IF(I0.NE.NOR) GO TO 33
     WRITE(6,45)
45   FORMAT(/,2X,2HNO,24X,1HX,24X,1HY,/,60(1H*),/)
     DO 44 I=1,NN
     XX=X(I)+U(2*I-1)
     YY=Y(I)+U(2*I)
     NO=0
     SUM1=0.0
     SUM2=0.0
     SUM3=0.0
     DO 62 N=1,NE
     IF(NI(N).EQ.I) GO TO 63
     IF(NJ(N).EQ.I) GO TO 63
     IF(NK(N).EQ.I) GO TO 63
```

```
GO TO 62
63 NO=NO+1
SUM1=SUM1+TSS(N)
SUM2=SUM2+TSTP(N)
S1=SS(1,N)$S2=SS(2,N)$S3=SS(3,N)
TA=SQRT((S1-S2)**2/4.0+S3**2)
SUM3=SUM3+TA
62 CONTINUE
SUM1=SUM1/FLOAT(NO)
SUM2=SUM2/FLOAT(NO)
SUM3=SUM3/FLOAT(NO)
V1=U(2*I-1)$V2=U(2*I)$V3=DU(2*I-1)$V4=DU(2*I)
WRITE(6,46)(I,XX,YY)
46 FORMAT(1X,I3,10X,E15.5,10X,E15.5)
WRITE(2,102) I,X(I),Y(I),V1,V2,V3,V4,SUM1,SUM2,SUM3
102 FORMAT(I10,9(E10.3))
44 CONTINUE
33 RETURN
END
SUBROUTINE SOLVE(U,F)
DIMENSION SKI(230,40),FI(230),F(230),U(230)
COMMON /C1/ NE,NN,NB,NEQ,X(115),Y(115),NI(162),NJ(162),NK(162),AI(
*162),AJ(162),AK(162),BI(162),BJ(162),BK(162),AREA(162),NP(230),NP1
*(162),NP2(162),NX(30),NY(30),EP(3,3,162),B(3,6)
*,E1,XU,H,G,NOR
COMMON /C2/ SK(230,40),SKET(6,6,162)
COMMON /C3/ DST(3,162),SS(3,162),DSS(3,162),TSTP(162),DTSTP(162),T
*SS(162),DTSS(162)
DO 1 I=1,NEQ
IF(NP(I).EQ.0) FI(I)=F(I)
IF(NP(I).EQ.1) FI(I)=SK(I,1)*U(I)*10.0E20
IF(NP(I).EQ.1.AND.U(I).EQ.0.0) FI(I)=SK(I,1)*10.0E10
DO 2 J=1,NB
2 SKI(I,J)=SK(I,J)
IF(NP(I).EQ.1) SKI(I,1)=SKI(I,1)*10.0E20
1 CONTINUE
DO 300 N=1,NEQ
I=N
DO 290 L=2,NB
I=I+1
IF(SKI(N,L)) 240,290,240
240 C=SKI(N,L)/SKI(N,1)
J=0
DO 270 K=L,NB
J=J+1
IF(SKI(N,K)) 260,270,260
260 SKI(I,J)=SKI(I,J)-C*SKI(N,K)
270 CONTINUE
280 SKI(N,L)=C
FI(I)=FI(I)-C*FI(N)
290 CONTINUE
300 FI(N)=FI(N)/SKI(N,1)
N=NEQ
350 N=N-1
IF(N) 500,500,360
360 L=N
DO 400 K=2,NB
```

```
L=L+1
IF(SKI(N,K)) 370,400,370
370 FI(N)=FI(N)-SKI(N,K)*FI(L)
400 CONTINUE
GO TO 350
500 TT=0.0
DO 3 N=1,NEQ
IF(NP(N).EQ.1) GO TO 3
U(N)=FI(N)
3 CONTINUE
DO 4 N=1,NEQ
IF(NP(N).EQ.0) GO TO 4
SUM=0.0
K=N+1
L=0
DO 5 J=1,NB
K=K-1
L=L+1
IF(K.EQ.0) GO TO 6
5 SUM=SUM+SK(K,L)*U(K)
6 TT=0.0
DO 7 J=2,NB
IF(SK(N,J).EQ.0.0) GO TO 7
SUM=SUM+SK(N,J)*U(N-1+J)
7 CONTINUE
F(N)=SUM
4 CONTINUE
RETURN
END
SUBROUTINE SADD(N,SKE)
DIMENSION NO(3),SKE(6,6)
COMMON /C1/ NE,NN,NB,NEQ,X(115),Y(115),NI(162),NJ(162),NK(162),AI(
*162),AJ(162),AK(162),BI(162),BJ(162),BK(162),AREA(162),NP(230),NP1
*(162),NP2(162),NX(30),NY(30),EP(3,3,162),B(3,6)
*,E1,XU,H,G,NOR
COMMON /C2/ SK(230,40),SKET(6,6,162)
NO(1)=NI(N)
NO(2)=NJ(N)
NO(3)=NK(N)
DO 1 JJ=1,3
NROW=(NO(JJ)-1)*2
DO 1 J=1,2
NROW=NROW+1
I=(JJ-1)*2+J
DO 2 KK=1,3
NCOLB=(NO(KK)-1)*2
DO 3 K=1,2
L=(KK-1)*2+K
NCOL=NCOLB+K+1-NROW
IF(NCOL)3,3,4
4 IF(L.LT.I) SKE(I,L)=SKE(L,I)
SK(NROW,NCOL)=SK(NROW,NCOL)+SKE(I,L)
3 CONTINUE
2 CONTINUE
1 CONTINUE
RETURN
END
```

```

SUBROUTINE MULTI(A,B,C,M,N,L)
DIMENSION A(M,N),B(N,L),C(M,L)
DO 1 I=1,M
DO 1 J=1,L
C(I,J)=0.0
DO 1 K=1,N
1 C(I,J)=C(I,J)+A(I,K)*B(K,J)
RETURN
END
```

APPENDIX 'B'

LISTING OF THE COMPUTER  
PROGRAM EPFEA 2  
USING QUADRILATERAL ELEMENTS  
(COMPRISING OF FOUR TRIANGULAR ELEMENTS)

NOMENCLATURE

Variable	Place in labelled common	Definition
NE	C1	Number of elements
NN	"	Number of nodes
NB	"	Band width of the overall stiffness matrix
NEQ	"	Number of equations
X,Y	"	Coordinates of nodal points
NOP	"	Nodal connection of elements
AI,AJ,AK, BI,BJ,BK	"	Local coordinates of elements
AREA	"	Area of elements
NP	"	Pointer vector for imposing boundary conditions
NP1,NP2	"	Pointer vectors for indicating state of elements
NX,NY	"	Peripheral nodal points matrices, due to the side and upper segments
EP	"	Stress-strain matrix of elements
SK	C2	Overall stiffness matrix
SKEQ	"	Stiffness matrices of quadrilateral elements
DST	C3	Strain-increment of elements
SS	"	Stress of elements
DSS	"	Stress-increment of elements
TSTP	"	Effective plastic strain of elements
DTSTP	"	Effective plastic strain-increment of elements
TSS0	C4	Yield strength of elements
SSZ	"	Stress of elements in the z-direction
DSSZ	"	Stress-increment of elements in the z-direction
EPZ	C4	Stress-strain matrix in the z-direction
SM	C6	9th and 10th equations of eliminated element stiffness matrices for recovery of internal nodes



XU	C7	Poisson's ratio
E1	"	Modulus of elasticity
H1,H2	"	Tangent moduli of stress-strain curve
YS1,YS2	"	Yield stresses of stress-strain curve at breaking points
NEQ1	"	Number of degree of freedom of internal nodes
NT	"	Number of triangular elements
G	"	Shear modulus of elasticity
NOR	"	Number of load increments

Local Variable	Place in Subroutine	Definition
D	GDATA	Elastic material matrix
SK10	SKFORM	Stiffness matrix of four triangular elements comprising a quadrilateral
SK	"	Stiffness matrix of a triangular element
NO	"	Nodal connection of a triangular element

Variables of main program	Definition
U	Displacement of nodal points
F	Force of nodal points
DU	Displacement-increment of nodal points
DF	Force-increment of nodal points
UM	Displacement of internal nodal points
VM	Displacement-increment of internal nodal points

PROGRAM 'EPFEA2'  
\*\*\*\*\*

```
C*****
C***** MAIN PROGRAM *****
C***** ELASTIC-PLASTIC FINITE ELEMENT ANALYSIS *****
C***** WRITTEN BY ALI NAJAFI-SANI IN THE FIRST SEMESTER OF 1978 *****
C***** DEVELOPED FOR QUADRILATERAL ELEMENTS *****
C*****
PROGRAM EPFEA2(INPUT, OUTPUT, TAPE5=INPUT, TAPE6=OUTPUT, TAPE1=113B,
*TAPE2=113B)
DIMENSION U(174),DU(174),F(174),DF(174),D(3,3)
DIMENSION UM(174),VM(174)
COMMON /C1/ NE,NN,NB,NEQ,X(87),Y(87),NOP(4,67),AI(268),AJ(268),AK(
*268),BI(268),BJ(268),BK(268),AREA(268),NP(174),NP1(268),NP2(268),N
*X(12),NY(12),EP(3,3,268),B(3,6)
COMMON /C2/ SK(174,34),SKEQ(8,8,67)
COMMON /C3/ DST(3,268),SS(3,268),DSS(3,268),TSTP(268),DTSTP(268),T
*SS(268),DTSS(268)
COMMON /C4/ TSSO(268),SSZ(268),DSSZ(268),EPZ(3,268)
COMMON /C5/ KS,LS
COMMON /C6/ SM(2,10,67)
COMMON /C7/ XU,E1,H1,H2,YS1,YS2,SP2,NEQ1,NT,KKU,G,NOR,A,B1,C
C*****
C***** INPUT OF DATA *****
CALL GDATA(D)
C*****
C***** GENERATION AND ASSEMBLY OF STIFFNESS MATRICES *****
CALL SKFORM(D)
C*****
C***** INPUT OF INITIAL BOUNDARY CONDITIONS *****
CALL BOND1(U,F,UM)
C*****
C***** INITIATION OF PLASTIC DEFORMATION *****
CALL YIELD1(U,F,DU,DF,D,UM,VM)
NOR=1500
C*****
C***** INITIATION OF LOAD INCREMENTS *****
DO 1 I=1,NOR
C*****
C***** UPDATE OF GEOMETRICAL MATRICES *****
CALL CHANGE(D,U,UM)
C*****
C***** INPUT OF INSTANTANEOUS BOUNDARY CONDITIONS *****
CALL BOND2(I,U,F,DU,DF,UM,VM)
C*****
C***** INITIATION OF INCREMENTAL PLASTIC DEFORMATION *****
CALL YIELD2(U,F,DU,DF,D,I,UM,VM)
1 CONTINUE
STOP
END
SUBROUTINE GDATA(D)
COMMON /C1/ NE,NN,NB,NEQ,X(87),Y(87),NOP(4,67),AI(268),AJ(268),AK(
```

```
*268),BI(268),BJ(268),BK(268),AREA(268),NP(174),NP1(268),NP2(268),N
*X(12),NY(12),EP(3,3,268),B(3,6)
COMMON /C2/ SK(174,34),SKEQ(8,8,67)
COMMON /C3/ DST(3,268),SS(3,268),DSS(3,268),TSTP(268),DTSTP(268),T
*SS(268),DTSS(268)
COMMON /C4/ TSSO(268),SSZ(268),DSSZ(268),EPZ(3,268)
COMMON /C7/XU,E1,H1,H2,YS1,YS2,SP2,NEQ1,NT,KKU,G,NOR,A,B1,C
DIMENSION D(3,3)
DATA NP/174*0/,NP1/268*1/,NP2/268*0/,NE/67/,NN/87/,NB/34/,NEQ/17
*4/
DATA NY/80,81,82,83,84,85,86,87,78,79,64,65/
DATA NX/9,18,20,32,31,43,42,51,50,58,65,64/
XU=0.345 $ E1=0.7E06 $ YS1=400.0 $ YS2=900.0 $ SP2=0.1 $ H1=5000.0
H2=750.0
SP2=0.09
XU=0.431 $ E1=0.1E06 $ YS1=60.0 $ YS2=150.0 $ SP2=0.05
H1=1800.0 $H2=260.0
SP2=0.045
NEQ1=2*NE $ NT=4*NE
WRITE(6,1)
1 FORMAT(////////,1X,28HINDENTATION OF ROUND BILLETS,/,30(1H*))
READ(5,3)((NOP(1,I),NOP(2,I),NOP(3,I),NOP(4,I)),I=1,NE)
3 FORMAT(4I5)
READ(5,2)((M,X(M),Y(M)),I=1,NN)
2 FORMAT(2(I2,3X,2F10.2))
R=14.0
DO 22 N=1,NN
IF(Y(N).EQ.1.0) Y(N)=SQRT(R**2-X(N)**2)
IF(X(N).EQ.1.0) X(N)=SQRT(R**2-Y(N)**2)
22 CONTINUE
SC=R
DO 12 K=1,NN
X(K)=X(K)/SC
Y(K)=Y(K)/SC
12 CONTINUE
N=0
DO 5 NQ=1,NE
XM=(X(NOP(1,NQ))+X(NOP(2,NQ))+X(NOP(3,NQ))+X(NOP(4,NQ)))/4.0
YM=(Y(NOP(1,NQ))+Y(NOP(2,NQ))+Y(NOP(3,NQ))+Y(NOP(4,NQ)))/4.0
DO 50 M=1,4
N=N+1
I=NOP(M,NQ)
IF(M.LT.4) J=NOP(M+1,NQ)
IF(M.EQ.4) J=NOP(1,NQ)
AI(N)=XM-X(J)
AJ(N)=X(I)-XM
AK(N)=X(J)-X(I)
BI(N)=Y(J)-YM
BJ(N)=YM-Y(I)
BK(N)=Y(I)-Y(J)
AREA(N)=0.5*(AK(N)*BJ(N)-AJ(N)*BK(N))
IF(AREA(N).GT.0.0) GO TO 50
WRITE(6,6) N
6 FORMAT(1X,I5,26HELEMENT WITH NEGATIVE AREA)
STOP
50 CONTINUE
5 CONTINUE
```

```
WRITE (6, 7)
7  FORMAT (///, 2X, 2HNO, 24X, 1HX, 24X, 1HY, /, 60(1H*), //)
   WRITE (6, 8) ((I, X(I), Y(I)), I=1, NN)
8  FORMAT (1X, I3, 10X, E15.5, 10X, E15.5)
   WRITE (6, 9)
9  FORMAT (//, 2X, 2HNO, 9X, 1HI, 9X, 1HJ, 9X, 1HK, , 9X, 1HP, /, 60(1H*), //)
   WRITE (6, 10) (I, NOP(1, I), NOP(2, I), NOP(3, I), NOP(4, I), I=1, NE)
10  FORMAT (1X, I3, 7X, I3, 7X, I3, 7X, I3, 7X, I3)
    FACT=E1*(1.0-XU)/(1.0+XU)/(1.0-2.0*XU)
    D(1, 1)=FACT
    D(2, 2)=FACT
    D(1, 2)=FACT*XU/(1.0-XU)
    D(2, 1)=D(1, 2)
    D(1, 3)=0.0
    D(3, 1)=0.0
    D(2, 3)=0.0
    D(3, 2)=0.0
    D(3, 3)=E1/2.0/(1.0+XU)
    N=0
    DO 11 NQ=1, NE
    DO 11 MO=1, 4
    N=N+1
    EPZ(1, N)=D(1, 2)
    EPZ(2, N)=D(1, 2)
    EPZ(3, N)=0.0
    DO 11 K=1, 3
    DO 11 M=1, 3
11  EP(K, M, N)=D(K, M)
    RETURN
    END
    SUBROUTINE SKFORM(D)
    DIMENSION SKE(6, 6), D(3, 3), W4(3, 6), W5(3, 6), W6(6, 3)
    DIMENSION SK10(10, 10), NO(3)
    COMMON /C1/ NE, NN, NB, NEQ, X(87), Y(87), NOP(4, 67), AI(268), AJ(268), AK(
    *268), BI(268), BJ(268), BK(268), AREA(268), NP(174), NP1(268), NP2(268), N
    *X(12), NY(12), EP(3, 3, 268), B(3, 6)
    COMMON /C2/ SK(174, 34), SKEQ(8, 8, 67)
    COMMON /C3/ DST(3, 268), SS(3, 268), DSS(3, 268), TSTP(268), DTSTP(268), T
    *SS(268), DTSS(268)
    COMMON /C6/ SM(2, 10, 67)
    DO 4 I=1, NEQ
    DO 4 J=1, NB
4  SK(I, J)=0.0
    DO 2 I=1, 2
    DO 2 J=1, 6
2  B(I, J)=0.0
    N=0
    DO 1 NQ=1, NE
    DO 12 I=1, 10
    DO 12 J=I, 10
12  SK10(I, J)=0.0
    DO 11 MO=1, 4
    N=N+1
    B(1, 1)=BI(N)
    B(1, 3)=BJ(N)
    B(1, 5)=BK(N)
    B(2, 2)=AI(N)
```

```
B(2,4)=AJ(N)
B(2,6)=AK(N)
B(3,1)=AI(N)
B(3,2)=BI(N)
B(3,3)=AJ(N)
B(3,4)=BJ(N)
B(3,5)=AK(N)
B(3,6)=BK(N)
CALL MULT1(D,B,W5,3,3,6)
TT=4.0*AREA(N)
DO 13 K=1,6
DO 13 M=K,6
SKE(K,M)=0.0
DO 14 L=1,3
14 SKE(K,M)=SKE(K,M)+B(L,K)*W5(L,M)
SKE(K,M)=SKE(K,M)/TT
13 CONTINUE
NO(1)=MO $ NO(2)=MO+1 $ NO(3)=5
IF(MO.EQ.4) NO(2)=1
DO 350 JJ=1,3
NROWB=(NO(JJ)-1)*2
DO 350 J=1,2
NROWB=NROWB+1
I=(JJ-1)*2+J
DO 330 KK=1,3
NCOLB=(NO(KK)-1)*2
DO 320 K=1,2
L=(KK-1)*2+K
NCOL=NCOLB+K
IF(NCOL+1-NROWB) 320,320,310
310 IF(L.LT.I) SKE(I,L)=SKE(L,I)
SK10(NROWB,NCOL)=SK10(NROWB,NCOL)+SKE(I,L)
320 CONTINUE
330 CONTINUE
350 CONTINUE
11 CONTINUE
SK10(10,9)=SK10(9,10)
DO 400 I=1,2
K=I+8
DO 300 J=1,10
300 SM(I,J,NQ)=SK10(J,K)
400 CONTINUE
DO 200 K=1,2
LL=10-K
KK=LL+1
DO 200 L=1,LL
T=SK10(L,KK)/SK10(KK,KK)
DO 100 M=L,LL
100 SK10(L,M)=SK10(L,M)-SM(3-K,M,NQ)*T
IF(L.NE.9) GO TO 200
DO 2567 M=1,9
2567 SM(1,M,NQ)=SM(1,M,NQ)-T*SM(2,M,NQ)
200 CONTINUE
DO 500 I=1,8
DO 500 J=I,8
SKEQ(I,J,NQ)=SK10(I,J)
500 CONTINUE
```

```
CALL SADD(NQ, SK10)
1 CONTINUE
  RETURN
  END
  SUBROUTINE BOND1(U, F, UM)
    DIMENSION U(174), F(174), UM(174)
    COMMON /C1/ NE, NN, NB, NEQ, X(87), Y(87), NOP(4, 67), AI(268), AJ(268), AK(
*268), BI(268), BJ(268), BK(268), AREA(268), NP(174), NP1(268), NP2(268), N
*X(12), NY(12), EP(3, 3, 268), B(3, 6)
    NEQ1=2*NE      $      NT=4*NE
    ND=5
    NP(2)=1$NP(4)=1$NP(6)=1$NP(8)=1$NP(10)=1$NP(12)=1$NP(14)=1
    NP(16)=1$NP(18)=1$NP(20)=1$NP(22)=1$NP(24)=1$NP(26)=1$NP(28)=1
    NP(30)=1$NP(32)=1$NP(34)=1$NP(36)=1$NP(38)=1$NP(40)=1$NP(42)=1
    NP(44)=1$NP(46)=1$NP(48)=1$NP(50)=1$NP(52)=1$NP(54)=1$NP(56)=1
    NP(58)=1$NP(60)=1$NP(62)=1$NP(64)=1$NP(66)=1$NP(68)=1$NP(70)=1
    NP(72)=1$NP(74)=1$NP(76)=1$NP(78)=1$NP(80)=1$NP(82)=1$NP(84)=1
    NP(86)=1$NP(88)=1$NP(90)=1$NP(92)=1$NP(94)=1$NP(96)=1$NP(98)=1
    NP(100)=1$NP(102)=1$NP(104)=1$NP(106)=1$NP(108)=1$NP(110)=1
    NP(112)=1$NP(114)=1$NP(116)=1$NP(118)=1$NP(120)=1$NP(122)=1
    NP(124)=1$NP(126)=1$NP(128)=1$NP(130)=1$NP(132)=1$NP(134)=1
    NP(136)=1$NP(138)=1$NP(140)=1$NP(142)=1$NP(144)=1$NP(146)=1
    NP(148)=1$NP(150)=1$NP(152)=1$NP(154)=1$NP(156)=1$NP(158)=1
    NP(160)=1$NP(162)=1$NP(164)=1$NP(166)=1$NP(168)=1$NP(170)=1
    NP(172)=1$NP(174)=1
    DO 1 I=1, NEQ
      U(I)=0.0
1    F(I)=0.0
    DO 2 I=1, NEQ1
2    UM(I)=0.0
      KK=2*NY(1)
      U(KK)=- (Y(NY(1))-Y(NY(2)))/FLOAT(ND)
      JJ=2*NX(1)-1
      U(JJ)=U(KK)
    RETURN
  END
  SUBROUTINE YIELD1(U, F, DU, DF, D, UM, VM)
    DIMENSION U(174), DU(174), UM(174), VM(174), F(174), DF(174)
    DIMENSION D(3, 3), SSD(1, 3), TSSD(3, 1), W1(1, 1), W2(1, 3), W3(3, 1), W4(3, 3
*) , W5(3, 6), W6(6, 3), SKEO(6, 6), SKE(6, 6), SK10(10, 10), ST(3, 268), TST(268
*) , NO(3)
    COMMON /C1/ NE, NN, NB, NEQ, X(87), Y(87), NOP(4, 67), AI(268), AJ(268), AK(
*268), BI(268), BJ(268), BK(268), AREA(268), NP(174), NP1(268), NP2(268), N
*X(12), NY(12), EP(3, 3, 268), B(3, 6)
    COMMON /C2/ SK(174, 34), SKEQ(8, 8, 67)
    COMMON /C3/ DST(3, 268), SS(3, 268), DSS(3, 268), TSTP(268), DTSTP(268), T
*SS(268), DTSS(268)
    COMMON /C4/ TSSO(268), SSZ(268), DSSZ(268), EPZ(3, 268)
    COMMON /C6/ SM(2, 10, 67)
    COMMON /C7/ XU, E1, H1, H2, YS1, YS2, SP2, NEQ1, NT, KCU, G, NOR, A, B1, C
    DO 300 I=1, NT
300  TSSO(I)=YS1
      CALL SOLVE(U, F)
      BIG=0.0
      N=0
      DO 1 NQ=1, NE
        DO 5002 J=1, 2
          JJ=8+J
          SUM=0.0
          K=JJ-1
          DO 5003 I=1, 4
5003  SUM=SUM+SM(J, 2*I-1, NQ)*U(NOP(I, NQ)*2-1)+SM(J, 2*I, NQ)*U(NOP(I, NQ)*2
*)
          IF(K.EQ.9) SUM=SUM+SM(2, 9, NQ)*UM(NQ*2-1)
5002  UM(NQ*2-2+J)=-SUM/SM(J, JJ, NQ)
          DO 5005 MO=1, 4
            N=N+1
```

```

I=NOP(MO,NQ)      $      K=NQ
IF(MO.LT.4) J=NOP(MO+1,NQ)
IF(MO.EQ.4) J=NOP(1,NQ)
ST(1,N)=0.5*(BI(N)*U(2*I-1)+BJ(N)*U(2*J-1)+BK(N)*UM(2*K-1))/AREA(N
*)
ST(2,N)=0.5*(AI(N)*U(2*I)+AJ(N)*U(2*J)+AK(N)*UM(2*K))/AREA(N)
ST(3,N)=0.5*(AI(N)*U(2*I-1)+BI(N)*U(2*I)+AJ(N)*U(2*J-1)+BJ(N)*U(2*
*J)+AK(N)*UM(2*K-1)+BK(N)*UM(2*K))/AREA(N)
SS(1,N)=D(1,1)*ST(1,N)+D(1,2)*ST(2,N)+D(1,3)*ST(3,N)
SS(2,N)=D(2,1)*ST(1,N)+D(2,2)*ST(2,N)+D(2,3)*ST(3,N)
SS(3,N)=D(3,1)*ST(1,N)+D(3,2)*ST(2,N)+D(3,3)*ST(3,N)
SSZ(N)=EPZ(1,N)*ST(1,N)+EPZ(2,N)*ST(2,N)+EPZ(3,N)*ST(3,N)
TSS(N)=SQRT((SS(1,N)-SS(2,N))**2+(SS(1,N)-SSZ(N))**2+(SS(2,N)-SSZ(
*N))**2+6.0*SS(3,N)**2)/SQRT(2.0)
TST(N)=TSS(N)/E1
IF(BIG.LT.TSS(N)) BIG=TSS(N)
5005 CONTINUE
1 CONTINUE
YP=TSSO(1)/BIG
IF(Y(NY(1))+U(2*NY(1)).GT.Y(NY(2))+U(2*NY(2))) GO TO 38
YP1=(Y(NY(1))-Y(NY(2)))/(U(2*NY(2))-U(2*NY(1)))
IF(YP1.LT.YP) YP=YP1
38 IF(NP(2*NX(1)-1).EQ.0) GO TO 39
IF(X(NX(1))+U(2*NX(1)-1).GT.X(NX(2))+U(2*NX(2)-1)) GO TO 39
TT=U(2*NX(2)-1)-U(2*NX(1)-1)
YP1=(X(NX(1))-X(NX(2)))/TT
IF(YP1.LT.YP) YP=YP1
39 TT=0.0
N=0
DO 2 NQ=1,NE
DO 2 MO=1,4
N=N+1
ST(1,N)=YP*ST(1,N)
ST(2,N)=YP*ST(2,N)
ST(3,N)=YP*ST(3,N)
SS(1,N)=YP*SS(1,N)
SS(2,N)=YP*SS(2,N)
SS(3,N)=YP*SS(3,N)
SSZ(N)=SSZ(N)*YP
TST(N)=YP*TST(N)
TSS(N)=YP*TSS(N)
IF(TSS(N)/TSSO(1).GE.0.995) NP2(N)=1
IF(NP2(N).EQ.1) NP1(N)=0
2 CONTINUE
DO 6 I=1,NEQ
DU(I)=0.0
DF(I)=0.0
U(I)=YP*U(I)
6 F(I)=YP*F(I)
DO 141 I=1,NEQ1
141 VM(I)=0.0
WRITE(6,10000)
10000 FORMAT(//,2X,2HNO,23X,2HUX,23X,2HUY,23X,2HFX,23X,2HFY,/,120(1H*),/
*/)
L=0
DO 20000 N=1,NEQ,2
L=L+1

```

```
X1=U(N)
X2=U(N+1)
Y1=F(N)
Y2=F(N+1)
WRITE(6,30000)L,X1,X2,Y1,Y2
30000 FORMAT(1X,I3,10X,4(E15.5,10X))
20000 CONTINUE
DO 100 K=1,NT
DTSTP(K)=0.0
TSTP(K)=0.0
100 CONTINUE
G=E1/2.0/(1.0+XU)
A=E1/(1.0+XU)
B1=(1.0-XU)/(1.0-2.0*XU)
C=XU/(1.0-2.0*XU)
N=0
DO 14 NQ=1,NE
IF(NP2(N+1).EQ.1.OR.NP2(N+2).EQ.1.OR.NP2(N+3).EQ.1.OR.NP2(N+4).EQ.
*1) GO TO 1409
N=N+4
GO TO 14
1409 TT=0.0
DO 1009 I=1,10
DO 1009 J=I,10
1009 SK10(I,J)=0.0
DO 1004 MO=1,4
N=N+1
IF(NP2(N).EQ.0) GO TO 140
S=2.0/3.0*TSS(N)*TSS(N)*(1.0+H1/3.0/G)
SH=(SS(1,N)+SS(2,N)+SSZ(N))/3.0
S1=SS(1,N)-SH
S2=SS(2,N)-SH
S3=SS(3,N)
S4=SSZ(N)-SH
EP(1,1,N)=A*(B1-S1*S1/S)
EP(2,1,N)=A*(C-S1*S2/S)
EP(2,2,N)=A*(B1-S2*S2/S)
EP(3,1,N)=-A*S1*S3/S
EP(3,2,N)=-A*S2*S3/S
EP(3,3,N)=A*(0.5-S3*S3/S)
EP(1,2,N)=EP(2,1,N)
EP(1,3,N)=EP(3,1,N)
EP(2,3,N)=EP(3,2,N)
EPZ(1,N)=A*(C-S1*S4/S)
EPZ(2,N)=A*(C-S2*S4/S)
EPZ(3,N)=-A*S3*S4/S
DO 8 K=1,3
DO 8 M=1,3
8 W4(K,M)=EP(K,M,N)
B(1,1)=BI(N)
B(1,3)=BJ(N)
B(1,5)=BK(N)
B(2,2)=AI(N)
B(2,4)=AJ(N)
B(2,6)=AK(N)
B(3,1)=AI(N)
B(3,2)=BI(N)
```



```
B(3,3)=AJ(N)
B(3,4)=BJ(N)
B(3,5)=AK(N)
B(3,6)=BK(N)
CALL MULT1(W4,B,W5,3,3,6)
TT=4.0*AREA(N)
DO 11 K=1,6
DO 11 M=K,6
SKE(K,M)=0.0
DO 118 L=1,3
118 SKE(K,M)=SKE(K,M)+B(L,K)*W5(L,M)
SKE(K,M)=SKE(K,M)/TT
11 CONTINUE
GO TO 151
140 TT=0.0
B(1,1)=BI(N) $ B(1,3)=BJ(N) $ B(1,5)=BK(N)
B(1,1)=BI(N) $ B(1,3)=BJ(N) $ B(1,5)=BK(N)
B(2,2)=AI(N) $ B(2,4)=AJ(N) $ B(2,6)=AK(N)
B(3,1)=AI(N) $ B(3,2)=BI(N) $ B(3,3)=AJ(N)
B(3,4)=BJ(N) $ B(3,5)=AK(N) $ B(3,6)=BK(N)
CALL MULT1(D,B,W5,3,3,6)
TT=4.0*AREA(N)
DO 101 K=1,6
DO 101 M=K,6
SKE(K,M)=0.0
DO 1019 L=1,3
1019 SKE(K,M)=SKE(K,M)+B(L,K)*W5(L,M)
SKE(K,M)=SKE(K,M)/TT
101 CONTINUE
151 TT=0.0
NO(1)=MO $ NO(2)=MO+1 $ NO(3)=5
IF(MO.EQ.4) NO(2)=1
DO 3500 JJ=1,3
NROWB=(NO(JJ)-1)*2
DO 3500 J=1,2
NROWB=NROWB+1
I=(JJ-1)*2+J
DO 3300 KK=1,3
NCOLB=(NO(KK)-1)*2
DO 3200 K=1,2
L=(KK-1)*2+K
NCOL=NCOLB+K
IF(NCOL+1-NROWB) 3200,3200,3100
3100 IF(L.LT.I) SKE(I,L)=SKE(L,I)
SK10(NROWB,NCOL)=SK10(NROWB,NCOL)+SKE(I,L)
3200 CONTINUE
3300 CONTINUE
3500 CONTINUE
1004 CONTINUE
SK10(10,9)=SK10(9,10)
DO 3001 I=1,2
K=8+I
DO 3001 J=1,10
3001 SM(I,J,NQ)=SK10(J,K)
DO 2081 K=1,2
LL=10-K
KK=LL+1
```

```
DO 2081 L=1,LL
T=SK10(L, KK)/SK10(KK, KK)
DO 2001 M=L, LL
SK10(L, M)=SK10(L, M)-SM(3-K, M, NQ)*T
2001 CONTINUE
IF(L.NE.9) GO TO 2081
DO 2567 M=1, 9
2567 SM(1, M, NQ)=SM(1, M, NQ)-T*SM(2, M, NQ)
2081 CONTINUE
DO 6001 I=1, 8
DO 6001 J=I, 8
SK10(I, J)=SK10(I, J)-SKEQ(I, J, NQ)
SKEQ(I, J, NQ)=SKEQ(I, J, NQ)+SK10(I, J)
6001 CONTINUE
CALL SADD(NQ, SK10)
14 CONTINUE
RETURN
END
SUBROUTINE CHANGE(D, U, UM)
DIMENSION U(174), UM(174)
COMMON /C1/ NE, NN, NB, NEQ, X(87), Y(87), NOP(4, 67), AI(268), AJ(268), AK(
*268), BI(268), BJ(268), BK(268), AREA(268), NP(174), NP1(268), NP2(268), N
*X(12), NY(12), EP(3, 3, 268), B(3, 6)
N=0
DO 5 NQ=1, NE
XM=(X(NOP(1, NQ))+X(NOP(2, NQ))+X(NOP(3, NQ))+X(NOP(4, NQ)))/4.0
YM=(Y(NOP(1, NQ))+Y(NOP(2, NQ))+Y(NOP(3, NQ))+Y(NOP(4, NQ)))/4.0
DO 50 M=1, 4
N=N+1
IF(NP2(N).NE.1) GO TO 50
I=NOP(M, NQ)
IF(M.LT.4) J=NOP(M+1, NQ)
IF(M.EQ.4) J=NOP(1, NQ)
AI(N)=(XM+UM(2*NQ-1))- (X(J)+U(2*J-1))
AJ(N)=(X(I)+U(2*I-1))- (XM+UM(2*NQ-1))
AK(N)=(X(J)+U(2*J-1))- (X(I)+U(2*I-1))
BI(N)=(Y(J)+U(2*J))- (YM+UM(2*NQ))
BJ(N)=(YM+UM(2*NQ))- (Y(I)+U(2*I))
BK(N)=(Y(I)+U(2*I))- (Y(J)+U(2*J))
AREA(N)=0.5*(AK(N)*BJ(N)-AJ(N)*BK(N))
50 CONTINUE
5 CONTINUE
RETURN
END
SUBROUTINE BOND2(IO, U, F, DU, DF, UM, VM)
DIMENSION U(174), DU(174), UM(174), VM(174), F(174), DF(174)
COMMON /C1/ NE, NN, NB, NEQ, X(87), Y(87), NOP(4, 67), AI(268), AJ(268), AK(
*268), BI(268), BJ(268), BK(268), AREA(268), NP(174), NP1(268), NP2(268), N
*X(12), NY(12), EP(3, 3, 268), B(3, 6)
COMMON /C5/ KS, LS
IF(IO.NE.1)GO TO 1
KS=1
LS=1
1 DELTA=0.0002
DO 10 KK=1, 12
DI=Y(NY(1))+U(2*NY(1))-Y(NY(KK))-U(2*NY(KK))
IF(DI.LT.0.00000001) KS=KK
```

```

IF(DI.LT.0.00000001) DU(2*NY(KK))=-DELTA
IF(DI.LT.0.00000001) NP(2*NY(KK))=1
IF(DI.LT.0.00000001) DU(2*NY(KK)-1)=0.0
IF(DI.LT.0.00000001) NP(2*NY(KK)-1)=1
10 CONTINUE
IF(NP(2*NX(1)-1).EQ.0) GO TO 7
DO 20 KK=1,12
DI=X(NX(1))+U(2*NX(1)-1)-X(NX(KK))-U(2*NX(KK)-1)
IF(DI.LT.0.00000001) LS=KK
IF(DI.LT.0.00000001) DU(2*NX(KK)-1)=-DELTA
IF(DI.LT.0.00000001) NP(2*NX(KK)-1)=1
IF(DI.LT.0.00000001) DU(2*NX(KK))=0.0
IF(DI.LT.0.00000001) NP(2*NX(KK))=1
20 CONTINUE
7 RETURN
END
SUBROUTINE YIELD2(U,F,DU,DF,D,IO,UM,VM)
DIMENSION U(174),DU(174),UM(174),VM(174),F(174),DF(174)
DIMENSION NO(3)
DIMENSION D(3,3),SSD(1,3),TSSD(3,1),W1(1,1),W2(1,3),W3(3,1),W4(3,3
*),W5(3,6),W6(6,3),SKEO(6,6),SKE(6,6),SK10(10,10)
COMMON /C1/ NE,NN,NB,NEQ,X(87),Y(87),NOP(4,67),AI(268),AJ(268),AK(
*268),BI(268),BJ(268),BK(268),AREA(268),NP(174),NP1(268),NP2(268),N
*X(12),NY(12);EP(3,3,268),B(3,6)
COMMON /C2/ SK(174,34),SKEQ(8,8,67)
COMMON /C3/ DST(3,268),SS(3,268),DSS(3,268),TSTP(268),DTSTP(268),T
*SS(268),DTSS(268)
COMMON /C4/ TSSO(268),SSZ(268),DSSZ(268),EPZ(3,268)
COMMON /C5/ KS,LS
COMMON /C6/ SM(2,10,67)
COMMON /C7/ XU,E1,H1,H2,YS1,YS2,SP2,NEQ1,NT,KKU,G,NOR,A,B1,C
YP=1000.0
CALL SOLVE(DU,DF)
N=0
DO 1 NQ=1,NE
DO 5002 J=1,2
JJ=8+J
SUM=0.0
K=JJ-1
DO 5003 I=1,4
SUM=SUM+SM(J,2*I-1,NQ)*DU(NOP(I,NQ)*2-1)+SM(J,2*I,NQ)*DU(NOP(I,NQ)
**2)
5003 CONTINUE
IF(K.EQ.9) SUM=SUM+SM(2,9,NQ)*VM(NQ*2-1)
5002 VM(NQ*2-2+J)=-SUM/SM(J,JJ,NQ)
DO 1001 M=1,4
N=N+1
I=NOP(M,NQ)
IF(M.LT.4) J=NOP(M+1,NQ)
IF(M.EQ.4) J=NOP(1,NQ)
K=NQ
DST(1,N)=0.5*(BI(N)*DU(2*I-1)+BJ(N)*DU(2*J-1)+BK(N)*VM(2*K-1))/ARE
*A(N)
DST(2,N)=0.5*(AI(N)*DU(2*I)+AJ(N)*DU(2*J)+AK(N)*VM(2*K))/AREA(N)
DST(3,N)=0.5*(AI(N)*DU(2*I-1)+BI(N)*DU(2*I)+AJ(N)*DU(2*J-1)+BJ(N)*
*DU(2*J)+AK(N)*VM(2*K-1)+BK(N)*VM(2*K))/AREA(N)
DSS(1,N)=EP(1,1,N)*DST(1,N)+EP(1,2,N)*DST(2,N)+EP(1,3,N)*DST(3,N)

```

```

DSS(2,N)=EP(2,1,N)*DST(1,N)+EP(2,2,N)*DST(2,N)+EP(2,3,N)*DST(3,N)
DSS(3,N)=EP(3,1,N)*DST(1,N)+EP(3,2,N)*DST(2,N)+EP(3,3,N)*DST(3,N)
DSSZ(N)=EPZ(1,N)*DST(1,N)+EPZ(2,N)*DST(2,N)+EPZ(3,N)*DST(3,N)
IF(NP2(N).EQ.1.AND.TSTP(N).GE.SP2) GO TO 1001
TT=SQRT((SS(1,N)+DSS(1,N)-SS(2,N)-DSS(2,N))**2+(SS(1,N)+DSS(1,N)-S
*SZ(N)-DSSZ(N))**2+(SS(2,N)+DSS(2,N)-SSZ(N)-DSSZ(N))**2+6.0*(SS(3,N
*)+DSS(3,N))**2)/SQRT(2.0)-TSS(N)
IF(TT.LT.0.0) GO TO 1001
A1=(DSS(1,N)-DSS(2,N))**2+(DSS(1,N)-DSSZ(N))**2+(DSS(2,N)-DSSZ(N)
)**2+6.0*DSS(3,N)**2
B2=DSS(3,N)*SS(3,N)*6.0+(DSS(1,N)-DSS(2,N))*(SS(1,N)-SS(2,N))+DSS
*(1,N)-DSSZ(N))*(SS(1,N)-SSZ(N))+DSS(2,N)-DSSZ(N))*(SS(2,N)-SSZ(N)
*)
C1=2.0*(TSS(N)**2-TSSO(N)**2)
BIG=(-B2+SQRT(B2**2-A1*C1))/A1
IF(BIG.LT.YP) YP=BIG
IF(YP.LT.0.0) WRITE(6,103) KKU,NQ
1001 CONTINUE
1 CONTINUE
103 FORMAT(//,20X,A12,4X,I4,2(2X,E10.3),/,50(1H*))
IF(YP.LT.0.0) STOP
IF(YP.GT.1.0) YP=1.0
DO 180 KK=2,12
IF(NP(2*NY(KK)).EQ.1) GO TO 180
IF((Y(NY(1))+U(2*NY(1))+DU(2*NY(1))).GT.(Y(NY(KK))+U(2*NY(KK))+DU(
*2*NY(KK)))) GO TO 180
YP1=(Y(NY(1))+U(2*NY(1))-Y(NY(KK))-U(2*NY(KK)))/(DU(2*NY(KK))-DU(2
**NY(1)))
IF(YP1.GT.0.0.AND.YP1.LT.YP) YP=YP1
180 CONTINUE
IF(NP(2*NX(1)-1).EQ.0) GO TO 39
DO 190 KK=2,12
IF(NP(2*NX(KK)-1).EQ.1) GO TO 190
TT=X(NX(1))+U(2*NX(1)-1)+DU(2*NX(1)-1)
IF(TT.GT.(X(NX(KK))+U(2*NX(KK)-1)+DU(2*NX(KK)-1)))GO TO 190
TT=DU(2*NX(KK)-1)-DU(2*NX(1)-1)
YP1=(X(NX(1))-X(NX(KK))-U(2*NX(KK)-1))/TT
IF(YP1.GT.0.0.AND.YP1.LT.YP) YP=YP1
190 CONTINUE
39 TT=0.0
N=0
DO 2 NQ=1,NE
DO 5004 M=1,4
N=N+1
DST(1,N)=DST(1,N)*YP
DST(2,N)=DST(2,N)*YP
DST(3,N)=DST(3,N)*YP
DSS(1,N)=DSS(1,N)*YP
DSS(2,N)=DSS(2,N)*YP
DSS(3,N)=DSS(3,N)*YP
DSSZ(N)=DSSZ(N)*YP
5004 CONTINUE
2 CONTINUE
N=0
DO 3 NQ=1,NE
DO 3 M=1,4
N=N+1

```

```
4   DTSS(N)=SQRT((SS(1,N)+DSS(1,N)-SS(2,N)-DSS(2,N))**2+(SS(1,N)+DSS(1
*,N)-SSZ(N)-DSSZ(N))**2+(SS(2,N)+DSS(2,N)-SSZ(N)-DSSZ(N))**2+6.0*(S
*S(3,N)+DSS(3,N))**2)/SQRT(2.0)-TSS(N)
   IF(NP2(N).EQ.0) GO TO 5
   IF(DTSS(N).GE.0.0) GO TO 6
   TSSO(N)=TSS(N)
   NP2(N)=0
   NP1(N)=1
   DO 15 K=1, 3
15  DSS(K,N)=D(K,1)*DST(1,N)+D(K,2)*DST(2,N)+D(K,3)*DST(3,N)
   DSSZ(N)=D(1,2)*DST(1,N)+D(1,2)*DST(2,N)
   GO TO 4
6   IF(TSTP(N).LT.SP2) DTSTP(N)=DTSS(N)/H1
   IF(TSTP(N).GE.SP2) DTSTP(N)=DTSS(N)/H2
   GO TO 3
5   DTSTP(N)=0.0
3   CONTINUE
   DO 9001 I=1, NEQ1
9001 UM(I)=UM(I)+YP*VM(I)
   DO 90 N=1, NEQ
   U(N)=U(N)+YP*DU(N)
   IF(NP(N).EQ.1) F(N)=F(N)+YP*DF(N)
90  DF(N)=0.0
   N=0
   DO 11 NQ=1, NE
   DO 11 M=1, 4
   N=N+1
   TSS(N)=TSS(N)+DTSS(N)
   TSTP(N)=TSTP(N)+DTSTP(N)
   SSSZ(N)=SSZ(N)+DSSZ(N)
   DO 110 K=1, 3
   SS(K,N)=SS(K,N)+DSS(K,N)
110 CONTINUE
11  CONTINUE
   N=0
   DO 12 NQ=1, NE
   IF(NP2(N+1).EQ.1.OR.NP2(N+2).EQ.1.OR.NP2(N+3).EQ.1.OR.NP2(N+4).EQ.
*1) GO TO 999
   IF(DTSS(N+1).LT.0.0.OR.DTSS(N+2).LT.0.0.OR.DTSS(N+3).LT.0.0.OR.DTS
*S(N+4).LT.0.0) GO TO 999
   KN=0
   IF(TSS(N+1)/TSSO(N+1).GE.0.995) KN=1
   IF(TSS(N+2)/TSSO(N+2).GE.0.995) KN=1
   IF(TSS(N+3)/TSSO(N+3).GE.0.995) KN=1
   IF(TSS(N+4)/TSSO(N+4).GE.0.995) KN=1
   IF(KN.EQ.1) GO TO 999
   N=N+4
   GO TO 12
999 TT=0.0
   DO 456 I=1, 10
   DO 456 J=I, 10
456 SK10(I,J)=0.0
   DO 5005 MO=1, 4
   N=N+1
   IF(NP2(N).EQ.1) GO TO 14
   IF(DTSS(N).LT.0.0) GO TO 2345
   IF(TSS(N)/TSSO(N).GE.0.995) NP2(N)=1
```

```
IF(NP2(N).EQ.1) NP1(N)=0
IF(NP2(N).EQ.1) GO TO 14
IF(DTSS(N).GE.0.0) GO TO 120
2345 TT=0.0
EPZ(1,N)=D(1,2)
EPZ(2,N)=D(1,2)
EPZ(3,N)=0.0
DO 13 K=1,3
DO 13 M=1,3
EP(K,M,N)=D(K,M)
13 W4(K,M)=D(K,M)
GO TO 19
14 IF(TSTP(N).LT.SP2) TSSO(N)=YS2
IF(TSTP(N).LT.SP2) S=2.0/3.0*TSS(N)*TSS(N)*(1.0+H1/3.0/G)
IF(TSTP(N).GE.SP2) S=2.0/3.0*TSS(N)*TSS(N)*(1.0+H2/3.0/G)
SH=(SS(1,N)+SS(2,N)+SSZ(N))/3.0
S1=SS(1,N)-SH
S2=SS(2,N)-SH
S3=SS(3,N)
S4=SSZ(N)-SH
EP(1,1,N)=A*(B1-S1*S1/S)
EP(2,1,N)=A*(C-S1*S2/S)
EP(2,2,N)=A*(B1-S2*S2/S)
EP(3,1,N)=-A*S1*S3/S
EP(3,2,N)=-A*S2*S3/S
EP(3,3,N)=A*(0.5-S3*S3/S)
EP(1,2,N)=EP(2,1,N)
EP(1,3,N)=EP(3,1,N)
EP(2,3,N)=EP(3,2,N)
EPZ(1,N)=A*(C-S1*S4/S)
EPZ(2,N)=A*(C-S2*S4/S)
EPZ(3,N)=-A*S3*S4/S
DO 16 K=1,3
DO 16 M=1,3
16 W4(K,M)=EP(K,M,N)
19 B(1,1)=BI(N)
B(1,3)=BJ(N)
B(1,5)=BK(N)
B(2,2)=AI(N)
B(2,4)=AJ(N)
B(2,6)=AK(N)
B(3,1)=AI(N)
B(3,2)=BI(N)
B(3,3)=AJ(N)
B(3,4)=BJ(N)
B(3,5)=AK(N)
B(3,6)=BK(N)
CALL MULT1(W4,B,W5,3,3,6)
TT=4.0*AREA(N)
DO 18 K=1,6
DO 18 M=K,6
SKE(K,M)=0.0
DO 1888 L=1,3
1888 SKE(K,M)=SKE(K,M)+B(L,K)*W5(L,M)
SKE(K,M)=SKE(K,M)/TT
18 CONTINUE
GO TO 151
```

```
120  TT=0.0
      B(1,1)=BI(N) $ B(1,3)=BJ(N) $ B(1,5)=BK(N)
      B(2,2)=AI(N) $ B(2,4)=AJ(N) $ B(2,6)=AK(N)
      B(3,1)=AI(N) $ B(3,2)=BI(N) $ B(3,3)=AJ(N)
      B(3,4)=BJ(N) $ B(3,5)=AK(N) $ B(3,6)=BK(N)
      CALL MULT1(D,B,W5,3,3,6)
      TT=4.0*AREA(N)
      DO 101 K=1,6
      DO 101 M=K,6
      SKE(K,M)=0.0
      DO 1012 L=1,3
1012  SKE(K,M)=SKE(K,M)+B(L,K)*W5(L,M)
      SKE(K,M)=SKE(K,M)/TT
101  CONTINUE
151  TT=0.0
      NO(1)=MO $ NO(2)=MO+1 $ NO(3)=5
      IF(MO.EQ.4) NO(2)=1
      DO 3500 JJ=1,3
      NROWB=(NO(JJ)-1)*2
      DO 3500 J=1,2
      NROWB=NROWB+1
      L=(JJ-1)*2+J
      DO 3300 KK=1,3
      NCOLB=(NO(KK)-1)*2
      DO 3200 K=1,2
      I=(KK-1)*2+K
      NCOL=NCOLB+K
      IF(NCOL+1-NROWB) 3200,3200,3100
3100  IF(L.LT.I) SKE(I,L)=SKE(L,I)
      SK10(NROWB,NCOL)=SK10(NROWB,NCOL)+SKE(I,L)
3200  CONTINUE
3300  CONTINUE
3500  CONTINUE
5005  CONTINUE
      SK10(10,9)=SK10(9,10)
      DO 3001 I=1,2
      K=8+I
      DO 3001 J=1,10
3001  SM(I,J,NQ)=SK10(J,K)
      DO 2001 K=1,2
      LL=10-K
      KK=LL+1
      DO 2001 L=1,LL
      T=SK10(L,KK)/SK10(KK,KK)
      DO 1501 M=L,LL
1501  SK10(L,M)=SK10(L,M)-SM(3-K,M,NQ)*T
      IF(L.NE.9) GO TO 2001
      DO 2567 M=1,9
2567  SM(1,M,NQ)=SM(1,M,NQ)-T*SM(2,M,NQ)
2001  CONTINUE
      DO 6001 I=1,8
      DO 6001 J=I,8
      SK10(I,J)=SK10(I,J)-SKEQ(I,J,NQ)
      SKEQ(I,J,NQ)=SKEQ(I,J,NQ)+SK10(I,J)
6001  CONTINUE
      CALL SADD(NQ,SK10)
12   CONTINUE
```

```
IF(MOD(I0,10).NE.0) GO TO 80
SUM1=ABS(U(2*NY(1)))
SUM6=ABS(U(2*NX(1)-1))
SUM2=0.0
SUM20=0.0
SUM3=0.0
SUM30=0.0
DO 220 KK=1,12
SUM2=SUM2+F(2*NY(KK))
IF(KK.EQ.1) GO TO 212
SUM20=SUM20+F(2*NY(KK)-1)
SUM30=SUM30+F(2*NX(KK))
212 TT=0.0
220 SUM3=SUM3+F(2*NX(KK)-1)
SUM2=ABS(SUM2)
SUM3=ABS(SUM3)
SUM20=ABS(SUM20)
SUM30=ABS(SUM30)
SUM4=X(NY(KS))+U(2*NY(KS)-1)
SUM5=Y(NX(LS))+U(2*NX(LS))
WRITE(1,230) SUM1,SUM2,SUM3,SUM4,SUM5,SUM6,SUM20,SUM30
230 FORMAT(8(E12.5))
80 TT=0.0
IF(MOD(I0,20).NE.0) GO TO 330
WRITE(6,26)I0
26 FORMAT(/,1X,13HLOADING STEP=,I4)
WRITE(6,4000)
4000 FORMAT(/,50X,13HPLASTIC ZONES,/,120(1H*))
WRITE(6,4081)((N,NP2(N)),N=1,NT)
4081 FORMAT(7(I4,4X,I2,8X))
WRITE(6,1990)
1990 FORMAT(/)
WRITE(6,10000)
10000 FORMAT(2X,2HNO,16X,2HUX,16X,2HUY,16X,2HFX,16X,2HFY,13X,5HDTSTP,14X
*,4HTSTP,15X,3HTSS,/,130(1H*))
N=0
DO 420 NQ=1,NE
SUM1=0.0
SUM2=0.0
SUM3=0.0
DO 42 MO=1,4
N=N+1
SUM1=SUM1+TSS(N)
SUM2=SUM2+TSTP(N)
SUM3=SUM3+DTSTP(N)
42 CONTINUE
SUM1=SUM1/4.0 $ SUM2=SUM2/4.0 $ SUM3=SUM3/4.0
X1=U(2*NQ-1) $ X2=U(2*NQ) $ Y1=F(2*NQ-1) $ Y2=F(2*NQ)
WRITE(6,32)(NQ,X1,X2,Y1,Y2,SUM3,SUM2,SUM1)
420 CONTINUE
32 FORMAT(I4,7(6X,E12.5))
K1=NE+1 $ K2=NN
DO 430 I=K1,K2
X1=U(2*I-1)
X2=U(2*I)
Y1=F(2*I-1)
Y2=F(2*I)
```



```
WRITE(6, 32)(I, X1, X2, Y1, Y2)
430 CONTINUE
330 IF(ABS(U(2*NY(1))).LT.0.08) GO TO 33
WRITE(6, 45)
45 FORMAT(///, 2X, 2HNO, 24X, IHX, 24X, IHY, /, 60(1H*), ///)
N=0
DO 44 NQ=1, NE
I=NQ
XX=X(I)+U(2*I-1)
YY=Y(I)+U(2*I)
SUM1=0.0 $ SUM2=0.0 $ SUM3=0.0
DO 62 MO=1, 4
N=N+1
SUM1=SUM1+TSS(N)
SUM2=SUM2+TSTP(N)
S1=SS(1, N)$S2=SS(2, N)$S3=SS(3, N)
TA=SQRT((S1-S2)**2/4.0+S3**2)
SUM3=SUM3+TA
62 CONTINUE
SUM1=SUM1/4.0 $ SUM2=SUM2/4.0 $ SUM3=SUM3/4.0
V1=U(2*I-1)$V2=U(2*I)$V3=DU(2*I-1)$V4=DU(2*I)
V5=UM(2*I-1) $ V6=UM(2*I)
WRITE(6, 46)(I, XX, YY)
46 FORMAT(1X, I3, 10X, E15.5, 10X, E15.5)
WRITE(2, 102) I, X(I), Y(I), V1, V2, V3, V4, V5, V6, SUM1, SUM2, SUM3
102 FORMAT(I10, 11(E10.3))
44 CONTINUE
K1=NE+1 $ K2=NN
DO 63 I=K1, K2
XX=X(I)+U(2*I-1)
YY=Y(I)+U(2*I)
V1=U(2*I-1)$V2=U(2*I)$V3=DU(2*I-1)$V4=DU(2*I)
WRITE(6, 46)(I, XX, YY)
WRITE(2, 102) I, X(I), Y(I), V1, V2, V3, V4
63 CONTINUE
STOP
33 RETURN
END
SUBROUTINE SADD(N, SKE)
DIMENSION SKE(10, 10)
COMMON /C1/ NE, NN, NB, NEQ, X(87), Y(87), NOP(4, 67), AI(268), AJ(268), AK(
*268), BI(268), BJ(268), BK(268), AREA(268), NP(174), NP1(268), NP2(268), N
*X(12), NY(12), EP(3, 3, 268), B(3, 6)
COMMON /C2/ SK(174, 34), SKEQ(8, 8, 67)
DO 1 JJ=1, 4
NROW=(NOP(JJ, N)-1)*2
DO 1 J=1, 2
NROW=NROW+1
I=(JJ-1)*2+J
DO 2 KK=1, 4
NCOLB=(NOP(KK, N)-1)*2
DO 3 K=1, 2
L=(KK-1)*2+K
NCOL=NCOLB+K+1-NROW
IF(NCOL)3, 3, 4
4 IF(L.LT.I) SKE(I, L)=SKE(L, I)
SK(NROW, NCOL)=SK(NROW, NCOL)+SKE(I, L)
```

```
3 CONTINUE
2 CONTINUE
1 CONTINUE
  RETURN
  END
  SUBROUTINE SOLVE(U,F)
  DIMENSION SKI(174,34),FI(174),F(174),U(174)
  COMMON /C1/ NE,NN,NB,NEQ,X(87),Y(87),NOP(4,67),AI(268),AJ(268),AK(
*268),BI(268),BJ(268),BK(268),AREA(268),NP(174),NP1(268),NP2(268),N
*X(12),NY(12),EP(3,3,268),B(3,6)
  COMMON /C2/ SK(174,34),SKEQ(8,8,67)
  COMMON /C3/ DST(3,268),SS(3,268),DSS(3,268),TSTP(268),DTSTP(268),T
*SS(268),DTSS(268)
  DO 1 I=1,NEQ
  IF(NP(I).EQ.0) FI(I)=F(I)
  IF(NP(I).EQ.1) FI(I)=SK(I,1)*U(I)*10.0E20
  IF(NP(I).EQ.1.AND.U(I).EQ.0.0) FI(I)=SK(I,1)*10.0E10
  DO 2 J=1,NB
2 SKI(I,J)=SK(I,J)
  IF(NP(I).EQ.1) SKI(I,1)=SKI(I,1)*10.0E20
1 CONTINUE
  DO 300 N=1,NEQ
  I=N
  DO 290 L=2,NB
  I=I+1
  IF(SKI(N,L)) 240,290,240
240 C=SKI(N,L)/SKI(N,1)
  J=0
  DO 270 K=L,NB
  J=J+1
  IF(SKI(N,K)) 260,270,260
260 SKI(I,J)=SKI(I,J)-C*SKI(N,K)
270 CONTINUE
280 SKI(N,L)=C
  FI(I)=FI(I)-C*FI(N)
290 CONTINUE
300 FI(N)=FI(N)/SKI(N,1)
  N=NEQ
350 N=N-1
  IF(N) 500,500,360
360 L=N
  DO 400 K=2,NB
  L=L+1
  IF(SKI(N,K)) 370,400,370
370 FI(N)=FI(N)-SKI(N,K)*FI(L)
400 CONTINUE
  GO TO 350
500 TT=0.0
  DO 3 N=1,NEQ
  IF(NP(N).EQ.1) GO TO 3
  U(N)=FI(N)
3 CONTINUE
  DO 4 N=1,NEQ
  IF(NP(N).EQ.0) GO TO 4
  SUM=0.0
  K=N+1
  L=0
```

```
DO 5 J=1,NB
K=K-1
L=L+1
IF(K.EQ.0) GO TO 6
5 SUM=SUM+SK(K,L)*U(K)
6 TT=0.0
DO 7 J=2,NB
IF(SK(N,J).EQ.0.0) GO TO 7
SUM=SUM+SK(N,J)*U(N-1+J)
7 CONTINUE
F(N)=SUM
4 CONTINUE
RETURN
END
SUBROUTINE MULT1(A,B,C,M,N,L)
DIMENSION A(M,N),B(N,L),C(M,L)
DO 1 I=1,M
DO 1 J=1,L
C(I,J)=0.0
DO 1 K=1,N
1 C(I,J)=C(I,J)+A(I,K)*B(K,J)
RETURN
END
```

APPENDIX 'C'

LISTING OF THE COMPUTER  
PROGRAM EPFEA 3  
USING ISOPARAMETRIC ELEMENTS

NOMENCLATURE

Variable	Place in labelled common	Definition
NE	C1	Number of elements
NN	"	Number of nodes
NB	"	Band width of the overall stiffness matrix
NEQ	"	Number of equations
X,Y	"	Coordinates of nodal points
NOP	"	Nodal connection of elements
NP	"	Pointer vector for imposing boundary conditions
NP1, NP2	"	Pointer vectors for indicating state of elements
NX, NY	"	Periphery nodal-points matrices, due to the side and upper segments
EP	"	Stress-strain matrix of elements
SI, TI	"	Natural coordinates of the Gaussian points
SII, TII	"	Natural coordinates of element nodal points
WG	"	Weight coefficient of the Gaussian quadrature formula
SK	C2	Overall stiffness matrix
SKEQ	"	Stiffness matrices of quadrilateral elements
DST	C3	Strain-increment of elements
SS	"	Stress of elements
DSS	"	Stress-increment of elements
TSTP	"	Effective plastic strain of elements
DTSTP	"	Effective plastic strain-increment of elements
TSS	"	Effective stress of elements
DTSS	"	Effective stress-increment of element
TSS0	C4	Yield strength of elements
SSZ	"	Stress of elements in the z-direction
DSSZ	"	Stress-increment of elements in the z-direction

EPZ	"	Stress-strain matrix in the z-direction
XF,YF	C5	Current coordinates of nodal points

Local Variable	Place in Subroutine	Definition
D	GDATA	Elastic material matrix
SK8	"	Element stiffness matrix
SHP	YIELD 1	Matrix of shape functions and their derivatives
XS	SHAPE	Jacobain matrix
S	STIFF	Element stiffness matrix

Variables of main program	Definition
U	Displacement of nodal points
F	Force of nodal points
DU	Displacement-increment of nodal points
DF	Force-increment of nodal points

PROGRAM 'EPFEA3'  
\*\*\*\*\*

```
C*****
C***** MAIN PROGRAM *****
C***** ELASTIC-PLASTIC FINITE ELEMENT ANALYSIS *****
C***** WRITTEN BY ALI NAJAFI-SANI IN THE FIRST SEMESTER OF 1978 *****
C***** DEVELOPED FOR ISOPARAMETRIC QUADRILATERAL ELEMENTS *****
C*****
PROGRAM EPFEA3(INPUT,OUTPUT,TAPE5=INPUT,TAPE6=OUTPUT,TAPE1=113B,
*TAPE2=113B)
DIMENSION U(174),DU(174),F(174),DF(174),D(3,3)
COMMON /C1/ NE,NN,NB,NEQ,X(87),Y(87),NOP(4,67),NP(174),NP1(268),NP
*2(268),NX(12),NY(12),EP(3,3,268),SI(4),TI(4),SII(4),TII(4),WG(4)
COMMON /C2/ SK(174,34),SKEQ(8,8,67)
COMMON /C3/ DST(3,268),SS(3,268),DSS(3,268),TSTP(268),DTSTP(268),T
*SS(268),DTSS(268)
COMMON /C4/ TSSO(268),SSZ(268),DSSZ(268),EPZ(3,268)
COMMON/C5/KS,LS,XF(87),YF(87)
C*****
C***** INPUT OF DATA AND *****
C***** GENERATION AND ASSEMBLY OF STIFFNESS MATRICES *****
CALL GDATA(D)
C*****
C***** INPUT OF INITIAL BOUNDARY CONDITIONS *****
CALL BOND1(U,F)
C*****
C***** INITIATION OF PLASTIC DEFORMATION *****
CALL YIELD1(U,F,DU,DF,D)
NOR=1500
C*****
C***** INITIATION OF LOAD INCREMENTS *****
DO 1 I=1,NOR
C*****
C***** UPDATE OF GEOMETRICAL MATRICES *****
CALL CHANGE(D,U)
C*****
C***** INPUT OF INSTANTANEOUS BOUNDARY CONDITIONS *****
CALL BOND2(I,U,F,DU,DF)
C*****
C***** INITIATION OF INCREMENTAL PLASTIC DEFORMATION *****
CALL YIELD2(U,F,DU,DF,D,I)
1 CONTINUE
REWIND 3
REWIND 4
STOP
END
SUBROUTINE GDATA(D)
DIMENSION D(3,3),SK8(8,8)
COMMON /C1/ NE,NN,NB,NEQ,X(87),Y(87),NOP(4,67),NP(174),NP1(268),NP
```

```
*2(268),NX(12),NY(12),EP(3,3,268),SI(4),TI(4),SII(4),TII(4),WG(4)
COMMON /C2/ SK(174,34),SKEQ(8,8,67)
COMMON /C3/ DST(3,268),SS(3,268),DSS(3,268),TSTP(268),DTSTP(268),T
*SS(268),DTSS(268)
COMMON /C4/ TSSO(268),SSZ(268),DSSZ(268),EPZ(3,268)
COMMON/C5/KS,LS,XF(87),YF(87)
DATA NP/174*0/,NP1/268*1/,NP2/268*0/,NE/67/,NN/87/,NB/34/,NEQ/17
$4/
DATA NY/80,81,82,83,84,85,86,87,78,79,64,65/
DATA NX/9,18,20,32,31,43,42,51,50,58,65,64/
DATA SI/-0.5,0.5,0.5,-0.5/,TI/-0.5,-0.5,0.5,0.5/
DATA SII/-1.0,1.0,1.0,-1.0/,TII/-1.0,-1.0,1.0,1.0/
DATA WG/4*1.0/
WRITE(6,1)
1 FORMAT(////////,1X,28HINDENTATION OF ROUND BILLETS,/,30(1H*))
READ(5,3)((NOP(1,I),NOP(2,I),NOP(3,I),NOP(4,I)),I=1,NE)
3 FORMAT(4I5)
READ(5,2)((M,X(M),Y(M)),I=1,NN)
2 FORMAT(2(I2,3X,2F10.5))
R=14.0
DO 22 N=1,NN
IF(Y(N).EQ.1.0) Y(N)=SQRT(R**2-X(N)**2)
IF(X(N).EQ.1.0) X(N)=SQRT(R**2-Y(N)**2)
22 CONTINUE
SC=R
DO 12 K=1,NN
Y(K)=Y(K)/SC $ X(K)=X(K)/SC
XF(K)=X(K) $ YF(K)=Y(K)
12 CONTINUE
DO 13 I=1,4
SII(I)=SII(I)/SQRT(3.0)
13 TII(I)=TII(I)/SQRT(3.0)
XU=0.345 $ E1=0.7E06 $ H1=0.86E03 $ H=H1
WRITE(6,7)
7 FORMAT(///,2X,2HNO,24X,1HX,24X,1HY,/,60(1H*),//)
WRITE(6,8)((I,X(I),Y(I)),I=1,NN)
8 FORMAT(1X,I3,10X,E15.5,10X,E15.5)
WRITE(6,9)
9 FORMAT(//,2X,2HNO,9X,1HI,9X,1HJ,9X,1HK,,9X,1HP,/,60(1H*),//)
WRITE(6,10)(I,NOP(1,I),NOP(2,I),NOP(3,I),NOP(4,I),I=1,NE)
10 FORMAT(1X,I3,7X,I3,7X,I3,7X,I3,7X,I3)
FACT=E1*(1.0-XU)/(1.0+XU)/(1.0-2.0*XU)
D(1,1)=FACT
D(2,2)=FACT
D(1,2)=FACT*XU/(1.0-XU)
D(2,1)=D(1,2)
D(1,3)=0.0
D(3,1)=0.0
D(2,3)=0.0
D(3,2)=0.0
D(3,3)=E1/2.0/(1.0+XU)
N=0
DO 11 NQ=1,NE
DO 11 MO=1,4
N=N+1
EPZ(1,N)=D(1,2)
EPZ(2,N)=D(1,2)
```



```

      EPZ(3,N)=0.0
      DO 11 K=1,3
      DO 11 M=1,3
11     EP(K,M,N)=D(K,M)
      DO 15 I=1,NEQ
      DO 15 J=1,NB
15     SK(I,J)=0.0
      DO 5 NQ=1,NE
C*****
C***** EVALUATION OF THE ELEMENTAL STIFFNESS MATRIX *****
      CALL STIFF(NQ,SK8)
      CALL SADD(NQ,SK8)
      DO 14 I=1,8
      DO 14 J=I,8
14     SKEQ(I,J,NQ)=SK8(I,J)
5     CONTINUE
      RETURN
      END
      SUBROUTINE BOND1(U,F)
      COMMON /C1/ NE,NN,NB,NEQ,X(87),Y(87),NOP(4,67),NP(174),NP1(268),NP
*2(268),NX(12),NY(12),EP(3,3,268),SI(4),TI(4),SII(4),TII(4),WG(4)
      DIMENSION U(174),F(174)
      ND=5
      NP(2)=1$NP(4)=1$NP(6)=1$NP(8)=1$NP(10)=1$NP(12)=1$NP(14)=1
      NP(16)=1$NP(18)=1$NP(1)=1$NP(19)=1$NP(41)=1$NP(65)=1$NP(87)=1
      NP(103)=1$NP(117)=1$NP(131)=1$NP(141)=1$NP(159)=1$NP(160)=1
      NP(17)=1
      DO 1 I=1,NEQ
      U(I)=0.0
1     F(I)=0.0
      KK=2*NY(1)
      U(KK)=- (Y(NY(1))-Y(NY(2)))/FLOAT(ND)
      RETURN
      END
      SUBROUTINE YIELD1(U,F,DU,DF,D)
      DIMENSION U(174),DU(174),F(174),DF(174),SHP(3,4)
      DIMENSION D(3,3),SSD(1,3),TSSD(3,1),W1(1,1),W2(1,3),W3(3,1),W4(3,3
*) ,W5(3,6),W6(6,3),SKEO(6,6),SKE(6,6),SK8(8,8),ST(3,268),TST(268)
      COMMON /C1/ NE,NN,NB,NEQ,X(87),Y(87),NOP(4,67),NP(174),NP1(268),NP
*2(268),NX(12),NY(12),EP(3,3,268),SI(4),TI(4),SII(4),TII(4),WG(4)
      COMMON /C2/ SK(174,34),SKEQ(8,8,67)
      COMMON /C3/ DST(3,268),SS(3,268),DSS(3,268),TSTP(268),DTSTP(268),T
*SS(268),DTSS(268)
      COMMON /C4/ TSSO(268),SSZ(268),DSSZ(268),EPZ(3,268)
      XU=0.345 $ E1=0.7E06 $ H =0.86E03
      NT=4*NE
      YSR=500.0
      DO 300 I=1,NT
300     TSSO(I)=YSR
      CALL SOLVE(U,F)
      BIG=0.0
      N=0
      DO 1 NQ=1,NE
      DO 5005 L=1,4
      N=N+I
      DO 5003 I=1,3
5003     ST(I,N)=0.0
```

```
SB=SII(L) $ TB=TII(L)
CALL SHAPE(SB, TB, XSJ, SHP, NQ)
DO 5002 J=1, 4
ST(1, N)=ST(1, N)+SHP(1, J)*U(NOP(J, NQ)*2-1)
ST(2, N)=ST(2, N)+SHP(2, J)*U(NOP(J, NQ)*2)
5002 ST(3, N)=ST(3, N)+SHP(1, J)*U(NOP(J, NQ)*2)+SHP(2, J)*U(NOP(J, NQ)*2-1)
SS(1, N)=D(1, 1)*ST(1, N)+D(1, 2)*ST(2, N)+D(1, 3)*ST(3, N)
SS(2, N)=D(2, 1)*ST(1, N)+D(2, 2)*ST(2, N)+D(2, 3)*ST(3, N)
SS(3, N)=D(3, 1)*ST(1, N)+D(3, 2)*ST(2, N)+D(3, 3)*ST(3, N)
SSZ(N)=EPZ(1, N)*ST(1, N)+EPZ(2, N)*ST(2, N)+EPZ(3, N)*ST(3, N)
TSS(N)=SQRT((SS(1, N)-SS(2, N))**2+(SS(1, N)-SSZ(N))**2+(SS(2, N)-SSZ(
*N))**2+6.0*SS(3, N)**2)/SQRT(2.0)
TST(N)=TSS(N)/E1
IF(BIG.LT.TSS(N)) BIG=TSS(N)
5005 CONTINUE
1 CONTINUE
YP=TSSO(1)/BIG
N=0
DO 2 NQ=1, NE
DO 2 MO=1, 4
N=N+1
ST(1, N)=YP*ST(1, N)
ST(2, N)=YP*ST(2, N)
ST(3, N)=YP*ST(3, N)
SS(1, N)=YP*SS(1, N)
SS(2, N)=YP*SS(2, N)
SS(3, N)=YP*SS(3, N)
SSZ(N)=SSZ(N)*YP
TST(N)=YP*TST(N)
TSS(N)=YP*TSS(N)
IF(TSS(N)/TSSO(1).GE.0.995) NP2(N)=1
IF(NP2(N).EQ.1) NP1(N)=0
2 CONTINUE
DO 6 I=1, NEQ
DU(I)=0.0
DF(I)=0.0
U(I)=YP*U(I)
6 F(I)=YP*F(I)
WRITE(6, 10000)
10000 FORMAT(//, 2X, 2HNO, 23X, 2HUX, 23X, 2HUY, 23X, 2HFX, 23X, 2H FY, /, 120(1H*), /
*/)
L=0
DO 20000 N=1, NEQ, 2
L=L+1
X1=U(N)
X2=U(N+1)
Y1=F(N)
Y2=F(N+1)
WRITE(6, 30000)L, X1, X2, Y1, Y2
30000 FORMAT(1X, I3, 10X, 4(E15.5, 10X))
20000 CONTINUE
DO 100 K=1, NT
DTSTP(K)=0.0
TSTP(K)=0.0
100 CONTINUE
G=E1/2.0/(1.0+XU)
A=E1/(1.0+XU)
```

```
B1=(1.0-XU)/(1.0-2.0*XU)
C=XU/(1.0-2.0*XU)
N=0
DO 14 NQ=1,NE
  IF(NP2(N+1).EQ.1.OR.NP2(N+2).EQ.1.OR.NP2(N+3).EQ.1.OR.NP2(N+4).EQ.
*1) GO TO 1409
  N=N+4
  GO TO 14
1409 TT=0.0
  DO 1004 MO=1,4
  N=N+1
  IF(NP2(N).EQ.0) GO TO 1004
  S=2.0/3.0*TSS(N)*TSS(N)*(1.0+H/3.0/G)
  SH=(SS(1,N)+SS(2,N)+SSZ(N))/3.0
  S1=SS(1,N)-SH
  S2=SS(2,N)-SH
  S3=SS(3,N)
  S4=SSZ(N)-SH
  EP(1,1,N)=A*(B1-S1*S1/S)
  EP(2,1,N)=A*(C-S1*S2/S)
  EP(2,2,N)=A*(B1-S2*S2/S)
  EP(3,1,N)=-A*S1*S3/S
  EP(3,2,N)=-A*S2*S3/S
  EP(3,3,N)=A*(0.5-S3*S3/S)
  EP(1,2,N)=EP(2,1,N)
  EP(1,3,N)=EP(3,1,N)
  EP(2,3,N)=EP(3,2,N)
  EPZ(1,N)=A*(C-S1*S4/S)
  EPZ(2,N)=A*(C-S2*S4/S)
  EPZ(3,N)=-A*S3*S4/S
1004 CONTINUE
  CALL STIFF(NQ,SK8)
  DO 6001 I=1,8
  DO 6001 J=I,8
  SK8(I,J)=SK8(I,J)-SKEQ(I,J,NQ)
  SKEQ(I,J,NQ)=SKEQ(I,J,NQ)+SK8(I,J)
6001 CONTINUE
  CALL SADD(NQ,SK8)
14 CONTINUE
  RETURN
  END
  SUBROUTINE CHANGE(D,U)
  DIMENSION U(174)
  COMMON /C1/ NE,NN,NB,NEQ,X(87),Y(87),NOP(4,67),NP(174),NP1(268),NP
*2(268),NX(12),NY(12),EP(3,3,268),SI(4),TI(4),SII(4),TII(4),WG(4)
  COMMON /C5/ KS,LS, XF(87), YF(87)
  INTEGER P
  DO 5 NQ=1,NE
  I=NOP(1,NQ) $ J=NOP(2,NQ) $ K=NOP(3,NQ) $ P=NOP(4,NQ)
  XF(I)=X(I)+U(2*I-1) $ XF(J)=X(J)+U(2*J-1)
  XF(K)=X(K)+U(2*K-1) $ XF(P)=X(P)+U(2*NQ-1)
  YF(I)=Y(I)+U(2*I) $ YF(J)=Y(J)+U(2*J)
  YF(K)=Y(K)+U(2*K) $ YF(P)=Y(P)+U(2*P)
5 CONTINUE
  RETURN
  END
  SUBROUTINE BOND2(IO,U,F,DU,DF)
```

```

DIMENSION U(174),DU(174),F(174),DF(174)
COMMON /C1/ NE,NN,NB,NEQ,X(87),Y(87),NOP(4,67),NP(174),NP1(268),NP
*2(268),NX(12),NY(12),EP(3,3,268),SI(4),TI(4),SII(4),TII(4),WG(4)
COMMON/C5/KS,LS,XF(87),YF(87)
DELTA=0.0002
DO 10 KK=1,12
DI=Y(NY(1))+U(2*NY(1))-Y(NY(KK))-U(2*NY(KK))
IF(DI.LT.0.00000001) KS=KK
IF(DI.LT.0.00000001) DU(2*NY(KK))=-DELTA
IF(DI.LT.0.00000001) NP(2*NY(KK))=1
10 CONTINUE
IF(NP(2*NX(1)-1).EQ.0) GO TO 7
DO 20 KK=1,12
DI=X(NX(1))-X(NX(KK))-U(2*NX(KK)-1)
IF(DI.LT.0.00000001) LS=KK
IF(DI.LT.0.00000001) DU(2*NX(KK)-1)=0.0
IF(DI.LT.0.00000001) NP(2*NX(KK)-1)=1
20 CONTINUE
7 RETURN
END
SUBROUTINE YIELD2(U,F,DU,DF,D,IO)
DIMENSION U(174),DU(174),F(174),DF(174)
DIMENSION D(3,3),SSD(1,3),TSSD(3,1),W1(1,1),W2(1,3),W3(3,1),W4(3,3
*),W5(3,6),W6(6,3),SKE0(6,6),SKE(6,6),SK8(8,8),SHP(3,4)
COMMON /C1/ NE,NN,NB,NEQ,X(87),Y(87),NOP(4,67),NP(174),NP1(268),NP
*2(268),NX(12),NY(12),EP(3,3,268),SI(4),TI(4),SII(4),TII(4),WG(4)
COMMON /C2/ SK(174,34),SKEQ(8,8,67)
COMMON /C3/ DST(3,268),SS(3,268),DSS(3,268),TSTP(268),DTSTP(268),T
*SS(268),DTSS(268)
COMMON /C4/ TSS0(268),SSZ(268),DSSZ(268),EPZ(3,268)
COMMON/C5/KS,LS,XF(87),YF(87)
IF(IO.EQ.1) KKN=0
KKU=10H YP LT 0
NOR=60
NT=4*NE
YP=1000.0
XU=0.345 $ E1=0.7E06 $ H1=0.86E03 $ H=H1
G=E1/2.0/(1.0+XU)
CALL SOLVE(DU,DF)
N=0
DO 1 NQ=1,NE
DO 1001 L=1,4
N=N+1
SB=SII(L) $ TB=TII(L)
CALL SHAPE(SB,TB,XSJ,SHP,NQ)
DO 5003 I=1,3
5003 DST(I,N)=0.0
DO 5002 J=1,4
DST(1,N)=DST(1,N)+SHP(1,J)*DU(NOP(J,NQ)*2-1)
DST(2,N)=DST(2,N)+SHP(2,J)*DU(NOP(J,NQ)*2)
5002 DST(3,N)=DST(3,N)+SHP(1,J)*DU(NOP(J,NQ)*2)+SHP(2,J)*DU(NOP(J,NQ)*
*2-1)
DSS(1,N)=EP(1,1,N)*DST(1,N)+EP(1,2,N)*DST(2,N)+EP(1,3,N)*DST(3,N)
DSS(2,N)=EP(2,1,N)*DST(1,N)+EP(2,2,N)*DST(2,N)+EP(2,3,N)*DST(3,N)
DSS(3,N)=EP(3,1,N)*DST(1,N)+EP(3,2,N)*DST(2,N)+EP(3,3,N)*DST(3,N)
DSSZ(N)=EPZ(1,N)*DST(1,N)+EPZ(2,N)*DST(2,N)+EPZ(3,N)*DST(3,N)
IF(NP2(N).EQ.1) GO TO 1001
```

```
TT=SQRT((SS(1,N)+DSS(1,N)-SS(2,N)-DSS(2,N))**2+(SS(1,N)+DSS(1,N)-S
*SZ(N)-DSSZ(N))**2+(SS(2,N)+DSS(2,N)-SSZ(N)-DSSZ(N))**2+6.0*(SS(3,N
*)+DSS(3,N))**2)/SQRT(2.0)-TSS(N)
IF(TT.LT.0.0) GO TO 1001
A=(DSS(1,N)-DSS(2,N))**2+(DSS(1,N)-DSSZ(N))**2+(DSS(2,N)-DSSZ(N))*
**2+6.0*DSS(3,N)**2
B1=DSS(3,N)*SS(3,N)*6.0+(DSS(1,N)-DSS(2,N))*(SS(1,N)-SS(2,N))+DSS
*(1,N)-DSSZ(N))*(SS(1,N)-SSZ(N))+DSS(2,N)-DSSZ(N))*(SS(2,N)-SSZ(N)
*)
C=2.0*(TSS(N)**2-TSSO(N)**2)
BIG=(-B1+SQRT(B1**2-A*C))/A
IF(BIG.LT.YP) YP=BIG
IF(YP.LT.0.0) WRITE(6,103) Kku,NQ,A,C
1001 CONTINUE
1 CONTINUE
103 FORMAT(//,20X,A12,4X,I4,2(2X,E10.3),/,50(1H*))
IF(YP.LT.0.0) STOP
DO 180 KK=2,12
IF(NP(2*NY(KK)).EQ.1) GO TO 180
IF((Y(NY(1))+U(2*NY(1))+DU(2*NY(1))).GT.(Y(NY(KK))+U(2*NY(KK))+DU(
*2*NY(KK)))) GO TO 180
YP1=(Y(NY(1))+U(2*NY(1))-Y(NY(KK))-U(2*NY(KK)))/(DU(2*NY(KK))-DU(2
**NY(1)))
IF(YP1.GT.0.0.AND.YP1.LT.YP) YP=YP1
180 CONTINUE
IF(NP(2*NX(1)-1).EQ.0) GO TO 39
DO 190 KK=2,12
IF(NP(2*NX(KK)-1).EQ.1) GO TO 190
IF(X(NX(1)).GT.(X(NX(KK))+U(2*NX(KK)-1)+DU(2*NX(KK)-1)))GO TO 190
YP1=(X(NX(1))-X(NX(KK))-U(2*NX(KK)-1))/DU(2*NX(KK)-1)
IF(YP1.GT.0.0.AND.YP1.LT.YP) YP=YP1
190 CONTINUE
39 TT=0.0
IF(YP.GT.1.0) YP=1.0
N=0
DO 2 NQ=1,NE
DO 5004 M=1,4
N=N+1
DST(1,N)=DST(1,N)*YP
DST(2,N)=DST(2,N)*YP
DST(3,N)=DST(3,N)*YP
DSS(1,N)=DSS(1,N)*YP
DSS(2,N)=DSS(2,N)*YP
DSS(3,N)=DSS(3,N)*YP
DSSZ(N)=DSSZ(N)*YP
5004 CONTINUE
2 CONTINUE
N=0
DO 3 NQ=1,NE
DO 3 M=1,4
N=N+1
4 DTSS(N)=SQRT((SS(1,N)+DSS(1,N)-SS(2,N)-DSS(2,N))**2+(SS(1,N)+DSS(1
*,N)-SSZ(N)-DSSZ(N))**2+(SS(2,N)+DSS(2,N)-SSZ(N)-DSSZ(N))**2+6.0*(S
*S(3,N)+DSS(3,N))**2)/SQRT(2.0)-TSS(N)
IF(NP2(N).EQ.0) GO TO 5
H=H1
IF(DTSS(N).GE.0.0) GO TO 6
```

```
TSSO(N)=TSS(N)
NP2(N)=0
NP1(N)=1
DO 15 K=1, 3
15 DSS(K,N)=D(K,1)*DST(1,N)+D(K,2)*DST(2,N)+D(K,3)*DST(3,N)
DSSZ(N)=D(1,2)*DST(1,N)+D(1,2)*DST(2,N)
GO TO 4
6 DTSTP(N)=DTSS(N)/H
GO TO 3
5 DTSTP(N)=0.0
3 CONTINUE
DO 90 N=1, NEQ
90 U(N)=U(N)+YP*DU(N)
F(N)=F(N)+YP*DF(N)
N=0
DO 11 NQ=1, NE
DO 11 M=1, 4
N=N+1
TSS(N)=TSS(N)+DTSS(N)
TSTP(N)=TSTP(N)+DTSTP(N)
SSZ(N)=SSZ(N)+DSSZ(N)
DO 110 K=1, 3
SS(K,N)=SS(K,N)+DSS(K,N)
110 CONTINUE
11 CONTINUE
A=E1/(1.0+XU)
B1=(1.0-XU)/(1.0-2.0*XU)
C=XU/(1.0-2.0*XU)
N=0
DO 12 NQ=1, NE
IF(NP2(N+1).EQ.1.OR.NP2(N+2).EQ.1.OR.NP2(N+3).EQ.1.OR.NP2(N+4).EQ.
*1) GO TO 999
KN=0
IF(TSS(N+1)/TSSO(N+1).GE.0.995) KN=1
IF(TSS(N+2)/TSSO(N+2).GE.0.995) KN=1
IF(TSS(N+3)/TSSO(N+3).GE.0.995) KN=1
IF(TSS(N+4)/TSSO(N+4).GE.0.995) KN=1
IF(KN.EQ.1) GO TO 999
N=N+4
GO TO 12
999 TT=0.0
DO 5005 MO=1, 4
N=N+1
IF(NP2(N).EQ.1) GO TO 14
IF(TSS(N)/TSSO(N).GE.0.995) NP2(N)=1
IF(NP2(N).EQ.1) NP1(N)=0
IF(NP2(N).EQ.1) GO TO 14
IF(DTSS(N).GE.0.0) GO TO 5005
EPZ(1,N)=D(1,2)
EPZ(2,N)=D(1,2)
EPZ(3,N)=0.0
DO 13 K=1, 3
DO 13 M=1, 3
13 EP(K,M,N)=D(K,M)
GO TO 5005
14 TT=0.0
S=2.0/3.0*TSS(N)*TSS(N)*(1.0+H/3.0/G)
```

```
SH=(SS(1,N)+SS(2,N)+SSZ(N))/3.0
S1=SS(1,N)-SH
S2=SS(2,N)-SH
S3=SS(3,N)
S4=SSZ(N)-SH
EP(1,1,N)=A*(B1-S1*S1/S)
EP(2,1,N)=A*(C-S1*S2/S)
EP(2,2,N)=A*(B1-S2*S2/S)
EP(3,1,N)=-A*S1*S3/S
EP(3,2,N)=-A*S2*S3/S
EP(3,3,N)=A*(0.5-S3*S3/S)
EP(1,2,N)=EP(2,1,N)
EP(1,3,N)=EP(3,1,N)
EP(2,3,N)=EP(3,2,N)
EPZ(1,N)=A*(C-S1*S4/S)
EPZ(2,N)=A*(C-S2*S4/S)
EPZ(3,N)=-A*S3*S4/S
5005 CONTINUE
CALL STIFF(NQ,SK8)
DO 6001 I=1,8
DO 6001 J=I,8
SK8(I,J)=SK8(I,J)-SKEQ(I,J,NQ)
SKEQ(I,J,NQ)=SKEQ(I,J,NQ)+SK8(I,J)
6001 CONTINUE
CALL SADD(NQ,SK8)
12 CONTINUE
IF(MOD(I0,10).NE.0) GO TO 80
SUM1=ABS(U(2*NY(1)))
SUM6=ABS(U(2*NX(1)-1))
SUM2=0.0
SUM20=0.0
SUM3=0.0
SUM30=0.0
DO 220 KK=1,12
SUM2=SUM2+F(2*NY(KK))
IF(KK.EQ.1) GO TO 212
SUM20=SUM20+F(2*NY(KK)-1)
SUM30=SUM30+F(2*NX(KK))
212 TT=0.0
220 SUM3=SUM3+F(2*NX(KK)-1)
SUM2=ABS(SUM2)
SUM3=ABS(SUM3)
SUM20=ABS(SUM20)
SUM30=ABS(SUM30)
SUM4=X(NY(KS))+U(2*NY(KS)-1)
SUM5=Y(NX(LS))+U(2*NX(LS))
WRITE(3,230) SUM1, SUM2, SUM3, SUM4, SUM5, SUM6, SUM20, SUM30
230 FORMAT(8(E12.5))
80 TT=0.0
IF(MOD(I0,10).NE.0) GO TO 330
WRITE(6,26)I0
26 FORMAT(/,1X,13HLOADING STEP=,I4)
WRITE(6,4000)
4000 FORMAT(/,50X,13HPLASTIC ZONES,/,120(1H*))
WRITE(6,4081)((N, NP2(N)),N=1,NT)
4081 FORMAT(7(I4,4X,I2,8X))
WRITE(6,1990)
```

```
1990 FORMAT(/)
      WRITE(6,10000)
10000 FORMAT(2X,2HNO,16X,2HUX,16X,2HUY,16X,2HFX,16X,2HFY,13X,5HDTSTP,14X
*,4HTSTP,15X,3HTSS,/,130(1H*))
      N=0
      DO 420 NQ=1,NE
      SUM1=0.0
      SUM2=0.0
      SUM3=0.0
      DO 42 MO=1,4
      N=N+1
      SUM1=SUM1+TSS(N)
      SUM2=SUM2+TSTP(N)
      SUM3=SUM3+DTSTP(N)
42    CONTINUE
      SUM1=SUM1/4.0 $ SUM2=SUM2/4.0 $ SUM3=SUM3/4.0
      X1=U(2*NQ-1) $ X2=U(2*NQ) $ Y1=F(2*NQ-1) $ Y2=F(2*NQ)
      WRITE(6,32)(NQ,X1,X2,Y1,Y2,SUM3,SUM2,SUM1)
420   CONTINUE
32    FORMAT(I4,7(6X,E12.5))
      K1=NE+1 $ K2=NN
      DO 430 I=K1,K2
      X1=U(2*I-1)
      X2=U(2*I)
      Y1=F(2*I-1)
      Y2=F(2*I)
      WRITE(6,32)(I,X1,X2,Y1,Y2)
430   CONTINUE
330   IF(I0.NE.NOR) GO TO 33
      WRITE(6,45)
45    FORMAT(///,2X,2HNO,24X,1HX,24X,1HY,/,60(1H*),//)
      N=0
      DO 44 NQ=1,NE
      I=NQ
      XX=X(I)+U(2*I-1)
      YY=Y(I)+U(2*I)
      SUM1=0.0 $ SUM2=0.0 $ SUM3=0.0
      DO 62 MO=1,4
      N=N+1
      SUM1=SUM1+TSS(N)
      SUM2=SUM2+TSTP(N)
      S1=SS(1,N)$S2=SS(2,N)$S3=SS(3,N)
      TA=SQRT((S1-S2)**2/4.0+S3**2)
      SUM3=SUM3+TA
62    CONTINUE
      SUM1=SUM1/4.0 $ SUM2=SUM2/4.0 $ SUM3=SUM3/4.0
      V1=U(2*I-1)$V2=U(2*I)$V3=DU(2*I-1)$V4=DU(2*I)
      V5=0.0 $ V6=0.0
      WRITE(6,46)(I,XX,YY)
46    FORMAT(1X,I3,10X,E15.5,10X,E15.5)
      WRITE(4,102) I,X(I),Y(I),V1,V2,V3,V4,V5,V6,SUM1,SUM2,SUM3
102   FORMAT(I10,11(E10.3))
44    CONTINUE
      K1=NE+1 $ K2=NN
      DO 63 I=K1,K2
      XX=X(I)+U(2*I-1)
      YY=Y(I)+U(2*I)
```



```

V1=U(2*I-1)$V2=U(2*I)$V3=DU(2*I-1)$V4=DU(2*I)
WRITE(6,46)(I,XX,YY)
WRITE(4,102) I,X(I),Y(I),V1,V2,V3,V4
63  CONTINUE
33  RETURN
    END
C*****
C*****  EVALUATION OF THE SHAPE FUCTION AT POINT (S,T) *****
    SUBROUTINE SHAPE(S,T,XSJ,SHP,N)
    DIMENSION XS(2,2),SHP(3,4)
    COMMON /C1/ NE,NN,NB,NEQ,X(87),Y(87),NOP(4,67),NP(174),NP1(268),NP
*2(268),NX(12),NY(12),EP(3,3,268),SI(4),TI(4),SII(4),TII(4),WG(4)
    COMMON/C5/KS,LS,XF(87),YF(87)
    DO 100 I=1,4
    SHP(3,I)=(0.5+SI(I)*S)*(0.5+TI(I)*T)
    SHP(1,I)=SI(I)*(0.5+TI(I)*T)
100  SHP(2,I)=TI(I)*(0.5+SI(I)*S)
    DO 200 I=1,2
    DO 200 J=1,2
    XS(I,J)=0.0
    DO 200 K=1,4
    IF(J.EQ.1) TT=XF(NOP(K,N))
    IF(J.EQ.2) TT=YF(NOP(K,N))
200  XS(I,J)=XS(I,J)+TT*SHP(I,K)
    XSJ=XS(1,1)*XS(2,2)-XS(1,2)*XS(2,1)
    DO 300 I=1,4
    TEMP=(XS(2,2)*SHP(1,I)-XS(1,2)*SHP(2,I))/XSJ
    SHP(2,I)=(-XS(2,1)*SHP(1,I)+XS(1,1)*SHP(2,I))/XSJ
300  SHP(1,I)=TEMP
    RETURN
    END
C*****
C*****  EVALUATION OF THE ELEMENTAL STIFFNESS MATRIX *****
    SUBROUTINE STIFF(NQ,S)
    DIMENSION S(8,8),SHP(3,4)
    COMMON /C1/ NE,NN,NB,NEQ,X(87),Y(87),NOP(4,67),NP(174),NP1(268),NP
*2(268),NX(12),NY(12),EP(3,3,268),SI(4),TI(4),SII(4),TII(4),WG(4)
    DO 50 I=1,8
    DO 50 J=I,8
50  S(I,J)=0.0
    S(2,1)=0.0 $ S(3,2)=0.0 $ S(4,3)=0.0 $ S(5,4)=0.0 $ S(6,5)=0.0
    S(7,6)=0.0 $ S(8,7)=0.0
    DO 100 L=1,4
    SB=SII(L) $ TB=TII(L)
    CALL SHAPE(SB,TB,XSJ,SHP,NQ)
    DV=XSJ*WG(L)
    N=4*(NQ-1)+L
    D11=EP(1,1,N)*DV $ D12=EP(1,2,N)*DV $ D13=EP(1,3,N)*DV
    D22=EP(2,2,N)*DV $ D23=EP(2,3,N)*DV $ D33=EP(3,3,N)*DV
    DO 100 J=1,4
    DB11=D11*SHP(1,J)+D13*SHP(2,J) $ DB12=D12*SHP(2,J)+D13*SHP(1,J)
    DB21=D12*SHP(1,J)+D23*SHP(2,J) $ DB22=D22*SHP(2,J)+D23*SHP(1,J)
    DB31=D13*SHP(1,J)+D33*SHP(2,J) $ DB32=D23*SHP(2,J)+D33*SHP(1,J)
    DO 100 I=1,J
    S(I+I-1,J+J-1)=S(I+I-1,J+J-1)+SHP(1,I)*DB11+SHP(2,I)*DB31
    S(I+I-1,J+J)=S(I+I-1,J+J)+SHP(1,I)*DB12+SHP(2,I)*DB32
    S(I+I,J+J-1)=S(I+I,J+J-1)+SHP(1,I)*DB31+SHP(2,I)*DB21

```

```
100  S(I+I ,J+J )=S(I+I, J+J )+SHP(1, I)*DB 32+SHP(2, I)*DB 22
      RETURN
      END
      SUBROUTINE SADD(N, SKE)
      DIMENSION SKE(8, 8)
      COMMON /C1/ NE, NN, NB, NEQ, X(87), Y(87), NOP(4, 67), NP(174), NP1(268), NP
*2(268), NX(12), NY(12), EP(3, 3, 268), SI(4), TI(4), SII(4), TII(4), WG(4)
      COMMON /C2/ SK(174, 34), SKEQ(8, 8, 67)
      DO 1 JJ=1, 4
      NROW=(NOP(JJ, N)-1)*2
      DO 1 J=1, 2
      NROW=NROW+1
      I=(JJ-1)*2+J
      DO 2 KK=1, 4
      NCOLB=(NOP(KK, N)-1)*2
      DO 3 K=1, 2
      L=(KK-1)*2+K
      NCOL=NCOLB+K+1-NROW
      IF(NCOL)3, 3, 4
4      IF(L.LT.I) SKE(I, L)=SKE(L, I)
      SK(NROW, NCOL)=SK(NROW, NCOL)+SKE(I, L)
3      CONTINUE
2      CONTINUE
1      CONTINUE
      RETURN
      END
      SUBROUTINE SOLVE(U, F)
      DIMENSION SKI(174, 34), FI(174), F(174), U(174)
      COMMON /C1/ NE, NN, NB, NEQ, X(87), Y(87), NOP(4, 67), NP(174), NP1(268), NP
*2(268), NX(12), NY(12), EP(3, 3, 268), SI(4), TI(4), SII(4), TII(4), WG(4)
      COMMON /C2/ SK(174, 34), SKEQ(8, 8, 67)
      COMMON /C3/ DST(3, 268), SS(3, 268), DSS(3, 268), TSTP(268), DTSTP(268), T
*SS(268), DTSS(268)
      DO 1 I=1, NEQ
      IF(NP(I).EQ.0) FI(I)=F(I)
      IF(NP(I).EQ.1) FI(I)=SK(I, 1)*U(I)*10.0E20
      IF(NP(I).EQ.1.AND.U(I).EQ.0.0) FI(I)=SK(I, 1)*10.0E10
      DO 2 J=1, NB
2      SKI(I, J)=SK(I, J)
      IF(NP(I).EQ.1) SKI(I, 1)=SKI(I, 1)*10.0E20
1      CONTINUE
      DO 300 N=1, NEQ
      I=N
      DO 290 L=2, NB
      I=I+1
      IF(SKI(N, L)) 240, 290, 240
240  C=SKI(N, L)/SKI(N, 1)
      J=0
      DO 270 K=L, NB
      J=J+1
      IF(SKI(N, K)) 260, 270, 260
260  SKI(I, J)=SKI(I, J)-C*SKI(N, K)
270  CONTINUE
280  SKI(N, L)=C
      FI(I)=FI(I)-C*FI(N)
290  CONTINUE
300  FI(N)=FI(N)/SKI(N, 1)
```

```

      N=NEQ
350  N=N-1
      IF(N) 500,500,360
360  L=N
      DO 400 K=2,NB
          L=L+1
          IF(SKI(N,K)) 370,400,370
370  FI(N)=FI(N)-SKI(N,K)*FI(L)
400  CONTINUE
      GO TO 350
500  TT=0.0
      DO 3 N=1,NEQ
          IF(NP(N).EQ.1) GO TO 3
          U(N)=FI(N)
3    CONTINUE
      DO 4 N=1,NEQ
          IF(NP(N).EQ.0) GO TO 4
          SUM=0.0
          K=N+1
          L=0
          DO 5 J=1,NB
              K=K-1
              L=L+1
              IF(K.EQ.0) GO TO 6
5          SUM=SUM+SK(K,L)*U(K)
6          TT=0.0
          DO 7 J=2,NB
              IF(SK(N,J).EQ.0.0) GO TO 7
              SUM=SUM+SK(N,J)*U(N-1+J)
7          CONTINUE
          F(N)=SUM
4          CONTINUE
      RETURN
      END
      SUBROUTINE MULT1(A,B,C,M,N,L)
      DIMENSION A(M,N),B(N,L),C(M,L)
      DO 1 I=1,M
          DO 1 J=1,L
              C(I,J)=0.0
          DO 1 K=1,N
1          C(I,J)=C(I,J)+A(I,K)*B(K,J)
      RETURN
      END
```

REFERENCES

1. Fuchs, F.J., High pressure continuous extrusion. Research Report, Western Electric Co., Princeton, New Jersey, U.S.A.
2. Fuchs, F.J., Apparatus and method for continuous extrusion. U.S. Patent No. 3.740.985, June 1975.
3. Green, D., Continuous extrusion-forming of wire sections. J. Inst. of Metals, 100, P. 295, 1972.
4. Avitzur, B., Extrolling: A concept for continuous wire making machines. Soc. of Manufacturing Engineers, MF 75-140, 1975.
5. Voorhes, W.G., Extrusion Process. U.S. Patent No. 3.922.898, December 1975.
6. Lengyel, B., Continuous extrusion. Provisional British Patent Specification No. 262, 1976.
7. Mendelson, A. and S.S. Manson, Practical solution of plastic deformation problems in the elastic-plastic range. NASA TR-28, 1959.
8. Gallagher, R.H., J. Padlog and P.P. Biljaard, Stress analysis of heated complex shapes. ARS Journal, 32, 700-707, 1962.
9. Argyris, J.H., S. Kelsey and H. Kamel, Matrix methods of structural analysis. AGARD-Ograph, Pergamon press, 1963 (edited by Fraeijs de veubeke).
10. Pope, G.G. , A discrete element method for the analysis of plane elasto-plastic stress problems. Royal Aircraft Establishment, TR 65028, 1965.
11. Marcal, P.V., The elastic-plastic straining of some shells of revolution with special reference to expansion belows. Ph.D. Thesis, Univ. of London, 1965.

12. Marcal, P.V. and C.E. Turner, Elasti-plastic behaviour of axisymmetrically loaded shells of revolution. *J. Mech. Eng. Sci.*, 5, P. 232, 1963.
13. Marcal, P.V., A stiffness method for elastic-plastic problems. *Int. J. Mech. Sci.*, 7, 229-238, 1965.
14. Marcal, P.V. and I.P. King, Elastic-plastic analysis of two-dimensional stress systems by the finite element method. *Int. J. Mech. Sci.*, 9, 143-155, 1967.
15. Akyuz, F.A. and J.E. Merwin, Solution of non-linear problems of elasto-plasticity by the finite element method. *AIAA Journal*, 6, 1825-1831, 1968.
16. Lee, C.H. and S. Kobayashi, Elasto-plastic analysis of plane strain and axisymmetric flat punch indentation by the finite element method. *Int. J. Mech. Sci.*, 12, 349-370, 1970.
17. Lee, C.H. and S. Kobayashi, Analysis of axisymmetric upsetting and plane strain side-pressing of solid cylinders by the finite element method. *J. Eng. for Ind.*, 93, 445-454, 1971.
18. Scharpf, D.W., Die Frage der Konvergnz bei der Berechnung Elasto-plastisch deformierbarer Tragwerke und Kontinua. Doctoral Thesis, Stuttgart Univ., 1969.
19. Argyris, J.H. and D.W. Scharpf, Methods of elasto-plastic analysis. *ZAMP*, 23, 517-552, 1972.
20. Yamada, Y., N. Yoshimura and T. Sakurai, Plastic stress-strain matrix and its application for the solution of elastic-plastic problems by the finite element method. *Int. J. Mech. Sci.*, 10, 343-354, 1968.
21. Blomfield, J.L., A review of the methods for calculating elastic-plastic strains in general and in particular in pipe

- bends and shells of revolution. To be published.
22. Marcal, P.V., Comparative study of numerical methods of elastic-plastic analysis. AIAA Journal, 6, 157-158, 1968.
  23. Iwata, K., K. Osakada and S. Fujino, Analysis of hydrostatic extrusion by the finite element method. J. Eng. for Ind., 64, 697-703, 1972.
  24. Nagamatsu, A., T. Murota and T. Jimma, On the non-uniform deformation of block in plane strain caused by friction. Bulletin of the JSME, 13, 1385-1402, 1970.
  25. Nagamatsu, A., T. Murota and T. Jimma, On the non-uniform deformation of material in axially symmetric compression caused by friction. Bulletin of the JSME, 14, 331-347, 1971.
  26. Mallett, R.H. and P.V. Marcal, Finite element analysis of non-linear structures. J. Struct, Div. of ASCE, 94, 2081-2105, 1968.
  27. Felippa, C.A, Refined finite element analysis of linear and non-linear two-dimensional structures. Ph.D. Thesis, Univ, of California, 1966.
  28. Turner, M.J., E.H. Dill, H.C. Martin and R.J. Melosh, Large deflection analysis of complex structures subjected to heating and external loads. J. Aero. Space Sci., 27, 97-106, 1960.
  29. Zienkiewicz, O.C., S. Valliapan and I.P. King, Elastic-plastic solutions of engineering problems, Initial stress finite element approach. Int. J. Num. Methods, 1, 75-100, 1969.
  30. Nayak, G.C. and O.C. Zienkiewicz, Elastic-plastic stress analysis. Int. J. Num. Methods, 5, 113-135, 1972.

31. Nayak, G.C., Plasticity and large deformation problems by the finite element method. Ph.D. Thesis, Univ. of Wales, Swansea, 1971.
32. Pian, P.H.H. and Pin Tong, Basis of finite element methods for solid continua. Int. J. Num. methods, 1, 3-28, 1968.
33. Yaghmai, S., Incremental analysis of large deformations in mechanics of solids with applications to axisymmetric shells of revolution. Ph.D. Thesis, Univ. of California, NASA CR-1350, 1969.
34. Oden, J.T., A general theory of finite elements. Int. J. Num. Methods, 1, 205-221, 1969.
35. Marcal, P.V., Finite element analysis of combined problems of non-linear material and geometric behaviour. Procs. ASME Joint Computer Conference on computational Approach to Applied Mechanics, 133-149, 1969.
36. Hibbitt, D.H., P.V. Marcal and J.R. Rice, A finite element formulation for problems of large strain and large displacement. Int. J. Sols. Structs., 6, 1069-1086, 1970.
37. Gordon, J.L. and A.S. Weinstein, A finite element analysis of the plane-strain drawing problem. Procs. 2nd. North-American Metalworking Research Conf., 194-208, Univ. Wisconsin, Madison, 1974.
38. Biot, M.A., Mechanics of incremental deformations. Wiley, New York, 1965.
39. Kudo, H. and S. Matsubara, The use of finite element method in the analysis of plastic deformation of some metal forming processes. Keynote paper to 24th. CIRP General Assembly, Tokyo, 1974.
40. Kitagawa, H., Y. Seguchi and Y. Tomita, An incremental theory of large

- displacements and its finite element formulation.  
Ing. Archiv., 41, 313-224, 1972.
41. Osias, J.R., Finite element formulation of elastic-plastic solids.  
NASA CR-2199, 1973.
42. Osias, J.R. and J.L. Swedlow, Finite elasto-plastic deformation,  
I-Theory and numerical examples. Int. J. Sol. Struct.,  
10, 321-339, 1974.
43. Osias, J.R. and J.L. Swedlow, Finite elasto-plastic deformation,  
II-Necking in tensile bars. Report SM-73-4, Dept. Mech.  
Eng., Carnegie Mellon Univ., 1973.
44. Swedlow, J.L., Character of the equations of elastic-plastic flow in  
three independent variables. Int. J. Non-linear Mech.,  
3, 325-336, 1968.
45. Swedlow, J.L., Approaches to non-linear problems. Procs. ASME Joint  
Computer Conf. on Computational Approach to Appl.  
Mech., 191-199, 1969.
46. Swedlow, J.L., A review of developments in the theory of elastic-  
plastic flow. NASA CR-2321, 1973.
47. Swedlow, J.L., A procedure for solving problems of elastic-plastic  
flow. Comps. and Structs., 3, 879-898, 1973.
48. Zienkiewicz, O.C. and P.N. Godbole, Flow of plastic and visco-  
plastic solids with special reference to extrusion  
and forming processes. Int. J. Num. Methods, 8,  
3-16, 1974.
49. Zienkiewicz, O.C. and I.C. Corneum, Visco-plasticity, plasticity  
and creep in elastic solids. Int. J. Num. Methods, 8,  
821-845, 1974.
50. Corneau, I., Numerical stability in quasi-static elasto-visco-



- plasticity. Int. J. Num. Methods, 9, 109-127, 1975.
51. Gotoh, M., A finite element analysis of general deformation of sheet metals. Int. J. Num. Methods, 8, 731-741, 1974.
52. Dieterle, K., Faltenbildung als verfahrensgrenze beim Stauchen von Hohlkörpern. Bericht Nr. 30, Institut für Umformtechnik (Univ. Stuttgart), Verlag Girardet, Essen, 1975.
53. Gunasekera, J.S. and J.M. Alexander, Matrix analysis of the large deformation of an elastic-plastic axially symmetric continuum. Symp. on Foundations of plasticity, 125-146, Noordhoff, Leyden, 1973.
54. Blass, A., A finite element approach in metal-working and its application to the radial upsetting process, Ph.D. Thesis, Imperial College of London, 1976.
55. Lee, E.H., Elastic-plastic deformation of finite strain. J. Appl. Mech., 36, 1-6, 1969.
56. Argyris, J.H., Elasto-plastic matrix displacement analysis of three dimensional continua. J. Royal Aero. Soc., 69, 663-635, 1965.
57. Jain, S.C. and S. Kobayashi, Deformation and fracture of an aluminium alloy in plane-strain side-pressing, presented at the 11th International Machine Tool Design and Research Conference, Birmingham, England, 14-18, 1970.
58. Male, A.T. and Cockcroft, A method for the determination of the coefficient of friction of metals under conditions of bulk plastic deformation, I. Inst. Met., 93, 38-46, 1964-65.

59. Hartley, P., C.E.N. Sturgess and G.W. Rowe, Friction in finite element analysis of metalforming processes, Int. J. Mech. Sci., 21, 301-311, 1979.
60. Chitkara, N.R., W. Johnson, M. Ueda, Incremental forging of balls from cylindrical specimens and of rollers from rectangular solids, Presented at the 16th International Machine Tool Design and Research Conference, 431-446, 1975.